Special Issue Reprint

Bio-Active Products from Mangrove Ecosystems

Edited by
Wenhan Lin, Guoqiang Li and Jing Xu

www.mdpi.com/journal/marinedrugs

MDPI

Bio-Active Products from Mangrove Ecosystems

Bio-Active Products from Mangrove Ecosystems

Editors

Wenhan Lin
Guoqiang Li
Jing Xu

MDPI

Editors

Wenhan Lin
Peking University,
Beijing, China

Guoqiang Li
Ocean University of China,
Qingdao, China

Jing Xu
Hainan University,
Haikou, China

This is a reprint of articles from the Special Issue published online in the open access journal *Marine Drugs* (ISSN 1660-3397) (available at: https://www.mdpi.com/journal/marinedrugs/special_issues/mangrove_ecosystems).

For citation purposes, cite each article independently as indicated on the article page online and as indicated below:

LastName, A.A.; LastName, B.B.; LastName, C.C. Article Title. *Journal Name* **Year**, *Volume Number*, Page Range.

Contents

About the Editors

Wenhan Lin

Wenhan Lin received his BS at the Department of Chemistry at Wenzhou University in 1982. He received the MS and PhD degrees during 1985–1990 from Shanghai Institute of Materia Medica, Chinese Academy of Sciences, where he studied phytochemistry including the isolation and structural characterization of bioactive natural products from medicinal plants. Then, he accepted a position for the postdoctoral fellowship (1990–1992) at Beijing Medical University (Medical Health Center, Peking University). After he was promoted as an associate professor at the same university in 1993, he visited the Federal University of Rio de Janeiro in Brazil as a guest researcher for one year (1993), Toho University of Japan as an oversea special researcher (1994), San Paolo University of Brazil as a guest researcher (1995), and Duesseldorf University of Germany as a visiting professor (2000–2001). From 1996 until now, he has been a full professor of medicinal chemistry at the School of Pharmaceutical Sciences of Peking University. For the last two decades, his research topic mainly focuses on the bioactive and structurally novel metabolites derived from marine organisms (sponges and corals), and their associated microorganisms. He has published around 350 peer-reviewed papers in scientific journals, and applied more than 20 patents.

Guoqiang Li

Guoqiang Li is currently a professor of medicinal chemistry at the Ocean University of China. He obtained his master's degree in 1992 from Lanzhou University, mentored by Prof. Zhongjian Jia, and his doctoral degree in 2004 from the Ocean University of China (jointly trained by Peking University) under the supervision of Prof. Huashi Guan and Prof. Wenhan Lin. In 2004, he joined the Ocean University of China at the School of Medicine and Pharmacy. His research interests include bioactive marine natural product discovery and structural optimization.

Jing Xu

Jing Xu obtained her BS and MS degrees from Hainan University. Since 2006, she has carried out doctoral research with Professor Huashi Guan at the College of Medicine and Pharmaceutics, Ocean University of China. Since 2007, she has continued doctoral research in the group of Prof. Peter Proksch and received her PhD degree in 2010 at Heinrich-Heine-Universität Düsseldorf, Germany, where she sparked an interest in mangrove microbial natural products with a particular focus on bioactive molecules, which has continued to this day. She joined the faculty of Hainan University after her graduation, where she is currently a Professor on Pharmaceutical Chemistry. She undertook a postdoctoral appointment at Nanjing University simultaneously, with Prof. Renxiang Tan, during 2011–2014. She spent 2016 working with Prof. Dr. Peter Leadley at the University of Cambridge as visiting scholar.

MDPI

Editorial

Bio-Active Products from Mangrove Ecosystems

Wenhan Lin [1,*], Guoqiang Li [2,*] and Jing Xu [3,*]

[1] State Key Laboratory of Natural and Biomimetic Drugs, Institute of Ocean Research, Peking University, Beijing 100191, China

[2] Key Laboratory of Marine Drugs, Chinese Ministry of Education, School of Medicine and Pharmacy, Ocean University of China, Qingdao 266003, China

[3] Collaborative Innovation Center of Ecological Civilization, School of Chemical Engineering and Technology, Hainan University, Haikou 570228, China

[*] Correspondence: whlin0526@126.com (W.L.); liguoqiang@ouc.edu.cn (G.L.); happyjing3@163.com (J.X.)

Mangrove communities represent the coastal habitats located in intertidal zones or brackish waters of tropical and subtropical coastal areas in over 118 countries [1]. Typical mangrove ecosystems including highly saline or brackish water, high solar irradiation, and tidal gradients, inducing mangrove residents to evolve biodiversity for environmental adaptations. Mangrove plants and the associated microorganisms encode unique biosynthetic genes which have the potential to generate chemical diversity and novelty with promising pharmaceutical applications. In recent decades, numerous metabolites with uncommon structures and efficacious bioactivities have been discovered from mangrove hosts and their associated microorganisms.

The emergence of drug-resistance and rising pathogen mutations attenuates the potency of current antimicrobial drugs. Thus, mining structurally novel and pharmacologically potent natural products from mangrove ecosystems has attracted a great deal of attention from chemists and pharmacologists. Additionally, a broad range of chemical structures with unique scaffolds imply that their biogenesis involves novel functional genes and corresponding enzymes with unique catalytic functions.

This Special Issue "Bio-Active Products from Mangrove Ecosystems" (https://www.mdpi.com/journal/marinedrugs/special_issues/mangrove_ecosystems, accessed on 3 March 2022) contains ten peer-reviewed articles, including three comprehensive reviews and seven research papers on different topics related to new approaches and information on bioactive compounds with privileged scaffolds, such as polyketides, alkaloids and terpenoids, derived from mangrove fungi with potential for anticancer, antimicrobial, antioxidant, antidiabetic, and immunosuppressive activities, and elucidation of ecological defense functions. Herein, we introduce a brief overview of the main achievements contributed by each study.

A review by Wu et al. [2] introduces unusual secondary metabolites from mangrove ecosystems, reporting 134 metabolites, which are classified into two major families in terms of the biological sources and 15 subfamilies according to the chemical structures, covering the period from 2010 to 2022. The structures, biological activities, biosynthesis, and total chemical syntheses of some unique compounds are included. A majority of these compounds are produced by mangrove-associated microorganisms, and more than 70% were isolated from endophyte fungi, indicating a remarkable chemical diversity of the microbial community. In addition, these compounds display diverse and remarkable biological activities and are frequently reported as antimicrobial and cytotoxic compounds. Structurally diverse secondary metabolites play a crucial role in the discovery of new natural products with interesting pharmacophores. Secondary metabolites featuring new scaffolds, unique ring systems, or unusual functional groups might merit the attention of chemists and biologists and could be a source of fresh pharmacophores with biological activity for the creation of drugs based on natural products.

The second review by Sulaiman et al. [3] provides a comprehensive review of antibacterial, antifungal, and antiviral natural products from the mangrove plants in Asia and the Pacific reported from 1968 to 2022. Among the 286 plant species, 119 exhibited antimicrobial effects, and a total of 114 antimicrobial natural products have been identified including 12 with MIC values below 1 µg/mL. A vast array of antimicrobial secondary metabolites that could be further examined for development of anti-infectives to mitigate infectious diseases such as the White Spot Syndrome Virus infection in aquaculture is described. In parallel, the use and promotion of mangrove plants in aquacultures are beneficial as the rise in the global population which requires a huge supply shrimps, prawns, crabs, and fish globally necessitates the preservation of mangroves.

Small molecules with different mechanisms of fibrinolysis action are desired for new antithrombotics and thrombolytics. Hang et al. [4] list a series of bioactive staplabin congeners which not only possess fibrinolytic activity but also exhibit various effects, such as anti-inflammatory, neuroprotective, and anti-cancer properties. The authors focused on the diverse biological activities of SMTP-7 (compound 1, also known as FGFC1), an isoindolone alkaloid from the marine fungi *Starchbotrys longispora* FG216 and *Stachybotrys microspora* IFO 30018, that possesses diverse bioactivities such as thrombolytic, anti-inflammatory, and anti-oxidative properties and selective anti-cancer activity. These properties make SMTP-7 an attractive option for the development of drugs for the treatment of various diseases, including cerebral infarction, stroke, ischemia/reperfusion damage, acute kidney injury, non-small cell lung cancer, and especially for cerebral infarction. The recent progress in structure–function relationships, preparation methods, identification of diverse biological activities and mechanism of SMTP-7 and its congeners is summarized, thereby illustrating its high therapeutic potential.

Cai et al. [5] reported 6 novel isocoumarins, namely talaromarins A-F, along with 17 known analogues from the mangrove-derived fungus *Talaromyces flavus* TGGP35. Their structures were elucidated by extensive analysis of spectroscopic data, modified Mosher's method, and ECD spectra. Eleven compounds (including talaromarin F) showed similar or better antioxidant activity compared with the positive control trolox, of which 6,8-dihydroxy-3-(2-hydroxypropyl)-7-methyl-1*H*-isochromen-1-one was the most active and showed ABTS radical scavenging capacity with an IC_{50} value of 0.009 mM. Moreover, 5,6-dihydroxy-3-(4-hydroxypentyl)-isochroman-1-one, peniciisocoumarin D, penicimarin N, and pestalotiorin exhibited strong inhibitory activity against α-glucosidase with IC_{50} values ranging from 0.10 to 0.62 mM, while the positive control acarbose showed an IC_{50} value of 0.5 mM.

Four previously unreported drimane sesquiterpenoids, named ustusol F, 9-deoxyustusol F, ustusol G, ustusolate H, in addition to ustusolate I, ustusolate J, and ustusol B, were isolated and structurally characterized from the fermentation broth of the mangrove-derived *Aspergillus ustus* 094102 by Gui et al. [6]. Ustusolate I has two pairs of enantiomers of the gem diol in the side chain, namely (2*E*, 4*E*; 6,7-erythro)-ustusolate I and (2*E*, 4*E*; *ent*-6,7-*erythro*)-ustusolate I, and (2*E*, 4E, 6*R*, 7*R*)- ustusolate I and (2*E*, 4E, 6*S*, 7*S*)-ustusolate I, which were purified using HPLC. The antiproliferative activities of the isolated compounds were evaluated against 29 human cancer cell lines and a non-cancer cell line, of which ustusolate I showed an antiproliferative effect against the human tumor cells CAL-62 and MG-63 with IC_{50} values of 16.3 and 10.1 µM, respectively.

Wang et al. [7] first systematically evaluated the diversity of cultivable fungi associated with the medicinal mangrove *Acanthus ilicifolius* collected from the South China Sea. A total of 102 fungal strains were isolated from *A. ilicifolius* and 84 independent culturable isolates were identified using a combination of morphological characteristics and internal transcribed spacer (ITS) sequence analyses, of which 37 strains were selected for phylogenetic analysis. The identified fungi belonged to 22 genera within seven taxonomic orders of one phyla, of which four genera *Verticillium*, *Neocosmospora*, *Valsa*, and *Pyrenochaeta* were first isolated from mangroves. Thirty-one strains of fungi displayed strong cytotoxicity to different human cancer cell lines: A-549, HeLa, HepG, and Jurkat. Integrating a cytotoxic

activity-guided strategy and fingerprint analysis, a well-known natural Golgi-disruptor and Arf-GEF inhibitor, brefeldin A, was quickly isolated from the active strains.

Feng et al. [8] reported three previously undescribed cytochalasins, namely phomoparagins A-C, together with five previously reported analogs from the mangrove-derived endophytic fungus *Phomopsis asparagi* DHS-48. Notably, phomoparagin A possessed an unprecedented 5/6/5/8/5-fused pentacyclic skeleton. These compounds were tested for their inhibitory activity against concanavalin A (ConA)/lipopolysaccharide (LPS)-induced spleen lymphocyte proliferation and the calcineurin (CN) enzyme. Phomoparagin B, phomopchalasins A and B, as well as cytochalasin H exhibited robust inhibitory activities with a relatively low toxicity. Moreover, phomoparagin B was shown to inhibit ConA-stimulated activation of NFAT1 dephosphorylation and block NFAT1 translocation in vitro, subsequently inhibiting the transcription of interleukin-2 (IL-2), whereas it directly inhibited calcineurin and did not require a matchmaker protein, such as the clinical immunosuppressants CsA and FK506.

Epigenetic manipulation was described as an effective method to stimulate gene clusters which are 'silent', 'orphan', and 'cryptic' for enhancing secondary metabolite expression without altering genes or causing the hereditable manipulation of microorganisms. Feng et al. [9] conducted an epigenetic manipulation of the aforementioned *Phomopsis asparagi* DHS-48 with the histone deacetylase (HDAC) inhibitor sodium butyrate and the DNA methyltransferase (DNMT) inhibitor 5-azacytidine (5-Aza). Based on the colony growth, dry biomass, HPLC, and ^{1}H NMR analyses, the fungal chemical profile was significantly different compared to the control, and an optional modifier (50 μM sodium butyrate) was selected for the follow up fermentation. Two undescribed compounds, named phaseolorin J and phomoparagin D, along with three previously reported chromones and previously described cytochalasins, were isolated from the culture treated with sodium butyrate. Their structures, including absolute configurations, were elucidated using a combination of detailed HRESIMS, NMR, and ECD analyses and ^{13}C NMR calculations. Phaseolorin J and phaseolorin J2 were found to be moderate immunosuppressants, inhibiting the proliferation of ConA (concanavalin A)-induced T and LPS (lipopolysaccharide)-induced B murine spleen lymphocytes. Additionally, phomoparagin D exhibited significant in vitro cytotoxicity against the human cancer cell lines Hela and HepG2.

Cai et al. [10] described two previously undescribed chlorinated metabolites, 8-chlorine-5-hydroxy-2,3-dimethyl-7-methoxychromone and 3,4-dichloro-1*H*-pyrrole-2,5-dione, together with eight known polyketides from the mangrove sediment-derived fungus Mollisia sp. SCSIO4140. X-ray single-crystal diffraction allowed the assignment of its absolute configuration of (4*S*, 5*S*, 13*R*, 14*R*, 17*R*, 18*R*, 21*R*)-stemphone C for the first time. 3,4-Dichloro-1*H*-pyrrole-2,5-dione and stemphone C showed different degrees of antimicrobial activity against several pathogenic fungi and bacteria, and antiproliferative activities against two human prostate cancer cell lines, PC-3 and 22Rv1. Furthermore, stemphone C was found to exhibit antiproliferative activity against two prostate cancer cell lines (PC-3 and 22Rv1) along with HepG2, WPMY-1, and MC3T3-E1. This compound reduced PC-3 cell colony formation, inducing apoptosis, and blocked the cell cycle at *S*-phase in a dose-dependent manner, revealing its use as a potential antiproliferative agent and a promising anti-prostate cancer agent.

Red yeast rice (*Monascus*-fermented rice, also called anka or koji) has been used as a natural food coloring additive and in traditional Chinese medicine since ancient times due to its ability to ease digestion and antiseptic effects. A novel strain *Monascus purpureus* wmd2424 was isolated from the mangrove in Chiayi Wetland. It was identified by colony culture morphology, microstructural characteristics, and partial sequence analysis of the β-tubulin gene fragments by Wu et al. [11]. The authors described the isolation of five previously unreported compounds, named monascuspurins A–E from the EtOAc extract of wmd2424 cultured in RGY medium. Of these, monascuspurins C–E exhibited mild antifungal activity against the tested *Aspergillus niger*, *Penicillium italicum*, *Candida albicans*, and *Saccharomyces cerevisiae*.

We would like to thank all the authors for their contribution to this Special Issue. The articles on the topic presented in this Special Issue revealed that mangrove ecosystems is especially attractive due to its abundant microbial communities, such as diverse strains of endophytic fungi from mangrove vegetation and sediments that produce various secondary metabolites with unusual skeletons. These compounds usually possess highly selective and specific biological activities with unique mechanisms of action, offering a promising prospect of mangrove ecosystems to serve as an unlimited reservoir for lead discovery and drug development. Biogenetic manipulation to stimulate silent or cryptic biosynthetic genes offers an effective strategy for mining untapped natural products from microorganisms. Nevertheless, the biosynthesis of most of the natural products derived from mangrove-associated microorganisms and their corresponding biosynthetic gene clusters in the mentioned microbial strains remain elusive.

Conflicts of Interest: The authors declare no conflict of interest.

References

1. Xu, J. *Mangrove Microbial Natural Product Chemistry*; Science Press: Beijing, China, 2014; ISBN 978-7-03-041971-2.
2. Wu, M.J.; Xu, B.; Guo, Y.W. Unusual secondary metabolites from the mangrove ecosystems: Structures, bioactivities, chemical, and bio-syntheses. *Mar. Drugs* **2022**, *20*, 535. [CrossRef] [PubMed]
3. Sulaiman, M.; Nissapatorn, V.; Rahmatullah, M.; Paul, A.K.; Rajagopal, M.; Rusdi, N.A.; Seelan, J.S.S.; Suleiman, M.; Zakaria, Z.A.; Wiart, C. Antimicrobial secondary metabolites from the mangrove plants of Asia and the Pacific. *Mar. Drugs* **2022**, *20*, 643. [CrossRef] [PubMed]
4. Hang, S.; Chen, H.; Wu, W.; Wang, S.; Fang, Y.; Sheng, R.; Tu, Q.; Guo, R. Progress in isoindolone alkaloid derivatives from marine microorganism: Pharmacology, preparation, and mechanism. *Mar. Drugs* **2022**, *20*, 405. [CrossRef] [PubMed]
5. Cai, J.; Zhu, X.-C.; Zeng, W.-N.; Wang, B.; Luo, Y.-P.; Liu, J.; Chen, M.-J.; Li, G.-Y.; Huang, G.-L.; Chen, G.-Y.; et al. Talaromarins A–F: Six new isocoumarins from mangrove-derived fungus *Talaromyces flavus* TGGP35. *Mar. Drugs* **2022**, *20*, 361. [CrossRef] [PubMed]
6. Gui, P.; Fan, J.; Zhu, T.; Fu, P.; Hong, K.; Zhu, W. Sesquiterpenoids from the mangrove-derived *Aspergillus ustus* 094102. *Mar. Drugs* **2022**, *20*, 408. [CrossRef] [PubMed]
7. Wang, C.-F.; Ma, J.; Jing, Q.-Q.; Cao, X.-Z.; Chen, L.; Chao, R.; Zheng, J.-Y.; Shao, C.-L.; He, X.-X.; Wei, M.-Y. Integrating activity-guided strategy and fingerprint analysis to target potent cytotoxic brefeldin a from a fungal library of the medicinal mangrove *Acanthus ilicifolius*. *Mar. Drugs* **2022**, *20*, 432. [CrossRef]
8. Feng, Z.; Zhang, X.; Wu, J.; Wei, C.; Feng, T.; Zhou, D.; Wen, Z.; Xu, J. Immunosuppressive cytochalasins from the mangrove endophytic fungus *Phomopsis asparagi* DHS-48. *Mar. Drugs* **2022**, *20*, 526. [CrossRef] [PubMed]
9. Feng, T.; Wei, C.; Deng, X.; Chen, D.; Wen, Z.; Xu, J. Epigenetic manipulation induced production of immunosuppressive chromones and cytochalasins from the mangrove endophytic fungus *Phomopsis asparagi* DHS-48. *Mar. Drugs* **2022**, *20*, 616. [CrossRef] [PubMed]
10. Cai, J.; Wang, X.; Gan, X.; Zhou, Q.; Luo, X.; Yang, B.; Liu, Y.; Ratnasekera, D.; Zhou, X. New chlorinated metabolites and antiproliferative polyketone from the mangrove sediments-derived fungus *Mollisia* sp. SCSIO41409. *Mar. Drugs* **2023**, *21*, 32. [CrossRef] [PubMed]
11. Wu, M.D.; Chen, J.J.; Cheng, M.J. Secondary metabolites with antifungal activities from mangrove derived fungus *Monascus purpureus* WMD2424. *Mar. Drugs* **2023**, *21*, 200. [CrossRef]

Review

Unusual Secondary Metabolites from the Mangrove Ecosystems: Structures, Bioactivities, Chemical, and Bio-Syntheses

Meng-Jun Wu [1,2], Baofu Xu [1,3,*] and Yue-Wei Guo [1,2,3,*]

1   State Key Laboratory of Drug Research, Shanghai Institute of Materia Medica, Chinese Academy of Sciences, 555 Zu Chong Zhi Road, Shanghai 201203, China

2   Collaborative Innovation Center of Yangtze River Delta Region Green Pharmaceuticals and College of Pharmaceutical Science, Zhejiang University of Technology, Hangzhou 310014, China

3   Shandong Laboratory of Yantai Drug Discovery, Bohai Rim Advanced Research Institute for Drug Discovery, Yantai 264117, China

*   Correspondence: bfxu@simm.ac.cn (B.X.); ywguo@simm.ac.cn (Y.-W.G.)

Abstract: Mangrove ecosystems are widely distributed in the intertidal zone of tropical and sub-tropical estuaries or coasts, containing abundant biological communities, for example, mangrove plants and diverse groups of microorganisms, featuring various bioactive secondary metabolites. We surveyed the literature from 2010 to 2022, resulting in a collection of 134 secondary metabolites, and classified them into two major families in terms of the biological sources and 15 subfamilies according to the chemical structures. To highlight the structural diversity and bioactivities of the mangrove ecosystem-associated secondary metabolites, we presented the chemical structures, bioactivities, biosynthesis, and chemical syntheses.

Keywords: mangrove ecosystems; secondary metabolites; novel carbon skeletons

1. Introduction

Identifying lead compounds is one of the biggest challenges in drug discovery. Natural products (NPs) and their intricate molecular frameworks have a long tradition as valuable starting points for drug development (for example, artemisinins, taxol, camptothecin, and penicillins). To date, NPs remain a significant source of new compounds, providing a wide range of structural diversities with multiple privileged scaffolds for drug discovery either directly, semi-synthetically, or as a source of inspiration [1–5]. However, discovering new bioactive NPs is generally time-consuming and laborious. Only a few new NP drug pharmacophores have been found over the past 20 years, representing critical issues for NPs-driven lead discovery campaigns.

Mangrove forests are complex ecosystems widely distributed in tropical and subtropical estuaries or coastal intertidal zones. These forests contain diverse biological communities, including mangrove plants and numerous groups of microorganisms. The environment of the mangrove system harbors unique traits, for instance, high salinity, low oxygen, tidal gradients, high temperature, and excessively intense light, resulting in an active ecosystem with various microorganisms [1–5]. Mangrove-associated microorganisms have been demonstrated to be a reliable source of bioactive metabolites and have likewise drawn the attention of NP researchers [6–12]. A large number of structurally unusual and bioactive NPs have been discovered from the mangrove-associated microorganisms, including fungal and bacterial endophytes isolated from the mangrove plants' leaves, branches, and roots [13,14]. In addition, Mangrove sediments-derived microbes, a rich reservoir of NP diversity, could be utilized to explore new drugs [15].

The bioactive NPs solely from the true mangrove and semi-mangrove floras worldwide have been summarized in several review papers in 2010 [16,17]. However, the investigation of the mangrove ecosystem is mainly focused on the mangrove-associated microorganism

but less on the mangrove flora in recent years. Three comprehensive reviews have recently focused on the NPs from mangrove-associated fungi and mangrove sediments-derived microbes [6,14,15]. However, to our knowledge, no review has been published on the secondary metabolites with unusual skeletons from the mangrove ecosystem. They might merit the attention of chemists and biologists and could be a source of fresh pharmacophores with biological activity for the creation of drugs based on natural products.

In this review, we focus on the mangrove ecosystem-associated NPs featuring new carbon scaffolds, unique ring systems, or unusual functional moieties covering from 2010 to 2022. The structures, biological activities, biosynthesis, and total chemical syntheses of exampled unique compounds were included.

The references were searched using the following keywords as the subject search: natural products/secondary metabolites, mangrove, via Web of Science, Chemical Abstracts, and PubMed databases covering from 2010 to 2022, resulting in a collection of 134 unusual secondary metabolites. We classified them into two major families in terms of biological sources.

2. Unusual Natural Products from Mangrove Flora

2.1. Limonoids

Limonoids are natural tetranortriterpenoids containing a four-ring structure with a 17β-furyl ring mainly distributed in the Meliaceae and Rutaceae families [18]. In the mangrove flora, they are especially abundant and structurally diversified in the genus *Xylocarpus moluccensis* and *X. grantum* (family Meliaceae). Up to 2021, approximately 2700 limonoids have been identified. Moreover, owing to their widespread distribution and substantial content in Meliaceae plants, and active biosynthetic pathways, more than 1600, including 30 types of unique rearrangement skeletons, have been isolated and identified in the last 10 years [19]. Among them, nearly 233 new limonoids with 14 kinds of novel skeletons were isolated from mangrove *Xylocarpus*.

Thaixylomolin A (**1**), isolated from the seeds of a Thai mangrove *Xylocarpus moluccensis* collected at the Trang province, was obtained similar to the cleavage of C-6/C-7 by Baeyer–Villiger (BV) oxidation [20], and then the oxidized C-6 formed an unusual 6-oxabicyclo[3.2.1]octan-3-one motif with C-1 [21]. In 2016, the same research group isolated another analogue from *X. moluccensis*, thaixylomolin R (**2**) [22], whose C-8 is decarboxylated compared with **1** (Figure 1).
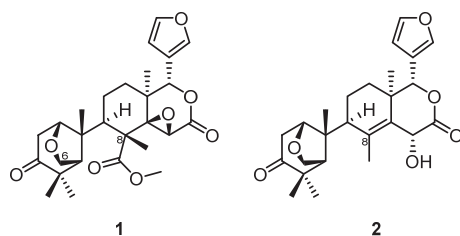
Figure 1. Structures of compounds **1** and **2**.

Xylomexicanin F (**3**) [23], hainangrantums I and J (**4** and **5**) [24] (Figure 2) are the second examples of a limonoid with an unusual 9, 10-*seco* and C-9-C-30 linkage, isolated from the seeds of the Chinese mangrove *X. granatum*. Among them, **3** showed moderate activity against the A549 and RERF cell lines with IC$_{50}$ values of 18.83 μM and 15.83 μM, respectively. However, the first reported analogue, xylogranatin D, was concluded as an artifact [25,26].
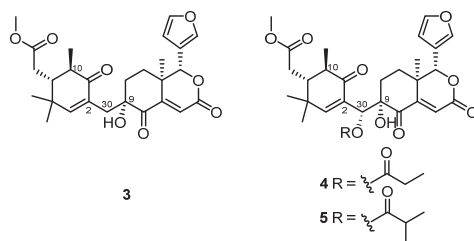
Figure 2. Structures of compounds **3–5**.

Chemical investigation of the seeds from a Trang (Thailand) mangrove *X. moluccensis* yielded five structurally intriguing limonoids, namely, trangmolins A–E (**6–10**) [27] (Figure 3). Notably, compounds **6–8** consist of unprecedented ring A/B-fused bicyclic moieties, and compound **10** represents the first example of the oxidative cleavage of the C2-C3 bond among limonoids. In 2021, a trangmolin A derivative krishnolide J (**11**) was isolated from seeds of the India Krishna mangrove *X. moluccensis* [28]. The biosynthetic origins of **6–11** could be traced back to a proposed andirobin-type limonoid with 1,2-bisketone groups [18]. Taking andirobin as the starting point, scientists from the Wu group proposed a biosynthetic pathway characterized by a highly divergent biosynthetic assembly line (Scheme 1) [27]. The three forks of the biosynthetic pathway obtain C-1/C-30 linkage (**6–8**, **11**), C-3/C-30 linkage (**9**), and C-2/C-30 linkage (**10**) based on the main mechanisms of electro- and nucleophilic enzymatic cascade reactions. The diverse cyclization patterns of **6–11** reveal the remarkable structural plasticity of rings A and B in limonoid biosynthesis.

6 R_1 = OAc, R_2 = OAc
7 R_1 = OH, R_2 = OAc
8 R_1 = OAc, R_2 = H
11 R_1 = S-Piv, R_2 = H
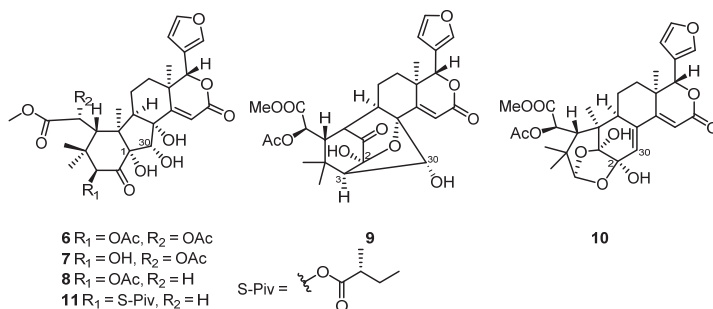
Figure 3. Structures of compounds **6–11**.

Andhraxylocarpins A–E (**12–16**) (Figure 4) were isolated and identified as three new types of limonoids from the seeds of two true mangroves, *X. granatum* (collected at the estuary of Krishna, India) and *X. moluccensis* (collected in the estuary of Godavari, India), respectively [29]. Among them, andhraxylocarpins A and B (**12 and 13**) contain an unprecedented 9-oxa-tricyclo-[3.3.2.1^{7,10}]undecan-2-ene motif, andhraxylocarpins C-D (**14 and 15**) harbor a rare (Z)-bicyclo[5.2.1]dec-3-en-8-one substructure, and andhraxylocarpin E (**16**) possesses a unique tricyclo[3.3.1.1^{3,6}]decan-9-one scaffold. In 2016, trangmolin F (**17**), which shared the same A/B fused carbobicyclic with **16**, was obtained from *X. moluccensis* by the same group [27] Wu et al. suggested a mexicanolide with a $\Delta^{8,30}$ double bond, derived from an andirobin by C-2/C-30 linkage and previously discovered among the genus *Xylocarpus*, may be the precursor of **12–16** [29] (Scheme 1). The presence of bridging rings (C10–C1–C2) in mexicanolide-type limonoids makes C-3 and C-30 close to each other in space, which leads to their coupling.
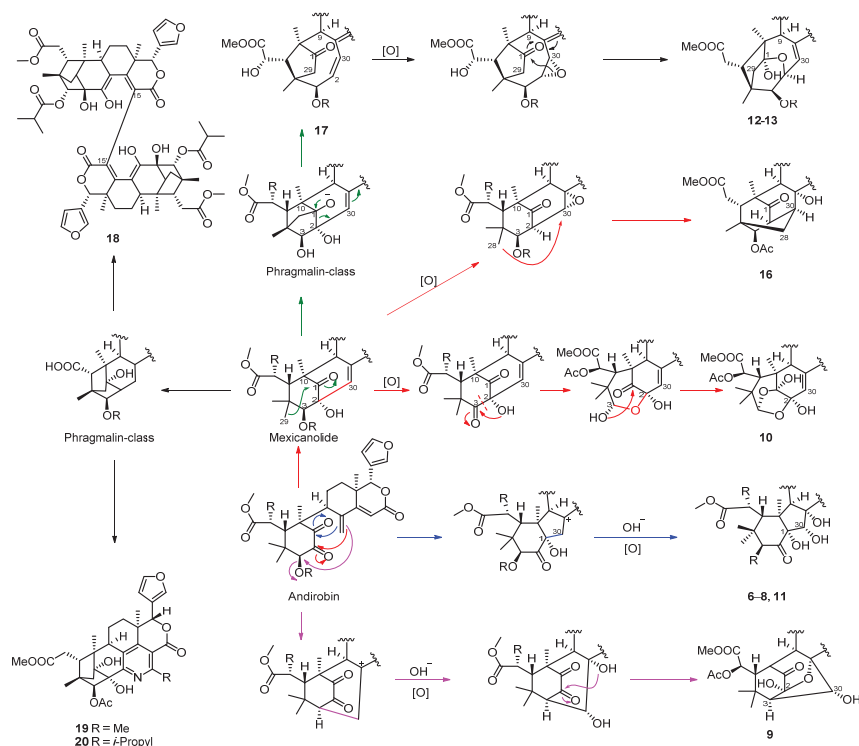
Scheme 1. Proposed biosynthetic pathway for compounds **6–20** [21,27,29,30].
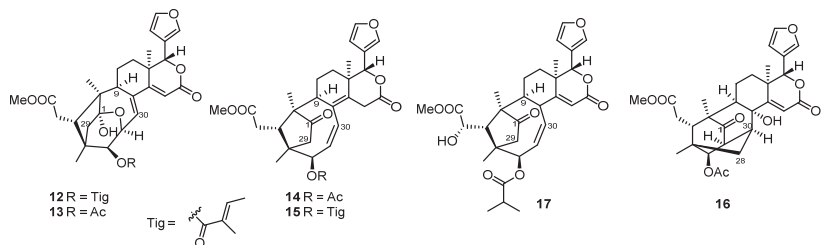
Figure 4. Structures of compounds **12–17**.

Krishnadimer A (**18**) (Figure 5) is the first dimeric limonoid isolated from the seeds of *X. moluccensis* with an unprecedented axial chirality architecture, with the C₂-symmetric architecture, with a *P*-configured central axis at the C15, C15′-positions of the monomeric units, represents a milestone during decades of work on natural limonoids [30]. It could be obtained by the intermolecular oxidative coupling of the phargmalin-class limonoid, which can be derived from andirobin through C-2/C-30 and C-1/C-29 linkage. (Scheme 1) The semisynthesis of the dimer was successfully conducted. Subsequently, eight new limonoid dimers of four skeletons (two symmetric and two nonsymmetric) were designed and synthesized by oxidative carbon-carbon radical coupling [31].
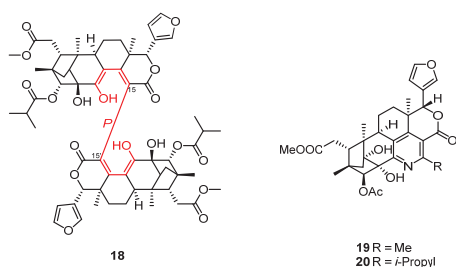
Figure 5. Structures of compounds **18–20**.

Two unprecedented limonoids, thaixylomolins B and C (**19** and **20**) (Figure 5), co-isolates with **1** [21], are limonoids containing a unique pentasubstituted pyridine scaffold that might be generated by aromatization into a pyridine ring from a phargmalin-class limonoid. (Scheme 1) Thaixylomolin B (**19**) exhibited inhibitory activity against nitric oxide production in lipopolysaccharide and IFN-γ-induced RAW264.7 murine macrophages with an IC_{50} value of 84.3 μM.

Two pyridine-containing limonoids, xylogranatopyridines A (**21**) and B (**22**) (Figure 6), were isolated from the twigs and leaves of *X. granatum*, collected from the seashore of Dongzhai, Hainan Province [32]. Compared to **21**, xylogranatopyridine B (**22**) possesses an unprecedented rearranged A-ring. Prexylogranatopyridine, a co-occurrence of limonoid with an unusual C-8-C-30 linkage, could be the common biosynthetic precursor of **21** and **22** (Scheme 2). Xylogranatopyridine A (**21**) exhibited significant inhibitory activity against protein tyrosine phosphatase 1B (PTP1B) with an IC_{50} value of 22.9 μM.
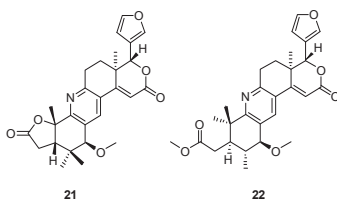
Figure 6. Structures of compounds **21** and **22**.
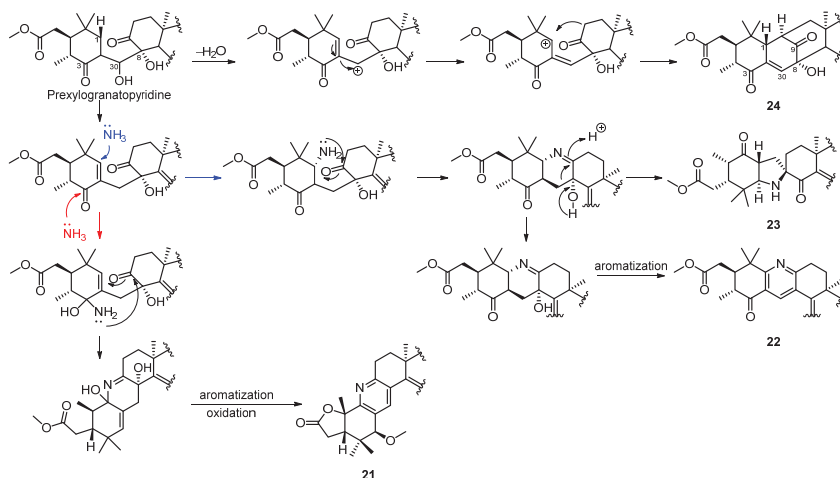
Scheme 2. Proposed biosynthetic pathway for compounds **21–24** [23,32,33].

An unusual tetranortriterpenoid, xylomexicanins E (**23**) (Figure 7), which is the first example of limonoid with azaspiro skeleton between B (pyrrolidine) and C rings, was isolated from the seeds of the Chinese mangrove, *X. granatum* [23]. The plausible biosynthetic routes are proposed, as shown in Scheme 2, starting from the limonoid prexylogranatopyridine.
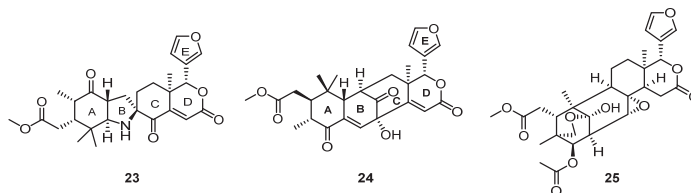
Figure 7. Structures of compounds **23**–**25**.

Further investigation of the seeds from the *X. granatum* led to the isolation of two new tetranortriterpenoids, xylomexicanins I and J (**24** and **25**) [33] (Figure 7). Notably, **24** represents an unprecedented limonoid with a bridged skeleton between the B- and C-rings, contrasting with analogues possessing bridged A- and B-rings (**25**). Wu et al. proposed that **24** was obtained from the same natural precursor as **22** after an enolate addition to the allylic alcohol moiety between C-3 and C-11 (Scheme 2).

Three new limonoids, entitled xylomolones A–C (**26**–**28**, respectively, Figure 8) were discovered from the seeds of the Thai mangrove *X. moluccensis*, as well as a vital biosynthetic precursor, xylomolone D (a new C11-terpenic acid methyl ester) [34]. Compared to **26**, compound **27** is the first 9,10-*seco* limonoid with a 3,4-dihydro-2H-pyran motif and possesses the reversed alignment of ring A. For the biosynthesis of xylomolone C (**28**), a five-membered A-ring could be built through a benzylic acid-like rearrangement, forming an unusual 3-oxabicyclo[3.2.1]octan-2,7-dione motif; the C-2 is excluded from the A-ring in the rearrangement process. Wu et al. proposed a novel convergent strategy for limonoid biosynthesis (Scheme 3).
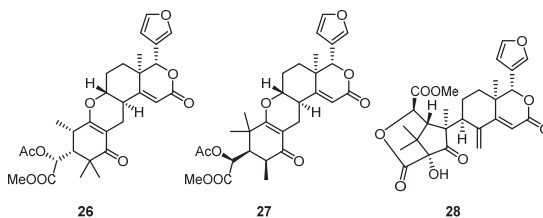
Figure 8. Structures of compounds **26**–**28**.
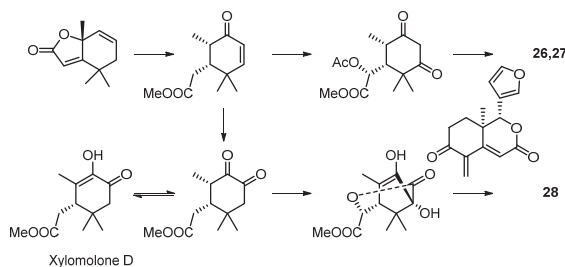
Scheme 3. Proposed biosynthetic pathway for compounds **26**–**28** [34].

2.2. Diterpenoids

Two new *ent*-isopimarane-type diterpenoids agallochaexcoerins D and E (**29** and **30**) [35] (Figure 9), possessing an unusual seven-membered lactone moiety, were isolated from

the wood of mangrove *Excoecaria agallocha*. Notably, **29** is the first report of *ent*-3,4-secoisopimaratriene diterpenoid with a rare seven-membered ring.
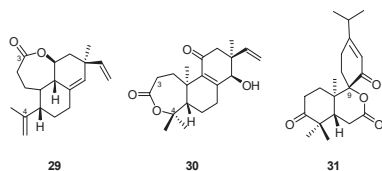
Figure 9. Structures of compounds **29–31**.

Decandrinin (**31**) (Figure 9), an unprecedented C-9-spiro-fused 7,8-*seco-ent*-abietane, was obtained from the bark of an Indian mangrove *Ceriops decandra* (collected in the estuary of Godavari, Andhra Pradesh) [36]. The biosynthetic precursor might be the naturally more prevalent occurring 7,13-*ent*-abietadien-3β-ol and the plausible biosynthetic was proposed (Scheme 4). The spiro ring could be formed by oxidative cleavage and lactonization.
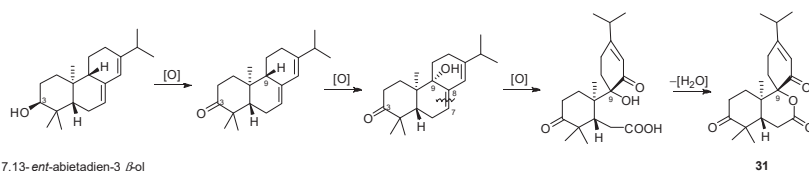
Scheme 4. Proposed biosynthetic pathway for compound **31** [36].

3. Unusual Natural Products from Mangrove-Associated Microorganisms

Previous chemical investigations of mangrove microbes especially mangrove-associated fungi resulted in the discovery of various bioactive secondary metabolites, including polyketides, terpenes, alkaloids, and peptides with diverse structural features.

3.1. Polyketides

Polyketides (PKs) are a large family of secondary metabolites with prominent structural diversity and various biological activities, isolated from diverse organisms. Polyketide synthases (PKSs) catalyze the sequential decarboxylative condensations of acyl-CoA thioesters to form structurally diverse PKs [37]. We direct readers to the fantastic reviews for more information on PKSs [38–41]. An even-increasing number of PKs from the mangrove-associated microorganisms are being reported.

3.1.1. Coumarins and Isocoumarins

Naturally occurring coumarins and isocoumarins are an essential class of benzopyrene derivatives and are present in remarkable amounts in plants, while only a few are found in microorganisms and animal sources.

Up to now, 12 new coumarin and 102 new isocoumarin derivatives have been obtained from mangrove-associated fungi [42,43]. Among them, Peniisocoumarin A and B (**32** and **33**, Figure 10), a pair of unusual dimeric isocoumarin-type diastereoisomers containing a symmetric four-membered core at C-9/9′ and C-10/10′ were obtained from the fermentation of *Penicillium commune* QQF-3 (isolated from fresh fruit of the mangrove plant *Kandelia candel*) [44]. The structures of **32** and **33** were unanimously defined by X-ray diffraction analysis using Cu Kα radiation. In 2015, Darsih et al., discovered penicilliumolide A (**34**) (Figure 10), an unusual tetracyclic isocoumarin containing a γ-lactone ring fused with a unique spiro framework, from the mangrove endophytic fungus *Penicillium chermesinum* HLit-ROR2 [45].
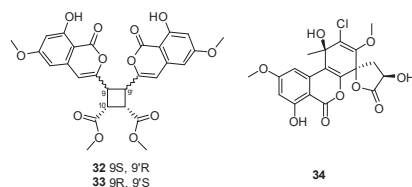
Figure 10. Structures of compounds **32–34**.

3.1.2. Chromones

The chromone and its derivatives have been identified as the central backbone in several functional organic compounds, with strategic importance in many research and industrial domains. Until now, 85 new chromone derivatives have been identified from mangrove-associated fungal species.

In 2019, two new polycyclic chromones, penixanthones C (**35**) and D (**36**) (Figure 11), possessing an unprecedented 6/6/6/5 polycyclic skeleton with a signature C_2 bridge, were isolated from the mangrove sediment-derived fungus *Penicillium* sp. SCSIO041218 [46]. However, **35** and **36** only showed weak cytotoxicity. Furthermore, the configurations of **35** and **36** remain elusive.
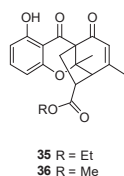
Figure 11. Structures of compounds **35** and **36**.

3.1.3. Azaphilones

Azaphilones or azaphilonoids are a structurally variable family of fungal polyketide metabolites harboring a highly oxygenated pyranoquinone bicyclic core [47]. In recent years, about 31 azaphilones with unusual structures and remarkable bioactivities were reported from mangrove-associated fungi, including genera *Aspergillus*, *Diaporthe*, *Penicillium*, and *Talaromyces*.

Two new citrinin derivatives, penicitol A (**37**) and penicitol B (**38**) (Figure 12) were identified from *Penicillium chrysogenum* ML226 obtained from the rhizosphere soil of the mangrove plant *Acanthus ilicifolius* [48]. The citrinin derivatives are a family of azaphilones, with the first one, namely citrinin, isolated from a *P. citrinum* strain in 1931 [49]. Penicitol A (**37**) is the first reported citrinin derivative with an unusual tetracyclic skeleton, and **38** is the first citrinin dimer with a single oxygen bridging center. **37** and **38** exhibited potent cytotoxic activities against HeLa, BEL-7402, HEK-293, HCT-116, and A-549 cell lines with IC_{50} values of 4.6–10.5 and 3.4–9.6 μM, respectively. In 2011, Hosokawa et al. reported the first total synthesis of penicitol A (**37**), achieved by acetalization [50].
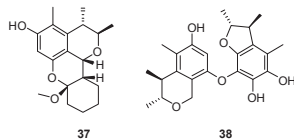
Figure 12. Structures of compounds **37** and **38**.

3.1.4. Benzophenones Derivatives

Benzophenones (BPs) are widely distributed NPs possessing a diphenyl ketone moiety [51]. Given the presence of the chemically active carbonyl group, which can efficiently

react with a variety of functional groups, diverse novel skeletons such as isobenzofuran, isoindolinone, and 3-dihydro-1H-indene, etc., could be formed. There are 12 members of BPs that are discovered from mangrove-associated fungi.

Four unusual 2,3-dihydro-1H-indene isomers, diaporindenes A–D (**39–42**) (Figure 13), and an unusual isoprenylisobenzofuran A (**43**) were isolated from *Diaporthe* sp. SYSU-HQ3, a fungus obtained from the branches of the mangrove plant *Excoecaria agallocha* collected from Zhuhai in Guangdong province, China [52]. Compounds **39–42** feature a 2,3-dihydro-1H-indene ring and a 1,4-benzodioxan moiety. Isoprenylisobenzofuran A (**43**) represented the first example of an isoprenylisobenzofuran nucleus possessing a rare 1,4-benzodioxan moiety. Biosynthetically, compounds **39–43** could be derived from co-occurrence benzophenone type metabolites such as tenellone B, which is formed by acetyl-CoA and malonyl-CoA through the catalysis of PKSs [53] (Scheme 5). In a bioassay, compounds **39–43** were found to exhibit significant inhibitory effects against nitric oxide production with IC$_{50}$ values from 4.2–9.0 μM and selective index (SI) values from 3.5 to 6.9.
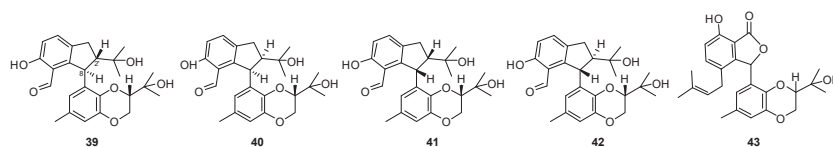
Figure 13. Structures of compounds **39–43**.
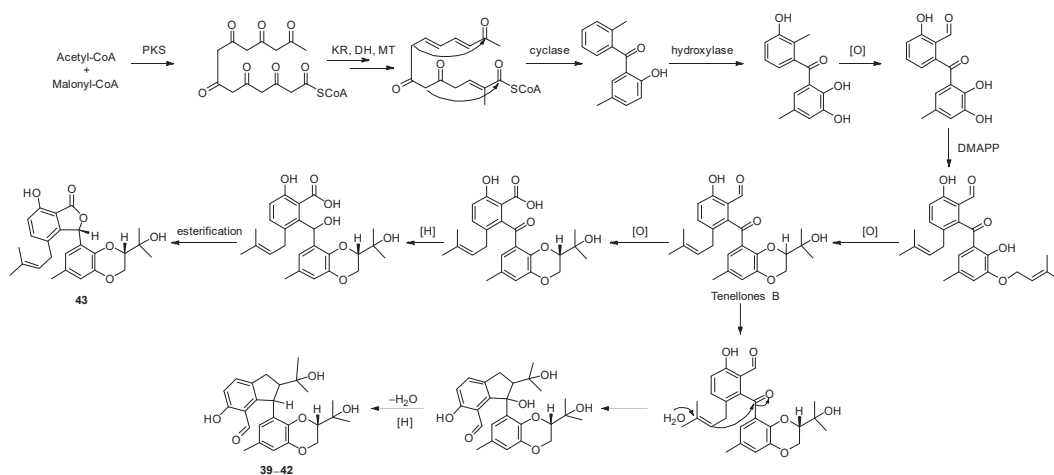
Scheme 5. Proposed biosynthetic pathway for compounds **39–43** [53].

3.1.5. Macrolides

Macrolides, especially those possessing 10- to 19-membered ring systems, have diversified structural features and constitute a prominent group of active secondary metabolites. Since the discovery of well-known progenitor macrolide antibiotic pikromycin in 1950 and the second generation of macrolides such as azithromycin and clarithromycin, naturally occurring macrolides have been found today due to their diverse structures and promising biological properties [54]. A total of 63 macrolides have been isolated from the mangrove-associated fungi.

Sumalarins A−C (**44**−**46**) (Figure 14) were identified from the cytotoxic extract of *Penicillium. sumatrense* MA-92 from the rhizosphere of the mangrove *Lumnitzera racemose*. Notably, they were the unusual and rare examples of sulfur-containing curvularin derivatives isolated for the first time from natural sources [55]. Compounds **44**−**46** displayed

cytotoxic activities against Du145, HeLa, Huh 7, MCF-7, NCI-H460, SGC-7901, and SW1990 cell lines with IC$_{50}$ values ranging from 3.8 μM to 10 μM. Compound **44** is likely formed via Michael's addition of 3-mercaptolactate to the double bond $\Delta^{10,11}$ of dehydrocurvularin. Esterification or acylation of **45** probably leads to the biosynthesis of **44** and **46** [55].

44 R = CH3
45 R = H

46

Dehydrocurvularin
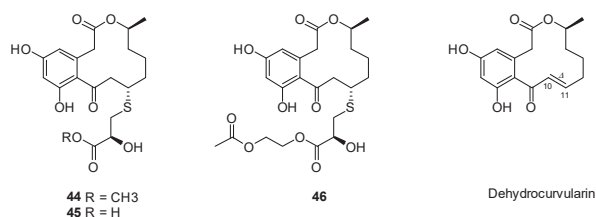
Figure 14. Structures of compounds **44–46** and dehydrocurvularin.

Ansamycins are characterized by an aromatic nucleus connected with a polyketide chain back to a nonadjacent position through an amide bond. Hertweck et al. isolated four unusual ansa macrolides, compounds **47–50** (Figure 15), from *Streptomyces* sp. HKI0576, a bacterial endophyte separated from the stem of mangrove *Bruguiera gymnorrhiza* [56]. This was the first report on discovering ansamycins from a plant endophyte. In addition, the degree of "in-built diversification" of these four compounds is unprecedented for complex polyketides. Among them, divergolide A (**47**) represents an unusual type of ansa macrolide with an unusual branched side chain and a disrupted polyketide backbone. Furthermore, the tricyclic chromophore is unprecedented for macrolides, and related *O*-heterocyclic substructures are only known from aromatic polyketides, such as the nogalamycin aglycone [57] and chaetoxanthone [58]. Divergolide B (**48**) represents another unusual type of ansa macrolide featuring a novel benzopyran/chromene core as the first congener of **47**. In addition, compounds **49** and **50** share substructures with **47** and **48** but feature structurally intriguing tetracyclic scaffolds. Furthermore, the ansa macrolides display significant antimicrobial and cytotoxic activities, probably regulating the immunity of the mangrove tree. Compounds **47–50** are biosynthesized from a common linear polyketide using 3-amino-5-hydroxybenzoic acid (AHBA) as a primer unit. Various reactions, including an optional acyl migration, generate the diverse multicyclic structures [56,59] (Scheme 6).

47   **48**   **49**   **50**   **51**
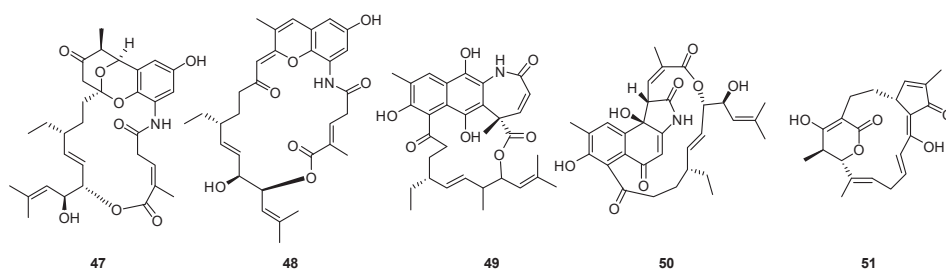
Figure 15. Structures of compounds **47–51**.

In 2014, Shen et al., cloned the biosynthetic gene cluster involved in the biosynthesis of the divergolides from the endophytic *Streptomyces* sp. W112 isolated from *Camptotheca acuminata*. Following gene disruption, gene overexpression, and bioinformatics analysis, they laid the foundation for further elucidation of the biosynthetic pathway as well as titer improvement [60]. In addition, Zhong et al. [61] conducted genome sequencing, bioinformatics analysis, and further isolations of four new divergolide congeners with a similar endophytic bacteria, *Streptomyces* sp. from *Bruguiera gymnorrhiza*. They showed that specialized acyltransferase domains are for selecting extender units, and the branched isobutylmalonyl-CoA is involved.
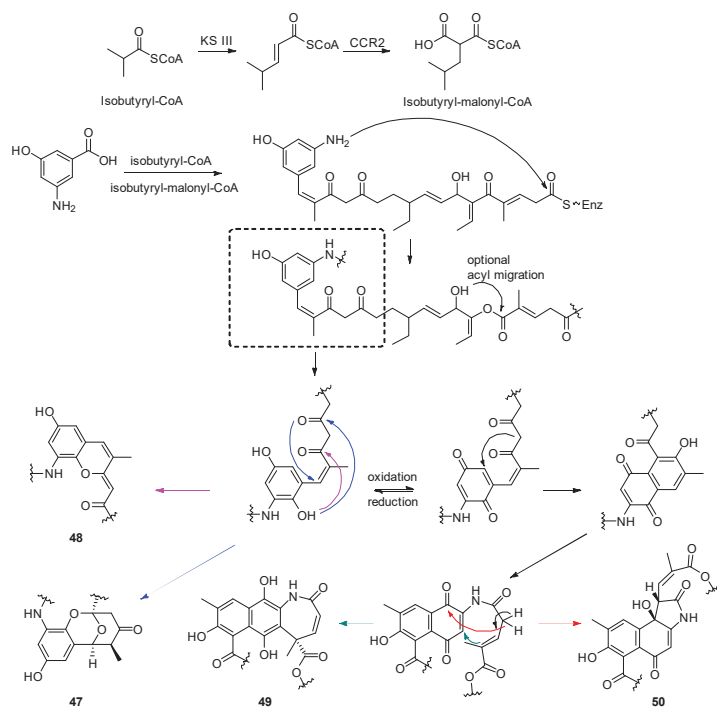
Scheme 6. Proposed biosynthetic pathway for compounds **46–49** [56].

The total synthesis of divergolide A using the ring-closing metathesis (RCM) approach was published by Dai et al., in 2012 [62]. Subsequently, Rasapalli et al. synthesized the western section of divergolides C (**49**) and D (**50**) and demonstrated the robustness of C4-C5 as an appropriate approach for the further total synthesis of divergolides C and D in 2013 [63]. This chemical method was also conducted for divergolides A and B. Studies on the total synthesis of divergolides A-D using inexpensive, readily available starting materials and simple operations have also been constantly reported in recent years [64–66].

A macrocyclic polyketide with an unusual carbon skeleton, namely hainanmycin A (**51**) (Figure 15), was isolated from *Streptomyces* sp. 219807 (from mangrove soil collected in Sanya) [67]. Compound **51** featured an unprecedented structural skeleton of a 17-membered carbocyclic framework. The cyclo-heptadeca framework containing a cyclopentenone ring substituted with a naturally occurring bridgehead enol motif is unique among NPs. It represents a new subgroup, a minor family of carbocyclic polyketide macrolides. Hong et al. [67] proposed a plausible biosynthetic pathway for **51** based on the biosynthesis of akaeolide [68], an analogue of **51**. Shortly, the PKS condenses acetyl-CoA and other building units (e.g., methylmalonyl-CoA and malonyl-CoA) to a linearized polyketide backbone. A thioesterase (TE) then releases the backbone with the formation of a δ-lactone ring. Further construction of the C-C bonds of C-16/C-12 and C-18/C-2 generate the structural core. Notably, a C-18 aldehyde intermediate (**S1**) might be involved in the C-18/C-12 carbon bond formation (Scheme 7).
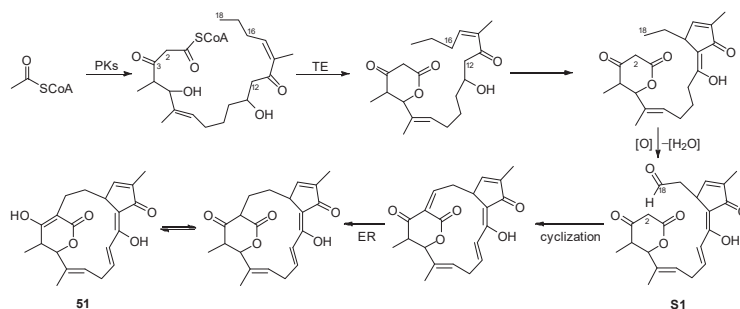
Scheme 7. Proposed biosynthetic pathway for compound **51** [67].

3.1.6. Others

Eight new compounds, streptoglycerides A–H (**52–59**) (Figure 16) possessing a unique ring system, were obtained from *Streptomyces* sp. isolated from a mangrove sample collected on Kosrae Island [69,70]. This is the first report to describe a rare 6/5/5 tricyclic ring system consisting of a glycerol moiety from marine organisms. Streptoglyceride C (**54**) showed a weak inhibitory effect on nitric oxide production in BV-2 microglia cells. Compounds **56–59** showed significant anti-inflammatory activity by inhibiting lipopolysaccharide (LPS)-induced nitric oxide (NO) production in Raw 264.7 cells with IC_{50} values ranging from 3.5 to 10.9 μM. It should be noted that **57** suppressed the transcription of iNOS and IL-6 without cytotoxicity.
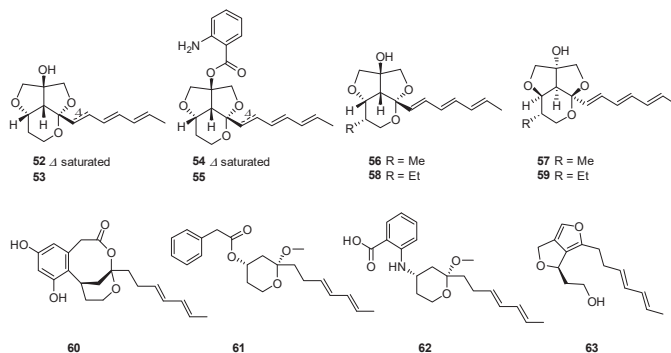
Figure 16. Structures of compounds **52–63**.

Upon further investigation of the unusual strain, four new compounds, miharadienes A–D (**60–63**), possessing unique ring systems and a rare diene side chain, were isolated [71]. A plausible biosynthetic pathway of miharadienes and related compounds, streptoglycerides is proposed in the literature (Scheme 8a) [71]. However, the formation of **52–55** from **63** by attacking the nucleophilic hydroxy on the electron-rich furan ring seems inapplicable. Therefore, we proposed an optional pathway for **52–55** (Scheme 8b). In short, the starting lauryl alcohol derivative appears to react with dihydroxyacetone, an oxidation product of glycerol, to form the intermediate **int i** through Aldol type reaction of the C-4 active methylene of lauryl alcohol derivative with the carbonyl of the dihydroxyacetone. Then the hemiketal formation gives the tetrahydrofuran ring, and ether formation forms the other tetrahydrofuran ring. Afterward, the ketal formation by the interaction of the terminal hydroxyethylene with the hemiketal provides the pyran ring and affords the intermediate **int ii**, which could be further converted into **52–55**, possessing a rare 6/5/5 ring system.
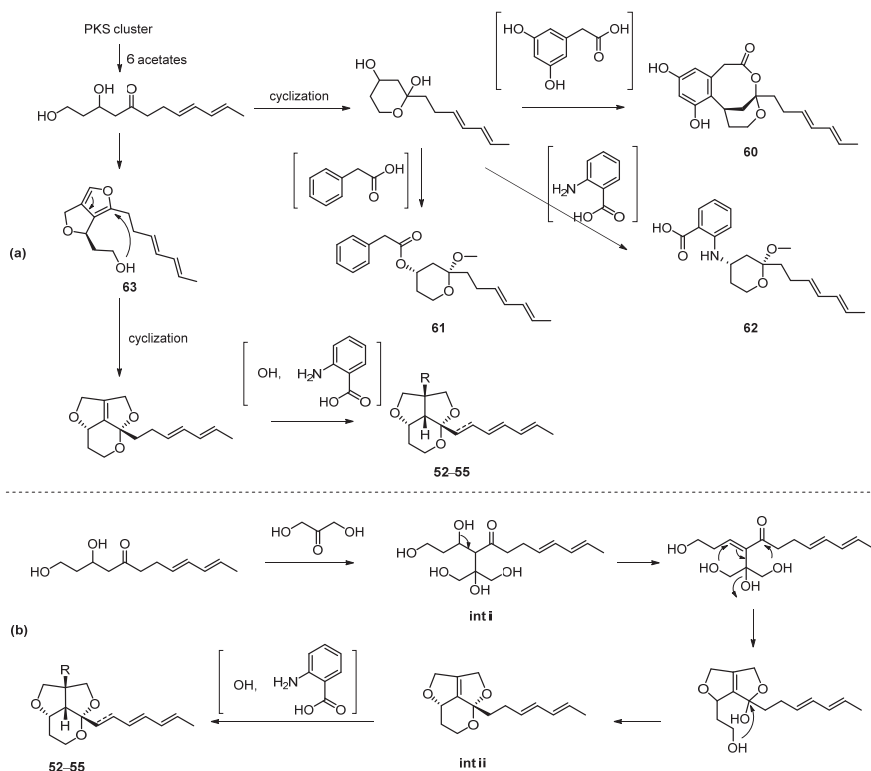
Scheme 8. (**a**) Proposed biosynthetic pathway for compounds **52–55** and **60–63** in the literature [71]; (**b**) proposed biosynthetic pathway for **52–55** in this review.

3.2. Terpenoids

The new terpenoids from mangrove fungi can be divided into seven groups based on their chemical structures and biosynthetic pathways: monoterpenes, sesquiterpenes, diterpenes, sesterterpenes, triterpenes, and meroterpenes. Sesquiterpenes (138), sesterterpenes (36), and meroterpenes (72) comprise the most significant proportions of new terpenes from mangrove fungi. However, monoterpenes, diterpenes, and triterpenes were rarely isolated from mangrove fungi, and no new skeleton was discovered.

3.2.1. Sesquiterpenoids

Sesquiterpenoids are the largest group of known terpenoids [72]. The mangrove fungi-derived sesquiterpenoids possess a variety of carbon skeletons, including monocyclic, bicyclic, and tricyclic types [73].

One tricyclic and three spirobicyclic norsesquiterpenoids (**64–67**) (Figure 17) were isolated from the endophytic fungus *Pseudolagarobasidium acaciicola* (from the mangrove *Bruguiera gymnorrhiza*) [74,75]. Among them, acaciicolin A (**64**) possesses a previously unknown skeleton with a uniquely connected 6/5/5 ring system and three consecutive oxygenated sp³ quaternary carbons at C-7, C-8, and C-8a. The norsesquiterpene skeleton of **64** was named "acaciicolane", and was different from the three known sesquiterpene skeletons with 6/5/5 ring systems: cedrane, prezizaane, and zizaane (Figure 18). Spiroa-caciicolides A–C (**65–67**) has a hitherto unobserved 5/6 fused spirobicyclic ring system. The absolute configurations of the new compounds **64–66** were determined by single-crystal

X-ray analysis (Cu-Kα radiation). **64–67** could originate from chamigrane endoperoxide A [76] (Scheme 9).
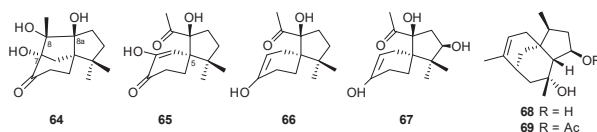
Figure 17. Structures of compounds **64–69**.
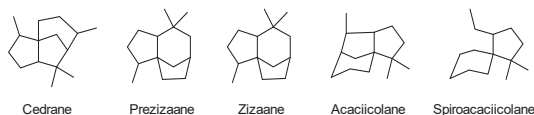
Figure 18. Structures of five sesquiterpene skeletons.
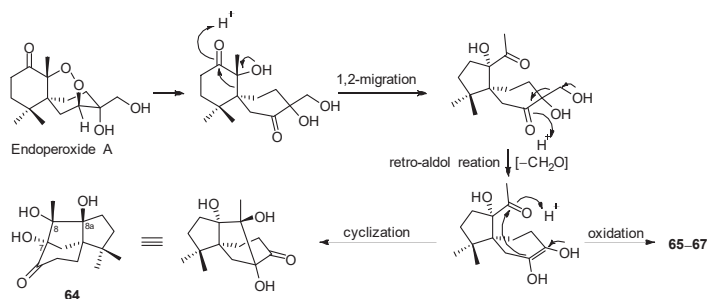
Scheme 9. Proposed biosynthetic pathway for compounds **63–66** [74].

Penicibilaenes A (**68**) and B (**69**) (Figure 17), two sesquiterpenes possessing a tricyclo[6.3.1.0^{1,5}]dodecane skeleton constituted by [3.3.1]-bridged and [4.3.0]-fused junctions, were characterized from *Penicillium bilaiae* MA-267, a fungus obtained from the rhizospheric soil of the mangrove plant *Lumnitzera racemosa* [77]. An X-ray crystallographic study determined the structure and configuration. The hypothetical biosynthetic pathway starting from *cis*-farnesyl pyrophosphate (FPP) was proposed (Scheme 10). Notably, Compounds **68** and **69** exhibited selective activity against the plant pathogenic fungus *Colletotrichum gloeosporioides* (MIC = 1.0 and 0.125 μg/mL, respectively).
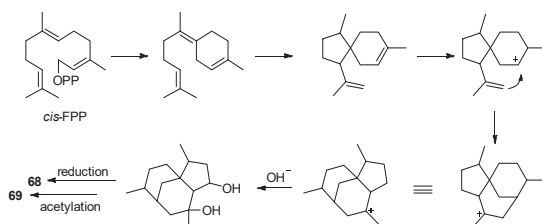
Scheme 10. Proposed biosynthetic pathway for compounds **68** and **69** [77].

The first total synthesis of **68** and **69** in their racemic forms was reported by Dong et al. in 2021 [78]. The approach featured a rhodium-catalyzed deconstructive formation of a tricyclic skeleton by C–C activation of cyclobutanone derivatives, generating ($\pm$)-**68** and ($\pm$)-**69** in 13 and 14 steps with 0.56% and 0.49% overall yields, respectively. In the same year, K Sugita described another more efficient synthetic pathway for the total practical

synthesis of (±)-**68** and (±)-**69** from commercially available 3-ethoxycyclohex-2-en-1-one with 4.0% overall yields for both compounds [79].

3.2.2. Sesterterpenoids

Sesterterpenoids are a relatively small and rare group of terpenoids found in widespread sources. They always possess interesting carbon skeletons, including linear, monocyclic, polycyclic, and miscellaneous. In addition, they exhibit diverse biological activities such as antimicrobial, cytotoxicity, anti-inflammatory, and protein tyrosine phosphatase B inhibition.

The group of She has been dedicated to the search for structurally unique and biologically active compounds from the mangrove plant-derived fungal endophytes. Five sesterterpenoids of three kinds of carbon skeletons, asperterpenoid A (**70**) (Figure 19), asperterpenols A and B (**71** and **72**), and aspterpenacids A and B (**73** and **74**), have been isolated and characterized from *Aspergillus* sp. Among them, asperterpenoid A (**70**), possessing a new 5/7/(3)6/5 pentacyclic carbon skeleton, exhibited potent inhibitory activity against *Mycobacterium tuberculosis* protein tyrosine phosphatase B (mPTPB) with an IC$_{50}$ value of 2.2 μM [80].
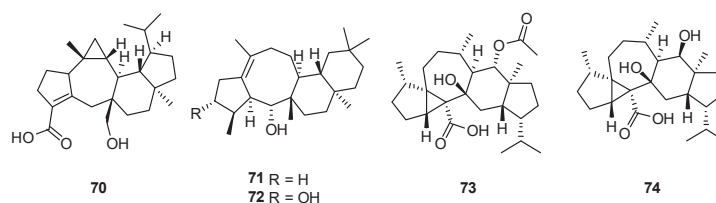
Figure 19. Structures of compounds **70–74**.

In addition, asperterpenol A (**71**) and asperterpenol B (**72**), two sesterterpenoids with an unusual 5/8/6/6 tetracyclic ring skeleton, showed inhibitory effects on acetylcholinesterase (AChE) with IC$_{50}$ values of 2.3 μM and 3.0 μM, respectively [81]. Furthermore, the two unusual pentacarbocyclic sesterterpenoids, aspterpenacids A (**73**) and B (**74**), with an unusual carbocyclic skeleton containing an unprecedented 5/3/7/6/5 ring system, showed no antibacterial and cytotoxic activities [82]. The structures of **69–73** were elucidated based on spectroscopic methods, and the absolute configurations of **70–73** were determined by single-crystal X-ray diffraction analysis. She et al. proposed a hypothetical biosynthetic pathway for **70–74** [80–82]. In brief, they are derived from geranylfarnesyl pyrophosphate (GFPP), followed by cyclization rearrangement and redox reactions (Scheme 11).

3.2.3. Meroterpenoids

Meroterpenoids are secondary metabolites with structures consisting of at least two parts: a terpenoid fragment (mainly mevalonate pathway) and a nonterpenoid fragment [83]. The different nonterpenoid moiety based on the biosynthetic pathway, various terpenoid (the length of the terpenoid chain and its cyclization mode), and the tailoring reactions make the chemical diversity of meroterpenoids.

Chermebilaene A (**75**) (Figure 20), an unprecedented acorane-type sesquiterpene hybridized with an octadecadienoic acid skeleton, together with an unusual orthoester meroterpenoid, chermebilaene B (**76**) were isolated from the co-culture extract of *P. bilaiae* MA-267 (from the rhizosphere of the mangrove *Lumnitzera racemosa*) and *P. chermesinum* EN-480 (from the fresh tissue of marine red algal *Pterocladiella tenuis*) [84]. Compound **75** showed potent inhibitory activities against *Ceratobasidium cornigerum* and *Edwardsiella tarda*, and may prove helpful as an antibiotic against aquatic or plant pathogens.
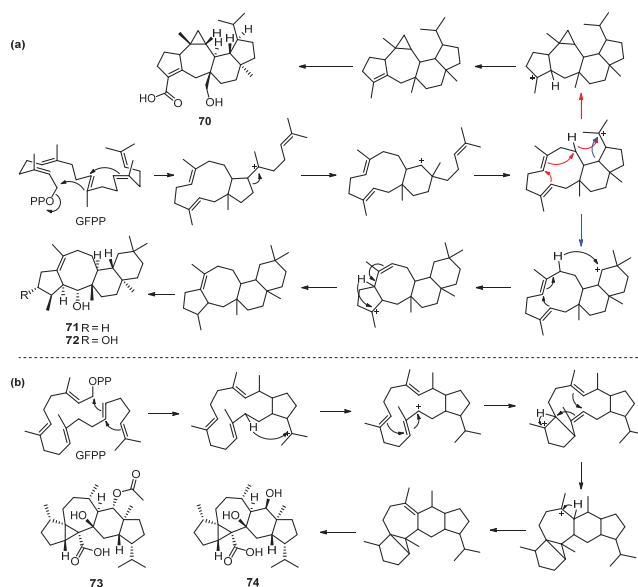
Scheme 11. (**a**) Proposed biosynthetic pathway for compounds **70**–**72** [80,81]; (**b**) Proposed biosynthetic pathway for compounds **73**–**74** [82].
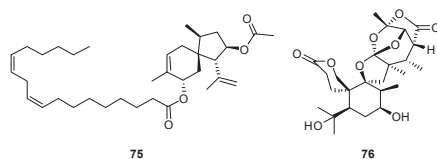
Figure 20. Structures of compounds **75** and **76**.

Simpterpenoid A (**77**) (Figure 21), an unconventional meroterpenoid containing a highly functionalized cyclohexadiene moiety with *gem*-propane-1,2-dione and methyl-formate groups, was isolated from the fungal strain *Penicillium simplicissimum* MA-332, obtained from the rhizospheric soil of the mangrove plant *Bruguiera sexangular* var. *rhynchopetala* [85]. The intricate polycyclic skeleton is unique in natural sources. Compound **77** exhibited potent inhibitory activity against influenza neuraminidase with an IC_{50} value of 8.1 nM.
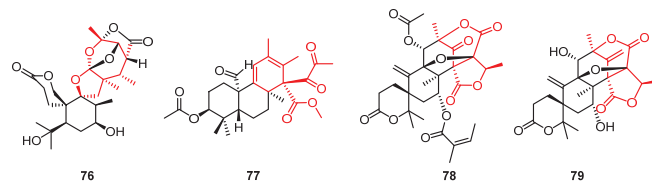
Figure 21. Structures of compounds **76**–**79**.

Two new meroterpenoids, penicianstinoids A and B (**78** and **79**, Figure 21), were obtained from the mangrove-derived fungus *Penicillium* sp. TGM112 isolated from the mangrove *Bruguiera sexangula* var. *rhynchopetala* [86]. Compared with **79**, compound **78** represents an austinoid-like meroterpenoid that is reported for the second time [87], in which a carbon−carbon double bond at C-1′−C-2′ was oxidized to a carbonyl group at

C-1′−C-2′. Compounds **78** and **79** showed growth inhibition activity against newly hatched larvae of *Helicoverpa armigera* (Hubner) with IC$_{50}$ values of 200 μg/mL. In addition, **78** and **79** displayed insecticidal activity against *Caenorhabditis elegans* with EC$_{50}$ values of 9.4 (±1.0) and 9.9 (±0.0) μg/mL, respectively. Biogenetically, compounds **76–79** are derived from the same intermediate **S2**, which is produced by the combination of a polyketide intermediate 3,5-dimethylorsellinicacid (DMOA) and the terpenoid precursor farnesyl pyrophosphate (FPP), following by a series of further modifications to generate a profile of meroterpenoids with diverse skeletons bearing polycyclic cores. DMOA-based meroterpenoids exhibit diverse structures due to the cyclization of the terpenoid moiety, divergence of post-cyclization modification reactions, and various tailoring reactions (Scheme 12) [83].

Scheme 12. Proposed biosynthetic pathway for compounds **76–79** [83].

Two hybrid sesquiterpene-cyclopaldic acid metabolites with an unusual carbon scaffold, namely pestalotiopens A and B (**80** and **81**) (Figure 22), were obtained from the endophytic fungus *Pestalotiopsis* sp. (from the leaves of the Chinese mangrove *Rhizophora mucronate*), together with the known phytotoxin altiloxin B [88]. A plausible biosynthetic pathway of **80** and **81** is proposed (Scheme 13). The cyclopaldic acid and altiloxin B were deduced as precursors.

Figure 22. Structures of compounds **80** and **81**.

Scheme 13. Proposed biosynthetic pathway for compounds **80** and **81** [88].

Indole terpenoids are structurally diverse meroterpenoids containing an indole ring from tryptophan and cyclic sesquiterpenes or diterpene backbone moiety [83].

Three indole sesquiterpenes, indotertine A (**82**) [89] and indotertine B (**83a/83b**) [90] (Figure 23) were discovered from actinomycete *Streptomyces* sp. CHQ-64 (derived from the rhizosphere soil of reeds). They possess an unusual skeleton with a condensed ring system made up of a tryptophan-derived indole moiety and a sesquiterpene unit, which represents a new subgroup of indole terpenoids combining amino acid and mevalonate pathways. Indotertine B (**83a/83b**) exists as a pair of rotamers about the N−C(O) bond with a 2:1 ratio, inseparable by HPLC because of the dynamic interconversion. The analysis of the NOESY spectrum implied that the formyl−N-1 amide bond was *S-trans* in **83a** and *S-cis* in **83b**. Compound **83** displays cytotoxic activities against HCT-8 and A549 tumor cell lines

with IC$_{50}$ values of 6.96 and 4.88 μM. Further chemical investigation of this fungal strain led to the isolation of drimentine I (**84**) [91], containing a rare heptacyclic skeleton formed via two bridging linkages. The pentacyclic product indotertine A (**82**) was hypothetically synthesized by iminium-olefin cyclization. In contrast, tetracyclic product drimentine F could take place from amidic nitrogen by nucleophilic addition to the α-position of the indole moiety (Scheme 14). However, cyclization of **84** happened on indol-NH to afford the linkage between C-14 and N-6 of drimentine F. Compound **84** was found to have weak activity against human cervical carcinoma cell line HeLa, with IC$_{50}$ values of 16.73 μM.
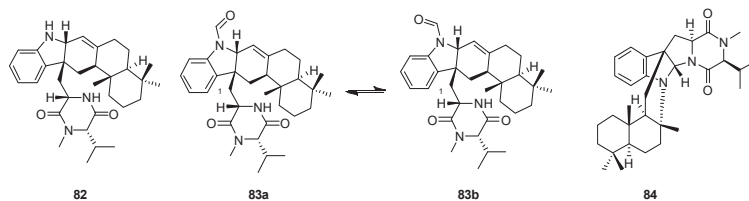
Figure 23. Structures of compounds **82–84**.
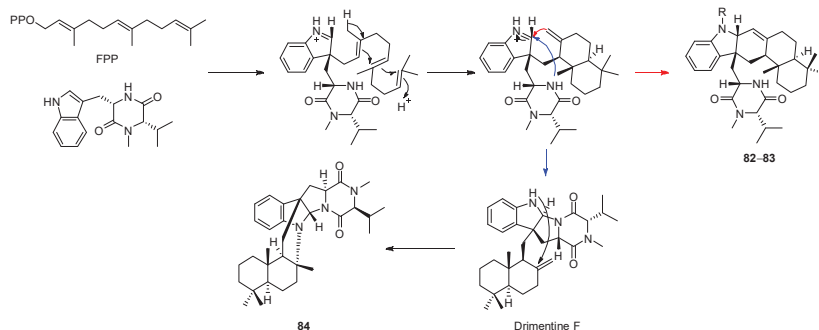
Scheme 14. Proposed biosynthetic pathway for compounds **82–84** [89].

Secopaxilline A (**85**) [92] (Figure 24) is the first example of indole diterpenoid derivatives possessing a carbon-nitrogen bond cleavage skeleton, which was isolated from metabolites of the aciduric fungus *Penicillium camemberti* OUCMDZ-1492 (separated from the soil and mud around the roots of *Rhizophora apiculata*). A plausible biosynthetic pathway for secopaxilline A (**85**) from paxilline was postulated, (Scheme 15), and the process has been conducted by chemical reactions with a 45% overall yield. Paxilline was derived from the common indole-diterpenoid precursor 3-geranylgeranylindole (GGI) derived from geranylgeranyl pyrophosphate (GGPP) and indole-3-glycerol phosphate [93] (Scheme 15).
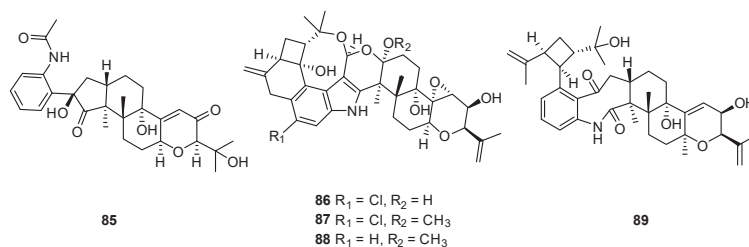
Figure 24. Structures of compounds **85–89**.
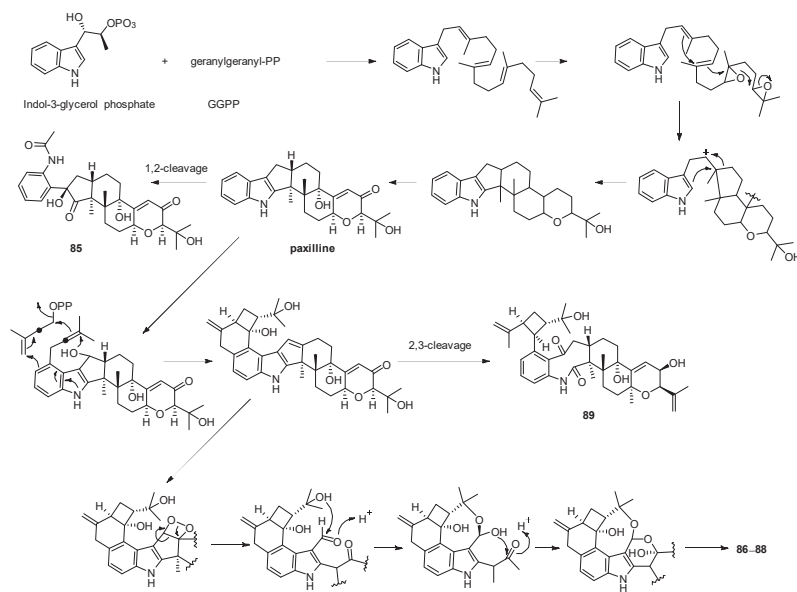
Scheme 15. Proposed biosynthetic pathway for compounds **86–89** [93].

The fungus *Mucor irregularis*, isolated from the fresh inner tissue of the mangrove *Rhizophora stylosa*, yields three unusual indole-diterpenes, rhizovarin A–C (**86–88**, Figure 24) [94], which represent the most complex members of the reported indole-diterpenes. Even though the main structural elements resemble those of other reported indole diterpenes, the presence of an unusual acetal linked to a hemiketal (**86**) or a ketal (**87** and **88**) unit in an unprecedented 4,6,6,8,5,6,6,6,6-fused indole-diterpene ring system makes them chemically unique. Their structures and absolute configurations were elucidated by spectroscopic analysis, modified Mosher's method, and chemical calculations. For rhizovarin A (**86**), the biosynthetic pathway may involve more oxidative steps than penitrem A, a known indole-diterpene derived from a paxilline and two isopentenyl-diphosphate units. (Scheme 15) The biosynthetic pathway has been elucidated by reconstitution of the biosynthetic genes in *Aspergillus oryzae* [95]. Another unusual indole-diterpene, containing a complex 6,8,6,6,6-fused ring system, rhizovarin D (**89**), was also obtained in this study. NOESY experiments determined the relative configuration for the stereogenic centers of **89**. Each isolated compound was evaluated for antitumor activity against HL-60 and A-549 cell lines. Compounds **86** and **87** showed activities against the human A-549 and HL-60 cancer cell lines (IC$_{50}$ < 10 μM).

Bioassay-guided fractionation of the bacterial strain *Erythrobacter* sp. SNB-035 (from mangrove sediments) led to the isolation of erythrazoles A and B (**90** and **91**) [96] (Figure 25). Structurally, **90** and **91** possess an abenzothiazole moiety, which is rare among NPs. Furthermore, **91** arises from four biosynthetic pathways: NRPS, terpene, shikimate, and polyketide. Although combinations of two of the four pathways are common among NPs, four biosynthetic pathways simultaneously involved are extremely rare (Scheme 16).
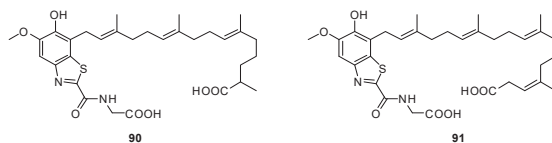
Figure 25. Structures of compounds **90** and **91**.
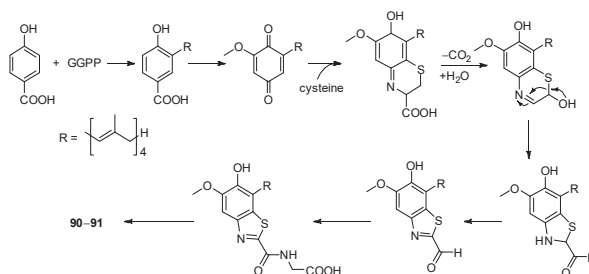
Scheme 16. Proposed biosynthetic pathway for compounds **90** and **91** [96].

3.3. Alkaloids and Other Nitrogen-Containing Metabolites

3.3.1. Diketopiperazines

Diketopiperazines (DKPs) are an essential group of structurally diverse cyclic dipeptides with significant biological properties [97].

Effusin A (**92**) (Figure 26) is a spirobicyclic *N,O*-acetal derivative with an unprecedented 3′,3a′,5′,6′-tetrahydrospiro-[piperazine-2,2′-pyrano[2,3,4-*de*]chromene] ring system. Besides this, a spiro-polyketide-diketopiperazine hybrid dihydrocryptoechinulin D (**93**) were isolated from a mangrove rhizosphere soil-derived fungus *Aspergillus effuses* H1-1 [98]. Compounds **92** and **93** occurred as racemates. The enantiomers were separated and characterized by online HPLC-ECD analysis, and their absolute configurations were determined by the TDDFT ECD calculation approach. The spirobicyclic *N,O*-acetal moiety of **92** could be obtained through a domino ring-closure reaction between the substituted salicylaldehyde moiety in aspergin and the eneamide moiety of the diketopiperazine unit in neoechinulin B [98]. On the contrary, the spirobicycle of **93** is produced by an enzyme-catalyzed regiospecific [4 + 2] Diels Alder reaction (Scheme 17). The cytotoxic effects of **92**–**93** were evaluated, **93** showed potent activity on P388 cells with an IC$_{50}$ value of 1.83 μM. The target of racemic **93** was also evaluated, and the (12*R*,28*S*,31*S*)-**93** enantiomer (**93a**) showed selectivity against topoisomerase I.

92a 12*R*, 21*R*, 28*R*, 29*R*
92b 12*S*, 21*S*, 28*S*, 29*S*

93a 12*R*, 28*S*, 31*S*
93b 12*S*, 28*R*, 31*R*
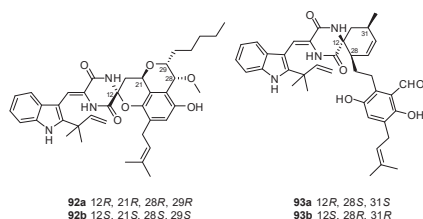
Figure 26. Structures of compounds **92** and **93**.
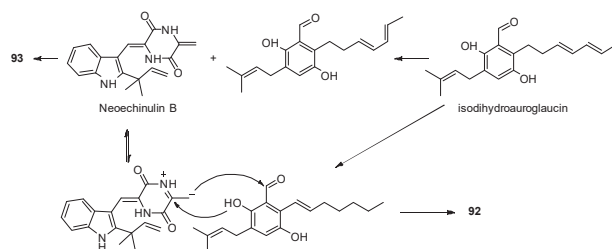
Scheme 17. Proposed biosynthetic pathway for compounds **92** and **93** [98].

Using the OSMAC (one strain many compounds) approach, a metabolically rich strain of *Penicillium brocae* MA-231 (isolated from mangrove *Avicennia marina*) could produce two

new diketopiperazines, spirobrocazines A–B (**94**–**95**) (Figure 27), which had a 6/5/6/5/6 cyclic system with a rare spirocyclic center at C-2 [99]. In addition, a deep-sea sediment-derived fungus *Eutypella* sp. Also yields three new spirocyclic DKPs, eutypellazines N–P (**96**–**98**) [100]. Compound **96** was determined as the C-2′ isomer of spirobrocazine A (**91**). Notably, **97** and **98** are the first compounds isolated from a wild-type fungus to contain a spirocyclic tetrahydrobenzothiophene motif. Furthermore, eight new dioxopiperazines **99**–**106** (penispirozines A-H) were discovered from the mangrove-derived fungus *Penicillium janthinellum* HDN13-309 [101]. The structures of **99**–**104** were similar to eutypellazines O–P (**97**–**88**). They were distinguished by not only the existence of a spiro-thiophane or spiro-furan ring system but also the chirality of the pentacyclic moiety. Moreover, penispirozine A (**99**) had an unusual pyrazino[1,2]oxazadecaline coupled with a thiophane ring system, while penispirozine B (**100**) possessed a 6/5/6/5/6 pentacyclic ring system with two rare spirocyclic centers. Biosynthetically, the precursor to these structurally diverse penispirozines was considered to be the diketopiperazine cyclo-L-Phe-L-Phe (Scheme 18). In addition, compounds **101** and **102** increased the expression of the two relevant phase-II detoxifying enzymes, SOD2 and HO-1, at 10 μM.
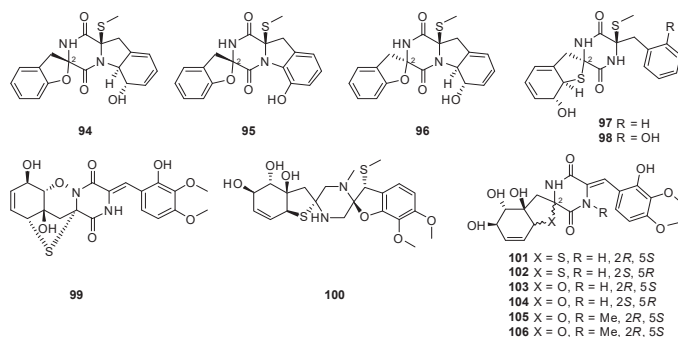
Figure 27. Structures of compounds **94**–**106**.
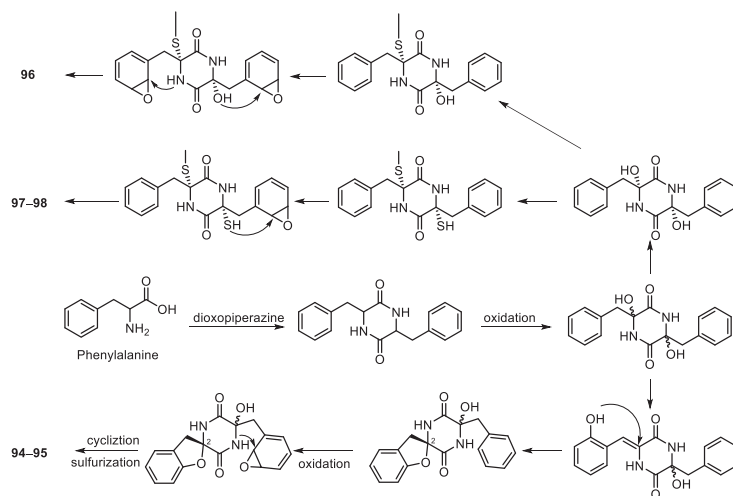
Scheme 18. Proposed biosynthetic pathway for compounds **94**–**98** [99,100].

A pair of unusual enantiomeric indole diketopiperazine alkaloid dimers, (±)-asperginulin A (**107a/b**) (Figure 28), with an unprecedented 6/5/4/5/6 pentacyclic skeleton, were

discovered from the mangrove endophytic fungus *Aspergillus* sp. SK-28, guided by UPLC-HRMS [102]. Chiral-phase HPLC separated the enantiomeric dimers. Their structures, including the absolute configurations, were elucidated by spectroscopic analysis, X-ray diffraction, and quantum chemical calculation. (+)-Asperginulin A (**107b**) exhibited antifouling activity against the barnacle *Balanus reticulatus*. **107** was possibly derived, in vivo, from intermolecular [2 + 2] cycloaddition of its monomer precursor by nonenzymatic processes (Scheme 19).
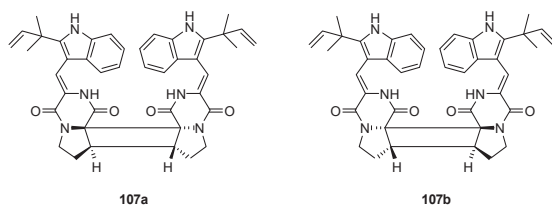
Figure 28. Structures of compounds **107a/b**.
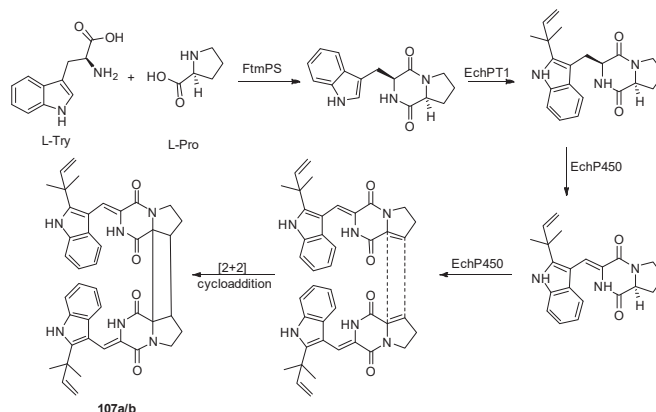
Scheme 19. Proposed biosynthetic pathway for compounds **107a/b** [102].

A class of pyrazinopyrimidine-type alkaloids, namely pyrasplorines A–C (**108**–**110**) (Figure 29) were discovered from the fungus *Aspergillus versicolor* HDN11-84 [103]. Pyrasplorine A (**105**) represents the first compound with spiro-cyclopentane in pyrazinopyrimidine-type alkaloids. The cyclopentane moiety is common in terpenes but rare in alkaloids and diketopiperazines, and it is only found in maremycins [104]. The structure is probably constructed by the condensation of anthranilic acid with diketopiperazine and followed by successive steps to yield the key intermediate **S3**. Then, compound **108** was derived from the **S3** via a series of reactions [105] (Scheme 20).
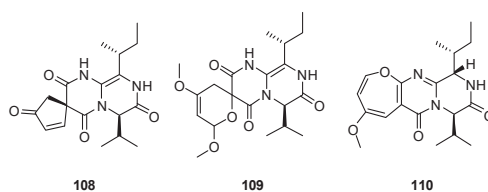
Figure 29. Structures of compounds **108**–**110**.
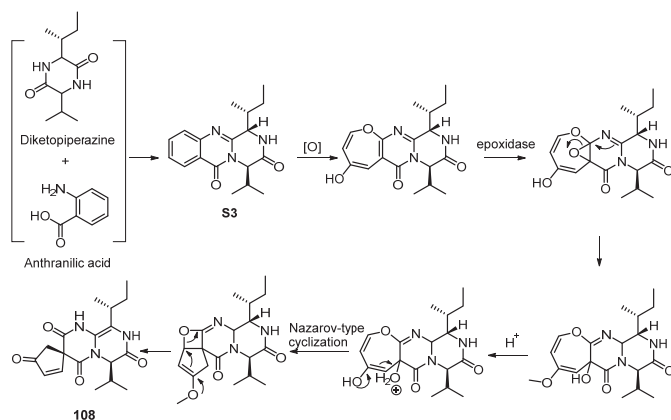
Scheme 20. Proposed biosynthetic pathway for compound **108** [105].

3.3.2. Indole and Isoindole Alkaloids Derivatives

Various mangrove fungi produce indole and isoindole alkaloids with a plethora of biologically active. The indole-terpenes which also belong to meroterpenes have been described in Section 3.2.3.

Cytochalasan alkaloid usually consists of a 10-(indol-3-yl) group, a macrocyclic ring, and a perhydroisoindolone moiety. Chaetoglobosin is one class of cytochalasan alkaloid. The mangrove endophytic fungus *Penicillium chrysogenum* V11 afforded two unusual new Chaetoglobosins, penochalasin I and K (**111** and **112**) [106,107] (Figure 30), with an unprecedented six-cyclic 6/5/6/5/6/13 fused ring system formed by the connection of C-5 and C-2′ of the chaetoglobosin class. Additionally, the biomimetic semi-synthesis of **111** and **112** was successfully carried out from the corresponding co-occurrence analogue chaetoglobosin C and chaetoglobosin A, respectively [107]. Compound **112** displayed significant inhibitory activities against *Colletotrichum gloeosporioides* and *Rhizoctonia solani* (MICs = 6.13 μM, 12.26 μM, respectively), which was better than those of control carbendazim. It also exhibited potent cytotoxicity against MDA-MB-435, SGC-7901, and A549 cells (IC$_{50}$ < 10 μM). In addition, compound **111** exhibited significant cytotoxicity against MDA-MB-435 and SGC-7901 cells (IC$_{50}$ < 10 μM).
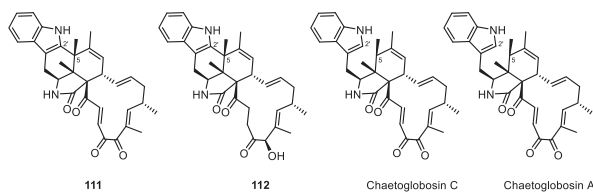
Figure 30. Structures of compounds **111** and **112**, chaetoglobosin A and C.

The typical paraherquamides (PHQs) are prenylated indole alkaloids with diverse ring systems. PHQs are derived from three building blocks: *L*-tryptophan, acyclic amino acid (either proline, β-methyl proline, or pipecolic acid), and one or two isoprenyl units. Interestingly, compounds **113–115** (Figure 31) (mangrovamides A–C, isolated from the *Penicillium* sp. Separated from a mangrove sediment sample of the South China Sea) feature a bicyclo [2.2.2] diazaoctane core and contain the first documented examples of isoprene derived dimethyl γ-pyrone and γ-methyl proline, instead of the usual β-methyl proline in the PHQ family [108]. A plausible biosynthetic pathway starting from L-ornithine to account for the formation of the observed γ-methyl proline is outlined (Scheme 21). Moreover, the X-ray data determined the absolute configuration of all chiral centers in **113**.

In an activity assay, **115** showed a moderate acetylcholinesterase inhibitory effect with an IC$_{50}$ value of 58.0 μM.
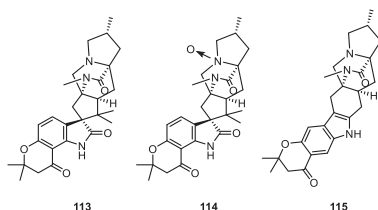
Figure 31. Structures of compounds **113–115**.
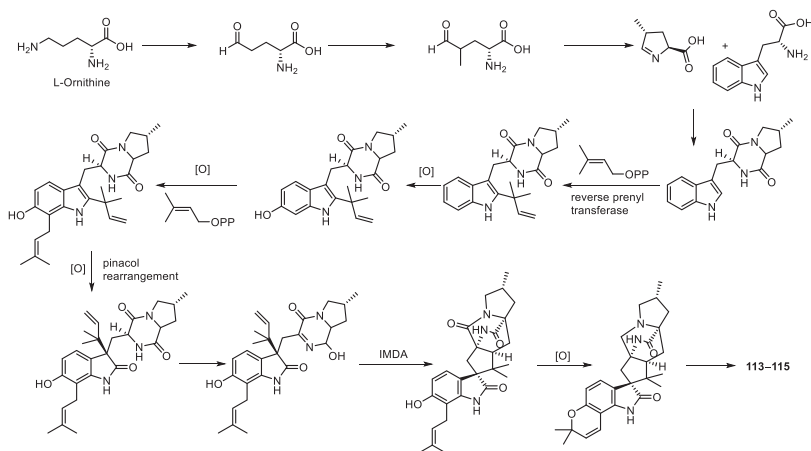
Scheme 21. Proposed biosynthetic pathway for compounds **113–115** [108].

Diaporisoindoles A and B (**116** and **117**) [109], and D and E (**118** and **119**) [52] (Figure 32), isolated from the mangrove endophytic fungus *Diaporthe* sp. SYSU-HQ3 (from a fresh branch of the mangrove plant *Excoecaria agallocha*) and could be derived from tenellone B, are the first reported examples of isoprenylisoindole alkaloids with a rare 1,4-benzodioxan moiety. In addition, siaporisoindole A (**116**) showed significant inhibitory activity against *Mycobacterium tuberculosis* protein tyrosine phosphatase B with IC$_{50}$ 4.2 μM compared to 22.1 μM for the positive control (oleanolic acid,). Furthermore, **116** and **117** exhibited potent inhibitory activity against NO production in RAW 264.7 cells with IC$_{50}$ values less than 10 μM. Then She et al. continued an extensive study of isolating an unusual diisoprenylisoindole dimer diaporisoindole C (**120**). It was presumed to be derived from compounds **116** or **117** via addition reaction, dehydration, and aromatization (Scheme 22).
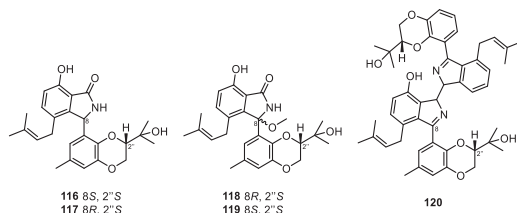
Figure 32. Structures of compounds **116–120**.
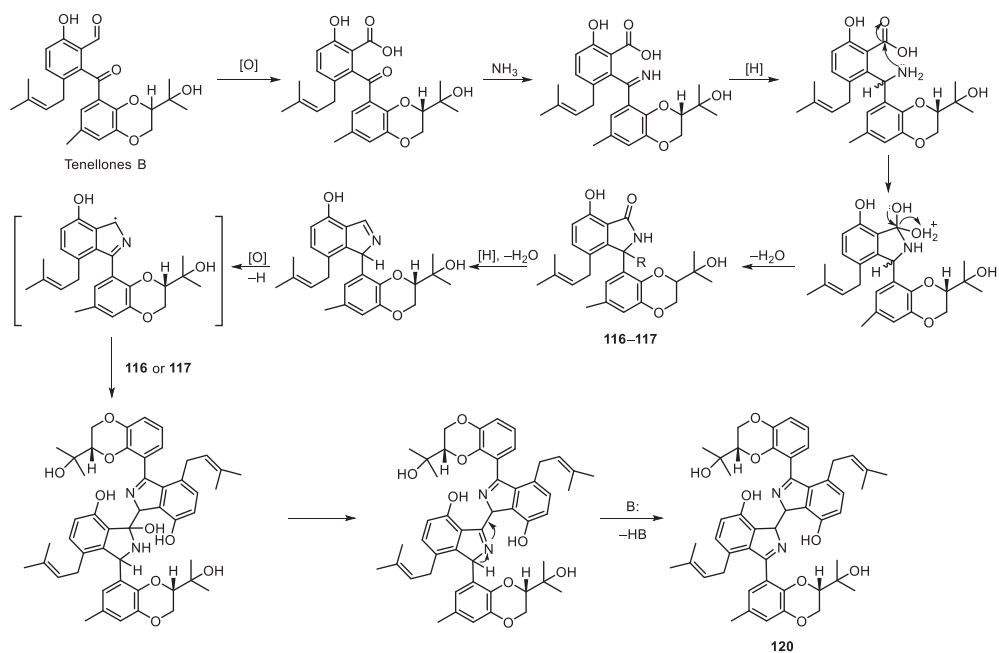
Scheme 22. Proposed biosynthetic pathway for compounds **116–120** [109].

Quinazoline containing indole alkaloids have pyrimidine [2, 1-b] quinazoline and imidazole [1, 2-a] indole groups linked by methylene (and, in some cases, further linked by additional helical Bridges). Two unusual quinazoline-containing indole alkaloids neosartoryadins A and B (**121** and **122**) (Figure 33) along with fiscalin C (a known compound to be related to biosynthesis) were identified from the mangrove endophytic fungus *Neosartorya udagawae* HDN13-313 [110]. Compounds **121** and **122** is a quinazoline-containing indole alkaloid featuring a unique 6/6/6/5 quinazoline ring directly linked to the 6/5/5 imidazolinone ring. **121** and **122** differs from conventional fumiquinazoline alkaloids such as fiscalin C by the unprecedented pyrido[2, 1-b]- quinazoline moiety, which binds to a pyridine (C ring) rather than a pyrimidine ring, in addition to the presence of a unique tetrahydrofuran ring (D ring). It is speculated that **121** and **122** are biosynthesized from *L*-tryptophan, anthranilic acid (ATA), L-valine, and 2-aminoisobutyric acid (Aib). The unprecedented C ring was formed by the key intermediate fiscalin C through further modification by oxidation, hydrolysis, water nucleophilic attack, dehydration, deprotonation, and subsequent aldol reaction (Scheme 23).

121 R = H
122 R = OH
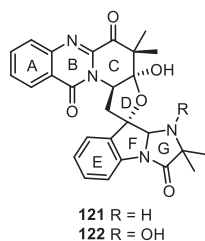
Figure 33. Structures of compounds **121** and **122**.
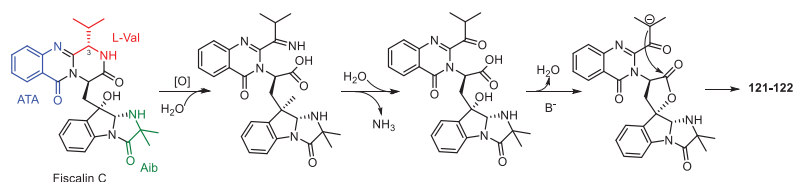
Scheme 23. Proposed biosynthetic pathway for compounds **121** and **122** [110].

Streptocarbazoles, the staurosporine analogues with extraordinary cyclic N-glycosidic connections between 1,3-carbon atoms of the glycosyl moiety and two indole nitrogen atoms of the indolocarbazole core, have also been produced by mangrove actinomycetes.

Streptomyces sp. FMA, isolated from mangrove soil collected in Sanya, Hainan Province of China provided streptocarbazoles A (**123**) and B (**124**) [111] (Figure 34). Compound **123** was cytotoxic to HL60, A549, P338, and HeLa cells with IC$_{50}$ values of 1.4, 5.0, 18.9, and 34.5 μM, respectively, while compound **124** was active against P388 and HeLa cells with IC$_{50}$ values of 12.8 and 22.5 μM, respectively. In addition, it was demonstrated that streptocarbazoles A arrest the HeLa cells in the G2/M phase at 10 μM. A plausible biogenetic pathway of **123** and **124** was postulated (Scheme 24). The indolocarbazole unit (K252c) was derived from tryptophan, while the glycosyl moiety was probably developed from 2-deoxy-D-pyranoglucose. Subsequently, the first cloning and characterization of an indolocarbazole gene cluster isolated from *Streptomyces sanyensis* FMA were reported. Indolocarbazole biosynthesis was confirmed by gene inactivation and heterologous expression in *Streptomyces coelicolor* M1152 [112].

123 R = OH
124 R = H
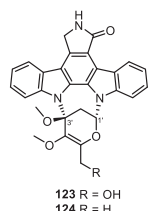
Figure 34. Structures of compounds **123** and **124**.
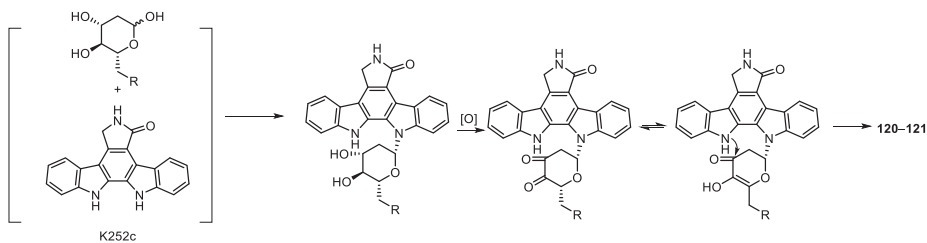
Scheme 24. Proposed biosynthetic pathway for compounds **123** and **124** [111].

3.3.3. Pyridines

Piericidins feature a 4-pyridinol core linked with a variable methylated polyene side chain. The strain *Streptomyces iakyrus* SCSIO NS104, isolated from a mangrove sediment sample collected from the Pearl River estuary to the South China Sea, yielded four new piericidin analogues, iakyricidins A–D (**125**–**128**) [113]. Iakyricidins B–D (**126**–**128**) represent a new subgroup of piericidin with C-C cyclization and double bond rearrangements in the polyene side chain. In addition, oxidized side chain piericidin analogue iakyricidin A (**125**) displayed potent antiproliferative activity against human renal carcinoma cell lines ACHN

cell with an IC$_{50}$ value of 20 nM. Compound **125** might be derived by oxidative cleavage between C-13 and C-14 of the precursor. In the plausible biosynthetic pathways of **126–128**, the most crucial step would be the yet-to-be-identified enzymatic C8-C12 cyclization from the co-occurrence precursor (Scheme 25).
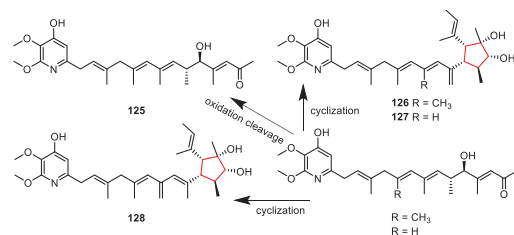
Scheme 25. Proposed biosynthetic pathway for compounds **125–128** [113].

Chemical investigation of the endophytic fungus *Campylocarpon* sp. HDN13-307, obtained from the root of mangrove plant *Sonneratia caseolaris* led to the isolation of four new 4-hydroxy-2-pyridone alkaloids, namely campyridones A–D (**129–132**) [114] (Figure 35), which existed as two pairs of diastereoisomers, featuring an additional C ring between the decalin and pyridone units, represented new ring systems for this family of alkaloids. A plausible biosynthetic pathway for **129–132** is postulated with the co-occurrence ilicicolin H as a critical intermediate. Ilicicolin H is a typical 4-hydroxy-2-pyridone alkaloid which was considered to be biosynthesized via tetramic acids formed by hybridizing a polyketide unit to a tyrosine (Scheme 26). Compound **132** exhibited activity against Hela cells with IC$_{50}$ values of 8.8 μM.
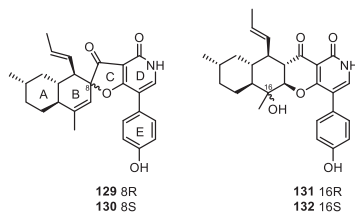
Figure 35. Structures of compounds **129–132**.
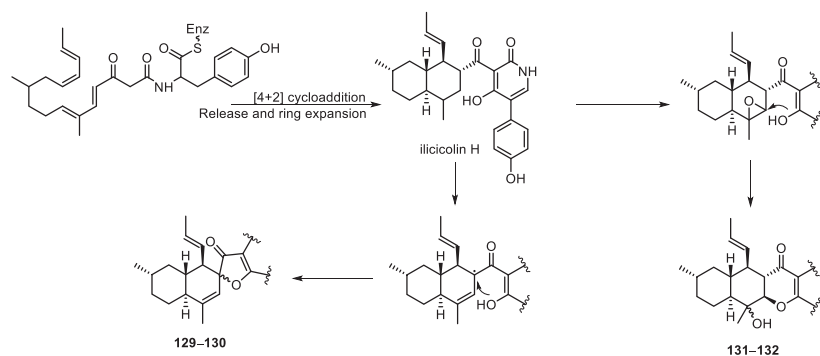
Scheme 26. Proposed biosynthetic pathway for compounds **129–132** [114].

3.3.4. Others

A chemical investigation of the fermentation of *Penicillium* sp. GD6, associated with the Chinese mangrove *Bruguiera gymnorrhiza*, resulted in the isolation of an unusual

pyrrolizidine alkaloid, penibruguieramine A (**133**) (Figure 36), characterized by an unprecedented 1-alkenyl-2-methyl-8-hydroxymethyl pyrrolizidin-3-one skeleton [115] (Scheme 27).
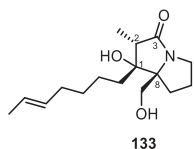
Figure 36. Structure of compound **133**.
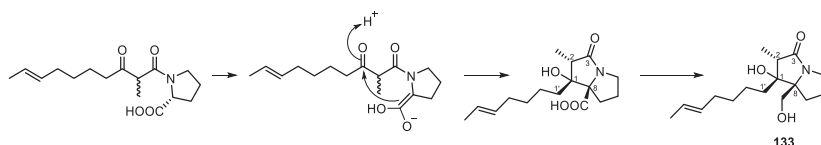
Scheme 27. Proposed biosynthetic pathway for compound **133** [115].

Talaramide A (**134**) (Figure 37) is the second example of an alkaloid with a unique oxidized tricyclic system resembling a bird cage, which was obtained from the mangrove endophytic fungus *Talaromyces* sp [116]. The first example was rubrobramide, obtained from the fungus *Cladobotryum ubrobrunnes*cens [117]. **134** was a PKS-NRPS hybrid metabolite derived from acetyl acid, malonic acid, and *L*-leucine. A series of polymerizations, cyclizations, rearrangements, and redox reactions finally afforded the unique oxidized tricyclic skeleton of **134** (Scheme 28).
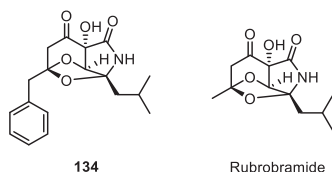
Figure 37. Structures of compound **134** and rubrobramide.
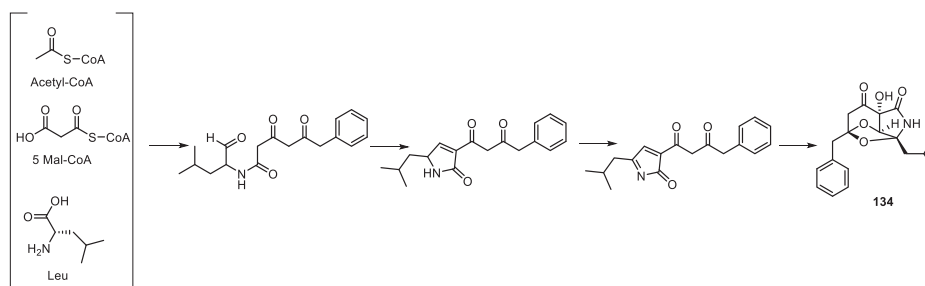
Scheme 28. Proposed biosynthetic pathway for compound **134** [116].

4. Conclusions

In this review, we presented the chemical constituents of the mangrove-associated ecosystem and showcased the diversity of the chemical structures, biological activities, chemical syntheses, and (proposed) biosynthetic pathways.

Structurally diverse secondary metabolites play a crucial role in the discovery campaigns for new NP drug pharmacophores. The mangrove ecosystem is producing various

structurally novel compounds that could provide a potent compound library for the identification of lead compounds. Herein, we presented a comprehensive review of 134 mangrove-derived NPs with new carbon skeletons, unique ring systems, or uncommon structural moieties. The majority of them were produced by mangrove-associated microorganisms, and more than 70% were isolated from endophyte fungus, indicating remarkable chemical diversity and interesting bioactivity of the microbial community. The structural novelty and diversity of these metabolites result from the enormous variety of mangrove ecosystems in combination with their potential biosynthetic capabilities. In addition, they display diverse and remarkable biological activities and are frequently reported as antimicrobial and cytotoxic compounds (Tables 1 and 2), which might attract researchers for further investigations toward chemical synthesis and biosynthesis. Mangrove ecosystems are a rewarding source for producing bioactive substances with novel carbon frameworks and discovering drug lead compounds, attracting pharmaceutical scientists for more in vivo and preclinical studies on these compounds.

Table 1. Structurally unusual secondary metabolites from mangrove flora.

Source	Secondary Metabolites	Reported Activities	Ref
X. moluccensis	Thaixylomolin A–C (**1**, **19** and **20**)	Anti-inflammatory	[21]
X. moluccensis	Thaixylomolin R (**2**)	NR [a]	[22]
X. granatum	Xylomexicanins E and F (**23** and **3**)	Cytotoxicity	[23]
X. granatum	Hainangrantum I and J (**4** and **5**)	NR	[24]
X. moluccensis	Trangmolins A–F (**6–10**, **17**)	NR	[27]
X. moluccensis	Krishnolide J (**11**)	NR	[28]
X. moluccensis	Andhraxylocarpins A and C (**12**, **14**)	NR	[29]
X. granatum	Andhraxylocarpins A–B and D–E (**12–13** and **15–16**)	NR	[29]
X. moluccensis	Krishnadimer A (**18**)	NR	[30]
X. granatum	Xylogranatopyridines A and B (**21** and **22**)	PTP1B inhibitory	[32]
X. granatum	Xylomexicanins I and J (**24** and **25**)	NR	[33]
X. moluccensis	Xylomolones A–C (**26–28**)	NR	[34]
Excoecaria agallocha	Agallochaexceorins D–E (**29–30**)	NR	[35]
Ceriops decandra	Decandrinin (**31**)	NR	[36]

[a] NR: not reported in references.

Table 2. Structurally unusual secondary metabolites from mangrove-associated microorganisms.

Microorganisms	Hosts	Secondary Metabolites	Reported Activities	Ref
Penicillium commune	*Kandelia candel*	Peniisocoumarins A and B (**32** and **33**)	NR [a]	[44]
Penicillium chermesinum	Mangrove forest	Penicilliumolide A (**34**)	NR	[45]
Penicillium sp.	Mangrove sediment	Penixanthones C and D (**35** and **36**)	NR	[46]
Penicillium chrysogenum	*Acanthus ilicifolius*	Penicitols A and B (**37-38**)	Cytotoxicity	[48]
Diaporthe sp.	*Excoecaria agallocha*	Diaporindenes A–D (**39-42**)	Anti-inflammatory	[52]
Diaporthe sp.	*Excoecaria agallocha*	Isoprenylisobenzofuran A (**43**)	Anti-inflammatory	[52]
Penicillium sumatrense	*Lumnitzera racemose*	Sumalarins A−C (**44–46**)	Cytotoxicity	[55]
Streptomyces sp.	*Bruguiera gymnorrhiza*	Divergolide A-D (**47–50**)	Antimicrobial, cytotoxicity	[56]
Streptomyces sp.	Mangrove soil	Hainanmycin A (**51**)	NR	[67]
Streptomyces sp.	Mangrove sample	Streptoglycerides A–H (**52–59**)	Anti-inflammatory	[69,70]
Streptomyces sp.	Mangrove sample	Miharadiened A–D (**60–63**)	NR	[71]
Pseudolagarobasidium acaciicola	*Bruguiera gymnorrhiza*	Acaciicolin A (**64**), Spiroacaciicolides A–C (**65–67**)	NR	[74,75]
Penicillium bilaiae	*Lumnitzera racemosa*	Penicibilaenes A–B (**68–69**)	Anti-fungal	[77]

[a] NR: not reported in references.

Table 2. *Cont.*

Microorganisms	Hosts	Secondary Metabolites	Reported Activities	Ref
Aspergillus sp.	Mangrove endophytic	Asperterpenoid A (**70**)	Antituberculosis	[80]
Aspergillus sp.	Mangrove endophytic	Asperterpenols A–B (**71–72**)	Acetylcholinesterase inhibition	[81]
Aspergillus terreus	*Kandelia obovate*	Aspterpenacids A–B (**73–74**)	NR	[82]
Penicillium bilaiae	*Lumnitzera racemosa*	Chermebilaenes A–B (**75–76**)	Antibiotic	[84]
Penicillium simplicissimum	*Bruguiera sexangula*	Simpterpenoid A (**77**)	Antiviral	[85]
Penicillium sp.	*Bruguiera sexangula*	Penicianstinoids A–B (**78–79**)	Insecticidal activity	[86]
Pestalotiopsis sp.	*Rhizophora mucronata*	Pestalotiopens A–B (**80–81**)	NR	[88]
Streptomyces sp.	Mangrove rhizosphere soil	Indotertine A (**82**), indotertine B (**83a/83b**)	Antitumor	[89,90]
Streptomyces sp.	Mangrove rhizosphere soil	Drimentine I (**84**)	Antitumor	[91]
Penicillium camemberti	Rhizosphere soil of *Rhizophora apiculata*	Secopaxilline A (**85**)	NR	[92]
Mucor irregularis	*Rhizophora stylosa*	Rhizovarin A–D (**86–89**)	Antitumor	[94]
Erythrobacter sp.	Mangrove sediment	Erythrazoles A–B (**90–91**)	NR	[96]
Aspergillus effuses	Mangrove rhizosphere soil	Effusin A (**92**), dihydrocryptoechinulin D (**93**)	Cytotoxicity	[98]
Penicillium brocae	*Avicennia marina*	Spirobrocazines A–B (**94–95**)	NR	[99]
Eutypella sp.	Deep sea sediment	Eutypellazines N–P (**96–98**)	NR	[100]
Penicillium janthinellum	Mangrove	Penispirozines A–H (**99–106**)	Antioxidant	[101]
Aspergillus sp.	Mangrove endophytic	(±)-Aspergulin A (**107a/b**)	Antifouling	[102]
Aspergillus versicolor	Rhizosphere soil of *Thespesia populnea*	Pyrasplorines A–C (**108–110**)	NR	[103]
Penicillium chrysogenum	Mangrove endophytic	Penochalasin I and K (**111–112**)	Antibiotic, cytotoxicity	[106,107]
penicillium sp.	Mangrove sediment	Mangrovamides A–C (**113–115**)	Acetylcholinesterase inhibition	[108]
Diaporthe sp.	*Excoecaria agallocha*	Diaporisoindoles A–B (**116–117**), diaporisoindoles D–E (**118–119**), diaporisoindole C (**120**)	Antituberculosis, anti-inflammatory	[52,109]
Neosartorya udagawae	Mangrove endophytic	Neosartoryadins A–B (**121–122**)	NR	[110]
Streptomyces sp.	Mangrove soil	Streptocarbazoles A–B (**123–124**)	Antitumor	[111]
Streptomyces iakyrus	Mangrove sediment	Iakyricidins A–D (**125–128**)	NR	[113]
Campylocarpon sp.	*Sonneratia caseolaris*	Campyridones A–D (**129–132**)	Antitumor	[114]
Penicillium sp.	*Bruguiera gymnorrhiza*	Penibruguieramine A (**133**)	NR	[115]
Talaromyces sp.	Mangrove endophytic	Talaramide A (**134**)	NR	[116]

[a] NR: not reported in references.

In conclusion, through this review, we conveyed that (1) the mangrove-associated ecosystem is still an abundant source of bioactive NPs providing leads for drug development, (2) chemical syntheses of several of the mangrove-associated NPs are completed, but more NPs are to be synthesized and more efficient routes are to be developed, and (3) the biosynthesis of most of the mangrove-associated NPs remain unclear.

References

1. Zhou, J.; Feng, Z.; Zhang, W.; Xu, J. Evaluation of the antimicrobial and cytotoxic potential of endophytic fungi extracts from mangrove plants *Rhizophora stylosa* and *R. mucronata*. *Sci. Rep.* **2022**, *12*, 2733–2744. [CrossRef] [PubMed]
2. Ser, H.L.; Tan, L.T.; Law, J.W.; Chan, K.-G.; Duangjai, A.; Saokaew, S.; Pusparajah, P.; Mutalib, N.-S.; Khan, T.M.; Goh, B.-H.; et al. Focused Review: Cytotoxic and Antioxidant Potentials of Mangrove-Derived *Streptomyces*. *Front. Microbiol.* **2017**, *8*, 2065–2075. [CrossRef]
3. Azman, A.-S.; Othman, I.; Velu, S.S.; Chan, K.-G.; Lee, L.-H. Mangrove rare actinobacteria: Taxonomy, natural compound, and discovery of bioactivity. *Front. Microbiol.* **2015**, *6*, 856–870. [CrossRef] [PubMed]
4. Nicoletti, R.; Salvatore, M.M.; Andolfi, A. Secondary Metabolites of Mangrove-Associated Strains of *Talaromyces*. *Mar. Drugs* **2018**, *16*, 12–26. [CrossRef]
5. Xu, J. Bioactive natural products derived from mangrove-associated microbes. *RSC Adv.* **2015**, *5*, 841–892. [CrossRef]
6. Chen, S.; Cai, R.; Liu, Z.; Cui, H.; She, Z. Secondary metabolites from mangrove-associated fungi: Source, chemistry and bioactivities. *Nat. Prod. Rep.* **2022**, *39*, 560–595. [CrossRef]
7. Ancheeva, E.; Daletos, G.; Proksch, P. Lead Compounds from Mangrove-Associated Microorganisms. *Mar. Drugs* **2018**, *16*, 319–349. [CrossRef]
8. Zeng, W.; Huang, G.; Wang, B.; Cai, J.; Zheng, C. Secondary Metabolites and Bioactivities of *Penicillium* sp. Sourced from Mangrove from 2007 to 2020. *Chin. J. Org. Chem.* **2021**, *41*, 4255–4278. [CrossRef]
9. Xu, D.B.; Ye, W.-W.; Han, Y.; Deng, Z.-X.; Hong, K. Natural products from mangrove actinomycetes. *Mar. Drugs* **2014**, *12*, 2590–2613. [CrossRef]
10. Deshmukh, S.K.; Gupta, M.K.; Prakash, V.; Reddy, M.S. Mangrove-Associated Fungi: A Novel Source of Potential Anticancer Compounds. *J. Fungi* **2018**, *4*, 101–139. [CrossRef] [PubMed]
11. Wang, X.; Mao, Z.-G.; Song, B.-B.; Chen, C.-H.; Xiao, W.-W.; Hu, B.; Wang, J.-W.; Jiang, X.-B.; Zhu, Y.-H.; Wang, H.-J. Advances in the study of the structures and bioactivities of metabolites isolated from mangrove-derived fungi in the South China Sea. *Mar. Drugs* **2013**, *11*, 3601–3616. [CrossRef] [PubMed]
12. Manohar, S.M. A Review of the Botany, Phytochemistry and Pharmacology of Mangrove *Lumnitzera racemosa* Willd. *Pharmacogn. Rev.* **2021**, *15*, 107–116. [CrossRef]
13. Wang, K.-W.; Wang, S.-W.; Wu, B.; Wei, J.-G. Bioactive Natural Compounds from the Mangrove Endophytic Fungi. *Mini. Rev. Med. Chem.* **2014**, *14*, 370–391. [CrossRef] [PubMed]
14. Cadamuro, R.D.; Bastos, I.M.A.S.; Silva, I.T.; Cruz, A.C.C.; Robl, D.; Sandjo, L.P.; Alves, S.; Lorenzo, J.M.; Rodríguez-Lázaro, D.; Treichel, H.; et al. Bioactive Compounds from Mangrove Endophytic Fungus and Their Uses for Microorganism Control. *J. Fungi* **2021**, *7*, 455–473. [CrossRef]
15. Li, K.; Chen, S.; Pang, X.; Cai, J.; Zhang, X.; Liu, Y.; Zhu, Y.; Zhou, X. Natural products from mangrove sediments-derived microbes: Structural diversity, bioactivities, biosynthesis, and total synthesis. *Eur. J. Med. Chem.* **2022**, *230*, 114117–114157. [CrossRef]
16. Wu, J.; Xiao, Q.; Xu, J.; Li, M.-Y.; Pan, J.-Y.; Yang, M.-H. Natural products from true mangrove flora: Source, chemistry and bioactivities. *Nat. Prod. Rep.* **2008**, *25*, 955–981. [CrossRef]
17. Li, M.Y.; Xiao, Q.; Pan, J.-Y.; Wu, J. Natural products from semi-mangrove flora: Source, chemistry and bioactivities. *Nat. Prod. Rep.* **2009**, *26*, 281–298. [CrossRef]
18. Fang, X.; Di, Y.T.; Hao, X.J. The Advances in the Limonoid Chemistry of the Meliaceae Family. *Curr. Org. Chem.* **2011**, *15*, 1363–1391. [CrossRef]
19. Luo, J.; Sun, Y.; Kong, L. Research progress of meliaceous limonoids from 2011 to 2021. *Nat. Prod. Rep.* **2022**, *39*, 1325–1365. [CrossRef]
20. Tan, Q.-G.; Luo, X.-D. Meliaceous limonoids: Chemistry and biological activities. *Chem. Rev.* **2011**, *111*, 7437–7522. [CrossRef]
21. Li, J.; Li, M.-Y.; Bruhn, T.; Katele, F.X.; Xiao, Q.; Pedpradab, P.; Wu, J.; Bringmann, G. Thaixylomolins A-C: Limonoids Featuring Two New Motifs from the Thai *Xylocarpus Moluccensis*. *Org. Lett.* **2013**, *15*, 3682–3685. [CrossRef]
22. Dai, Y.-G.; Li, W.-S.; Pedpradab, P.; Liu, J.-J.; Wu, J.; Shen, L. Thaixylomolins O–R: Four new limonoids from the Trang mangrove, *Xylocarpus moluccensis*. *RSC Adv.* **2016**, *6*, 85978–85984. [CrossRef]
23. Wu, Y.-B.; Qing, X.; Huo, C.-H.; Yan, H.-M.; Shi, Q.-W.; Sauriol, F.; Gu, Y.-C.; Kiyota, H. Xylomexicanins E-H, new limonoids from *Xylocarpus granatum*. *Tetrahedron* **2014**, *70*, 4557–4562. [CrossRef]
24. Pan, J.-Y.; Chen, S.-L.; Li, M.-Y.; Li, J.; Yang, M.-H.; Wu, J. Limonoids from the Seeds of a Hainan Mangrove, *Xylocarpus Granatum*. *J. Nat. Prod.* **2010**, *73*, 1672–1679. [CrossRef] [PubMed]
25. Wu, J.; Zhang, S.; Bruhn, T.; Xiao, Q.; Ding, H.; Bringmann, G. Xylogranatins F-R: Antifeedants from the Chinese mangrove, *Xylocarpus granatum*, a new biogenetic pathway to tetranortriterpenoids. *Chem. Eur. J.* **2008**, *14*, 1129–1144. [CrossRef]
26. Sheng, Y.; Yin, S.; Wang, X.-N.; Lin, L.-P.; Ding, J.; Yue, J.-M. Xylogranatins A−D: Novel Tetranortriterpenoids with an Unusual 9,10-seco Scaffold from Marine Mangrove *Xylocarpus granatum*. *Org. Lett.* **2006**, *8*, 4935–4938. [CrossRef]
27. Li, W.-S.; Shen, L.; Bruhn, T.; Pedpradab, P.; Wu, J.; Bringmann, G. Trangmolins A-F with an Unprecedented Structural Plasticity of the Rings A and B: New Insight into Limonoid Biosynthesis. *Chem. Eur. J.* **2016**, *22*, 11719–11727. [CrossRef]
28. He, C.L.; Li, W.-S.; Wu, J.; Shen, L. Krishnolides E-K: New limonoids from the Krishna mangrove *Xylocarpus moluccensis*. *Fitoterapia* **2021**, *150*, 104835–104843. [CrossRef]

29. Li, J.; Li, M.-Y.; Bruhn, T.; Gotz, D.C.G.; Xiao, Q.; Satyanandamurty, T.; Wu, J.; Bringmann, G. Andhraxylocarpins A-E: Structurally intriguing limonoids from the true mangroves *Xylocarpus granatum* and *Xylocarpus moluccensis*. *Chem. Eur. J.* **2012**, *18*, 14342–14351. [CrossRef]
30. Li, W.-S.; Wu, J.; Li, J.; Satyanandamurty, T.; Shen, L.; Bringmann, G. Krishnadimer A, an Axially Chiral Non-biaryl Natural Product: Discovery and Biomimetic Synthesis. *Org. Lett.* **2017**, *19*, 182–185. [CrossRef]
31. Li, W.-S.; Yang, Y.; Liu, J.-J.; Shen, L.; Shi, Z.; Wu, J. Scaffold diversity-oriented synthesis of limonoid dimers: Discovery of an axially chiral agent within vivoanti-breast cancer activity. *Org. Chem. Front.* **2018**, *5*, 1079–1091. [CrossRef]
32. Zhou, Z.-F.; Liu, H.-L.; Zhang, W.; Kurtán, T.; Mándi, A.; Bényei, A.; Li, J.; Taglialatela-Scafati, O.; Guo, Y.-W. Bioactive rearranged limonoids from the Chinese mangrove *Xylocarpus granatum* Koenig. *Tetrahedron* **2014**, *70*, 6444–6449. [CrossRef]
33. Wu, Y.-B.; Wang, Y.-Z.; Ni, Z.-Y.; Qing, X.; Shi, Q.-W.; Sauriol, F.; Vavricka, C.J.; Gu, Y.-C.; Kiyota, H. Xylomexicanins I and J: Limonoids with Unusual B/C Rings from *Xylocarpus granatum*. *J. Nat. Prod.* **2017**, *80*, 2547–2550. [CrossRef]
34. Li, W.-S.; Mandi, A.; Liu, J.-J.; Shen, L.; Kurtan, T.; Wu, J. Xylomolones A-D from the Thai *Mangrove Xylocarpus moluccensis*: Assignment of Absolute Stereostructures and Unveiling a Convergent Strategy for Limonoid Biosynthesis. *J. Org. Chem.* **2019**, *84*, 2596–2606. [CrossRef] [PubMed]
35. Ponnapalli, M.G.; Ankireddy, M.; Annam, S.C.V.A.R.; Ravirala, S.; Sukki, S.; Tuniki, V.R. Unusual *ent*-isopimarane-type diterpenoids from the wood of *Excoecaria agallocha*. *Tetrahedron Lett.* **2013**, *54*, 2942–2945. [CrossRef]
36. Wang, H.; Li, M.-Y.; Katele, F.Z.; Satyanandamurty, T.; Wu, J.; Bringmann, G. Decandrinin, an unprecedented C9-spiro-fused 7,8-*seco-ent*-abietane from the Godavari mangrove *Ceriops decandra*. *Beilstein J. Org. Chem.* **2014**, *10*, 276–281. [CrossRef]
37. Chooi, Y.-H.; Tang, Y. Navigating the fungal polyketide chemical space: From genes to molecules. *J. Org. Chem.* **2012**, *77*, 9933–9953. [CrossRef] [PubMed]
38. Vederas, J.C. Explorations of fungal biosynthesis of reduced polyketides—A personal viewpoint. *Nat. Prod. Rep.* **2014**, *31*, 1253–1259. [CrossRef]
39. Hang, L.; Liu, N.; Tang, Y. Coordinated and Iterative Enzyme Catalysis in Fungal Polyketide Biosynthesis. *ACS Catal.* **2016**, *6*, 5935–5945. [CrossRef]
40. Zhang, X.; Guo, J.; Cheng, F.; Li, S. Cytochrome P450 enzymes in fungal natural product biosynthesis. *Nat. Prod. Rep.* **2021**, *38*, 1072–1099. [CrossRef]
41. Little, R.F.; Hertweck, C. Chain release mechanisms in polyketide and non-ribosomal peptide biosynthesis. *Nat. Prod. Rep.* **2022**, *39*, 163–205. [CrossRef] [PubMed]
42. Goncalves, G.A.; Spillere, A.R.; Neves, G.M.; Kagami, L.P.; Poser, G.L.; Canto, R.F.S.; Eifler-Lima, V.L. Natural and synthetic coumarins as antileishmanial agents: A review. *Eur. J. Med. Chem.* **2020**, *203*, 112514–112533. [CrossRef] [PubMed]
43. Shabir, G.; Saeed, A.; El-Seedi, H.R. Natural isocoumarins: Structural styles and biological activities, the revelations carry on. *Phytochemistry* **2021**, *181*, 112568–112590. [CrossRef]
44. Cai, R.; Wu, Y.; Chen, S.; Cui, H.; Liu, Z.; Li, C.; She, Z. Peniisocoumarins A-J: Isocoumarins from *Penicillium commune* QQF-3, an Endophytic Fungus of the Mangrove Plant *Kandelia candel*. *J. Nat. Prod.* **2018**, *81*, 1376–1383. [CrossRef]
45. Darsih, C.; Prachyawarakorn, V.; Wiyakrutta, S.; Mahidol, C.; Ruchirawat, S.; Kittakoop, P. Cytotoxic metabolites from the endophytic fungus *Penicillium chermesinum*: Discovery of a cysteine-targeted Michael acceptor as a pharmacophore for fragment-based drug discovery, bioconjugation and click reactions. *RSC Adv.* **2015**, *5*, 70595–70603. [CrossRef]
46. Huang, J.; She, J.; Yang, X.; Liu, J.; Zhou, X.; Yang, B. A New Macrodiolide and Two New Polycyclic Chromones from the Fungus *Penicillium* sp. SCSIO041218. *Molecules* **2019**, *24*, 1686–1692. [CrossRef]
47. Gao, J.-M.; Yang, S.-X.; Qin, J.-C. Azaphilones: Chemistry and biology. *Chem. Rev.* **2013**, *113*, 4755–4811. [CrossRef] [PubMed]
48. Guo, W.; Li, D.; Peng, J.; Zhu, T.; Gu, Q.; Li, D. Penicitols A-C and penixanacid A from the mangrove-derived *Penicillium chrysogenum* HDN11-24. *J. Nat. Prod.* **2015**, *78*, 306–310. [CrossRef]
49. Blanc, P.J.; Laussac, J.P.; Bars, J.L.; Bars, P.L.; Loret, M.O.; Pareilleux, A.; Prome, D.; Prome, J.C.; Santerre, A.L.; Goma, G. Characterization of monascidin A from Monascus as citrinin. *Int. J. Food Microbiol.* **1995**, *27*, 201–213. [CrossRef]
50. Ohashi, T.; Hosokawa, S. Total Syntheses of Stoloniferol B and Penicitol A, and Structural Revision of Fusaraisochromanone. *Org. Lett.* **2018**, *20*, 3021–3024. [CrossRef]
51. Wu, S.-B.; Long, C.; Kennelly, E.J. Structural diversity and bioactivities of natural benzophenones. *Nat. Prod. Rep.* **2014**, *31*, 1158–1174. [CrossRef] [PubMed]
52. Cui, H.; Liu, Y.; Li, J.; Huang, X.; Yan, T.; Cao, W.; Liu, H.; Long, Y.; She, Z. Diaporindenes A-D: Four Unusual 2,3-Dihydro-1 H-indene Analogues with Anti-inflammatory Activities from the Mangrove Endophytic Fungus *Diaporthe* sp. SYSU-HQ3. *J. Org. Chem.* **2018**, *83*, 11804–11813. [CrossRef] [PubMed]
53. Zhang, C.; Ondeyka, J.G.; Herath, K.B.; Guan, Z.; Collado, J.; Platas, G.; Pelaez, F.; Leavitt, P.S.; Gurnett, A.; Nare, B.; et al. Tenellones A and B from a *Diaporthe* sp.: Two Highly Substituted Benzophenone Inhibitors of Parasite cGMP-Dependent Protein Kinase Activity. *J. Nat. Prod.* **2005**, *68*, 611–613. [CrossRef] [PubMed]
54. Dinos, G.P. The macrolide antibiotic renaissance. *Br. J. Pharmacol.* **2017**, *174*, 2967–2983. [CrossRef]
55. Meng, L.-H.; Li, X.-M.; Lv, C.-T.; Li, C.-S.; Xu, G.-M.; Huang, C.-G.; Wang, B.-G. Sulfur-containing cytotoxic curvularin macrolides from *Penicillium sumatrense* MA-92, a fungus obtained from the rhizosphere of the mangrove *Lumnitzera racemosa*. *J. Nat. Prod.* **2013**, *76*, 2145–2149. [CrossRef]

56. Ding, L.; Maier, A.; Fiebig, H.-H.; Gorls, H.; Lin, W.-H.; Peschel, G.; Hertweck, G. Divergolides A-D from a mangrove endophyte reveal an unparalleled plasticity in ansa-macrolide biosynthesis. *Angew. Chem. Int. Ed.* **2011**, *50*, 1630–1634. [CrossRef]

57. Wiley, P.F.; Kelly, R.B.; Caron, E.L.; Wiley, V.H.; Johnson, J.H.; MacKellar, F.A.; Mizsak, S.A. Structure of Nogalamycin. *J. Am. Chem. Soc.* **1977**, *99*, 542–549. [CrossRef]

58. Pontius, A.; Krick, A.; Kehraus, S.; Brun, R.; König, G.M. Antiprotozoal Activities of Heterocyclic-Substituted Xanthones from the Marine-Derived Fungus *Chaetomium* sp. *J. Nat. Prod.* **2008**, *71*, 1579–1584. [CrossRef]

59. Xu, Z.; Baunach, M.; Ding, L.; Peng, H.; Franke, J.; Hertweck, C. Biosynthetic code for divergolide assembly in a bacterial mangrove endophyte. *ChemBioChem* **2014**, *15*, 1274–1279. [CrossRef]

60. Li, S.-R.; Zhao, G.-S.; Sun, M.-W.; He, H.-G.; Wang, H.-X.; Li, Y.-Y.; Lu, C.-H.; Shen, Y.-M. Identification and characterization of the biosynthetic gene cluster of divergolides from *Streptomyces* sp. W112. *Gene* **2014**, *544*, 93–99. [CrossRef]

61. Zhao, G.; Li, S.; Guo, Z.; Sun, M.; Lu, C. Overexpression of div8 increases the production and diversity of divergolides in *Streptomyces* sp. W112. *RSC Adv.* **2015**, *5*, 98209–98214. [CrossRef]

62. Zhao, G.; Wu, J.; Dai, W.-M. Toward a Total Synthesis of Divergolide, A.; Synthesis of the Amido Hydro-quinone Core and the C10–C15 Fragment. *Synlett* **2012**, *23*, 2845–2849. [CrossRef]

63. Rasapalli, S.; Jarugumilli, G.; Yarrapothu, G.R.; Golen, J.A.; Rheingold, A.L. Studies toward Total Synthesis of Divergolides C and D. *Org. Lett.* **2013**, *15*, 1736–1739. [CrossRef] [PubMed]

64. Nawrat, C.C.; Kitson, R.R.; Moody, C.J. Toward the total synthesis of hygrocin B and divergolide C: Construction of the naphthoquinone-azepinone core. *Org. Lett.* **2014**, *16*, 1896–1899. [CrossRef]

65. Trauner, D.; Hager, A.; Kuttruff, C.; Hager, D.; Terwilliger, D. Toward the Total Synthesis of Divergolides C and D. *Synlett* **2013**, *24*, 1915–1920. [CrossRef]

66. Rasapalli, S.; Jarugumilli, G.; Yarrapothu, G.R.; Golen, J.A.; Rheingold, A.L. Synthesis of the naphthoquinone core of divergolides (C–D) and model studies for elaboration of the ansabridge. *Tetrahedron Lett.* **2013**, *54*, 2615–2618. [CrossRef]

67. Tian, E.-L.; Gu, B.-B.; Han, Y.; Qu, X.-D.; Lin, H.-W.; Deng, Z.-X.; Hong, K. Hainanmycin A, a cyclo-heptadeca macrolide bearing a cyclopentenone moiety from the mangrove-derived *Streptomyces* sp. 219807. *Tetrahedron Lett.* **2017**, *58*, 4348–4351. [CrossRef]

68. Zhou, T.; Komaki, H.; Ichikawa, N.; Hosoyama, A.; Sato, S.; Igarashi, Y. Biosynthesis of akaeolide and lorneic acids and annotation of type I polyketide synthase gene clusters in the genome of *Streptomyces* sp. NPS554. *Mar. Drugs* **2015**, *13*, 581–596. [CrossRef]

69. Choi, B.-K.; Park, S.-Y.; Choi, D.-K.; Shin, B.; Shin, Y.-H.; Oh, D.-C.; Lee, H.-S.; Lee, H.-S.; Lee, Y.-J.; Lee, J.S.; et al. Streptoglycerides A-D with a Rare 6/5/5 Tricyclic Ring Skeleton from a Marine Actinomycete *Streptomyces* species. *Org. Lett.* **2018**, *20*, 6037–6040. [CrossRef]

70. Shin, H.J.; Heo, C.-S.; Anh, C.V.; Yoon, Y.D.; Kang, J.S. Streptoglycerides E-H, Unsaturated Polyketides from the Marine-Derived Bacterium *Streptomyces specialis* and Their Anti-Inflammatory Activity. *Mar. Drugs* **2022**, *20*, 44–55. [CrossRef]

71. Choi, B.-K.; Cho, D.-Y.; Choi, D.-K.; Shin, H.J. Miharadienes A–D with unique cyclic skeletons from a marine-derived *Streptomyces miharaensis*. *Org. Chem. Front.* **2021**, *8*, 4845–4852. [CrossRef]

72. Zhao, W.-Y.; Yi, J.; Chang, Y.-B.; Sun, C.-P.; Ma, X.-C. Recent studies on terpenoids in *Aspergillus* fungi: Chemical diversity, biosynthesis, and bioactivity. *Phytochemistry* **2022**, *193*, 113011–113035. [CrossRef]

73. Jiang, M.; Wu, Z.; Guo, H.; Liu, L.; Chen, S. A Review of Terpenes from Marine-Derived Fungi: 2015–2019. *Mar. Drugs* **2020**, *18*, 321–368. [CrossRef] [PubMed]

74. Wibowo, M.; Prachyawarakorn, V.; Aree, T.; Wiyakrutta, S.; Mahidol, C.; Ruchirawat, S.; Kittakoop, P. Tricyclic and Spirobicyclic Norsesquiterpenes from the Endophytic Fungus *Pseudolagarobasidium acaciicola*. *Eur. J. Org. Chem.* **2014**, *19*, 3976–3980. [CrossRef]

75. Wibowo, M.; Prachyawarakorn, V.; Aree, T.; Mahidol, C.; Ruchirawat, S.; Kittakoopet, P. Cytotoxic sesquiterpenes from the endophytic fungus *Pseudolagarobasidium acaciicola*. *Phytochemistry* **2016**, *122*, 126–138. [CrossRef]

76. Liu, D.-Z.; Dong, Z.-J.; Wang, F.; Liu, J.-K. Two novel norsesquiterpene peroxides from basidiomycete *Steccherinum ochraceum*. *Tetrahedron Lett.* **2010**, *51*, 3152–3153. [CrossRef]

77. Meng, L.-H.; Li, X.-M.; Liu, Y.; Wang, B.-G. Penicibilaenes A and B, sesquiterpenes with a tricyclo[6.3.1.0^{1,5}]dodecane skeleton from the marine isolate of *Penicillium bilaiae* MA-267. *Org. Lett.* **2014**, *16*, 6052–6255. [CrossRef]

78. Xue, Y.; Dong, G. Total Synthesis of Penicibilaenes via C-C Activation-Enabled Skeleton Deconstruction and Desaturation Relay-Mediated C-H Functionalization. *J. Am. Chem. Soc.* **2021**, *143*, 8272–8277. [CrossRef]

79. Matsuo, R.; Watanabe, A.; Kamo, S.; Matsuzawa, A.; Sugita, K. Total syntheses of (±)-penicibilaenes A and B *via* intramolecular aldol condensation. *Org. Chem. Front.* **2021**, *8*, 6063–6066. [CrossRef]

80. Huang, X.; Huang, H.; Li, H.; Sun, X.; Huang, H.; Lu, Y.; Lin, Y.; Long, Y.; She, Z. Asperterpenoid A, a New Sesterterpenoid as an Inhibitor of *Mycobacterium tuberculosis* Protein Tyrosine Phosphatase B from the Culture of *Aspergillus* sp. 16-5c. *Org. Lett.* **2013**, *15*, 721–723. [CrossRef]

81. Xiao, Z.; Huang, H.; Shao, C.; Xia, X.; Ma, L.; Huang, X.; Lu, Y.; Lin, Y.; Long, Y.; She, Z. Asperterpenols A and B, New Sesterterpenoids Isolated from a Mangrove Endophytic Fungus *Aspergillus* sp. 085242. *Org. Lett.* **2013**, *15*, 2522–2525. [CrossRef] [PubMed]

82. Liu, Z.; Chen, Y.; Chen, S.; Liu, Y.; Lu, Y.; Chen, D.; Lin, Y.; Huang, X.; She, Z. Aspterpenacids A and B, Two Sesterterpenoids from a Mangrove Endophytic Fungus *Aspergillus terreus* H010. *Org. Lett.* **2016**, *18*, 1406–1409. [CrossRef] [PubMed]

83. Jiang, M.; Wu, Z.; Liu, L.; Chen, S. The chemistry and biology of fungal meroterpenoids (2009–2019). *Org. Biomol. Chem.* **2021**, *19*, 1644–1704. [CrossRef]

84. Meng, L.-H.; Li, X.-M.; Li, H.-L.; Wang, B.-G. Chermebilaenes A and B, New Bioactive Meroterpenoids from Co-Cultures of Marine-Derived Isolates of *Penicillium bilaiae* MA-267 and *Penicillium chermesinum* EN-480. *Mar. Drugs* **2020**, *18*, 339–348. [CrossRef] [PubMed]

85. Li, H.-L.; Xu, R.; Li, X.-M.; Yang, S.-Q.; Meng, L.-H.; Wang, B.-G. Simpterpenoid A, a Meroterpenoid with a Highly Functionalized Cyclohexadiene Moiety Featuring *gem*-Propane-1,2-dione and Methylformate Groups, from the Mangrove-Derived *Penicillium simplicissimum* MA-332. *Org. Lett.* **2018**, *20*, 1465–1468. [CrossRef]

86. Bai, M.; Zheng, C.-J.; Huang, G.-L.; Mei, R.-Q.; Wang, B.; Luo, Y.-P.; Zheng, C.; Niu, Z.-G.; Chen, G.-Y. Bioactive Meroterpenoids and Isocoumarins from the Mangrove-Derived Fungus *Penicillium* sp. TGM112. *J. Nat. Prod.* **2019**, *82*, 1155–1164. [CrossRef] [PubMed]

87. Horikoshi, A.; Tsuchida, M.; Tsujiuchi, T.; Oyama, K.; Mitomi, M. Substance, Its Production Method, Production Strain, and Agricultural and Horticultural Insecticide Containing the Same as an Active Ingredient. JP Patent JP-2010018586-A, 10 July 2008.

88. Hemberger, Y.; Xu, J.; Wray, V.; Proksch, P.; Wu, J.; Bringmann, G. Pestalotiopens A and B: Stereochemically Challenging Flexible Sesquiterpene-Cyclopaldic Acid Hybrids from *Pestalotiopsis* sp. *Chem. Eur. J.* **2013**, *19*, 15556–15564. [CrossRef] [PubMed]

89. Che, Q.; Zhu, T.; Qi, X.; Mándi, A.; Kurtán, T.; Mo, X.; Li, J.; Gu, Q.; Li, D. Hybrid Isoprenoids from a Reeds Rhizosphere Soil Derived Actinomycete *Streptomyces* sp. CHQ-64. *Org. Lett.* **2012**, *14*, 3438–3441. [CrossRef]

90. Che, Q.; Zhu, T.; Keyzers, R.A.; Liu, X.; Li, J.; Gu, Q.; Li, D. Polycyclic hybrid isoprenoids from a reed rhizosphere soil derived *Streptomyces* sp. CHQ-64. *J. Nat. Prod.* **2013**, *76*, 759–763. [CrossRef]

91. Che, Q.; Li, J.; Li, D.; Gu, Q.; Zhu, T. Structure and absolute configuration of drimentine I, an alkaloid from *Streptomyces* sp. CHQ-64. *J. Antibiot.* **2016**, *69*, 467–469. [CrossRef] [PubMed]

92. Fan, Y.; Wang, Y.; Fu, P.; Chairoungdua, A.; Piyachaturawat, P.; Zhu, W. Secopaxilline A, an indole-diterpenoid derivative from an aciduric Penicillium species, its identification and semisynthesis. *Org. Chem. Front.* **2018**, *5*, 2835–2839. [CrossRef]

93. Byrne, K.M.; Smith, S.K.; Ondeyka, J.G. Biosynthesis of Nodulisporic Acid A: Precursor Studies. *J. Am. Chem. Soc.* **2002**, *124*, 7055–7060. [CrossRef]

94. Gao, S.-S.; Li, X.-M.; Williams, K.; Proksch, P.; Ji, N.-Y.; Wang, B.-G. Rhizovarins A-F, Indole-Diterpenes from the Mangrove-Derived Endophytic Fungus *Mucor irregularis* QEN-189. *J. Nat. Prod.* **2016**, *79*, 2066–2074. [CrossRef] [PubMed]

95. Jesus, A.D.; Gorst-Allman, C.P.; Steyn, P.S.; Heerden, F.V.; Vleggaar, R.; Wessels, P.L.; Hull, W.E. Tremorgenic Mycotoxins from *Penicillium crustosum.* Biosynthesis of Penitrem A. *J. Chem. Soc.* **1983**, 1863. [CrossRef]

96. Hu, Y.; MacMillan, J.B. Erythrazoles A-B, Cytotoxic Benzothiazoles from a Marine-Derived *Erythrobacter* sp. *Org. Lett.* **2011**, *13*, 6580–6583. [CrossRef] [PubMed]

97. Huang, R.M.; Yi, X.-X.; Zhou, Y.; Su, X.; Peng, Y.; Gao, C.-H. An update on 2,5-diketopiperazines from marine organisms. *Mar. Drugs* **2014**, *12*, 6213–6235. [CrossRef]

98. Gao, H.; Liu, W.; Zhu, T.; Mo, X.; Mándi, A.; Kurtán, T.; Li, J.; Ai, J.; Gu, Q.; Li, D. Diketopiperazine alkaloids from a mangrove rhizosphere soil derived fungus *Aspergillus effuses* H1-1. *Org. Biomol. Chem.* **2012**, *10*, 9501–9506. [CrossRef]

99. Meng, L.-H.; Wang, C.Y.; Mándi, A.; Li, X.-M.; Hu, X.-Y.; Kassack, M.U.; Kurtán, T.; Wang, B.-G. Three Diketopiperazine Alkaloids with Spirocyclic Skeletons and One Bisthiodiketopiperazine Derivative from the Mangrove-Derived Endophytic Fungus *Penicillium brocae* MA-231. *Org. Lett.* **2016**, *18*, 5304–5307. [CrossRef]

100. Niu, S.; Liu, D.; Shao, Z.; Proksch, P.; Lin, W. Eutypellazines N−S, new thiodiketopiperazines from a deep sea sediment derived fungus *Eutypella* sp. with anti-VRE activities. *Tetrahedron Lett.* **2017**, *58*, 3695–3699. [CrossRef]

101. Zhu, M.; Yang, Z.; Wang, H.; Gan, Q.; Zhang, G.; Che, Q.; Zhu, T.; Gu, Q.; Han, B.; Li, D. Penispirozines A-H, Three Classes of Dioxopiperazine Alkaloids with Spirocyclic Skeletons Isolated from the Mangrove-Derived *Penicillium janthinellum*. *J. Nat. Prod.* **2020**, *83*, 2647–2654. [CrossRef] [PubMed]

102. Cai, R.; Jiang, H.; Xiao, Z.; Cao, W.; Yan, T.; Liu, Z.; Lin, S.; Long, Y.; She, Z. (−)- and (+)-Asperginulin A, a Pair of Indole Diketopiperazine Alkaloid Dimers with a 6/5/4/5/6 Pentacyclic Skeleton from the Mangrove Endophytic Fungus *Aspergillus* sp. SK-28. *Org. Lett.* **2019**, *21*, 9633–9636. [CrossRef] [PubMed]

103. Li, F.; Sun, C.; Che, Q.; Zhu, T.; Gu, Q.; Guan, H.; Zhang, G.; Li, D. Pyrazinopyrimidine alkaloids from a mangrove-derived fungus *Aspergillus versicolor* HDN11-84. *Phytochemistry* **2021**, *188*, 112817–112823. [CrossRef]

104. Duan, Y.; Liu, Y.; Huang, T.; Zou, Y.; Huang, T.; Hu, K.; Deng, Z.; Lin, S. Divergent biosynthesis of indole alkaloids FR900452 and spiro-maremycins. *Org. Biomol. Chem.* **2018**, *16*, 5446–5451. [CrossRef]

105. Luo, X.; Chen, C.; Tao, H.; Lin, X.; Yang, B.; Zhou, X.; Liu, Y. Structurally diverse diketopiperazine alkaloids from the marine-derived fungus *Aspergillus versicolor* SCSIO 41016. *Org. Chem. Front.* **2019**, *6*, 736–740. [CrossRef]

106. Huang, S.; Chen, H.; Li, W.; Zhu, X.; Ding, W.; Li, C. Bioactive Chaetoglobosins from the Mangrove Endophytic Fungus *Penicillium chrysogenum*. *Mar. Drugs* **2016**, *14*, 172–183. [CrossRef] [PubMed]

107. Zhu, X.; Zhou, D.; Liang, F.; Wu, Z.; She, Z.; Li, C. Penochalasin K, a new unusual chaetoglobosin from the mangrove endophytic fungus *Penicillium chrysogenum* V11 and its effective semi-synthesis. *Fitoterapia* **2017**, *123*, 23–28. [CrossRef]

108. Yang, B.; Dong, J.; Lin, X.; Zhou, X.; Zhang, Y.; Liu, Y. New prenylated indole alkaloids from fungus *Penicillium* sp. derived of mangrove soil sample. *Tetrahedron* **2014**, *70*, 3859–3863. [CrossRef]

109. Cui, H.; Lin, Y.; Luo, M.; Lu, Y.; Huang, X.; She, Z. Diaporisoindoles A-C: Three Isoprenylisoindole Alkaloid Derivatives from the Mangrove Endophytic Fungus *Diaporthe* sp. SYSU-HQ3. *Org. Lett.* **2017**, *19*, 5621–5624. [CrossRef]

110. Yu, G.; Zhou, G.; Zhu, M.; Wang, W.; Zhu, T.; Gu, Q.; Li, D. Neosartoryadins A and B, Fumiquinazoline Alkaloids from a Mangrove-Derived Fungus *Neosartorya udagawae* HDN13-313. *Org. Lett.* **2016**, *18*, 244–247. [CrossRef]

111. Fu, P.; Yang, C.; Wang, Y.; Liu, P.; Ma, Y.; Xu, L.; Su, M.; Hong, K.; Zhu, W. Streptocarbazoles A and B, Two Novel Indolocarbazoles from the Marine-Derived Actinomycete Strain *Streptomyces* sp. FMA. *Org. Lett.* **2012**, *14*, 2422–2425. [CrossRef] [PubMed]

112. Li, T.; Du, Y.; Cui, Q.; Zhang, J.; Zhu, W.; Hong, K.; Li, W. Cloning, characterization and heterologous expression of the indolocarbazole biosynthetic gene cluster from marine-derived *Streptomyces sanyensis* FMA. *Mar. Drugs* **2013**, *11*, 466–488. [CrossRef] [PubMed]

113. Li, K.; Liang, Z.; Chen, W.; Luo, X.; Fang, W.; Liao, S.; Lin, X.; Yang, B.; Wang, J.; Tang, L.; et al. Iakyricidins A-D, antiproliferative piericidin analogs bearing carbonyl group or cyclic skeleton from *Streptomyces iakyrus* SCSIO NS104. *J. Org. Chem.* **2019**, *84*, 12626–12631. [CrossRef] [PubMed]

114. Zhu, M.; Zhang, X.; Feng, H.; Che, Q.; Zhu, T.; Gu, Q.; Li, D. Campyridones A–D, pyridone alkaloids from a mangrove endophytic fungus *Campylocarpon* sp. HDN13-307. *Tetrahedron* **2016**, *72*, 5679–5683. [CrossRef]

115. Zhou, Z.-F.; Kurtán, T.; Yang, X.-H.; Mándi, A.; Geng, M.-Y.; Ye, B.-P.; Taglialatela-Scafati, O.; Guo, Y.-W. Penibruguieramine A, a novel pyrrolizidine alkaloid from the endophytic fungus *Penicillium* sp. GD6 associated with Chinese mangrove *Bruguiera gymnorrhiza*. *Org. Lett.* **2014**, *16*, 1390–1393. [CrossRef]

116. Chen, S.; He, L.; Chen, D.; Cai, R.; Long, Y.; Lu, Y.; She, Z. Talaramide A, an Unusual Alkaloid from the Mangrove Endophytic Fungus *Talaromyces* sp. (HZ-YX1) as Inhibitor of Mycobacterial PknG. *New J. Chem.* **2017**, 4273–4277. [CrossRef]

117. Gressler, M.; Zaehle, C.; Scherlach, K.; Hertweck, C.; Brock, M. Multifactorial induction of an orphan PKS-NRPS gene cluster in *Aspergillus terreus*. *Chem. Biol.* **2011**, *18*, 198–209. [CrossRef]

Review

Antimicrobial Secondary Metabolites from the Mangrove Plants of Asia and the Pacific

Mazdida Sulaiman [1], Veeranoot Nissapatorn [2], Mohammed Rahmatullah [3], Alok K. Paul [4], Mogana Rajagopal [5], Nor Azizun Rusdi [6], Jaya Seelan Sathya Seelan [6], Monica Suleiman [6], Zainul Amiruddin Zakaria [7] and Christophe Wiart [6,*

[1] Department of Chemistry, Faculty of Science, University of Malaya, Kuala Lumpur 50603, Malaysia
[2] School of Allied Health Sciences and World Union for Herbal Drug Discovery (WUHeDD), Walailak University, Nakhon Si Thammarat 80160, Thailand
[3] Department of Biotechnology & Genetic Engineering, University of Development Alternative, Dhaka 1207, Bangladesh
[4] School of Pharmacy and Pharmacology, University of Tasmania, Hobart, TAS 7001, Australia
[5] Faculty of Pharmaceutical Sciences, UCSI University, Kuala Lumpur 56000, Malaysia
[6] Institute for Tropical Biology & Conservation, University Malaysia Sabah, Kota Kinabalu 88400, Malaysia
[7] Department of Biomedical Sciences, Faculty of Medicine and Health Sciences, University Malaysia Sabah, Kota Kinabalu 88400, Malaysia
* Correspondence: christophewiart@ums.edu.my

Abstract: Microbes such as the White Spot Syndrome Virus account for severe losses in the shrimp farming industry globally. This review examines the literature on the mangrove plants of Asia and the Pacific with antibacterial, antifungal, or antiviral activities. All of the available data published on this subject were collected from Google Scholar, PubMed, Science Direct, Web of Science, ChemSpider, PubChem, and a library search from 1968 to 2022. Out of about 286 plant species, 119 exhibited antimicrobial effects, and a total of 114 antimicrobial natural products have been identified including 12 with MIC values below 1 µg/mL. Most of these plants are medicinal. The mangrove plants of Asia and the Pacific yield secondary metabolites with the potential to mitigate infectious diseases in shrimp aquaculture.

Keywords: mangrove plants; shrimp farming; natural products; antibacterial; antifungal; antiviral; Asia; Pacific

1. Introduction

The global shrimp and prawn aquaculture industry is regularly threatened by outbreaks of microbial infections [1] that require antibiotics, antifungals, and antiviral agents participating in the selection of multidrug-resistant strains of microbes, pausing the grim scenario of the emergence of a "superbug" that could wipe out the global supply of penaeids [2]. In this context, there is an urgent necessity to search for antimicrobial agents with original chemical frameworks, and such molecules could come from the flora of Asia and the Pacific, which is the oldest, largest, and richest on Earth, especially seashores, tidal rivers, and mangrove plants.

Mangroves are ecosystems of the tropical and subtropical seashores, estuaries, and tidal rivers characterized by a halophytic flora of mainly trees and shrubs divided into true mangrove or mangrove-associated species. True mangrove species are restricted to mangroves whereas mangrove-associated species are found along the seashores, and even inland. There are estimates of about 54 true mangrove plant species and 60 mangrove-associated species globally, which are home to shrimps, prawns, crabs, and fish [3]. Most mangrove species grow in Asia and the Pacific [4]. Examples of true mangrove plant species are *Excoecaria agallocha* L. (land zone), *Bruguiera gymnorhiza* (L.) Savigny, *Rhizophora stylosa* Griff. (intermediate zone), *Avicennia alba* Bl., and *Aegiceras corniculatum* (L.) Blanco

(fringing zone) [5]. Even though most of the global fish catches are directly or indirectly dependent on mangroves, these are on their way to extinction due to logging, agriculture, aquaculture, and urbanization, with an estimate of about 2–8% loss of surface per year [6]. Shrimps, prawns, and fish farming are the greatest threat to mangroves with, for example, approximately half of the 279,000 ha of mangroves in the Philippines lost from 1951 to 1988 [7]. Another aggravating factor is global warming, and consequently, a rise in sea levels that interfere with the growth of true mangrove plants.

Most plants in mangroves are Angiosperms organized phylogenetically into 11 major taxa or clades organized in three groups: (i) Basal Angiosperms: Protomagnoliids, Magnoliids, Monocots, Eudicots; (ii) Core Angiosperms: Core Eudicots, Rosids, Fabids, Malvids; and (iii) Upper Angiosperms: Asterids, Lamiids, and Campanulids. Within each clade, plants yield specific secondary metabolites to control and even communicate with phytopathogenic bacteria and fungi. Plants are challenged by phytopathogenic bacteria, fungi, and viruses and produce a vast array of antimicrobial secondary metabolites [8]. These antimicrobial principles fall into two main categories: phytoanticipins and phytoalexins. Phytoanticipins are antimicrobials present in plant tissues before pathogen challenges or inactive immediate precursors of phytoalexins [8].

Phytoanticipins and phytoalexins are mainly either phenolics, terpenes, or alkaloids with various levels of solubility in water and are extractable with water, polar organic (methanol, ethanol), mid-polar solvents (chloroform, dichloromethane, ethyl acetate), and non-polar solvents (hexane, petroleum ether) [9]. The measurement of the antibacterial and antifungal strength of extracts and secondary metabolites *in vitro* is quantitatively based on the minimum inhibiting concentration (MIC) and several thresholds of activity have been proposed [10]. Qualitatively, antibacterial and antifungal strength are appreciated by halos developed around a paper disc or an agar well expressed in the inhibition zone diameter (IZD) [10].

Colette et al. (2022) noted that the presence of *Atriplex jubata* S. Moore evoked some levels of remediation in the shrimp farms of New Caledonia [11] and this review aims to attempt to answer the following points: What is the current knowledge on the distribution of antibacterial, antifungal, and antiviral principles from the mangrove plants of Asia and the Pacific? What are the strongest antimicrobial principles isolated thus far from these plants? What is the spectrum of activity of the antimicrobial principles? What are the medicinal values of these plants? What is the potential usefulness of these plants as remediation of shrimp farming? We hypothesize that a shrimp or prawn farming system preserving healthy mangroves could be a mean to solve the increasing problem of infection.

2. Distribution of Antibacterial, Antifungal, and Antiviral Principles Various Mangrove Plants

The enumeration of mangrove and mangrove-associated plants is provided in Table S1, and the chemical structures of the antimicrobial secondary metabolites identified from these plants is given Figure S1.

2.1. Subclass Lycopodidae

The only lycopod associated with mangroves is *Lycopodium carinatum* Desv. ex Poir., for which no antimicrobial activities have been recorded thus far.

2.2. Subclass Polypodiidae

Aqueous and polar organic extracts of ferns of the mangrove are moderately broad-*spectrum* antibacterial and antifungal (Table 1). Data on the antiviral properties of ferns are lacking. The methanol extract of *Stenochlaena palustris* (Burm. f.) Bedd. (25 μL/6 mm disc of a 100 mg/mL solution) evoked halos against *Staphylococcus aureus*, *Bacillus subtilis*, *Escherichia coli*, *Klebsiella pneumoniae*, *Salmonella typhi*, *Penicillium chrysogenum*, *Aspergillus niger*, and *Saccharomyces cerevisae* [12]. From the leaves of this fern was identified the flavonol glycoside stenopalustroside A (**1**), which strongly repressed the *Staphylococcus epidermidis* [13].

Antimicrobials in this subclass are mainly phenolics. Other ferns with broad-spectrum antibacterial and antifungal properties are *Nephrolepis biserrate* (Sw.) Schott, *Drynaria quercifolia* (L.) J. Sm., *Drymoglossum piloselloides* (L.) Presl., *Pyrrosia piloselloides* (L.) Farw., *Microsorum punctatum* (L.) Copel. [14–16], *Phymatosorus scolopendria* (Burm. f.) Pic. Serm. [17], *Platycerium coronarium* (O.F. Müll.) Desv. [18], and the true mangrove fern *Acrostichum aureum* L. [19–21]. Of note, the ethyl acetate extract of roots of *Acrostichum speciosum* L., which is a true mangrove fern, was bactericidal for *E. coli* with the MIC/MBC of 40/40 µg/mL [21].

Table 1. Ferns and cycads from the mangroves, tidal rivers, and the seashores of Asia and the Pacific with antibacterial and/or antifungal activity.

FAMILY Genus, Species	Extract		Secondary Metabolite Identified
	Antibacterial	Antifungal	
SUBCLASS POLYPODIIDAE			
BLECHNACEAE *Stenochlaena palustris* (Burm. f.) Bedd.	+	+	*Antibacterial:* Stenopalustroside A (1), *S. epidermidis* (MIC = 2 µg/mL) [13].
NEPHROLEPIDACEAE *Nephrolepis biserrata* (Sw.) Schott	+	+	
POLYPODIACEAE *Drynaria quercifolia* (L.) J. Sm.	+	+	
Drymoglossum piloselloides (L.) Presl.	+	+	
Microsorum punctatum (L.) Copel.	+	+	
Platycerium coronarium (O.F. Müll.) Desv.	+		
Pyrrosia piloselloides (L.) M.G. Price)	+	+	
PTERIDACEAE *Acrostichum aureum* L.	+	+	
Acrostichum speciosum Willd.	+		
SUBCLASS CYCADIIDAE			
CYCADACEAE *Cycas rumphii* Miq.	+		

Bold: true mangrove plants [3]. +: Activity of extract(s) reported in the literature.

2.3. Subclass Cycadaceae

The ethyl acetate extract of *Cycas rumphii* Miq. developed halos against *Staphylococcus albus* whereas the methanol extract (20 mg/mL solution per disc) hampered the growth of *S. aureus* and *E. coli* [22]. Later, the methanol extract of leaves (paper disc impregnated with 20 mg/mL solution) repressed *S. aureus* (ATCC 25953) [22]. Note that the Cycadaceae have not been much studied for their antimicrobial effects (Table 1) [23].

2.4. Subclass Magnoliidae

Mangrove plants in this subclass produce most of, and a broad spectrum of antimicrobial secondary metabolites.

2.4.1. Clade Protomagnoliids

Plants in the clade are not found in mangroves.

2.4.2. Clade Magnoliids

Plants in this clade are not common in mangroves and principally yield antimicrobial isoquinoline alkaloids and lignans (Table S2). In the Lauraceae, the filamentous climber *Cassytha filiformis L. yields* the aporphine dicentrine (**2**), which inhibits the growth

of *Cladosporium clodosporioides* (Table S2) [24]. *Hernandia nymphaeifolia* (C. presl.) Kubitzki (Hernandiaceae) produces the dibenzyl butyrolactone lignan deoxypodophyllotoxin (**3**), which is strongly active against HSV (Table S2) [25]. In the family Annonaceae, the hexane extract of stem bark of *Annona glabra* L. exhibited antibacterial and antifungal properties on account of kaurane diterpenes (Table S2) [26].

2.4.3. Clade Monocots

Plants in this clade are mainly mangrove-associated with organic extracts being moderately broad-spectrum antibacterial and antifungal and producing mainly antimicrobial phenolics (Table 2). For instance, the ethanol extract of rhizomes of *Lasia spinosa* (L.) Thwaites developed halos with *S. aureus*, *S. epidermidis*, *S. pyogenes*, *S. dysenteriae*, *E. coli*, *V. cholerae*, *E. aerogenes*, *P. aeruginosa*, *C. albicans*, *A. niger*, and *S. cerevisae* (500 µg/disc) [27,28]. Other instances are *Phoenix paludosa* Roxb. [29,30], *Saribus rotundifolius* (Lam.) Bl. [31], *Cyperus scariosus* R. Br. [32], *Eleocharis dulcis* (Burm. f.) Trin. ex Hensch. [33,34], *Pandanus tectorius* Parkinson [35], the true mangrove *Nypa fruticans* Wurm. [35], *Areca catechu* L. [31], *Phragmites vallatoria* Veldkamp [36], *Ruppia maritima* L. [37], and *Flagellaria indica* L. [38]. The ethanol extract of *Flagellaria indica* L. at the concentration of 12.5 µg/mL repressed DV by 45.5% [39,40]. In the family Orchidaceae, an aqueous extract of *Aerides odoratum* Reinw. ex Bl. repressed the *E. coli* [41] and the chloroform extract of pseudobulbs of *Cymbidium finlaysonianum* Wall. ex Lindl. moderately retrained *T. Mentagrophytes* (MIC: 250 µg/mL) [42]. From this orchid, the phytoalexin stilbene batatasin III (**4**) was active against Gram-positive bacteria [43] as well as phytopathogenic filamentous fungi [44]. Gigantol (**5**) and batatasin III exhibited meek activity with HSV-1 and -2 [45]. The phenanthrene moscatin (**6**) from *Dendrobium moschatum* (Buch. -Ham.) Sw. is a moderate antibacterial [46]. Other examples of antibacterial and antifungal phenolics from the Monocots are meridinol (**7**) [47], tricin (**8**) [48,49], and naringenin (**9**) [50,51] (Table 2).

2.4.4. Clade Core Eudicots

Plants in this clade are not found in mangroves.

2.4.5. Clade Core Eudicots

Plants in this clade are not found in mangroves.

2.4.6. Clade Rosids

The ethanol extract of the leaves of *Cayratia trifolia* (L.) Domin (*Vitaceae)* inhibited the growth of *S. aureus* [52]. This climber produces antibacterial and antifungal as well as antivirals as in ε-viniferin (**12**) piceid (**13**), and resveratrol (**14**) (Table S2), [53–59].

2.4.7. Clade Fabids

Fabids principally yield antimicrobial phenolics (Table S2).

Order Malpighiales: Organic polar, mid-polar, and non-polar extracts of *Calophyllum inophyllum* L. (Clusiaceae) are broadly antimicrobial [60–62]. Of note, the methanol extract of latex very strongly hindered *S. aureus* with an IC$_{50}$ of 1.1 µg/mL and *Trichophyton rubrum* with an IC$_{50}$ of 3.3 µg/mL [63]. The hexane extract of seeds strongly restrained HIV-1 at the concentration of 10 µg/mL [64]. Inophyllum B (**15**), inophyllum B acetate (**16**), and inophyllum P (**17**) from the leaves blocked HIV reverse transcriptase respectively, while inophyllum B (**15**) and P (**17**) inhibited HIV with IC$_{50}$ values of 1.4 and 1.6 µM, respectively (Table S2) [61].

In the Euphorbiaceae, extracts of leaves of *Excoecaria agallocha* L. moderately repressed a broad array of bacteria and yeasts [64–67]. The ethanol extract of leaves inhibited the replication of the ECMV (EC$_{50}$:16.7 µg/mL), HIV (EC$_{50}$: 7.3 µg/mL), NDV, and SFV [68]. This vesicant tree yields 12-deoxyphorbol 13-(3*E*,5*E*-decadienoate) (**18**) with very strong antiretroviral effects (Table S2) [69]. *Suregada glomerulata* (Bl.) Baill. yields the alkaloid

5β-carboxymethyl-3α-hydroxy-2β-hydroxymethyl-1- methylpyrrolidine (**19**), which curbed HIV-1 replication (Table S2) [70].

Table 2. Monocots from the mangroves, tidal rivers, and the seashores of the Asia and the Pacific with antibacterial, antifungal, and/or antiviral activity.

FAMILY Genus, Species (Synonym)	Extracts			Antimicrobial Principle(s)
	Antibacterial	**Antifungal**	**Antiviral**	
ARACEAE *Lasia spinosa* (L.) Thwaites	+	+		*Antibacterial:* Meridinol (7) (100 µg/disc) [47]. *Antifungal:* Meridinol (7) (100 µg/disc) [47].
ARECACEAE *Phoenix paludosa* Roxb.	+	+		*Antibacterial:*3′-Acetoxy-6,7-dimetoxy-4′ (2″,3″,4″,6″- tetraacetylglucopyranosyl)flavone (10), *P. aeruginosa, E. coli, S flexneri*, MIC= 8, 4, and 8 µg/mL, respectively [47]. Tricin (8), *P. aeruginosa, E. coli, S. flexneri*, MIC = 4, 2, and 2 µg/mL, respectively [47]. Cinnamic acid (11), *P. aeruginosa, E. coli, S. flexneri*, MIC = 64, 16, and 16µg/mL, respectively [47]. *Antifungal:* 3′-Acetoxy-6,7-dimetoxy-4′ (2″,3″,4″,6″- tetraacetylglucopyranosyl)flavone (10): *C. neoformans, C. albicans, C. parapsilosis*, MIC: of 16, 8, and 8 µg/mL, respectively [47]. Tricin (8), *C. neoformans, C. albicans, C. parapsilosis*, MIC = 8, 4, and 4 µg/mL, respectively [47]. Cinnamic acid (11), *C. neoformans, C. albicans, C. parapsilosis*, MIC = 64, 32, and 32 µg/mL, respectively [47].
Saribus rotundifolius (Lam.) Bl.	+	+		
CYPERACEAE *Cyperus scariosus* R. Br.		+		
Eleocharis dulcis (Burm. f.) Trin. ex Hensch	+			
Rhynchospora corymbosa (L.) Britton				
FLAGELLARIACEAE *Flagellaria indica* L.	+	+		*Antiviral:* Tricin (8), IVA, IC$_{50}$ = 4.6 µM, HIV-1, IC$_{50}$ = 14.4 µg/mL [49].
ORCHIDACEAE *Aerides odoratum* Reinw. ex Bl.	+			
Cymbidium finlaysonianum Wall. ex Lindl.		+		*Antibacterial:* Batatasin III (4), *S. aureus, B. subtilis*, MRSA, MIC = 250, 500, and 500 µg/mL, respectively [43]. *Antifungal:* Batatasin III (4), *A. brassicicola, P. parasitica, C. capsici, B. oryzae, D.medusaea, C. paradoxa moreau, E.turcicum, P. theae, A. citri* [44]. *Antiviral:* Batatasin III (4), HSV-1, HSV-2, IC$_{50}$ = 341.5 and 384.2 µM, respectively [45]. Gigantol (5), HSV-1 and HSV-2, IC$_{50}$ = 304.1 and 319.3 µM, respectively [45].
Dendrobium moschatum (Buch. -Ham.) Sw.				*Antibacterial:* Moscatin (6), *V. parahemolyticus, S. gallinarum, S. aureus, S. agalactiae, E. faecalis, B. subtilis, R. anatipestifer*, MIC = 96, 72, 72, 48, 96, 72, and 72 µg/mL, respectively [46].
PANDANACEAE *Nypa fruticans* Wurmb.	+			*Antiviral:* Naringenin (9), SARS-CoV, 65.2 µM [51]; YFV, EC$_{50}$: 0.001 M; ZKV [50]
Pandanus tectorius Parkinson				
POACEAE *Phragmites vallatoria* Veldkamp	+	+		
RUPPIACEAE *Ruppia maritima* L.	+			

+: Activity of extract(s) reported in the literature.

Plants in the Rhizophoraceae are tanniferous and have antibacterial activities as in *Bruguiera cylindrica* (L.) Bl. [71], *Bruguiera gymnorhiza* (L.) Savigny [72], *Bruguiera sexangula* (Lour.) Poir., *Ceriops decandra* Griff.) Ding Hou [28,63], *Ceriops tagal* (Perr.) C.B. Rob. [71], *Kandelia candel* (L.) Druce [73,74], *Rhizophora apiculata* Bl. [75], and *Rhizophora stylosa*

Griff. [71,76]. The hydrolysable tannin fraction of the bark of the latter weakly inhibited the growth of *A. calcoaceticus*, *B. licheniformis*, *P. mirabilis*, and *S. saprophyticus* [77]. Other antibacterials in this family are 2,6-dimethoxy-*p*-benzoquinone (**20**) as well as gallic acid (**21**) [78,79] (Table S2), [78–93].

16-Hydroxypimar-8(14)-en-15-one (**22**) from the roots of *Ceriops tagal* (Perr.) C.B. Rob. Moderately restrained a broad-spectrum of bacteria (Table S2) [80]. Diterpenes are often liposoluble, explaining perhaps the suppression of a broad-spectrum of bacteria and fungi including *B. pumilus* with a MIC value of 15.6 µg/mL by the benzene extract of the wood of *C. decandra* [94]. The presence of tannins and phenolics most probably account for the antiviral effects observed in *B. cylindrica*, *Rhizophora mucronata* Lam., *R. apiculata*, *B. gymnorhiza* [72], *C. decandra* [68]. Other examples of water soluble antibacterials are the cyclohexylideneacetonitrile derivatives from *B. gymnorhiza*, which strongly repressed HBV [69].

Order Fabales: Aqueous, polar and mid-polar extracts of Fabaceae are moderately broad-spectrum antibacterial and antifungal, as observed with *Caesalpinia bonduc* (L.) Roxb [95] (Table S2) [96]. The methanol extract of the seed coat of this climber strongly restrained *P. aeruginosa*, *S. aureus*, and *B. cereus* (MIC: 22 µg/mL) [97]. *This extract given to Wistar rats* subcutaneously at a dose of 25 mg/kg body weight once a day for 10 days evoked a reduction in lung abscesses induced by *P. aeruginosa* [97]. The active principle here are diterpenes including bondenolide (**23**) [96] and neocaesalpin P (**24**) [98].Other examples of Fabaceae yielding antibacterial or antifungal organic polar or mid-polar extracts are- *Canavalia maritima* Thouars [99], the true mangrove tree *Cynometra iripa* Kostel. [100], *Cynometra* ramiflora Miq. [101], *Derris scandens* (Aubl.) Pittier [17], *Derris trifoliata* Lour. [102], *Inocarpus fagifer* (Parkinson) Fosb. [17], *Sindora siamensis* Teysm. ex Miq. [103], *Pongamia pinnata* (L.) Pierre [104], and *Cathormion umbellatum* (Vahl) Kosterm. [105]. *Plants in this family yield antibacterial and/or antifungal* isoflavonoids such as lupalbigenin (**25**) and derrisisoflavone A (**26**) from *Derris scandens* (Aubl.) Pittier [106–109] (Table S2) [107,109,110]. Other examples are santal (**27**), scandenin A (**28**) dalpanitin (**29**), vicenin 3 (**30**), derrisisoflavone C (**31**), and 5,7,4′-trihydroxy-6,8-diprenylisoflavone (**32**) [107]. Organic and aqueous extracts in this family are often antiviral, as in *D. scandens* with HSV-1 (IC$_{50}$: 60 µg/mL) PV and MV as well as *Cynometra ramiflora* Miq. with DV-2 [111], and *Derris trifoliata* Lour. with HIV [112,113]. As for antiviral principles, isoflavone deguelin (**33**) was active against HCMV [113,114] whereas rotenone (**34**) restrained HSV-1 and -2. *D. trifoliata* yields the strong antibacterial and anticandidal lupinifolin (**35**) (Table S2) [115–117].

Order Fagales: Organic polar and mid-polar extract of fruits and leaves of the tanniferous *Casuarina equisetifolia* L. (Casuarinaceae) are broadly antibacterial and antifungal [118–120].

Order Rosales: In the Moraceae, the methanol extract of the bark of *Ficus microcarpa* L.f. (40 µL of a 10 mg/mL solution on 6 mm disc) developed halos with *B. brevis*, *B. cereus*, *B. subtilis*, *E. coli*, and *A. polymorph* [121]. From this tree, the flavanols (+) (2*R*,3*S*) afzelechin (**36**) and (-)(2*R*,3*R*) epiafzelechin (**37**) weakly repressed HSV-1 (Table S2) [122].

2.4.8. Clade Malvids

Antimicrobials in this vast Clade are diverse (Table S2).

Order Myrtales: Polar and mid-polar organic extracts of *Combretum quadrangulare* Kurz (Combretaceae) [123] and *Terminalia catappa* L. (Combretaceae) are antibacterial and anticandidal [124,125] probably due to ellagitannins such as corilagin (**38**) [81,126] (Table S2) [127,128] and other phenolics. Phenolic fraction from the fruits of *T. catappa* strongly repressed *S. aureus*, *B. subtilis*, *E. faecalis*, and *L. monocytogenes* with the MIC values of 15.6, 15.6, 7.8, and 15.6 µg/mL, respectively [129]. Other antimicrobials in this family are triterpenes, probably explaining the strong activity of the hexane extract of *Lumnitzera racemosa* Willd. with *B. cereus* and *E. coli* [21]. The ethanol extract of barks of this shrub repressed NVD, VV, EMCV, and SFV [130]. Aqueous extracts from Combretaceae plants are often antiviral, as in the pericarps of *T. catappa* with HSV-2 [131] or *C. quadrangulare* blocking HIV integrase with the IC$_{50}$ of 2.9 µg/mL [132].

The methanol extract of the true mangrove shrub *Pemphis acidula* J.R. & G. Forst (Lythraceae) hindered a broad-spectrum of bacteria [133,134]. Essential oils of *Melaleuca cajuputi* Roxb. and *Melaleuca quinquenervia* (Cav.) S.T. Blake (*Myrtaceae*) are strongly and broadly antibacterial and antifungal [135–138]. The essential oil of *M. quinquenervia* repressed *Phytophthora cactorum* [139] and was strongly fungicidal for filamentous fungi [140].

In the family Sonneratiaceae, polar and mid-polar organic and aqueous extracts of the true mangrove trees *Sonneratia apetala* Buch-Ham., *Sonneratia griffithii* Kurtz., and *Sonneratia ovata* Back. are bacterial and antifungal [21,141–145]. *S. griffithii* yields strongly antibacterial lupane triterpenes such as 3β-hydroxy-lup-9(11),12-diene, 28-oic acid (**39**), lupeol (**40**), and lupan-3β-ol (**41**) (Table S2) [146]. Antiviral triterpenes are present in Sonneratiaceae plants [147].

Order Brassicales: Polar organic extracts of *Azima sarmentosa* (Bl.) B. & H and *Azima tetracantha* Lam. (Salvadoraceae) inhibited the growth of bacteria and fungi [148,149].

Order Malvales: In the family Malvaceae, organic polar extracts of *Hibiscus tiliaceus* L. and *Thespesia populnea* (L.) Soland. ex Correa restrained a broad array of bacteria [150,151]. *T. populnea* yields the cadalane sesquiterpenes populene C (**42**) and D (**43**), mansonone D (**44**) and E (**45**), 7-hydroxycadalene (**46**), gossypol (**47**), and (+) 6,6′-methoxygossypol (**48**) with strong activity toward Gram-positive bacteria (Table S2) [152]. The ethanol extract of flowers of *T. populnea* strongly hindered VSV, CV B4, and RSV (EC$_{50}$: 20 μg/mL) [153] whereas the methanol extract of *Malachra capitata (L.) L.* was active against the FMDV [154]. The petroleum ether extract of the leaves of *Kleinhovia hospita* L. strongly retrained *E. coli* and *A. jejunii* with the MIC values of 35.7 and 38 μg/mL, respectively [155,156], while the ethanol extract of the bark yielded a MIC value of 4 μg/mL with *S. aureus* [17]. From this plant, the steroids (9*R*,10*R*, 23*R*)-21,23:23,27-diepoxycycloarta-1,24-diene-3,27-dione (**49**) and (9*R*,10*R*,21*S*,23*R*)-21/23,23/27-diepoxy-21-methoxycycloartan-1,24-diene-3,27-dione (**50**) are strongly active (Table S2) [156].

Sterculiaceae plants are often antimicrobial as in the dichloromethane extract *Heritiera littoralis* Aiton with *M. madagascariense* and *M. indicus* [157,158]. From this tree, the flavonol glycoside afzelin (**51**) is strongly antibacterial and antiviral (Table S2) [55,159–163].

Other antimicrobial principles in this true mangrove tree are taraxerol (**52**), friedelin (**53**), and astilbin (**54**) [164]. The ethanol extract of the bark of *Heritiera fomes* Buch. Ham. developed halos with *S. epidermidis*, *S. pyogenes*, *E. coli*, *E. aerogenes*, *Pseudomonas sp*. [28], and *K. rhizophilia* [164].

Order Sapindales: Organic polar extracts of the true mangrove trees *Aglaia cucullata* Pellegr., *Xylocarpus granatum* J. Koenig, and *Xylocarpus moluccensis* (Lam.) M. Roem (Meliaceae) displayed antibacterial properties [28,165,166] (Table S2) [144–146,148]. Phytoalexins in this family are limonoids such as in the antiretroviral sundarbanxylogranin B (**55**) from the seeds of *X. granatum* [167] or thaixylomolin I (**56**) and K (**57**) isolated from the seeds of *X. moluccensis* [168]. Another example is krishnolide A (**58**) [169]. From the latter, moluccensin I from the fruits moderately inhibited the growth of *S. hominis* and *E. faecalis* [170]. The limonoid catabolite dihydrofuranone 3-(1-hydroxyethyl)-2,2-dimethyl-4-butyrolactone (**59**) from the leaves of *X. granatum* is a strong repressor of the phytopathogenic fungi *Blumeria graminis* [171].

In the Rutaceae, essential oils of *Acronychia pedunculata* (L.) Miq. and *Limnocitrus littoralis* (Miq.) Swingle are antibacterial and antifungal [172–174]. The ethanol extract of the former was active toward *C. albicans*, *A. niger*, and *C. neoformans* [175]. The acridone pharmacophore [176] intercalates into microbial DNA [177] and represses WSSV [178]. *A. pedunculata* yields very strong antistaphylococcal acridone alkaloids [179] as well as the prenylated acetophloroglucinol acrovestone (**60**) [177] (Table S2) [180].

Antimicrobials in the family Sapindaceae are mainly triterpene saponins and triterpenes the later soluble lipid. The petroleum ether of *Allophylus cobbe* (L.) Raeusch strongly inhibited the growth of *Shigella sonnei, Salmonella paratyphi*, and *C. neoformans* with the MIC values of 31.2 μg/mL [178–181]. The methanol extract of the leaves of *Harpullia arborea* (Blanco) Radlk repressed a broad-spectrum of bacteria and fungi [182] whereas the ethanol

extract of leaves was active against HCV [183] on probable account of simple phenolic glycosides [184].

The methanol extract of leaves of *Quassia indica* (Gaertn.) Nooteboom (Simaroubaceae) developed halos with *E. coli*, *S. aureus*, *A. Niger*, and *C. albicans* [185].

Order Santalales: Plants in the Loranthaceae generate antimicrobial phenolics such as the flavonol glycoside quercitrin isolated from the leaves of *Dendrophthoe pentandra* (L.) Miq. (100 μg/mL/6 mm disc) [186]. These are soluble in methanol explaining the antibacterial properties of *Macrosolen cochinchinensis* (Lour.) Tiegh [187] or *Viscum orientale* Willd. [188]. The organic polar extracts of *Olax scandens* Roxb. and *Ximenia americana* L. (Olacaceae) are antibacterial and antifungal [189–191]. Phytoalexins here are often polyacetylene fatty acids extractable with non-polar solvent from which the halos developed against *B. subtilis*, *Enterococcus faecalis*, *P. aeruginosa*, and *K. pneumoniae* with the hexane extract of the leaves of *Olax scandens* Roxb. [192]. The methanol extract of the stembark of *X. americana* strongly inhibited the replication of HIV [193].

Order Caryophyllales: In the order Caryophyllales, a fatty acid fraction of *Sesuvium portulacastrum* (L.) L. (Aizoaceae) as well as the essential oil moderately hindered a broad-spectrum of bacteria and fungi [194,195]. The ethanol extract of leaves was active against HBV [130]. The polar organic extract of *Salicornia brachiata* Miq. and *Suaeda maritima* (L.) Dumort. (Chenopodiaceae) displayed broad-spectrum antibacterial, antifungal, and antiviral properties [196,197]. The fatty acid fraction of the aerial parts of *S. brachiata* Miq. moderately restrained *B. subtilis S. aureus* and methicillin-resistant *S. aureus* [198]. The ethanol extract of the leaves of *S. maritima* was active against the EMCV [130]. The organic polar extract of the true mangrove tree *Aegialitis rotundifolia* Roxb. and *Limonium tetragonium* Bullock (Plumbaginaceae) are antibacterial and antifungal [199,200]. The methanol extract of the roots of *L. tetragonium* Bullock blocked HIV-1 reverse transcriptase [201].

2.4.9. Clade Asterids

Plants in this clade yield antimicrobial triterpenes (Table S2).

In the order Ericales, the ethanol extract of the bark of the true mangrove tree *Diospyros littorea* (R. Br.) Kosterm. (Ebenaceae) developed halos with *Streptococcus* sp., *S. aureus*, *Aeromonas hydrophila*, and *Vibrio parahaemolyticus* [62].

Antimicrobial principles in the Lecythidaceae are mainly triterpene saponins that are soluble in polar organic and aqueous extracts, explaining why plants in the genus *Barringtonia* J.R. Forst. & G. Forst. are antibacterial and antifungal. The methanol extract of leaves of *Barringtonia acutangula* (L.) Gaertn. hindered *C. albicans* and *Candida tropicalis* with the MIC values of 31.2 and 62.5 μg/mL, respectively [202,203]. Other examples include the methanol extract of *Barringtonia asiatica* (L.) Kurz [204] or *Barringtonia racemosa* (L.) Spreng [205,206]. Other antimicrobial principles are oleanane triterpenes such as germanicol caffeoyl ester (**61**), camelliagenone (**62**), and germanicol (**63**) in *B. asiatica* (Table S2) [207] or lupeol (**40**) (Table S2) [208]. These are mainly lipophilic, where activities in non-polar extracts as exemplified with the petroleum ether extract of the stem bark of *B. asiatica* that strongly restrained *B. subtilis* with the MIC value of 25 μg/mL, respectively [209]. Other lipophilic to mid-polar principles in *B. racemosa* are neo-clerodane diterpenes such as nasimalun A (**64**) [204,208,210]. The aqueous extract suppressed HSV-1 (IC$_{50}$: 23 μg/mL) [211].

The ethanol extract of the bark (500 μg/disc) of the true mangrove tree *Aegiceras corniculatum* (L.) Blanco (Aegicerataceae) developed a halo with a broad spectrum of bacteria [28], while the hexane extract of leaves inhibited the growth of *Mycobacterium tuberculosis* (H$_{37}$R$_v$) with the MIC value of 50 μg/mL [212]. The oleanane triterpene acornine 2 (**65**) isolated from the bark hindered yeasts and filamentous fungi (Table S2) [212]. The ethanol extract of fruits inhibited NDV and SFV [130].

2.4.10. Clade Lamiids

The Lamiids produce various types of antimicrobials (Table S2).

Order Boraginales: The *Cordia dichotoma* G. Forst. (Boraginaceae) methanol extract restrained *S. pyogenes*, *S. aureus*, *E. coli*, *P. aeruginosa*, *A. niger*, and *C. albicans* [213]. *Merrilliodendron megacarpum* Sleumer (Icacinaceae) yields the strongly antifungal pyranoindolizinoquinoline alkaloid camptothecin (**66**) which also restrains a broad spectrum of virus in vitro (Table S2) [214–219].

Order Gentianales: Plants in the genus *Cerbera* L. (Apocynaceae) are antimicrobial. The ethanol extract of *Cerbera manghas* L. very strongly restrained *E. coli* and *P. aeruginosa* (MIC: 4 μg/mL) [17] and VSV (IC$_{50}$: 0.01 μg/mL) [220]. The methanol extract of seeds of *Cerbera odollam* Gaertn. developed halos with a broad-spectrum of bacteria [221] and the ethanol extract of fruits suppressed *Aspergillus flavus*, *Fusarium oxysporum*, and *Penicillium citrum* [222]. Note that Apocynaceous indole alkaloids are often antistaphylococcal [223]. The ethanol extract of the leaves (500 μg/well) of *Hoya parasitica* (Roxb.) Wall. ex Wight (Asclepiadaceae) inhibited the growth of *S. aureus*, *Proteus sp.*, *E. coli*, and *S. sonnei*, and *Shigella dysenteriae* with the IZD of 23, 19, 10, 8, and 20 mm, respectively [224].

In the Rubiaceae, the organic polar and mid-polar extracts of *Guettarda speciosa* L., *Hydnophytum formicarum* Jack, *Morinda citrifolia* L., and *Myrmecodia tuberosa* Jack, and *Guettarda speciosa* L. are antibacterial and antifungal [82,225–228] (Table S2) [81,162,229–231]. Plants in this family yield antimicrobial water soluble iridoid glycosides such as in loganic acid (**67**) from *G. speciosa,* which strongly repressed HCV [228], and asperuloside (**68**) from *M. citrifolia* (Table S2) [77,91,93,220,232–234]. Other antimicrobial principles are caffeic acid derivatives including the antiviral 4,5-di-*O*-caffeoylquinic acid (**69**) [229,235] as well as 5,4′-dihydroxy-6,7,8,-trimethoxyflavone (**70**) in *Gardenia lucida Roxb*. [91,234,236], antimycobacterial monoterpene indole alkaloids [230], the chalcone butein (**71**) from *H. formicarum* [22] (Table S2) [88,237], and the anthraquinones damnacanthal (**72**) and 1,3-dihydroxy-5-methoxy-2,6-bismethoxymethyl-9,10-anthraquinone [233] (Table S2) [81,229,230,232]. (*E*)-phytol (**73**) is strongly antimycobacterial [232]. The ethanol extract of *M. citrifolia* is weakly active with the FMDV [238] and the methanol extract of *Psychotria serpens* L. with HSV [155]. The essential oil of the latter is strongly bactericidal with *S. aureus* (MIC/MBC: 39/39 μg/mL) [239].

Order Lamiales: In the family Acanthaceae, the chloroform extract of the leaves of *Acanthus ebracteatus* Vahl inhibited the growth of *B. cereus*, *S. aureus*, *P. aeruginosa*, and *Proteus vulgaris*, *C. albicans*, *Aspergillus fumigatus*, and *A. niger* [240]. This true mangrove herb yields the antibacterial 3,5-dimethoxy-4-hydroxy methyl benzoic acid (**74**), (Z)-4-coumaric acid 4-*O*-β-D-glucopyranoside (**75**), and 6-hydroxy-benzoxazolinone (**76**) (Table S2) [241]. The alcohol extract given to ducklings orally at a dose of 2 g/kg/day for 14 days evoked a decrease in serum hepatitis B surface antigen, AST, ALT, and improved the hepatic cytoarchitecture [242]. The ethanol extract of roots inhibited the replication of the NDV, Vaccinia virus, ECMV, and SFV [130].

Avicennia species (Avicenniaceae) are true mangrove trees yielding broad-spectrum antibacterials [243–245] such as the diterpenes excoecarin A (**77**), *ent*-16-hydrozy-3-oxo-13-*epi*-manoyl-oxide (**78**), *ent*-15-hydroxy-labda-8(17), 13*E*-dien-3-one (**79**), which repressed *Rhizopus orizae* and *A. niger* and rhizophorin B with *B. subtilis* (Table S2) [246]. The ethanol extract of *Avicennia alba* L. and *Avicennia officinalis* L. restrained ECMV [130].

Dolichandrone spathacea (Burm. f.) Bedd. (Bignoniaceae) is a true mangrove tree yielding the hydroxycinnamic acid glycoside derivatives decaffeoyl acteoside (**80**) and verbascoside (**81**) active against *E. faecalis* (ATCC 1034) and *S. sonnei* (Table S2) [247]. Verbascoside (**81**) very strongly hindered RSV (Table S2) [248].

An extract of the stems and leaves of *Myoporum bontioides* (Siebold & Zucc.) A. Gray (Myoporaceae) moderately inhibited the growth of *F. oxysporum*, *Pestalotia mangiferae*, *Thielaviopsis paradoxa*, *Colletotrichum musae*, *Alternaria alternata*, *Mycosphaerella sentina*, and *Sphaceloma fawcettii* [249]. From this plant, the sesquiterpenes myoporumine A (**82**) and B (**83**), (-)-epingaione (**84**), and (–)-dehydroepingaione (**85**) strongly repressed MRSA (Table S2) [250]. (-)-Epingaione is a strong inhibitor of filamentous fungi [249]. Other antifungal principles in this plant are homomonoterpenes (Table S2) [251]

In the Verbenaceae, *Premna odorata* Blanco produces the strong antimycobacterial long chain alkane 1-heneicosyl formate (**86**) (Table S2) [252]. *Essential oil of plants in this family like in the Lamiaceae are often antifungal* [253]. *The methanol extract (200 μg/disc) developed halos with A. niger and Penicillium cyclopium* [254,255].

Order Solanales: The ethanol extract of the flowers of *Ipomoea pes-caprae* (L.) R. Br. (Convolvulaceae) inhibited the growth of *S. aureus*, *B. subtilis*, *Streptococcus mutans*, *P. vulgaris*, *K. pneumoniae*, *E. coli*, *A. flavus*, *A. niger*, and *Penicillium* sp [256]. The methanol extract of the leaves of *Solanum viride* R. Br. (Solanaceae) was weakly active against *S. aureus* and *C. albicans* [257].

2.4.11. Clade Campanulids

The ethanol extract of the roots of *Pluchea indica* (L.) Less. (Asteraceae) repressed *E. coli*, *B. cereus*, *Pseudomonas fluorescens*, *S. aureus*, and *S. typhimurium* [258]. The aqueous extract of leaves inhibited HIV-1 [259]. The aqueous extract of berries of *Scaevola taccada* (Gaertn.) Roxb. (Goodeniaceae) restrained HIV-1 [259]. The methanol extract of leaves (500 μg/well) evoked halos with *V. cholerae*, *K. pneumoniae*, *S. typhi*, *S. sonnei*, *F. oxysporum*, *Fusarium solani*, *Rhizoctonia solani*, and *Odium monilioides* [260]. This coastal shrub yields the strong antifungal furanocoumarin scataccanol (**87**) as well as 4-formylsyringol (**88**) (Table S2) [261].

3. Antimicrobial Extracts and Compounds from Mangrove and Mangrove-Associated Plants with the Potential to Be Used for Shrimp Farming

According to Kuete (2010), crude extracts with MIC values less than 100 μg/mL are antimicrobial [10]. Here, we define a very strongly active extract with a MIC value below 10 μg/mL. An isolated compound is defined as very strongly active for a MIC value below or equal to 1 μg/mL (as well as less than 1 μg/thin layer chromatography), strongly antibacterial (or antifungal) for a MIC value above 1 μg/mL and equal to or below 50 μg/mL, moderately antibacterial (or antifungal) for a MIC from 50 and below 100 μg/mL, weakly antibacterial (or antifungal) for a MIC from 100 and below 500 μg/mL, very weakly antibacterial (or antifungal) for a MIC ranging from 500 to below 2500 μg/mL, and inactive for a MIC value above 2500 μg/mL.

For antiviral principles, we suggest that a compound with an IC_{50} value below or equal to 1 μg/mL is very strongly active, for an IC_{50} value above 1 and equal to or below 20 μg/mL strongly antiviral, for an IC_{50} above 20 and below or equal to 100 μg/mL moderately antiviral, for an IC_{50} above 100 and below or equal to 500 μg/mL weakly antiviral, for an IC_{50} ranging from above 500 to below or equal to 2500 μg/mL very weakly antiviral, and inactive with an IC_{50} value above 2500 μg/mL.

Using these criteria, the strongest antimicrobial extracts from mangrove and mangrove-associated plants that could be of value for shrimp farming are from *C. inophyllum* (*S. aureus*, *T. rubrum*) [63], *T. catappa* (*E. faecalis*) [129]., *C. manghas* (*E. coli*, *P. aeruginosa*, VSV) [17,220], and *C. odollam* (HSV) [223].

The strongest antimicrobial principles identified from the mangrove and mangrove-associated plants that could be of value for shrimp farming are as follows (Figure 1):

(i) Antibacterial: Lupinifolin (**35**) (Gram-positive and Gram-negative) [116]; 7-hydroxycadalene (**46**) [152].

(ii) Antifungal: Lupinifolin (**35**) (Yeasts) [116].

(iii) Antiviral: Naringenin (**9**) [50], verbascoside (**81**) [248], inophyllum B (**15**) [61], 12-deoxyphorbol 13-(3*E*,5*E*-decadienoate) (**18**) [69], 5*β*-carboxymethyl-3*α*-hydroxy-2*β*-hydroxymethyl-1- methylpyrrolidine (**19**) [70], deguelin *(***33***)* [117], deoxypodophyllotoxin (**3**) [25,116] (9*R*,10*R*, 23*R*)-21,23:23,27-diepoxycycloarta-1,24-diene-3,27-dione (**49**) [156], gallic acid (**21**) [83], and 4,5-di-*O*-caffeoylquinic acid (**69**).

(iv) We note that most of these principles are hydrophilic or amphiphilic (Figure 1).
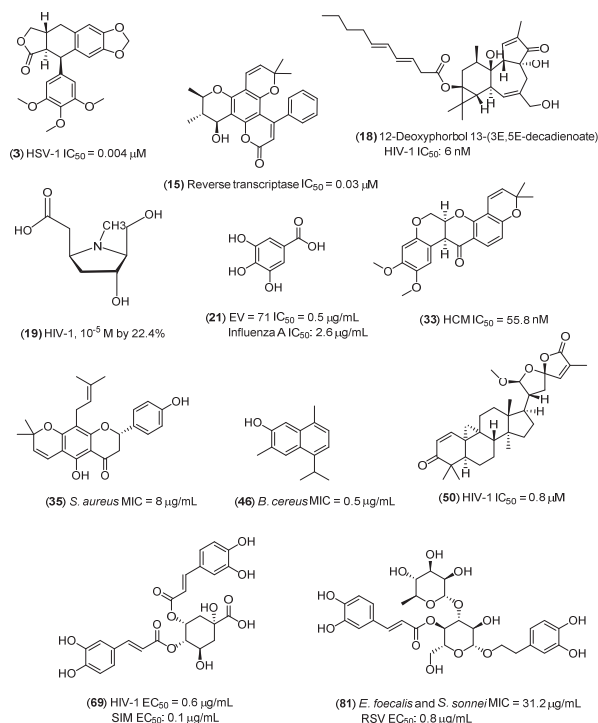
Figure 1. Natural products from mangrove plants with very strong antimicrobial activities.

4. Spectrum of Activity of Antimicrobial Extracts and Principles from Mangrove and Mangrove-Associated Plants

The following observations can be made:

(i)   No reports on the only lycopod associated with mangrove are available.

(ii)   Of the 26 ferns, nine had antibacterial effects and six are antifungal, and no antiviral activities were reported. The only antimicrobial principle from ferns thus far is the strong antibacterial (Gram-positive) stenopalustroside A [13] (Table 1).

(iii) The cycad associated with mangroves has antibacterial effects.

(iv)   No reports on the only pine tree associated with mangrove are available.

(v)   Of the 51 monocots, 11 displayed antimicrobial effects, of which eight had antibacterial activity, six with antiviral activity, and none reported with antiviral properties. Active principles isolated were phenolics such as the flavanol naringenin (**9**) in the Pandanaceae, antibacterial, antifungal, and antiviral orchidaceous phenanthrenes as well as the flavones and antifungal hydroxycinnamic acid of Poaceae (Table 2)

(vi)   Of the 207 dicots, 92 had antimicrobial effects including 78 antibacterial, 39 antifungal, and 25 antiviral effects. A total of about 80 antimicrobial principles were isolated (Table S2).

(vii) Aqueous and organic polar extracts of plants from the mangrove presented activity against Gram-positive and Gram-negative bacteria, filamentous fungi and yeasts, enveloped and non-enveloped viruses, DNA, and RNA viruses (Table S2).

(viii) The extract of *P. pinnata* [262] and gallic acid (**21**) abounds notably in the true mangrove trees *Rhizophora apiculata* Bl. and *Aegiceras corniculatum* (L.) Blanco is a protected shrimp against WSSV [84] as well as an aqueous extract of the true mangrove tree *C. tagal* (Perr.) C.B. Rob. [263]

5. Medicinal Use of Mangrove and Mangrove-Associated Plants

One could suggest the use of medicinal plants as a more sustainable alternative to chemotherapy in paenid aquaculture. Therefore, the possible beneficial effect of mangrove and mangrove-associated plants for the sanitation of shrimp farms is reinforced by the observation that 85 plants were used for the treatment of infectious diseases including mainly diarrhea, dysentery, and wounds [264–294] (Table S1). The pharmacological effect of these plants involves active principles that are potentially able to act on paenids, which could be examined further.

6. Mangrove and Mangrove-Associate Plants as Remediation of Shrimp Farming?

Shrimp and prawn farms are regularly affected by (+)-RNA viruses such as the Taura syndrome virus, Yellow head virus, and Gill-associated virus as well as DNA viruses (WSSV, Monodon Baculovirus) and Gram-negative bacteria such as *Hepatobacterium penaei* and *Vibrio* spp. [295]. Synthetic drugs are being used in an attempt to evade economic losses but threaten the environment and contribute to the selection of multidrug-resistant pathogenic microorganisms. Being able to produce antimicrobial principles (some of them water soluble like ellagic acid), mangrove and mangrove-associated plants could be used as a source of natural agents and/or afford ecological systems to combat the infections with shrimps and prawns. Polar organic and aqueous extracts of most mangrove and mangrove-associated plants exhibit broad-spectrum antibacterial, antifungal, or antiviral properties in vitro, suggesting that antimicrobial secondary metabolites from plants and plant litter in the sea and brackish waters could afford some control against the overgrowth of pathogenic microbes. Of note, *P. pinnata* ethanol extract of leaves given to Penaeus monodon as part of feed at the dose of 300 μg/g of body weight/day evoked some levels of protection against WSSV [262]. Gallic acid (**21**), which abounds notably in the true mangrove trees *R. apiculata* and *A. corniculatum* is strongly antiviral and protected shrimps against WSSV [84]. Gallic acid (**21**) may, at least in part, account for the fact the aqueous extract of the true mangrove tree *C. tagal* given at the dose of 10% of the body weight, twice a day, protected shrimps against WSSV [263]. Furthermore, gallic acid (**21**) decreases microbial proliferation in mangrove soil [296] as well as the growth of microalgae [297], which contribute to a decreased production in shrimp aquaculture [298], at least in part, to the alteration in the shrimp's immune system [299]. The control of pathogenic bacteria may have some beneficial effects for the symbiotic bacteria of shrimp against pathogenic microorganisms [300]. Furthermore, phenolic acids from mangrove and mangrove-associated plants could, by chelation, protect shrimps against toxic metals including cadmium [301,302]. Therefore, it is possible to extend the protective effect of mangrove and mangrove-associated plants to fisheries and crab farming, the latter being affected by *Vibrio* species [165]. Another interesting feature of mangrove plants is that they are a host for microorganisms for Actinomyces producing antibacterial principles [303].

7. Conclusions

Plants from the Mangroves of Asia and the Pacific produce a vast array of antimicrobial secondary metabolites that could be further examined for their possible development into medications to control microbial outbreaks in aquaculture. In parallel, growing plant mangroves in aquacultures and promoting mangrove-associated aquaculture could be beneficial. The rise in the global population and the imperative to supply shrimps, prawns, crabs, and fish globally requires the preservation of mangroves.

References

1. Lightner, D.V.; Redman, R.M.; Pantoja, C.R.; Tang, K.F.J.; Noble, B.L.; Schofield, P.; Mohney, L.L.; Nunan, L.M.; Navarro, S.A. Historic emergence, impact and current status of shrimp pathogens in the Americas. *J. Invertebr. Pathol.* **2012**, *110*, 174–183. [CrossRef]
2. Thornber, K.; Verner-Jeffreys, D.; Hinchliffe, S.; Rahman, M.M.; Bass, D.; Tyler, C.R. Evaluating antimicrobial resistance in the global shrimp industry. *Rev. Aquacult.* **2020**, *12*, 966–986. [CrossRef]
3. Giesen, W.; Wulffraat, S.; Zieren, M.; Scholten, L. *Mangrove Guidebook for Southeast Asia*; FAO: Bangkok, Thailand; Wetlands International: Wageningen, The Netherlands, 2007.
4. Ricklefs, R.E.; Latham, R.E. Global patterns of diversity in mangrove floras. In *Species Diversity in Ecological Communities: Historical and Geographical Perspectives*; University of Chicago Press: Chicago, IL, USA, 1993; pp. 215–229.
5. Stewart, M.; Fairfull, S. Mangroves. In *Industries*; NDOP, Ed.; NSW Government: Parramatta, Sydney, 2008.
6. Polidoro, B.A.; Carpenter, K.E.; Collins, L.; Duke, N.C.; Ellison, A.M.; Ellison, J.C.; Farnsworth, E.J.; Fernando, E.S.; Kathiresan, K.; Koedam, N.E.; et al. The loss of species: Mangrove extinction risk and geographic areas of global concern. *PLoS ONE* **2010**, *5*, e10095. [CrossRef] [PubMed]
7. Rafael, A.; Calumpong, H.P. Fungal infections of mangroves in natural forests and reforestation sites from Philippines. *Aquacul Aquar. Conserv. Legisl.* **2019**, *12*, 2062–2074.
8. Tiku, A.R. Antimicrobial compounds (phytoanticipins and phytoalexins) and their role in plant defense. In *Co-Evolution of Secondary Metabolites*; Springer: Cham, Switzerland, 2020.
9. Wang, Z.; Li, S.; Ge, S.; Lin, S. Review of distribution, extraction methods, and health benefits of bound phenolics in food plants. *J. Agric. Food Chem.* **2020**, *68*, 3330–3343. [CrossRef] [PubMed]
10. Kuete, V. Potential of Cameroonian plants and derived products against microbial infections: A review. *Planta Med.* **2010**, *76*, 1479–1491. [CrossRef] [PubMed]
11. Colette, M.; Guentas, L.; Gunkel-Grillon, P.; Callac, N.; Della Patrona, L. Is halophyte species growing in the vicinity of the shrimp ponds a promising agri-aquaculture system for shrimp ponds remediation in New Caledonia? *Marine Pollution Bull.* **2022**, *177*, 13563. [CrossRef]
12. Zuraini, Z.; Sasidharan, S.; Kaur, S.R.; Nithiyayini, M. Antimicrobial and antifungal activities of local edible fern *Stenochlaena palustris* (Burm. F.) Bedd. *Pharmacol.Online* **2010**, *1*, 233–237.
13. Liu, H.; Orjala, J.; Sticher, O.; Rali, T. Acylated flavonol glycosides from leaves of *Stenochlaena palustris*. *J. Nat. Prod.* **1999**, *62*, 70–75. [CrossRef] [PubMed]
14. Padhy, R.; Dash, S.K. Antibacterial evaluation of methanolic Rhizome extract from an in vivo and in vitro grown Pteridophyte, *Drynaria quercifolia* (Linn.) J. Smith. *Asian J. Pharm. Clin. Res.* **2015**, *8*, 130–138.
15. Amoroso, V.B.; Antesa, D.A.; Buenavista, D.P.; Coritico, F.P. Antimicrobial, antipyretic, and anti-inflammatory activities of selected Philippine medicinal pteridophytes. *Asian J. Biodivers.* **2014**, *5*, 1. [CrossRef]
16. Somchit, M.N.; Hassan, H.; Zuraini, A.; Chong, L.C.; Mohamed, Z.; Zakaria, Z.A. In vitro anti-fungal and anti-bacterial activity of *Drymoglossum piloselloides* L. Presl. against several fungi responsible for athletes foot and common pathogenic bacteria. *Afr. J. Microbiol. Res.* **2011**, *5*, 3537–3541.
17. Frankova, A.; Vistejnova, L.; Merinas-Amo, T.; Leheckova, Z.; Doskocil, I.; Soon, J.W.; Kudera, T.; Laupua, F.; Alonso-Moraga, A.; Kokoska, L. In vitro antibacterial activity of extracts from Samoan medicinal plants and their effect on proliferation and migration of human fibroblasts. *J. Ethnopharmacol.* **2021**, *264*, 113220. [CrossRef]
18. Desnilasari, D.; Iwansyah, A.C.; Fauziah, R. From local wisdom: Preliminary antibacterial activity of "Tanduk rusa" Fern (*Platycerium coronarium*). In Proceedings of the 1st International Conference on Appropriate Technology Development 2015, Bandung, Indonesia, 5–7 October 2015.

19. Thomas, T. In vitro evaluation of antibacterial activity of *Acrostichum aureum* Linn. *Ind. J. Nat. Prod.* **2012**, *3*, 135–138.
20. Shamsuddin, A.A.; Najiah, M.; Suvik, A.; Azariyah, M.N.; Kamaruzzaman, B.Y.; Effendy, A.W.; John, B.A. Antibacterial properties of selected mangrove plants against Vibrio species and its cytotoxicity against *Artemia salina*. *World Appl. Sci. J.* **2013**, *25*, 333–340.
21. Saad, S.; Taher, M.; Susanti, D.; Qaralleh, H.; Awang, A.F.I.B. In vitro antimicrobial activity of mangrove plant *Sonneratia alba*. *Asian Pacific J. Trop. Biomed.* **2012**, *2*, 427–429. [CrossRef]
22. Khan, A.V.; Ahmed, Q.U.; Khan, A.A.; Shukla, I. Antibacterial activity of *Cycas rumphii* Miq. leaves extracts against some tropical human pathogenic bacteria. *Res. J. Microbiol.* **2011**, *6*, 761. [CrossRef]
23. Amin, E. Phytochemical content and biological activity of the genus Cycas, Family Cycadaceae: A review. *Pharm. Sci. Asia* **2021**, *4*, 300–319.
24. Puvanendran, S.; Wickramasinghe, A.; Karunaratne, D.N.; Carr, G.; Wijesundara, D.S.A.; Andersen, R.; Karunaratne, V. Antioxidant constituents from *Xylopia championii*. *Pharm. Biol.* **2008**, *46*, 352–355. [CrossRef]
25. Sudo, K.; Konno, K.; Shigeta, S.; Yokota, T. Inhibitory effects of podophyllotoxin derivatives on herpes simplex virus replication. *Antiv. Chem. Chemothery* **1998**, *9*, 263–267. [CrossRef]
26. Padmaja, V.; Thankamany, V.; Hara, N.; Fujimoto, Y.; Hisham, A. Biological activities of *Annona glabra*. *J. Ethnopharmacol.* **1995**, *48*, 21–24. [CrossRef]
27. Uddin, S.J.; Rouf, R.; Shilpi, J.A.; Alamgir, M.; Nahar, L.; Sarker, S.D. Screening of some Bangladeshi medicinal plants for in vitro antibacterial activity. *Orient. Pharm. Exp. Med.* **2008**, *8*, 316–321. [CrossRef]
28. Goshwami, D.; Rahman, M.M.; Muhit, M.A.; Islam, M.S.; Anasri, M. Antioxidant property, cytotoxicity and antimicrobial activity of *Lasia spinosa* leaves. *Nepal J. Sci. Technol.* **2012**, *13*, 215–218. [CrossRef]
29. Mondal, B.; Hore, M.; Baishakhi, F.S.; Ramproshad, S.; Sadhu, S.K. Study of antioxidant, antidiabetic and antibacterial activities of mangrove plant *Phoenix paludosa*. *Asian J. Med. Health Res.* **2018**, *3*, 12.
30. Paul, S.R.; Sayeed, M.; Hakim, M. Antibacterial and cytotoxic activity of the bark of *Phoenix paludosa* in different solvents. *Jordan J. Biol. Sci.* **2017**, *10*, 213–217.
31. Essien, E.E.; Antia, B.S.; Etuk, E.I. Phytoconstituents, antioxidant and antimicrobial activities of *Livistona chinensis* (Jacquin), *Saribus rotundifolius* (Lam.) Blume and *Areca catechu* Linnaeus Nuts. *Pharm. Biosci. J.* **2017**, *10*, 59–67. [CrossRef]
32. Khan, W.U.; Khan, R.A.; Ahmed, M.; Khan, L.U.; Khan, M.W. Pharmacological evaluation of methanolic extract of *Cyperus scariosus*. *Bangladesh J. Pharmacol.* **2016**, *11*, 353–358. [CrossRef]
33. Zhan, G.; Pan, L.Q.; Mao, S.B.; Zhang, W.; Wei, Y.Y.; Tu, K. Study on antibacterial properties and major bioactive constituents of Chinese water chestnut (*Eleocharis dulcis*) peels extracts/fractions. *Eur. Food Res. Technol.* **2014**, *238*, 789–796. [CrossRef]
34. Ramadhani, D.A.; Novita, H.; Rajamuddin, M.A.L.; Elya, B. Chemical compounds screening of leaves extract from *Eleocharis dulcis* (Burm. f.) trin. ex hensch and in vitro antibacterial pathogenic test for fish. *AACL Bioflux.* **2020**, *13*, 2770–2778.
35. Ebana, R.U.B.; Etok, C.A.; Edet, U.O. Phytochemical screening and antimicrobial activity of *Nypa fruticans* harvested from Oporo River in the Niger Delta Region of Nigeria. *Int. J. Innov. Appl. Stud.* **2015**, *10*, 1120.
36. Joshi, B.; Panda, S.K.; Jouneghani, R.S.; Liu, M.; Parajuli, N.; Leyssen, P.; Neyts, J.; Luyten, W. Antibacterial, antifungal, antiviral, and anthelmintic activities of medicinal plants of Nepal selected based on ethnobotanical evidence. *Evidence-Based Compl. Alt. Med.* **2020**, *2020*, 1–13. [CrossRef] [PubMed]
37. Bushmann, P.J.; Ailstock, M.S. Antibacterial compounds in estuarine submersed aquatic plants. *J. Exp. Marine Biol. Ecol.* **2006**, *331*, 41–50. [CrossRef]
38. Nugraha, A.S.; Permatasari, A.E.N.; Kadarwenny, C.P.; Pratoko, D.K.; Triatmoko, B.; Rosyidi, V.A.; Norcahyanti, I.; Dewi, I.P.; Dianasari, D.; Sary, I.P.; et al. Phytochemical screening and the antimicrobial and antioxidant activities of medicinal plants of Meru Betiri National park–Indonesia. *J. Herbs Spices Med. Plants* **2020**, *26*, 303–314. [CrossRef]
39. Klawikkan, N.; Nukoolkarn, V.; Jirakanjanakit, N.; Yoksan, S.; Wiwat, C. Effect of Thai medicinal plant extracts against Dengue virus in vitro. *Mahidol Univ. J. Pharm. Sci.* **2011**, *38*, 13–18.
40. Kaushik, S.; Kaushik, S.; Sharma, V.; Yadav, J. Antiviral and therapeutic uses of medicinal plants and their derivatives against Dengue viruses. *Pharm. Rev.* **2018**, *12*, 13–18.
41. Paul, P.; Chowdhury, A.; Nath, D.; Bhattacharjee, M.K. Antimicrobial efficacy of orchid extracts as potential inhibitors of antibiotic resistant strains of *E. coli*. *Asian J. Pharm. Clin. Res.* **2013**, *6*, 108–111.
42. Juneja, R.K.; Sharma, S.C.; Tandon, J.S. Two substituted bibenzyls and a dihydrophenanthrene from *Cymbidium aloifolium*. *Phytochemistry* **1987**, *26*, 1123–1125. [CrossRef]
43. Jiang, S.; Wang, M.; Jiang, L.; Xie, Q.; Yuan, H.; Yang, Y.; Zafar, S.; Liu, Y.; Jian, Y.; Li, B.; et al. The medicinal uses of the genus *Bletilla* in traditional Chinese medicine: A phytochemical and pharmacological review. *J. Ethnopharmacol.* **2021**, *280*, 114263. [CrossRef]
44. Zhou, X.M.; Zheng, C.J.; Gan, L.S.; Chen, G.Y.; Zhang, X.P.; Song, X.P.; Li, G.N.; Sun, C.G. Bioactive phenanthrene and bibenzyl derivatives from the stems of *Dendrobium nobile*. *J. Nat. Prod.* **2016**, *79*, 1791–1797. [CrossRef]
45. Sukphan, P.; Sritularak, B.; Mekboonsonglarp, W.; Lipipun, V.; Likhitwitayawuid, K. Chemical constituents of *Dendrobium venustum* and their antimalarial and anti-herpetic properties. *Nat. Prod. Commun.* **2014**, *9*, 1934578X1400900625. [CrossRef]
46. Ren, J.; Qian, X.P.; Guo, Y.G.; Li, T.; Yan, S.K.; Jin, H.Z.; Zhang, W.D. Two new phenanthrene glycosides from *Liparis regnieri* Finet and their antibacterial activities. *Phytochem. Lett.* **2016**, *18*, 64–67. [CrossRef]

47. Hasan, C.M.; Alam, F.; Haque, M.; Sohrab, M.H.; Monsur, M.A.; Ahmed, N. Antimicrobial and cytotoxic activity from *Lasia spinosa* and isolated lignan. *Lat. Am. J. Pharm.* **2011**, *30*, 550–553.
48. Pagning, A.L.N.; Lateef, M.; Tapondjou, L.A.; Kuiate, J.R.; Ngnokam, D.; Ali, M.S. New triterpene and new flavone glucoside from *Rhynchospora corymbosa* (Cyperaceae) with their antimicrobial, tyrosinase and butyrylcholinesterase inhibitory activities. *Phytochem. Lett.* **2016**, *2016*, 121–128. [CrossRef]
49. Yazawa, K.; Kurokawa, M.; Obuchi, M.; Li, Y.; Yamada, R.; Sadanari, H.; Matsubara, K.; Watanabe, K.; Koketsu, M.; Tuchida, Y.; et al. Anti-influenza virus activity of tricin, 4′, 5, 7-trihydroxy-3′, 5′-dimethoxyflavone. *Antiv. Chem. Chemother.* **2011**, *22*, 1–11. [CrossRef]
50. Castrillo, M.; Córdova, T.; Cabrera, G.; Rodríguez-Ortega, M. Effect of naringenin, hesperetin and their glycosides forms on the replication of the 17D strain of yellow fever virus. *Av. Biomed.* **2015**, *4*, 69–78.
51. Clementi, N.; Scagnolari, C.; D'Amore, A.; Palombi, F.; Criscuolo, E.; Frasca, F.; Pierangeli, A.; Mancini, N.; Antonelli, G.; Clementi, M.; et al. Naringenin is a powerful inhibitor of SARS-CoV-2 infection in vitro. *Pharmacol. Res.* **2021**, *163*, 105255. [CrossRef]
52. Sari, R.S.E.; Soegianto, L.; Liliek, S. Uji aktivitas antimikroba ekstrak etanol daun *Cayratia trifolia* terhadap *S. aureus* dan *Candida albicans*. *J. Farm. Sains Dan Terap.* **2018**, *5*, 23–29.
53. Nguyen, T.N.A.; Dao, T.T.; Tung, B.T.; Choi, H.; Kim, E.; Park, J.; Lim, S.I.; Oh, W.K. Influenza A (H1N1) neuraminidase inhibitors from *Vitis amurensis*. *Food Chem.* **2011**, *124*, 437–443. [CrossRef]
54. Lee, S.; Mailar, K.; Kim, M.I.; Park, M.; Kim, J.; Min, D.H.; Heo, T.H.; Bae, S.K.; Choi, W.; Lee, C. Plant-derived purification, chemical synthesis, and in vitro/in vivo evaluation of a resveratrol dimer, viniferin, as an HCV replication inhibitor. *Viruses* **2019**, *11*, 890. [CrossRef]
55. Aguilar-Guadarrama, B.; Navarro, V.; Leon-Rivera, I.; Rios, M.Y. Active compounds against tinea pedis dermatophytes from *Ageratina pichinchensis* var. bustamenta. *Nat. Prod. Res.* **2009**, *23*, 1559–1565. [CrossRef]
56. Sahidin, I.; Wahyuni, W.; Malaka, M.H.; Imran, I. Antibacterial and cytotoxic potencies of stilbene oligomers from stem barks of baoti (*Dryobalanops lanceolata*) growing in Kendari, Indonesia. *Asian J. Pharm. Clin. Res.* **2017**, *10*, 139–143.
57. Basri, D.F.; Xian, L.W.; Abdul Shukor, N.I.; Latip, J. Bacteriostatic antimicrobial combination: Antagonistic interaction between epsilon-viniferin and vancomycin against methicillin-resistant *Staphylococcus aureus*. *BioMed Res. Int.* **2014**, *2014*, 461756. [CrossRef] [PubMed]
58. Yim, N.; Trung, T.N.; Kim, J.P.; Lee, S.; Na, M.; Jung, H.; Kim, H.S.; Kim, Y.H.; Bae, K. The antimicrobial activity of compounds from the leaf and stem of *Vitis amurensis* against two oral pathogens. *Bioorg. Med. Chem. Lett.* **2010**, *20*, 1165–1168. [CrossRef]
59. Mattio, L.M.; Dallavalle, S.; Musso, L.; Filardi, R.; Franzetti, L.; Pellegrino, L.; D'Incecco, P.; Mora, D.; Pinto, A.; Arioli, S. Antimicrobial activity of resveratrol-derived monomers and dimers against foodborne pathogens. *Sci. Rep.* **2019**, *9*, 7843. [CrossRef]
60. Yimdjo, M.C.; Azebaze, A.G.; Nkengfack, A.E.; Meyer, A.M.; Bodo, B.; Fomum, Z.T. Antimicrobial and cytotoxic agents from *Calophyllum inophyllum*. *Phytochemistry* **2004**, *65*, 2789–2795. [CrossRef]
61. Patil, A.D.; Freyer, A.J.; Eggleston, D.S.; Haltiwanger, R.C.; Bean, M.F.; Taylor, P.B.; Caranfa, M.J.; Breen, A.L.; Bartus, H.R. The inophyllums, novel inhibitors of HIV-1 reverse transcriptase isolated from the Malaysian tree, *Calophyllum inophyllum* Linn. *J. Med. Chem.* **1993**, *36*, 4131–4138. [CrossRef]
62. Hamdillah, A.; Isnansetyo, A.; Istiqomah, I.; Puspita, I.D.; Handayani, D.P.; Kaneko, T. Antibacterial activity of coastal plants and marine sponges from Kei Island Indonesia against bacterial fish pathogens. *Pharmacog. J.* **2019**, *11*, 812–817. [CrossRef]
63. Cuesta-Rubio, O.; Oubada, A.; Bello, A.; Maes, L.; Cos, P.; Monzote, L. Antimicrobial assessment of resins from *Calophyllum antillanum* and *Calophyllum inophyllum*. *Phytother. Res.* **2015**, *29*, 1991–1994. [CrossRef] [PubMed]
64. Spino, C.; Dodier, M.; Sotheeswaran, S. Anti-HIV coumarins from *Calophyllum* seed oil. *Bioorg. Med. Chem. Lett.* **1998**, *8*, 475–3478. [CrossRef]
65. Agoramoorthy, G.; Chandrasekaran, M.; Venkatesalu, V.; Hsu, M.J. Antibacterial and antifungal activities of fatty acid methyl esters of the blind-your-eye mangrove from India. *Braz. J. Microbiol.* **2007**, *38*, 739–742. [CrossRef]
66. Ravikumar, S.; Gnanadesigan, M.; Vijayakumar, V. In vitro antibacterial activity of diterpene and benzoxazole derivatives from *Excoecaria agallocha* L. *Int. J. Biol. Chem. Sci.* **2010**, *4*, 692–701.
67. Sabu, K.R.; Sugathan, S.; Idhayadhulla, A.; Woldemariam, M.; Aklilu, A.; Biresaw, G.; Tsegaye, B.; Manilal, A. Antibacterial, antifungal, and cytotoxic activity of *Excoecaria agallocha* leaf extract. *J. Exp. Pharmacol.* **2022**, *14*, 692–707.
68. Premanathan, M.; Rajendran, S.; Ramanathan, T.; Kathiresan, K. A survey of some Indian medicinal plants for anti-human immunodeficiency virus (HIV) activity. *Indian. J. Med. Res.* **2000**, *112*, 73. [PubMed]
69. Erickson, K.L.; Beutler, J.A.; Cardellina, J.H.; McMahon, J.B.; Newman, D.J.; Boyd, M.R. A novel phorbol ester from *Excoecaria agallocha*. *J. Nat. Prod.* **1995**, *58*, 769–772. [CrossRef]
70. Yan, R.Y.; Wang, H.Q.; Liu, C.; Chen, R.Y.; Yu, D.Q. Three new water-soluble alkaloids from the leaves of *Suregada glomerulata* (Blume) Baill. *Fitoter* **2011**, *82*, 247–250. [CrossRef] [PubMed]
71. Millat, M.S.; Islam, S.; Hussain, M.S.; Moghal, M.M.R.; Islam, T. Antibacterial profiling of *Launaea sarmentosa* (Willd.) and *Bruguiera cylindrica* (L.): Two distinct ethno medicinal plants of Bangladesh. *Eur. Exp. Biol.* **2017**, *7*, 1–5.

72. Bibi Sadeer, N.; Haddad, J.G.; Oday Ezzat, M.; Desprès, P.; Abdallah, H.H.; Zengin, G.; Uysal, A.; El Kalamouni, C.; Gallo, M.; Montesano, D.; et al. *Bruguiera gymnorhiza* (L.) Lam. at the forefront of pharma to confront Zika virus and microbial infections—An in vitro and in silico perspective. *Molecules* **2021**, *26*, 5768. [CrossRef] [PubMed]
73. Ravikumar, S.; Gnanadesigan, M.; Suganthi, P.; Ramalakshmi, A. Antibacterial potential of chosen mangrove plants against isolated urinary tract infectious bacterial pathogens. *Int. J. Med. Sci.* **2010**, *2*, 94–99.
74. Jasna, T.K.; Khaleel, K.M.; Rajina, M. In vitro antibacterial activity of mangrove plant *Kandelia candel* (L.) druce (Rhizophoraceae). *World J. Pharma Res.* **2017**, *6*, 470–477.
75. Mahalakshmi, G.; Vengadeshkumar, L.; Rajamohan, K.; Sanjaygandhi, S.; Sharmila, A.M. Leaf extract of *Rhizophora apiculata* as a potential bio-inducer of early blight disease resistance in tomato plant. *Nov. Res. Microbiol. J.* **2020**, *4*, 714.
76. Burhanuddin, B.; Saru, A.; Rantetondok, A.; Zainuddin, E.N. Antibacterial activity Rhizophora stylosa and *Avicennia marina* of mangrove fruit extraction on vibriosis of mangrove crab larvae (*Scylla serrata* Forsskal). *Int. J. Environ. Agric. Biotechnol.* **2019**, *4*, 1242–1248. [CrossRef]
77. Lim, S.H.; Darah, I.; Jain, K. Antimicrobial activities of tannins extracted from *Rhizophora apiculata* barks. *J. Trop. Forest Sci.* **2006**, *18*, 59–65.
78. Kokpol, U.; Chavasiri, W.; Chittawong, V.; Bruce, M.; Cunningham, G.N.; Miles, D.H. Long chain aliphatic alcohols and saturated carboxylic acids from heartwood of *Rhizophora apiculata*. *Phytochemistry* **1993**, *33*, 1129–1131. [CrossRef]
79. Thiem, B.; Goślińska, O. Antimicrobial activity of *Rubus chamaemorus* leaves. *Fitoter* **2004**, *75*, 93–95. [CrossRef] [PubMed]
80. Chacha, M.; Mapitse, R.; Afolayan, A.J.; Majinda, R.R. Antibacterial diterpenes from the roots of *Ceriops tagal*. *Nat. Prod. Commun.* **2008**, *3*, 17–20. [CrossRef]
81. Fogliani, B.; Raharivelomanana, P.; Bianchini, J.P.; Bouraı̈, S.; Hnawia, E. Bioactive ellagitannins from *Cunonia macrophylla*, an endemic Cunoniaceae from New Caledonia. *Phytochem.* **2005**, *66*, 241–247. [CrossRef] [PubMed]
82. Jayaraman, S.K.; Manoharan, M.S.; Illanchezian, S. Antibacterial, antifungal and tumor cell suppression potential of *Morinda citrifolia* fruit extracts. *Int. J. Integr. Biol.* **2008**, *3*, 44–49.
83. Choi, H.J.; Song, J.H.; Bhatt, L.R.; Baek, S.H. Anti-human rhinovirus activity of gallic acid possessing antioxidant capacity. *Phytother. Res.* **2010**, *24*, 1292–1296. [CrossRef] [PubMed]
84. Shan, L.P.; Zhang, X.; Hu, Y.; Liu, L.; Chen, J. Antiviral activity of esculin against white spot syndrome virus: A new starting point for prevention and control of white spot disease outbreaks in shrimp seedling culture. *J. Fish Dis.* **2022**, *45*, 59–68. [CrossRef]
85. Hatano, T.; Kusuda, M.; Hori, M.; Shiota, S.; Tsuchiya, T.; Yoshida, T. Theasinensin A, a tea polyphenol formed from Epigallocate-chin gallate, suppresses antibiotic resistance of methicillin-resistant *S. aureus*. *Planta Med.* **2003**, *69*, 984–989. [PubMed]
86. Xu, T.; Wang, Z.; Lei, T.; Lv, C.; Wang, J.; Lu, J. New flavonoid glycosides from *Sedum aizoon* L. *Fitoter* **2015**, *101*, 125–132. [CrossRef] [PubMed]
87. Hafid, A.F.; Wahyuni, T.S.; Tumewu, L.; Apryani, E.V.H.Y.; Permanasari, A.A.; Adianti, M.; Kawahara, N. Antihepatitis C virus activity of Indonesian Mahogany (*Toona Sureni*). *Asian J. Pharm. Clin. Res.* **2018**, *11*, 87–90. [CrossRef]
88. Hsu, W.C.; Chang, S.P.; Lin, L.C.; Li, C.L.; Richardson, C.D.; Lin, C.C.; Lin, L.T. *Limonium sinense* and gallic acid suppress hepatitis C virus infection by blocking early viral entry. *Antiv. Res.* **2015**, *118*, 139–147. [CrossRef]
89. You, H.L.; Huang, C.C.; Chen, C.J.; Chang, C.C.; Liao, P.L.; Huang, S.T. Anti-pandemic influenza A (H1N1) virus potential of catechin and gallic acid. *J. Chin. Med. Assoc.* **2018**, *81*, 458–468. [CrossRef] [PubMed]
90. Weng, J.R.; Lin, C.S.; Lai, H.C.; Lin, Y.P.; Wang, C.Y.; Tsai, Y.C.; Wu, K.C.; Huang, S.H.; Lin, C.W. Antiviral activity of *Sambucus ormosana* Nakai ethanol extract and related phenolic acid constituents against human coronavirus NL63. *Virus Res.* **2019**, *273*, 197767. [CrossRef] [PubMed]
91. Afifi, F.Ü.; Al-Khalil, S.; Abdul-Haq, B.K.; Mahasneh, A.; Al-Eisawi, D.M.; Sharaf, M.; Wong, L.K.; Schiff, P.L., Jr. Antifungal flavonoids from Varthemia iphionoides. *Phytother. Res.* **1991**, *5*, 173–175. [CrossRef]
92. Wang, J.; Qin, X.; Chen, Z.; Ju, Z.; He, W.; Tan, Y.; Zhou, X.; Tu, Z.; Lu, F.; Liu, Y. Two new anthraquinones with antiviral activities from the barks of *Morinda citrifolia* (Noni). *Phytochem. Lett.* **2016**, *15*, 13–15. [CrossRef]
93. Saludes, J.P.; Garson, M.J.; Franzblau, S.G.; Aguinaldo, A.M. Antitubercular constituents from the hexane fraction of *Morinda citrifolia* Linn. (Rubiaceae). *Phytother. Res.* **2002**, *16*, 683–685. [CrossRef]
94. Simlai, A.; Mukherjee, K.; Mandal, A.; Bhattacharya, K.; Samanta, A.; Roy, A. Partial purification and characterization of an antimicrobial activity from the wood extract of mangrove plant *Ceriops decandra*. *EXCLI J.* **2016**, *15*, 103–112.
95. Saeed, M.A.; Sabir, A.W. Antibacterial activity of *Caesalpinia bonducella* seeds. *Fitoter* **2001**, *72*, 807–809. [CrossRef]
96. Simin, K.; Khaliq-uz-Zaman, S.M.; Ahmad, V.U. Antimicrobial activity of seed extracts and bondenolide from *Caesalpinia bonduc* (L.) Roxb. *Phytother. Res.* **2001**, *15*, 437–440. [CrossRef] [PubMed]
97. Arif, T.; Mandal, T.K.; Kumar, N.; Bhosale, J.D.; Hole, A.; Sharma, G.L.; Padhi, M.M.; Lavekar, G.S.; Dabur, R. In vitro and in vivo antimicrobial activities of seeds of *Caesalpinia bonduc* (Lin.) Roxb. *J. Ethnopharmacol.* **2009**, *123*, 177–180. [CrossRef] [PubMed]
98. Ata, A.; Udenigwe, C.C.; Gale, E.M.; Samarasekera, R. Minor chemical constituents of *Caesalpinia bonduc*. *Nat. Prod. Commun.* **2009**, *4*, 311–314. [CrossRef]
99. Idrus, I.; Kurniawan, F.; Mustapa, F.; Wibowo, D. Concentration Effect of Leaf Extract from Kekara Laut (*Canavalia Maritima* Thou.) in Inhibiting of *Staphylococcus Epidermidis* Bacteria With a Statistical Science Approach. *Indo. J. Chem. Res.* **2021**, *8*, 180–185. [CrossRef]
100. Powar, P. Antifungal activity of Mangrove bark. *Int. J. Pharm. Bio. Sci.* **2011**, *4*, 484–488.

101. Suhendi, A.; Indrayudha, P.; Azizah, T. Antibacterial activity of ethanol extract of steam bark of *Cynometra ramiflora* Linn against various bacterial. *Open Conf. Proc. J.* **2013**, *4*, 1. [CrossRef]

102. Kumar, V.A.; Ammani, K.; Siddhardha, B. In vitro antimicrobial activity of leaf extracts of certain mangrove plants collected from Godavari estuarine of *Konaseema delta*, India. *Int. J. Med. Arom. Plants.* **2011**, *1*, 132–136.

103. Xin, L.Y.; Min, T.H.; Zin, P.N.L.M.; Pulingam, T.; Appaturi, J.N.; Parumasivam, T. Antibacterial potential of Malaysian ethnomedicinal plants against methicillin-susceptible Staphylococcus aureus (MSSA) and methicillin-resistant *Staphylococcus aureus* (MRSA). *Saudi J. Biol.Sci.* **2021**, *28*, 5884–5889. [CrossRef]

104. Gunasekara, T.D.C.P.; Radhika, N.D.M.; Ragunathan, K.K.; Gunathilaka, D.P.P.; Weerasekera, M.M.; Hewageegana, H.G.S.P.; Arawwawala, L.A.D.M.; Fernando, S.S.N. Determination of antimicrobial potential of five herbs used in ayurveda practices against *Candida albicans*, *Candida parapsilosis* and methicillin resistant *S. aureus*. *Anc. Sci. Life.* **2017**, *36*, 187. [CrossRef]

105. Rattanasuk, S.; Boongapim, R.; Phiwthong, T. Antibacterial activity of *Cathormion umbellatum*. *Bangladesh J. Pharmacol.* **2021**, *16*, 91–95. [CrossRef]

106. Hamburger, M.O.; Cordell, G.A.; Tantivatana, P.; Ruangrungsi, N. Traditional medicinal plants of Thailand, VIII. Isoflavonoids of *Dalbergia candenatensis*. *J. Nat. Prod.* **1987**, *50*, 696–699. [CrossRef] [PubMed]

107. Sekine, T.; Inagaki, M.; Ikegami, F.; Fujii, Y.; Ruangrungsi, N. Six diprenylisoflavones, derrisisoflavones A–F, from *Derris scandens*. *Phytochemistry* **1999**, *52*, 87–94. [CrossRef]

108. Hussain, H.; Al-Harrasi, A.; Krohn, K.; Kouam, S.F.; Abbas, G.; Shah, A.; Raees, M.A.; Ullah, R.; Aziz, S.; Schulz, B. Phytochemical investigation and antimicrobial activity of *Derris scandens*. *J. King Saud Univ.-Sci.* **2015**, *27*, 375–378. [CrossRef]

109. Mohotti, S.; Rajendran, S.; Muhammad, T.; Strömstedt, A.A.; Adhikari, A.; Burman, R.; De Silva, E.D.; Göransson, U.; Hettiarachchi, C.M.; Gunasekera, S. Screening for bioactive secondary metabolites in Sri Lankan medicinal plants by microfractionation and targeted isolation of antimicrobial flavonoids from *Derris scandens*. *J. Ethnopharmacol.* **2020**, *246*, 112158. [CrossRef]

110. Mahabusarakam, W.; Deachathai, S.; Phongpaichit, S.; Jansakul, C.; Taylor, W.C. A benzil and isoflavone derivatives from *Derris scandens* Benth. *Phytochemistry* **2004**, *65*, 1185–1191. [CrossRef] [PubMed]

111. Mathaiyan, M.; Suresh, A.; Balamurugan, R. Binding property of HIV p24 and reverse transcriptase by chalcones from *Pongamia pinnata* seeds. *Bioinformation* **2018**, *14*, 279–284. [CrossRef] [PubMed]

112. Nukui, M.; O'Connor, C.M.; Murphy, E.A. The natural flavonoid compound deguelin inhibits HCMV lytic replication within fibroblasts. *Viruses* **2018**, *10*, 614. [CrossRef]

113. Yusuf, A.I.; Dewi, B.E.; Sjatha, F. Antiviral activity of *Cynometra ramiflora* Linn leaves extract against replication of Dengue virus serotype 2 on Huh 7.5 cell in vitro. In Proceedings of the BROMO Conference (BROMO 2018)—Symposium on Natural Product and Biodiversity, Surabaya, Indonesia, 11–12 July 2018; pp. 1–4.

114. Takatsuki, A.; Nakatani, N.; Morimoto, M.; Tamura, G.; Matsui, M.; Arima, K.; Yamaguchi, I.; Misato, T. Antiviral and antitumor antibiotics. XX. Effects of rotenone, deguelin, and related compounds on animal and plant viruses. *Appl. Microbiol.* **1969**, *18*, 660–667. [CrossRef]

115. Yusook, K.; Weeranantanapan, O.; Hua, Y.; Kumkrai, P.; Chudapongse, N. Lupinifolin from Derris reticulata possesses bactericidal activity on S. aureus by disrupting bacterial cell membrane. *J. Nat. Med.* **2017**, *71*, 357–366. [CrossRef]

116. Mazimba, O.; Masesane, I.B.; Majinda, R.R. A flavanone and antimicrobial activities of the constituents of extracts from *Mundulea sericea*. *Nat. Prod. Res.* **2012**, *26*, 1817–1823. [CrossRef]

117. Phrutivorapongkul, A.; Lipipun, V.; Ruangrungsi, N.; Watanabe, T.; Ishikawa, T. Studies on the constituents of seeds of *Pachyrrhizus erosus* and their anti herpes simplex virus (HSV) activities. *Chem. Pharm. Bull.* **2002**, *50*, 534–537. [CrossRef] [PubMed]

118. Nehad, M.G.; Abdulrahaman, S.H. Antimicrobial efficacy of *Casuarina equisetifolia* extracts against some pathogenic microorganisms. *J. Med. Plants Res.* **2012**, *6*, 5819–5825.

119. Lagnika, L.; Amoussa, A.M.O.; Oketokoun, S.A.; Adjovi, Y.; Sanni, A. In vitro antifungal and antioxidant activities of two Benin medicinal plants. *J. Med. Plants Res.* **2014**, *8*, 513–519.

120. Kumar, U.M.N.; Panneerselvam, T. Efficacy of aqueous and ethanol extracts *Casuarina equisetifolia* for potential antimicrobial activity. *World J. Pharm. Pharm. Sci.* **2015**, *4*, 1877–1882.

121. Ao, C.; Li, A.; Elzaawely, A.A.; Xuan, T.D.; Tawata, S. Evaluation of antioxidant and antibacterial activities of *Ficus microcarpa* L. fil. extract. *Food Control* **2008**, *19*, 940–948. [CrossRef]

122. Hu, Y.; Wu, X.; Liu, N.; Zhang, F.; Lu, Y.; Zhang, Y.; Fu, L. Flavans with anti-HSV activity from the leaves of *Ficus microcarpa* L. *J. Trop. Subtrop. Bot.* **2010**, *18*, 559–563.

123. Nantachit, K.; Sirilun, S.; Nobsathian, S.; Rungjang, S. Three new polycyclic containing sulfur compounds from the seeds of *Combretum quadrangulare* kurz (Combretaceae), antifungal and anti-mycobacterium activities. *Chiang Mai J. Sci.* **2017**, *44*, 157–167.

124. Pawar, S.P.; Pal, S.C. Antimicrobial activity of extracts of *Terminalia catappa* root. *Indian J Med. Sci.* **2002**, *56*, 276–278.

125. Terças, A.G.; Monteiro, A.D.S.; Moffa, E.B.; Dos Santos, J.R.; Sousa, E.M.D.; Pinto, A.R.; Costa, P.C.; Borges, A.C.; Torres, L.; Barros Filho, A.K.; et al. Phytochemical characterization of *Terminalia catappa* linn. extracts and their antifungal activities against candida spp. *Front. Microbiol.* **2017**, *8*, 595. [CrossRef]

126. Adesina, S.K.; Idowu, O.; Ogundaini, A.O.; Oladimeji, H.; Olugbade, T.A.; Onawunmi, G.O.; Pais, M. Antimicrobial constituents of the leaves of *Acalypha wilkesiana* and *Acalypha hispida*. *Phytother. Res.* **2000**, *14*, 371–374. [CrossRef]

127. Yeo, S.G.; Song, J.H.; Hong, E.H.; Lee, B.R.; Kwon, Y.S.; Chang, S.Y.; Kim, S.H.; Won Lee, S.; Park, J.H.; Ko, H.J. Antiviral effects of *Phyllanthus urinaria* containing corilagin against human enterovirus 71 and Coxsackievirus A16 in vitro. *Arch. Pharm. Res.* **2015**, *38*, 193–202. [CrossRef] [PubMed]
128. Dao, N.T.; Jang, Y.; Kim, M.; Nguyen, H.H.; Pham, D.Q.; Le Dang, Q.; Van Nguyen, M.; Yun, B.S.; Pham, Q.M.; Kim, J.C.; et al. Chemical constituents and anti-influenza viral activity of the leaves of Vietnamese plant *Elaeocarpus tonkinensis*. *Rec. Nat. Prod.* **2019**, *13*, 71–80. [CrossRef]
129. Aman, S.; Naim, A.; Siddiqi, R.; Naz, S. Antimicrobial polyphenols from small tropical fruits, tea and spice oilseeds. *Food Sci. Technol. Int.* **2014**, *20*, 241–251. [CrossRef] [PubMed]
130. Premnathan, M.; Chandra, K.; Bajpai, S.K.; Kathiresan, K. A survey of some Indian marine plants for antiviral activity. *Bot. Mar.* **1992**, *35*, 321–324. [CrossRef]
131. Arunkumar, J.; Rajarajan, S.A. Study on the in vitro Cytotoxicity and Anti-HSV-2 Activity of lyophilized extracts of Terminalia catappa Lin., Mangifera indica Lin. and phytochemical compound mangiferin. *Int. J. Med. Pharm. Virol.* **2015**, *2*, 22–26.
132. Tewtrakul, S.; Miyashiro, H.; Nakamura, N.; Hattori, M.; Kawahata, T.; Otake, T.; Yoshinaga, T.; Fujiwara, T.; Supavita, T.; Yuenyongsawad, S.; et al. HIV-1 integrase inhibitory substances from *Coleus parvifolius*. *Phytother. Res.* **2003**, *17*, 232–239. [CrossRef] [PubMed]
133. Hardjito, L. Antibacterial, antioxidant and topoisomerase-I inhibitor activities of the coastal ethnomedicinal plant *Pemphis acidula*. *BIOTROPIA-Southeast Asian J. Trop. Biol.* **2007**, *14*, 43–51.
134. Samidurai, K.; Saravanakumar, A. Antibacterial activity of *Pemphis acidula* Forst. *Glob. J. Pharmacol.* **2009**, *3*, 113–115.
135. Abd Wahab, N.Z.; Ja'afar, N.S.A.; Ismail, S.B. Evaluation of antibacterial activity of essential oils of *Melaleuca cajuputi* Powell. *J. Pure Appl. Microbiol.* **2022**, *16*, 549–557. [CrossRef]
136. Bua, A.; Molicotti, P.; Donadu, M.G.; Usai, D.; Le, L.S.; Tran, T.T.T.; Ngo, V.Q.T.; Marchetti, M.; Usai, M.; Cappuccinelli, P.; et al. "In vitro" activity of *Melaleuca cajuputi* against mycobacterial species. *Nat. Prod. Res.* **2020**, *34*, 1494–1497. [CrossRef]
137. Yala, J.F.; Mabika, R.M.; Camara, B.; Tuo, S.; Souza, A.; Lepengue, A.N.; Koné, D.; M'batchi, B. Assessment of the antibacterial activity of four essential oils and the biobactericide Neco. *Int. J. Phytomed* **2017**, *9*, 443–450. [CrossRef]
138. Keereedach, P.; Hrimpeng, K.; Boonbumrung, K. Antifungal activity of Thai cajuput oil and its effect on efflux-pump gene expression in fluconazole-resistant *Candida albicans* clinical isolates. *Int. J. Microbiol.* **2020**, *2020*, 1–10. [CrossRef]
139. Lee, Y.S.; Kim, J.; Shin, S.C.; Lee, S.G.; Park, I.K. Antifungal activity of Myrtaceae essential oils and their components against three phytopathogenic fungi. *Flav. Frag. J.* **2008**, *23*, 23–28. [CrossRef]
140. Pino, O.; Sánchez, Y.; Rojas, M.M.; Rodríguez, H.; Abreu, Y.; Duarte, Y.; Martínez, B.; Peteira, B.; Correa, T.M.; Martínez, D. Composición química y actividad plaguicida del aceite esencial de *Melaleuca quinquenervia* (Cav) ST Blake. *Rev. Protección Veg.* **2011**, *26*, 177–186.
141. Hossain, S.J.; Basar, M.H.; Rokeya, B.; Arif, K.M.T.; Sultana, M.S.; Rahman, M.H. Evaluation of antioxidant, antidiabetic and antibacterial activities of the fruit of *Sonneratia apetala* (Buch.-Ham.). *Oriental Pharm. Exp. Med.* **2013**, *13*, 95–102. [CrossRef]
142. Afzali, S.F.; Wong, W.L. In vitro screening of *Sonneratia alba* extract against the oomycete fish pathogen, Aphanomyces invadans. *Iran. J. Fish. Sci.* **2017**, *16*, 1333–1340.
143. Bobbarala, V.; Vadlapudi, V.; Naidu, K.C. Mangrove plant *Sonneratia apetala* antimicrobial activity on selected pathogenic microorganisms. *Orient. J. Chem.* **2009**, *25*, 445–447.
144. Khumaidah, L.; Purnomo, A.S.; Fatmawati, S. Antimicrobial activity of *Sonneratia ovata* backer. *Hayati J. Biosci.* **2019**, *26*, 152. [CrossRef]
145. Limbago, J.S.; Sosas, J.; Gente, A.A.; Maderse, P.; Rocamora, M.M.; Gomez, D.K. Antibacterial effects of mangrove ethanolic leaf extract against zoonotic fish pathogen *Salmonella arizonae*. *J. Fish.* **2021**, *9*, 92205. [CrossRef]
146. Harizon Pujiastuti, B.; Kurnia, D.; Sumiarsa, D.; Shiono, Y.; Supratman, U. Antibacterial triterpenoids from the bark of *Sonneratia alba* (Lythraceae). *Nat. Prod. Comm.* **2015**, *10*, 277–280.
147. Gong, K.K.; Li, P.L.; Qiao, D.; Zhang, X.W.; Chu, M.J.; Qin, G.F.; Tang, X.L.; Li, G.Q. Cytotoxic and antiviral triterpenoids from the mangrove plant *Sonneratia paracaseolaris*. *Molecules* **2017**, *22*, 1319. [CrossRef] [PubMed]
148. Moe, T.S.; Win, H.H.; Hlaing, T.T.; Lwin, W.W.; Htet, Z.M.; Mya, K.M. Evaluation of in vitro antioxidant, antiglycation and antimicrobial potential of indigenous Myanmar medicinal plants. *J. Integr. Med.* **2018**, *16*, 358–366. [CrossRef] [PubMed]
149. Duraipandiyan, V.; Gnanasekar, M.; Ignacimuthu, S. Antifungal activity of triterpenoid isolated from *Azima tetracantha* leaves. *Folia Histochem. Cytobiol* **2010**, *48*, 311–313. [CrossRef] [PubMed]
150. Sumardi, S.; Basyuni, M.; Wati, R. Antimicrobial activity of polyisoprenoids of sixteen mangrove species from North Sumatra, Indonesia. *Biodiversitas J. Biol. Divers* **2018**, *19*, 1243–1248. [CrossRef]
151. Abdul-Awal, S.M.; Nazmir, S.; Nasrin, S.; Nurunnabi, T.R.; Uddin, S.J. Evaluation of pharmacological activity of *Hibiscus tiliaceus*. *Springerplus* **2016**, *5*, 1–6. [CrossRef] [PubMed]
152. Boonsri, S.; Karalai, C.; Ponglimanont, C.; Chantrapromma, S.; Kanjana-Opas, A. Cytotoxic and antibacterial sesquiterpenes from *Thespesia populnea*. *J. Nat. Prod.* **2008**, *71*, 1173–1177. [CrossRef] [PubMed]
153. Arthanari, S.K.; Vanitha, J.; Ganesh, M.; Venkateshwaran, K.; Clercq, D. Evaluation of antiviral and cytotoxic activities of methanolic extract of *S. grandiflora* (Fabaceae) flowers. *Asian Pac. J. Trop. Biomed.* **2012**, *2*, S855–S858. [CrossRef]
154. Chungsamarnyart, N.; Sirinarumitr, T.; Chumsing, W.; Wajjawalku, W. In vitro study of antiviral activity of plant crude-extracts against the foot and mouth disease virus. *Agric. Nat. Res.* **2007**, *41*, 97–103.

155. Dey, M.C.; Roy, R.N.; Sinhababu, A. Fatty acid composition and antibacterial activity of the leaf oil of *Kleinhovia hospita* Linn. *J. Nat. Prod.* **2017**, *10*, 378–384.

156. Rahim, A.; Saito, Y.; Miyake, K.; Goto, M.; Chen, C.H.; Alam, G.; Morris-Natschke, S.; Lee, K.H.; Nakagawa-Goto, K. Kleinhospitine E and cycloartane triterpenoids from *Kleinhovia hospita*. *J. Nat. Prod.* **2018**, *81*, 1619–1627. [CrossRef] [PubMed]

157. Al Muqarrabun, L.M.R. and Ahmat, N.Medicinal uses, phytochemistry and pharmacology of family Sterculiaceae: A review. *Eur. J. Med. Chem.* **2015**, *92*, 514–530. [CrossRef]

158. Christopher, R.; Nyandoro, S.S.; Chacha, M.; De Koning, C.B. A new cinnamoylglycoflavonoid, antimycobacterial and antioxidant constituents from *Heritiera littoralis* leaf extracts. *Nat. Prod. Res.* **2014**, *28*, 351–358. [CrossRef] [PubMed]

159. Tatsimo, S.J.N.; de Dieu Tamokou, J.; Havyarimana, L.; Csupor, D.; Forgo, P.; Hohmann, J.; Kuiate, J.R.; Tane, P. Antimicrobial and antioxidant activity of kaempferol rhamnoside derivatives from *Bryophyllum pinnatum*. *BMC Res. Notes* **2012**, *5*, 158. [CrossRef] [PubMed]

160. De Almeida, A.P.; Miranda, M.M.F.S.; Simoni, I.C.; Wigg, M.D.; Lagrota, M.H.C.; Costa, S.S. Flavonol monoglycosides isolated from the antiviral fractions of *Persea americana* (Lauraceae) leaf infusion. *Phytother. Res.* **1998**, *12*, 562–567. [CrossRef]

161. Kuspradini, H.; Mitsunaga, T.; Ohashi, H. Antimicrobial activity against Streptococcus sobrinus and glucosyltransferase inhibitory activity of taxifolin and some flavanonol rhamnosides from kempas (*Koompassia malaccensis*) extracts. *J. Wood Sci.* **2009**, *55*, 308–313. [CrossRef]

162. Jiang, R.W.; Ma, S.C.; He, Z.D.; Huang, X.S.; But, P.P.H.; Wang, H.; Chan, S.P.; Ooi, V.E.C.; Xu, H.X.; Mak, T.C. Molecular structures and antiviral activities of naturally occurring and modified cassane furanoditerpenoids and friedelane triterpenoids from *Caesalpinia minax*. *Bioorg. Med. Chem.* **2002**, *10*, 2161–2170. [CrossRef]

163. Chang, F.R.; Yen, C.T.; Ei-Shazly, M.; Lin, W.H.; Yen, M.H.; Lin, K.H.; Wu, Y.C. Anti-human coronavirus (anti-HCoV) triterpenoids from the leaves of *Euphorbia neriifolia*. *Nat. Prod. Commun.* **2012**, *7*, 1415–1417. [CrossRef]

164. Wangensteen, H.; Dang, H.C.T.; Uddin, S.J.; Alamgir, M.; Malterud, K.E. Antioxidant and antimicrobial effects of the mangrove tree *Heritiera fomes*. *Nat. Prod. Comm.* **2009**, *4*, 371–376. [CrossRef]

165. Choudhury, S.; Sree, A.; Mukherjee, S.C.; Pattnaik, P.; Bapuji, M. In vitro antibacterial activity of extracts of selected marine algae and mangroves against fish pathogens. *Asian Fish. Sci.* **2005**, *18*, 285. [CrossRef]

166. Veni, P.S.; Sunita, S.; Srinivasulu, A. Antibacterial and phytochemical screening of *Xylocarpus moluccensis* leaf and stem on selected drug resistant and sensitive bacteria. *Int. J. Microbiol. Res. IJMR* **2014**, *5*, 30–34.

167. Dai, Y.G.; Wu, J.; Padmakumar, K.P.; Shen, L. Sundarbanxylogranins A–E, five new limonoids from the Sundarban Mangrove, *Xylocarpus granatum*. *Fitoter* **2017**, *122*, 85–89. [CrossRef]

168. Li, W.; Jiang, Z.; Shen, L.; Pedpradab, P.; Bruhn, T.; Wu, J.; Bringmann, G. Antiviral limonoids including khayanolides from the Trang mangrove plant *Xylocarpus moluccensis*. *J. Nat. Prod.* **2015**, *78*, 1570–1578. [CrossRef]

169. Zhang, Q.; Satyanandamurty, T.; Shen, L.; Wu, J. Krishnolides A–D: New 2-ketokhayanolides from the Krishna mangrove, *Xylocarpus moluccensis*. *Mar. Drugs* **2017**, *15*, 333. [CrossRef] [PubMed]

170. Pudhom, K.; Sommit, D.; Nuclear, P.; Ngamrojanavanich, N.; Petsom, A. Moluccensins H− J, 30-Ketophragmalin Limonoids from *Xylocarpus moluccensis*. *J. Nat. Prod.* **2010**, *73*, 263–266. [CrossRef] [PubMed]

171. Du, S.; Wang, M.; Zhu, W.; Qin, Z. A new fungicidal lactone from *Xylocarpus granatum* (Meliaceae). *Nat. Prod. Res.* **2009**, *23*, 1316–1321. [CrossRef] [PubMed]

172. Lesueur, D.; De Rocca Serra, D.; Bighelli, A.; Minh Hoi, T.; Huy Thai, T.; Casanova, J. Composition and antimicrobial activity of the essential oil of *Acronychia pedunculata* (L.) Miq. from Vietnam. *Nat. Prod. Res.* **2008**, *22*, 393–398. [CrossRef] [PubMed]

173. Thirugnanasampandan, R.; Gunasekar, R.; Gogulramnath, M. Chemical composition analysis, antioxidant and antibacterial activity evaluation of essential oil of *Atalantia monophylla* Correa. *Pharmacog. Res.* **2015**, *7*, S52. [CrossRef] [PubMed]

174. Trong Le, N.; Viet Ho, D.; Quoc Doan, T.; Tuan Le, A.; Raal, A.; Usai, D.; Sanna, G.; Carta, A.; Rappelli, P.; Diaz, N.; et al. Biological activities of essential oils from leaves of *Paramignya trimera* (Oliv.) Guillaum and *Limnocitrus littoralis* (Miq.) Swingle. *Antibiotics* **2020**, *9*, 207. [CrossRef]

175. Reddy, K.H.; Sharma, P.V.G.K.; Reddy, O.V.S. A comparative in vitro study on antifungal and antioxidant activities of *Nervilia aragoana* and *Atlantia monophylla*. *Pharm. Biol.* **2010**, *48*, 595–602. [CrossRef]

176. Wainwright, M. Acridine—a neglected antibacterial chromophore. *J. Antimicrob. Chemother.* **2001**, *47*, 1–13. [CrossRef]

177. Thimmaiah, K.; Ugarkar, A.G.; Martis, E.F.; Shaikh, M.S.; Coutinho, E.C.; Yergeri, M.C. Drug–DNA interaction studies of acridone-based derivatives. *Nucleosides Nucleotides Nucleic Acids* **2015**, *34*, 309–331. [CrossRef] [PubMed]

178. Manimaran, M.; Rajkumar, T.; Vimal, S.; Taju, G.; Majeed, S.A.; Hameed, A.S.; Kannabiran, K. Antiviral activity of 9 (10H)-Acridanone extracted from marine Streptomyces fradiae strain VITMK2 in Litopenaeus vannamei infected with white spot syndrome virus. *Aquaculture* **2018**, *488*, 66–73. [CrossRef]

179. Sripisut, T.; Deachathai, S.; Chang, L.C.; Laphookhieo, S. Antibacterial compounds from *Atalantia monophylla* roots and stems. *Planta Med.* **2013**, *79*, PN11. [CrossRef]

180. Wisetsai, A.; Lekphrom, R.; Suebrasri, T.; Schevenels, F.T. Acroflavone A, a new prenylated flavone from the fruit of *Acronychia pedunculata* (L.) Miq. *Nat. Prod. Res.* **2021**, *36*, 5330–5336. [CrossRef] [PubMed]

181. Islam, M.T.; Noor, M.A.; Karon, B.; de Freitas, R.M. In vitro antimicrobial and brine shrimp lethality of *Allophylus cobbe* L. *Ayu* **2012**, *33*, 299. [CrossRef]

182. Raghavendra, H.L.; Prashith kekuda T., R.; Karthik K., N.; Ankith G., N. Antiradical, antibacterial, and antifungal activity of *Harpullia arborea* (Blanco) Radlk. (Sapindaceae). *Int. J. Curr. Pharm. Res.* **2017**, *9*, 32–36.

183. Tumewu, L.; Apryiani, E.; Santi, M.R. Anti Hepatitis C virus activity screening on *Harpullia arborea* extracts and isolated compound. In *Proceeding the 1st International Conference on Pharmaceutics and Pharmaceutical Sciences*; Fakultas Farmasi Universitas Airlangga: Surabaya, Indonesia, 2014; pp. 165–167.

184. Abdelkader, M.S.A.; Rateb, M.E.; Mohamed, G.A.; Jaspars, M. Harpulliasides A and B: Two new benzeneacetic acid derivatives from Harpullia pendula. *Phytochem. Lett.* **2016**, *15*, 131–135. [CrossRef]

185. Anusha, P.; Sudha Bai, R. Phytochemical profile and antimicrobial potential of methanolic extracts of bark and leaf of *Quassia indica* (Gaertn.) Nooteb. *J. Phytopharmacol.* **2017**, *6*, 269–276. [CrossRef]

186. Hardiyanti, R.; Marpaung, L.; Adnyana, I.K.; Simanjuntak, P. Isolation of quercitrin from *Dendrophthoe pentandra* (L.) Miq leaves and it's antioxidant and antibacterial activities. *Rasayan J. Chem.* **2019**, *12*, 1822–1827. [CrossRef]

187. Tripathi, S.; Ray, S.; Das, P.K.; Mondal, A.K.; Verma, N.K. Antimicrobial activities of some rare aerial hemi parasitic taxa of south West Bengal, India. *Int. J. Phytopharm.* **2013**, *4*, 106–112.

188. Satish, S.; Raveesha, K.A.; Janardhana, G.R. Antibacterial activity of plant extracts on phytopathogenic *Xanthomonas campestris* pathovars. *Lett. Appl. Microbiol.* **1999**, *28*, 145–147. [CrossRef]

189. Omer, M.E.F.A.; Elnima, E.I. Antimicrobial activity of *Ximenia americana*. *Fitoter* **2003**, *74*, 122–126. [CrossRef]

190. Owk, A.K.; Lagudu, M.N. Evaluation of antimicrobial activity and phytochemicals in *Olax scandens* Roxb. roots. *Pharma Sci. Monit.* **2016**, *7*, 232–239.

191. Kone, W.M.; Atindehou, K.K.; Terreaux, C.; Hostettmann, K.; Traore, D.; Dosso, M. Traditional medicine in North Côte-d'Ivoire: Screening of 50 medicinal plants for antibacterial activity. *J. Ethnopharmacol.* **2004**, *93*, 43–49. [CrossRef]

192. Duraipandiyan, V.; Ayyanar, M.; Ignacimuthu, S. Antimicrobial activity of some ethnomedicinal plants used by Paliyar tribe from Tamil Nadu, India. *BMC Compl. Altern. Med.* **2006**, *6*, 1–7. [CrossRef]

193. Asres, K.; Bucar, F.; Kartnig, T.; Witvrouw, M.; Pannecouque, C.; De Clercq, E. Antiviral activity against human immunodeficiency virus type 1 (HIV-1) and type 2 (HIV-2) of ethnobotanically selected Ethiopian medicinal plants. *Phytother. Res.* **2001**, *15*, 62–69. [CrossRef]

194. Chandrasekaran, M.; Senthilkumar, A.; Venkatesalu, V. Antibacterial and antifungal efficacy of fatty acid methyl esters from the leaves of *Sesuvium portulacastrum* L. *Eur. Rev. Med. Pharmacol. Sci.* **2011**, *15*, 775–780.

195. Magwa, M.L.; Gundidza, M.; Gweru, N.; Humphrey, G. Chemical composition and biological activities of essential oil from the leaves of *Sesuvium portulacastrum*. *J. Ethnopharmacol.* **2006**, *103*, 85–89. [CrossRef]

196. Bhosale, S.H.; Jagtap, T.G.; Naik, C.G. Antifungal activity of some marine organisms from India, against food spoilage *Aspergillus* strains. *Mycopathologia* **1999**, *147*, 133–138. [CrossRef]

197. Banerjee, M.B.; Ravikumar, S.; Gnanadesigan, M.; Rajakumar, B.; Anand, M. Antiviral, antioxidant and toxicological evaluation of mangrove associate from South East coast of India. *Asian Pac. J. Trop. Biomed.* **2012**, *2*, S1775–S1779. [CrossRef]

198. Chandrasekaran, M.; Kannathasan, K.; Venkatesalu, V. Antimicrobial activity of fatty acid methyl esters of some members of Chenopodiaceae. *Z. Nat. C* **2008**, *63*, 331–336. [CrossRef]

199. Ghosh, D.; Mondal, S.; Ramakrishna, K. Spectroscopic characterization of phytoconstituents isolated from a rare mangrove *Aegialitis rotundifolia* Roxb., leaves and evaluation of antimicrobial activity of the crude extract. *Asian J. Pharm. Clin. Res.* **2019**, *12*, 220–224. [CrossRef]

200. Sett, S.; Hazra, J.; Datta, S.; Mitra, A.; Mitra, A.K. Screening the Indian Sundarban mangrove for antimicrobial activity. *Int. J. Sci. Innov. Disc.* **2014**, *4*, 17–25.

201. Min, B.S.; Kim, Y.H.; Tomiyama, M.; Nakamura, N.; Miyashiro, H.; Otake, T.; Hattori, M. Inhibitory effects of Korean plants on HIV-1 activities. *Phytother. Res.* **2001**, *15*, 481–486. [CrossRef] [PubMed]

202. Sahoo, S.; Panda, P.K.; Mishra, S.R.; Parida, R.K.; Ellaiah, P.; Dash, S.K. Antibacterial activity of *Barringtonia acutangula* against selected urinary tract pathogens. *Indian J. Pharma Sci.* **2008**, *70*, 677. [CrossRef] [PubMed]

203. Mishra, S.; Sahoo, S.; Mishra, S.K.; Rout, K.K.; Nayak, S.K.; Panda, P.K.; Dhal, N.K. Antimicrobial investigation of leaves of *Barringtonia acutangula* Linn. *Med. Aromat. Plant Sci. Biotechnol.* **2009**, *3*, 55–58.

204. Khan, M.R.; Omoloso, A.D. Antibacterial, antifungal activities of *Barringtonia asiatica*. *Fitoter* **2002**, *73*, 255–260. [CrossRef]

205. Hussin, N.M.; Muse, R.; Ahmad, S.; Ramli, J.; Mahmood, M.; Sulaiman, M.R.; Shukor, M.Y.A.; Rahman, M.F.A.; Aziz, K.N.K. Antifungal activity of extracts and phenolic compounds from *Barringtonia racemosa* L.(Lecythidaceae). *African J. Biotechnol.* **2009**, *8*, 2835–2842.

206. Saha, S.; Sarkar, K.K.; Hossain, M.L.; Hossin, A.; Barman, A.K.; Ahmed, M.I.; Sadhu, S.K. Bioactivity studies on *Barringtonia racemosa* (Lam.) bark. *Pharmacologyonline* **2013**, *1*, 93–100.

207. Ragasa, C.Y.; Espineli, D.L.; Shen, C.C. New triterpenes from *Barringtonia asiatica*. *Chem. Pharm. Bull.* **2011**, *59*, 778–782. [CrossRef] [PubMed]

208. Bonvicini, F.; Antognoni, F.; Mandrone, M.; Protti, M.; Mercolini, L.; Lianza, M.; Gentilomi, G.A.; Poli, F. Phytochemical analysis and antibacterial activity towards methicillin-resistant *Staphylococcus aureus* of leaf extracts from *Argania spinosa* (L.) Skeels. *Plant Biosystem.* **2017**, *151*, 649–656. [CrossRef]

209. Rahman, M.M.; Polfreman, D.; MacGeachan, J.; Gray, A.I. Antimicrobial activities of *Barringtonia acutangula*. *Phytother. Res.* **2005**, *19*, 543–545. [CrossRef] [PubMed]

210. Pefile, S.C. A Study of the Antiherpes Simplex Virus Type 1 Properties of *Barringtonia racemosa*. Ph.D. Thesis, University of Cape, Cape Town, Africa, 2001.
211. Janmanchi, H.; Raju, A.; Degani, M.S.; Ray, M.K.; Rajan, M.G.R. Antituberculosis, antibacterial and antioxidant activities of *Aegiceras corniculatum*, a mangrove plant and effect of various extraction processes on its phytoconstituents and bioactivity. *S. Afr. J. Bot.* **2017**, *113*, 421–427. [CrossRef]
212. Gupta, V.K.; Mukherjee, K.; Roy, A. Two novel antifungals, acornine 1 and acornine 2, from the bark of mangrove plant *Aegiceras corniculatum* (Linn.) Blanco from Sundarban Estuary. *Pharmacog. Mag.* **2014**, *10*, S342.
213. Nariya, P.B.; Bhalodia, N.R.; Shukla, V.J.; Acharya, R.N. Antimicrobial and antifungal activities of *Cordia dichotoma* (Forster F.) bark extracts. *Ayu* **2011**, *32*, 585. [CrossRef] [PubMed]
214. Li, S.; Zhang, Z.; Cain, A.; Wang, B.; Long, M.; Taylor, J. Antifungal activity of camptothecin, trifolin, and hyperoside isolated from *Camptotheca acuminata*. *J. Agric. Food Chem.* **2005**, *53*, 32–37. [CrossRef]
215. Horwitz, S.B.; Chang, C.K.; Grollman, A.P. Antiviral action of camptothecin. *Antimicrob. Agents Chemother.* **1972**, *2*, 395–401. [CrossRef] [PubMed]
216. Wu, K.X.; Chu, J.J.H. Antiviral screen identifies EV71 inhibitors and reveals camptothecin-target, DNA topoisomerase 1 as a novel EV71 host factor. *Antiv. Res.* **2017**, *143*, 122–133. [CrossRef] [PubMed]
217. Kelly, D.C.; Avery, R.J.; Dimmock, N.J. Camptothecin: An inhibitor of influenza virus replication. *J. Gen. Virol.* **1974**, *25*, 427–432. [CrossRef] [PubMed]
218. Rubinstein, L.; Rein, A. Effect of camptothecin on Simian virus 40 DNA. *Nature* **1974**, *248*, 226–228. [CrossRef]
219. Pantazis, P. Camptothecin: A promising antiretroviral drug. *J. Biomed. Sci.* **1996**, *3*, 14–19. [CrossRef] [PubMed]
220. Ali, A.M.; Mackeen, M.M.; El-Sharkawy, S.H.; Hamid, J.A.; Ismail, N.H.; Ahmad, F.; Lajis, N.H. Antiviral and cytotoxic activities of some plants used in Malaysian indigenous medicine. *Pertanika J. Trop. Agric. Sci.* **1996**, *19*, 129–136.
221. Ahmed, F.; Amin, R.; Shahid, I.Z.; Sobhani, M.M.E. Antibacterial, cytotoxic and neuropharmacological activities of *Cerbera odollam* seeds. *Adv. Trad. Med.* **2008**, *8*, 323–328. [CrossRef]
222. Chu, S.Y.; Singh, H.; Ahmad, M.S.; Mamat, A.S. Phytochemical screening of antifungal biocompounds from fruits and leaves extract of *Cerbera odollam* Gaertn. *Malays. Appl. Biol.* **2015**, *44*, 75–79.
223. Pájaro-González, Y.; Cabrera-Barraza, J.; Martelo-Ramírez, G.; Oliveros-Díaz, A.F.; Urrego-Álvarez, J.; Quiñones-Fletcher, W.; Díaz-Castillo, F. In Vitro and In Silico Antistaphylococcal Activity of Indole Alkaloids Isolated from Tabernaemontana cymosa Jacq (Apocynaceae). *Sci. Pharm.* **2022**, *90*, 38. [CrossRef]
224. Ahmed, F.; Reza, M.S.H.; Shahid, I.Z.; Khatun, A.; Islam, K.K.; Ali, M.R. Antibacterial and antinociceptive activity of *Hoya parasitica*. *Hamdard Med.* **2008**, *51*, 22–26.
225. Muangrom, W.; Vajrodaya, S. Comparative phytochemistry and antibacterial properties of *Guettarda speciosa* L. In Proceedings of the 56th Kasetsart University Annual Conference, Bangkok, Thailand, 30 January–2 February 2018.
226. Prachayasittikul, S.; Buraparuangsang, P.; Worachartcheewan, A.; Isarankura-Na-Ayudhya, C.; Ruchirawat, S.; Prachayasittikul, V. Antimicrobial and antioxidative activities of bioactive constituents from *Hydnophytum formicarum* Jack. *Molecules* **2008**, *13*, 904–921. [CrossRef] [PubMed]
227. Bachala, T. Antibacterial and Antifungal activities of various extracts of *Guettarda speciosa* L. *Int. J. Phytopharmacol.* **2010**, *1*, 20–22.
228. Zhang, H.; Rothwangl, K.; Mesecar, A.D.; Sabahi, A.; Rong, L.; Fong, H.H. Lamiridosins, hepatitis C virus entry inhibitors from *Lamium album*. *J. Nat. Prod.* **2009**, *72*, 2158–2162. [CrossRef]
229. Ge, L.; Wan, H.; Tang, S.; Chen, H.; Li, J.; Zhang, K.; Zhou, B.; Fei, J.; Wu, S.; Zeng, X. Novel caffeoylquinic acid derivatives from *Lonicera japonica* Thunb. flower buds exert pronounced anti-HBV activities. *RSC Adv.* **2018**, *8*, 35374–35385. [CrossRef] [PubMed]
230. De Carvalho Junior, A.R.; Oliveira Ferreira, R.; de Souza Passos, M.; da Silva Boeno, S.I.; Glória das Virgens, L.D.L.; Ventura, T.L.B.; Calixto, S.D.; Lassounskaia, E.; de Carvalho, M.G.; Braz-Filho, R.; et al. Antimycobacterial and nitric oxide production inhibitory activities of triterpenes and alkaloids from *Psychotria nuda* (Cham. & Schltdl.) Wawra. *Molecules* **2019**, *24*, 1026.
231. Hanh, N.P.; Phan, N.H.T.; Thuan, N.T.D.; Hanh, T.T.H.; Vien, L.T.; Thao, N.P.; Thanh, N.V.; Cuong, N.X.; Binh, N.Q.; Nam, N.H.; et al. Two new simple iridoids from the ant-plant *Myrmecodia tuberosa* and their antimicrobial effects. *Nat. Prod. Res.* **2016**, *30*, 2071–2076. [CrossRef]
232. Kapadia, G.J.; Sharma, S.C.; Tokuda, H.; Nishino, H.; Ueda, S. Inhibitory effect of iridoids on Epstein-Barr virus activation by a short-term in vitro assay for anti-tumor promoters. *Cancer Lett.* **1996**, *102*, 223–226. [CrossRef]
233. Pollo, L.A.; Martin, E.F.; Machado, V.R.; Cantillon, D.; Wildner, L.M.; Bazzo, M.L.; Waddell, S.J.; Biavatti, M.W.; Sandjo, L.P. Search for antimicrobial activity among fifty-two natural and synthetic compounds identifies anthraquinone and polyacetylene classes that inhibit *Mycobacterium tuberculosis*. *Front. Microbiol.* **2021**, *11*, 622629. [CrossRef] [PubMed]
234. Manzione, M.G.; Martorell, M.; Sharopov, F.; Bhat, N.G.; Kumar, N.V.A.; Fokou, P.V.T.; Pezzani, R. Phytochemical and pharmacological properties of asperuloside, a systematic review. *Eur. J. Pharmacol.* **2020**, *883*, 173344. [CrossRef]
235. Mahmood, N.; Moore, P.S.; De Tommasi, N.; De Simone, F.; Colman, S.; Hay, A.J.; Pizza, C. Inhibition of HIV infection by caffeoylquinic acid derivatives. *Antiv. Chem. Chemother.* **1993**, *4*, 235–240. [CrossRef]
236. Ticona, L.A.; Bermejo, P.; Guerra, J.A.; Abad, M.J.; Beltran, M.; Lázaro, R.M.; Alcamí, J.; Bedoya, L.M. Ethanolic extract of *Artemisia campestris* subsp. glutinosa (Besser) Batt. inhibits HIV–1 replication in vitro through the activity of terpenes and flavonoids on viral entry and NF–κB pathway. *J. Ethnopharmacol.* **2020**, *263*, 113163. [CrossRef]

237. Chokchaisiri, R.; Suaisom, C.; Sriphota, S.; Chindaduang, A.; Chuprajob, T.; Suksamrarn, A. Bioactive flavonoids of the flowers of *Butea monosperma*. *Chem. Pharm. Bull.* **2009**, *57*, 428–432. [CrossRef]
238. Kuo, Y.C.; Chen, C.C.; Tsai, W.J.; Ho, Y.H. Regulation of herpes simplex virus type 1 replication in Vero cells by *Psychotria serpens*: Relationship to gene expression, DNA replication, and protein synthesis. *Antiv. Res.* **2001**, *51*, 95–109. [CrossRef]
239. Yu, S.; Liu, B.C.; Lai, P.X. Chemical composition, antibacterial and antioxidant activities of the essential oil of *Psychotria serpens*. *Chem. Nat. Comp.* **2020**, *56*, 748–750. [CrossRef]
240. Bose, S.; Bose, A. Antimicrobial activity of *Acanthus ilicifolius* (L.). *Indian J. Pharm. Sci.* **2008**, *70*, 821. [CrossRef] [PubMed]
241. Ravikumar, S.; Raja, M.; Gnanadesigan, M. Antibacterial potential of benzoate and phenylethanoid derivatives isolated from *Acanthus ilicifolius* L. leaf extracts. *Nat. Prod. Res.* **2012**, *26*, 2270–2273. [CrossRef] [PubMed]
242. Wei, P.H.; Wu, S.Z.; Mu, X.M.; Xu, B.; Su, Q.J.; Wei, J.L.; Yang, Y.; Qin, B.; Xie, Z.C. Effect of alcohol extract of *Acanthus ilicifolius* L. on anti-duck hepatitis B virus and protection of liver. *J. Ethnopharmacol.* **2015**, *160*, 1–5. [CrossRef] [PubMed]
243. Illian, D.N.; Basyuni, M.; Wati, R.; Hasibuan, P.A.Z. Polyisoprenoids from *Avicennia marina* and *Avicennia lanata* inhibit WiDr cells proliferation. *Pharmacog. Mag.* **2018**, *14*, 513.
244. Lalitha, P.; Parthiban, A.; Sachithanandam, V.; Purvaja, R.; Ramesh, R. Antibacterial and antioxidant potential of GC-MS analysis of crude ethyl acetate extract from the tropical mangrove plant *Avicennia officinalis* L. *S. Afr. J. Bot.* **2021**, *142*, 149–155. [CrossRef]
245. Vadlapudi, V.; Naidu, K.C. Bioactivity of marine mangrove plant *Avicennia alba* on selected plant and oral pathogens. *Int. J. ChemTech Res.* **2009**, *1*, 1213–1216.
246. Subrahmanyam, C.; Kumar, S.R.; Reddy, G.D. Bioactive diterpenes from the mangrove *Avicennia officinalis* Linn. *Indian J. Chem.* **2006**, *45*, 2556–2557. [CrossRef]
247. Nguyen, T.S.; Xia, N.H.; Van Chu, T.; Van Sam, H. Ethnobotanical study on medicinal plants in traditional markets of Son La province, Vietnam. *For. Soc.* **2019**, *3*, 171–192. [CrossRef]
248. Chen, J.L.; Blanc, P.; Stoddart, C.A.; Bogan, M.; Rozhon, E.J.; Parkinson, N.; Ye, Z.; Cooper, R.; Balick, M.; Nanakorn, W.; et al. New iridoids from the medicinal plant *Barleria prionitis* with potent activity against respiratory syncytial virus. *J. Nat. Prod.* **1998**, *61*, 1295–1297. [CrossRef]
249. Yecheng, D.; Zhen, Y.; Yanzhen, Y.; Xiulian, B. Inhibitory activity against plant pathogenic fungi of extracts from *Myoporum bontioides* A. Gray and indentification of active ingredients. *Pest Manag. Sci.* **2008**, *64*, 203–207. [CrossRef]
250. Dong, L.M.; Huang, L.L.; Dai, H.; Xu, Q.L.; Ouyang, J.K.; Jia, X.C.; Gu, W.X.; Tan, J.W. Anti-MRSA sesquiterpenes from the semi-mangrove plant *Myoporum bontioides* A. Gray. *Mar. Drugs* **2018**, *16*, 438. [CrossRef] [PubMed]
251. Minh, T.T.; Toan, H.K.; Quang, L.D.; Hoang, V.D. Myobontioids AD and antifungal metabolites from the leaves of *Myoporum bontioides* A. Gray. *Nat. Prod. Res.* **2021**, 1–7. [CrossRef] [PubMed]
252. Lirio, S.B.; Macabeo, A.P.G.; Paragas, E.M.; Knorn, M.; Kohls, P.; Franzblau, S.G.; Wang, Y.; Aguinaldo, M.A.M. Antitubercular constituents from *Premna odorata* Blanco. *J. Ethnopharmacol.* **2014**, *154*, 471–474. [CrossRef] [PubMed]
253. Tangarife-Castaño, V.; Roa-Linares, V.; Betancur-Galvis, L.A.; Durán García, D.C.; Stashenko, E.; Mesa-Arango, A.C. Antifungal activity of Verbenaceae and Labiatae families essential oils. *Pharmacologyonline* **2012**, *1*, 133–145.
254. Rahman, A.; Shanta, Z.S.; Rashid, M.A.; Parvin, T.; Afrin, S.; Khatun, M.K.; Sattar, M.A. In vitro antibacterial properties of essential oil and organic extracts of *Premna integrifolia* Linn. *Arabian J. Chem.* **2016**, *9*, S475–S479. [CrossRef]
255. Nguyen, Q.V.; Eun, J.B. Antimicrobial activity of some Vietnamese medicinal plants extracts. *J. Med. Plants Res.* **2013**, *4*, 2597–2605.
256. Sheeba, S.N.; Ariharan, V.N.; Mary, J.V.J.; Bai, S.M.M.; Paul, J.V. Phytochemical and biological screening of organic Solvent extracts of *Ipomoea pes-caprae* flower. *Ann. Rom. Soc. Cell Biol.* **2021**, *25*, 7800–7821.
257. Ryan, D.H.; Katherine, H.H.; Taylor, J.W.; Gajendra, S. Traditional Tongan treatments for infections: Bioassays and ethnobotanical leads for activity. *J. Med. Plants Res.* **2014**, *8*, 1215–1222.
258. Srimoon, R.; Ngiewthaisong, S. Antioxidant and antibacterial activities of Indian marsh fleabane (*Pluchea indica* (L.) Less). *Asia-Pac. J. Sci. Technol.* **2015**, *20*, 144–154.
259. Locher, C.P.; Witvrouw, M.; De Béthune, M.P.; Burch, M.T.; Mower, H.F.; Davis, H.; Lasure, A.; Pauwels, R.; De Clercq, E.; Vlietinck, A.J. Antiviral activity of Hawaiian medicinal plants against human immunodeficiency virus type-1 (HIV-1). *Phytomed* **1996**, *2*, 259–264. [CrossRef]
260. Manimegalai, B.; Inbathamizh, L.; Ponnu, T.M. In vitro studies on antimicrobial activity and phytochemical screening of leaf extracts of *Scaevola taccada*. *Int. J. Pharm. Pharm. Sci.* **2012**, *4*, 367–370.
261. Suthiwong, J.; Thongsri, Y.; Yenjai, C. A new furanocoumarin from the fruits of *Scaevola taccada* and antifungal activity against *Pythium insidiosum*. *Nat. Prod. Res.* **2017**, *31*, 453–459. [CrossRef] [PubMed]
262. Rameshthangam, P.A.; Ramasamy, P. Antiviral activity of bis (2-methylheptyl) phthalate isolated from *Pongamia pinnata* leaves against White Spot Syndrome Virus of *Penaeus monodon* Fabricius. *Virus Res.* **2007**, *126*, 38–44. [CrossRef] [PubMed]
263. Sudheer, N.S.; Philip, R.; Singh, I.B. In vivo screening of mangrove plants for anti WSSV activity in *Penaeus monodon*, and evaluation of *Ceriops tagal* as a potential source of antiviral molecules. *Aquacult* **2011**, *311*, 36–41. [CrossRef]
264. Rahmawati, N.; Mustofa, F.I.; Haryanti, S. Diversity of medicinal plants utilized by To Manui ethnic of Central Sulawesi, Indonesia. *Biodiversitas J. Biol. Divers.* **2020**, *21*, 375–392. [CrossRef]
265. Chusri, S.; Sinvaraphan, N.; Chaipak, P.; Luxsananuwong, A.; Voravuthikunchai, S.P. Evaluation of antibacterial activity, phytochemical constituents, and cytotoxicity effects of Thai household ancient remedies. *J. Altern. Compl. Med.* **2014**, *20*, 909–918. [CrossRef]

266. Swamy, V.; Ninge, K.; Sudhakar, R. Antimicrobial activity of *Casuarina equisetifolia*. *Int. J. Innov. Pharm. Dev.* **2013**, *1*, 49–57.
267. Buenz, E.J. Hepatocytes detoxify *Atuna racemosa* extract. *Exp. Biol. Med.* **2006**, *231*, 1739–1743. [CrossRef]
268. Wiart, C. *Medicinal Plants in the Asia Pacific for Zoonotic Pandemics*; CRC Press: Boca Raton, FL, USA, 2021.
269. Brijesh, S.; Daswani, P.G.; Tetali, P.; Rojatkar, S.R.; Antia, N.H.; Birdi, T.J. Studies on *Pongamia pinnata* (L.) Pierre leaves: Understanding the mechanism(s) of action in infectious diarrhea. *J. Zhejiang Univ. Sci. B.* **2006**, *7*, 665–674. [CrossRef]
270. Thaman, R.R.; Thomson, L.A.; DeMeo, R.; Areki, F.; Elevitch, C.R. Intsia bijuga (vesi). In *Species Profiles for Pacific Island Agroforestry*; Academic Publishing: Cambridge, MA, USA, 2006.
271. Islam, A.R.; Hasan, M.M.; Islam, M.T.; Tanaka, N. Ethnobotanical study of plants used by the Munda ethnic group living around the Sundarbans, the world's largest mangrove forest in southwestern Bangladesh. *J. Ethnopharmacol.* **2022**, *285*, 114853. [CrossRef]
272. Walker, T. *An Examination of Medicinal Ethnobotany and Biomedicine Use in Two Villages on the Phnom Kulen Plateau*; Hollins University: Roanoke, VA, USA, 2017.
273. Li, D.L.; Xing, F.W. Ethnobotanical study on medicinal plants used by local Hoklos people on Hainan Island, China. *J. Ethnopharmacol.* **2016**, *194*, 358–368. [CrossRef] [PubMed]
274. Duraipandiyan, V.; Ignacimuthu, S. Antifungal activity of traditional medicinal plants from Tamil Nadu, India. *Asian Pac. J. Trop. Biomed* **2011**, *1*, S204–S215. [CrossRef]
275. Ju, S.K.; Semotiuk, A.J.; Krishna, V. Indigenous knowledge on medicinal plants used by ethnic communities of South India. *Ethnobot. Res. Appl.* **2019**, *18*, 1–112.
276. Janni, K. Plants in Samoan Culture. The Ethnobotany of Samoa. *Econ. Bot.* **2002**, *56*, 100. [CrossRef]
277. Herlina, R.; Rahayuningsih, M.; Iswari, R.S. Species richness of medicinal plants in the Dieng Plateau. *J. Innov. Sci. Educ.* **2019**, *8*, 116–122.
278. Uy, M.M.; Garcia, K.I. Evaluation of the antioxidant properties of the leaf extracts of Philippine medicinal plants *Casuarina equisetifolia* Linn, *Cyperus brevifolius* (Rottb) Hassk, *Drymoglossum piloselloides* Linn, *Ixora chinensis* Lam, and *Piper abbreviatum* Opiz. *Adv. Agric. Bot.* **2015**, *7*, 71–79.
279. Tomar, S.; Jawanjal, P. Overview of *Pentatropis capensis* (Asclepiadaceae)—An extra pharmacopoeial plant. *J. Ayu Herb. Med.* **2019**, *5*, 66–69. [CrossRef]
280. Wiart, C. *Medicinal Plants of Asia and the Pacific; Drugs for the Future?* World Scientific Publishing Co. Inc.: Singapore, 2006.
281. Thomson, L.A.; Englberger, L.; Guarino, L.; Thaman, R.R.; Elevitch, C.R. Pandanus tectorius (pandanus). In *Species Profiles for Pacific Island Agroforestry*; ResearchGate GmbH: Berlin, Germany, 2006; p. 28.
282. Medhi, R.P.; Chakrabarti, S. Traditional knowledge of NE people on conservation of wild orchids. *Indian J. Tradit. Knowl.* **2009**, *8*, 11–16.
283. Akhter, M.; Hoque, M.M.; Rahman, M.; Huda, M.K. Ethnobotanical investigation of some orchids used by five communities of Cox's Bazar and Chittagong hill tracts districts of Bangladesh. *J. Med. Plants Stud.* **2017**, *5*, 265–268.
284. Rahmatullah, M.; Mollik, M.A.H.; Islam, M.K.; Islam, M.R.; Jahan, F.I.; Khatun, Z.; Seraj, S.; Chowdhury, M.H.; Islam, F.; Miajee, Z.U.M.; et al. A survey of medicinal and functional food plants used by the folk medicinal practitioners of three villages in Sreepur Upazilla, Magura district, Bangladesh. *Am. Eurasian J. Sustain. Agric.* **2010**, *4*, 363–373.
285. Primavera, J.; Sadaba, R.; Lebata, M.; Hazel, J.; Altamirano, J. *Handbook of Mangroves in the Philippines-Panay*; Aquaculture Department, Southeast Asian Fisheries Development Center: Tigbauan, Philippines, 2004.
286. Latayada, F.S.; Uy, M.M. Screening of the antioxidant properties of the leaf extracts of Philippine medicinal plants *Ficus nota* (Blanco) Merr., *Metroxylon sagu* Rottb., *Mussaenda philippica* A. Rich., *Inocarpus fagifer*, and *Cinnamomum mercadoi* Vidal. *Bull. Environ. Pharmacol. Life Sci.* **2016**, *5*, 18–24.
287. Wiart, C. *Ethnopharmacology of Medicinal Plants: Asia and the Pacific*; Springer Science & Business Media: Berlin/Heidelberg, Germany, 2007.
288. Motley, T.J. The ethnobotany of Fagraea Thunb. (Gentianaceae): The timber of malesia and the scent of polynesia. *Econ. Bot.* **2004**, *58*, 396–409. [CrossRef]
289. Paramita, S. Tahongai (*Kleinhovia hospita* L.): Review sebuah tumbuhan obat dari Kalimantan Timur. *Indones. J. Plant Med.* **2016**, *9*, 29–36. [CrossRef]
290. Duke, N.C. *Australia's Mangroves: The Authoritative Guide to Australia's Mangrove Plants*; MER: Brisbane, Australia, 2006.
291. Liebezeit, G.; Rau, M.T. New Guinean mangroves—Traditional usage and chemistry of natural products. *Senckenberg. Marit.* **2006**, *36*, 1–10. [CrossRef]
292. Cambie, R.C.; Ash, J. *Fijian Medicinal Plants*; CSIRO Publishing: Clayton, Australia, 1994.
293. Khare, C.P. *Indian Medicinal Plants: An Illustrated Dictionary*; Springer Science & Business Media: Berlin/Heidelberg, Germany, 2008.
294. Reverter, M.; Bontemps, N.N.; Lecchini, D.; Banaigs, B.; Sasal, P. Use of plant extracts in fish aquaculture as an alternative to chemotherapy: Current status and future perspectives. *Aquaculture* **2014**, *433*, 50–61. [CrossRef]
295. Soto-Rodriguez, S.A.; Gomez-Gil, B.; Lozano, R.; del Rio-Rodríguez, R.l.; Diéguez, A.L.; Romalde, J.L. Virulence of *Vibrio harveyi* responsible for the "Bright-red" Syndrome in the Pacific white shrimp *Litopenaeus vannamei*. *J. Invertebr. Pathol.* **2012**, *109*, 307–317. [CrossRef]
296. Davies, T.K.; Lovelock, C.E.; Pettit, N.E.; Grierson, P.F. Short-term microbial respiration in an arid zone mangrove soil is limited by availability of gallic acid, phosphorus and ammonium. *Soil Biol. Biochem.* **2017**, *115*, 73–81. [CrossRef]

297. Liu, Y.; Li, F.; Huang, Q. Allelopathic effects of gallic acid from Aegiceras corniculatum on *Cyclotella caspia*. *J. Env. Sci.* **2013**, *25*, 776–784. [CrossRef]

298. Alonso-Rodrıguez, R.; Páez-Osuna, F. Nutrients, phytoplankton and harmful algal blooms in shrimp ponds: A review with special reference to the situation in the Gulf of California. *Aquaculture* **2003**, *219*, 317–336. [CrossRef]

299. Gao, J.; Zuo, H.; Yang, L.; He, J.H.; Niu, S.; Weng, S.; He, J.; Xu, X. Long-term influence of cyanobacterial bloom on the immune system of *Litopenaeus vannamei*. *Fish Shellfish. Immunol.* **2017**, *61*, 79–85. [CrossRef] [PubMed]

300. Gil-Turnes, M.S.; Hay, M.E.; Fenical, W. Symbiotic marine bacteria chemically defend crustacean embryos from a pathogenic fungus. *Science* **1989**, *246*, 116–118. [CrossRef]

301. Haoliang, L.; Chongling, Y.; Jingchun, L. Low-molecular-weight organic acids exuded by Mangrove (*Kandelia candel* (L.) Druce) roots and their effect on cadmium species change in the rhizosphere. *Environ. Exp. Bot.* **2007**, *61*, 159–166. [CrossRef]

302. White, S.L.; Rainbow, P.S. Regulation and accumulation of copper, zinc and cadmium by the shrimp *Palaemon elegans*. *Mar. Ecol. Prog. Ser.* **1982**, *8*, 95–101. [CrossRef]

303. Rozirwan, R.; Muda, H.I.; Ulqodry, T.Z. Antibacterial potential of *Actinomycetes* isolated from mangrove sediment in Tanjung Api-Api, South Sumatra, Indonesia. *Biodiversitas J. Biol. Divers* **2020**, *21*, 5723–5728. [CrossRef]

Review

Progress in Isoindolone Alkaloid Derivatives from Marine Microorganism: Pharmacology, Preparation, and Mechanism

Sijin Hang [1,†], Hui Chen [2,†], Wenhui Wu [1], Shiyi Wang [3], Yiwen Fang [4], Ruilong Sheng [5], Qidong Tu [6,*] and Ruihua Guo [1,7,8,*]

[1] College of Food Science and Technology, Shanghai Ocean University, Shanghai 201306, China; sjhang2022@163.com (S.H.); whwu@shou.edu.cn (W.W.)
[2] Shanghai Engineering Center of Hadal Science and Technology, College of Marine Sciences, Shanghai Ocean University, Shanghai 201306, China; h-chen@shou.edu.cn
[3] AIEN Institute, Shanghai Ocean University, Shanghai 201306, China; may.canali@163.com
[4] Department of Chemistry, College of Science, Shantou University, Shantou 515063, China; ywfang@stu.edu.cn
[5] CQM-Centro de Química da Madeira, Campus da Penteada, Universidade da Madeira, 9000-390 Funchal, Portugal; ruilong.sheng@staff.uma.pt
[6] Jiangxi Provincial Key Laboratory of Drug Design and Evaluation, School of Pharmacy, Jiangxi Science & Technology Normal University, Nanchang 330013, China
[7] Shanghai Engineering Research Center of Aquatic-Product Processing & Preservation, Shanghai 201306, China
[8] Laboratory of Quality and Safety Risk Assessment for Aquatic Products on Storage and Preservation (Shanghai), Ministry of Agriculture, Shanghai 201306, China
[*] Correspondence: 1020100994@jxstnu.edu.cn (Q.T.); rhguo@shou.edu.cn (R.G.)
[†] These two authors contributed equally to this work.

Abstract: Compound **1** (SMTP-7, also FGFC1), an isoindolone alkaloid from marine fungi *Starchbotrys longispora* FG216 and fungi *Stachybotrys microspora* IFO 30018, possessed diverse bioactivities such as thrombolysis, anti-inflammatory and anti-oxidative properties, and so on. It may be widely used for the treatment of various diseases, including cerebral infarction, stroke, ischemia/reperfusion damage, acute kidney injury, etc. Especially in cerebral infarction, compound **1** could reduce hemorrhagic transformation along with thrombolytic therapy, as the traditional therapies are accompanied with bleeding risks. In the latest studies, compound **1** selectively inhibited the growth of NSCLC cells with EGFR mutation, thus demonstrating its excellent anti-cancer activity. Herein, we summarized pharmacological activities, preparation of staplabin congeners—especially compound **1**—and the mechanism of compound **1,** with potential therapeutic applications.

Keywords: FGFC1; thrombus; fibrinolytic; *Stachybotrys longispora* FG216; *Stachybotrys microspora* IFO 30018

1. Introduction

The hemostatic system, consisting of the coagulation and fibrinolytic systems, is a vital physiological function in inhibiting hemorrhage and accelerating wound healing [1,2]. Fibrinolysis is regulated by plasminogen and activated by physiologic plasminogen activators: tissue-type plasminogen activator (t-PA) and urokinase-type plasminogen activator (u-PA). Meanwhile, the level of activated plasmin could be inhibited through the block of plasminogen activation by several specific molecules [3,4]. However, various clinical cases indicated that hereditary or acquired factors would enhance or weaken fibrinolytic systems, causing the disorder between the coagulation and fibrinolytic systems, which led to hemorrhage or thrombosis. Compared with a hemorrhage, thrombus formation develops much more gradually and imperceptibly, leading many patients' deaths [5]. Current drugs on thrombosis include aspirin, ticlopidine, warfarin, and heparin; however, the risk of bleeding is a concern [6]. Therefore, small molecules, with different mechanisms of fibrinolysis action, are desired for new antithrombotics and thrombolytics.

Natural products, historically, possess various bioactivities for the treatment of human diseases [7–12]. Marine products, due to the unique marine environments, provide special structures of compounds differing from terrestrial ones. Up to now, over 28,175 chemical entities have been identified, with hundreds of new compounds discovered every year [13]. Numerous marine molecules have been approved for clinical treatments, such as anticancer cytarabine and analgesic ziconotide [14–16].

In 1996, Kohyama et al. isolated SMTP-1 from fungi *Stachybotrys microspora* IFO 30018, with 20–30% higher plasminogen-fibrin binding action than staplabin, indicating the potential for thrombolysis therapy [17–19]. Staplabin, a triprenyl phenol, was the basic core of the SMTP family, and SMTP-1, as well as other congeners, were variants of staplabin (Figure 1) [17,20]. Then, a series of congeners, containing a tricyclic γ-lactam moiety, a geranylmethyl side-chain, and an N-linked side-chain, were isolated and showed plasminogen activation [21]. Compound **1** (Figure 2), with two staplabin cores bridged by ornithine, could increase urokinase-catalyzed plasminogen activation, fibrin binding of plasminogen, and fibrinolysis mediated by urokinase and plasminogen [20]. Meanwhile, it showed excellent clot clearance activity in vivo [22,23]. In a rat pulmonary embolism model, compound **1** (5 mg/kg) enhanced, by three-fold, the clot clearance rate above the spontaneous clearance group. Moreover, clot clearance of compound **1** was enhanced, further, in combination with u-PA [23].
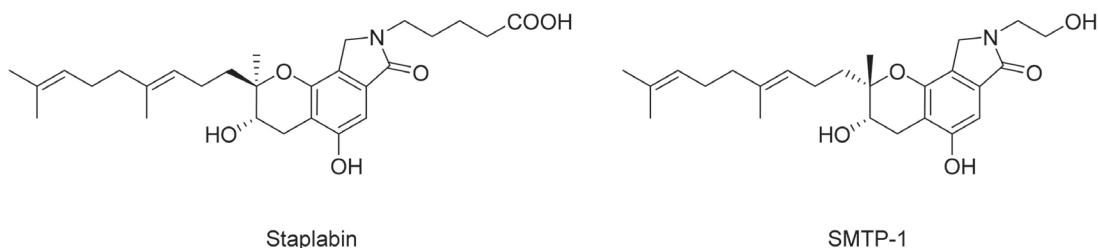
Staplabin   SMTP-1

Figure 1. Structures of staplabin and SMTP-1.

At present, more than 60 congeners of staplabin have been isolated, which not only performed fibrinolysis activity but also exhibited various effects, such as anti-inflammatory, neuroprotection, and anti-cancer properties [1]. Other modified derivatives and structure–function relationships of compound **1** have also been studied. Scientists also confirmed the absolute configuration and preparation methods of congeners and derivatives, which shared similar absolute configuration (8S, 9S) and a staplabin core. Meanwhile, most monomeric analogues could be obtained by replacing the ornthine with non-basic amino acids or simple amines [24,25]. Herein, we focused on the diverse biological activities of compound **1**, which is a congener of staplabin (Figure 2).

Figure 2. *Cont.*

9, SMTP-6D

10, SMTP-16

11, SMTP-19

12, SMTP-22

13, SMTP-25

14, SMTP-26

15, SMTP-28

16, SMTP-33

17, SMTP-43

18, SMTP-44D

19, SMTP-54

20, SMTP-55
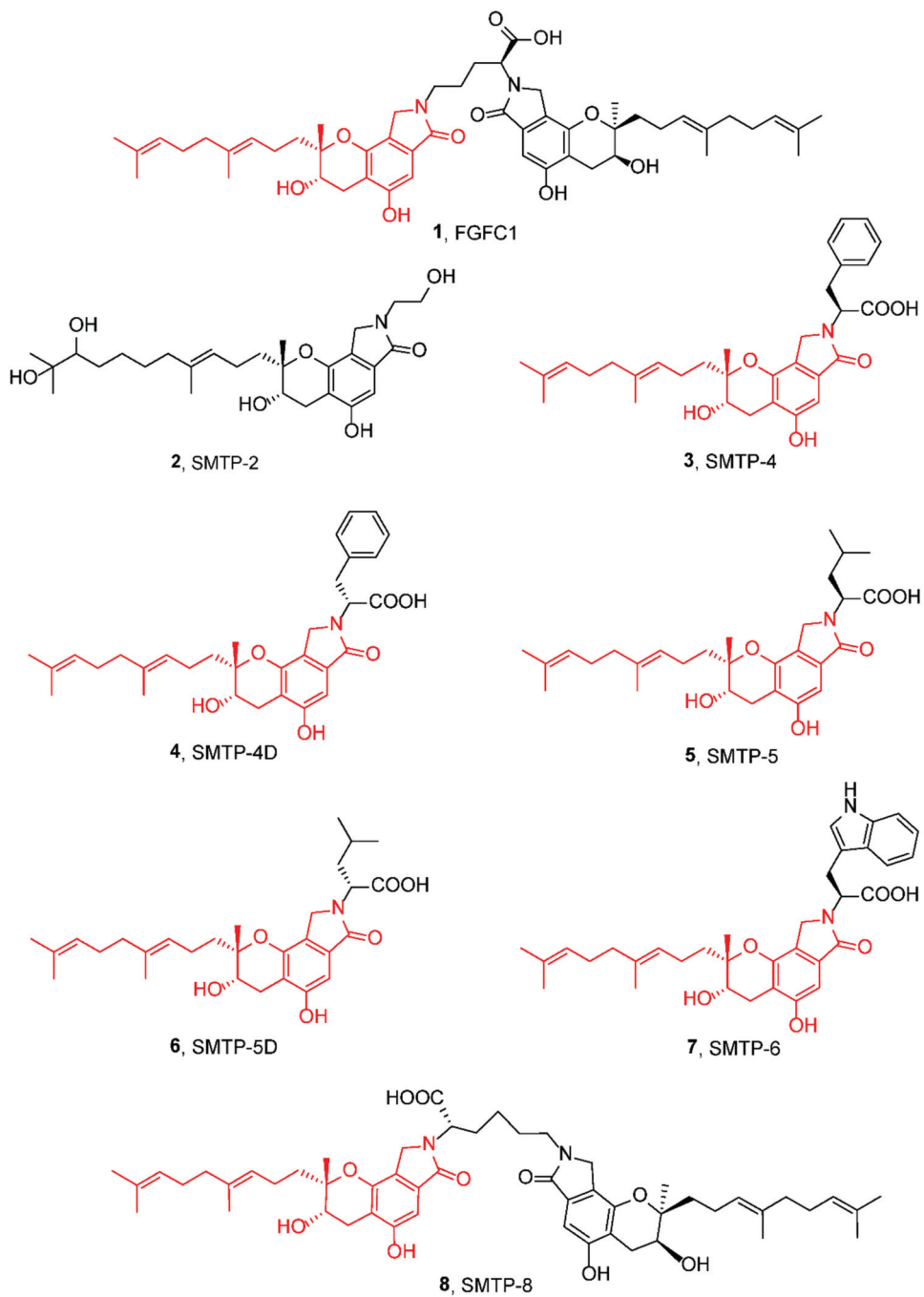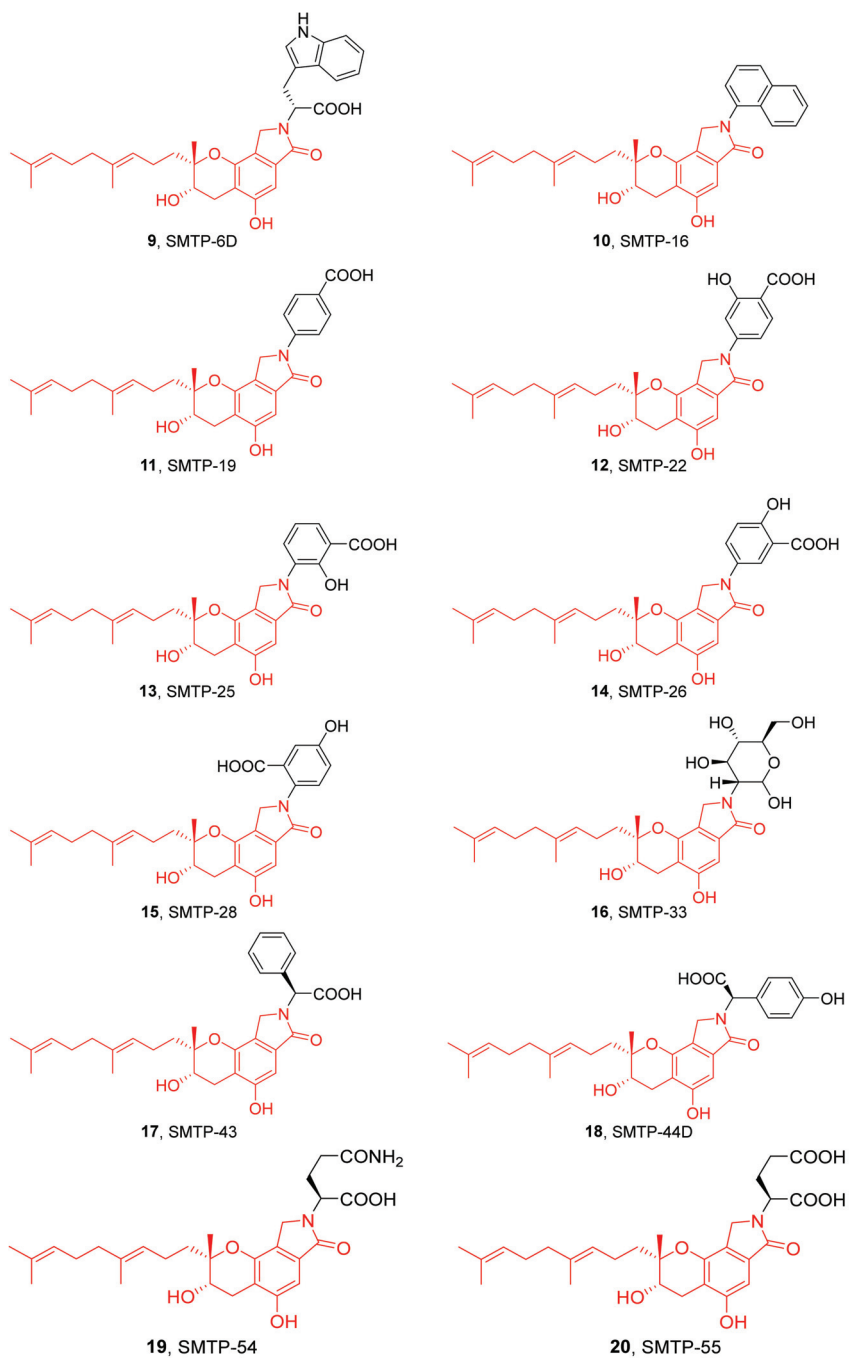
Figure 2. *Cont.*
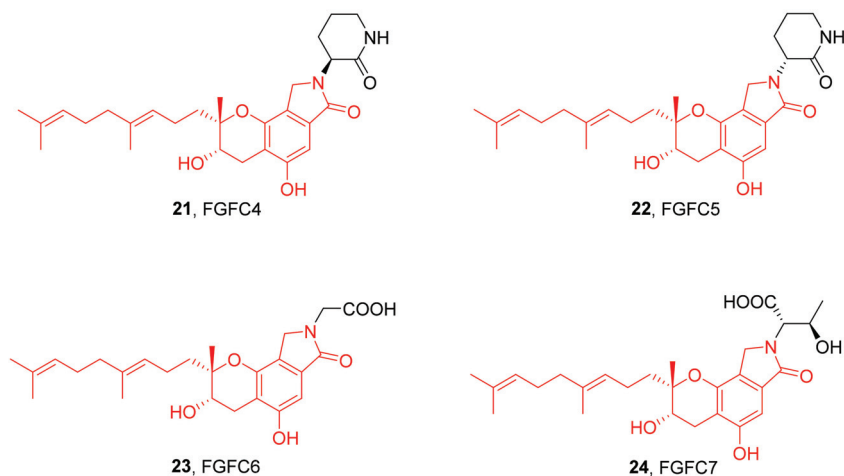
Figure 2. Structures of congeners and derivatives of staplabin.

2. Pharmacological Activity

2.1. Thrombolytic Activity

Thromboembolic disease is a main cause of mortality and disability. For instance, stroke is responsible for 5.2% of all mortalities in the world [26]. Most of them are ischemic strokes, which would trigger transient or permanent occlusion of cerebral vessels causing brain infarcts, cerebral tissue death, and focal neuronal damage after blocking for 6 h [27]. Therefore, the key to saving stroke patients is solving thromboembolism in an efficient way. It is needed to search for more potent and safer drugs for the inhibition and treatment of ischemic symptoms.

In 1999, Hu et al. isolated compound **1** from the fungus *S. microspora* IFO 30018, with a preliminary determination for its plasminogen activation and fibrinolysis activity at 80–150 μM in vitro [20]. In 2010, Hashimoto et al. established a novel cerebral infarction model for predicting cerebral infarction, in which generated embolus transferred to the brain in the right common carotid artery of Mongolian gerbils, induced by acetic acid [28]. In the same year, they assessed the therapeutic effect of compound **1** and t-PA in the cerebral infarction model [29]. The fibrinolytic activity of compound **1** (<20% of positive control) was lower than t-PA (>140% of positive control) in the 3 h after administration, but the activity of compound **1** increased about 3.5-fold during 1–3 h and was higher than t-PA after 3 h. It was attributed that the activity of compound **1** gradually increased. Meanwhile, compound **1** extended the therapeutic time window. Compared with a clear infarct in the cerebral hemisphere by t-PA (10 mg/kg) treatment, there was no visible infarction in the group of compound **1** at 3 h after ischemia. More importantly, there was little hemorrhagic region with 10 mg/kg of compound **1**, suggesting that it is a latent safe cerebral infarction therapy method. Hu et al., (2012) disclosed that compound **1** enhanced plasmin generation in vivo [20]. The level of plasmin-α2-antiplasmin complex, an indicator of plasmin formation, increased by 1.5-fold in male ICR mice after the treatment with 5 and 10 mg/kg of compound **1**. In 2014, the antithrombotic activity of compound **1** was further demonstrated in the male cynomolgus monkey model [30,31], which achieved excellent effects (Table 1). In addition, Ito et al. found that the combination therapy with warfarin and compound **1**, in the middle cerebral artery occlusion, improved the treatment safety and reduced hemorrhagic transformation [32]. Compound **1**, as a safe thrombolytic agent, relieved the side effects, such as severe infarction, edema, and hemorrhage, induced by warfarin in the middle cerebral artery occlusion model. All mice treated with compound **1** survived and the hemorrhagic severity score (1.3 ± 0.5) indicated decreased hemorrhagic transformation.

Table 1. The antithrombotic effect of compound **1** in the severe embolic stroke monkey model.

The Antithrombotic Effects	Efficacy (10 mg/kg)
consistent clot clearance	$43.3 \pm 40.5\%$
thrombotic middle cerebral artery occlusion recanalization	32.5-fold
neurologic deficit amelioration	29%
cerebral infarct reduction	46%
cerebral hemorrhage decrease	51%
infarct, edema and clot sizes reduction	65%, 37%, and 55%, respectively

Then, Wang et al. isolated compound **1** from a rare marine fungus *Stachybotrys longispora* FG216 and evaluated its fibrinolysis activity [33]. Additionally, 0.1–0.4 mmol/L of compound **1** increased the Glu-plasminogen and Lys-plasminogen activation by 2.05–11.44 times in vitro. Meanwhile, 10 mg/kg compound **1** dissolved most pulmonary thrombus in the Wistar rat in vivo. Yan et al. further researched the thrombolysis and hemorrhagic activities of compound **1**, from *S. longispora* FG216, in vitro and on acute pulmonary embolism Wistar rat model in vivo [34]. Compound **1**, from 5 to 25 μM, induced fibrin hydrolysis in vitro; moreover, its thrombolytic activity was evaluated with fluorescence lung tissues in vivo. It was observed that compound **1**, of 5 and 10 mg/kg, displayed effective dissolving capacity (less fluorescence halo). Meanwhile, the euglobulin lysis time (ELT) was shortened for 30 s by the treatment of compound **1** in the Wistar rat model. Shortening ELT was related to the activation of the fibrinolytic system. Therefore, compound **1** exhibited fibrinolytic activity in vivo. Compound **1** (5, 10, and 25 mg/kg), especially, did not induce fibrinogenolysis at 30 min and 2 h after administration, which suggested that compound **1** reduced the risk of hemorrhage. Thus, compound **1** was a potential thrombolytic agent without hemorrhage [34]. In 2021, Gao et al. detected that compound **1**, with low concentration (0.096 mM), enhanced fibrinolytic activity by 2.2-fold in vitro; however, it inhibited fibrinolytic activity at excess doses (above 0.24 mM) [35].

Congeners **3**, **5**, and **7** enhanced fibrinolysis activities at 0.25 mM, in the ^{125}I-Fibrin degradation experiment, by 2.3-fold, 1.9-fold, and 2.7-fold, respectively [36]. Congener **8** (80 μM) also increased fibrinolysis activity by eight-fold in the fibrin binding of ^{125}I-plasminogen [20]. In 2003, Hu et al. isolated congeners **4**, **6,** and **9** with the activation effect on the urokinase-catalyzed plasminogen in vitro [24]. In 2012, congeners **11**–**13**, isolated from *S. microspore*, showed similar plasminogen activation activities when compared with compound **1** [37]. In 2018, Shibata et al. evaluated fibrinolysis activities of congeners **12** and **17** in an acetic acid-induced cerebral infarction mouse model [38]. Compared with compound **1**, of 10 mg/kg, congeners **12** and **17** reduced the size of the infarction area, neurological score, and edema percentage (Table 2).

Table 2. The fibrinolysis activities of compound **1**, as well as congeners **12** and **17**.

Fibrinolysis Activities (10 mg/kg)	Infarction Area Size Reduction	Neurological Score Reduction	Edema Percentage Reduction
Compound **1**	$4.9 \pm 1.1\%$	$1.7 \pm 0.4\%$	$5.8 \pm 1.0\%$
Congener **12**	$4.4 \pm 0.5\%$	$1.7 \pm 0.4\%$	$4.6 \pm 1.0\%$
Congener **17**	$5.7 \pm 1.2\%$	$1.5 \pm 0.5\%$	$3.3 \pm 1.4\%$

To gain a deep insight into the antithrombotic effect, many studies attempted to illustrate the detailed mechanism for compound **1**. Hashimoto et al., firstly, confirmed excellent thrombolytic activity of compound **1** (no visible infarction area after treatment with 10 mg/kg for 3 and 6 h) in an acetic acid-induced novel embolic cerebral infarction model in vivo. They hypothesized that compound **1** could relieve cerebral infarction by combined effects, giving rise to studies on other activities of compound **1** [28]. In 2010, they demonstrated that compound **1** possessed thrombolytic and anti-inflammatory activities [29]. By the treatment with compound **1**, at 3 h after ischemia, mRNA expression of interleukin-1β (IL-1β), tumor necrosis factor-α (TNF-α), and interleukin-6 (IL-6) did not increase significantly. Therefore, compound **1** ameliorated hemorrhage and neurologic deficits, with a

wide therapeutic time window in thrombolysis, by inhibiting inflammation. One year later, Akamatsu et al. further completed the anti-inflammatory mechanism of compound **1** in fibrinolysis [39]. Matrix metalloproteinase-9 (MMP-9) was significantly inhibited (92 kDa band) with compound **1** in transient focal cerebral ischemia, suggesting a cerebral neuroprotective effect of compound **1**, on ischemia/reperfusion injury, and a reduction risk for hemorrhagic transformation. Moreover, compound **1** inhibited the expression of an early superoxide anion and nitrotyrosine for 2 h after ischemia/reperfusion, so it showed anti-oxidative activity to reduce ischemia/reperfusion damage [39]. In 2014, Hanshimoto et al. observed that reactive oxygen species could cause overexpression of proinflammatory cytokines [40]. Compound **1** inhibited the overexpression of a signal transducer and activator of transcription 3, to extend the therapeutic time window in thrombolysis therapy, by exhibiting its anti-oxidative effect. In addition, Huang et al. observed the inhibitory activity of compound **1** on pro-MMP-9, which inhibited the degradation of the basal membrane and the blood–brain barrier, reducing the risk of hemorrhage [41]. Moreover, Koyanagi et al., (2014) found compound **1** performed better plasminogen activation activity with the presence of physiological cofactors [42]. Compound **1**, of 20–60 μmol/L, promoted the activation of Glu-plasminogen, by 10-fold, with phosphatidylcholine and phosphatidylserine. Meanwhile, compound **1** also showed promoted plasminogen activation activity, with the presence of gangliosides and oleic acid released from thrombus in the process of clot lysis. These endogenous cofactors might change the fifth kringle domain conformation of plasminogen to induce the interactions between compound **1** and the plasminogen, whose mechanism could be elucidated in detail in future.

Wu group also investigated the thrombolytic mechanism of compound **1**. Compound **1** of 0.1–0.4 mmol/L activated the Glu-plasminogen and Lys-plasminogen (2.05–11.44 folds), but it had no fibrinolytic activity in the absence of u-PA or a plasminogen in vitro [33]. Meanwhile, the treatment, with 10 mg/kg of compound **1** after 24 h, performed efficiently in the pulmonary embolism Wistar rat model, meaning that u-PA and plasminogen mediated its thrombolytic effect. Furthermore, Wu group detected enzymatic kinetic parameters of compound **1** by chromogenic-substrate associated with *p*-nitroaniline from the enzymatic reaction [43]. The results indicated that the increase in k_{cat} and k_{cat}/K_m activity was related to the concentration of compound **1**, which exhibited 26.5-fold and 22.8-fold activity at 40 μg/mL. Moreover, the affinity of plasminogen and pro-uPA to the enzyme substrate presented a faint decrease with an increasing concentration of compound **1**, as the K_m increased (from 0.413 to 0.484 μmol/L) along with the increasing concentration of compound **1** (0–40 μg/mL). The results further proved that reciprocal activation of pro-uPA and plasminogen was critical to the fibrinolysis activity of compound **1**, which enhanced the maximum catalytic efficiency and total catalytic activity of fibrinolysis. The fibrinolysis activity of compound **1** featured an enzymatic kinetic characteristic.

Wu group further studied the interaction mechanism between compound **1** and plasminogen [35]. The Glu-plasminogen, in the bloodstream, contains a Pan-apple domain (PAp), five kringle domains (KR1-KR5), and a serine protease domain (SP). Lysine-binding sites (LBS), in kringle domains of plasminogen, were essential for the interaction of plasminogen and compound **1** [44–46]. Compound **1**, firstly, bound the LBS of KR1, while KR1 activated and mediated the interaction between plasminogen and the C-terminal lysine moiety on fibrin. KR5 dropped from PAp and was exposed to closed plasminogen temporarily [36]. Then, compound **1** formed hydrogen bonds with Asp518 and Asp534 in KR5, which induced conformational change and structural rearrangement. After that, additional LBSs on kringle domains were exposed, leading the movement of PAp. Therefore, these additional LBSs interacted with compound **1**, causing an open conformation of plasminogen, which could be easily activated by u-PA (Figure 3). The theoretical binding mode showed that compound **1** formed a stable complex with Glu39, Thr41, and Arg43 in plasminogen with hydrogen bonds (Figure 4).
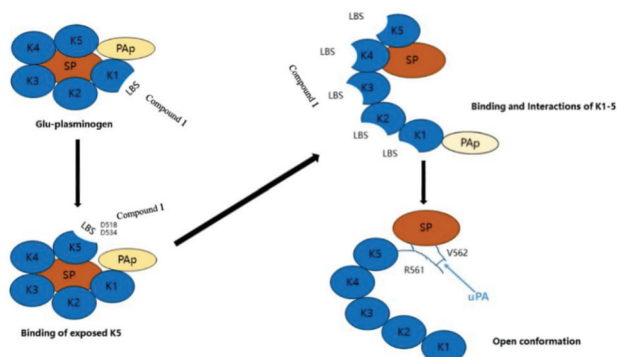
Figure 3. The mechanism of plasminogen activation by compound **1**.

(a)   (b)
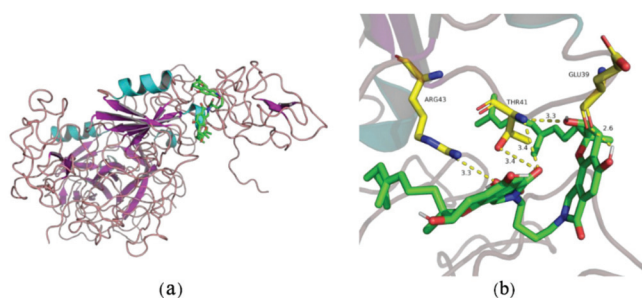
Figure 4. The interactions between compound **1** and plasminogen: (**a**) binding site; (**b**) the 3D docking model of compound **1** with plasminogen.

The structure–activity relationships of the plasminogen modulator compound **1** and its congeners have been studied in detail. Most congeners contain the same geranylmethyl side-chain, but they bear different *N*-linked side-chains. Congener **2** possessed a hydroxylated geranylmethyl side-chain [17] and could not enhance plasminogen binding to the activated plasminogen. Thus, the side-chain of geranylmethyl plays a key role in promoting plasminogen activation. In 2016, Otake et al. found that the geranylmethyl side-chain of congeners was critical to inhibitory activity of soluble epoxide hydrolase (sEH), an enzyme mediating anti-inflammatory action [47]. sEH lost inhibitory activity with the increasing number of hydroxyl groups on geranylmethyl side-chains or missing geranylmethyl side-chains, and the terminal hydroxy group of side-chain led to the damage of cellular localization. For the *N*-linked side-chain, Hasumi et al. isolated the simplest congener (SMTP-0) without an *N*-linked side-chain, which had no plasminogen activation effect [48] (Figure 5). It can be concluded that the *N*-linked side-chain was essential for plasminogen-modulating activity. In 2010, Hasegawa et al. confirmed the crucial role of the *N*-linked side chain in modulating plasminogen [21]. The congeners, without ionizable groups in *N*-linked side-chain, were inactive in plasminogen activation, such as with congener **10**. Moreover, the congeners, with an aromatic group and a negatively ionizable group on the side-chain, were more active for the enhancement of plasminogen activation than those with an aliphatic group and a negatively ionizable group, such as congener **3** (E_{max} = 15-fold). Koide et al. further isolated a series of SMTP congeners with different *N*-linked side-chains and evaluated their bioactivities. Congeners **11** (E_{max} = 126-fold) and **12** (E_{max} = 159-fold) were as potent as compound **1** (E_{max} = 102-fold) in plasminogen-modulating activity [37]. Only these congeners could express higher plasminogen-modulating and anti-oxidative activities, and other isomers or phenolic hydroxy groups, at different positions, did not

present satisfactory activities in plasminogen activation. Moreover, the congeners with *N*-linked side-chains showed anti-oxidative activities too. All the congeners bearing a phenolic hydroxy group and a carboxylic acid group displayed higher anti-oxidative activities. Congener **12**, especially, possessed more than 1.7 times the anti-oxidative activity in comparison to compound **1** (Figure 5).
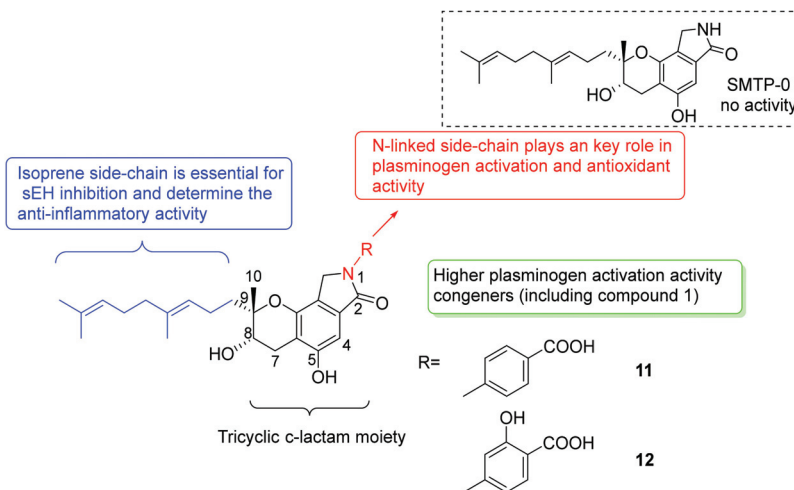
Figure 5. Structure–activity relationships of congeners **11** and **12**.

Pharmacokinetics is an essential evaluation system for the development of new drugs, which finally determines the metabolism and efficacy of drugs in vivo [49]. In 2013, Su et al. observed the pharmacokinetics and tissue distribution of compound **1** in Wistar rats [50]. Compound **1** had a half-life ($t_{1/2}$) of ca. 22.37 min, and it was suitable for two-compartment models, by intravenous administration, for 10 and 20 mg/kg. From the viewpoint of tissue distribution, compound **1** was present in the highest concentration in the liver, but it had low or undetectable concentrations in the brain, suggesting that compound **1** did not cross the blood–brain barrier (the results were wrong, and compound **1** could cross the blood–brain barrier). In 2019, Ma et al. evaluated pharmacokinetic properties in beagle dogs and permeability characterization in Caco-2 cells [51]. $t_{1/2}$ of compound **1** was determined in dogs' brains, and $t_{1/2}$, in beagle dogs, was about two times longer than in Wistar rats (48.7 min in average). Moreover, compound **1** performed low penetrability in a human Caco-2 cell's monolayer model and the rapid distribution into organs, suggesting intravenous injection was more appropriate than oral. In addition, absorption and transportation characteristics of compound **1** had been studied [52]. In Caco-2 cells model, compound **1** expressed passive diffusion of the absorption pattern, and it was not the substrate of P-gp, indicating that compound **1** could cross the blood–brain barrier. Therefore, compound **1** had the potential to be a thrombolytic agent for the treatment of occluded cerebral vessels.

The modification of compound **1** enhanced fibrinolytic activity to access more efficient and safer thrombolytic agents. In 2021, Wang et al. synthesized a series of compound **1** derivatives through the modification of phenyl groups, at the C2-OH and C2′-OH positions on compound **1**, and evaluated their fibrinolytic activities (Figure 6) [53] (The compound, modified by Wang et al., was the enantiomer of compound **1** (8S, 9S)). Derivative **a**, with methyl, and derivative **b,** with *para*-bromobenzyl, presented significant fibrinolytic activity with the EC$_{50}$ values of 59.7 µM and 42.3 µM, respectively. Derivative **b** showed rapidly increasing fibrinolytic activity in the early stage (0–40 min), dose-dependently. Furthermore, derivative **b** displayed weak activities of inducing apoptosis and anti-inflammation on HeLa cells, suggesting that derivative **b** was a potential antithrombotic agent.

1   R = OH   (115.0 μM)

a   R = Me   (59.7 μM)

b   R = *para*-bromobenzyl   (42.3μM)
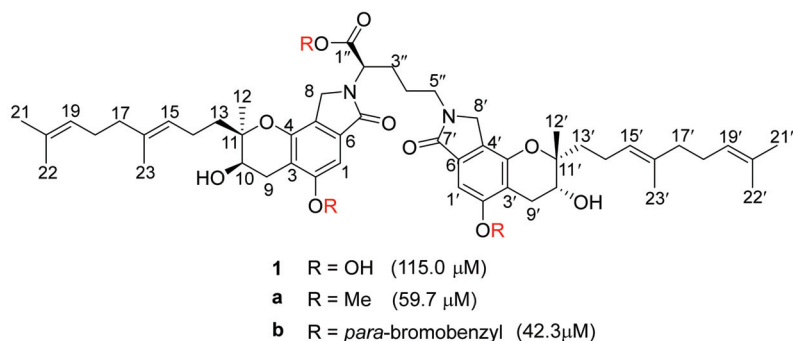
Figure 6. The modification of compound **1**.

2.2. Effects on Inflammation and Oxidant Related Damage: In Reperfusion of Occluded Vessels

A large portion of tissue damage in diseases is caused by inflammation. In 2000, it had already been confirmed that inflammation could affect the coagulation system and regulation, which was responsible for thrombotic complications in vivo [54]. In 2005, it was found that patients with inflammatory diseases were more likely to develop thrombosis. For instance, the patients with inflammatory bowel disease suffered from a three-fold risk of pulmonary embolism or vein thrombosis [55]. In 2008, the unique role of inflammation was focused in the formation of venous thrombus [56]. Thus, researchers investigated the relationship between the reduced damage of ischemia/reperfusion and anti-inflammatory activity by the treatment of compound **1**.

Mammalian sEH contributes to inflammatory response through hydrolyzing lipid signaling molecules, and it has been developed as a potential therapeutic target [57,58]. More than 100 sEH inhibitor patents have been published for the treatment of diabetes, hypertension, pain, and cardiovascular diseases [59,60]. The geranylmethyl side-chain of compound **1** is crucial to the inhibitory activity of sEH [47]. Therefore, compound **1** and other staplabin congeners possessed great anti-inflammatory potential.

sEH is a bifunctional enzyme with a C-terminal domain (Cterm-EH) and an N-terminal domain (Nterm-phos). Cterm-EH catalyzes hydrolysis of epoxyeicosatrienoic acids (EETs, an endogenous signaling molecule involved anti-inflammation), and Nterm-phos hydrolyzes lipid phosphates [60–62]. Therefore, the inhibition to Cterm-EH is the key to inhibit inflammation. Mastsumoto et al. performed sEH inhibition kinetic analysis of congeners [63]. Congeners **14** (IC_{50} = 12 ± 1) and **15** (IC_{50} = 5 ± 2) had better Cterm-EH inhibitory activities in comparison to congeners **10** (IC_{50} > 100) and **16** (IC_{50} > 100). Therefore, although the geranylmethyl side-chain was essential to the inhibitory activity, the nature of *N*-linked side chains also affected the inhibitory potency of sEH (Figure 7). Compound **1** inhibited the hydrolysis of EETs with IC_{50} of 6.5 μM. SMTP-0 (IC_{50} = 1.2 μM) and congener **18** (IC_{50} = 9.2 μM) were also efficient for inhibiting the hydrolysis of EETs [63]. Meanwhile, both 10 mg/kg of compound **1** and congener **18** improved neuritis symptoms in a rat Guillain–Barré syndrome model, and they alleviated symptoms of ulcerative colitis and Crohn's disease in mice. The results proved that compound **1** and staplabin congeners possessed great anti-inflammatory potential [63].
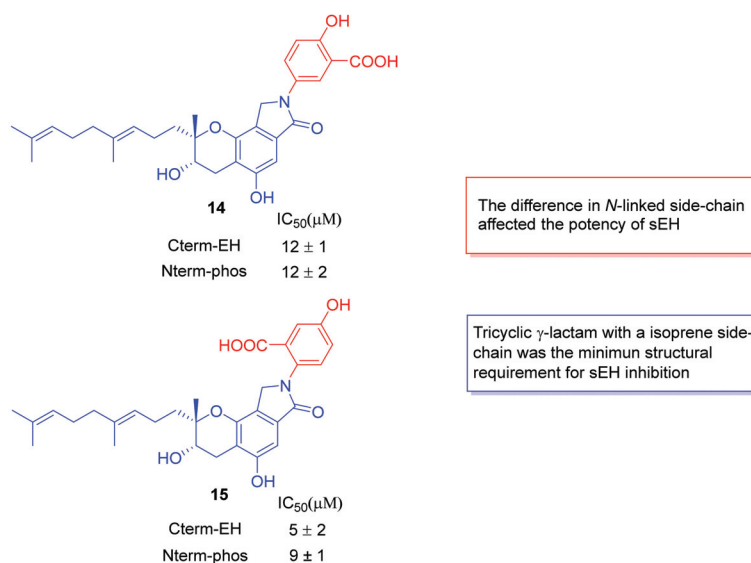
Figure 7. The structure of congeners **14**, **15,** and the SARs study of inhibitory effect on Cterm-EH and Nterm-phos.

Occluded vessels reperfusion could produce reactive oxygen species (ROS), which would stimulate ischemic cells, secreting excessive pro-inflammatory and inflammatory cytokines, such as IL-6, IL-1β, and TNF-α. The overexpressed cytokines cause damage, hemorrhage, and even inflammation in cerebral vessels, which is a major factor in ischemic brain injury [64]. Shibata et al. observed little hemorrhagic region with compound **1** (10 mg/kg), in the model of cerebral infarction mice, in comparison with 10 mg/kg t-PA treatment; moreover, they investigated the involved mechanism [29]. mRNA expression of IL-6, IL-1β, and TNF-α were not increased by the treatment of compound **1**, in comparison to t-PA treatment, at 3 h after ischemia. Hashimoto et al. found that compound **1** decreased expression of IL-6, the signal transducer and activator of transcription 3, S100 calcium binding protein A8, and MMP-9 by microarray and RT-PCR analysis [40]. Therefore, compound **1** inhibited the secretion of pro-inflammatory and inflammatory cytokines to improve the hemorrhage and ischemic brain injury. Meanwhile, Akamatsu et al. detected that superoxide anions (one ROS in cerebral ischemia) were observed by hydroethidine signals at 2 h after reperfusion [39]. Hydroethidine signal was reduced by the treatment of compound **1** in comparison to the vehicle group, meaning that compound **1** inhibited the production of ROS to decrease reperfusion damage. In addition, the treatment of compound **1** reduced the expression of nitrotyrosine and MMP-9, causing attenuated ischemic neuronal damage. Moreover, inflammatory tissue could release proteolytic enzymes of MMP-9, which is associated with blood–brain barrier breakdown and hemorrhagic complications in cerebral infarction [65]. Ito et al. indicated that compound **1** inhibited the activation of MMP-9 to protect the blood–brain barrier from destruction and hemorrhagic transformation (pro-MMP-9: 88.9 ± 34.2; MMP-9: 5.0 ± 1.6) in mice [32]. Besides, Huang et al. suggested that compound **1** could inhibit oxidative stress to reduce ischemia/reperfusion injury [41]. Compound **1** decreased the expression of 4-hydroxy-2-nonenal (4-NHE), 3-nitrotyrosine, and 8-hydroxy-2′-deoxyguanosine (8-OHdG) significantly, which provided therapeutic benefits for ischemic stroke. Therefore, compound **1** possessed anti-inflammatory and anti-oxidative activities in the reperfusion of occluded vessels (Figure 8).
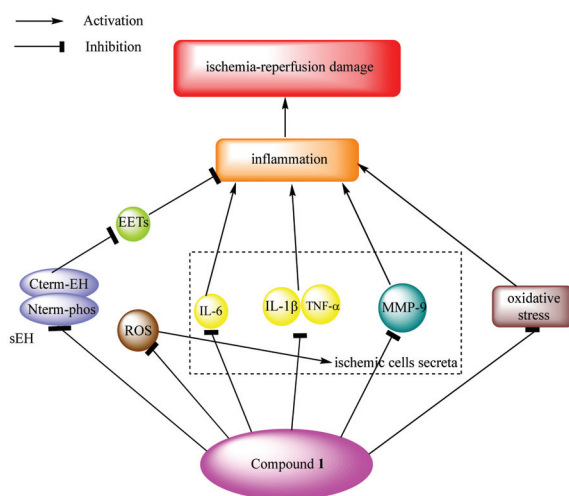
Figure 8. The anti-inflammatory and anti-oxidative mechanisms of compound **1** in ischemia–reperfusion damage.

2.3. Neuroprotective Activity

In 2011, Akamatsu et al. first confirmed the intrinsic neuroprotective effect of compound **1** [39]. In the photochemical-induced thrombotic occlusion model of cynomolgus monkeys, compound **1** of 10 mg/kg improved the neurologic deficit by 29% and cerebral hemorrhage by 51%, after treatment for 24 h, in comparison to the saline control group [29]. Then, Shibata et al. further explored the mechanism of reducing brain damage [66]. Compound **1** inhibited the expression of 4-NHE and neutrophil cytosolic factor 2 (Ncf2) after treatment for 1–3 h. Additionally, 4-NHE is an oxidized product of lipid peroxidation, Ncf2 can stimulate the NADPH oxidase complex to produce SOD, and their levels would increase in the infarction area [67]. Therefore, compound **1** reduced lipid peroxidation and the generation of SOD, in cerebral infarction, to possess neuroprotective activity [66]. Moreover, Ito et al. evaluated the activation of MMP-9 with compound **1** treatment in a mouse model. Compared with the control group, compound **1**, of 10 mg/kg, inhibited the expression of MMP-9, which could digest the endothelial basal lamina and open the blood–brain barrier, causing neuro-inflammation [32]. Compound **1** showed less basal membrane damage and functional breakdown of the blood–brain barrier. Therefore, compound **1** reduced neuronal damage by inhibiting MMP-9 expression. In 2018, Huang et al. investigated the anti-inflammatory and antiapoptosis mechanisms of compound **1** for neuroprotective effects [68]. Compound **1**, of 10 mg/kg, decreased the expression of NF-κB, TNF-α, and NLRP3-positive cells, which involved the alleviation of neuroinflammation. Meanwhile, compound **1** reduced the expression of cleaved-caspase-3, suggesting the inhibition in cell death progress. Therefore, compound **1** treatment demonstrated less necrosis of neurons and high neuroprotective activity in the peri-ischemic area. The results showed that the neuroprotective activity of compound **1** was attributed to the anti-oxidative, anti-inflammatory, and anti-apoptosis mechanisms in cerebral infarction.

In 2014, Matsumoto et al. found that congener **18** (10 mg/kg) (Figure 9) alleviated neuritis symptoms in a rat model presenting neuroprotective activity [63]. Shi et al. investigated the therapeutic effect of congener **18** in the neurovascular unit (NVU) and neurovascular trophic coupling damage [69]. Congener **18** ameliorated the NVU dissociation between pericyte, basal lamina, and astrocytic foot. It also improved the endothelial neuroprotective support for the outsider neurons. Moreover, congener **18** decreased the expression of TNF-α, 4-HNE, 8-OHdG, and cleaved caspase-3. Therefore, neuroprotective activity of congener **18** was due to its anti-inflammatory, anti-oxidative, and anti-apoptotic

mechanisms. Congener **18**, especially, had therapeutic potential for diabetic neuropathy symptoms [70]. Congener **18** (30 mg/kg) improved the mechanical allodynia, thermal hyperalgesia symptoms, and neurological degeneration of DN in a streptozotocin-induced diabetes mouse model.
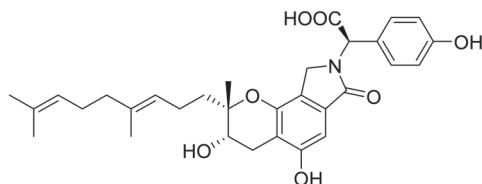
18

Figure 9. The structure of congener **18**.

2.4. Effects on IgA Nephropathy and Acute Kidney Injury

IgA nephropathy (IgAN) has become a primary chronic glomerulonephritis worldwide, featuring mesangial cell proliferation and the deposition of IgA [71]. It causes a gradual decline in renal function, and 30% of patients will develop to the end stage of renal disease [72–74]. Kemmochi et al., (2012) investigated the therapeutic effects of compound **1** against IgAN [75]. In a mouse IgAN model, compound **1** (10 mg/kg) slightly reduced the deposition of IgA, but it had no effect on the serum concentration of IgA. The results suggested that compound **1** might inhibit the progression of IgAN through reducing the deposition of IgA in the glomerular mesangium. However, it was not effective in decreasing IgA production and treatment for terminal IgAN, indicating the limited therapeutic ability in IgAN.

Unlike IgAN, acute kidney injury (AKI) could cause rapid reduction in renal function [76]. The pathological condition of the kidney retained toxins and wastes, causing toxicosis and disorder in fluid, electrolyte, and acid–base balance [77]. It is estimated that 22% of hospitalized adults suffered from AKI [78]. Compound **1** showed less damage of ischemia-reperfusion in thrombolysis therapy. Meanwhile, ischemia-reperfusion played a major role in AKI renal damage. Therefore, in 2021, Shibata et al. studied the efficacy of compound **1** in renal damage [79]. Compound **1** improved the parameters of renal function (blood–urea nitrogen, creatinine levels in serum, creatinine clearance, and fractional excretion of sodium) and renal tubule damage. The therapeutic effect of compound **1** was derived from anti-inflammatory and anti-oxidative activities. The inhibition to sEH elevated the EET level, which inhibited tubular dysfunction and inflammatory factors, such as NF-κB, TNF-α, IL-6, and IL-1β. ROS production was also reduced after compound **1** treatment. Thus, the suppression of peroxidation led to less renal cell injury.

2.5. Effects on Cancer: Non-Small Cell Lung Cancer

The essence of cancer is the abnormal proliferation and differentiation of cells, which are dependent on angiogenesis [80]. Therefore, anti-cancer agents could identify and inhibit angiogenesis, thus representing an approach for cancer therapy [81]. Many patents on angiogenesis inhibitors have been published, such as angiostatin, endostatin, and thrombospondin. Therein, angiostatin is a hidden fragment of plasminogen with great antiangiogenic properties [82]. Congener **7** reduced vascular formation, along with proliferation and migration, to inhibit tumor growth and possessed plasminogen activation activity, causing a conformational change of plasminogen to dissolve thrombus [83]. Ohyama et al., (2004) reported that congener **7** also promoted the autoproteolytic of plasmin, inducing extensive fragmentation of the catalytic domain [83]. After urokinased-catalyzed plasminogen was activated by congener **7**, the catalytic domain of plasmin (activated plasminogen) rapidly degraded into 68–77 kDa fragments. These fragments blocked proliferation, migration, and

vascular formation of endothelial cells, at concentrations of 0.3–10 μg/mL, meaning they provide potential applications of congener **7** for cancer treatment.

As the most common cell lung cancer, non-small cell lung cancer (NSCLC) accounts for approximately 80–85% of lung cancer diseases [84]. The clinical drugs for treating NSCLC are the epidermal growth factor receptor (EGFR) and EGFR-targeted tyrosine kinase inhibitors (TKIs). However, more than 80% patients gradually showed drug resistance after about 1 year of treatment with EGFR-TKI. Thus, it is necessary to discover new anti-tumor agents for treating NSCLC [85]. In 2022, Yan et al. observed the effects of compound **1** on erlotinib-resistant NSCLC and explored the underlying mechanism [86]. NSCLC cells were sensitive to compound **1** with $IC_{50} = 7.45 \pm 0.57$ μM in vitro, especially for erlotinib-resistant NSCLC H1975 cells ($IC_{50} = 9.22 \pm 0.84$ μM); meanwhile, compound **1** was relatively safe for normal cells. The accumulation of cleaved-PARP, cleaved-caspase-3, Bax, and the reduction in Bcl-2 revealed that compound **1** induced the cell apoptosis of NSCLC cells [86]. Then, they discovered the underlying mechanism of treating erlotinib-resistant NSCLC. Compound **1** induced mitochondria-mediated apoptosis, leading to increased ROS and reduced GSH. Thus, compound **1** caused apoptosis of erlotinib-resistant NSCLC cells [86,87]. In addition, compound **1** also inhibited the PI3K/Akt signaling pathway and the EGFR/PI3K/Akt/mTOR pathway. The abnormal activation of the PI3K/Akt pathway could cause TKI resistance, as well as invasiveness and migration of NSCLC [85]. Moreover, compound **1** showed high binding affinity to EGFR$^{T790M/L858R}$ in molecular modeling, meaning compound **1** selectively exhibited anticancer activity on erlotinib-resistant NSCLC cells. Finally, compound **1** (10 mg/kg) had consistent anti-cancer effects in nude mice, meaning that it showed potential for erlotinib-resistant NSCLC therapy. In 2022, Feng et al. further observed that compound **1** downregulated the levels of CD4K and Cyclin D1 to arrest the cell cycle of PC9 cells at the G0/G1 phase [88]. Compound **1**, especially, inhibited the viability and proliferation of PC9 cells through the inhibition of the NF-κB signaling pathway. The results indicated that compound **1** had excellent anti-cancer activity on *EGFR*-mutant NSCLC cells, but it had weak or no effect on wild-type EGFR cells. It can be concluded that compound **1** might depend on the EGFR status to induce apoptosis of NSCLC cells.

3. Preparation of Compound 1 and Staplabin Congeners

Hu et al. isolated SMTP congeners from *S. microspora* in 2001 [25]. They found that the use of amino acids and amino alcohols significantly increased the production of congeners, and the obtained products were related to the type of added amino acid. The production of compound **1** and congeners **3**, **5**, and **7** increased by 7 to 45-fold, with the addition of Orn, Phe, Leu, Trp, and Lys at 100 mg/mL, which acted as precursors in culture. Therefore, the addition of precursors was an important procedure in the preparation of compound **1** and staplabin congeners.

In 2012, Nishimura et al. isolated a new compound designated pre-SMTP from fungus *S. microspora*, which directly afforded SMTP congeners by reacting nonenzymatically (phthalaldehydes reaction) [89,90]. Pre-SMTP accumulated, with limited amounts of amine, in medium with *S. microspora*, and it consumed rapidly after increased amine feeding. Meanwhile, SMTP-0, as well as congeners **3**, **7**, **19**, and **20** were afforded, by reaction of pre-SMTP, with ammonium chloride, *L*-phenylalanine, *L*-tryptophan, L-glutamine, and L-glutamic acid, respectively. Thus, it is available to synthesize a variety of congeners, with different *N*-linked side-chain structures, through nonenzymatic reaction between pre-SMTP and an amine (Figure 10).

In 2013, Su et al. investigated the fermentation conditions of compound **1** isolated from *S. longispora* FG216 [91]. The results showed that the optimized fermentation conditions were as follows: 0.5% ornithine hydrochloride addition, 28 °C culture temperature, and 7 d (Figure 11a). The yield of compound **1** increased up to 1.98 g/L. In 2015, Wang et al. designed a metabolic regulation strategy to improve the production of compound **1** [92]. The results indicated that the carbon skeleton of compound **1** was synthesized through

the shikimate and mevalonate pathways. Therefore, the addition of precursor shikimic acid and precursor sodium acetate increased the yield of compound **1** by 10.4%–14.6% (Figure 11b,c). Glucose and ornithine were the essential skeleton and structural core of compound **1**, respectively, which involved the synthesis of compound **1**. Along with 20 g/L glucose and 4.32 g/L *L*-ornithine provision, compound **1** increased up to 82.2 and 95.9 g/L (Figure 11d). During the fermentation, a transformation was observed from ornithine, FGFC3, and FGFC2 into compound **1**. Further research is needed for promoting transformation from ornithine to compound **1**, which will be able to increase production substantially (Figure 11e).
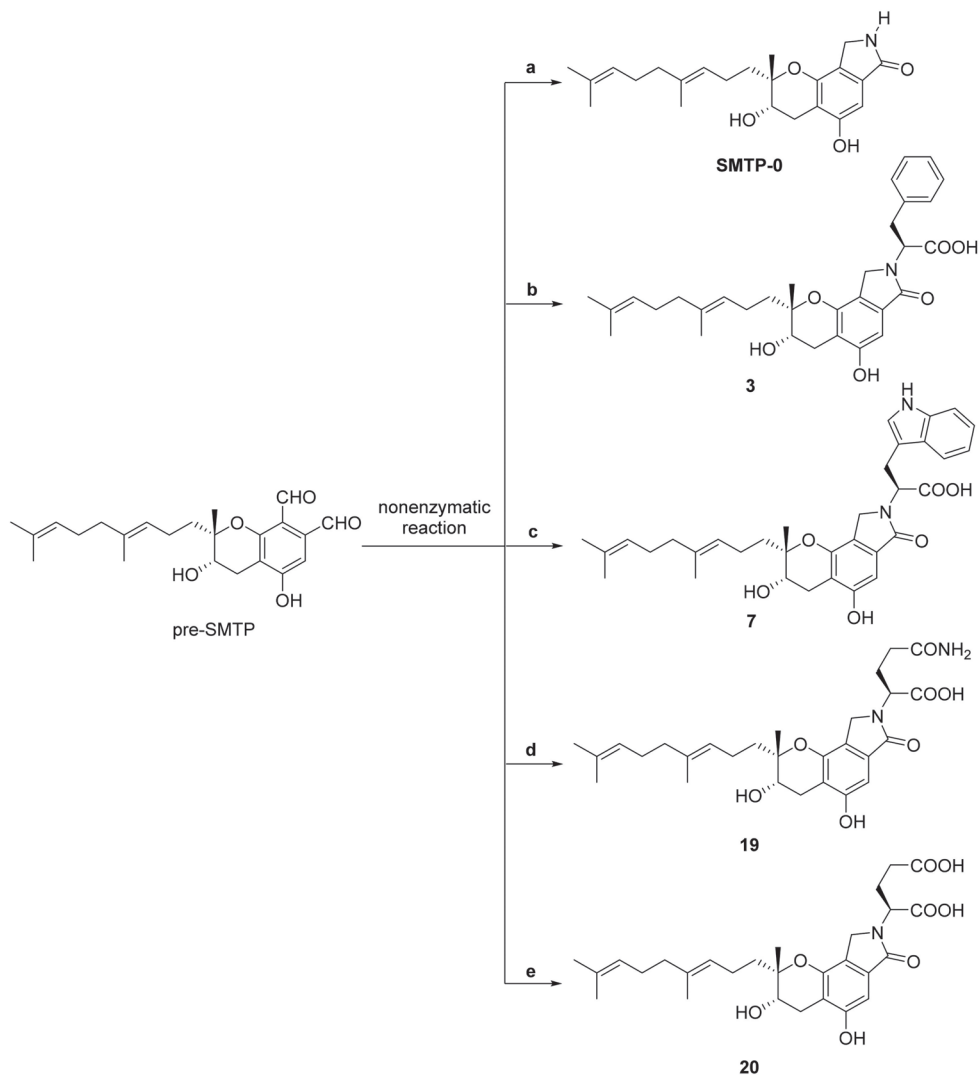
Figure 10. Synthesis of SMTP-0, as well as congeners **3**, **7**, **19**, and **20,** based on pre-SMTP (phthalaldehydes reaction). Pre-SMTP (100 µg/mL in acetone) was incubated with (**a**) 5 mg/mL ammonium acetate in acetic acid (1.5%, *v/v*); (**b**) 5 mg/mL *L*-phenylalanine in acetic acid (1.5%, *v/v*); (**c**) 5 mg/mL *L*-tryptophan in acetic acid (1.5%, *v/v*); (**d**) 5 mg/mL *L*-glutamine in acetone-water-acetic acid (50:50:1); (**e**) 5 mg/mL *L*-glutamic acid in acetone-water-acetic acid (50:50:1).

Optimized fermentation method for compound **1**:

Compound **1**

a Optimize fermentation condition:
0.5% ornithine hydrochloride addition, 28°C, 7d

b Enhance compound **1** metabolic pathways:
i. 0.1 g/L shikimic acid (shikimate pathway)
ii. 3 mmol/L sodium acetate (mevalonate pathway)

c Inhibit bypass metabolic pathways:
0.09 mmol/L cerulenin (polyketide pathway)

d Increase key precursor:
i. 20 g/L glucose
ii. 4.32 g/L L-ornithine
iii. glucose and L-ornithine (further experiments needed)

e Transform precursor completely
(further studies needed)

Figure 11. The optimized method for a compound **1** culture. On fermentaion basal medium, inducers (or precursor), and conditions: (**a**) 0.5% ornithine hydochloride, 28 °C, 7 d, 1.98 g/L; (**b**) (i) 0.1 g/L shikimic acid, yield increased by 10.4%; (ii) 3 mmol/L sodium acetate, yield increased; (**c**) 0.09 mmol/L cerulenin, yield increased by 14.6%; (**d**) (i) 20 g/L glucose, 82.2 g/L; (ii) 4.32 g/L, L-ornithine, 95.9 g/L; (iii) and (**e**) need further research.

Yin et al., (2017) studied the biosynthesis pathway in *S. longispora* FG216 [93]. The results were that three reported core genes and the nitrate reductase (NR) gene copy were the isoindolinone biosynthetic gene cluster in *S. longispora* FG216. NR is the rate-limiting enzyme of nitrate reduction. Therefore, nitrate reductase possibly played a role in the balance of ammonium ion concentration. Moreover, four new derivatives, **21**–**24**, were obtained by various amino supplements in *S. longispora* FG216 (Figure 12).

21
amino: 0.2% (3S)-3-amino-2-piperidinone
yield: 163 mg/100mL broth

22
amino: 0.2% (3R)-3-amino-2-piperidinone
yield: 40 mg/100mL broth

23
amino: 0.5% glycine
yield: 62 mg/100mL broth

24
amino: 0.5% L-threonine
yield: 72 mg/100mL broth

various amino supplements resulted different derivatives

Figure 12. The structures of derivatives **21**–**24**.

4. Conclusions

Compound **1** possesses rich bioactivities, such as excellent fibrinolytic, anti-inflammatory, and anti-oxidative activities. Compared with other anti-thrombotic agents, such as warfarin, compound **1** exhibits less hemorrhage risk for the treatment of thrombosis because it changes the conformation of plasminogen, in the presence of uPA, to activate the plasminogen. Moreover, the inhibition to sEH reduces inflammatory response, causing neuroprotection and less damage from the reperfusion of occluded vessels. The structure–activity relationships of compound **1** indicate that the *N*-linked side chain determines plasminogen activation activity, and the geranylmethyl side chain is essential for anti-inflammatory activity. Recent studies show that compound **1** possesses, surprisingly, anti-cancer activity toward EGFR-TKI-resistant NSCLC cells. Furthermore, the satisfactory pharmacokinetic property and optimized culture methods show that compound **1** has potential as a promising agent. Some modifications of compound **1** and staplabin congeners perform better in fibrinolytic or neuroprotective activity, thereby illustrating the high therapeutic potential.

References

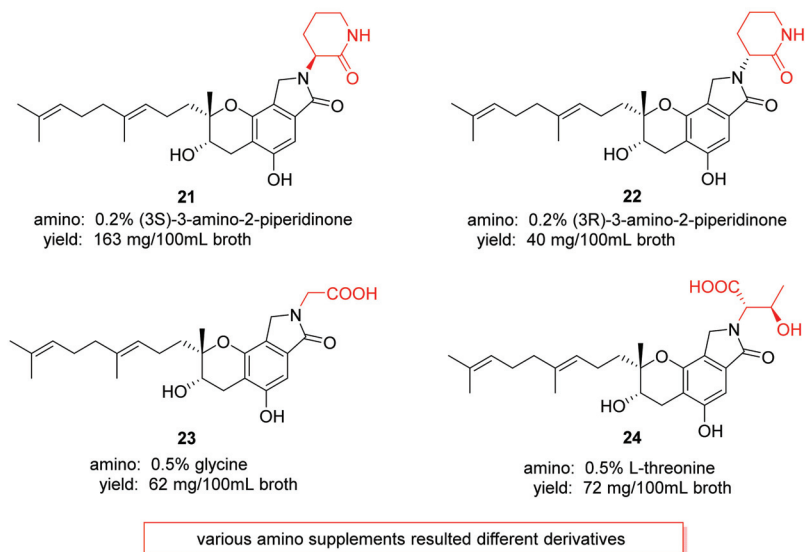1. Hasumi, K.; Suzuki, E. Impact of SMTP targeting plasminogen and soluble epoxide hydrolase on thrombolysis, inflammation, and ischemic stroke. *Int. J. Mol. Sci.* **2021**, *22*, 954. [CrossRef] [PubMed]
2. Hasumi, K.; Yamamichi, S.; Harada, T. Small-molecule modulators of zymogen activation in the fibrinolytic and coagulation systems. *FEBS J.* **2010**, *277*, 3675–3687. [CrossRef]
3. Rijken, D.C.; Lijnen, H.R. New insights into the molecular mechanisms of the fibrinolytic system. *J. Thromb. Haemost.* **2009**, *7*, 4–13. [CrossRef] [PubMed]
4. Chang, Y.; Dabiri, G.; Damstetter, E.; Ebot, E.B.; Powers, J.G.; Phillips, T. Coagulation disorders and their cutaneous presentations: Pathophysiology. *J. Am. Acad. Dermatol.* **2016**, *74*, 783–792. [CrossRef]
5. Booth, N.A. Fibrinolysis and thrombosis. *Bailliere's Best Pract. Res. Clin. Haematol.* **1999**, *12*, 423–433. [CrossRef] [PubMed]
6. Sashidhara, K.V.; Kumar, A.; Kumar, M.; Singh, S.; Jain, M.; Dikshit, M. Synthesis of novel 3-carboxamide-benzocoumarin derivatives as orally active antithrombotic agents. *Bioorg. Med. Chem. Lett.* **2011**, *21*, 7034–7040. [CrossRef] [PubMed]
7. Waluyo, D.; Prabandari, E.E.; Pramisandi, A.; Hidayati, D.N.; Chrisnayanti, E.; Puspitasari, D.J.; Dewi, D.; Suryani; Kristiningrum; Oktaviani, A.N.; et al. Exploring natural microbial resources for the discovery of anti-malarial compounds. *Parasitol. Int.* **2021**, *85*, 102432. [CrossRef]

8. Jing, L.; Luohao, L.; Runqing, Z.; Vuanghao, L.; Qianqian, S.; Lizhen, F. Natural products from the genus *Daldinia* and their bioactivities. *Med. Res.* **2021**, *5*, 210005.
9. Xiaojing, S.; Hong, W.; Jiao, C.; Zhubin, Z.; Fanqiu, N. Chemical constituents and bioactivities of *Aconitum episcopale*. *Med. Res.* **2021**, *5*, 210001.
10. Romano, G.; Costantini, M.; Sansone, C.; Lauritano, C.; Ruocco, N.; Ianora, A. Marine microorganisms as a promising and sustainable source of bioactive molecules. *Mar. Environ. Res.* **2017**, *128*, 58–69. [CrossRef]
11. Hui, H.; Junwen, W.; Xueyan, L.; Wenhui, W.; Kejin, S.; Chaoyan, Z. Renoprotective effect of sulphate polysaccharide from brown algae on ethylene glycol-induced renal damage in rats. *Med. Res.* **2020**, *4*, 190010.
12. Junwen, W.; Xueyan, L.; Chaoyan, Z. Recent advances on bioactivity of seaweed polysaccharides. *Med. Res.* **2019**, *3*, 200003.
13. Malve, H. Exploring the ocean for new drug developments: Marine pharmacology. *J. Pharm. BioAllied Sci.* **2016**, *8*, 83–91. [CrossRef]
14. Phuphanich, S.; Maria, B.; Braeckman, R.; Chamberlain, M. A pharmacokinetic study of intra-CSF administered encapsulated cytarabine (DepoCyt) for the treatment of neoplastic meningitis in patients with leukemia, lymphoma, or solid tumors as part of a phase III study. *J. Neuro-Oncol.* **2007**, *81*, 201–208. [CrossRef]
15. Jimenez, P.C.; Wilke, D.V.; Branco, P.C.; Bauermeister, A.; Rezende-Teixeira, P.; Gaudêncio, S.P.; Costa-Lotufo, L.V. Enriching cancer pharmacology with drugs of marine origin. *Br. J. Pharmacol.* **2020**, *177*, 3–27. [CrossRef]
16. Martinez, A. Marine-derived drugs in neurology. *Curr. Opin. Investig. Drugs* **2007**, *8*, 525–530.
17. Kohyama, T.; Hasumi, K.; Hamanaka, A.; Endo, A. SMTP-1 and -2, novel analogs of staplabin produced by *Stachybotrys microspora* IFO30018. *J. Antibiot.* **1997**, *50*, 172–174. [CrossRef]
18. Takayasu, R.; Hasumi, K.; Shinohara, C.; Endo, A. Enhancement of fibrin binding and activation of plasminogen by staplabin through induction of a conformational change in plasminogen. *FEBS Lett.* **1997**, *18*, 58–62. [CrossRef]
19. Shinohara, C.; Hasumi, K.; Hatsumi, W.; Endo, A. Saplabin, a novel fungal triprenyl phenol which stimulates the binding of plasminogen to fibrin and U937 Cells. *J. Antibiot.* **1996**, *49*, 961–966. [CrossRef]
20. Hu, W.; Ohyama, S.; Hasumi, K. Activation of fibrinolysis by SMTP-7 and -8, novel staplabin analogs with a pseudosymmetric structure. *J. Antibiot.* **2000**, *53*, 241–247. [CrossRef]
21. Hasegawa, K.; Koide, H.; Hu, W.; Nishimura, N.; Narasaki, R.; Kitano, Y.; Hasumi, K. Structure-activity relationships of 11 new congeners of the SMTP plasminogen modulator. *J. Antibiot.* **2010**, *63*, 589–593. [CrossRef]
22. Miyazaki, T.; Kimura, Y.; Ohata, H.; Hashimoto, T.; Shibata, K.; Hasumi, K.; Honda, K. Distinct effects of tissue-type plasminogen activator and SMTP-7 on cerebrovascular inflammation following thrombolytic reperfusion. *Stroke* **2011**, *42*, 1097–1104. [CrossRef]
23. Hu, W.; Narasaki, R.; Nishimura, N.; Hasumi, K. SMTP (*Stachybotrys microspora* triprenyl phenol) enhances clot clearance in a pulmonary embolism model in rats. *Thromb. J.* **2012**, *10*, 2. [CrossRef]
24. Hu, W.; Kitano, Y.; Hasumi, K. SMTP-4D, -5D, -6D, -7D and -8D, a new series of the non-lysine-analog plasminogen modulators with a D-amino acid moiety. *J. Antibiot.* **2003**, *56*, 832–837. [CrossRef]
25. Hu, W.; Narasaki, R.; Ohyama, S.; Hasumi, K. Selective production of staplabin and SMTPs in cultures of *Stachybotrys microspora* fed with precursor amines. *J. Antibiot.* **2001**, *54*, 962–966. [CrossRef]
26. Benjamin, E.J.; Blaha, M.J.; Chiuve, S.E.; Cushman, M.; Das, S.R.; Deo, R.; de Ferranti, S.D.; Floyd, J.; Fornage, M.; Gillespie, C.; et al. Heart disease and stroke statistics—2017 update: A report from the American Heart Association. *Circulation* **2017**, *135*, e146–e603. [CrossRef]
27. Zhao, Y.; Zhang, X.; Chen, X.; Wei, Y. Neuronal injuries in cerebral infarction and ischemic stroke: From mechanisms to treatment (review). *Int. J. Mol. Med.* **2022**, *49*, 15. [CrossRef]
28. Hashimoto, T.; Shibata, K.; Nobe, K.; Hasumi, K.; Honda, K. A novel embolic model of cerebral infarction and evaluation of *Stachybotrys microspora* triprenyl phenol-7 (SMTP-7), a novel fungal triprenyl phenol metabolite. *J. Pharmacol. Sci.* **2010**, *114*, 41–49. [CrossRef] [PubMed]
29. Shibata, K.; Hashimoto, T.; Nobe, K.; Hasumi, K.; Honda, K. A novel finding of a low-molecular-weight compound, SMTP-7, having thrombolytic and anti-inflammatory effects in cerebral infarction of mice. *Naunyn-Schmiedeberg's Arch. Pharmacol.* **2010**, *382*, 245–253. [CrossRef] [PubMed]
30. Sawada, H.; Nishimura, N.; Suzuki, E.; Zhuang, J.; Hasegawa, K.; Takamatsu, H.; Honda, K.; Hasumi, K. SMTP-7, a novel small-molecule thrombolytic for ischemic stroke: A study in rodents and primates. *J. Cereb. Blood Flow Metab.* **2014**, *34*, 235–241. [CrossRef] [PubMed]
31. Suzuki, E.; Nishimura, N.; Yoshikawa, T.; Kunikiyo, Y.; Hasegawa, K.; Hasumi, K. Efficacy of SMTP-7, a small-molecule anti-inflammatory thrombolytic, in embolic stroke in monkeys. *Pharmacol. Res. Perspect.* **2018**, *6*, e00448. [CrossRef]
32. Ito, A.; Niizuma, K.; Shimizu, H.; Fujimura, M.; Hasumi, K.; Tominaga, T. SMTP-7, a new thrombolytic agent, decreases hemorrhagic transformation after transient middle cerebral artery occlusion under warfarin anticoagulation in mice. *Brain Res.* **2014**, *1578*, 38–48. [CrossRef]
33. Wang, G.; Wu, W.; Zhu, Q.; Fu, S.; Wang, X.; Hong, S.; Guo, R.; Bao, B. Identification and fibrinolytic evaluation of an isoindolone derivative isolated from a rare marine fungus *Stachybotrys longispora* FG216. *Chin. J. Chem.* **2015**, *33*, 1089–1095. [CrossRef]
34. Yan, T.; Wu, W.; Su, T.; Chen, J.; Zhu, Q.; Zhang, C.; Wang, X.; Bao, B. Effects of a novel marine natural product: Pyrano indolone alkaloid fibrinolytic compound on thrombolysis and hemorrhagic activities in vitro and in vivo. *Arch. Pharmacal. Res.* **2015**, *8*, 1530–1540. [CrossRef]

35. Gao, C.; Shen, Q.; Tang, P.; Cao, Y.; Lin, H.; Li, B.; Sun, P.; Bao, B.; Wu, W. In vitro study of the fibrinolytic activity via single chain urokinase-type plasminogen activator and molecular docking of FGFC1. *Molecules* **2021**, *26*, 1816. [CrossRef]

36. Hasumi, K.; Ohyama, S.; Kohyama, T.; Ohsaki, Y.; Takayasu, R.; Endo, A. Isolation of SMTP-3, 4, 5 and -6, novel analogs of staplabin, and their effects on plasminogen activation and fibrinolysis. *J. Antibiot.* **1998**, *51*, 1059–1068. [CrossRef]

37. Koide, H.; Hasegawa, K.; Nishimura, N.; Narasaki, R.; Hasumi, K. A new series of the SMTP plasminogen modulators with a phenylamine-based side chain. *J. Antibiot.* **2012**, *65*, 361–367. [CrossRef]

38. Shibata, K.; Hashimoto, T.; Hasumi, K.; Honda, K.; Nobe, K. Evaluation of the effects of a new series of SMTPs in the acetic acid-induced embolic cerebral infarct mouse model. *Eur. J. Pharmacol.* **2018**, *818*, 221–227. [CrossRef]

39. Akamatsu, Y.; Saito, A.; Fujimura, M.; Shimizu, H.; Mekawy, M.; Hasumi, K.; Tominaga, T. *Stachybotrys microspora* triprenyl phenol-7, a novel fibrinolytic agent, suppresses superoxide production, matrix metalloproteinase-9 expression, and thereby attenuates ischemia/reperfusion injury in rat brain. *Neurosci. Lett.* **2011**, *503*, 110–114. [CrossRef]

40. Hashimoto, T.; Shibata, K.; Ohata, H.; Hasumi, K.; Honda, K. Altered gene expression in an embolic stroke model after thrombolysis with tissue plasminogen activator and *Stachybotrys microspora* triprenyl phenol-7. *J. Pharmacol. Sci.* **2014**, *125*, 99–106. [CrossRef]

41. Huang, Y.; Ohta, Y.; Shang, J.; Li, X.; Liu, X.; Shi, X.; Feng, T.; Yamashita, T.; Sato, K.; Takemoto, M.; et al. Reduction of ischemia reperfusion-related brain hemorrhage by *Stachybotrys microspora* triprenyl phenol-7 in mice with antioxidant effects. *J. Stroke Cerebrovasc. Dis.* **2018**, *27*, 3521–3528. [CrossRef]

42. Koyanagi, K.; Narasaki, R.; Yamamichi, S.; Suzuki, E.; Hasumi, K. Mechanism of the action of SMTP-7, a novel small-molecule modulator of plasminogen activation. *Blood Coagul. Fibrinolysis* **2014**, *25*, 316–321. [CrossRef]

43. Guo, R.H.; Duan, D.; Hong, S.T.; Zhou, Y.; Wang, F.; Wang, S.J.; Wu, W.H.; Bao, B. A marine fibrinolytic compound FGFC1 stimulating enzymatic kinetic parameters of a reciprocal activation system based on a single chain urokinase-type plasminogen activator and plasminogen. *Process Biochem.* **2018**, *68*, 190–196. [CrossRef]

44. Rahman, M.N.; Becker, L.; Petrounevitch, V.; Hill, B.C.; Jia, Z.; Koschinsky, M.L. Comparative analyses of the lysine binding site properties of apolipoprotein(a) kringle IV types 7 and 10. *Biochemistry* **2002**, *41*, 1149–1155. [CrossRef]

45. Xue, Y.; Bodin, C.; Olsson, K. Crystal structure of the native plasminogen reveals an activation-resistant compact conformation. *J. Thromb. Haemostasis.* **2012**, *10*, 1385–1396. [CrossRef]

46. Law, R.H.P.; Abu-Ssaydeh, D.; Whisstock, J.C. New insights into the structure and function of the plasminogen/plasmin system. *Curr. Opin. Struct. Biol.* **2013**, *23*, 836–841. [CrossRef]

47. Otake, S.; Ogawa, N.; Kitano, Y.; Hasumi, K.; Suzuki, E. Isoprene side-chain of SMTP is essential for soluble epoxide hydrolase inhibition and cellular localization. *Nat. Prod. Commun.* **2016**, *11*, 223–227. [CrossRef]

48. Hasumi, K.; Hasegawa, K.; Kitano, Y. Isolation and absolute configuration of SMTP-0, a simplest congener of the SMTP family nonlysine-analog plasminogen modulators. *J. Antibiot.* **2007**, *60*, 463–468. [CrossRef]

49. Yellepeddi, V.; Rower, J.; Liu, X.; Kumar, S.; Rashid, J.; Sherwin, C.M.T. State-of-the-art review on physiologically based pharmacokinetic modeling in pediatric drug development. *Clin. Pharmacokinet.* **2019**, *58*, 1–13. [CrossRef]

50. Su, T.; Wu, W.; Yan, T.; Zhang, C.; Zhu, Q.; Bao, B. Pharmacokinetics and tissue distribution of a novel marine fibrinolytic compound in Wistar rat following intravenous administrations. *J. Chromatogr. B Anal. Technol. Biomed. Life Sci.* **2013**, *942*, 77–82. [CrossRef]

51. Ma, Z.; Guo, R.; Elango, J.; Bao, B.; Wu, W. Evaluation of marine diindolinonepyrane in vitro and in vivo: Permeability characterization in Caco-2 cells monolayer and pharmacokinetic properties in Beagle dogs. *Mar. Drugs* **2019**, *17*, 651. [CrossRef] [PubMed]

52. You, H.S.; Zhang, H.F.; Dong, Y.L.; Chen, S.Y.; Wang, M.Y.; Dong, W.H.; Xing, J.F. Absorption and transportation characteristics of scutellarin and scutellarein across Caco-2 monolayer model. *Zhongxiyi Jiehe Xuebao* **2010**, *8*, 863–869. [CrossRef] [PubMed]

53. Wang, Y.; Chen, H.; Sheng, R.; Fu, Z.; Fan, J.; Wu, W.; Tu, Q.; Guo, R. Synthesis and bioactivities of marine pyran-isoindolone derivatives as potential antithrombotic agents. *Mar. Drugs* **2021**, *19*, 218. [CrossRef] [PubMed]

54. Esmon, C.T. Does inflammation contribute to thrombotic events? *Haemostasis* **2000**, *30*, 34–40. [CrossRef] [PubMed]

55. Irving, P.M.; Pasi, K.J.; Rampton, D.S. Thrombosis and inflammatory bowel disease. *Clin. Gastroenterol. Hepatol.* **2005**, *3*, 617–628. [CrossRef]

56. Wakefield, T.W.; Myers, D.D.; Henke, P.K. Mechanisms of venous thrombosis and resolution. *Arterioscler. Thromb. Vasc. Biol.* **2008**, *28*, 387–391. [CrossRef]

57. Harris, T.R.; Hammock, B.D. Soluble epoxide hydrolase: Gene structure, expression and deletion. *Gene* **2013**, *526*, 61–74. [CrossRef]

58. Morisseau, C.; Hammock, B.D. Impact of soluble epoxide hydrolase and epoxyeicosanoids on human health. *Annu. Rev. Pharmacol. Toxicol.* **2013**, *53*, 37–58. [CrossRef]

59. Shen, H.C.; Hammock, B.D. Discovery of inhibitors of soluble epoxide hydrolase: A target with multiple potential therapeutic indications. *J. Med. Chem.* **2012**, *55*, 1789–1808. [CrossRef]

60. Newman, J.W.; Morisseau, C.; Hammock, B.D. Epoxide hydrolases: Their roles and interactions with lipid metabolism. *Prog. Lipid Res.* **2005**, *44*, 1–51. [CrossRef]

61. Thomson, S.J.; Askari, A.; Bishop-Bailey, D. Anti-inflammatory effects of epoxyeicosatrienoic acids. *Int. J. Vasc. Med.* **2012**, *2012*, 605101. [CrossRef]

62. Ulu, A.; Harris, T.R.; Morisseau, C.; Miyabe, C.; Inoue, H.; Schuster, G.; Dong, H.; Iosif, A.M.; Liu, J.Y.; Weiss, R.H.; et al. Anti-inflammatory effects of ω-3 polyunsaturated fatty acids and soluble epoxide hydrolase inhibitors in angiotensin-II-dependent hypertension. *J. Cardiovasc. Pharmacol.* **2013**, *62*, 285–297. [CrossRef]

63. Matsumoto, N.; Suzuki, E.; Ishikawa, M.; Shirafuji, T.; Hasumi, K. Soluble epoxide hydrolase as an anti-inflammatory target of the thrombolytic stroke drug SMTP-7. *J. Biol. Chem.* **2014**, *289*, 35826–35838. [CrossRef]

64. Dirnagl, U.; Iadecola, C.; Moskowitz, M.A. Pathobiology of ischemic stroke: An integrated view. *Trends Neurosci.* **1999**, *22*, 391–397. [CrossRef]

65. Rosell, A.; Cuadrado, E.; Ortega-Aznar, A.; Hernández-Guillamon, M.; Lo, E.H.; Montaner, J. MMP-9-positive neutrophil infiltration is associated to blood-brain barrier breakdown and basal lamina type IV collagen degradation during hemorrhagic transformation after human ischemic stroke. *Stroke* **2008**, *39*, 1121–1126. [CrossRef]

66. Shibata, K.; Hashimoto, T.; Nobe, K.; Hasumi, K.; Honda, K. Neuroprotective mechanisms of SMTP-7 in cerebral infarction model in mice. *Naunyn-Schmiedeberg's Arch. Pharmacol.* **2011**, *384*, 103–108. [CrossRef]

67. Adibhatla, R.M.; Hatcher, J.F. Phospholipase A2, reactive oxygen species, and lipid peroxidation in cerebral ischemia. *Free Radic. Biol. Med.* **2006**, *40*, 376–387. [CrossRef]

68. Huang, Y.; Ohta, Y.; Shang, J.; Morihara, R.; Nakano, Y.; Fukui, Y.; Liu, X.; Shi, X.; Feng, T.; Yamashita, T.; et al. Antineuroinflammatory effect of SMTP-7 in ischemic mice. *J. Stroke Cerebrovasc. Dis.* **2018**, *27*, 3084–3094. [CrossRef]

69. Shi, X.; Ohta, Y.; Shang, J.; Morihara, R.; Nakano, Y.; Fukui, Y.; Liu, X.; Feng, T.; Huang, Y.; Sato, K.; et al. Neuroprotective effects of SMTP-44D in mice stroke model in relation to neurovascular unit and trophic coupling. *J. Neurosci. Res.* **2018**, *96*, 1887–1899. [CrossRef]

70. Shinouchi, R.; Shibata, K.; Hashimoto, T.; Jono, S.; Hasumi, K.; Nobe, K. SMTP-44D improves diabetic neuropathy symptoms in mice through its antioxidant and anti-inflammatory activities. *Pharmacol. Res. Perspect.* **2020**, *8*, e00648. [CrossRef]

71. Pop-Busui, R.; Boulton, A.J.; Feldman, E.L.; Bril, V.; Freeman, R.; Malik, R.A.; Sosenko, J.M.; Ziegler, D. Diabetic neuropathy: A position statement by the American Diabetes Association. *Diabetes Care* **2017**, *40*, 136–154. [CrossRef] [PubMed]

72. Tesfaye, S.; Boulton, A.J.; Dickenson, A.H. Mechanisms and management of diabetic painful distal symmetrical polyneuropathy. *Diabetes Care* **2013**, *36*, 2456–2465. [CrossRef]

73. Tomino, Y. IgA nephropathy: Lessons from an animal model, the ddY mouse. *J. Nephrol.* **2008**, *21*, 463–467. [PubMed]

74. Mubarak, M. IgA nephropathy: An update on pathogenesis and classification. *J. Coll. Physicians Surg. Pak.* **2011**, *21*, 230–233. [PubMed]

75. Kemmochi, S.; Hayashi, H.; Taniai, E.; Hasumi, K.; Sugita-Konishi, Y.; Kumagai, S.; Mitsumori, K.; Shibutani, M. Protective effect of *Stachybotrys microspora* triprenyl phenol-7 on the deposition of IgA to the glomerular mesangium in nivalenol-induced IgA nephropathy using BALB/c mice. *J. Toxicol. Pathol.* **2012**, *25*, 149–154. [CrossRef] [PubMed]

76. Abuelo, J.G. Normotensive ischemic acute renal failure. *N. Engl. J. Med.* **2007**, *357*, 797–805. [CrossRef] [PubMed]

77. Bonventre, J.V.; Yang, L. Cellular pathophysiology of ischemic acute kidney injury. *J. Clin. Investig.* **2011**, *121*, 4210–4221. [CrossRef]

78. Susantitaphong, P.; Cruz, D.N.; Cerda, J.; Abulfaraj, M.; Alqahtani, F.; Koulouridis, I.; Jaber, B.L.; Acute Kidney Injury Advisory Group of The American Society of Nephrology. World incidence of AKI: A meta-analysis. *Clin. J. Am. Soc. Nephrol.* **2013**, *8*, 1482–1493. [CrossRef]

79. Shibata, K.; Hashimoto, T.; Hasumi, K.; Nobe, K. Potent efficacy of *Stachybotrys microspora* triprenyl phenol-7, a small molecule having anti-inflammatory and antioxidant activities, in a mouse model of acute kidney injury. *Eur. J. Pharmacol.* **2021**, *910*, 174496. [CrossRef]

80. Ross, R. Successful growth of tumours. *Nature* **1989**, *339*, 16–17. [CrossRef]

81. Gately, S.; Twardowski, P.; Stack, M.S.; Cundiff, D.L.; Grella, D.; Castellino, F.J.; Enghild, J.; Kwaan, H.C.; Lee, F.; Kramer, R.A.; et al. The mechanism of cancer-mediated conversion of plasminogen to the angiogenesis inhibitor angiostatin. *Proc. Natl. Acad. Sci. USA* **1997**, *94*, 10868–10872. [CrossRef] [PubMed]

82. Dhanabal, M.; Sethuraman, N. Endogenous angiogenesis inhibitors as therapeutic agents: Historical perspective and future direction. *Recent Pat. Anti-Cancer Drug Discov.* **2006**, *1*, 223–236. [CrossRef] [PubMed]

83. Ohyama, S.; Harada, T.; Chikanishi, T.; Miura, Y.; Hasumi, K. Nonlysine-analog plasminogen modulators promote autoproteolytic generation of plasmin(ogen) fragments with angiostatin-like activity. *Eur. J. Biochem.* **2004**, *271*, 809–820. [CrossRef] [PubMed]

84. Miller, K.D.; Fidler-Benaoudia, M.; Keegan, T.H.; Hipp, H.S.; Jemal, A.; Siegel, R.L. Cancer statistics for adolescents and young adults, 2020. *CA-Cancer J. Clin.* **2020**, *70*, 443–459. [CrossRef]

85. Chan, S.K.; Gullick, W.J.; Hill, M.E. Mutations of the epidermal growth factor receptor in non-small cell lung cancer—Search and destroy. *Eur. J. Cancer* **2006**, *42*, 17–23. [CrossRef]

86. Yan, S.; Zhang, B.; Feng, J.; Wu, H.; Duan, N.; Zhu, Y.; Zhao, Y.; Shen, S.; Zhang, K.; Wu, W.; et al. FGFC1 selectively inhibits erlotinib-resistant non-small cell lung cancer via elevation of ROS mediated by the EGFR/PI3K/Akt/mTOR pathway. *Front. Pharmacol.* **2021**, *12*, 764609. [CrossRef]

87. Joseph, B.; Marchetti, P.; Formstecher, P.; Kroemer, G.; Lewensohn, R.; Zhivotovsky, B. Mitochondrial dysfunction is an essential step for killing of non-small cell lung carcinomas resistant to conventional treatment. *Oncogene* **2017**, *36*, 4818. [CrossRef]

88. Feng, J.; Li, S.; Zhang, B.; Duan, N.; Zhou, R.; Yan, S.; Elango, J.; Liu, N.; Wu, W. FGFC1 exhibits anti-cancer activity via inhibiting NF-κB signaling pathway in *EGFR*-mutant NSCLC cells. *Mar. Drugs* **2022**, *20*, 76. [CrossRef]

89. Nishimura, Y.; Suzuki, E.; Hasegawa, K.; Nishimura, N.; Kitano, Y.; Hasumi, K. Pre-SMTP, a key precursor for the biosynthesis of the SMTP plasminogen modulators. *J. Antibiot.* **2012**, *65*, 483–485. [CrossRef]
90. Do Minh, T.; Johnson, A.L.; Jones, J.E.; Senise, P.P., Jr. Reactions of phthalaldehyde with ammonia and amines. *J. Org. Chem.* **1977**, *42*, 4217–4221. [CrossRef]
91. Su, T.; Bao, B.; Yan, T.; Zhang, C.; Bu, Y.; Wu, W. Response surface methodology to optimize marine microbe culture for producing fungi fibrinolytic compound. *Chin. J. Biotechnol.* **2013**, *29*, 857–861.
92. Wang, M.; He, H.; Na, K.; Cai, M.; Zhou, X.; Zhao, W.; Zhang, Y. Designing novel glucose/ornithine replenishment strategies by biosynthetic and bioprocess analysis to improve fibrinolytic FGFC1 production by the marine fungus *Stachybotrys longispora*. *Process Biochem.* **2015**, *50*, 2012–2018. [CrossRef]
93. Yin, Y.; Fu, Q.; Wu, W.; Cai, M.; Zhou, X.; Zhang, Y. Producing novel fibrinolytic isoindolinone derivatives in marine fungus *Stachybotrys longispora* FG216 by the rational supply of amino compounds according to its biosynthesis pathway. *Mar. Drugs* **2017**, *15*, 214. [CrossRef]

Talaromarins A–F: Six New Isocoumarins from Mangrove-Derived Fungus *Talaromyces flavus* TGGP35

Jin Cai [1,2,†], Xiao-Chen Zhu [3,†], Wei-Nv Zeng [1,2], Bin Wang [1,2], You-Ping Luo [1,2], Jing Liu [1,2], Min-Jing Chen [1,2], Gao-Yu Li [1,2], Guo-Lei Huang [1,2], Guang-Ying Chen [1,2], Jing Xu [3,*] and Cai-Juan Zheng [1,2,*]

[1] Key Laboratory of Tropical Medicinal Resource Chemistry of Ministry of Education, College of Chemistry and Chemical Engineering, Hainan Normal University, Haikou 571158, China; caijin20210207@163.com (J.C.); z17889949296@163.com (W.-N.Z.); 15180328507@163.com (B.W.); lyp188089688692022@163.com (Y.-P.L.); liujing3182799099@163.com (J.L.); cmj19151835730@163.com (M.-J.C.); qqwbma_999@163.com (G.-Y.L.); 070333@hainnu.edu.cn (G.-L.H.); chgying@163.com (G.-Y.C.)
[2] Key Laboratory of Tropical Medicinal Plant Chemistry of Hainan Province, Haikou 571158, China
[3] Key Laboratory of Advanced Materials of Tropical Island Resources of Ministry of Education, School of Chemical Engineering and Technology, Hainan University, Haikou 570228, China; zhuxiaochenlucky@163.com
[*] Correspondence: happyjing3@hainanu.edu.cn (J.X.); caijuan2002@163.com (C.-J.Z.)
[†] These authors contributed equally to this work.

Abstract: Six new isocoumarin derivative talaromarins A-F (**1–6**), along with 17 known analogues (**7–23**), were isolated from the mangrove-derived fungus *Talaromyces flavus* (Eurotiales: Trichocomaceae) TGGP35. Their structures were identified by detailed IR, UV, 1D/2D NMR and HR-ESI-MS spectra. The absolute configurations of new compounds were determined by the modified Mosher's method and a comparison of their CD spectra with dihydroisocoumarins described in the literature. The antioxidant, antibacterial, anti-phytopathogenic and inhibitory activity against α-glucosidase of all the isolated compounds were tested. Compounds **6–11**, **17–19** and **21–22** showed similar or better antioxidant activity than the IC_{50} values ranging from 0.009 to 0.27 mM, compared with the positive control trolox (IC_{50} = 0.29 mM). Compounds **10**, **18**, **21** and **23** exhibited strong inhibitory activities against α-glucosidase with IC_{50} values ranging from 0.10 to 0.62 mM, while the positive control acarbose had an IC_{50} value of 0.5 mM. All compounds showed no antibacterial or anti-phytopathogenic activity at the concentrations of 50 µg/mL and 1 mg/mL, respectively. These results indicated that isocoumarins will be useful to developing antioxidants and as diabetes control agents.

Keywords: *Talaromyces flavus*; isocoumarins; antioxidant; antibacterial; α-glucosidase inhibitory activity; anti-phytopathogenic

1. Introduction

Marine fungi, particularly the mangrove-derived fungi, have proven to be a prolific source of structurally novel and biologically active secondary metabolites, which increasingly attracted the attention of both pharmaceutical and natural product chemists [1–3]. Up to now, more than 1400 new secondary metabolites produced by mangrove-derived fungi have been reported, including polyketides, alkaloids, terpenes and so on, and more than 40% of secondary metabolites displayed cytotoxic, antibacterial and insecticidal activities etc. [3–8]. Among them, isocoumarins are lactone-type derivatives derived from the polyketide pathway [9,10], and they possess a wide range of pharmacological activities such as antibacterial 7-hydroxyoospolactone and parapholactone [11], anti-inflammatory (±)-prunomarin A [12], cytotoxic lunatinin [13], insecticidal peniciisocoumarins A and B, antiplasmodial monocerin [14], antioxidant and α-glucosidase inhibitory penicimarin N [15], brine shrimp (*Artemia salina*) lethal and broad-spectrum antimicrobial penicimarins G–K [16,17], penicoffrazins B and C [18].

The genus of *Talaromyces* has been studied and applied as a biocontrol agent, as a rich source of chitinolytic enzymes and producer of secondary metabolites [19–21]. Different classes of bioactive secondary metabolites have been found from the genus of *Talaromyces* [19–21], including some bioactive isocoumarins, such as selective antimigratory talarolactone A [22], α-glucosidase inhibitory sescandelin B and 3,4-dimethyl-6,8-dihydroxyisocoumarin [23], antibacterial tratenopyrone [24], antibacteria and antifungi (-)-8-hydroxy-3-(4-hydroxypentyl)-3,4-dihydroisocoumarin [25]. These results indicated that the genus of *Talaromyces* can be used for the control of pathogenic bacteria, phytopathogenic microorganisms, diabetes control agents and so on [19,26].

As part of our continuing exploration of structurally novel and biologically interesting secondary metabolites from mangrove-derived fungi [27–33], a fungus *Talaromyces flavus* TGGP35 obtained from the medicinal mangrove plant *Acanthus ilicifolius* attracted our attention, because of the EtOAc extract of *T. flavus* TGGP35 showed potent antioxidant activity. A chemical investigation of this fungus led to the identification of six new isocoumarins talaromarins A-F (**1–6**) and 17 known analogues (**7–23**) (Figure 1). Herein, we report the isolation, structure identification, and bioactivities of these compounds.
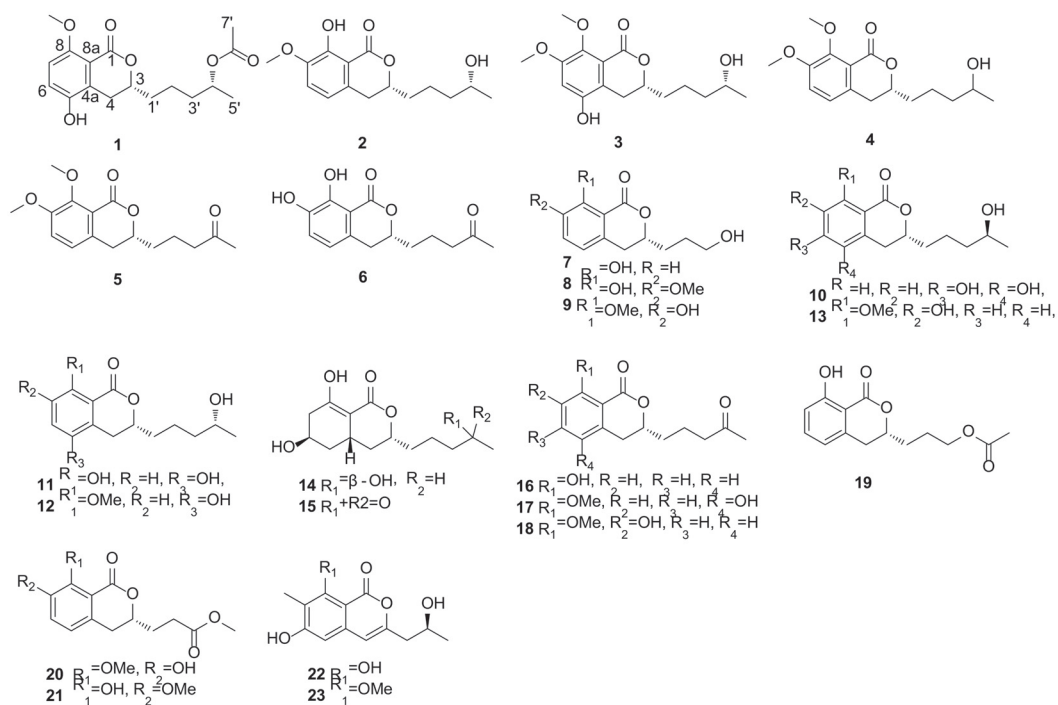
Figure 1. The structures of compounds **1–23**.

2. Results and Discussion

Compound **1** was isolated as a colorless oil. The molecular formula of **1** was established as $C_{17}H_{22}O_6$ (seven degrees of unsaturation) by its HR-ESI-MS spectrum at m/z 323.1475 $[M + H]^+$ (calcd for $C_{17}H_{23}O_6$, 323.1472). The IR spectrum showed the presence of a hydroxyl group (3432 cm^{-1}) and an aromatic ring (1743, 1618 and 1388 cm^{-1}) in **1**. The ^{1}H-NMR data (Table 1) displayed a pair of ortho coupled aromatic protons at δ_H 7.00 (d, J = 8.8 Hz) and 6.78 (d, J = 8.8 Hz), one methoxyl group at δ_H 3.88 (s), two oxygenated methine groups at δ_H 4.90 (m) and 4.34 (m), four methylene groups at δ_H [3.08 (m) and 2.64 (m)], 1.85 (m), 1.57 (m) and 1.52 (m), one methyl group at δ_H 1.22 (d, J = 6.4 Hz).

The combination of ^{13}C NMR and DEPT data (Table 2) exhibited 17 carbon resonances, including two ester carbonyls at δ_C (171.1 and 163.1), six aromatic carbons at δ_C (155.5, 145.3, 128.4, 121.2, 114.6 and 111.5), one methoxyl group at δ_C (56.6), two oxygenated methine groups at δ_C (77.4 and 70.9), four methylene groups at δ_C (35.7, 34.7, 28.0 and 21.0), two methyl groups at δ_C (21.6 and 20.1). The above 1D NMR spectroscopic data indicated that **1** had an isocoumarin skeleton structure, and **1** is similar to penicimarin G (**12**) [16]. The major difference was the presence of an acetoxy group at [(δ_C 171.1 (C), 21.6 (CH$_3$) and δ_H 2.04, (s)] in **1**, indicating that the hydroxyl group in **12** was replaced by an acetoxy group in **1**. The ^{1}H-^{1}H COSY correlations of CH$_2$(2′)–CH$_2$(3′)−CH(4′)−CH$_3$(5′), combined with the HMBC correlations from H-5′ to C-4′/C-3′ (Figure 2), confirmed the acetoxy group connected at C-4′ in **1**, and the planar structure of **1** was determined (Figure 1).

Table 1. 1H NMR spectroscopic data (400/600 MHz) (δ in ppm, *J* in Hz) for **1–6** in CDCl$_3$.

Position	1	2	3	4	5	6
3	4.34, m	4.54, m	4.35, m	4.36, m	4.37, m	4.58, m
4	2.64, dd (16.4, 11.6) 3.08, dd (16.4, 2.8)	2.86, m	2.56, m 2.98, m	2.82, m	2.82, m	2.87, m
5		6.62, d (8.0)		6.91, d (8.0)	6.91, d (8.4)	6.61, d (8.0)
6	7.00, d (8.8)	6.98, d (8.4)	6.67, s	7.06, d (8.0)	7.06, d (8.0)	7.07, d (8.0)
7	6.78, d (8.8)					
7-OH						5.53, s
7-OMe		3.87, s	3.84, s	3.88, s	3.88, s	
8-OMe	3.88, s		3.89, s	3.96, s	3.95, s	
8-OH		11.18, s				11.00, s
1′	1.85, m	1.87, m	1.85, m	1.88, m	1.82, m	1.78, m
2′	1.57, m	1.58, m	1.60, m	1.58, m	1.78, m	1.80, m
3′	1.52, m	1.47, m	1.50, m	1.51, m	2.52, t (6.4)	2.53, m
4′	4.90, m	3.80, m	3.82, m	3.83, m		
5′	1.22, d (6.4)	1.19, d (6.4)	1.21, d (6.0)	1.21, d (4.0)	2.16, s	2.15, m
7′	2.04, s					

Table 2. 13C NMR spectroscopic data (100/150 MHz) for **1–6** in CDCl$_3$.

Position	1	2	3	4	5	6
1	163.1, C	170.4, C	162.7, C	162.6, C	162.5, C	170.2, C
3	77.4, CH	80.4, CH	78.3, CH	78.5, CH	78.3, CH	80.6, CH
4	28.0, CH$_2$	32.4, CH$_2$	27.4, CH$_2$	33.8, CH$_2$	33.7, CH$_2$	32.2, CH$_2$
4a	128.4, C	130.1, C	119.9, C	132.3, C	132.2, C	129.7, C
5	145.3, C	117.1, CH	147.7, CH	122.4, CH	122.4, CH	117.9, CH
6	121.2, CH	117.5, CH	106.1, C	117.5, CH	117.4, CH	120.8, CH
7	111.5, CH	147.4, C	153.1, C	153.0, C	153.0, C	143.9, C
8	155.5, C	152.5, C	142.9, C	151.6, C	151.5, C	149.1, C
8a	114.6, C	108.6, C	117.7, C	119.6, C	119.5, C	108.4, C
7-OMe		56.4, CH$_3$	56.6, CH$_3$	56.5, CH$_3$	56.5, CH$_3$	
8-OMe	56.6, CH$_3$		61.8, CH$_3$	61.7, CH$_3$	61.7, CH$_3$	
1′	34.7, CH$_2$	34.8, CH$_2$	34.9, CH$_2$	34.8, CH$_2$	34.0, CH$_2$	34.1, CH$_2$
2′	21.0, CH$_2$	21.3, CH$_2$	21.5, CH$_2$	21.5, CH$_2$	19.4, CH$_2$	19.2, CH$_2$
3′	35.7, CH$_2$	38.9, CH$_2$	39.1, CH$_2$	39.1, CH$_2$	43.2, CH$_2$	43.0, CH$_2$
4′	70.9, CH	67.9, CH	68.2, CH	68.1, CH	208.7, C	208.6, C
5′	20.1, CH$_3$	23.7, CH$_3$	23.8, CH$_3$	23.8, CH$_3$	30.1, CH$_3$	30.1, CH$_3$
6′	171.1, C					
7′	21.6, CH$_3$					
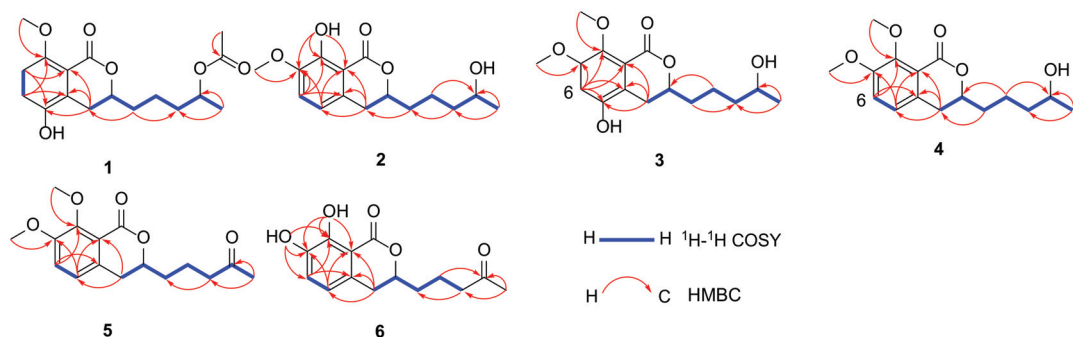
Figure 2. ^{1}H-^{1}H COSY and key HMBC correlations for compounds **1–6**.

The absolute configurations of C-3 and C-4′ in **1** were determined by chemical hydrolysis, modified Mosher's method and a comparison of CD spectra with dihydroisocoumarins described in the literature [28,34]. The major hydrolysis product (**1a**) of **1** was obtained with K$_2$CO$_3$ and anhydrous ethanol at 28 °C for 1.5 h (Figure 3), and **1a** showed the same planar structure with **12** [16]. The modified Mosher's method was used to determine the configuration of C-4′ for **1a**. The differences in ^{1}H NMR chemical shifts of **1a** between (*S*)- and (*R*)-MTPA esters ($\Delta\delta = \delta_S - \delta_R$) were calculated to assign the absolute configuration of C-4′ to be *R* (Figure 4), the same as **12** [16]. The negative cotton effect at 266 nm suggested the *R* configuration at C-3 (Figure 5), by comparison with data for dihydroisocoumarins described in the literature [34]. Thus, the structure of **1** was determined and named talaromarin A.
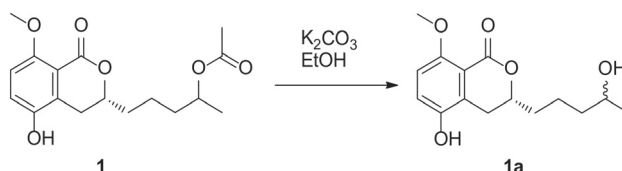
Figure 3. Reaction route of hydrolysis for compound **1**.
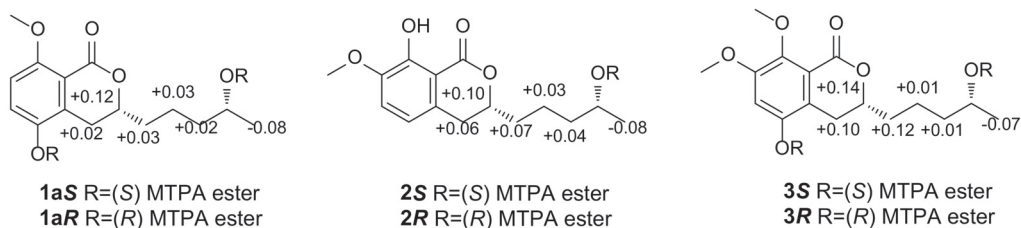
Figure 4. $\Delta\delta$ (=$\delta_S - \delta_R$) values for (*S*)- and (*R*)-MTPA esters of compounds **1–3**.

Compound **2** was isolated as a white powder. The molecular formula was deduced to be C$_{15}$H$_{20}$O$_5$ on the basis of HR-ESI-MS spectrum, implying six degrees of unsaturation. According to the IR spectrum, the hydroxyl group (3414 cm^{-1}) and aromatic rings (1668, 1619, 1586, 1502 and 1442 cm^{-1}) were observed. The ^{1}H and ^{13}C NMR spectroscopic data (Tables 1 and 2) revealed that **2** also belonged to the isocoumarin class and had a similar structural relationship to penicimarin M [17], except for the presence of one oxygenated methine at [δ_H 3.80 (m), δ_C 67.9 (CH)] for C-4′, and the absence of a carbonyl group at δ_C 208.4 (C) in **2**. The above results suggested a carbonyl group in penicimarin M was

replaced by an oxygenated methine group in **2**. Furthermore, the ^{1}H-^{1}H COSY correlations of H-5′ to H-4′ and H-3′ to H-2′/H-4′, and the HMBC correlations from the methyl H-5′ to C-3′/C-4′ established the oxygenated methine at C-4′ (Figure 2). The absolute configuration of C-4′ was determined as *R* by Mosher's method [28] (Figure 4). The negative cotton effect at 265 nm suggested the *R* configuration at C-3 (Figure 5), by comparison with data for dihydroisocoumarins described in the literature [34]. Thus, the absolute configuration of **2** was established as 3*R*,4′*R* and named talaromarin B.
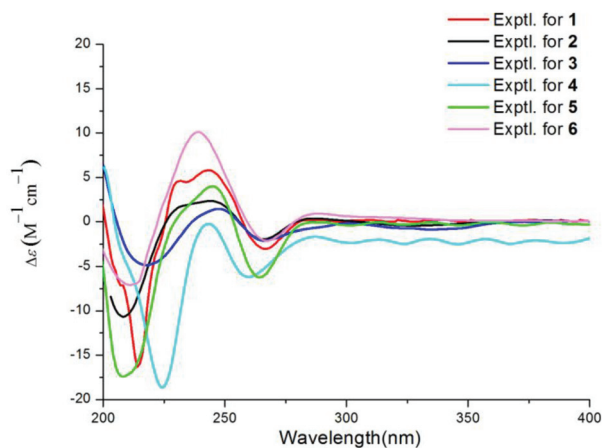
Figure 5. The experimental CD spectra of compounds **1**–**6**.

Compound **3** was isolated as a yellow oil, with the molecular formula $C_{16}H_{22}O_6$ (six degrees of unsaturation) by the HR-ESI-MS spectrum. The IR spectrum indicated that **3** had hydroxyl group (3415 cm^{-1}) and aromatic ring (1638, 1618 and 1384 cm^{-1}). The ^{1}H, ^{13}C NMR data (Tables 1 and 2) and HR-ESI-MS data revealed that **3** closely resembled those of **2**, the main differences were the presence of a methoxyl group at [δ_H 3.89 (s), δ_C 61.8 (CH$_3$)] in **3**, and an aromatic proton signal at δ_H 6.62 (d, *J* = 8.0 Hz) was absented in **3**. Moreover, the chemical shift of C-5 at δ_C (117.1) in **2** was downfield-shifted to δ_C (147.7) in **3**. The HMBC correlations from 8-OCH$_3$ to C-8, 7-OCH$_3$ to C-7 and H-6 to C-8/C-7/C-4a (Figure 2), indicated the additional methoxyl group was attached to C-8 and the hydroxyl group was connected to C-5 (Figure 2). The absolute configurations of C-3 and C-4′ were determined to be the same *R* by comparison with CD data described in the literature [34] and Mosher's method [28] (Figures 4 and 5). Thus, the structure of **3** was determined and named talaromarin C.

Compound **4** was isolated as a yellow oil, and the molecular formula was established as $C_{16}H_{22}O_5$ (six degrees of unsaturation) on the basis of its HR-ESI-MS spectrum. The IR spectrum of **4** displayed absorption bands for hydroxyl (3475 cm^{-1}), carbonyl (1706 cm^{-1}) and aromatic (1637 and 1617 cm^{-1}) groups. The ^{1}H and ^{13}C NMR spectroscopic data (Tables 1 and 2) suggested that **4** was very similar to those of **2**, the only difference was the presence of a methoxyl group at [δ_H 3.96 (s) and δ_C 61.7 (CH$_3$)] in **4**. The location of the methoxyl groups at C-7 and C-8 were established by HMBC correlations from 7-OCH$_3$ to C-7, 8-OCH$_3$ to C-8, H-6 to C-8/C-4a and H-5 to C-7/C-8a/C-4 (Figure 2). The ^{1}H-^{1}H COSY, HMQC, and HMBC spectra established the complete assignment for **4** (Figure 2). Mosher's method was tried to determine the absolute configuration of C-4′ in **4** [28]; unfortunately, the reaction failed. The negative cotton effect at 259 nm suggested the *R* configuration at C-3 (Figure 5) [34]. Thus, the structure of **4** was determined and named talaromarin D.

Compound **5** was isolated as a colorless oil and had the molecular formula of $C_{16}H_{20}O_5$ as determined by HR-ESI-MS and NMR data, requiring seven degrees of unsaturation. The presence of an aromatic ring (1638, 1617 cm^{-1}) was observed in the IR spectrum. The ^{1}H

and [^13]C NMR data (Tables 1 and 2) of **5** were structurally similar to those of **4**, except for the presence of a ketone carbonyl carbon at δ_C 208.7 (C) and the absence of one oxygenated methine carbon at [δ_C 68.1 (CH), δ_H 3.83 (m)] at C-4′ in **5**, indicating that the oxygenated methine group in **4** was replaced by a carbonyl group for C-4′ in **5**. The HMBC correlations from H-3′ to C-1′, H-5′ to C-4′/C-3′ further confirmed **5** with a carbonyl unit at C-4′ (Figure 2). The whole structure was further determined by the 2D NMR spectra (Figure 2). The absolute configuration of C-3 was determined as *R* by CD spectra (Figure 5) [34], and **5** was named talaromarin E.

Compound **6** was isolated as a yellow oil. The molecular formula of **6** was established as $C_{14}H_{16}O_5$ (seven degrees of unsaturation) on the basis of its HR-ESI-MS data. The IR spectrum of **6** showed the hydroxyl group at 3461 and 3407 cm^{-1} and the aromatic rings at 1736 and 1671 cm^{-1}. The [^1]H and [^13]C NMR spectroscopic data (Tables 1 and 2) revealed that **6** was an isocoumarin derivative, with a similar structural relationship to peniciisocoumarin D (**18**), the obvious difference was that **6** lacked a methoxy group at C-8. The methoxy group (8-OMe) in **18** was replaced by a hydroxy group (8-OH) in **6**, which was supported by the appearance of a hydrogen-bonded hydroxyl group at δ_H 11.00 (s). The HMBC correlations from the hydroxyl group 8-OH to C-8a/C-8/C-7 further confirmed the 8-OH was connected at C-8 (δ_C 149.1) (Figure 2). The [^1]H-[^1]H COSY, HMQC, and HMBC spectra determined the complete assignment for **6** (Figure 2). The absolute configuration of C-3 was determined as *R* by CD spectroscopy (Figure 5) [34] and **6** was named talaromarin F.

By comparing physical and spectroscopic data with the literature, the 17 known homologues were identified as (*R*)-3-(3-hydroxypropyl)-8-hydroxy-3,4-dihydroisocoumarin (**7**) [35], peniciisocoumarin C (**8**) [28], 7-hydroxy-3-(3-hydroxypropyl)-8-methoxyisochroman-1-one (**9**) [34], 5,6-dihydroxy-3-(4-hydroxypentyl)-isochroman-1-one (**10**) [23], peniciisocoumarin F (**11**) [28], penicimarin G (**12**) [16], penicimarin C (**13**) [36], peniciisocoumarin A (**14**) [28], peniciisocoumarin B (**15**) [28], aspergillumarin A (**16**) [37], penicimarin H (**17**) [16], peniciisocoumarin D (**18**) [28], peniciisocoumarin G (**19**) [28], peniciisocoumarin E (**20**) [28], penicimarin N (**21**) [15], 6,8-dihydroxy-3-(2-hydroxypropyl)-7-methyl-1*H*-isochromen-1-one (**22**) [38] and pestalotiorin (**23**) [39].

The plausible biosynthetic pathways of compounds **1–23** were also proposed (Scheme 1). Isocoumarins were originated from the acetate-malonate or the polyketide synthase (PKS) pathway [10]. Peniciisocoumarin C (**8**), penicimarin C (**13**) and peniciisocoumarin A (**14**) would be biosynthesized from malonyl-CoA and acetyl-CoA and can be considered as intermediates which would be transformed to other isolated compounds from the fungus TGGP35. Compound **8** would be transformed to **7**, **9** and **20–23** by condensation, aromatization, esterification, dihydroxylation, methoxylation reaction and so on. Compound **13** would be transformed to **10** by dehydroxylation, demethoxylation and dehydroxylation reaction. Compounds **1–6**, **10–15** and **17–19** would be deduced from **14** with dihydroxylation, methoxylation, methylation, hydroxylation, esterification, acetylation, Baeyer–Viliger oxidation reaction, etc.

The antioxidant activities of compounds **1–23** were evaluated. Compounds **6–11**, **17–19** and **22** exhibited potent antioxidant activity with the IC$_{50}$ values ranging from 0.009 to 0.27 mM, while the positive control trolox was IC$_{50}$ = 0.29 mM (Table 3).

Table 3. Antioxidant activity for compounds **2**, **6–11**, **17–19**, **21** and **22**.

Compound	2	6	7	8	9	10	11	17	18	19	21	22	Trolox [a]
IC$_{50}$ (mM)	28.39	0.14	0.17	0.13	0.10	0.11	0.12	0.12	0.16	0.15	20.66	0.009	0.29

[a] Trolox was used as a positive control.
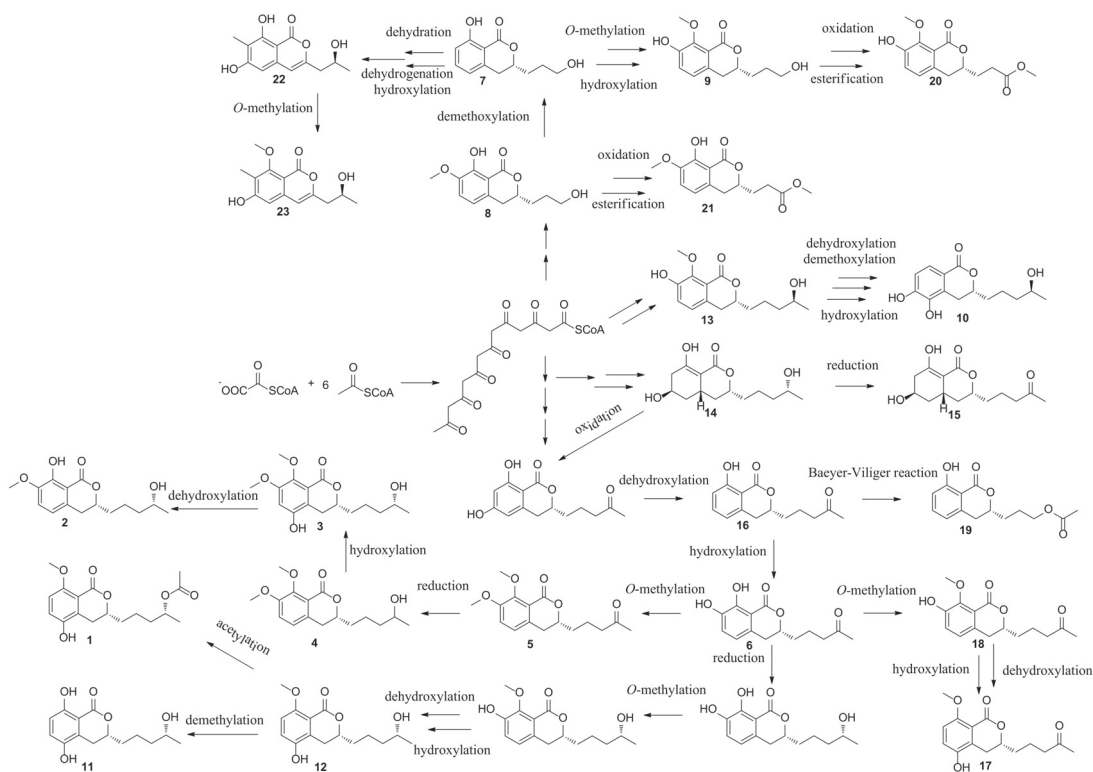
Scheme 1. Plausible biosynthetic pathways of compounds **1–23**.

The preliminary structure–activity relationship of the isolated isocoumarins was discussed. The substitution site, orientation of hydroxyl and methoxy groups on the skeleton of isocoumarins, and the substitution of different groups by side chain C-4′ can affect their antioxidant activity. Compound **2** which possesses a hydroxyl group on C-8, showed better antioxidant activity than that of **3** and **4**, indicating that the chelated hydroxyl group at C-8 is important in enhancing antioxidant activity. Compound **6** possesses two hydroxyl groups at C-7 and C-8, which showed higher antioxidant activity than **16** (only one hydroxyl group on C-8), indicating that the hydroxyl group at C-7 is an important antioxidant activity site. Compounds **17** and **18** possess a ketone group at C-4′, which showed higher antioxidant activity than **12** and **13,** which have an oxygenated methine at C-4′, suggesting that the substitution of different groups by side chain at C-4′ can affect antioxidant activity. Compound **22** possesses a hydroxyl group at C-8, showed higher antioxidant activity than **23**, suggesting that the chelated hydroxyl group at C-8 is important in enhancing antioxidant activity. Furthermore, compounds **7**, **8**, **19** and **21** show antioxidant activities, which may be due to the existence of a chelated hydroxyl group.

Compounds **10**, **18**, **21**, and **23** showed strong inhibitory activity against α-glucosidase with the IC_{50} values of 0.10, 0.38, 0.62 and 0.54 mM, respectively (the positive control acarbose with the IC_{50} value of 0.5 mM).

All compounds were tested for their antibacterial activities against *Staphylococcus. aureus*, *Escherichia coli*, *S. epidermidis* and *Pseudomonas aeruginosa*; however, all compounds showed no antibacterial activity at the concentration of 50 μg/mL. All compounds showed no biological activity against five phytopathogens (*Colletotrichum asianum*, *C. acutatum*,

Fusarium oxysporum, *Pyricularia oryzae* and *Curvularia australiensis*) at the concentration of 1 mg/mL.

3. Materials and Methods

3.1. General Experimental Procedures

Optical rotations were measured on a JASCO P-1020 digital polarimeter (JASCO, Tokyo, Japan). IR spectra were recorded on a Thermo Nicolet 6700 (using KBr disks) spectrophotometer. UV spectra were measured on a PERSEE TU-1990 spectrophotometer. CD spectra were recorded on a Mos-450 spectrometer and 1D and 2D NMR spectra were recorded on a Bruker AV spectrometer (400 MHz for ^{1}H and 100 MHz for ^{13}C) and a JNM-ECZS spectrometer (600 HMz for ^{1}H and 125 MHz for ^{13}C). HR-ESI-MS spectra were obtained on a Q-TOF Ultima Global GAA076 LC mass spectrometer. ESI-MS spectra were recorded on a MAT-95-MS mass spectrometer. HPLC were used for the Agilent 1100 prep-HPLC system with an Agilent C18 analytical (9.4 × 250 mm, 5 μm) HPLC column. Silical gel (200−300 mesh, Qingdao Marine Chemical Factory, Qingdao, China) were used for column chromatography (CC). Sephadex LH-20 gel column (GE Healthcare, Bio-Sciences Corp, Piscataway, NJ, USA) were used for CC. Biological activities were tested on an ultra-clean workbench (Suzhou Sujing Company, Suzhou, China) and the biological activities' results were tested with a full wavelength multifunctional microplate reader (Bio-Tek Instruments, Winooski, VT, USA). Methanol, ethyl acetate, petroleum ether, chloroform, dimethyl sulfoxide and other conventional chemical reagents were used in the experimental operation (Guangzhou Xilong Chemical Reagent Factory, Guangzhou, China).

3.2. Fungal Materials

The fungus TGGP35 was isolated from the stem of the mangrove plant *Acanthus ilicifolius*, which were collected in the Dongzhai Port, Haikou, Hainan Province in August, 2015. The fungus was identified according to its morphological characteristics and a molecular biological protocol by 18S rRNA amplification and sequencing of the ITS region. The sequence data have been submitted to GeneBank, with accession number MT071116, and the fungal strain was identified as *Talaromyces flavus* (Eurotiales: Trichocomaceae). The strains have been stored in the Key Laboratory of Tropical Medicinal Resources Chemistry of the Ministry of Education, School of Chemistry and Chemical Engineering, Hainan Normal University (PDA medium, stored at 4 °C).

3.3. Fermentation, Extraction and Isolation

The seed culture was prepared in potato liquid medium (6 g sea salt and 10 g peptone in 2 L of potato infusion, in 1 L × 4 erlenmeyer flasks each containing 500 mL seed medium), and incubated on a rotary shaker (170 rpm) for 4 days at 28 °C. In total, 20 mL seed culture was then transferred into 1 L erlenmeyer flasks with solid rice medium with a total of 100 bottles of fermentation (each flask contained 60 mL rice, 0.6 g sea salt and 1.0 g peptone) at 28 °C for 4 weeks. The whole rice fermented material was extracted three times with EtOAc, and then concentrated in vacuo to yield crude extracts (120.8 g). The total crude extracts were subjected to silica gel column chromatography (CC) eluted with petroleum ether/EtOAc (*v/v*, gradient 100:0–0:100) and EtOAc/MeOH (*v/v*, gradient 100:0–70:30) to generate fifteen fractions (Fr. A-Fr. L). Fr. F (20.5 g) was fractionated by silica gel CC (200-300 mesh) using a gradient elution of petroleum ether/EtOAc system (7:1–0:1) to obtain ten fractions (Fr. F1-Fr. F10) by the TLC analysis. Fr. F2 (10.3 g) was subjected to Sephadex LH-20 (Petroleum ether-CHCl$_3$-MeOH, 2:1:1, *v/v*), and then to semi-preparative HPLC (MeOH-H$_2$O, 70:30, *v/v*) to give compounds **1** (4.2 mg), **2** (5.5 mg), **3** (3.8 mg), **5** (4.5 mg) and **7** (4.7 mg). Subfraction Fr. F3 was further separated by semi-preparative HPLC (MeOH-H$_2$O, 60:40, *v/v*) for four subfractions Fr. F3a-3d. Compounds **6** (4.7 mg), **8** (5.5 mg), **9** (5.8 mg), and **10** (3.5 mg) were isolated from subfraction Fr. F3a. Compounds **11** (3.7 mg), **14** (4.7 mg), **16** (5.5 mg), **17** (5.8 mg) and **19** (3.5 mg) for subfraction Fr. F3b. Compounds **12** (6.3 mg), **13** (3.2 mg) and **15** (5.7 mg) for subfraction Fr. F3c, and compounds

18 (6.8 mg), **19** (6.2 mg) and **21** (3.6 mg) for subfraction Fr. F3d. Fr. F4 (5.4 g) were subjected to Sephadex LH-20 (CHCl$_3$-MeOH, 1:1, v/v), then used for semi-preparative HPLC (MeOH-H$_2$O, 65:35, v/v) to give compound **20** (3.0 mg). Fr. F5 (2.4 g) was subjected to Sephadex LH-20 (CHCl$_3$-MeOH, 1:1, v/v), then used for semi-preparative HPLC (MeOH-H$_2$O, 35:65, v/v) to give compounds **22** (3.4 mg) and **23** (2.7 mg).

Talaromarin A (**1**): yellow oil; $[\alpha]^{25}_D$ −21.4 (*c* 0.10, MeOH); UV (MeOH) λ_{max} (log ε) 330, 221 nm; IR (KBr) ν_{max} 3432, 1716, 1618, 1383 cm^{-1}; CD (*c* 0.05, MeOH) λ_{max} ($\Delta\varepsilon$) 243 (+5.68), 266 (−2.89) nm; ^{1}H and ^{13}C NMR data see Tables 1 and 2; HR-ESI-MS *m/z*: 323.1475 [M + H]$^+$, (C$_{17}$H$_{23}$O$_6$, calcd. for 323.1472).

Talaromarin B (**2**): white powder; $[\alpha]^{25}_D$ −23.6 (*c* 0.10, MeOH); UV (MeOH) λ_{max} (log ε) 330, 255, 223 nm; IR (KBr) ν_{max} 3414, 1668, 1619, 1586, 1502, 1442 cm^{-1}; CD (*c* 0.05, MeOH) λ_{max} ($\Delta\varepsilon$) 244 (+2.27), 265 (−2.17) nm; ^{1}H and ^{13}C NMR data see Tables 1 and 2; HR-ESI-MS *m/z*: 279.1240 [M − H]$^-$, (C$_{15}$H$_{19}$O$_5$, calcd. for 279.1239).

Talaromarin C (**3**): yellow oil; $[\alpha]^{25}_D$ −22.0 (*c* 0.10, MeOH); UV (MeOH) λ_{max} (log ε) 317, 215 nm; IR (KBr) ν_{max} 3415, 1638, 1618, 1384 cm^{-1}; CD (*c* 0.05, MeOH) λ_{max} ($\Delta\varepsilon$) 248 (+1.36), 266 (−2.01) nm; ^{1}H and ^{13}C NMR data see Tables 1 and 2; HR-ESI-MS *m/z*: 311.1485 [M + H]$^+$, (C$_{16}$H$_{23}$O$_6$, calcd. for 311.1482).

Talaromarin D (**4**): yellow oil; $[\alpha]^{25}_D$ −21.8 (*c* 0.10, MeOH); UV (MeOH) λ_{max} (log ε) 313, 222 nm; IR (KBr) ν_{max} 3475, 1706, 1637, 1617 cm^{-1}; CD (*c* 0.05, MeOH) λ_{max} ($\Delta\varepsilon$) 243 (−0.31), 259 (−6.25) nm; ^{1}H and ^{13}C NMR data see Tables 1 and 2; HR-ESI-MS *m/z*: 295.1527 [M + H]$^+$, (C$_{16}$H$_{23}$O$_5$, calcd. for 295.1524).

Talaromarin E (**5**): colorless oil; $[\alpha]^{25}_D$ −24.4 (*c* 0.10, MeOH); UV (MeOH) λ_{max} (log ε) 314, 219 nm; IR (KBr) ν_{max} 1638,1617 cm^{-1}; CD (*c* 0.05, MeOH) λ_{max} ($\Delta\varepsilon$) 245 (+3.93), 264 (−11.89) nm; ^{1}H and ^{13}C NMR data see Tables 1 and 2; HR-ESI-MS *m/z*: 293.1370 [M + H]$^+$, (C$_{16}$H$_{21}$O$_5$, calcd. for 293.1374).

Talaromarin F (**6**): yellow oil; $[\alpha]^{25}_D$ −21.2 (*c* 0.10, MeOH); UV (MeOH) λ_{max} (log ε) 328, 254, 223 nm; IR (KBr) ν_{max} 3481, 3407, 1736, 1671 cm^{-1}; CD (*c* 0.05, MeOH) λ_{max} ($\Delta\varepsilon$) 238 (+10.12), 267 (−2.07) nm; ^{1}H and ^{13}C NMR data see Tables 1 and 2; HR-ESI-MS *m/z*: 265.1050 [M + H]$^+$, (C$_{14}$H$_{17}$O$_5$, calcd. for 265.1053).

3.4. Preparations of the (S)- and (R)-MTPA Esters of Compounds **1**, **2** and **3**

Compound **1** was hydrolyzed in anhydrous ethanol solution for 90 min with potassium carbonate in an equivalent ratio of 1:2; the mixed product after hydrolysis was purified by semi-preparative HPLC (MeOH-H$_2$O, 70:30, v/v) to obtain **1a**. The preparation of (*S*)- and (*R*)-MTPA ester derivatives of **1a**, **2** and **3** was performed as described previously [28].

Hydrolysate of **1** (**1a**): ^{1}H NMR (CDCl$_3$, 400 MHz): δ_H 6.99 (1H, d, *J* = 8.8 Hz H-6), 6.79 (1H, d, *J* = 8.8 Hz, H-7), 4.26 (1H, m, H-3), 3.83 (1H, m, H-4′), 3.10 and 2.63 (2H, m, H-4), 1.90 (2H, m, H-1′), 1.70 (2H, m, H-2′), 1.50 (2H, m, H-3′), 1.21 (3H, d, *J* = 6.0 Hz, H-5′); ^{13}C NMR (CDCl$_3$, 100 MHz): δ_C 163.3, 159.4, 151.5, 145.1, 135.0, 128.5, 121.2, 111.4, 68.2, 56.6, 39.1, 34.9, 28.0, 23.8, 21.4; ESI-MS *m/z* 281.1 [M + H]$^+$.

(*S*)-MTPA ester of **1a**: ^{1}H NMR (CDCl$_3$, 600 MHz): δ_H 7.29 (1H, d, *J* = 9.0 Hz, H-6), 6.94 (1H, d, *J* = 9.0 Hz, H-7), 5.12 (1H, m, H-4′), 4.21 (1H, m, H-3), 2.64 and 2.49 (2H, m, H-4), 1.86 (2H, m, H-1′), 1.67 (2H, m, H-2′), 1.55 (2H, m, H-3′), 1.25 (3H, d, *J* = 6.6 Hz, H-5′); ESI-MS *m/z* 758.2 [M + Na]$^+$.

(*R*)-MTPA ester of **1a**: ^{1}H NMR (CDCl$_3$, 600 MHz): δ_H 7.31 (1H, d, *J* = 9.0 Hz, H-6), 6.94 (1H, d, *J* = 9.0 Hz, H-7), 5.11 (1H, m, H-4′), 4.09 (1H, m, H-3), 2.62 and 2.41 (2H, m, H-4), 1.83 (2H, m, H-1′), 1.64 (2H, m, H-2′), 1.53 (2H, m, H-3′), 1.33 (3H, d, *J* = 6.0 Hz, H-5′); ESI-MS *m/z* 758.2 [M + Na]$^+$.

(*S*)-MTPA ester of **2**: ^{1}H NMR (CDCl$_3$, 600 MHz): δ_H 7.01 (1H, d, *J* = 7.8 Hz, H-5), 6.63 (1H, d, *J* = 7.8 Hz, H-6), 5.17 (1H, m, H-4′), 4.52 (1H, m, H-3), 2.82 (2H, m, H-4), 1.88 (2H, m, H-1′), 1.62 (2H, m, H-2′), 1.50 (2H, m, H-3′), 1.29 (3H, d, *J* = 6.0 Hz, H-5′); ESI-MS *m/z* 758.3 [M + Na]$^+$.

(*R*)-MTPA ester of **2**: ^{1}H NMR (CDCl$_3$, 600 MHz): δ_H 7.01 (1H, d, *J* = 8.4 Hz, H-5), 6.62 (1H, d, *J* = 8.4 Hz, H-6), 5.16 (1H, m, H-4′), 4.42 (1H, m, H-3), 2.76 (2H, m, H-4), 1.81 (2H, m,

H-1′), 1.59 (2H, m, H-2′), 1.46 (2H, m, H-3′), 1.37 (3H, d, *J* = 6.0 Hz, H-5′); ESI-MS *m/z* 774.3 [M + K]$^+$.

(*S*)-MTPA ester of **3**: ^{1}H NMR (CDCl$_3$, 600 MHz): δ_H 6.88 (1H, s, H-6), 5.14 (1H, m, H-4′), 4.21 (1H, m, H-3), 2.43 (2H, m, H-4), 1.72 (2H, m, H-1′), 1.52 (2H, m, H-2′), 1.43 (2H, m, H-3′), 1.35 (3H, d, *J* = 9.4 Hz, H-5′); ESI-MS *m/z* 766.6 [M + Na]$^+$.

(*R*)-MTPA ester of **3**: ^{1}H NMR (CDCl$_3$, 600 MHz): δ_H 6.86 (1H, s, H-6), 5.13 (1H, m, H-4′), 4.07 (1H, m, H-3), 2.33 (2H, m, H-4), 1.65 (2H, m, H-1′), 1.51 (2H, m, H-2′), 1.42 (2H, m, H-3′), 1.28 (3H, d, *J* = 9.4 Hz, H-5′); ESI-MS *m/z* 766.0 [M + Na]$^+$.

3.5. Biological Assays

3.5.1. Antioxidant Activity

The antioxidant activity assay was based on the reported methods [15]. The assay was performed on a 96-well microplate, the reaction was initiated by adding 10 μL of sample solution to 200 μL of ABTS working solution. All test group gradients (including positive control) were of 2.0, 1.0, 0.5, 0.25 mg/mL, respectively. PBS buffer was used as the blank control, DMSO as the negative control, and trolox as the positive control (IC$_{50}$ = 0.29 mM). The antioxidant effect was evaluated by a full wavelength multifunctional microplate reader measurement at 734 nm. The inhibition rate of each sample was calculated according to the following formula: inhibition rate = [(A$_{blank}$ − A$_{compound}$)/A$_{blank}$] × 100%. Finally, the SPSS software was used to calculate the IC$_{50}$ value.

3.5.2. Antibacterial Activity

All compounds were determined against four pathogenic bacteria: *Staphylococcus aureus* (ATCC 25923), *Escherichia coli* (ATCC 25922), *S. epidermidis* (ATCC 17749) and *Pseudomonas aeruginosa* (ATCC 17749). The concentration value of the test group and positive control was 1mg/mL by the microplate assay method [28]. The antibacterial effect was evaluated by a full wavelength multifunctional microplate reader measurement at 630 nm; the broth medium containing pathogenic bacteria was used as the blank group and DMSO as the negative control, ciprofloxacin was used as the positive control. The positive control ciprofloxacin showed antibacterial activities against four pathogenic bacteria *S. aureus*, *E. coil*, *S. epidermidis* and *P. aeruginosa* with the MIC values of 0.097, 0.78, 0.195 and 0.78 μg/mL, respectively.

3.5.3. Anti-Phytopathogenic Activity

All compounds were tested against five plant pathogens (*Colletotrichum asianum*, *C. acutatum*, *Fusarium oxysporum*, *Pyricularia oryzae* and *Curvularia australiensis*) by disk method [40]. DMSO was used as a negative control, carbendazim as a positive control. The concentration values of all test groups, negative control and positive control were 1 mg/mL; the anti-phytopathogenic results were recorded on a vernier caliper.

3.5.4. Inhibitory Activity against α-Glucosidase

The α-glucosidase inhibitory activity of the tested compounds was determined using the method in [17], with modifications for carrying it out in 96-well plates. The initial concentration of all test samples (including positive control and negative control) was 1 mg/mL, the optimized method was a mixture of 0.1 mM potassium phosphate buffer (pH = 6.8, 0.5 mL) and 10 mg/L α-glucosidase (100 μL), the testing sample (0.5 mL) was incubated at 37 °C for 5 min, and the 2.5 mM (4-nitrophenyl-*β*-*D*-glucopyranoside) PNPG (0.5 mL) was added, followed by mixing. The reaction was carried out at 37 °C for 15 min and then stopped by adding 0.2 M solution of Na$_2$CO$_3$ (0.75 mL). The inhibitory activity against α-Glucosidase was evaluated by a full wavelength multifunctional microplate reader measurement at 405 nm. Finally, inhibition rate = [(A$_{control}$ − A$_{compound}$)/A$_{control}$] × 100%. The SPSS software was used to calculate the IC$_{50}$ value. DMSO was used as the negative control and acarbose was used as the positive control (IC$_{50}$ = 0.5 mM).

4. Conclusions

In summary, 23 secondary metabolites, including six new isocoumarin derivative talaromarins A-F (**1–6**) and 17 known analogues (**7–23**) were obtained from the mangrove-derived fungus *Talaromyces flavus* TGGP35. Compounds **6–11**, **17–19** and **22** exerted similar or better antioxidant activity than the positive control trolox (IC$_{50}$ = 0.29 mM), with IC$_{50}$ values ranging from 0.009 to 0.27 mM. Compounds **10**, **18**, **21** and **23** exhibited strong inhibitory activities against α-glucosidase with IC$_{50}$ values ranging from 0.10 to 0.62 mM, while the IC$_{50}$ value of positive control acarbose was 0.5 mM. All compounds showed no antibacterial or anti-phytopathogenic activity at the concentrations of 50 µg/mL and 1 mg/mL, respectively. Their plausible biosynthetic pathway and structure–activity relationships were also explored. Therefore, these findings demonstrate the potential of these active compounds as lead compounds for developing antioxidants and as diabetes control agents.

Supplementary Materials: The following supporting information can be downloaded at: https://www.mdpi.com/article/10.3390/md20060361/s1, D, 2D NMR and MS data of new compounds **1–6**.

Institutional Review Board Statement: Not applicable.

Informed Consent Statement: Not applicable.

Data Availability Statement: The data presented in this study are available in this article and Supplementary Material.

References

1. Carroll, A.R.; Copp, B.R.; Davis, R.A.; Keyzers, R.A.; Prinsep, M.R. Marine natural products. *Nat. Prod. Rep.* **2022**, *18*, 1R–49R. [CrossRef] [PubMed]
2. Xu, W.F.; Wu, N.N.; Wu, Y.W.; Qi, Y.X.; Wei, M.Y.; Pineda, L.M.; Ng, M.G.; Spadafora, C.; Zheng, J.Y.; Lu, L.; et al. Structure modifcation, antialgal, antiplasmodial, and toxic evaluations of a series of new marine-derived 14-membered resorcylic acid lactone derivatives. *Mar. Life Sci. Technol.* **2022**, *4*, 88–97. [CrossRef]
3. Chen, S.H.; Cai, R.L.; Liu, Z.M.; Gui, H.; She, Z.G. Secondary metabolites from mangrove-associated fungi: Source, chemistry and bioactivities. *Nat. Prod. Rep.* **2022**, *39*, 560–595. [CrossRef] [PubMed]
4. Jiang, H.M.; Cai, R.L.; Zang, Z.M.; Yang, W.C.; Wang, B.; Zhu, G.; Yuan, J.; She, Z.G. Azaphilone derivatives with anti-inflammatory activity from the mangrove endophytic fungus *Penicillium sclerotiorum* ZJHJJ-18. *Bioorg. Chem.* **2022**, *122*, 105721. [CrossRef]
5. Wu, Q.; Chang, Y.M.; Che, Q.; Li, D.H.; Zhang, G.J.; Zhu, T.J. Citreobenzofurans D-F and phomenones A-B: Five novel sesquiterpenoids from the mangrove-derived fungus *Penicillium* sp. HDN13-494. *Mar. Drugs* **2022**, *20*, 137. [CrossRef]
6. Qin, X.Y.; Huang, J.G.; Zhou, D.X.; Zhang, W.X.; Zhang, Y.J.; Li, J.; Yang, R.Y.; Huang, X.S. Polyketide derivatives, guhypoxylonols A-D from a mangrove endophytic fungus *Aspergillus* sp. GXNU-Y45 that inhibit nitric oxide production. *Mar. Drugs* **2022**, *20*, 5. [CrossRef]
7. Su, J.H.; Wang, M.Q.; Li, Y.Z.; Lin, Y.S.; Gu, J.Y.; Zhu, L.P.; Yang, W.Q.; Jiang, S.Q.; Zhao, Z.X.; Sun, Z.H. Rare cytochalasans isolated from the mangrove endophytic fungus *Xylaria arbuscular*. *Fitoterapia* **2022**, *157*, 105124. [CrossRef]
8. Zeng, W.N.; Huang, G.L.; Cai, J.; Zheng, C.J. Secondary metabolites and bioactivities of *Penicillium* sp. sourced from mangrove from 2007 to 2020. *Chin. J. Org. Chem.* **2021**, *41*, 4255–4278. [CrossRef]

9. Saeed, A. Isocoumarins, miraculous natural products blessed with diverse pharmacological activities. *Eur. J. Med. Chem.* **2016**, *116*, 290–317. [CrossRef]
10. Noor, A.O.; Almasri, D.M.; Bagalagel, A.A.; Abdallah, H.M.; Mohamed, S.G.A.; Mohamed, G.A.; Ibrahim, S.R.M. Naturally occurring isocoumarins derivatives from endophytic fungi: Sources, isolation, structural characterization, biosynthesis, and biological activities. *Molecules* **2020**, *25*, 395. [CrossRef]
11. Xu, X.L.; Li, J.P.; Zhang, K.; Wei, S.Z.; Lin, R.; Polyak, S.W.; Yang, N.; Song, F.H. New isocoumarin analogues from the marine-derived fungus *Paraphoma* sp. CUGBMF180003. *Mar. Drugs* **2021**, *19*, 313. [CrossRef] [PubMed]
12. Zhang, X.Q.; Lu, Z.H.; Xia, G.R.; Song, W.M.; Guo, Z.Y.; Proksch, P. (+)-/(−)-Prunomarin A and (+)-pestalactone B, three new isocoumarin derivatives from the endophytic fungus *Phomopsis prunorum*. *Tetrahedron. Lett.* **2021**, *75*, 153205. [CrossRef]
13. Ran, Y.Q.; Lan, W.J.; Qiu, Y.; Guo, Q.; Feng, G.K.; Deng, R.; Zhu, X.F.; Li, H.J.; Dong, J. Monarubins A-C from the marine shellfish-associated fungus *Monascus ruber* BB5. *Mar. Drugs* **2020**, *18*, 100. [CrossRef] [PubMed]
14. Coronado, L.; Zhang, X.Q.; Dorta, D.; Escala, N.; Pineda, L.M.; Ng, M.G.; Olmo, E.D.; Wang, C.Y.; Gu, Y.C.; Shao, C.L.; et al. Semisynthesis, antiplasmodial activity, and mechanism of action studies of isocoumarin derivatives. *J. Nat. Prod.* **2021**, *84*, 1434–1441. [CrossRef] [PubMed]
15. Zeng, W.N.; Cai, J.; Wang, B.; Chen, L.Y.; Pan, C.X.; Chen, S.J.; Huang, G.L.; Zheng, C.J. A new bioactive isocoumarin from the mangrove-derived fungus *Penicillium* sp. TGM112. *J. Asian Nat. Prod. Res.* **2021**, 1–6. [CrossRef]
16. Huang, G.L.; Zhou, X.M.; Bai, M.; Liu, Y.X.; Zhao, Y.L.; Luo, Y.P.; Niu, Y.Y.; Zheng, C.J.; Chen, G.Y. Dihydroisocoumarins from the mangrove-derived fungus *Penicillium citrinum*. *Mar. Drugs* **2016**, *14*, 177. [CrossRef]
17. Mei, R.Q.; Wang, B.; Zeng, W.N.; Huang, G.L.; Chen, G.Y.; Zheng, C.J. Bioactive isocoumarins isolated from a mangrove-derived fungus *Penicillium* sp. MGP11. *Nat. Prod. Res.* **2022**, *36*, 1260–1265. [CrossRef]
18. Cao, J.; Li, X.M.; Li, X.; Li, H.L.; Meng, L.H.; Wang, B.G. New lactone and isocoumarin derivatives from the marine mangrove-derived endophytic fungus *Penicillium coffeae* MA-314. *Phytochem. Lett.* **2019**, *32*, 1–5. [CrossRef]
19. Proksa, B. *Talaromyces flavus* and its metabolites. *Chem. Pap.* **2010**, *64*, 696–714. [CrossRef]
20. Nicoletti, R.; Trincone, A. Bioactive compounds produced by strains of *Penicillium* and *Talaromyces* of marine origin. *Mar. Drugs* **2016**, *14*, 37. [CrossRef]
21. Nicoletti, R.; Salvatore, M.M.; Andolfi, A. Secondary metabolites of mangrove-associated strains of *Talaromyces*. *Mar. Drugs* **2018**, *16*, 12. [CrossRef] [PubMed]
22. Yuan, W.H.; Teng, M.T.; Yun, Y.F.; Jiang, N.; Ma, L.; Sun, S.S.; Yuan, B.; Tang, J.; Wu, Q.Y.; Li, Q.; et al. Talarolactone A, an isocoumarin derivative fused with dihydrothiophene with selective antimigratory activity from the endolichenic fungus *Talaromyces* sp. *J. Nat. Prod.* **2020**, *83*, 1716–1720. [CrossRef] [PubMed]
23. Chen, S.H.; Liu, Y.Y.; Liu, Z.M.; Cai, R.L.; Lu, Y.J.; Huang, X.S.; She, Z.G. Isocoumarins and benzofurans from the mangrove endophytic fungus *Talaromyces amestolkiae* possess α-glucosidase inhibitory and antibacterial activities. *RSC Adv.* **2016**, *6*, 26412–26420. [CrossRef]
24. Buttachon, S.; May, Z.; War, W.; Dethoup, T.; Gales, L.; Pereira, J.A.; Silva, A.M.S.; Kijjoa, A. Secondary metabolites from the culture of the marine sponge-associated fungi *Talaromyces tratensis* and *Sporidesmium circinophorum*. *Planta Med.* **2016**, *82*, 888–896. [CrossRef] [PubMed]
25. Miao, F.; Yang, R.; Chen, D.D.; Wang, Y.; Qin, B.F.; Yang, X.J.; Zhou, L. Isolation, identification and antimicrobial activities of two secondary metabolites of *Talaromyces verruculosus*. *Molecules* **2012**, *17*, 14091–14098. [CrossRef]
26. Duo-Chuan, L.I.; Chen, S.; Jing, L.U. Purification and partial characterization of two chitinases from the mycoparasitic fungus *Talaromyces flavus*. *Mycopathologia* **2005**, *159*, 223–229. [CrossRef]
27. Bai, M.; Zheng, C.J.; Chen, G. Austins-type meroterpenoids from a mangrove-derived *Penicillium* sp. *J. Nat. Prod.* **2021**, *84*, 2104–2110. [CrossRef]
28. Bai, M.; Zheng, C.J.; Huang, G.L.; Mei, R.Q.; Wang, B.; Luo, Y.P.; Zheng, C.; Niu, Z.G.; Chen, G.Y. Bioactive meroterpenoids and isocoumarins from the mangrove-derived fungus *Penicillium* sp. TGM112. *J. Nat. Prod.* **2019**, *82*, 1155–1164. [CrossRef]
29. Liao, H.X.; Shao, T.M.; Mei, R.Q.; Huang, G.L.; Zhou, X.M.; Zheng, C.J.; Wang, C.Y. Bioactive secondary metabolites from the culture of the mangrove-derived fungus *Daldinia eschscholtzii* HJ004. *Mar. Drugs* **2019**, *17*, 710. [CrossRef]
30. Bai, M.; Zheng, C.J.; Nong, X.H.; Zhou, X.M.; Luo, Y.P.; Chen, G.Y. Four new insecticidal xanthene derivatives from the mangrove-derived fungus *Penicillium* sp. JY246. *Mar. Drugs* **2019**, *17*, 649. [CrossRef]
31. Bai, M.; Huang, G.L.; Mei, R.Q.; Wang, B.; Luo, Y.P.; Nong, X.H.; Chen, G.Y.; Zheng, C.J. Bioactive lactones from the mangrove-derived fungus *Penicillium* sp. TGM112. *Mar. Drugs* **2019**, *17*, 433. [CrossRef] [PubMed]
32. Liao, H.X.; Zheng, C.J.; Huang, G.L.; Mei, R.Q.; Nong, X.H.; Shao, T.M.; Chen, G.; Wang, C.Y. Bioactive polyketide derivatives from the mangrove-derived fungus *Daldinia eschscholtzii* HJ004. *J. Nat. Prod.* **2019**, *82*, 2211–2219. [CrossRef] [PubMed]
33. Zheng, C.J.; Bai, M.; Zhou, X.M.; Huang, G.L.; Shao, T.M.; Luo, Y.P.; Niu, Y.Y.; Chen, G.Y.; Han, C.R. Penicilindoles A-C, cytotoxic indole diterpenes from the mangrove-derived fungus *Eupenicillium* sp. HJ002. *J. Nat. Prod.* **2018**, *81*, 1045–1049. [CrossRef] [PubMed]
34. Yan, Z.Y.; Wen, S.; Ding, M.; Guo, H.X.; Huang, G.Y.; Zhu, X.T.; Huang, J.Y.; She, Z.G.; Long, Y.H. The purification, characterization, and biological activity of new polyketides from mangrove-derived endophytic fungus *Epicoccum nigrum* SCNU-F0002. *Mar. Drugs* **2019**, *17*, 414. [CrossRef]

35. Sun, J.; Zhu, Z.X.; Song, Y.L.; Ren, Y.; Dong, D.; Zheng, J.; Liu, T.; Zhao, Y.F.; Tu, P.F.; Li, J. Anti-neuroinflammatory constituents from the fungus *Penicillium* purpurogenum MHZ 111. *Nat. Prod. Res.* **2017**, *31*, 562–567. [CrossRef]
36. Qi, J.; Shao, C.L.; Li, Z.Y.; Gan, L.S.; Fu, X.M.; Bian, W.T.; Zhao, H.Y.; Wang, C.Y. Isocoumarin derivatives and benzofurans from a sponge-derived *Penicillium* sp. fungus. *J. Nat. Prod.* **2013**, *76*, 571–579. [CrossRef]
37. Li, S.D.; Wei, M.Y.; Chen, G.Y.; Lin, Y.C. Two new dihydroisocoumarins from the endophytic fungus *Aspergillus* sp. collected from the South China Sea. *Chem. Nat. Compd.* **2012**, *48*, 371–373. [CrossRef]
38. Zin, W.W.M.; Buttachon, S.; Dethoup, T.; Pereira, J.A.; Gales, L.; Inacio, A.; Costa, P.M.; Lee, M.; Sekeroglu, N.; Silva, A.M.S.; et al. Antibacterial and antibiofilm activities of the metabolites isolated from the culture of the mangrove-derived endophytic fungus *Eurotium chevalieri* KUFA 0006. *Phytochemistry* **2017**, *141*, 86–97. [CrossRef]
39. Arunpanichlert, J.; Rukachaisirikul, V.; Phongpaichit, S.; Supaphon, O.; Sakayaroj, J. Meroterpenoid, isocoumarin, and phenol derivatives from the seagrass-derived fungus *Pestalotiopsis* sp. PSU-ES194. *Tetrahedron* **2015**, *71*, 882–888. [CrossRef]
40. He, J.; Yang, M.S.; Wang, W.X.; Li, Z.H.; Elkhateeb, W.A.M.; Wen, T.C.; Ai, H.L.; Feng, T. Anti-phytopathogenic sesquiterpenoid-xanthone adducts from potato endophytic fungus *Bipolaris eleusines*. *RSC Adv.* **2019**, *9*, 128–131. [CrossRef]

marine drugs

MDPI

Sesquiterpenoids from the Mangrove-Derived *Aspergillus ustus* 094102

Pengyan Gui [1,†], Jie Fan [1,2,†], Tonghan Zhu [1,3], Peng Fu [1,4], Kui Hong [5,*] and Weiming Zhu [1,4,*]

[1] Key Laboratory of Marine Drugs, Ministry of Education of China, School of Medicine and Pharmacy, Ocean University of China, Qingdao 266003, China; 11180811003@stu.ouc.edu.cn (P.G.); fj900622@163.com (J.F.); sdueduzth@126.com (T.Z.); fupeng@ouc.edu.cn (P.F.)

[2] Qingdao Marine Technical College, Qingdao 266590, China

[3] College of Civil Engineering and Architecture, Shandong University of Science and Technology, Qingdao 266590, China

[4] Laboratory for Marine Drugs and Bioproducts of Qingdao National Laboratory for Marine Science and Technology, Qingdao 266237, China

[5] Key Laboratory of Combinatorial Biosynthesis and Drug Discovery, Ministry of Education and School of Pharmaceutical Sciences, Wuhan University, Wuhan 430071, China

[*] Correspondence: kuihong31@whu.edu.cn (K.H.); weimingzhu@ouc.edu.cn (W.Z.); Tel./Fax: +86-532-82031268 (W.Z.)

[†] These authors contributed equally to this work.

Abstract: Four new drimane sesquiterpenoids (**1**–**4**) and three known ones (**5**–**7**) were isolated from the fermentation broth of the mangrove-derived *Aspergillus ustus* 094102. Compound **5** was further resolved as four purified compounds **5a**–**5d**. By means of extensive spectroscopic and ECD analysis as well as the chemical transformation, their structures were identified as (2R,3R,5S,9R,10S)-2,3,9,11-tetrahydroxydrim-7-en-6-one (ustusol F, **1**), (2R,3R,5R,9S,10R)-2,3,11-trihydroxydrim-7-en-6-one (9-deoxyustusol F, **2**), (3S,5R,9R,10R)-3,11,12-trihydroxydrim-7-en-6-one (ustusol G, **3**), (5S,6R,9S,10S,11R,2′E,4′E)-(11-dideoxy-11-hydroxystrobilactone A-6-yl)-5-carboxypenta-2,4-dienoate (ustusolate H, **4**), ((5S,6R,9S,10S)-strobilactone A-6-yl) (2E,4E)-6,7-dihydroxyocta-2,4-dienoate (ustusolate I, **5**), (2′E,4′E;6′,7′-*erythro*)-ustusolate I (**5a**) and (2′E,4′E;*ent*-6′,7′-*erythro*)-ustusolate I (**5b**), (2′E,4′E,6′R,7′R)-ustusolate I (**5c**) and (2′E,4′E,6′S,7′S)-ustusolate I (**5d**), (5S,6R,9S,10S,2′E,4′E)-(strobilactone A-6-yl)-5-carboxypenta-2,4-dienoate (ustusolate J, **6**), and (2S,5S,9R,10S)-2,9,11-trihydroxydrim-7-en-6-one (ustusol B, **7**), respectively. Compound **5** showed antiproliferation against the human tumor cells CAL-62 and MG-63 with the IC$_{50}$ values of 16.3 and 10.1 μM, respectively.

Keywords: drimane sesquiterpenoids; absolute configuration; antiproliferation; *Aspergillus ustus*; mangrove-derived fungus

1. Introduction

As well as we know, microbial metabolites are an important source of drug discovery and development [1]. However, with the deepening of research, many strains in the conventional environment have been repeatedly studied, resulting in the increase of the recurrence rate of known compounds and the decrease of the occurrence rate of new bioactive compounds [2]. Mangrove fungi have attracted much attention because of their special growth environment and unique metabolic mechanism, resulting in the diversity of the structure and bioactivity of their secondary metabolites, which has become a new hotspot in drug development [3,4]. Our previous work reported 9 drimane sesquiterpenoids, 8 benzofurans [4], and 18 ophiobolins [5] from mangrove-derived fungus *Aspergillus ustus* 094102, among which ustusorane E and ustusolate E exhibited cytotoxic activity against the HL-60 cells with IC$_{50}$ values of 0.13 and 9.0 μM, respectively [4]. In addition, more than 50 drimane sesquiterpenoids have been reported from fungi, including cytotoxic

strobilactones A and B from *Strobilurus ohshimae* [6], (6-strobilactone-B) ester of (*E,E*)-6-oxo-2,4-hexadienoic acid from marine sponge-derived *A. ustus* [7], (6-strobilactone-B) ester of (*E,E*)-6-carbon-7-hydroxy-2,4-octadienoic acid from mangrove-derived *A. ustus* [8], synergistic antibacterial ustusoic acid B from *A. ustus* [9], and ET-1 binding inhibitory (2′*E*,4′*E*,6′*E*)-6-(l′-carboxyocta-2′,4′,6′-triene)-9-hydroxydrim-7-ene-l l-al from *A. ustus* var. *pseudodeflectus* [10], etc. In order to further explore the new drimane sesquiterpenoids produced by *A. ustus* strain 094102, we continued to study its secondary metabolites. As a result, we isolated and identified four new drimane sesquiterpenoids (**1–4**), as well as three known analogues, (strobilactone A-6-yl) (2*E*,4*E*)-6,7-dihydroxyocta-2,4-dienoate (**5**) [7] that were further isolated as four isomers **5a–5d**, mono(6-strobilactone A) ester of (*E,E*)-2,4-hexadienedioic acid (**6**) [7], and 2α,9α,11-trihydroxy-6-oxodrim-7-ene (**7**) [7]. The structures elucidation including absolute configurations and the antiproliferative activity will be discussed here.

2. Results and Discussion

The bioactive EtOAc extract of the fermentation broth of the mangrove-derived fungus *Aspergillus ustus* 094102 was chromatographed on silica gel, Sephadex LH-20, and preparative HPLC columns to give compounds **1–7** (Figure 1).
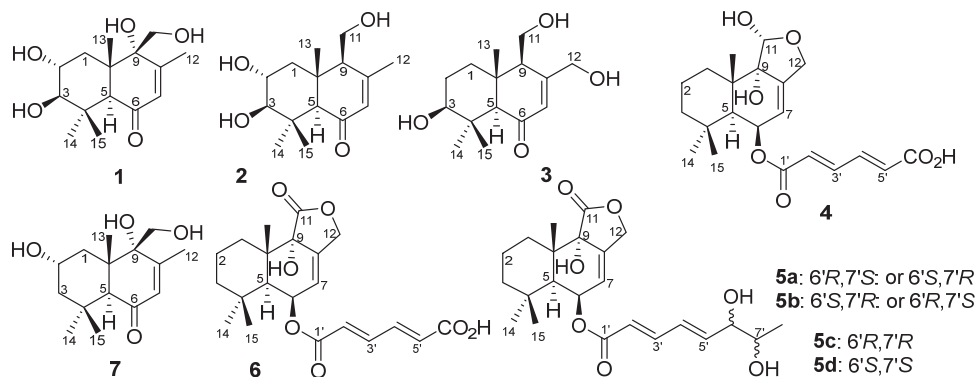
Figure 1. Structures of compounds **1–7** from *Aspergillus ustus* 094102.

Compound **1** was obtained as a colorless oily solid. Its molecular formula was determined as $C_{15}H_{24}O_5$ based on the high-resolution mass spectrometry (HRMS, ESI-Orbitrap) peak at m/z 285.1694 [M+H]$^+$ or 283.1547 [M–H]$^-$ (Figure S1), indicating 4 index of hydrogen deficiency (IHD). The IR spectrum at v_{max} 3399 and 1663 cm^{-1} (Figure S2), corresponded to a hydroxy and an α,β-unsaturated carbonyl group, respectively. The ^{1}H-NMR data (Table 1, Figure S3) of **1** revealed four tertiary methyl groups at δ_H 1.04 (s, H-13/15), 1.14 (s, H-14) and 1.96 (s, H-12), an oxymethylene signal at δ_H 3.53/3.64 (d/d, H-11), a methylene signal at δ_H 1.85/1.69 (dd/t, H-1), one olefinic proton signal at δ_H 5.61 (d, H-7), three methine signals at δ_H 3.47 (dt, H-2), 2.67 (d, H-3) and 2.81 (s, H-5), as well as four exchangeable proton signals at δ_H 4.48 (HO-3/2), 4.91 (HO-11) and 5.06 (HO-9). The ^{13}C-NMR and DEPT data (Table 1, Figures S4 and S5) of **1** revealed 15 carbon signals, including a ketone carbonyl signal at δ_C 199.2 (C-6), two olefinic carbons at δ_C 128.2/157.4 (C-7/C-8), four methyl signals at δ_C 16.7/19.1/19.2/29.3 (C-15/C-13/C-12/C-14), two methylenes at δ_C 38.6/61.9 (C-1/C-11), three methines at δ_C 55.0/66.4/81.6 (C-5/C-2/C-3) and three nonhydrogenated carbons at δ_C 37.8/45.4/74.6 (C-4/C-10/C-9). These NMR data (Table 1) were closely related to those of 3β,9α,11-trihydroxydrim-7-en-6-one (that is 3β,9α,11-trihydroxy-6-oxodrim-7-ene [7]), indicating the presence of a drimane sesquiterpene skeleton. The key difference was that compound **1** possessed an additional hydroxy group that resided at C-2 of ring A. On the basis of correlations in the COSY experiments between HO-3/H-3, H-3/H-2/H-1 and HO-11/H-11, as well

as the key HMBC correlations from H-1 to C-5/C-10/C-13, H-3 to C-4/C-14/C-15, H-5 to C-4/C-6/C-9/C-10/C-13/C-14/C-15, H-7 to C-5/C-9/C-12, H-11 to C-8/C-9/C-10, H-12 to C-7/C-8/C-9, H-13 to C-5/C-9/C-10, H-14 to C-3/C-4/C-5/C-15, and H-15 to C-3/C-4/C-14 (Figures 2 and S6–S8) further confirmed the constitution of **1** (Figure 1). The relative configuration was deduced from the NOESY spectrum (Figures 3 and S9), which showed correlations of H-1α to H-3/H-5/HO-9, H-11 to H-1β/H-2/H-13, and H-2 to H-13 indicated *cis*-orientation of HO-2/H-5/HO-9, and H-2/HO-3/CH$_3$-13/CH$_2$-11, and a *trans*-fused decalin nucleus. The absolute configuration of **1** was determined by its ECD spectrum. On the basis of the octant rule for cyclohexenones [11–13], the positive Cotton effect at λ_{max} 336 nm ($\Delta\varepsilon$ + 8.4) and the negative Cotton effect at λ_{max} 240 nm ($\Delta\varepsilon$ − 41.3) (Figures 3 and S10) indicated the (2*R*,3*R*,5*S*,9*R*,10*S*)-configuration, consistent with the core configuration of the drimane sesquiterpene, 9α,11-dihydroxydrim-7-en-6-one (that is 6-oxo-7-drimen-9α,11-diol [14]), whose absolute configurations have been established by chemical synthesis. Therefore, compound **1**, which we named ustusol F, was determined as (2*R*,3*R*,5*S*,9*R*,10*S*)-2,3,9,11-tetrahydroxydrim-7-en-6-one.

Table 1. ^{1}H (500 MHz) and ^{13}C (125 MHz) NMR Data for Compounds **1–3** and **7** (DMSO-d_6, TMS, δ ppm).

Position	1		2		3		7	
	δ_C, type	δ_H, Mult. (*J* in Hz)	δ_C, Type	δ_H, mult. (*J* in Hz)	δ_C, type	δ_H, Mult. (*J* in Hz)	δ_C, Type	δ_H, Mult. (*J* in Hz)
1	38.6, CH$_2$	β 1.69, dd (12.6, 4.6) α 1.85, dd (12.6, 12.1)	45.3, CH$_2$	2.09, dd (12.6, 4.3) 1.33, dd (12.6, 12.1)	36.6, CH$_2$	1.42–1.46, m 1.86–1.90, m	41.0, CH$_2$	1.71–1.65, m 1.76–1.71, m
2	66.4, CH	3.46–3.48, m	66.1, CH	3.42–3.47, m	26.7, CH$_2$	1.46–1.51, m, 2H	62.4, CH	3.68–3.72, m
3	81.6, CH	2.67, d (9.5)	81.6, CH	2.75, d (9.6)	76.8, CH	3.02, t (7.0)	51.7, CH$_2$	0.96, t (11.9) 1.50, dd (11.9, 3.8)
4	37.8, C		38.0, C		37.5, C		33.4, C	
5	55.0, CH	2.81, s	61.0, CH	2.22, s	62.0, CH	2.15, s	54.7, CH	2.70, s
6	199.2, C		198.6, C		199.4, C		199.6, C	
7	128.2, CH	5.61, d (1.4)	127.9, CH	5.71, s	123.7, CH	5.96, s	128.1, CH	5.61, s
8	157.5, C		159.0, C		162.3, C		157.6, C	
9	74.6, C		57.1, CH	2.29, br s	55.1, CH	2.31, br s	74.6, C	
10	45.4, C		42.3, C		41.7, C		46.2, C	
11	61.9, CH$_2$	3.53, d (11.5) 3.64, d (11.5)	57.9, CH$_2$	3.61, dd (11.0, 5.0) 3.74, br d (11.4)	57.7, CH$_2$	3.51–3.54, m 3.68, br d (10.9)	61.9, CH$_2$	3.53, d (11.5) 3.64, d (11.5)
12	19.2, CH$_3$	1.96, d (1.4)	21.5, CH$_3$	1.98, s	61.3, CH$_2$	4.19, d (18.1) 4.26, d (18.1)	19.2, CH$_3$	1.98, s
13	16.7, CH$_3$	1.04, s	16.7, CH$_3$	0.88, s	15.8, CH$_3$	0.80, s	18.9, CH$_3$	1.08, s
14	29.3, CH$_3$	1.14, s	28.7, CH$_3$	1.12, s	28.5, CH$_3$	1.10, s	33.8, CH$_3$	1.14, s
15	19.1, CH$_3$	1.04, s	16.5, CH$_3$	1.03, s	15.5, CH$_3$	0.99, s	22.7, CH$_3$	1.03, s
2-OH		4.47, s		4.47, s				4.39, s
3-OH				4.50, s				
9-OH		5.06, s						5.02, s
11-OH		4.91, s		4.68, s				
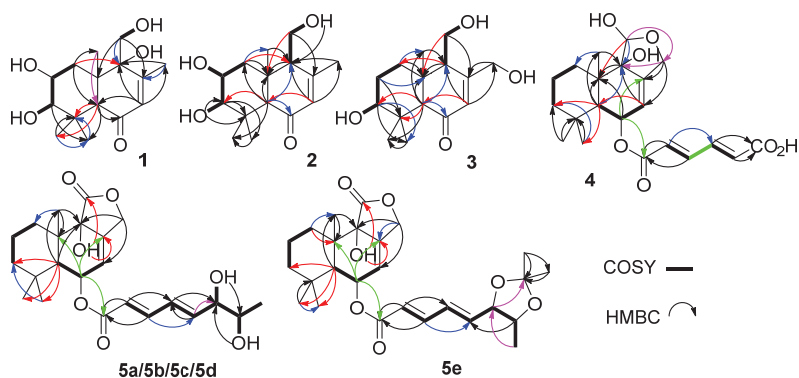
Figure 2. Key COSY and HMBC correlations of compounds **1–4** and **5a–5e**.
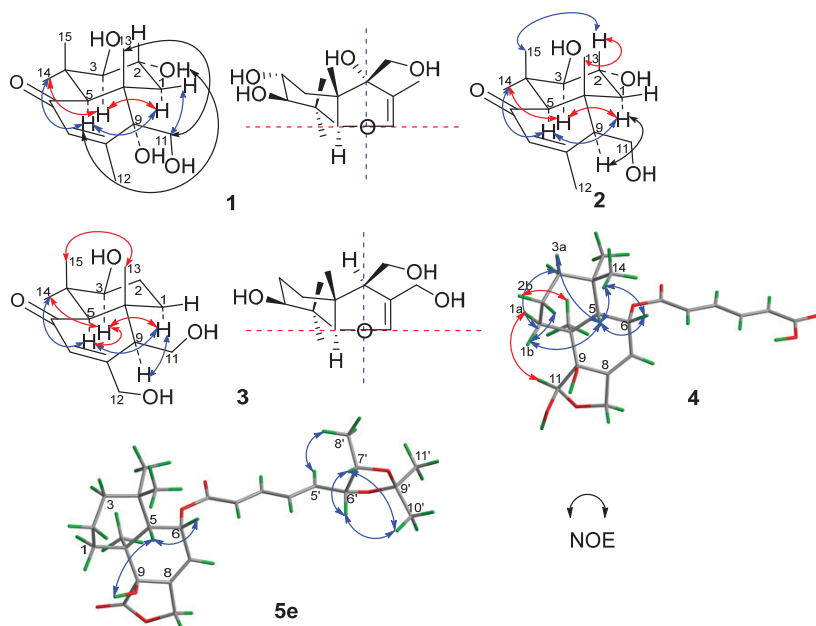
Figure 3. NOESY correlations of compounds **1–4** & **5e** and the octant rule for **1** and **3**.

Compound **2** was obtained as a light-yellow oil. Its molecular formula was determined as $C_{15}H_{24}O_4$ based on the HRESIMS peak at m/z 269.1751 [M+H]⁺ (Figure S11). The similar IR and UV absorptions to those of **1** implied that they shared the same molecular skeleton (Figure S12). The 1D NMR data (Table 1, Figures S13–S15) were also similar to **1** except for a methine signal at $\delta_{C/H}$ 57.1/2.29 which replaced the nonhydrogenated oxycarbon at δ_C 74.6, the disappearance of a hydroxy signal at δ_H 5.06 (HO-9), and the changes of chemical shifts around C-9. These data combined with the 16 amu less of molecular weight than **1** revealed compound **2** as the 9-deoxy derivative of compound **1**. Key COSY of H-9/H-11/HO-11 and HMBC of H-11 to C-8 and C-10 and H-9 to C-10 (Figures 2, S16 and S18) supported the inference. The same relative configuration to **1** was deduced from the NOESY correlations of H-2 (δ_H 3.45) to H-13 (δ_H 0.88), H-15 (δ_H 1.03) and H-1β (δ_H 2.09), H-1α (δ_H 1.33) to H-3 (δ_H 2.75), H-5 (δ_H 2.22) and H-9 (δ_H 2.29), and H-3 to H-14 (δ_H 1.12) (Figures 3, S16 and S18). The absolute configuration of the *threo*-2,3-diol in **2** was assigned

by a dimolybdenum-induced ECD method [15,16]. Upon addition of $Mo_2(OAc)_4$ to a DMSO solution of compound **2**, a chiral dimolybdenum complex was generated in situ as an auxiliary chromophore. Because the contribution from the inherent ECD was subtracted to give the induced ECD of the complex, the observed sign of the Cotton effect in the induced spectrum originates solely from the chirality of the *ortho*-diol moiety expressed by the sign of the O–C–C–O torsion angle. The positive Cotton effect at λ_{max} 332 ($\Delta\varepsilon$ + 6.8) nm (Figure S20) permitted us to assign the (2*R*,3*R*)-configuration on the basis of Snatzke's empirical rule [15]. In addition, compounds **1** and **2** also showed a similar ECD Cotton effect, indicating the same absolute configuration. Thus, compound **2,** which we named 9-deoxyustusol F, was determined as (2*R*,3*R*,5*R*,9*S*,10*R*)-2,3,11-trihydroxydrim-7-en-6-one.

Compound **3** was obtained as a colorless oily solid. Its molecular formula was determined as $C_{15}H_{24}O_4$ based on the HRESIMS peak at m/z 269.1750 [M+H]$^+$ (Figure S21), indicating an isomer of **2**. Similar 1D NMR data (Table 1, Figures S23–S25) with **2** were observed. In addition, a methylene signal ($\delta_{H/C}$ 1.47/26.7) and an oxymethylene signal ($\delta_{H/C}$ 4.19/4.26/61.3) replaced the methyl signal ($\delta_{H/C}$ 1.98/21.5) and oxymethine signal ($\delta_{H/C}$ 3.45/66.1). Key COSY of H-1/H2-2/H-3 as well as the HMBC of H2-12 (δ_H 4.19/4.26) to C-8 (δ_C 162.3), H-7 (δ_H 5.96) to C-12 (δ_C 61.3) and H2-2 (δ_H 1.47) to C-4 (δ_C 37.5) and C-10 (δ_C 41.7) revealed that 2-OH was moved to C-12 to form 2-CH$_2$ and 12-CH$_2$OH, respectively (Figures 2, S26 and S28). The relative configuration of compound **3** was deduced from the NOE difference (NOEdiff) experiment. NOEdiff of **3** showed that H-5 (δ_H 2.15) and H-1a (δ_H 1.44) were enhanced after the irradiation of H-9 (δ_H 2.31), while H-3 (δ_H 3.02) and H-9 (δ_H 2.31) were enhanced after the irradiation of H-5. The NOE enhancements of H-3 (δ_H 3.02) and H-5 (δ_H 2.15) were also observed after H-14 (δ_H 1.10) was irradiated, while H-13 (δ_H 0.80) was enhanced after the irradiation of H-15 (δ_H 0.99). H-1b (δ_H 1.88) and H-15 was enhanced after the irradiation of H-13 (Figure S29). These NOE data indicated the *cis*-orientation of H-3, H-5, H-9 and H-14 as well as H-13 and H-15, indicating the same relative configuration of **3** to **2** in the chiral centers of C-3, C-5, C-9, and C-10. The similar ECD spectrum to that of **2** implied the same absolute configuration, which was confirmed by octant rule for cyclohexanone [11–13], the positive Cotton effect at λ_{max} 335 nm ($\Delta\varepsilon$ + 10.6) and the negative Cotton effect at λ_{max} 241 nm ($\Delta\varepsilon$ – 19.1) (Figures 4 and S30). Accordingly, compound **3**, which we named ustusol G, was elucidated as (3*S*,5*R*,9*R*,10*R*)-3,11,12-trihydroxydrim-7-en-6-one.
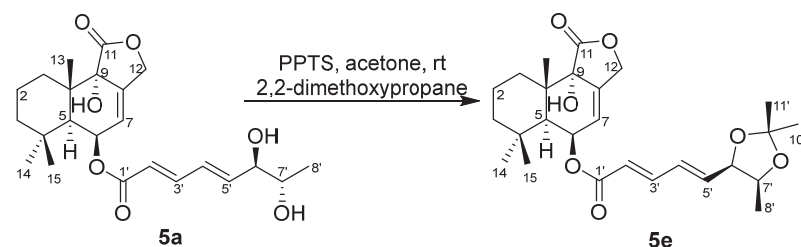
Figure 4. The preparation of acetonide **5e** from **5a**.

Compound **4** was obtained as a colorless solid. Its molecular formula was determined as $C_{21}H_{28}O_7$ based on the HRESIMS peak at m/z 391.1762 [M–H]$^-$, indicating 8 HIDs (Figure S32). The IR spectrum showed absorption bands of hydroxyl and conjugated carbonyl at ν_{max} 3434 and 1696 cm^{-1} (Figure S33), respectively. The 1D NMR spectra of **4** (Table 2, Figures S34–S36) were very similar to those of (2*E*,4*E*)-(strobilactone A-6-yl)-5-carboxypenta-2,4-dienoate (that is mono(6-strobilactone B) ester of (*E*,*E*)-2,4-hexadienedioic acid [7]), which we named ustusolate J (**6**) for convenience, suggesting that they shared the same molecular scaffold. The only difference was a replacement of the lactone carbonyl signal (δ_C 174.6 in **6**) by the hemiacetal methine group ($\delta_{C/H}$ 97.4/5.20 in **4**). In addition, the chemical shifts for C-9 and C-7 have a great increase and decrease, respectively (Table 2 and Figure S35). These data combined with a 2 amu more than **6** suggested that the γ-

lactone of **6** was reduced to the corresponding hemiacetal in **4**. The key HMBC correlations from hemiacetal proton (δ_{H-11} 5.20) to C-9 (δ_C 76.4)/C-10 (δ_C 38.0)/C-12 (δ_C 65.8), from H-12 (δ_H 4.08/4.38) to C-7 (δ_C 117.0)/C-8 (δ_C 143.2)/C-9/C-11 (δ_C 97.3), and from H-7 (δ_H 5.49) to C-5 (δ_C 45.1)/C-9 verified the deduction (Figures 2 and S39). Compound **4** displayed the key NOESY correlations of H-6 (δ_H 5.58) with H-5 (δ_H 2.07) and H-14 (δ_H 0.91), H-5 with H-1b (δ_H 1.86) and H-2a (δ_H 1.42), H-11 (δ_H 5.20) with H-1a (δ_H 1.22), as well as H-13 (δ_H 1.12) with H-2b (δ_H 1.58) (Figures 3 and S40), indicating *cis*-orientation of H-5 with H-6 and *trans*-orientation of H-5 with H-11 and H-13 which is the same relative configuration of **4** to **1** and **6** in the decalin (decahydronaphthalene) nucleus. The same relative configuration of HO-9 was deduced from the same biosynthetic pathway to those of compounds **1** and **5**–**7**. Subsequently, the same ECD pattern of **4**–**6** (Figure S78) implied the same absolute configuration of the drimane nucleus. Compound **4,** which we named ustusolate H, was thus elucidated as (5*S*,6*R*,9*S*,10*S*,11*R*,2′*E*,4′*E*)-(11-deoxy-11-hydroxystrobilactone A-6-yl)-5-carboxypenta-2,4-dienoate.

Table 2. ^{1}H (500 MHz) and ^{13}C (125 MHz) NMR Data for Compounds **4** and **6** (DMSO-d_6, TMS, δ ppm).

Position	4		6	
	δ_C, Type	δ_H, Mult. (*J* in Hz)	δ_C, Type	δ_H, Mult. (*J* in Hz)
1	31.6, CH$_2$	1.20–1.23, m 1.86, td (13.5, 4.1)	29.8, CH$_2$	1.82, br d (13.5) 1.95, td (13.5, 4.1)
2	17.8, CH$_2$	1.39–1.45, m 1.52–1.63, m	17.6, CH$_2$	1.43–1.50, m 1.54–1.64, m
3	44.5, CH$_2$	1.17–1.20, m 1.29–1.35, m	44.4, CH$_2$	1.19, d (12.5) 1.34, br d (12.5)
4	33.3, C		33.5, C	
5	45.1, CH	2.07, d (4.6)	44.6, CH	2.01, d (4.7)
6	67.3, CH	5.58, br s	68.4, CH	5.79, br s
7	117.0, CH	5.49, d (2.3)	121.3, CH	5.60, br s
8	143.2, C		142.3, C	
9	76.4, C		73.3, C	
10	38.0, C		37.4, C	
11	97.4, CH	5.20, s	174.6, C	
12	65.8, CH$_2$	4.08, d (13.0) 4.38, d (13.0)	66.6, CH$_2$	4.78, d (12.7) 4.87, d (12.7)
13	18.6, CH$_3$	1.12, s	18.5, CH$_3$	1.05, s
14	32.7, CH$_3$	0.91, s	24.5, CH$_3$	1.05, s
15	24.5, CH$_3$	1.06, s	32.3, CH$_3$	0.91, s
1′	165.0, C		165.0, C	
2′	128.2, CH	6.39, dd (11.6, 2.9)	127.9, CH	6.33–6.43, overlap [a]
3′	140.6, CH	7.32, dd (11.2, 2.9)	137.0, CH	7.27–7.35, overlap [b]
4′	141.9, CH	7.29, dd (11.2, 2.9)	140.6, CH	7.27–7.35, overlap [b]
5′	130.2, CH	6.35, dd (11.6, 2.9)	130.4, CH	6.33–6.43, overlap [a]
6′	166.9, C		166.9, C	

[a] Overlapping signals of H-2′ with H-5′; [b] Overlapping signals of H-3′ with H-4′.

Compound **5** was obtained as a yellow oil. Its molecular formula was determined as C$_{21}$H$_{28}$O$_7$ based on the ESIMS peak at *m/z* 419.1 for [M–H]$^-$ and *m/z* 464.9 for [M + HCO$_2$]$^-$(Figure S42), indicating 8 HIDs. A literature search verified that the constitution (planar structure) of compound **5** was the same as the (strobilactone A-6-yl) (2*E*,4*E*)-6,7-dihydroxyocta-2,4-dienoate (that is (6-strobilactone-B) esters of (*E*,*E*)-6,7-dihydroxy-2,4-octadienoic acid [7]), for almost the same NMR data. However, four sets of ^{13}C NMR signals of compound **5** (Figure S40) for the side chain at δ_C 165.51/165.50/165.49/165.47 (C-1′), 120.03/120.99/119.95/119.90 (C-2′), 145.41/145.37/145.34/145.26 (C-3′), 127.54/127.35/127.16/126.98 (C-4′), 146.18/146.12/145.48/145.45 (C-5′), 75.16/75.00/74.64/74.46 (C-6′), 69.64/69.62/69.33/69.32 (C-7′), and 19.34/19.26/18.26/18.24 (C-8′) were observed, indi-

cating four stereoisomers of **5** resulted from the *ortho*-diol chiral centers of the side chain. With the help of HPLC, compound **5**, which we named ustusolate I for convenience, was confirmed to have four baseline-separated peaks, then purified **5a**, **5b**, **5c**, and **5d** were obtained (Figure S83). The NMR differences of **5a–5d** were concentrated in the side chains (Tables 3 and 4, Figures S45–S60), and indicated that compounds **5a** and **5b**, **5c**, and **5d** were two pairs of enantiomers of the *ortho*-diol in the side chain. To elucidate the relative configuration of 6′,7′-diol moiety, the acetonide (**5e**) was prepared from **5a** (Figure 4). The 1D and 2D NMR spectra (Tables 3 and 4, Figures S66–S70), as well as the NOESY correlations of H-5′ (δ_H 6.24)/H$_3$-8′ (δ_H 1.01) and H$_3$-11′ (δ_H 1.40), H-6′ (δ_H 4.62)/H-7′ (δ_H 4.34) and H$_3$-10′ (δ_H 1.28) in **5e** (Figures 3 and S71) clearly suggested an *erythro*-6′,7′-diol in **5a** and **5b**, and a *threo*-6′,7′-diol in **5c** and **5d** was accordingly elucidated. This conclusion is consistent with the chemical shift rule of methyl carbon (δ_{CH3}) for 1-methyl-1,2-diol by chemical synthesis, that is 18.1–18.6 and 19.1–19.6 ppm for *threo*- and *erythro*-1,2-diol, respectively [17]. The absolute configuration of the *threo*-6′,7′-diol in **5c** and **5d** was assigned by a dimolybdenum-induced ECD method [15,16] in the same manner as that of compound **2**. Upon addition of Mo$_2$(OAc)$_4$ to a solution of compounds **5c** and **5d** in DMSO, a chiral dimolybdenum complex was generated in situ as an auxiliary chromophore. According to the negative ECD Cotton effects of **5c** at λ_{max} 303 ($\Delta\varepsilon$ − 7.9) nm and the positive ECD Cotton effects of compound **5d** at λ_{max} 305 ($\Delta\varepsilon$ +2.37) nm (Figures S73 and S74), the absolute configuration of *threo*-6′,7′-diol in **5c** and **5d** were determined to be (6′*R*,7′*R*) and (6′*S*,7′*S*), respectively. Thus, the structure of **5c** and **5d** was unambiguously determined as (2′*E*,4′*E*,6′*R*,7′*R*)-ustusolate I (**5c**) and (2′*E*,4′*E*,6′*S*,7′*S*)-ustusolate I (**5d**), respectively. Unfortunately, the absolute configuration of compounds **5a** and **5b** were not determined yet in this paper, which we tentatively named (2′*E*,4′*E*;6′,7′-*erythro*)-ustusolate I (**5a**) and (2′*E*,4′*E*; *ent*-6′,7′-*erythro*)-ustusolate I (**5b**), respectively.

Table 3. ^{1}H NMR Data for Compounds **5a–5e** (600 MHz, DMSO-d_6, TMS, δ ppm).

Position	5a	5b	5c	5d	5e
	δ_H, Mult. (*J* in Hz)	δ_H, Mult. (*J* in Hz)	δ_H, Mult. (*J* in Hz)	δ_H, Mult. (*J* in Hz)	δ_H, Mult. (*J* in Hz)
1a	1.83, d (13.6)	1.83, d (13.6)	1.84, d (13.6)	1.84, d (13.6)	1.83, d, (13.7)
1b	1.95, dd, (13.7, 4.3)	1.96, dd (13.7, 4.3)	1.96, dd (13.8, 4.2)	1.96, dd (13.7, 4.4)	1.96, dd (13.8, 4.4)
2a	1.48, dt (13.7, 3.9)	1.48, dt (13.7, 3.8)	1.48, dt (13.7, 3.8)	1.47, dt (13.7, 3.8)	1.45–1.49, m
2b	1.56–1.66, m	1.56–1.66, m	1.57–1.65, m	1.57–1.65, m	1.56–1.62, m
3a	1.21, td (13.3, 3.4)	1.21, td (13.3, 3.4)	1.20, td (13.3, 3.5)	1.21, td (13.3, 3.4)	1.18–1.23, m
3b	1.34, d (12.7)	1.34, d (12.7)	1.34, d (12.7)	1.34, d (12.7)	1.34, d (12.5)
5	2.02, d (4.9)	2.01, d (5.0)	2.01, d (5.0)	2.01, d (4.9)	2.01, d (5.0)
6	5.59, br s	5.59, br s	5.59, br s	5.59, br s	5.59, br s
7	5.79, br s	5.79, br s	5.79, br s	5.79, br s	5.79, br s
12a	4.79, d (12.6)	4.79, d (12.7)	4.79, d (12.6)	4.79, d (12.6)	4.78, d (12.7)
12b	4.88, dt (12.6, 2.4)	4.88, dt (12.6, 2.4)	4.88, dt (12.6, 2.4)	4.88, td (12.6, 2.4)	4.88, dt (12.6, 2.5)
13	1.06, s	1.06, s	1.06, s	1.06, s	1.06, s
14	0.92, s	0.92, s	0.92, s	0.92, s	0.92, s
15	1.07, s	1.07, s	1.07, s	1.07, s	1.07, s
2′	5.94, d (15.3)	5.94, d (15.3)	5.94, d (15.3)	5.94, d (15.3)	6.01, d (15.3)
3′	7.22, dd (15.3, 10.7)	7.22, dd (15.4, 10.7)	7.23, dd (15.3, 11.1)	7.23, dd (15.3, 11.1)	7.27, dd (15.3, 11.0)
4′	6.43, dd (15.3, 10.7)	6.42, dd (15.3, 10.8)	6.46, dd (15.3, 11.1)	6.45, dd (15.3, 11.2)	6.47, dd (15.2, 11.1)
5′	6.36, dd (15.3, 4.9)	6.34, dd (15.3, 5.1)	6.32, dd (15.3, 4.9)	6.30, dd (15.3, 5.1)	6.23, dd (15.2, 6.6)
6′	3.86, dd (10.2, 5.0)	3.84, dd (10.2, 5.1)	3.98, dd (10.2, 5.0)	3.96, dd (10.2, 5.1)	4.62, dd (12.8, 6.5)
7′	3.48, dq (11.6, 6.3)	3.48, dq (11.6, 6.3)	3.57, dq (11.6, 6.3)	3.57, dq (11.6, 6.3)	4.34, dq (12.8, 6.4)
8′	1.03, d (6.3)	1.03, d (6.3)	0.95, d (6.3)	0.95, d (6.3)	1.01, d (6.4)
9-OH	6.29, s	6.28, s	6.29, s	6.29, s	6.30, s
6′-OH	4.99, d (5.3)	5.00, d (5.2)	5.01, d (4.7)	5.02, d (4.7)	
7′-OH	4.60, d (5.3)	4.60, d (5.3)	4.66, d (4.7)	4.65, d (4.7)	
10′					1.28, s
11′					1.40, s

Table 4. ^{13}C NMR Data for Compounds **5a–5e** (150 MHz, DMSO-d_6, TMS, δ ppm).

Position	5a	5b	5c	5d	5e
	δ_C, Type	δ_C, Type	δ_C, Type	δ_C, Type	δ_C, Type
1	29.6, CH$_2$	29.6, CH$_2$	29.6, CH$_2$	29.6, CH$_2$	29.6, CH$_2$
2	17.5, CH$_2$	17.5, CH$_2$	17.5, CH$_2$	17.5, CH$_2$	17.5, CH$_2$
3	44.5, CH$_2$	44.5, CH$_2$	44.5, CH$_2$	44.5, CH$_2$	44.5, CH$_2$
4	33.3, C	33.3, C	33.4, C	33.4, C	33.4, C
5	44.2, CH	44.2, CH	44.2, CH	44.2, CH	44.2, CH
6	65.8, CH	65.8, CH	65.8, CH	65.8, CH	66.0, CH
7	121.4, CH	121.4, CH	121.4, CH	121.4, CH	121.3, CH
8	137.2, C	136.6, C	136.6, C	136.6, C	136.7, C
9	73.2, C	73.2, C	73.2, C	73.2, C	73.2, C
10	37.3, C	37.3, C	37.3, C	37.3, C	37.3, C
11	174.4, C	174.4, C	174.4, C	174.4, C	174.4, C
12	68.3, CH$_2$	68.2, CH$_2$	68.3, CH$_2$	68.3, CH$_2$	68.3, CH$_2$
13	18.3, CH$_3$	18.3, CH$_3$	18.3, CH$_3$	18.3, CH$_3$	18.3, CH$_3$
14	32.2, CH$_3$	32.2, CH$_3$	32.2, CH$_3$	32.2, CH$_3$	32.2, CH$_3$
15	24.3, CH$_3$	24.3, CH$_3$	24.3, CH$_3$	24.3, CH$_3$	24.3, CH$_3$
1′	165.5, C	165.4, C	165.5, C	165.5, C	165.4, C
2′	119.9, CH	120.0, CH	119.9, CH	120.0, CH	121.4, CH
3′	145.5, CH	145.4, CH	145.3, CH	145.3, CH	144.6, CH
4′	126.9, CH	127.1, CH	127.3, CH	127.5, CH	129.2, CH
5′	146.2, CH	146.1, CH	145.4, CH	145.4, CH	140.4, CH
6′	75.0, CH	75.1, CH	74.4, CH	74.6, CH	77.7, CH
7′	69.6, CH	69.6, CH	69.3, CH	69.3, CH	73.5, CH
8′	19.2, CH$_3$	19.3, CH$_3$	18.3, CH$_3$	18.3, CH$_3$	16.0, CH$_3$
9′					107.6, CH$_3$
10′					25.4, CH$_3$
11′					28.0, CH$_3$

Compounds **6** and **7** which could be a 3-deoxy derivative of ustusol F (**1**) were identified by respective comparison of NMR data with those of mono(6-strobilactone-B) ester of (*E*,*E*)-2,4-hexadienedioic acid [7] and 2α,9α,11-trihydroxy-6-oxodrim-7-ene [7]. The same ECD pattern of compound **6** with **5** (Figure S78) and compound **7** with **1** (Figure S31) indicated they shared the same absolute configuration. Thus, compounds **6** and **7** were respectively identified as (5*S*,6*R*,9*S*,10*S*,2′*E*,4′*E*)-(strobilactone A-6-yl)-5-carboxypenta-2,4-dienoate (ustusolate J, **6**) and (2*S*,5*S*,9*R*,10*S*)-2,9,11-trihydroxydrim-7-en-6-one (ustusol B, **7**) in this paper. In addition, compound **7** showed almost the same NMR data as our previously reported ustusol B [4] (Table S1) and displayed the same retention times in the co-HPLC (Figure S91). Thus, the structure of ustusol B was revised as structure **7**, which was named ustusol B.

The drimane sesquiterpenoids **1–7** were postulated to be biosynthesized from farnesyl-PP (**I**) which generated intermediate **II**, **III** and **IV** after cyclization and oxidation. The intermediates **II** and **III** were subjected to further oxidation to form compounds **1**, **2**, **3**, and **7**. The intermediate **II** was further oxidized to intermediate **IV**, and the latter was subjected to oxidation, hemi acetalization, and esterification to form compounds **4**, **5**, and **6** (Figure 5).

The antiproliferations of compounds **1–7** were evaluated against 29 human cancer cell lines and a normal cell line (the names of cell lines are listed in the Supplementary Files) by the cell counting Kit-8 (CCK-8) methods [18,19]. Only compound **5**, the mixture of **5a/5b/5c/5d**, showed antiproliferative activity against the human thyroid cancer cells (CAL-62) and human osteosarcoma cells (MG-63) with the IC$_{50}$ values of 16.28 ± 1.01 and 10.08 ± 0.04 μM, respectively, while the pure compounds **5a–5d** were inactive (IC$_{50}$ ≥ 50 μM). The IC$_{50}$ values of doxorubicin (positive control) against CAL-62 and MG-63 were 0.062 ± 0.022 and 0.096 ± 0.012 μM, respectively. The bacteriostatic activities of compounds **1–7** against 6 human pathogenic bacteria and 6 aquatic pathogenic bacteria (the names are listed in the Supplementary Files) were tested by the diffusion method of

filter paper, but no inhibition zone was observed at the concentration of 100 µg/mL for compounds **1**–**7**.

Figure 5. Proposed biosynthetic pathway for drimane sesquiterpenoids from *A. ustus* 094102.

3. Experimental Section

3.1. General Experimental Procedures

Optical rotations were measured with a JASCO P-1020 digital polarimeter. UV data were recorded with a Beckman DU 640 spectrophotometer, and ECD data were collected using a JASCO J-715 spectropolarimeter. IR spectra were taken on a Nicolet NEXUS 470 spectrophotometer as KBr disks. ^{1}H, ^{13}C, DEPT, HMQC, HMBC, COSY, and NOESY NMR spectra were recorded on a JEOL JNM-ECP 600 spectrometer or a Bruker Avance 500 spectrometer in DMSO-d_6 solution and were referenced to the corresponding residual solvent signals ($\delta_{H/C}$ 2.50/39.52 for DMSO-d_6). HRESIMS spectra were collected using a Q-TOF Ultima Global GAA076 LC mass spectrometer. ESIMS data were measured using a Waters ACQUITY SQD 2 UPLC/MS system with a reversed-phase C18 column (AC-QUITY UPLC BEH C18, 2.1 × 50 mm, 1.7 µm) at a flow rate of 0.4 mL/min. Semiprepar-ative HPLC was performed using an ODS column (YMC- pack ODS-A, 10 × 250 mm, 5 µm, 4 mL/min) and a phenyl column (YMC-pack Ph, 10 × 250 mm, 5 µm, 4 mL/min). Vacuum–liquid chromatography (VLC) utilized silica gel H (Qingdao Marine Chemical Factory, Qingdao, China). TLC were carried out by plates precoated with silica gel GF254 (10–40 µm, Qingdao Marine Chemical Factory) and Sephadex LH-20 (Amersham Pharmacia Biotech, Buckinghamshire, UK) were used for column chromatography (CC).

3.2. Fungal Material

The mangrove fungal strain *A. ustus* 094102 was isolated from the rhizosphere soil of the mangrove plant *Bruguiera gymnorrhiza* grown in Wenchang, Hainan Province of China. It was identified according to the morphological characteristics and the ITS sequences [4,5].

3.3. Cultivation and Extraction

The fungus *A. ustus* 094102 was statically cultured at 25 °C for 28 days in one hundred 1000 mL conical flasks, each containing 300 mL of the liquid medium that was prepared by dissolving maltose (20 g), mannitol (20 g), glucose (10 g), monosodium glutamate (10 g), yeast extract (3 g), corn steep liquor (1 g), CaCO$_3$ (2 g), KH$_2$PO$_4$ (0.5 g), MgSO$_4$·7H$_2$O (0.3 g), and sea salt (33 g) in 1 L of tap water (pH 7.0). The whole fermentation broth (30 L) was filtered by cheesecloth to separate the mycelia from the filtrate. The mycelia were extracted three times with an 80% volume of aqueous acetone. The acetone solution was concentrated under reduced pressure to give an aqueous solution. The aqueous solution was extracted three times with an equivalent volume of ethyl acetate (EtOAc), while the filtrate was extracted three times with an equivalent volume of EtOAc. All EtOAc extracts were combined and concentrated under vacuum to give 240 g of crude gum.

3.4. Purification

The crude gum (240 g) was separated into ten fractions (Fr1–Fr10) on a silica gel VLC column using a stepwise gradient elution of petroleum ether (PE), PE-CH$_2$Cl$_2$ (1:1–0:1) followed by CH$_2$Cl$_2$-MeOH (1:0–1:1). Fr9 (26 g) was fractionated on Sephadex LH-20, eluted with CH$_2$Cl$_2$-MeOH (1:1), to obtain three subfractions (Fr9.1–Fr9.3). Fr9.2 (8 g) was further separated into five subfractions (Fr9.2.1–Fr9.2.5) by VLC on the RP-18 column using a stepwise gradient elution of MeOH-H$_2$O (9:1–1:1), among which the elution of 40% MeOH–H$_2$O gave compound **7** (9.2 mg). Compounds **1** (6.2 mg, t$_R$ 11.8 min) and **2** (32 mg, t$_R$ 18.7 min) were obtained from Fr9.2.2 (1.7 g) by semipreparative HPLC over an ODS column eluting with 15% MeCN-H$_2$O containing 0.5‰ Et$_3$N. Fr7 (12 g) was fractionated on Sephadex LH-20, eluted with MeOH-CH$_2$Cl$_2$ (1:1), to obtain four subfractions (Fr7.1–Fr7.4). Fr7.4 (3.3 g) was further purified by semipreparative HPLC over an ODS column eluting with 40% MeCN-H$_2$O containing 0.5‰ TFA (trifluoroacetic acid) to yield compound **4** (7.6 mg, t$_R$ 16.5 min). Fr7.3 (1.3 g) was fractionated into four subfractions (Fr7.3.1–Fr7.3.5) on a RP-18 column using a stepwise gradient elution of MeOH-H$_2$O (1:9–2:3). Fr7.3.2 (300 mg) was further separated by semipreparative HPLC on an ODS column eluted with 20% MeCN-H$_2$O to yield compound **3** (3.1 mg, t$_R$ 7.8 min). Fr6 (17.6 g) was further fractionated on Sephadex LH-20 eluted with MeOH-CH$_2$Cl$_2$ (1:1) to afford four subfractions (Fr6.1–Fr6.4). Fr6.2 (1.1 g) was further separated by semipreparative HPLC on an ODS column eluted with 40% MeCN-H$_2$O containing 0.5‰ TFA to yield compound **6** (16.3 mg, t$_R$ 15 min), while compound **5** (860 mg, t$_R$ 17.0 min) was purified from Fr6.4 (9 g) by semipreparative HPLC on an ODS column eluted with 65% MeCN-H$_2$O. Pure compounds **5a** (8.8 mg, t$_R$ 39 min), **5b** (5.4 mg, t$_R$ 42 min), **5c** (7.3 mg, t$_R$ 44 min) and **5d** (6.8 mg, t$_R$ 46 min) were obtained from compound **5** by a careful separation on an ODS column eluted with 50% MeOH-H$_2$O.

3.5. The Preparation of Acetonide (5e) for Relative Configuration

According to our procedure [16], compound **5a** (5 mg) in acetone (3 mL) was added to the mixture of 2,2-dimethoxypropane (1 mL), pyridinium *p*-toluenesulfonate (PPTS, 26 mg) and *N*,*N*-dimethylformamide (DMF, 1 mL). The resulting solution was stirred at room temperature (rt) for 12 h, and then 5 mL of H$_2$O was added. The reaction solution was extracted with 15mL of CH$_2$Cl$_2$, and the organic phase was concentrated under reduced pressure. The residue was purified by semipreparative HPLC (95% MeOH-H$_2$O) to yield the acetonide **5e** (3.4 mg, t$_R$ 5.7 min). Its structure was identified by ESIMS (Figure S65) and NMR data (Tables 3 and 4, Figures 4 and S66–S71).

3.6. The Induced ECD Spectra of Compounds **2**, **5c**, *and* **5d** *for Absolute Configuration*

According to a published procedure [16,17], analytical pure DMSO was dried with 4 Å molecular sieves and was used to prepare 0.6 mg/mL of Mo$_2$(OAc)$_4$ solution. To three pieces of this solution (each 1 mL, 1.40 µmol), compounds **2** (0.5 mg, 1.86 µmol), **5c** (0.8 mg, 1.90 µmol), and **5d** (0.8 mg, 1.90 µmol) were respectively added and the first ECD spectra of the mixtures were recorded immediately. Then, ECD spectra were continuously recorded every 10 min until stationary. The inherent ECD spectrum was subtracted. The observed signs of the diagnostic bands in the region of λ_{max} 300–400 nm in the induced ECD spectra were correlated to the absolute configuration of the *ortho*-diol moiety.

(2*R*,3*R*,5*S*,9*R*,10*S*)-2,3,9,11-Tetrahydroxydrim-7-en-6-one (ustusol F, **1**): colorless oil; [α]$^{23}_D$ −56.0 (*c* 0.11, MeOH); UV (MeOH) λ_{max} (log ε) 232 (0.82) nm; ECD (1.76 mM, MeOH) λ_{max} (Δε) 336 (+8.4), 271 (−3.2), 240 (−41.3), 215 (−12.8) nm; IR (KBr) ν_{max} 3399, 2959, 1663, 1439, 1384, 1243, 1062, 1027 cm^{-1}; ^{1}H and ^{13}C NMR see Table 1; HRESIMS *m/z* 285.1694 [M+H]$^+$ (calcd for C$_{15}$H$_{24}$O$_5$, 285.1697), or 283.1547 [M–H]$^-$ (calcd for C$_{15}$H$_{23}$O$_5$, 283.1551).

(2*R*,3*R*,5*R*,9*S*,10*R*)-2,3,11-Trihydroxydrim-7-en-6-one (9-deoxyustusol F, **2**): yellow oil; [α]$^{23}_D$ −56 (*c* 0.06, MeOH); UV (MeOH) λ_{max} (log ε) 238 (1.65) nm; ECD (1.87 mM, MeOH) λ_{max} (Δε) 334 (+6.8), 264 (−1.3), 240 (−18.3), 220 (−14.3) nm; IR (KBr) ν_{max} 3398, 2942, 1659, 1440, 1382, 1237, 1152, 1060, 983 cm^{-1}; ^{1}H and ^{13}C NMR see Table 1; HRESIMS *m/z* 269.1751 [M+H]$^+$ (calcd for C$_{15}$H$_{24}$O$_4$, 269.1747).

(3*S*,5*R*,9*R*,10*R*)-3,11,12-Trihydroxydrim-7-en-6-one (ustusol G, **3**): colorless oil; [α]$^{23}_D$ −71 (*c* 0.04, MeOH); UV (MeOH) λ_{max} (log ε) 240 (1.60) nm; ECD (1.87 mM, MeOH) λ_{max} (Δε) 335 (+10.6), 265 (−2.6), 241 (−19.1), 205 (−71.7) nm; ^{1}H and ^{13}C NMR see Table 1; HRESIMS *m/z* 269.1750 [M+H]$^+$ (calcd for C$_{15}$H$_{24}$O$_4$, 269.1747).

(5*S*,6*R*,9*S*,10*S*,11*R*,2′*E*,4′*E*)-6-(11-Deoxy-11-hydroxystrobilactone A-6-yl)-5-carboxypenta-2,4-dienoate (ustusolate H, **4**): colorless solid; [α]$^{25}_D$ −96 (*c* 0.2, MeOH); UV (MeOH) λ_{max} (log ε) 264 (1.54) nm; ECD (0.64 mM, MeOH) λ_{max} (Δε) 264 (−6.2), 232 (−3.3), 205 (−11.1) nm; IR (KBr) ν_{max} 3434, 2953, 2926, 2856, 1684, 1640, 1460, 1398, 1310, 1260, 1208, 1136, 1028, 913 cm^{-1}; ^{1}H and ^{13}C NMR see Table 2; HRESIMS *m/z* 391.1762 [M–H]$^-$ (calcd for C$_{21}$H$_{27}$O$_7$, 391.1762).

((5*S*,6*R*,9*S*,10*S*)-Strobilactone A-6-yl) (2*E*,4*E*)-6,7-dihydroxyocta-2,4-dienoate (ustusolate I, **5**): light yellow oil; UV (MeOH) λ_{max} (log ε) 265 (4.15) nm. ^{1}H NMR (DMSO-*d*$_6$, 500 MHz) δ_H 1.83 (d, *J* = 13.6 Hz, 1H, H-1α), 1.95 (dd, *J* = 4.4, 13.6 Hz, 1H, H-1β); 1.59 (m, 1H, H-2α), 1.47 (m, 1H, H-2β); 1.20 (td, *J* = 3.2, 13.1 Hz, 1H, H-3α), 1.34 (d, *J* = 12.3 Hz, 1H, H-3β); 2.00 (d, *J* = 5.0 Hz, 1H, H-5); 5.59 (brs, 1H, H-6); 5.79 (brs, 1H, H-7); 4.88 (dt, *J* = 2.3, 12.6 Hz, 1H, H-12α), 4.78 (d, *J* = 12.6 Hz, 1H, H-12β); 1.06 (s, 3H, H-13); 0.92 (s, 3H, H-14); 1.07 (s, 3H, H-15); 5.94 (d, *J* = 15.3 Hz, 1H, H-2′); 7.20/7.23 (m, 1H, H-3′); 6.40/6.44 (m, 1H, H-4′); 6.30/6.34 (m, 1H, H-5′); 3.85/3.97 (m, 1H, H-6′); 3.49/3.56 (m, 1H, H-7′); 0.94/1.02 (d, *J* = 6.2 Hz, 3H, H-8′); 5.02 (brs, 1H, HO-6′); 4.61/4.66 (brs, 1H, HO-7′); ^{13}C NMR (DMSO-*d*$_6$,125 MHz) δ_C 29.6 (CH$_2$, C-1), 17.5 (CH$_2$, C-2), 44.5 (CH$_2$, C-3), 33.4 (C, C-4), 44.2 (CH, C-5), 65.8 (CH, C-6), 121.4 (CH, C-7), 136.6 (C, C-8), 73.2 (C, C-9), 37.3 (C, C-10), 174.4 (C, C-11), 68.3 (CH$_2$, C-12), 18.3 (CH$_3$, C-13), 32.2 (CH$_3$, C-14), 24.4 (CH$_3$, C-15), 165.51/165.50/165.49/165.47 (C, C-1′), 120.03/120.99/119.95/119.90 (CH, C-2′), 145.41/145.37/145.34/145.26 (CH, C-3′), 127.54/127.35/127.16/126.98 (CH, C-4′), 146.18/146.12/145.48/145.45 (CH, C-5′), 75.16/75.00/74.64/74.46 (CH, C-6′), 69.64/69.62/69.33/69.32 (CH, C-7′), and 19.34/19.26/18.26/18.24 (CH$_3$, C-8′); ESIMS peak at *m/z* 419.1 for [M–H]$^-$ and *m/z* 464.9 for [M + HCO$_2$]$^-$ (C$_{23}$H$_{32}$O$_7$).

(2′*E*,4′*E*;6′,7′-*erythro*)-Ustusolate I (**5a**): light yellow oil; [α]$^{23}_D$ −35 (*c* 0.30, MeOH); UV (MeOH) λ_{max} (log ε) 268 (4.15) nm; ECD (0.60 mM, MeOH) λ_{max} (Δε) 255 (−8.3), 236 (−8.9), 208 (−21.2) nm; ^{1}H and ^{13}C NMR see Tables 3 and 4; ESIMS *m/z* 421.2 [M+H]$^+$ (C$_{23}$H$_{32}$O$_7$).

(2′*E*,4′*E*;*ent*-6′,7′-*erythro*)-Ustusolate I (**5b**): light yellow oil; [α]$^{23}_D$ −42 (*c* 0.30, MeOH); UV (MeOH) λ_{max} (log ε) 261 (4.39) nm; ECD (0.60 mM, MeOH) λ_{max} (Δε) 256 (−11.0), 234 (−8.9), 209 (−21.4) nm; ^{1}H and ^{13}C NMR see Tables 3 and 4; ESIMS *m/z* 421.2 [M+H]$^+$ (C$_{23}$H$_{32}$O$_7$).

(2′*E*,4′*E*,6′*R*,7′*R*)-Ustusolate I (**5c**): light yellow oil; [α]$^{23}_D$ −105 (*c* 0.30, MeOH; UV (MeOH) λ$_{max}$ (log ε) 261 (4.42) nm; ECD (0.60 mM, MeOH) λ$_{max}$ (Δε) 256 (−8.6), 234 (−8.5), 208 (−22.9) nm; ^{1}H and ^{13}C NMR see Tables 3 and 4; ESIMS *m/z* 421.2 [M+H]$^+$ ($C_{23}H_{32}O_7$).

(2′*E*,4′*E*,6′*S*,7′*S*)-Ustusolate I (**5d**): light yellow oil; [α]$^{23}_D$ −79 (*c* 0.29, MeO; UV (MeOH) λ$_{max}$ (log ε) 262 (4.36) nm; ECD (0.60 mM, MeOH) λ$_{max}$ (Δε) 259 (−10.4), 234 (−8.2), 208 (−18.9) nm; ^{1}H and ^{13}C NMR see Tables 3 and 4; ESIMS *m/z* 421.2 [M+H]$^+$ ($C_{23}H_{32}O_7$).

(2′*E*,4′*E*;6′,7′-*erythro*)-Ustusolate I-6′,7′-acetonide (**5e**): light yellow oil; [α]$^{22}_D$ −102 (*c* 0.16, MeOH); UV (MeOH) λ$_{max}$ (log ε) 268 (4.15) nm; ECD (0.60 mM, MeOH) λ$_{max}$ (Δε) 256 (−15.1), 232 (−13.8), 210 (−39.4) nm; ^{1}H and ^{13}C NMR see Tables 3 and 4; ESIMS *m/z* 421.2 [M+H]$^+$ ($C_{26}H_{36}O_7$).

(5*S*,6*R*,9*S*,10*S*,2′*E*,4′*E*)-(Strobilactone A-6-yl)-5-carboxypenta-2,4-dienoate (ustusolate J, **6**): colorless solid; [α]$^{20}_D$ −280 (*c* 0.65, MeOH); UV (MeOH) λ$_{max}$ (log ε) 265 (1.84) nm; ECD (0.64 mM, MeOH) λ$_{max}$ (Δε) 261 (−11.4), 232 (−8.9), 207 (−23.2) nm; IR (KBr) ν$_{max}$ 3400, 3320, 2950, 2928, 1658, 1615, 1460, 1385, 1290,1208, 1155, 1078, 970 cm^{-1}; ^{1}H and ^{13}C NMR see Table 2; ESIMS *m/z* 459.5 [M−H]$^-$ ($C_{21}H_{26}O_7$).

(2*S*,5*S*,9*R*,10*S*)-2,9,11-Trihydroxydrim-7-en-6-one (ustusol B, **7**): light yellow solid; [α]$^{23}_D$ −140 (*c* 0.1, MeOH); UV (MeOH) λ$_{max}$ (log ε) 252 (1.33) nm; ECD (1.87 mM, MeOH) λ$_{max}$ (Δε) 335 (+11.9), 268 (−3.3), 241 (−66.9), 214 (−18.7) nm; IR (KBr) ν$_{max}$ 3400, 3320, 2950, 2928, 1658, 1615, 1460, 1385, 1290, 1208, 1155, 1078, 970 cm^{-1}; ^{1}H and ^{13}C NMR see Table 1; ESIMS *m/z* 269.2 [M+H]$^+$, 291.2 [M+Na]$^+$ ($C_{15}H_{24}O_4$).

4. Conclusions

In summary, we identified four unpublished drimane sesquiterpenoids (**1**–**4**) and three published analogues (**5**–**7**) from the mangrove-derived fungus *Aspergillus ustus* 094102. Their structures including absolute configurations of **1**–**7** were determined by spectroscopic analysis, chemical reaction, and ECD spectra. Compound **5,** containing four stereoisomers of the chiral *ortho*-diol in the side chain, was further purified as the pure isomers **5a**–**5d** for the first time, among which the absolute configuration of the *threo*-6,7-diol (**5c** and **5d**) in the side chain was also determined by a dimolybdenum ECD method for the first time. In addition, the absolute configurations of the published compounds **6** and **7** were also resolved in this paper. Unresolved compound **5** displayed selective antiproliferation against CAL-62 and MG-63 tumor cells with the IC$_{50}$ values of 16.3 and 10.1 μM, respectively, while the purified compounds **5a**–**5d** didn't show activity.

Institutional Review Board Statement: This research is not involving humans or animals.

Informed Consent Statement: This research is not involving humans or animals.

Data Availability Statement: This research is not involving humans or animals.

References

1. Cragg, G.M.; Grothaus, P.G.; Newman, D.J. New horizons for old drugs and drug leads. *J. Nat. Prod.* **2014**, *77*, 703–723. [CrossRef] [PubMed]
2. Meng, L.H.; Li, X.M.; Li, H.L.; Wang, B.G. Chermebilaenes A and B, new bioactive meroterpenoids from co-cultures of marine-derived isolates of *Penicillium bilaiae* MA-267 and *Penicillium chermesinum* EN-480. *Mar. Drugs* **2020**, *18*, 339. [CrossRef] [PubMed]
3. Bugni, T.S.; Ireland, C.M. Marine-derived fungi: A chemically and biologically diverse group of microorganisms. *Nat. Prod. Rep.* **2004**, *21*, 143–163. [CrossRef] [PubMed]
4. Lu, Z.; Wang, Y.; Miao, C.; Liu, P.; Hong, K.; Zhu, W. Sesquiterpenoids and benzofuranoids from the marine-derived fungus *Aspergillus ustus* 094102. *J. Nat. Prod.* **2009**, *72*, 1761–1767. [CrossRef] [PubMed]
5. Zhu, T.; Lu, Z.; Fan, J.; Wang, L.; Zhu, G.; Wang, Y.; Li, X.; Hong, K.; Piyachaturawat, P.; Chairoungdua, A.; et al. Ophiobolins from the mangrove fungus *Aspergillus ustus*. *J. Nat. Prod.* **2018**, *81*, 2–9. [CrossRef] [PubMed]
6. Shiono, Y.; Hiramatsu, F.; Murayama, T.; Koseki, T.; Funakoshi, T.; Ueda, K.; Yasuda, H. Two drimane-type sesquiterpenes, strobilactones a and b, from the liquid culture of the edible mushroom *Strobilurus ohshimae*. *Z. Naturforsch.* **2007**, *62b*, 1585–1589. [CrossRef]
7. Liu, H.; Edrada-Ebel, R.; Ebel, R.; Wang, Y.; Schulz, B.; Draeger, S.; Werner, E.G.M.; Wray, V.; Lin, W.; Proksch, P. Drimane sesquiterpenoids from the fungus *Aspergillus ustus* isolated from the marine sponge *Suberites domuncula*. *J. Nat. Prod.* **2009**, *72*, 1585–1588. [CrossRef] [PubMed]
8. Zhou, H.; Zhu, T.; Cai, S.; Gu, Q.; Li, D. Drimane sesquiterpenoids from the mangrove-derived fungus *Aspergillus ustus*. *Chem. Pharm. Bull.* **2011**, *59*, 762–766. [CrossRef] [PubMed]
9. Neuhaus, G.F.; Loesgen, S. Antibacterial drimane sesquiterpenes from *Aspergillus ustus*. *J. Nat. Prod.* **2021**, *84*, 37–45. [CrossRef] [PubMed]
10. Hayes, M.A.; Wrigley, S.K.; Chetland, I.; Reynolds, E.E.; Ainsworth, A.M.; Renno, D.V.; Latif, M.A.; Cheng, X.M.; Hupe, D.J.; Peter, C.; et al. Novel drimane sesquiterpene esters from *Aspergillus ustus* var. *pseudodeflectus* with endothelin receptor binding activity. *J. Antibiot.* **1996**, *49*, 505–512.
11. Mi, J.F.; Xu, R.S.; Yang, Y.P.; Yang, P.M. Studies on circular dichroism of diterpenoids from *Mallotus anomalus* and Sesquiterpenoid tussilagone. *Acta Pharm. Sin.* **1993**, *28*, 105–109.
12. Jiang, Y.; Liu, Y.; Guo, Q.; Jiang, Z.; Xu, C.; Zhu, C.; Yang, Y.; Lin, S.; Shi, J. Acetylenes and fatty acids from *Codonopsis pilosula*. *Acta Pharm. Sin. B* **2015**, *5*, 215–222. [CrossRef] [PubMed]
13. Ebel, R. Terpenes from marine-derived fungi. *Mar. Drugs* **2010**, *8*, 2340–2368. [CrossRef] [PubMed]
14. Garlaschelli, L.; Vidari, G. Synthetic studies on biologically active natural compounds. Part I. Stereospecific transformation of uvidin A into (-)-cinnamodial. *Tetrahedron* **1989**, *45*, 7371–7378. [CrossRef]
15. Bari, L.D.; Pescitelli, G.; Pratelli, C.; Pini, D.; Salvadori, P. Determination of absolute configuration of acyclic 1,2-diols with $Mo_2(OAc)_4$. 1. Snatzke's method revisited. *J. Org. Chem.* **2001**, *66*, 4819–4825. [CrossRef] [PubMed]
16. Fan, Y.; Wang, Y.; Liu, P.; Zhu, T.; Zhu, W. Indole-diterpenoids with anti-H1N1 activity from the aciduric fungus *Penicillium camemberti* OUCMDZ-1492. *J. Nat. Prod.* **2013**, *76*, 1328–1336. [CrossRef] [PubMed]
17. Wang, L.; Zhu, W. Versicolactones A and B: Total synthesis and structure revision. *Tetrahedron Lett.* **2013**, *54*, 6729–6731. [CrossRef]
18. Tominaga, H.; Ishiyama, M.; Ohseto, F.; Sasamoto, K.; Hamamoto, T.; Suzuki, T.; Watanabe, M. A water-soluble tetrazolium salt useful for colorimetric cell viability assay. *Anal. Commun.* **1999**, *36*, 47–50. [CrossRef]
19. Wang, D.; Wang, C.; Gui, P.; Liu, H.; Khalaf, S.M.H.; Elsayed, E.A.; Wadaan, M.A.M.; Hozzein, W.N.; Zhu, W. Identification, bioactivity, and productivity of *Actinomycins* from the marine-derived *Streptomyces heliomycini*. *Front. Microbiol.* **2017**, *8*, 1147. [CrossRef] [PubMed]

Integrating Activity-Guided Strategy and Fingerprint Analysis to Target Potent Cytotoxic Brefeldin A from a Fungal Library of the Medicinal Mangrove *Acanthus ilicifolius*

Cui-Fang Wang [1,2], Jie Ma [1,2], Qian-Qian Jing [1], Xi-Zhen Cao [1], Lu Chen [1], Rong Chao [1], Ji-Yong Zheng [2], Chang-Lun Shao [1,2,*], Xiao-Xi He [1,*] and Mei-Yan Wei [1,*]

[1] Key Laboratory of Marine Drugs, The Ministry of Education of China, School of Medicine and Pharmacy, College of Food Science and Engineering, Ocean University of China, Qingdao 266003, China; wangcuifang0115@163.com (C.-F.W.); majie346@163.com (J.M.); jingqianqian1231@163.com (Q.-Q.J.); caoxizhen2022@163.com (X.-Z.C.); cl2014049048@163.com (L.C.); chaorong1122@163.com (R.C.)

[2] State Key Laboratory for Marine Corrosion and Protection, Luoyang Ship Material Research Institute (LSMRI), Qingdao 266061, China; zhengjy@sunrui.net

* Correspondence: shaochanglun@163.com (C.-L.S.); hexiaoxi@ouc.edu.cn (X.-X.H.); mywei95@126.com (M.-Y.W.); Tel.: +86-532-8203-1381 (M.-Y.W.)

Abstract: Mangrove-associated fungi are rich sources of novel and bioactive compounds. A total of 102 fungal strains were isolated from the medicinal mangrove *Acanthus ilicifolius* collected from the South China Sea. Eighty-four independent culturable isolates were identified using a combination of morphological characteristics and internal transcribed spacer (ITS) sequence analyses, of which thirty-seven strains were selected for phylogenetic analysis. The identified fungi belonged to 22 genera within seven taxonomic orders of one phyla, of which four genera *Verticillium*, *Neocosmospora*, *Valsa*, and *Pyrenochaeta* were first isolated from mangroves. The cytotoxic activity of organic extracts from 55 identified fungi was evaluated against human lung cancer cell lines (A-549), human cervical carcinoma cell lines (HeLa), human hepatoma cells (HepG2), and human acute lymphoblastic leukemia cell lines (Jurkat). The crude extracts of 31 fungi (56.4%) displayed strong cytotoxicity at the concentration of 50 μg/mL. Furthermore, the fungus *Penicillium* sp. (HS-N-27) still showed strong cytotoxic activity at the concentration of 25 μg/mL. Integrating cytotoxic activity-guided strategy and fingerprint analysis, a well-known natural Golgi-disruptor and Arf-GEFs inhibitor, brefeldin A, was isolated from the target active strain HS-N-27. It displayed potential activity against A549, HeLa and HepG2 cell lines with the IC_{50} values of 101.2, 171.9 and 239.1 nM, respectively. Therefore, combining activity-guided strategy with fingerprint analysis as a discovery tool will be implemented as a systematic strategy for quick discovery of active compounds.

Keywords: *Acanthus ilicifolius*; endophytic fungi; fungal metabolites; cytotoxic activity; activity-guided strategy

1. Introduction

Cancer stands in the frontline among leading killers worldwide and the annual mortality rate is expected to reach 16.4 million by 2040 [1,2]. The marine environment has the potential to produce candidate compounds (structures) as leads to drugs, or actual drugs, as has been actively discussed for the last 50 or so years [3–5]. Nowadays, several compounds have led to drugs, especially in the area of cancer, such as trabectedin, and eribulin, which were discovered under the cytotoxic activity-guided approach [3–6]. Brefeldin A (BFA), a well-known natural Golgi-disruptor and Arf-GEFs inhibitor, was first isolated from *Penicillium decumbens* in 1958 [7,8] and subsequently identified only from the marine-derived genus *Penicillium* [9]. Previous studies reported that BFA showed strong anticancer activity in a variety of cancers, including colorectal, prostate, lung, and breast cancers [10,11]. BFA is considered as a promising leading molecule for developing anticancer drugs.

The mangrove forests are a complex ecosystem growing in tropical and subtropical intertidal estuarine zones and nourish a diverse group of microorganisms [12,13]. Microorganisms associated with mangrove environments are a major source of antimicrobial agents and also produce a wide range of important medicinal compounds, including enzymes, antitumor agents, insecticides, vitamins, immunosuppressants, and immune modulators [13–17]. Among the mangrove microbial community, mangrove associated fungi were the second-largest ecological group of the marine fungi [13,14]. Up to December 2020, at least 1387 new structures have been isolated and identified from a diverse range of mangrove-derived fungi (325 strains), which belong to about 69 genera. Furthermore, about 40.7% (530) of the 1300 new compounds displayed a wide range of pharmacological activities, and the antitumor (mainly cytotoxicity) function is noteworthy and visible, accounting for 34% (196 compounds) of the active compounds. Therefore, mangrove associated fungi are a rich source of structurally unique and diverse bioactive secondary metabolites [13].

Acanthus ilicifolius is widely distributed from India to southern China, tropical Australia and the Western Pacific islands, throughout Southeast Asia [18]. Various classes of bioactive compounds including alkaloids, benzoxazinoids, lignans, flavanoids, triterpenoids and steroids have been obtained from *A. ilicifolius* [18–20]. In addition, up to December 2020, a total of 22 strains belonging to 9 genera have been reported, which produced 95 new secondary metabolites. The endophytic fungi derived from *A. ilicifolius* are one of the most favored to be studied [13], yet little attention has been paid to the fungal communities associated with *A. ilicifolius*.

Investigating new bioactive natural products from marine fungi is a major and constant research focus in our laboratory [21–24]. Natural product researchers also face the challenge of targeting the discovery of bioactive compounds from a microbial resource library. The present work aims to integrate activity-guided strategy and fingerprint analysis to target the potent cytotoxic compounds from a fungal library of the medicinal mangrove *A. ilicifolius* (Figure 1). The cultivable fungi associated with the medicinal mangrove *A. ilicifolius* from the South China Sea were firstly systematic evaluated for their diversity. Furthermore, integrating the cytotoxic activity-guided strategy, the target active strains were quickly identified. Combined with fingerprint analysis, a potent cytotoxic activity compound, brefeldin A, was isolated from the target active strains. The combination of activity-guided strategy and fingerprint analysis could improve the efficiency of discovering active compounds in crude extracts from a complex and diverse fungal library.
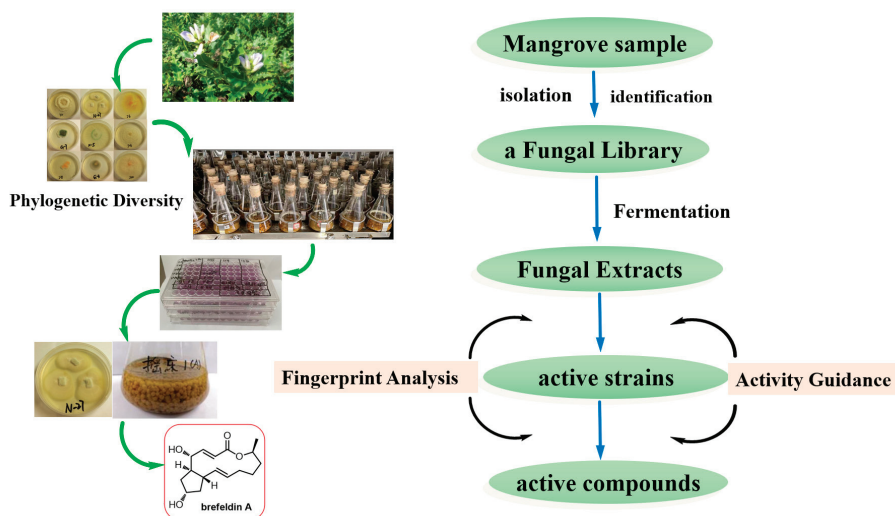

Figure 1. The detailed flowchart of this study.

2. Results

2.1. Cultivable Fungi's Phylogeny and Diversity

A total of 102 fungal isolates were obtained from *Acanthus ilicifolius* using the PDA medium with four salt gradients of 3%, 5%, 7% and 10%. Duplicated strains were removed using a detailed morphological approach. Consequently, eighty-four independent strains were selected for sequencing and identification based on ITS sequences. According to the sequences deposited into NCBI, the 84 strains belonged to the phylum Ascomycota including seven taxonomic orders: *Hypocreales, Xylariales, Diaporthales, Eurotiales, Pleosporales, Capnodiales, Botryosphaeriaceae* and 22 genera: *Trichoderma, Hypocrea, Acremonium, Verticillium, Fusarium, Neocosmospora, Pestalotiopsis, Diaporthe, Phomopsis, Valsa, Colletotrichum, Penicillium, Eupenicillium, Aspergillus, Talaromyces, Pyrenochaeta, Pleosporales, Curvularia, Alternaria, Cladosporium, Phyllosticta,* and *Lasiodiplodia* (Table 1). These identified fungi and their best matches in the NCBI database are summarized in Table S1. Most of the isolates matched their closest relatives with 98 to 100% similarity, except for HS-G-02 (97%) and HS-G-06 (95%), which indicated that they were new species. Both of the fungi HS-G-06 and HS-G-02 further enriched the diversity of mangrove fungi. Further analysis of the isolated fungi showed that *Eurotiales* was the dominant group with identified fungi, followed by *Hypocreales*. The fungal community was dominated by *Penicillium*, comprising 21 isolates, followed by *Fusarium, Aspergillus*, and *Eupenicillium* with 15, 14, and 10 isolates, respectively. Some of the genera, such as *Trichoderma, Phomopsis* and *Cladosporium* obtained six, five and five, respectively. Most of the remaining genera occurred as singletons or doubletons.

Table 1. The classification of cultivable fungi associated with *Acanthus ilicifolius*.

	Phylum	Class	Order	Genus	Number
	Ascomycota	Sordariomycetes	*Hypocreales*	*Trichoderma*	6
				Hypocrea	2
				Acremonium	2
				Verticillium	3
				Fusarium	15
				Neocosmospora	1
				Colletotrichum	3
			Xylariales	*Pestalotiopsis*	3
			Diaporthales	*Diaporthe*	2
				Phomopsis	5
				Valsa	2
		Eurotiomycetes	*Eurotiales*	*Penicillium*	21
				Eupenicillium	10
				Aspergillus	14
				Talaromyces	1
		Dothideomycetes	*Pleosporales*	*Pyrenochaeta*	1
				Pleosporales	1
				Curvularia	1
				Alternaria	1
			Capnodiales	*Cladosporium*	5
			Botryosphaeriaceae	*Phyllosticta*	1
				Lasiodiplodia	2
Total	**1**	**3**	**7**	**22**	**102**

In addition, the species of fungi isolated from different parts of *A. ilicifolius* were quite different (Figure 2). The results showed that some genera of fungi were isolated only from one part. For example, *Phomopsis* and *Acremonium* were isolated only from the stem. *Colletotrichum, Curvularia,* and *Alternaria* were isolated only from the leaf. *Valsa, Hypocrea,* and *Neocosmospora* were isolated only from the soil. *Diaporthe, Talaromyces,* and *Pyrenochaeta* were isolated only from the leaf.
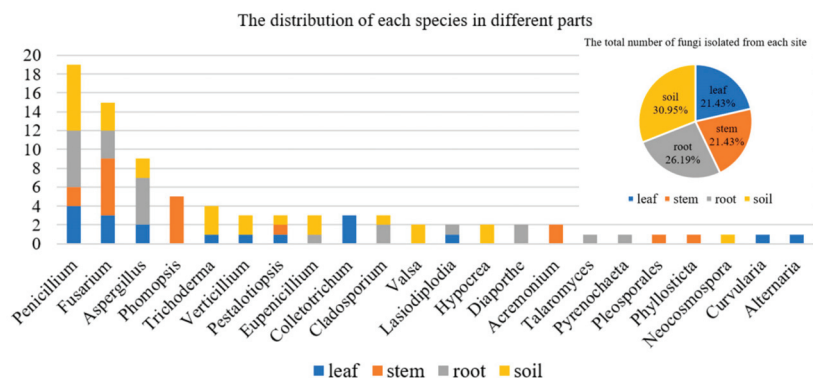
Figure 2. The distribution of each species in different parts.

Further phylogenetic analysis was carried out on 37 strains. These 37 independent individuals were selected as the representative strains because they belong to different fungal species after we aligned the sequences with the BioEdit software (Figure S1). The phylogenetic tree of fungi in the order *Hypocreales* based on ITS gene sequence is presented in Figure S2. Furthermore, the fingerprints of secondary metabolites of fungi from different species and genera were analyzed (Figure S4).

2.2. The Cytotoxicity of Cultivable Fungal Extracts

The organic extracts of 55 identified fungi were evaluated for their cytotoxic activities against human lung cancer cell line (A-549), human cervical carcinoma cell (HeLa), human hepatoma cells (HepG2) and Jurkat tumour cell lines at the concentration of 50 µg/mL (Figure 3a). To identify active strains for further research as potential cytotoxic strains, the relative inhibition rate of A-549, HeLa and HepG2 cell lines should greater than 70%, and the relative inhibition rate of Jurkat cell line should greater than 60%. The results showed that these fungi showed different inhibition rates to different cell lines. The number of the fungi showing activity against A-549, HeLa, HepG2, and Jurkat tumour cell lines were 17, 17, 19 and 24, respectively (Figure S3). The crude extracts of 31 fungi displayed cytotoxicity against the test cell lines, of which 21 fungi showed selective inhibitory activity on different tested cell lines,; for example, *Fusarium* sp. showed selective inhibitory activity on HeLa cell lines. Most fungi showed strong selective inhibitory activity on Jurkat cell lines. Interestingly, the remaining 10 fungi belonging to the two orders *Eurotiales* and *Hypocreales*, displayed a broad-spectrum strong cytotoxic activity, such as *Penicillium* sp. (HS-N-23, HS-N-27, HS-N-29, and HS-G-01), *Eupenicillium* sp. (HS-N-25), *Trichoderma* sp. (HS-01 and HS-N-04), *Aspergillus* sp. (HS-G-04 and HS-Y-27), and *Verticillium* sp. (HS-N-28).

The crude extracts were further reduced in concentration for the activity test. The results showed that only the two active strains of *Penicillium* sp. (HS-N-27 and HS-N-29) still showed strong inhibitory activity against all the texted cell lines at the concentration of 25 µg/mL. Cytotoxic metabolites were isolated from the endophytic fungus *Penicillium chermesinum*, leading to the discovery of a cysteine-targeted Michael acceptor as a pharmacophore for fragment-based drug discovery, bioconjugation and click reactions [25]. The heteroatom-containing new compounds 2-hydroxyl-3-pyrenocine-thio propanoic acid and 5,5-dichloro-1-(3,5-dimethoxyphenyl)-1,4-dihydroxypentan-2-one, which were isolated from a deep-sea *Penicillum citreonigrum* XT20-134, showed potent cytotoxicity to the human hepatoma tumor cell Bel7402 [26]. Additionally, the active strains HS-N-28, HS-G-01, and HS-N-25 showed strong selective inhibitory activity against A-549, HeLa and HepG2 cell lines. The active strains HS-Y-27, HS-N-23, HS-G-04, and HS-N-28 showed strong selective inhibitory activity against HeLa cell lines. The active strains HS-G-01, and HS-N-25 showed strong selective inhibitory activity against HepG2 and A549 cell lines. Obviously, these

active strains are important microbial resources and have the potential for interesting cytotoxic compounds (Figure 3b).
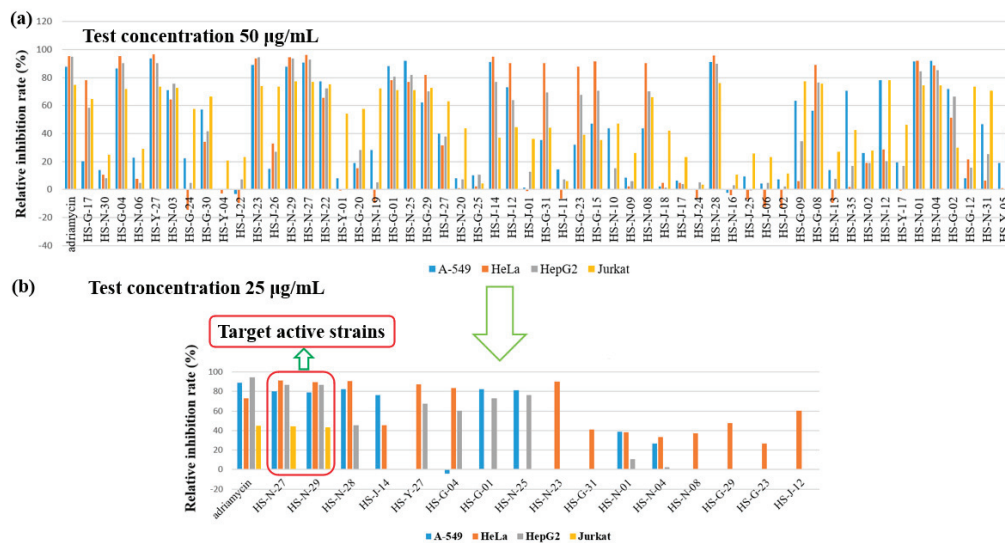

Figure 3. Cytotoxicity of organic extracts of 55 identified fungi. (**a**) The cytotoxic activities of 55 identified fungi against A-549, HeLa, HepG2 and Jurkat tumour cell lines at the concentration of 50 μg/mL. (**b**) The cytotoxic activities of the active strains at the concentration of 25 μg/mL.

2.3. Isolation and Identifcation of Compounds **1**–**7**

As the two active strains *Penicillium* sp. (HS-N-27 and HS-N-29) showed strong cytotoxic activity against all the tested cell lines at the concentration of 25 μg/mL, both of the *Penicillium* sp. fungi were selected as the target strains. Combining cytotoxic activity-guided strategy with fingerprint analysis, compound **1** was obtained from the fermentation broth of the two active strains HS-N-27 and HS-N-29. By comparison of NMR data with the reported literature, the structure was identified as brefeldin A (Figure 5), which was a 13-membered macrolactone with a cyclopentane substituent [7]. BFA is a well-known natural Golgi-disruptor and Arf-GEFs inhibitor [8]. Combining morphological characteristics and fingerprint analysis of metabolites (Figure S5), the two fungi HS-N-27 and HS-N-29 were identified as different individuals of the same *Penicillium* sp. species. The neighbor-joining of the phylogenetic tree of the target active strain *Penicillium* sp. (HS-N-27) in *Hypocreales* order fungi from *A. ilicifolius* based on ITS sequences is shown in Figure 4.

The genus *Aspergillus* is one of the dominant producers of new natural products [13]. The fingerprint analysis showed that the metabolites of *Aspergillus flavus* (HS-N-06) were relatively single and that *A. candidus* (HS-Y-23) was rich in metabolites with strong special UV absorption peak (Figure S4). The secondary metabolites of the two fungal strains were further studied. Under the guidance of chemical technology, 5-hydroxymethylfuran-3-carboxylic acid (**2**) was obtained from the fermentation broth of *A. flavus* (HS-N-06) [27]. Terphenyllin (**3**) was obtained from the fermentation broth of *A. candidus* (HS-Y-23), which showed weak cytotoxic activity against HeLa cell lines with the IC_{50} value of 19.0 μM [28]. In addition, 5-hydroxy-3-hydroxymethyl-2-methyl-7-methoxychromone (**4**), indolyl-3-carboxylic acid (**5**), and trichodermamides A (**6**) and D (**7**) were obtained from the fermentation broth of *Trichoderma harzianum* (HS-N-04) [29–31]. The structures of isolated and identified compounds were in Figure 5.
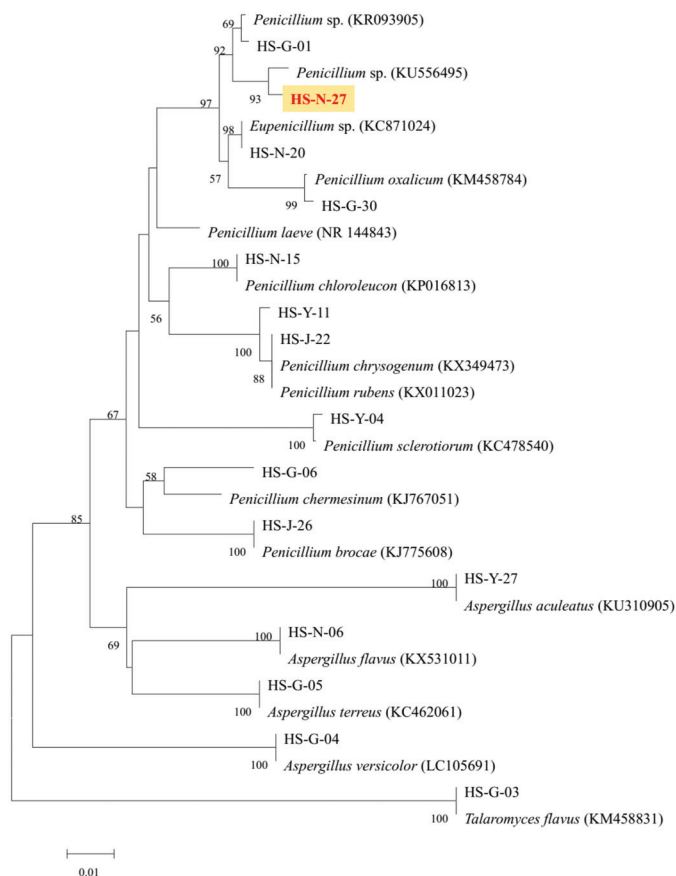
Figure 4. The neighbor-joining of phylogenetic tree of HS-N-27 fungi in *Hypocreales* order fungi. The values at each node represent the bootstrap values from 1000 replicates, and the scale bar = 0.01 substitutions per nucleotide.
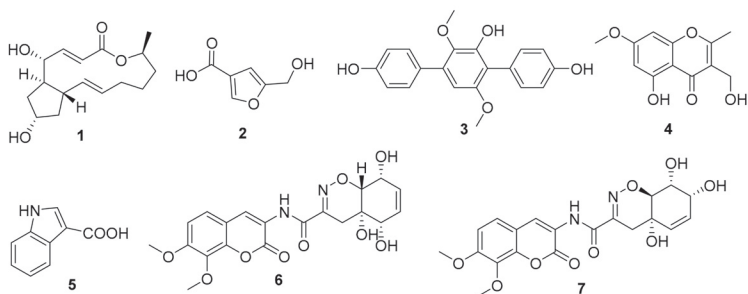

Figure 5. Structures of isolated and identified compounds.

3. Discussion

Mangrove-associated fungi are rich in diversity and can produce impressive quantities of metabolites with promising biological activities that may be useful to humans as novel physiological agents [13–17]. The phylogenetic diversity of culturable fungi derived mangrove species *Rhizophora stylosa* and *R. mucronata* collected from the South China Sea

has been reported [32]. The endophytic fungi derived from *A. ilicifolius* areamong the most favored to be studied. Up to December 2020, only 22 strains associated with *A. ilicifolius* belonging to 9 genera have been reported [13]. Investigation on phylogenetic diversity of *A. ilicifolius* associated fungi is relatively rare. In this study, 84 of the 102 isolates were successfully classified at the genus level based on ITS sequences with relatives in the NCBI database (Table S1). The identified fungi belonged to 22 genera, of which four genera *Verticillium*, *Neocosmospora*, *Valsa*, and *Pyrenochaeta* were first isolated from mangroves. (Table S1). Two strains HS-G-02 (97%) and HS-G-06 (95%) with low similarity indicated that they should be new species, which further enriched the diversity of mangrove fungi. The new strains may produce a variety of commercially interesting and potentially useful products. The above results indicated that a high diversity of fungi can be recovered from *A. ilicifolius* in the South China Sea.

Further analysis of the isolated fungi showed that *Eurotiales* was the dominant group with identified fungi accounted for 45.1%, followed by *Hypocreales*. The fungal community comprising *Penicillium* accounted for 20.6%, followed by *Fusarium*, and *Aspergillus*. It was reported that *Penicillium* (283, 20%), *Aspergillus* (246, 18%), and *Pestalotiopsis* (88, 6%) are the dominant producers of new natural products (1384) isolated from mangrove-associated fungi, comprising more than 45% of the total molecules [13]. The fungi obtained from *A. ilicifolius* could provide abundant microbial resources for the discovery of new compounds.

Natural product researchers face the challenge of maximizing the discovery of new or potent compounds from a microbial resource library. Combining activity-guided strategy with fingerprint analysis as a discovery tool will be implemented as a systematic strategy for quick discovery of active compounds. The crude extracts of 56.4% fungi displayed strong cytotoxicity. Interestingly, the remaining 10 fungi belonging to the two orders *Eurotiales* and *Hypocreales*, displayed a broad-spectrum strong cytotoxic activity. Furthermore, integrating cytotoxic activity-guided strategy and fingerprint analysis, a strong cytotoxic active compound brefeldin A was isolated from the target active strain HS-N-27. Brefeldin A is a well-known natural Golgi-disruptor and Arf-GEFs inhibitor, and shows strong anticancer activity in a variety of cancers [8–11]. BFA is considered as a promising leading molecule for developing anticancer drugs. As the metabolites of the fungi *Penicillium* sp. (HS-N-27) are relatively simple and BFA is easily separated and purified, this provides the source of compounds for the study of the medicinal properties of BFA. A series of BFA derivatives with antileukemia activity had been reported in terms of the semi-synthesis, cytotoxic evaluation, and structure-activity relationships [9]. This method, combining activity-guided strategy with fingerprint analysis, could improve the efficiency of discovering active compounds.

4. Materials and Methods

4.1. Sampling Site and Plant Material

The medicinal mangrove *A. ilicifolius*, which was authenticated by Prof. Fengqin Zhou (Shandong University of Traditional Chinese Medicine) was collected from the South China Sea. The samples were stored at the Key Laboratory of Marine Drugs, the Ministry of Education of China, School of Medicine and Pharmacy, Ocean University of China, Qingdao, China.

4.2. Isolation of Cultivable Fungi

To obtain the fungi associated with medicinal mangrove *A. ilicifolius* within different parts of the plant, the surface sterilization of each part from *A. ilicifolius* was carried out following an isolation as Qin et al. described with some modifications [33]. The root, stem and leaf of *A. ilicifolius* samples were washed with sterile artificial seawater for three times to remove the microorganisms and sediment attached to the surface. Appropriate samples were taken, using scissors or scalpel to cut all parts, including root, stem and leaf, with attention to the integrity of sampling. Then, the sample was soaked in 75% alcohol for 30 s,

and the water on the sample was sucked up with sterile filter paper. The sample was cut into 1 cm^3 pieces for fungal isolation.

The methods of tissue sectioning and tissue homogenization were used to isolate fungi. Tissue sectioning method: The tissues of 1 cm^3 pieces were inoculated into PDA medium (200.0 g of potato extract, 20.0 g of glucose in 1 L of seawater with four salinities of 3%, 5%, 7% and 10% respectively) in a sterile environment. In order to improve the utilization of the plate and to separate more microorganisms, the medium plate was generally divided into three areas, and 2–3 pieces of tissue were placed in each area of the PDA medium with four salt gradients of 3%, 5%, 7% and 10%. Tissue homogenization method: The tissue was ground in 2 mL of sterile artificial seawater with a mortar in a sterile environment, and then the resulting homogenate was diluted with sterile artificial seawater at three dilutions (1:10, 1:100, and 1:1000). 100 μL of each dilution was plated in quadruplicate onto corresponding medium for fungal cultivation. The inoculated plates were cultured at 25 °C for 2 days. The fungi were replated onto new PDA plates several times until the morphology of the fungi could be distinguished. The obtained fungal strains were deposited at the Key Laboratory of Marine Drugs, the Ministry of Education of China, School of Medicine and Pharmacy, Ocean University of China, Qingdao, China.

4.3. Genomic DNA Extraction, PCR Amplifcation, Sequencing and Phylogenetic Analysis

The genomic DNA extraction was conducted using the Fungal DNA kits (E.Z.N.A., Omega, Norcross, GA, USA) according to the manufacturer's protocol. The internal transcribed spacer (ITS1-5.8S-ITS2) regions of the fungi were amplified with the universal ITS primers, ITS1F (5′-CTTGGTCATTTAGAGGAAGTAA-3′) and ITS4 (5′-TCCTCCGCTTATTG ATATGC-3′) using the polymerase chain reaction (PCR) [34]. The PCR was performed through the following cycle: initial denaturation at 94 °C for 5 min, 30 cycles of 94 °C denaturation for 40 s min, 52 °C annealing for 40 s, 72 °C extension for 1 min; with a final extension at 72 °C for 10 min. Finally, the amplified products were submitted for sequencing (Invitrogen, Shanghai, China) and a BLASTN search was used to search for sequences of the closest match in the GenBank by Basic Local Alignment Search Tool (BLAST) programs database.

The sequences of fungal ITS regions obtained from *A. ilicifolius* were compared with the related sequences in the National Center for Biotechnology Information (NCBI). Each of these sequences was then aligned to sequences available in the NCBI database to determine the identity of the sequence, which further determined the species and genera of fungi. All fungal ITS sequences were aligned using the BioEdit software, applying the default parameters. The phylogenetic tree was generated using neighbor-joining (NJ) algorithms in the MEGA 7 software (version 7.0, Mega Limited) combined with bootstrap analysis using 1000 replicates incorporating fungal sequences showing the highest homology to sequences amplified.

4.4. General Experimental Procedures

The Agilent DD2 NMR spectrometer (JEOL, Tokyo, Japan) at 500 MHz and 125 MHz frequency was used for ^{1}H and ^{13}C NMR spectra respectively. The vacuum column chromatography silica gel (200–300 mesh, Qing Dao Hai Yang Chemical Group Co, Qingdao, China), silica gel plates for thin layer chromatography (G60, F-254, and Yan Tai Zi Fu Chemical Group Co, Yan Tai, China), and reverse phase octadecylsilyl silica gel column were used for the separation of compounds. UPLCMS spectra were measured on Waters UPLC®system (Waters Ltd., Milford, MA, USA) using a C$_{18}$ column (ACQUITY UPLC®BEH C$_{18}$, 2.1 × 50 mm, 1.7 μm; 0.5 mL/min) and ACQUITY QDA ESIMS scan from 150 to 1000 Da was used for the analysis of fungal extracts and ESI-MS spectra of the compounds. Semipreparative HPLC was performed on a Hitachi L-2000 system (Hi-tachi Ltd., Tokyo, Japan) using a C$_{18}$ column (Kromasil 250 × 10 mm, 5 μm, 2.0 mL/min).

4.5. Fungal Fermentation and Chemical Extraction

The 55 fungal isolates were fermented in a 500 mL conical flask containing 250 mL PDA liquid medium. The fungi were shaken at 28 °C, 120 rpm for 7 days. Each exper-iment was conducted in three parallels. The fermentation broth was extracted three times with an equal volume of EtOAc and the whole EtOAc solutions were evaporated under reduced pressure to give the dried extracts.

4.6. Cytotoxic Assay

The cytotoxic activity was evaluated against human lung cancer cell line (A-549), human cervical carcinoma cells (HeLa), human hepatoma cells (HepG2) and Jurkat tumor cell lines by the MTT method, with adriamycin as a positive control [35]. The organic extracts, and adriamycin (the positive control) were dissolved in DMSO with the concentration of 50 μg/mL, 25 μg/mL, and 1 μM, respectively for bioassay.

4.7. Extraction and Isolation of Compounds

The organic extract of *Penicillium* sp. (HS-N-27) showed strong cytotoxic activity. The organic extract of the *Penicillium* sp. (HS-N-27) was subjected to silica gel column chromatography (CC) and eluted by a gradient of petroleum ether (PE)/ethyl acetate (EA) and then EA/MeOH to generate nine fractions (Fr. 1–9). All the fractions were further evaluated for cytotoxic activity. The Fr. 5 showed strong cytotoxic activity. Combined with fingerprint analysis,-the composition of Fr. 5 is relatively simple (Figure S5); it was further purified by semipreparative HPLC (MeOH−H_2O, 80%; 2 mL/min) to obtain **1** (BFA) (19.0 mg).

The organic extract of the *Aspergillus flavus* (HS-N-06) was subjected to silica gel vacuum liquid chromatography (VLC) and eluted by a gradient of PE/EA and then EA/MeOH to afford four subfractions (Fr. 1−Fr. 4). Fr. 3 was separated by ODS CC (MeOH−H_2O, 30–50%) to afford **2** (17.0 mg).

The organic extract of the *A. aculeatus* (HS-Y-23) was subjected to silica gel vacuum liquid chromatography (VLC) and eluted by a gradient of PE/EA and then EA/MeOH to afford seven subfractions (Fr. 1−Fr. 7). Fr. 4 was separated by ODS CC (MeOH−H_2O, 30–100%) and then purified by semipreparative HPLC (MeOH−H_2O, 70%; 2 mL/min) to afford **3** (7.0 mg).

The organic extract of the *Trichoderma harzianum* (HS-N-04) was subjected to silica gel column chromatography (CC) and eluted by a gradient of PE/EA and then EA/MeOH to generate six fractions (Fr. 1–6). Fr. 2 was further purified by using CC to generate five fractions (Fr. 2-1–2-5). Fr.2-2 was separated by normal phase silica gel column chromatography and purified by semi preparative HPLC (MeOH−H_2O, 85%; 2 mL/min) to obtain **4** (10.0 mg). Fr.2-4 was separated by normal phase silica gel column chromatography and semipreparative HPLC to obtain **5** (2.4 mg). Fr.4 was separated into six fractions by Sephadex LH-20 eluting with MeOH gel column. Fr.4-2 was purified by semipreparative HPLC (MeOH−H_2O, 70%; 2 mL/min) to yield **6** (5.3 mg). Fr.4-4 was purified by semipreparative HPLC (MeOH−H_2O, 76%; 2 mL/min) to obtain **7** (5.0 mg).

5. Conclusions

This is the first systematic report on the phylogenetic diversity of fungi from mangrove *A. ilicifolius*. Four genera *Verticillium*, *Neocosmospora*, *Valsa*, and *Pyrenochaeta*, which were first isolated from mangroves, further enriched the diversity of mangrove fungi. Thirty-one strains of fungi displayed strong cytotoxicity to different cell lines, which was the important microbial resource for the discovery of cytotoxic compounds. Furthermore, by integrating cytotoxic activity-guided strategy and fingerprint analysis, a potent cytotoxic activity compound was quickly isolated from target active strains. This method, combining activity-guided strategy with fingerprint analysis, could improve the efficiency of discovering active compounds.

References

1. Sung, H.; Ferlay, J.; Siegel, R.L.; Laversanne, M.; Soerjomataram, I.; Jemal, A.; Bray, F. Global Cancer Statistics 2020: GLOBOCAN estimates of incidence and mortality worldwide for 36 cancers in 185 countries. *CA Cancer J. Clin.* **2021**, *71*, 209–249. [CrossRef] [PubMed]
2. Mohan, C.D.; Rangappa, S.; Nayak, S.C.; Jadimurthy, R.; Wang, L.; Sethi, G.; Garg, M.; Rangappa, K.S. *Bacteria as a treasure house of secondary metabolites with anticancer potential. Seminars in Cancer Biology*; Academic Press: Cambridge, MA, USA, 2021. [CrossRef]
3. Newman, D.J.; Cragg, G.M. Drugs and Drug Candidates from Marine Sources:An Assessment of the Current "State of Play". *Planta Med.* **2016**, *82*, 775–789. [CrossRef] [PubMed]
4. Newman, D.J.; Cragg, G.M. Natural Products as Sources of New Drugs over the Nearly Four Decades from 01/1981 to 09/2019. *J. Nat. Prod.* **2020**, *83*, 770–803. [CrossRef] [PubMed]
5. Jimenez, P.C.; Wilke, D.V.; Branco, P.C.; Bauermeister, A.; Rezende-Teixeira, P.; Gaudêncio, S.P.; Costa-Lotufo, L.V. Enriching cancer pharmacology with drugs of marine origin. *Br. J. Pharmacol.* **2020**, *177*, 3–27. [CrossRef]
6. Wright, A.E.; Forleo, D.A.; Gunawardana, G.P.; Gunasekera, S.P.; Koehn, F.E.; McConnell, O.J. Antitumor Tetrahydroisoquinoline Alkaloids from the Colonial Ascidian *Ecteinascidia turbinate*. *J. Org. Chem.* **1990**, *55*, 4509–4512. [CrossRef]
7. Singleton, V.L.; Bohonos, N.; Ullstrup, A.J. Decumbin, a new compound from a species of Penicillium. *Nature* **1958**, *181*, 1072–1073. [CrossRef]
8. Renault, L.; Guibert, B.; Cherfils, J. Structural snapshots of the mechanism and inhibition of a guanine nucleotide exchange factor. *Nature* **2003**, *426*, 525–530. [CrossRef]
9. Lu, X.X.; Jiang, Y.Y.; Wu, Y.W.; Chen, G.Y.; Shao, C.L.; Gu, Y.C.; Liu, M.; Wei, M.Y. Semi-Synthesis, Cytotoxic Evaluation, and Structure—Activity Relationships of Brefeldin a Derivatives with Antileukemia Activity. *Mar. Drugs* **2022**, *20*, 26. [CrossRef]
10. Prieto-Dominguez, N.; Parnell, C.; Teng, Y. Drugging the small GTPase pathways in cancer treatment: Promises and challenges. *Cells* **2019**, *8*, 255. [CrossRef]
11. Anadu, N.O.; Davisson, V.J.; Cushman, M. Synthesis and anticancer activity of Brefeldin A ester derivatives. *J. Med. Chem.* **2006**, *49*, 3897–3905. [CrossRef]
12. Wu, J.; Xiao, Q.; Xu, J.; Li, M.Y.; Pan, J.Y.; Yang, M.H. Natural products from true mangrove flora: Source, chemistry and bioactivities. *Nat. Prod. Rep.* **2008**, *25*, 955–981. [CrossRef]
13. Chen, S.; Cai, R.; Liu, Z.; Cui, H.; She, Z. Secondary metabolites from mangrove-associated fungi: Source, chemistry and bioactivities. *Nat. Prod. Rep.* **2022**, *39*, 560–595. [CrossRef]

14. Carroll, A.R.; Copp, B.R.; Davis, R.A.; Keyzers, R.A.; Prinsep, M.R. Marine natural products. *Nat. Prod. Rep.* **2021**, *38*, 362–413. [CrossRef]
15. Thatoi, H.; Behera, B.C.; Mishra, R.R.; Dutta, S.K. Biodiversity and biotechnological potential of microorganisms from mangrove ecosystems: A review. *Ann. Microbiol.* **2013**, *63*, 1–19. [CrossRef]
16. Ancheeva, E.; Daletos, G.; Proksch, P. Lead compounds from mangrove-associated microorganisms. *Mar. Drugs* **2018**, *16*, 319. [CrossRef]
17. Xu, J. Bioactive natural products derived from mangrove-associated microbes. *RSC Adv.* **2015**, *5*, 841–892. [CrossRef]
18. Wu, J.; Zhang, S.; Xiao, Q.; Li, Q.; Huang, J.; Long, L.; Huang, L. Phenylethanoid and aliphatic alcohol glycosides from *Acanthus ilicifolius*. *Phytochemistry* **2003**, *63*, 491–495. [CrossRef]
19. Rutvi, P.; Nilay, P.; Krushil, P.; Meet, P.; Kunj, P.; Preeti, V.; Mamta, S. *Acanthus ilicifolius*: A true mangrove with biomedical potential. *J. Pharm. Pharm. Sci.* **2020**, *9*, 472–489. [CrossRef]
20. Cai, Y.S.; Sun, J.Z.; Tang, Q.Q.; Fan, F.; Guo, Y.W. Acanthiline A, a pyrido[1,2-a]indole alkaloid from Chinese mangrove *Acanthus ilicifolius*. *J. Asian. Nat. Prod. Res.* **2018**, *20*, 1088–1092. [CrossRef]
21. Hai, Y.; Wei, M.Y.; Wang, C.Y.; Gu, Y.C.; Shao, C.L. The intriguing chemistry and biology of sulfur-containing natural products from marine microorganisms (1987–2020). *Mar. Life Sci. Technol.* **2021**, *3*, 488–518. [CrossRef]
22. Xu, W.F.; Wu, N.N.; Wu, Y.W.; Qi, Y.X.; Wei, M.Y.; Pineda, L.M.; Ng, M.G.; Spadafora, C.; Zheng, J.Y.; Lu, L.; et al. Structure modification, antialgal, antiplasmodial, and toxic evaluations of a series of new marine-derived 14-membered resorcylic acid lactone derivatives. *Mar. Life Sci. Technol.* **2022**, *4*, 88–97. [CrossRef]
23. Hai, Y.; Cai, Z.M.; Li, P.D.; Wei, M.Y.; Wang, C.Y.; Gu, Y.C.; Shao, C.L. Trends of antimalarial marine natural products: Progresses, challenges and opportunities. *Nat. Prod. Rep.* **2022**, *39*, 969–990. [CrossRef]
24. Guo, F.W.; Mou, X.F.; Qu, Y.; Wei, M.Y.; Chen, G.Y.; Wang, C.Y.; Gu, Y.C.; Shao, C.L. Scalable total synthesis of (+)-aniduquinolone A and its acid-catalyzed rearrangement to aflaquinolones. *Commun. Chem.* **2022**, *5*, 35. [CrossRef]
25. Darsih, C.; Prachyawarakorn, V.; Wiyakrutta, S.; Mahidol, C.; Ruchirawat, S.; Kittakoop, P. Cytotoxic metabolites from the endophytic fungus *Penicillium chermesinum*: Discovery of a cysteine-targeted Michael acceptor as a pharmacophore for fragment-based drug discovery, bioconjugation and click reactions. *RSC Adv.* **2015**, *5*, 70595–70603. [CrossRef]
26. Tang, X.X.; Liu, S.Z.; Yan, X.; Tang, B.W.; Fang, M.J.; Wang, X.M.; Wu, Z.; Qiu, Y.K. Two New Cytotoxic Compounds from a Deep-Sea *Penicillum citreonigrum* XT20-134. *Mar. Drugs* **2019**, *17*, 509. [CrossRef]
27. Ma, Y.M.; Ma, C.C.; Li, T.; Wang, J. A new furan derivative from an endophytic *Aspergillus flavus* of *Cephalotaxus fortunei*. *Nat. Prod. Res.* **2016**, *30*, 79–84. [CrossRef] [PubMed]
28. Takahashi, C.; Yoshihira, K.; Natori, S.; Umeda, M. The structures of toxic metabolites of *Aspergillus candidus*. I. The compounds A and E, cytotoxic *p*-terphenyls. *Chem. Pharm. Bull.* **1976**, *24*, 613–620. [CrossRef] [PubMed]
29. Takenaka, Y.; Tanahashi, T.; Nagakura, N.; Hamada, N. 2,3-dialkylchromones from mycobiont cultures of the lichen Graphis Scripta. *Heterocycles* **2000**, *53*, 1589–1593. [CrossRef]
30. Garo, E.; Starks, C.M.; Jensen, P.R.; Fenical, W.; Lobkovsky, E.; Clardy, J. Trichodermamides A and B, cytotoxic modified dipeptides from the marine-derived fungus Trichoderma virens. *J. Nat. Prod.* **2003**, *66*, 423–426. [CrossRef]
31. Zhu, M.; Yang, Z.; Feng, H.; Gan, Q.; Che, Q.; Zhu, T.; Gu, Q.; Han, B.; Li, D. Trichodermamides D–F, heterocyclic dipeptides with a highly functionalized 1, 2-oxazadecaline core isolated from the endophytic fungus *Penicillium janthinellum* HDN13-309. *RSC Adv.* **2017**, *7*, 48019–48024. [CrossRef]
32. Zhou, J.; Diao, X.; Wang, T.; Chen, G.; Lin, Q.; Yang, X.; Xu, J. Phylogenetic diversity and antioxidant activities of culturable fungal endophytes associated with the mangrove species *Rhizophora stylosa* and *R. mucronata* in the South China Sea. *PLoS ONE* **2018**, *13*, e0197359. [CrossRef]
33. Qin, X.Y.; Yang, K.L.; Li, J.; Wang, C.Y.; Shao, C.L. Phylogenetic diversity and antibacterial activity of culturable fungi derived from the Zoanthid *Palythoa haddoni* in the South China Sea. *Mar. Biotechnol.* **2015**, *17*, 99–109. [CrossRef]
34. Qadri, M.; Rajput, R.; Abdin, M.Z.; Vishwakarma, R.A.; Riyaz-Ul-Hassan, S. Diversity, molecular phylogeny, and bioactive potential of fungal endophytes associated with the Himalayan blue pine (*Pinus wallichiana*). *Microb. Ecol.* **2014**, *67*, 877–887. [CrossRef]
35. Scudiero, D.A.; Shoemaker, R.H.; Paul, K.D.; Monks, A.; Tierney, S.; Nofziger, T.H.; Currens, M.J.; Seniff, D.; Boyd, M.R. Evaluation of a soluble tetrazolium/formazan assay for cell growth and drug sensitivity in culture using human and other tumor cell lines. *Cancer Res.* **1988**, *48*, 4827–4833.

Zhao Feng †, Xuexia Zhang †, Jingwan Wu, Chengwen Wei, Ting Feng, Dongdong Zhou, Zhenchang Wen and Jing Xu *

School of Chemical Engineering and Technology, Hainan University, Haikou 570228, China
* Correspondence: happyjing3@hainanu.edu.cn; Tel.: +86-898-6627-9226
† These authors contributed equally to this work.

Abstract: Three new cytochalasins, phomoparagins A-C (**1**–**3**), along with five known analogs (**4**–**8**), were isolated from *Phomopsis asparagi* DHS-48, a mangrove-derived endophytic fungus. Their structures, including their absolute configurations, were elucidated using a combination of detailed HRESIMS, NMR, and ECD techniques. Notably, **1** possessed an unprecedented 5/6/5/8/5-fused pentacyclic skeleton. These compounds were tested for their inhibitory activity against concanavalin A (ConA)/lipopolysaccharide (LPS)-induced spleen lymphocyte proliferation and calcineurin (CN) enzyme. Several metabolites (**2** and **4**–**6**) exhibited fascinating inhibitory activities with a relatively low toxicity. Furthermore, **2** was demonstrated to inhibit ConA-stimulated activation of NFAT1 dephosphorylation and block NFAT1 translocation in vitro, subsequently inhibiting the transcription of interleukin-2 (IL-2). Our results provide evidence that **2** may, at least partially, suppress the activation of spleen lymphocytes via the CN/NFAT signaling pathway, highlighting that it could serve as an effective immunosuppressant that is noncytotoxic and natural.

Keywords: mangrove endophytic fungi; *Phomopsis* sp.; cytochalasins; immunosuppressive activity; CaN/NFAT signaling pathway

1. Introduction

Immunosuppressants are the main clinical drugs for the treatment of undesirable or abnormal activations in the body, such as immune system activation, which is associated with a variety of autoimmune diseases and allergic reactions, including rheumatoid arthritis, multiple sclerosis, systemic lupus erythematosus, and glomerulonephritis, and responses in organ transplantation recipients [1]. Most of the representative immunosuppressive drugs used in the clinic were developed from microbial secondary metabolites, such as cyclosporin A (CsA), tacrolimus (FK506), and rapamycin [2]. These drugs form complexes with intracellular immunophilin receptors. Among them, the CsA/cyclophilin and FK506/FKBP complexes share the same pharmacodynamic property of suppressing activated T cells by inhibiting the activity of calcineurin (CN) phosphatase; thus, these complexes prevent the dephosphorylation and nuclear translocation of activated T cell nuclear factor (NFAT) and NFAT-mediated transcription of a large number of cytokine genes, such as interleukin 2 (IL-2) [3,4]. However, despite their undeniable satisfactory therapeutic effects, the aforementioned immunosuppressive drugs have been found to cause dramatic side effects, such as nephrotoxicity, hepatotoxicity, neurotoxicity, malignancy, and other adverse effects [5,6]. Thus, the discovery of new clinically applied immunosuppressants with a high efficacy but no major cytotoxicity is urgently needed.

Endophytic fungi isolated from mangrove trees are one of the most pivotal and promising sources of bioactive natural products, presumably owing to their intriguing structural skeleton and the promising pharmacological effect of their secondary metabolites, making them attractive repositories for therapeutic agents and lead compounds [7,8]. Over

50% of mangrove-derived endophytic fungal bioactive secondary metabolites are produced by the genera *Aspergillus* and *Penicillium*, while *Pestalotiopsis*, *Alternaria*, and *Phomopsis* are considered the predominant producers [9]. The *Phomopsis* (teleomorph *Diaporthe*) fungi, which contains more than 900 species named from a wide range of hosts, have attracted considerable attention from natural product researchers in recent years [10,11]. Versatile bioactive metabolites, such as cytotoxic phomopchalasins B and C [12]; cytochalasins J_1–J_3, H_1, and H_2 [13]; dicerandrols [14]; antibiotic isopentylated diphenyl ethers [15], phomoxanthone A [16] and phompsichalasin [17]; β-site amyloid precursor protein cleaving enzyme 1 (BACE1) inhibitory protoilludane-type sesquiterpenoids [18]; and anti-Tobacco mosaic virus (TMV) cytosporone U [19] and arylbenzofurans [20] have been isolated from *Phomopsis* strains. Among them, cytochalasins are a diverse group of polyketide synthase nonribosomal peptide synthetase (PKS-NRPS)-derived fungal metabolites characterized by a perhydroisoindolone moiety, which is typically fused to a macrocyclic ring (ring size 9–14) [21]. Since the first representatives, cytochalasin A and B, were isolated in 1966 [22], the number of natural products belonging to this family has increased to over 200 [12]. As part of our research on mangrove-derived fungi, a series of structurally novel and biologically active metabolites have been discovered [23–27]. Our primary application of in vitro immunosuppressive activity screening indicated that the MeOH extracts from the endophytic fungus strain *Phomopsis asparagi* DHS-48, which were obtained from a fresh root of the mangrove plant *Rhizophora mangle*, strongly inhibited ConA/LPS-induced spleen lymphocyte proliferation and CN enzyme activity, with IC_{50} values of 6.20 ± 0.20 µg/mL, 10.28 ± 0.24 µg/mL, and 78.03 ± 0.45 µg/mL, respectively. Bioassay-guided investigation of the immunosuppressive constituents obtained from the large-scale fermentation of the abovementioned *P. asparagi* DHS-48 resulted in the isolation of three new cytochalasins, namely, phomoparagins A-C (**1**–**3**), along with five known analogs, phomopchalasin A and B (**4**,**5**) [12], cytochalasin H (**6**) [28], and J (**7**) [29] and fragiformin B (**8**) [30] (Figure 1). Herein, we report the isolation, structure elucidation, and immunosuppressive activity, as well as the plausible biosynthetic pathway, of the isolated compounds.
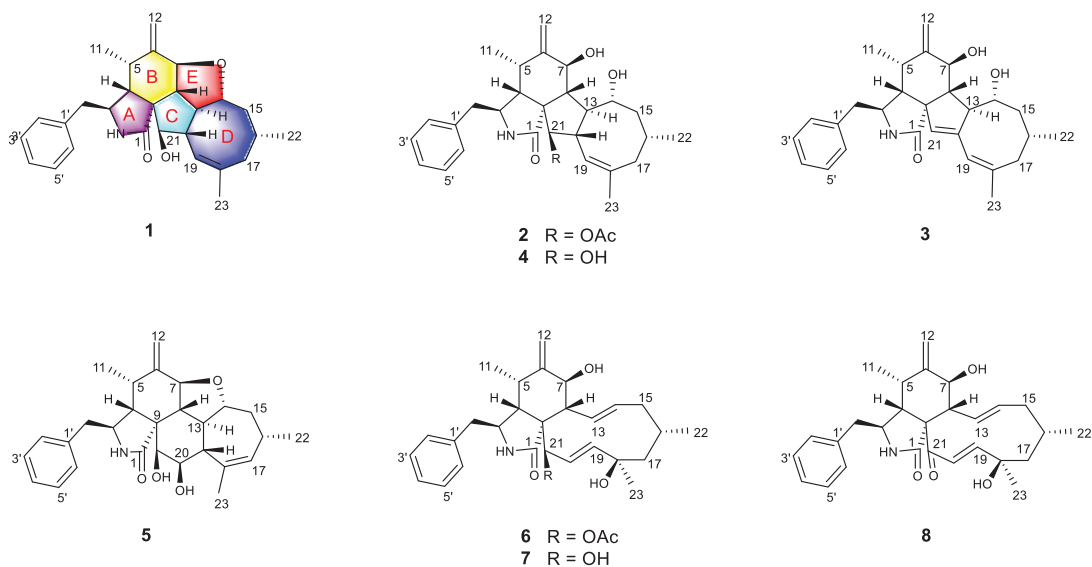

Figure 1. Structures of the isolated Compounds **1**–**8**.

2. Results

Phomoparagin A (**1**) was obtained as a colorless amorphous powder. Its molecular formula, $C_{28}H_{35}NO_3$ with 12 degrees of unsaturation, was established using the high-resolution-electrospray ionization mass spectrometry (HRESIMS) positive ion at *m/z* 434.2644 ([M+H]$^+$, calcd for 434.2695). The ^{1}H NMR data of **1** (Table 1), as well as the coupling constants of the connected protons, indicated the presence of a tertiary methyl at δ_H (1.74, 3H, s, H$_3$-23), two secondary methyl groups at δ_H (0.73, 3H, d, *J* = 6.1 Hz, H$_3$-11; 0.95, 3H, d, *J* = 6.7 Hz, H$_3$-22), an exocyclic methylene group at δ_H (5.13 and 4.96, 2H, both s, H$_2$-12), three oxygenated methine groups at δ_H (4.13, 1H, d, *J* = 9.8 Hz, H-7; 4.19, 1H, t, *J* = 9.7 Hz, H-14; 2.99, 1H, d, *J* = 2.4 Hz, H-21), an olefinic methine group at δ_H (5.28, 1H, br s, H-19), and typical resonance of a single substituted phenyl at δ_H (7.22–7.30, 5H). Its ^{13}C NMR spectrum (Table 2) disclosed 28 carbon resonances, including three sp^3 methyls, three sp^3 methylenes, 10 sp^3 methines, one sp^3 quaternary carbon, one sp^2 exocyclic methylene, six sp^2 olefinic methines, and four sp^2 quaternary carbons (three olefinic carbons and one amide carbonyl), as supported by the DEPT and HSQC spectra. The complete structure of **1** was established by extensive analysis of its 2D NMR spectra. The ^{1}H-^{1}H COSY (Figure 2) and HSQC spectra suggested the presence of the fragments CH$_2$(10)-CH(3)-CH(4)-CH(5)-CH$_3$(11)-, CH(7)-CH(8)-CH(13)-CH(14)-CH$_2$(15)-CH(16)-CH$_2$(17), incorporating CH$_3$-(22), which was coupled to CH-(16); -CH(7)-CH(8)-CH(13)-CH(20)-CH(21)-, incorporating CH-(19), which was coupled to CH-(20), and CH(2′) to CH(6′). In the HMBC spectrum (Figure 2), ^{13}C-^{1}H long-range correlations were observed from H-3 (δ_H 3.30, m) and H-4 (δ_H 2.64, m) to C-1 (δ_C 171.7); H-4 and H-5 (δ_H 2.65, m) to C-9 (δ_C 53.8); H-7 (δ_H 4.13, d, 9.8) to C-5(δ_C 33.4), C-6(δ_C 150.9), C-12(δ_C 113.4), C-14(δ_C 76.8), and C-8(δ_C 41.9), establishing the phenylalanine moiety (rings A and B). HMBC correlations from H-8 (δ_H 2.19, t, 10.0 Hz) to C-1, C-4 (δ_C 47.9), C-9 (δ_C 53.8), and H-4 (δ_H 2.49, m) to C-21 (δ_C 75.6) supported that the five-membered ring C was fused to ring B via C-8 and C-9. An eight-membered ring D was elucidated using the HMBC correlations from H-19 (δ_H 5.28, br s) to C-17 (δ_C 43.4), C-21 (δ_C 75.6), C-18 (δ_C 138.9), and C-23 (δ_C 27.7), and from H-22 (δ_H 0.95, d, 6.7) to C-15 (δ_C 44.4) and C-17 (δ_C 43.4). Additionally, H-10 (δ_H 2.76, 2.69) to C-3 (δ_C 54.5), C-4 (δ_C 47.6), C-1′ (δ_C 138.7), and C-2′/C-6′ (δ_C 131.1) revealed the connection of the phenyl to C-3 via C-10. Comparison of the ^{1}H and ^{13}C NMR spectra of **1** with those of phomopchalasin A (**4**), which was previously isolated from the endophytic fungus *Phomopsis* sp. shj2 associated with *Isodon eriocalyx* var. laxif lora. [12], indicated that these two compounds possessed the same 5/6/5/8-fused tetracyclic cytochalasan ring system (rings A-D). These two compounds are different, in that a new five-membered epoxy unit (ring E) was formed by the dehydration reaction between 7-OH and 14-OH. To confirm this observation, evidence was obtained from the chemical shifts of C-8 (δ_C 41.9) and C-13 (δ_C 42.5) in **1**, which were significantly shifted upfield compared with C-8 (δ_C 51.3) and C-13 (δ_C 51.7) in **4**, along with the HRESIMS data. Thus, the connection from C-7 to C-14 via an oxygen atom was deduced from the above evidence.
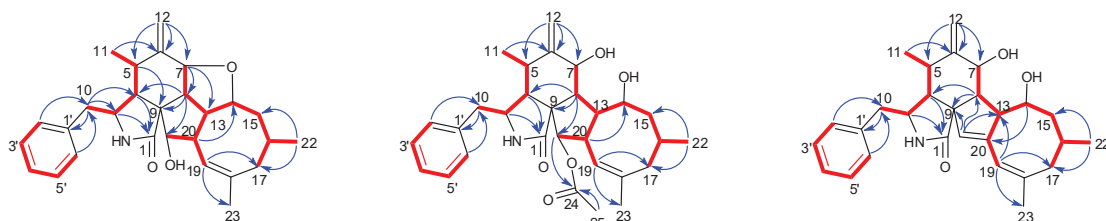

Figure 2. Key COSY and HMBC correlations of Compounds **1**–**3**.

Table 1. ^{1}H NMR data (δ) for **1–3** in CD$_3$OD (400 MHz) (δ in ppm, J in Hz).

No.	1	2	3
1			
3	3.30, m	3.43, q (5.0)	3.32, m
4	2.64, m	2.76, d (6.9)	2.67, m
5	2.65, m	2.53, m	2.70, m
6			
7	4.13, d (9.8)	4.19, d (8.3)	3.90, d (11.1)
8	2.19, t (10.0)	1.98, m	2.87, m
9			
10	2.76, dd (13.2, 5.7)	2.84, dd (12.6, 4.9)	2.83, m
	2.69, m	2.62, m	2.68, m
11	0.73, d (6.1)	0.59, d (6.9)	0.65, d (6.3)
12	5.13, s	4.97, s	5.09, s
	4.96, s	4.83, s	4.95, s
13	1.52, m	3.19, q (10.9)	3.19, brs
14	4.19, t (9.7)	4.65, t (9.0)	3.34, d (2.4)
15	2.36, d (13.5)	1.87, dt (14.2, 8.7)	2.31, dd (12.5, 6.9)
	1.03, qd (13.5, 2.4)	1.46, dd (14.2, 2.9)	1.73, dd (12.5, 9.9)
16	1.49, m	2.13, m	1.95, m
17	1.95, m	2.58, m	2.86, m
		1.99, m	1.48, dd (13.7, 3.2)
18			
19	5.28, brs	5.55, d (7.1)	5.18, d (6.0)
20	2.68, m	2.50, m	
21	2.99, d (2.4)	3.71, d (5.0)	5.53, s
22	0.95, d (6.7)	1.01, d (7.0)	0.94, d (6.8)
23	1.74, s	1.78, s	1.80, s
24			
25		1.99, s	
1′			
2′, 6′	7.22, d (7.1)	7.28, d (7.2)	7.23, d (7.2)
3′, 5′	7.30, t (7.2)	7.30, t (7.6)	7.25, d (7.2)
4′	7.24, t (6.4)	7.21, t (6.8)	7.24, d (6.4)

Table 2. ^{13}C NMR data (δ) for **1–3** in CD$_3$OD (100 MHz) (δ in ppm, J in Hz).

No.	1	2	3
1	179.1, C	181.9, C	179.1, C
3	54.5, CH	54.5, CH	54.0, CH
4	47.6, CH	44.4, CH	47.1, CH
5	33.4, CH	31.5, CH	33.1, CH
6	150.9, C	153.4, C	152.5, C
7	76.0, CH	74.1, CH	72.8, CH
8	41.9, CH	53.4, CH	38.2, CH
9	53.8, C	58.0, C	52.7, C
10	44.9, CH$_2$	43.9, CH$_2$	45.0, CH$_2$
11	13.1, CH$_3$	13.4, CH$_3$	13.0, CH$_3$
12	113.4, CH$_2$	111.8, CH$_2$	113.7, CH$_2$
13	42.5, CH	47.7, CH	47.5, CH
14	76.8, CH	80.7, CH	73.2, CH
15	44.4, CH$_2$	41.3, CH$_2$	42.3, CH$_2$
16	33.5, CH	32.0, CH	35.2, CH
17	43.4, CH$_2$	38.9, CH$_2$	37.5, CH$_2$
18	138.9, C	136.0, C	138.1, C
19	128.5, CH	129.1, CH	123.2, CH
20	43.4, CH	54.4, CH	137.9, C
21	75.6, CH	83.1, CH	120.1, CH
22	25.4, CH$_3$	24.8, CH$_3$	22.1, CH$_3$
23	27.7, CH$_3$	27.2, CH$_3$	28.2, CH$_3$
24		173.1, C	
25		21.9, CH$_3$	
1′	138.7, C	139.4, C	138.9, C
2′,6′	131.1, CH	130.8, CH	131.0, CH
3′,5′	129.5, CH	129.4, CH	129.5, CH
4′	127.7, CH	127.5, CH	127.7, CH

The relative configuration of **1** was subsequently established by analyzing the NOESY spectrum. The NOE crosspeaks (Figure 3) between H-8/H-14, H-14/H-20, and H-20/H-16 indicated that these protons have β orientations. H-7/H-13 and H-13/H-21 were observed, suggesting that these protons are cofacial and have α-orientations. Considering the above evidence, we assumed that the stereochemistry is the same as that reported for **4,** based on the similarity in the 2D NMR resonances and the shared biogenetic origin.
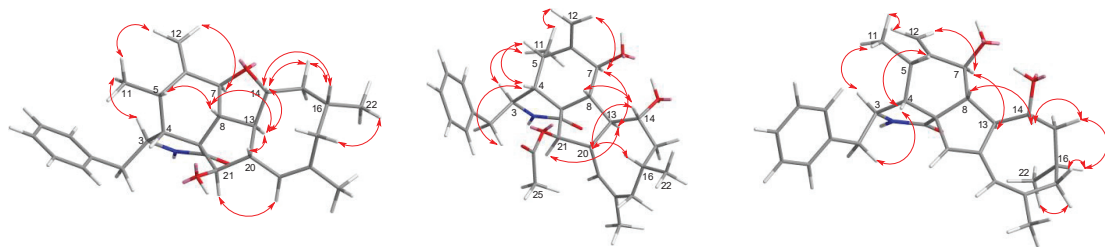
Figure 3. Key NOESY correlations of Compounds **1–3**.

The absolute configuration of **1** was determined by comparing experimental and calculated ECD spectra using time-dependent density-functional theory (TDDFT). Two feasible configurations, 3*S*, 4*R*, 5*S*, 7*S*, 8*R*, 9*R*, 13*R*, 14*R*, 16*R*, 20*S*, 21*R* and 3*R*, 4*S*, 5*R*, 7*R*, 8*S*, 9*S*, 13*S*, 14*S*, 16*S*, 20*R*, 21*S* (**1** and *ent*-**1**, respectively), were calculated at the B3LYP/6-31+G(d,p) level with a PCM solvent model for MeOH. The calculated ECD spectrum of **1** showed an excellent fit with the experimental spectrum (Figure 4), which indicated the absolute configuration to 3*S*, 4*R*, 5*S*, 7*S*, 8*R*, 9*R*, 13*R*, 14*R*, 16*R*, 20*S*, 21*R*. Thus, the complete structure of **1** was established.
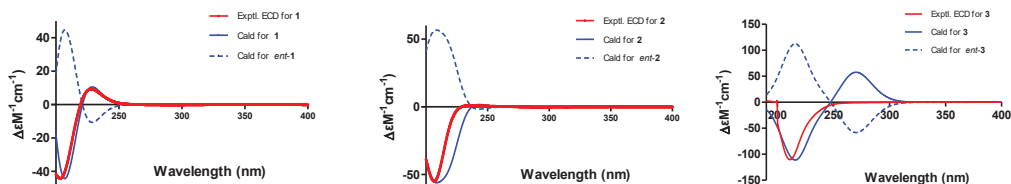

Figure 4. Experimental and calculated electronic circular dichroism (ECD) spectra of **1–3**.

Phomoparagin B (**2**) was obtained as colorless needles and has a molecular formula of $C_{30}H_{39}NO_5$ based on HRESIMS (*m/z* 516.2727, calcd for [M+Na]⁺ 516.2726), implying 12 degrees of unsaturation. The ¹H and ¹³C NMR spectra (Table 1 and 2) of **2** were similar to those of phomopchalasin A (**4**) [12], except that the hydroxyl group at C-21 of the latter was replaced by the acetoxy group of **2**. This was confirmed by the molecular weight difference of 42 amu observed between compounds **2** and **4**, along with the strong HMBC correlation (Figure 2) from the protons of the methyl ester group (δ 1.99, 3H, s) and H-21 (δ 3.71, 1H, *d*, 5.0) to C-24 (δ 173.1), which supports the presence of an acetoxy group at C-21 in **2**. The relative configuration of **2** was determined by interpreting the NOESY data (Figure 3). As expected, the experimental ECD spectrum (Figure 4) of **2** matched exactly with the calculated spectrum. Accordingly, the absolute configuration of **2** was determined to be 3*S*, 4*R*, 5*S*, 7*S*, 8*R*, 9*R*, 13*R*, 14*R*, 16*R*, 20*S*, 21*R*, and it was named phomoparagin B.

Phomoparagin C (**3**), a colorless amorphous powder, has a molecular formula of $C_{28}H_{35}NO_3$, as established by HRESIMS (*m/z* 434.2678, calcd for [M+H]⁺ 434.2695), corresponding to 12 degrees of unsaturation. The ¹H and ¹³C NMR data (Tables 1 and 2) of **3** were similar to those of **2**, except for the signals of the -OCOCH₃ substituent and an aliphatic methine proton within **2**, which were absent in **3**. Instead, signals of an olefinic double bond at (δ_C 137.9, s, C-20; δ_H 5.53, 1H, s; δ_C 120.1, d, CH-21) appeared, which

accounts for the molecular weight difference of 60 amu that was observed between the compounds. Conformational evidence was obtained from the HMBC correlations of H-21 to C-8(δ_C 38.2)/C-9(δ_C 52.7)/C-13(δ_C 47.5) (Figure 2). The relative stereochemistry of compound **3** was determined using the key NOSEY cross peaks (Figure 3) of H-3 with H₃-11; H-8 with H-4 and H-20; and H-14 with H-16 and H-20. The absolute configuration could be determined as 3*S*, 4*R*, 5*S*, 7*S*, 8*R*, 9*R*, 13*R*, 14*R*, 16*R*, by comparing the experimental and calculated ECD spectra using TDDFT (Figure 4). Thus, the structure of **3** was determined, and it was named phomoparagin C.

Previous isotope labeling experiments revealed that cyctochalasans might rationally share the same biosynthetic pathway, and it most likely originates from a polyketide synthase (PKS)/nonribosomal peptide synthetase (NRPS) hybrid machinery [31,32]. The stepwise assembly is realized from one activated acetyl-CoA starter, seven malonyl-CoA extender units and phenylalanine. An intramolecular aldol condensation generates pyrrolinone, which reacts via a [4 + 2]-cycloaddition, hydroxylation, and dehydrogenation to generate the same biosynthetic precursor **7**. Subsequent acetylation and oxidation of 7 formed **6** and **8**, respectively. Compound **5**, which contains a 5/6/6/7/5-fused pentacyclic ring system, might originate by dehydration, epoxidation, intramolecular nucleophilic addition, hydroxylation, and dehydration reactions. In another pathway, **7** undergoes dehydration, intramolecular rearrangement, and hydroxylation, to produce the 5/6/5/8-fused tetracyclic intermediate **4**. The subsequent intramolecular dehydration and acetylation led to the formation of **1**–**3** (Figure 5). Of these, **1** possesses an unprecedented 5/6/5/8/5-fused pentacyclic ring system.
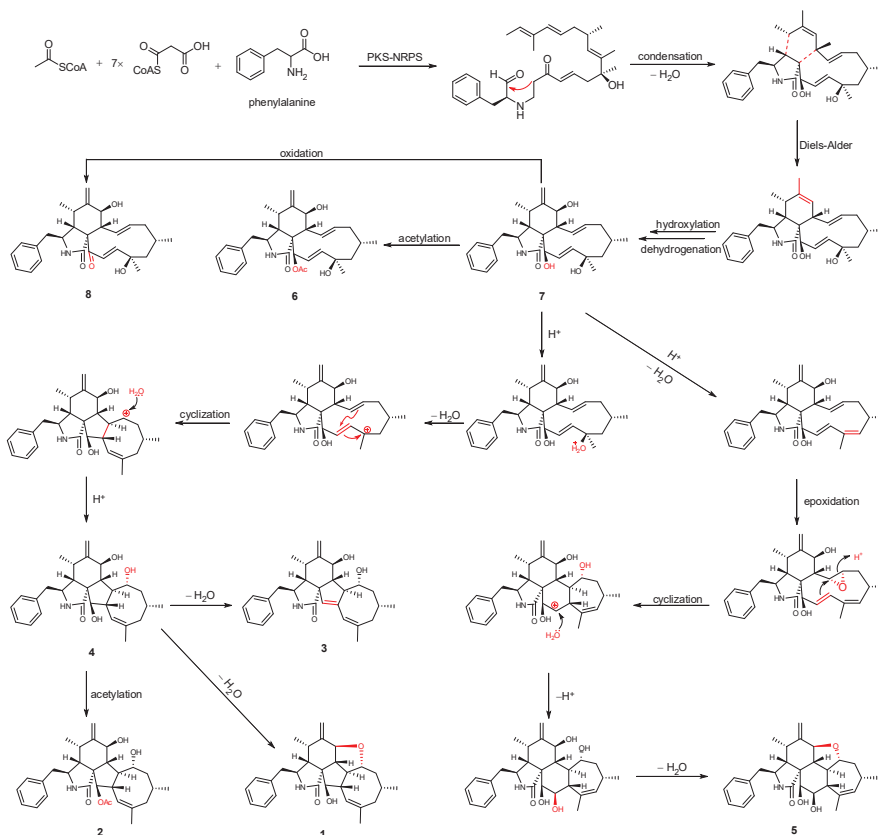

Figure 5. Plausible biogenetic relationship of isolated compounds.

The isolated compounds (**1–8**) were evaluated for their immunosuppressive activities against the proliferation of ConA-induced T and LPS-induced B murine splenic lymphocytes, according to previously described protocols [33–35]. The results showed that Compounds **2** and **4–6** remarkably inhibited the proliferation against splenic lymphocyte growth, with IC_{50} values ranging from 11.2 ± 0.3 μM to 154.4 ± 0.4 μM, of which **2** and **6** displayed the most promising inhibitory effects (Table 3). The cytotoxicity of immunosuppressive Compounds **2** and **4–6** was tested in murine splenocyte cultures for 72 h using the tetrazolium salt-based CCK-8 assay. The results (Table 4) showed that even **6** exhibited better suppression of the overproduction of the cell stimulated by ConA compared with that of **2**, but **2** exhibited relatively lower toxicity for the survival of normal splenocytes ($IC_{50} = 111.7 \pm 1.1$ μM) than that of **6** ($IC_{50} = 42.2 \pm 1.7$ μM) and it was approximately 11-fold lower in comparison with that of CsA ($IC_{50} = 10.9 \pm 0.8$ μM) and cytochalasin D ($IC_{50} = 1.0 \pm 0.0$ μM), indicating that the compound has a relatively low toxicity toward the survival of normal splenic cells. Thus, we selected this particular cytochalasin for the mechanism of action studies.

Table 3. Immunosuppressive activities of isolated compounds [a].

Compound	IC_{50} (μM) [b]	
	ConA-Induced T-Cell Proliferation	LPS-Induced B-Cell Proliferation
2	21.6 ± 1.7	78.5 ± 1.3
4	32.8 ± 2.4	144.9 ± 2.2
5	31.2 ± 2.5	154.4 ± 0.4
6	11.2 ± 0.3	102.8 ± 1.1
cyclosporin A [c]	4.4 ± 0.0	25.1 ± 0.4

[a] Compound **1**, **3**, **7–8** were inactive ($IC_{50} > 200$ μM). [b] Data are presented as mean $\pm$ SD from three separate experiments. [c] Positive control.

Table 4. Cytotoxicity data of immunosuppressive compounds [a].

Cell Line	Compound					
	2	4	5	6	CsA	Cytochalasin D
murine splenocytes	111.7 ± 1.1	373.7 ± 3.3	84.4 ± 0.3	42.17 ± 1.7	10.9 ± 0.8	1.0 ± 0.0

[a] Results are expressed as IC_{50} values of mean $\pm$ SD ($n = 7$) in μM.

To directly examine whether **2** specifically inhibits the CaN/NFAT pathway, we first investigated the CaN inhibition rate of **2**. As expected, **2** was found to be significantly active and inhibited CN in a dose-dependent manner with an IC_{50} value of 17.89 ± 0.40 μM, which has a greater potency than that of the clinically used immunosuppressant cyclosporine A (CsA, IC_{50} of 31.7 ± 0.7 μM) (Figure 6A). The effect of **2** on ConA-stimulated NFAT1 and NFAT-P expression was determined by Western blotting. In unstimulated cells, NFAT was found exclusively in the phosphorylated form, reflecting that calcineurin is inactive under resting conditions. In contrast, in the ConA-stimulated cells in the absence of **2**, the dephosphorylated form of NFAT1 was detected, as well as the phosphorylated form. The presence of 50 μM **2** strongly inhibited the dephosphorylation of NFAT (Figure 6B). Correspondingly, immunofluorescence analysis demonstrated that NFAT1 protein was diffusely distributed in the cytoplasm and was absent from the nucleus. After 48 h of stimulation with 5 μg/mL Con A, the fluorescent NFAT1 translocated to the nucleus. In contrast, the presence of **2** blocked the Con A-stimulated translocation of NFAT from the cytoplasm to the nucleus in a dose-dependent manner (Figure 6C). With respect to the effect of **2** on the expression levels of IL-2 mRNA, as determined by real-time quantitative PCR (q-PCR), the transcription level of Con A-stimulated IL-2 mRNA decreased with increasing concentrations of **2** (Figure 6D). ELISA experiments further confirmed the effects of **2** at the IL-2 protein level (Figure 6E). Molecular docking was then performed to further understand the possible binding modes and binding affinities of highly active **2** with the active sites of CN using AutoDock 4.2. As shown in Figure 6F, **2** formed four key hydrogen bonds with residues GLN-130 and HIS-339 with a binding energy of -5.92 kcal·mol^{-1}. In addition, **2** formed

hydrophobic interactions with residues ILE-436, ILE-474, ARG-477, VAL-490, and VAL-498 and intermolecular interactions with residues THR-126, GLN-127, ASP-313, and PRO-340. Therefore, the immunosuppressive activity of **2** is possibly, at least in part, mediated via CaN/NFAT signaling pathway-regulated Con A-stimulated activation of splenocytes (Figure 7), highlighting its potential for use as an effective noncytotoxic natural immunosuppressant.
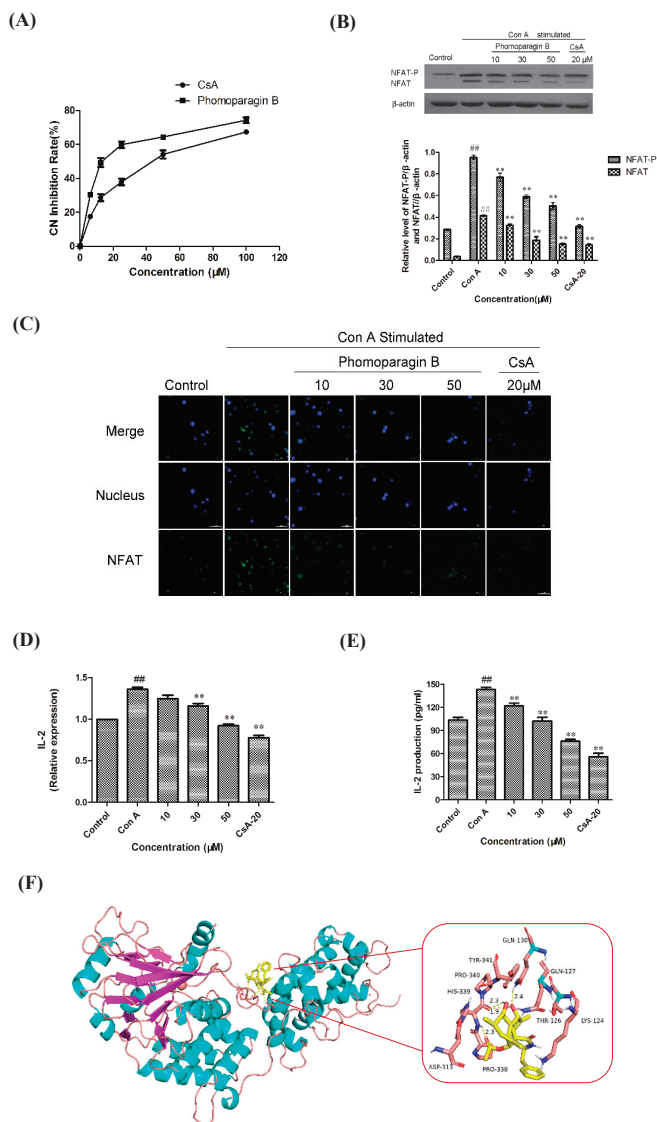
(A)

(B)

(C)

(D)

(E)

(F)

Figure 6. The effect of **2** on calcineurin activity (**A**). Effects of **2** on the expression of ConA-induced NFAT1 protein and analyzed by Western blot (**B**). Effects of **2** on the expression of ConA-induced NFAT protein and analyzed by Western blot (**C**). Effect of **2** in ConA-induced mouse T lymphocytes on IL-2 mRNA expression by q-PCR (**D**) and IL-2 secretion by ELISA (**E**). Molecular docking analysis of the binding of **2** to calcineurin (**F**). ** $p < 0.01$ compared to the stimulated group. ## $p < 0.01$ compared to the control group.
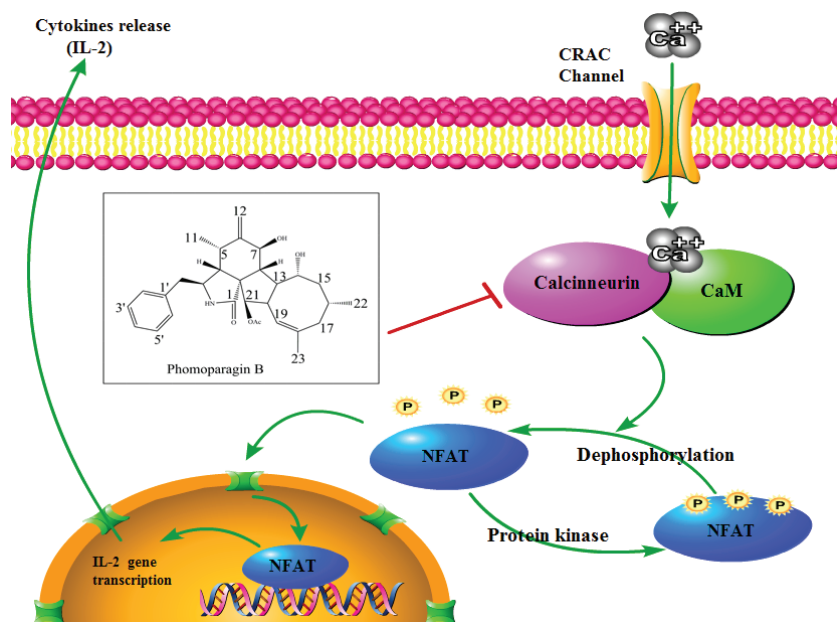
Figure 7. Schematic view of **2** acting on the CN/NFAT signaling pathway.

3. Materials and Methods

3.1. General Experimental Procedures

A WYA-2S digital Abbe refractometer (Shanghai Physico-optical Instrument Factory) was used to measure optical rotations. Circular dichroism (CD) spectra were measured on a JASCO J-715 spectra polarimeter. An LTQ Orbitrap XL instrument (Thermo Fisher Scientific, Bremen, Germany) was used to record HRESIMS data. 1D and 2D NMR spectra were recorded on a Bruker AV-400 spectrometer for ^{1}H nuclei and 100 MHz for ^{13}C nuclei in CD$_3$OD. An Agilent 1100 instrument was applied for HPLC analysis and semipreparative HPLC separation. Sephadex LH-20 (18−110 μm, Merck, Darmstadt, Germany), RP-18 gel (25–40 μm, Daiso Inc., Osaka, Japan), or silica gel (200–300 mesh, Qingdao Marine Chemical Inc., Qingdao, China) were employed for column chromatography. Thin-layer chromatography was performed over F$_{254}$ glass plates (200–400 mesh, Qingdao Marine Chemical Inc., Qingdao, China) and analyzed under UV light (254 and 366 nm). The purity of the isolated compounds was determined by high-performance liquid chromatography (HPLC), which was performed on an Agilent 1200 instrument and a reverse-phase column (4.6 × 150 mm, 5 μm). The UV wavelength for detection was 210 nm. All compounds were eluted with a flow rate of 0.7 mL·min^{-1} over a 15-min gradient, as follows: T = 0, 95% B; T = 15, 100% B (A, H$_2$O; B, MeOH) and the purity of tested compounds were proven to exceed 95% (Figure S43).

3.2. Fungal Material

The strain DHS-8 of *Phomopsis asparagi* was isolated from a healthy tree root of the mangrove plant *Rhizophora mangle*, which was collected in the Dong Zhai Gang-Mangrove Garden (110°320′–110°37′ E, 19°51′–20°01′ N) in Hainan Province in October 2015. The strain was isolated under sterile conditions from the inner tissue of the root, following an isolation protocol described previously [36] and identified using a molecular biological protocol by DNA amplification and sequencing of the ITS region (GenBank Accession no. MT126606). A voucher strain was preserved on potato dextrose agar slants stored at 4 °C at one of the authors' laboratory (J. X.).

3.3. Fermentation and Extraction

The fungus was fermented onto autoclaved rice solid-substrate medium (thirty 1000 mL Erlenmeyer flasks, each containing 100 g of rice and 100 mL of 0.3% saline water) and incubated for 28 days at 28 °C. In total, 140 flasks of culture were extracted three times with EtOAc, and the filtrate was evaporated under reduced pressure to yield crude extract (65 g).

3.4. Purification and Identification

The crude extract was partitioned with petroleum ether (PE), dichloromethane, ethyl acetate (EA), and *n*-butyl alcohol (BA). The dichloromethane fraction and ethyl acetate fraction were combined (30 g) and then subjected to silica gel column chromatography using gradient elution with CH_2Cl_2–MeOH mixtures of increasing polarity (100:0–0:100, *v/v*) to afford 8 fractions (Fr. 1–Fr. 8). Fr. 2 was subjected to open silica gel CC using gradient elution with CH_2Cl_2-EtOAc (4:1–1:1, *v/v*) to yield fractions Fr. 2.1–2.6. Then Fr. 2.3 and Fr. 2.4 were purified by semipreparative reversed-phase HPLC using MeOH–H_2O (50:50, *v/v*) to afford **3** (5.0 mg) (Figures S19–S27). Purification of Fr. 2.5 was conducted by CC over RP-18 with a MeOH–H_2O gradient (50:50–90:10, *v/v*) to yield **2** (8.0 mg) (Figures S10–S18) and **6** (119.2 mg) (Figures S34–S36). Fr. 2.6 was separated using Sephadex LH-20 CC with $CHCl_3$–MeOH (1:1, *v/v*) to afford **1** (105 mg) (Figures S1–S9). Fr. 4 was subjected to CH_2Cl_2-EtOAc (1:1, *v/v*) and further fractionated by RP C-18 CC eluted with CH_3OH-H_2O (70:30, *v/v*) to produce the major component **7** (818.3 mg) (Figures S37–S39). Fr. 5 was subjected to silica gel CC using CH_2Cl_2-CH_3OH as the eluent (100:4–100:6, *v/v*). The promising subfraction Fr. 5.1 was separated by semipreparative reversed-phase HPLC using MeOH–H_2O (60:40, *v/v*) to obtain **8** (2.7 mg) (Figures S40–S42). Separations of Fr. 5.4 following a procedure similar to that used for Fr. 5.1 gave **4** (semiprep. HPLC, MeOH–H_2O = 60:40, *v/v*, 120 mg) (Figures S28–S30). Fr. 6.2, collected from Fr. 6 was subjected to silica gel CC with CH_2Cl_2-EtOAc (100:10, *v/v*), followed by Sephadex LH-20 CC using $CHCl_3$–MeOH (1:1, *v/v*) as the eluent to yield **5** (6.1 mg) (Figures S31–S33).

Phomoparagin A (1): colorless amorphous residue (MeOH); $[\alpha]^{20}_D$ -13 (*c* 0.001, MeOH); UV (MeOH) λ_{max} 215 nm; ^1H and ^{13}C NMR data, see Table 1; HRESIMS *m/z* 434.2644 $[M + H]^+$ (calcd for C28H36NO3, 434.2695).
Phomoparagin B (2): colorless amorphous residue (MeOH); $[\alpha]^{20}_D$ +54 (*c* 0.001, MeOH); UV (MeOH) λ_{max} 212 nm; ^1H NMR data, see Table 1; HRESIMS *m/z* 516.2733 $[M + Na]^+$ (calcd for $C_{30}H_{39}NO_5Na$, 516.2726).
Phomoparagin C (3): colorless amorphous residue (MeOH); $[\alpha]^{20}_D$ -14 (*c* 0.001, MeOH); UV (MeOH) λ_{max} 212 nm; ^1H and ^{13}C NMR data, see Table 1; HRESIMS *m/z* 434.2678 $[M + H]^+$ (calcd for $C_{28}H_{36}NO_3$, 434.2695).

3.5. Electron Circular Dichroism Calculation

Monte Carlo conformational searches were run by employing Spartan's 14 software using the Merck Molecular Force Field (MMFF). Conformers with a Boltzmann population of over 0.4% were chosen for ECD calculations (Tables S1 and S2). Then, the conformers were initially optimized at the B3LYP/6-31 g level in gas using the PCM polarizable conductor calculation model. The theoretical calculation of ECD was conducted in MeOH using time-dependent density functional theory (TD-DFT) at the B3LYP/6-31+g (d, p) level for all conformers of Compounds **1–3**. Rotatory strengths for a total of 30 excited states were calculated. ECD spectra were generated using the program SpecDis 1.6 (University of Würzburg, Würzburg, Germany) and GraphPad Prism 5 (University of California San Diego, USA) from dipole-length rotational strengths by applying Gaussian band shapes with sigma = 0.3 eV.

3.6. Splenocyte Proliferation Assay

Spleen cells were collected from BALB/c mice under aseptic conditions, plated in a 96-well plate at a density of 1.5×10^6 cells/well and activated by Con A (5 µg/mL) or

LPS (10 μg/mL) in the presence of various concentrations of compounds or cyclosporine A (CsA) at 37 °C and 5% CO_2 for 48 h. Then, 20 μL CCK-8 was added to each well, 4 h before the end of the incubation. Absorbance at OD_{450} was measured on an ELISA reader, and the IC_{50} value was calculated from the correlation curve between the compound concentration and the OD_{450}.

3.7. Cell Viability Assessment

Cell viability was evaluated using the CCK-8 method. Spleen cells were plated in a 96-well plate at a density of 1.5×10^6 cells/well. Then, the cells were incubated with various concentrations of compounds or 0.1% DMSO at 37 °C and 5% CO_2 for 72 h. Proliferation was measured using the CCK-8 assay, as described above. Cyclosporin A (CsA) and cytochalasin D were used as positive controls.

3.8. CN Phosphatase Assay

A spectrophotometric assay was used to determine the activities of CN with 20 mM p-nitrophenyl phosphate (p-NPP) as the substrate in 1 mM $CaCl_2$, 0.5 mM $MnCl_2$, 2 mM CaM, 2 mM CNB, 1 mM DTT, 0.1 mg/mL bovine serum albumin (BSA), and 50 mM Tris-HCl (pH 7.4) at 4 °C. The reaction was initiated by the addition of CNA, various concentrations of compounds (6.25, 12.5, 25, 50 or 100 μM) were added, and the solution was preincubated for 10 min at 4 °C. The OD_{410} value was measured, and the inhibitory concentration (IC_{50}) was calculated. DMSO (2%) was used as a vehicle control. CsA was used as a positive control.

3.9. Western Blot Analysis

Splenocytes were washed with PBS and lysed in PMSF lysate. After centrifugation at 12,000 rpm for 5 min, the protein concentration was determined using a BSA Protein Assay Kit. Protein lysates were separated using 10% sodium dodecyl sulfate–polyacrylamide gel electrophoresis (SDS–PAGE) and transferred to polyvinylidene difluoride (PVDF) membranes. After blocking, the membranes were incubated overnight with the respective primary antibodies against NFAT1, NFAT-P, and β-actin in 5% BSA, and the secondary antibody was horseradish peroxidase (HRP)-conjugated goat anti-rabbit IgG. Immunoreactive bands were visualized by incubation with luminescent liquid and exposed to light-sensitive film.

3.10. Immunofluorescence

Splenocytes were seeded in a 24-well plate at a density of 5×10^6 cells/well, incubated with various concentrations of Compound **2** or CsA, and then activated by culturing with Con A (5 μg/mL) for 48 h. After treatment, the cells were fixed with 4% paraformaldehyde for 30 min, permeabilized in 0.5% Triton X-100 for 15 min, blocked with 5% BSA for 1 h, and then incubated overnight in the respective primary antibody; NFAT1 (D43B1) XP® Rabbit antibody was used at a 1:100 dilution in PBS. The corresponding fluorescent anti-rabbit IgG (H+L) secondary antibody was added for 1 h. Nuclear staining was performed with the addition of 300 μL DAPI for 5 min. Stained cells were washed with PBS and visualized using confocal microscopy.

3.11. Real-Time Quantitative PCR

Total cellular RNA was isolated from splenocytes (5×10^6 cells/well) treated with the indicated concentrations of compounds or cyclosporin A for 48 h and extracted using RNA isolate. The obtained total RNA (2 μg) was used for cDNA synthesis with a Servicebio®RT First Strand cDNA Synthesis Kit with random primers, according to the manufacturer's instructions. qPCR was performed ith SYBR Green qPCR Master Mix (High ROX) using ABI StepOne Plus Real-time Detection System and *β*-actin as internal control. The primers were as follows: IL-2 forward, 5′-TGTCACAAACAGTGCACCTACTTC-3′; IL-2 reverse, 5′-TGTGGCCTTCTTGGGCATGT-3′; *β*-actin forward, 5′-GTGACAGCAGTCGGTTGGAG-

3′; β-actin reverse, 5′-AGTGGGGTGGCTTTTAGGAT-3′. The expression levels of genes were normalized to the expression of β-actin mRNA and analyzed using the delta-delta CT method ($2^{-\Delta\Delta CT}$).

3.12. IL-2 ELISA Assay

Splenocytes were treated as described in the RT–qPCR section, and then the IL-2 levels in the obtained culture supernatants were measured using an enzyme-linked immunosorbent assay (ELISA) kit, according to the manufacturer's instructions. Cytokine standard curves were used to calculate the amount of IL-2, and the absorbance of each well was read at OD_{450} using an ELISA reader.

3.13. Molecular Docking Analysis

Molecular docking studies were performed to investigate the binding mode of Compound **2** with calcineurin using AutoDock 4.2 software. The crystallographic structure of calcineurin (PDB ID: 1AUI) was obtained from the Research Collaboratory for Structural Bioinformatics Protein Data Bank (RCSB PDB, http://www.rcsb.org, accessed on 17 December 2021). The structure file 1AUI was protonated, and water was deleted at pH 7 using the Clean Protein tool. The 3D structure of the small molecule was built using ChemBioDraw Ultra 14.0 (Cambridgesoft Corp., Cambridge, MA, USA) and optimized using MM2 and the steepest gradient method in Chem3D Ultra 14.0 (Cambridgesoft Corp., Cambridge, MA, USA). The Lamarckian genetic algorithm method was used in AutoDock 4.2 (Scripps Research, San Diego, CA, USA), and a docking site was defined as all residues within an RMS tolerance of 1.0 Å. The default parameters were used if no other parameters are mentioned. The obtained results were analyzed and visualized with PyMOL software (Schrödinger, New York, USA).

3.14. Statistical Analysis

All the results are presented as the mean $\pm$ SD, and the difference was considered significant at the $p < 0.05$ level. GraphPad Prism v5.0 (University of California San Diego, USA) was employed to analyze the data and draw plots. One-way analysis of variance (ANOVA) was used to determine the statistical significance of differences between means in SPSS13.0 (Chicago, IL, USA).

4. Conclusions

In summary, our chemical exploratory investigations on the mangrove-derived endophytic fungus *Phomopsis asparagi* DHS-48 led to the characterization of three new cytochalasins and five known analogs. Phomoparagin A (**1**) represents the first example of a cytochalasan that features an unprecedented 5/6/5/8/5-fused pentacyclic skeleton, and phomoparagin B (**2**) of the CN-NFAT signaling pathway was discovered and is a promising immunosuppressant, as it directly inhibited calcineurin and did not require a matchmaker protein, such as the clinical immunosuppressants CsA and FK506. The potent immunosuppressive activity and low toxicity of **2** collectively suggested that it is an attractive option for immunosuppressive drug development.

ZDKJ202018) and Key Research Program of Hainan Province (ZDYF2021SHFZ108) and Guangdong Key Laboratory of Marine Materia Medica Open Fund (LMM2021-4) are gratefully acknowledged.

Institutional Review Board Statement: All experiments conducted on animal material were approved by the Ethics Committee of the Hainan University (HNUAUCC-2021-00082, 17 February 2021), and all methods used were compliant with the regulations of the Ethics Committee.

Conflicts of Interest: The authors declare no conflict of interest.

References

1. Mika, A.; Stepnowski, P. Current methods of the analysis of immunosuppressive agents in clinical materials: A review. *J. Pharmaceut. Biomed.* **2016**, *127*, 207–231. [CrossRef] [PubMed]
2. Ho, S.; Clipstone, N.; Timmermann, L.; Northrop, J.; Graef, I.; Fiorentino, D.; Nourse, J.; Crabtree, G.R. The mechanism of action of cyclosporin A and FK506. *Clin. Immunol. Immunopathol.* **1996**, *80*, S40–S45. [CrossRef]
3. Liu, J.; Farmer, J.D.; Lane, W.S.; Friedman, J.; Schreiber, S.L. Calcineurin is a common target of cyclophilin-cyclosporin a and fkbp-fk506 complexes. *Cell* **1991**, *66*, 807–815. [CrossRef]
4. Clipstone, N.A.; Crabtree, G.R. Identification of calcineurin as a key signalling enzyme in t-lymphocyte activation. *Nature* **1992**, *357*, 695–697. [CrossRef]
5. Hackstein, H.; Thomson, A.W. Dendritic cells: Emerging pharmacological targets of immunosuppressive drugs. *Nat. Rev. Immunol.* **2004**, *4*, 24–34. [CrossRef] [PubMed]
6. Kahan, B.D. Individuality: The barrier to optimal immunosuppression. *Nat. Rev. Immunol.* **2003**, *3*, 831–838. [CrossRef]
7. Xu, J. Bioactive natural products derived from mangrove-associated microbes. *RSC Adv.* **2015**, *5*, 841–892. [CrossRef]
8. Xu, J. Biomolecules produced by mangrove-associated microbes. *Curr. Med. Chem.* **2011**, *18*, 5224–5266. [CrossRef]
9. Xu, J. Natural products of mangrove-derived microbes. *Toxicon* **2019**, *158*, S28–S29. [CrossRef]
10. Udayanga, D.; Liu, X.; McKenzie, E.H.C.; Chukeatirote, E.; Bahkali, A.H.A.; Hyde, K.D. The genus Phomopsis: Biology, applications, species concepts and names of common phytopathogens. *Fungal Divers.* **2011**, *50*, 189–225. [CrossRef]
11. Udayanga, D.; Liu, X.; Crous, P.W.; Mckenzie, E.H.C.; Chukeatirote, E.; Hyde, K.D. A multi-locus phylogenetic evaluation of diaporthe (phomopsis). *Fungal Divers.* **2012**, *56*, 157–171. [CrossRef]
12. Yan, B.C.; Wang, W.G.; Hu, D.B.; Sun, X.; Kong, L.M.; Li, X.N.; Du, X.; Luo, S.H.; Liu, Y.; Li, Y.; et al. Phomopchalasins A and B, two cytochalasans with polycyclic-fused skeletons from the endophytic fungus *Phomopsis* sp. shj2. *Org. Lett.* **2016**, *18*, 1108–1111. [CrossRef] [PubMed]
13. Shang, Z.; Raju, R.; Salim, A.A.; Khalil, Z.G.; Capon, R.J. Cytochalasins from an australian marine sediment-derived *Phomopsis* sp (cmb-m0042f): Acid-mediated intramolecular cycloadditions enhance chemical diversity. *J. Org. Chem.* **2017**, *82*, 9704–9709. [CrossRef] [PubMed]
14. Wagenaar, M.M.; Clardy, J. New Antibiotic and Cytotoxic Dimers Produced by the Fungus *Phomopsis* longicolla Isolated from an Endangered Mint. *J. Nat. Prod.* **2001**, *64*, 1006–1009. [CrossRef] [PubMed]
15. Li, Z.J.; Yang, H.Y.; Li, J.; Liu, X.; Ye, L.; Kong, W.S.; Tang, S.Y.; Du, G.; Liu, Z.H.; Zhou, M.; et al. Isopentylated diphenyl ether derivatives from the fermentation products of an endophytic fungus *phomopsis fukushii*. *J. Antibiot.* **2018**, *71*, 359–362. [CrossRef] [PubMed]
16. Elsässer, B.; Krohn, K.; Flörke, U.; Root, N.; Aust, H.J.; Draeger, S.; Schulz, B.; Antus, S.; Kurtán, T. X-ray Structure Determination, Absolute Configuration and Biological Activity of Phomoxanthone A. *Eur. J. Org. Chem.* **2005**, *2005*, 4563–4570. [CrossRef]
17. Horn, W.S.; Simmonds, M.S.J.; Schwartz, R.E.; Blaney, W.M. Phomopsichalasin, a novel antimicrobial agent from an endophytic *Phomopsis* sp. *Tetrahedron* **1995**, *51*, 3969–3978. [CrossRef]
18. Xie, S.; Wu, Y.; Qiao, Y.; Guo, Y.; Wang, J.; Hu, Z.; Zhang, Q.; Li, X.; Huang, J.; Zhou, Q.; et al. Protoilludane, illudalane, and botryane sesquiterpenoids from the endophytic fungus *Phomopsis* sp. tj507a. *J. Nat. Prod.* **2018**, *81*, 1311–1320. [CrossRef]
19. Tan, Q.W.; Fang, P.H.; Ni, J.C.; Gao, F.; Chen, Q.J. Metabolites Produced by an Endophytic *Phomopsis* sp. and Their Anti-TMV Activity. *Molecules* **2017**, *22*, 2073–2083. [CrossRef]
20. Du, G.; Wang, Z.C.; Hu, W.Y.; Yan, K.L.; Wang, X.L.; Yang, H.M.; Yang, H.Y.; Gao, Y.H.; Liu, Q.; Hu, Q.F. Three new 3-methyl-2-arylbenzofurans from the fermentation products of an endophytic fungus *Phomopsis* sp. and their anti-tmv activity. *Phytochem. Lett.* **2017**, *21*, 287–290. [CrossRef]
21. Speck, K.; Magauer, T. The chemistry of isoindole natural products. *Beilstein J. Org. Chem.* **2013**, *9*, 2048–2078. [CrossRef] [PubMed]
22. Rothweiler, W.; Tamm, C. Isolation and structure of Phomin. *Experientia* **1966**, *22*, 750–752. [CrossRef]
23. Hemberger, Y.; Xu, J.; Wray, V.; Proksch, P.; Wu, J.; Bringmann, G. Pestalotiopens A and B: Stereochemically Challenging Flexible Sesquiterpene-Cyclopaldic Acid Hybrids from *Pestalotiopsis* sp. *Chem. Eur. J.* **2013**, *19*, 15556–15564.
24. Xu, Z.Y.; Xiong, B.X.; Xu, J. Chemical Investigation of Secondary Metabolites Produced by Mangrove Endophytic Fungus *Phyllosticta Capitalensis*. *Nat. Prod. Res.* **2019**, *35*, 1561–1565. [CrossRef] [PubMed]
25. Zhou, J.; Li, G.; Deng, Q.; Zheng, D.Y.; Yang, X.B.; Xu, J. Cytotoxic constituents from the mangrove endophytic *Pestalotiopsis* sp. induce G(0)/G(1) cell cycle arrest and apoptosis in human cancer cells. *Nat. Prod. Res.* **2018**, *32*, 2968–2972. [CrossRef] [PubMed]

26. Xu, Z.Y.; Wu, X.; Li, G.; Feng, Z.; Xu, J. Pestalotiopisorin B, a new isocoumarin derivative from the mangrove endophytic fungus *Pestalotiopsis* sp. HHL101. *Nat. Prod. Res.* **2019**, *34*, 1002–1007. [CrossRef]

27. Deng, Q.; Li, G.; Sun, M.Y.; Yang, X.B.; Xu, J. A new antimicrobial sesquiterpene isolated from endophytic fungus *Cytospora* sp. from the Chinese mangrove plant *Ceriops tagal*. *Nat. Prod. Res.* **2018**, *34*, 1404–1408. [CrossRef]

28. Lee, J.; Yi, J.M.; Kim, H.; Lee, Y.J.; Park, J.S.; Bang, O.S.; Kim, N.S. Cytochalasin h, an active anti-angiogenic constituent of the ethanol extract of gleditsia sinensis thorns. *Biol. Pharm. Bull.* **2014**, *37*, 6–12. [CrossRef]

29. Izawa, Y.; Hirose, T.; Shimizu, T.; Koyama, K.; Natori, S. Six new 10-phenyl-[11] cytochalasins N-S from *Phomopsis* sp. *Tetrahedron* **1989**, *45*, 2323–2335. [CrossRef]

30. Stadler, M.; Quang, D.N.; Tomita, A.; Hashimoto, T.; Asakawa, Y. Changes in secondary metabolism during stromatal ontogeny of hypoxylon fragiforme. *Mycol. Res.* **2006**, *110*, 811–820. [CrossRef]

31. Vederas, J.C.; Graf, W.; David, L.; Tamm, C. Biosynthesis of cytochalasans. part 4. the mode of incorporation of common naturally-occurring carboxylic acids into cytochalasin d. *Helv. Chim. Acta.* **1975**, *58*, 1886–1897. [CrossRef]

32. Schümann, J.; Hertweck, C. Molecular basis of cytochalasan biosynthesis in fungi: Gene cluster analysis and evidence for the involvement of a pks-nrps hybrid synthase by rna silencing. *J. Am. Chem. Soc.* **2007**, *129*, 9564–9565. [CrossRef] [PubMed]

33. Xu, J.; Zhang, X.X.; Huang, F.L.; Li, G.; Leadlay, P.F. Efophylins A and B, two new C2-asymmetric macrodiolide immunosuppressants from *Streptomyces malaysiensis* DSM 4137. *J. Nat. Prod.* **2021**, *84*, 1579–1586. [CrossRef] [PubMed]

34. Zhang, X.X.; Li, G.; Deng, Q.; Xu, Z.Y.; Cen, J.R.; Xu, J. Vomifoliol isolated from mangrove plant *Ceriops tagal* inhibits the NFAT signaling pathway with CN as the target enzyme in vitro. *Bioorg. Med. Chem. Lett.* **2021**, *48*, 128235. [CrossRef] [PubMed]

35. Xu, Z.Y.; Zhang, X.X.; Ma, J.K.; Yang, Y.; Zhou, J.; Xu, J. Secondary metabolites produced by mangrove endophytic fungus *Aspergillus fumigatus* HQD24 with immunosuppressive activity. *Biochem. Syst. Ecol.* **2020**, *93*, 104166. [CrossRef]

36. Zhou, J.; Diao, X.; Wang, T.; Chen, G.; Lin, Q.; Yang, X.; Xu, J. Phylogenetic diversity and antioxidant activities of culturable fungal endophytes associated with the mangrove species *Rhizophora stylosa* and *R. mucronata* in the South China Sea. *PLoS ONE* **2018**, *13*, e0197359.

Article

Epigenetic Manipulation Induced Production of Immunosuppressive Chromones and Cytochalasins from the Mangrove Endophytic Fungus *Phomopsis asparagi* DHS-48

Ting Feng [†], Chengwen Wei [†], Xiaolin Deng, Dandan Chen, Zhenchang Wen and Jing Xu *

Collaborative Innovation Center of Ecological Civilization, School of Chemical Engineering and Technology, Hainan University, Haikou 570228, China
* Correspondence: happyjing3@hainanu.edu.cn; Tel.: +86-898-6627-9226
† These authors contributed equally to this work.

Abstract: A mangrove endophytic fungus *Phomopsis asparagi* DHS-48 was found to be particularly productive with regard to the accumulation of substantial new compounds in our previous study. In order to explore its potential to produce more unobserved secondary metabolites, epigenetic manipulation was used on this fungus to activate cryptic or silent genes by using the histone deacetylase (HDAC) inhibitor sodium butyrate and the DNA methyltransferase (DNMT) inhibitor 5-azacytidine (5-Aza). Based on colony growth, dry biomass, HPLC, and ^{1}H NMR analyses, the fungal chemical diversity profile was significantly changed compared with the control. Two new compounds, named phaseolorin J (**1**) and phomoparagin D (**5**), along with three known chromones (**2–4**) and six known cytochalasins (**6–11**), were isolated from the culture treated with sodium butyrate. Their structures, including their absolute configurations, were elucidated using a combination of detailed HRESIMS, NMR, and ECD and ^{13}C NMR calculations. The immunosuppressive and cytotoxic activities of all isolated compounds were evaluated. Compounds **1** and **8** moderately inhibited the proliferation of ConA (concanavalin A)-induced T and LPS (lipopolysaccharide)-induced B murine spleen lymphocytes. Compound **5** exhibited significant in vitro cytotoxicity against the tested human cancer cell lines Hela and HepG2, which was comparative to the positive control adriamycin and fluorouracil. Our finding demonstrated that epigenetic manipulation should be an efficient strategy for the induction of new metabolites from mangrove endophytic fungi.

Keywords: mangrove endophytic fungus; *Phomopsis asparagi*; epigenetic manipulation; chromones; cytochalasins

1. Introduction

Mangrove endophytic fungi, which adapted to extreme environmental stresses, such as high salinity, high temperature, high humidity, light, and air limitations, are considered to be a reliable source of unique metabolites [1–4]. Exploring the secondary metabolites with excellent biological activity and pharmacy value from mangrove-derived fungi has become a new hotspot in drug development [5]. Nevertheless, genome sequencing unveils that most mangrove endophytic fungi possess significantly more biosynthetic gene clusters than the number of compounds they produce under conventional culture conditions [6–10]. These facts inspire researchers to develop suitable strategies to stimulate these gene clusters described as 'silent', 'orphan', and 'cryptic' that could, therefore, provide access to an enormous reservoir of structurally novel secondary metabolites to enhance the potential pharmaceutical usage. Several approaches have been successfully used to elicit untapped metabolite profiles, such as OSMAC (One Strain of Many Compounds), which includes media composition, UV irradiation, shaking, incubation temperature, and epigenetic manipulation; and genome mining strategies, which include transcriptional regulator modulation, promoter engineering, and the heterologous expression [11–15].

The methods that use genetic engineering techniques require a relatively sophisticated knowledge of the biology of the producing or surrogate host organisms [16]. In contrast, epigenetic manipulation has been demonstrated to be an effective method for enhancing secondary metabolite expression without altering genes or causing the hereditable manipulation of organisms [17]. There are three main types of small molecule epigenetic regulators known to modulate secondary metabolite expression: DNA methyltransferase (DNMT) inhibitors, 5-azacytidine (5-aza) and *N*-phthalyl-L-tryptophan (RG108); histone deacetylase (HDAC) inhibitors, suberoylanilide hydroxamic acid (SAHA), suberoylbis hydroxamic acid (SBHA), nicotinamide, sodium butyrate, valproic acid, and octanoylhydroxamic acid, and histone acetyltransferase (HAT) inhibitor, and anacardic acid. These inhibitors have been added alone [18–23] or in combination [24–26] to culture media, successfully inducing or changing the metabolic pathways to enhance the production and/or accumulation of different compounds that are not detected in axenic cultures. For example, the production of cytosporones active against malaria and methicillin-resistant *Staphylococcus aureus* was enhanced, and a previously undescribed cytosporone R was isolated when the histone deacetylase inhibitor (HDAC) sodium butyrate and the DNA methyltransferase (DNMT) inhibitor 5-azacytidine (5-aza) were employed to activate the genes of the marine fungus *Leucostoma persoonii*, an endophyte of mangroves [27]. Baker's group screened the potential of mangrove-derived endophytic fungi as a source of new antibiotics when cultured in the presence and absence of small molecule epigenetic modulators. Of 1608 extracts from 530 fungal isolates, nearly half (44%) of those fungi producing active extracts only did so following sodium butyrate and 5-aza treatment [28]. These cases might validate that chemical epigenetic manipulation is feasible to efficiently uncover cryptic secondary metabolites from mangrove endophytic fungi. However, the successful examples of epigenetic manipulation applied to mangrove endophytic fungi are limited to confirm the conclusion.

The coelomycetous genus *Phomopsis* belongs to the family Diaporthaceae and consists of approximately 900 fungal species from a wide range of hosts [29]. The different species belonging to the genus *Phomopsis* are especially known for producing a wide variety of compounds with pharmacological properties, notably cytotoxic [30–32], antimicrobial [33–35], *β*-site amyloid precursor protein cleaving enzyme 1 (BACE1) inhibitory [36], anti-Tobacco mosaic virus (TMV) [37] and immunosuppressive activities [38]. As part of our research on discovering structurally novel and biologically active natural products from mangrove-derived endophytic fungal strains [39–48], a strain of *Phomopsis asparagi* DHS-48 isolated from the fresh root of *Rhizophora mangle* attracted our attention for the characterization of a series of immunosuppressive chromones [46] and cytochalasins [38]. In the present study, in order to tap the metabolic potential of this titled fungal strain, epigenetic manipulation was applied to activate its cryptic secondary biosynthetic pathways. The colony growth, dry biomass, ^{1}H NMR, and HPLC chromatogram were detected under the cultivation with small molecule epigenetic modifiers, the DNMT inhibitor 5-aza, the HDAC inhibitor sodium butyrate, and a combination of these inhibitors at various concentrations. A follow-up fermentation of an optional modifier (50 μM sodium butyrate) led to the isolation of two new compounds, phaseolorin J (**1**) and phomoparagin D (**5**), along with nine known phaseolorin D (**2**) [49], chaetochromone B (**3**) [50], pleosporalin D (**4**) [51], cytochalasins J, J1, J2, J3, H (**6–10**) [31] and phomopchalasin D (**11**) [38]. Herein, we report the epigenetic manipulation of this fungus, and the isolation, structural determination, and bioactivity evaluation of the induced products (Figure 1). A hypothetical biosynthetic pathway for the isolated metabolites is also discussed.
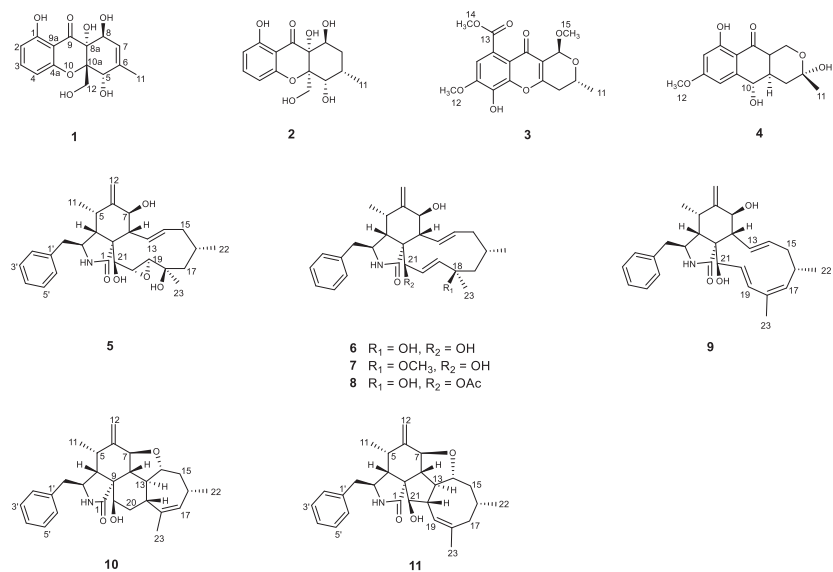
Figure 1. Structures of the isolated compounds **1–11**.

2. Results

2.1. Epigenetic Manipulation

The epigenetic manipulation of *Phomopsis asparagi* DHS-48 was conducted in both liquid medium and solid medium by using the DNMT inhibitor 5-aza, the HDAC inhibitor sodium butyrate, and the combination of these inhibitors at different concentrations (0, 10, 50, 100 μM). Cultivation without these epigenetic modifiers was used as a control. By comparing the colony growth on PDA (Figure 2a) and dry biomass (calibration graph Figure 2b) in PDA (Figure 2c) and PDB (Figure 2d), we found that the DNMT and HDAC inhibitors produced inconsistent results, and 50 μM sodium butyrate solid fermentation was preferable to induce more remarkable chemical diversity of the secondary metabolites. The HPLC analyses of the EtOAc extracts of *Phomopsis asparagi* DHS-48 cultivated in the presence of different epigenetic agents in all the cases further confirmed our deduction (Figure S44). Consequently, a scaled-up fermentation with 50 μM sodium butyrate was carried out.
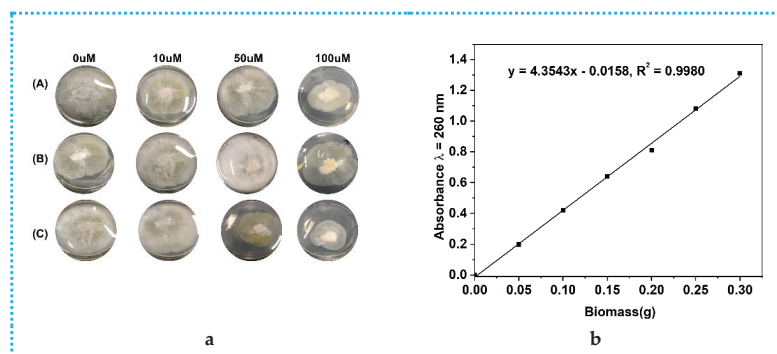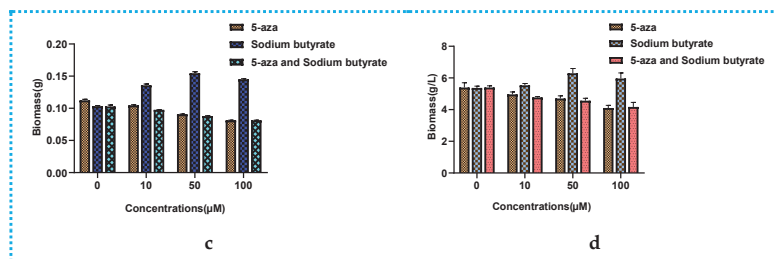

Figure 2. *Cont.*

Figure 2. Comparison of colony growth, dry biomass (in PDA and PDB) of *Phomopsis asparagi* DHS-48 in the presence of different concentrations (0, 10, 50, 100 μM) of 5-aza, sodium butyrate, and the combination of these inhibitors**:** (**a**) colony growth. In (A), 5-aza was added; in (B), sodium butyrate was added; in (C), the combination of these inhibitors was added; (**b**) calibration graph for calculating dry biomass based on nucleic acid contents with different epigenetic doses in PDA; (**c**) the dry biomass of fungi cultivated in PDA with different epigenetic doses; (**d**) the dry biomass of fungi cultivated in PDB with different epigenetic doses.

The EtOAc extracts of the mycelia and solid rice medium incubated with 50 μM sodium butyrate were subjected to HPLC analyses. By comparing with the blank control (Figures 3 and S45), the production levels of the known metabolites **6–8**, **10**, and **11** were considerably enhanced in the sodium-butyrate-inhibited fermentation at the same injection concentration. In addition, certain peaks of **1–5** and **9** appear to be present in the chromatograms from the 50 μM HDAC inhibitor that are absent in the control group. Continuously, these differences were also supported by the fact that the ^{1}H NMR metabolic profile (Figure 4) of EtOAc extracts showed several additional significant hydrogen resonances between 5.5 and 8.0 ppm, compared with the control group.
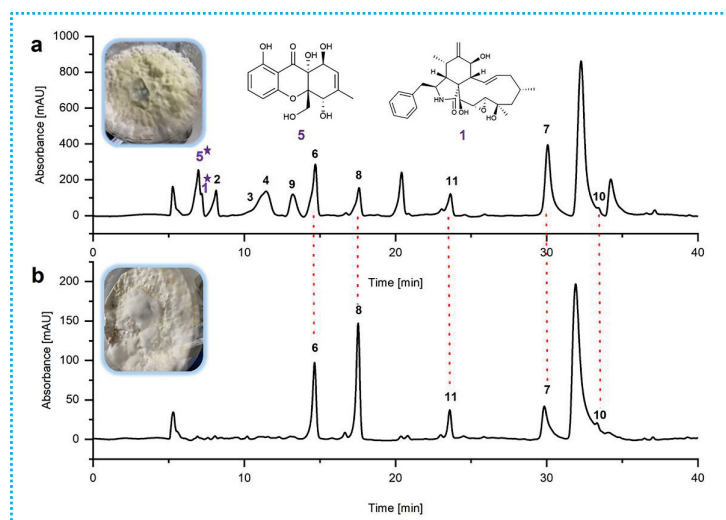

Figure 3. HPLC profiles of fungal EtOAc extracts (**a**) obtained from rice solid-substrate medium after 50 μM sodium butyrate treatment and (**b**) obtained from rice solid-substrate medium without epigenetic inhibitor treatment. HPLC chromatograms: C18 column (Agilent Technologies 10 mm × 250 mm). Solvents: A, H_2O; B, MeOH. Linear gradient: 0 min, 60% B; 40 min, 100% B. Temperature 25 °C. Flow rate 2 mL/min. UV detection at λ = 210 nm. Peaks **1–11** represent the isolated metabolites. ★ Compounds **1** and **5** in (**a**) represent the new compounds stimulated by epigenetic manipulation.
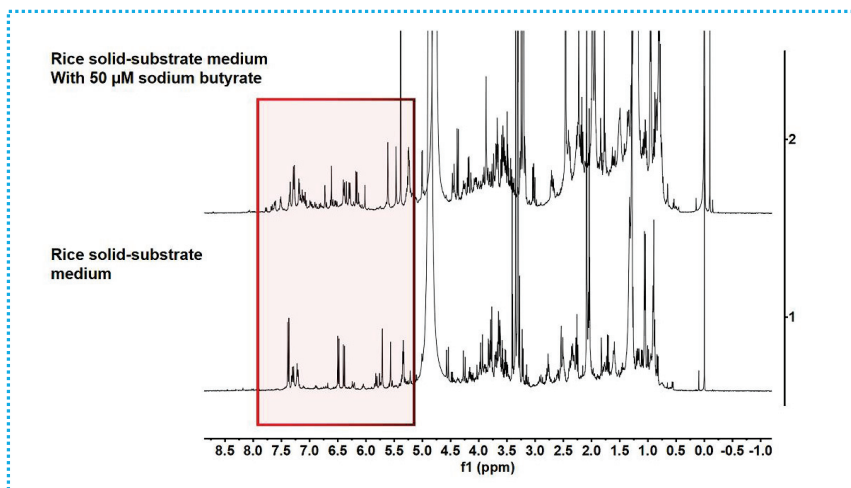
Figure 4. ^{1}H NMR spectra of EtOAc extracts of *Phomopsis asparagi* DHS-48 measured in CD$_3$OD at 400 MHz, chemical shifts (δ) presented in ppm.

2.2. Structure Elucidation of the New Compounds

Phaseolorin J (**1**) was isolated as a light yellow amorphous powder. Its molecular formula was determined as C$_{15}$H$_{16}$O$_7$ on the basis of HRESIMS data (*m/z* 331.0781 [M + Na] $^+$, calcd for C$_{15}$H$_{16}$O$_7$ Na 331.0788), which clearly indicated the presence of eight indices of unsaturation. The ^{1}H and ^{13}C NMR data of **1** (Table 1) and its ^{1}H-^{1}H COSY and HSQC spectra showed the presence of a series of characteristic signals for a 1,2,3-trisubstituted benzene ring (δ_H 6.43 (d, *J* = 8.2 Hz), δ_C 109.3, d, CH-2; δ_H 7.38 (t, *J* = 8.2 Hz), δ_C 138.9, d, CH-3; δ_H 6.52 (d, *J* = 8.2 Hz), δ_C 108.7, d, CH-4), one olefinic methine of a trisubstituted double bond (δ_H 5.61 (dq, *J* = 4.8, 1.7 Hz); δ_C 122.3, d, CH-7), a tertiary methyl (δ_H 1.86, 3H, d, 1.7; δ_C 19.2, q, CH$_3$-11), an oxygenated methylene (δ_H 4.12, (d, *J* = 13.2 Hz), δ_H 4.03 (d, *J* = 13.2 Hz); δ_C 64.1, t, CH$_2$-12), and two oxygenated methines (δ_H 4.69, 1H, br s, δ_C 74.5, d, CH-5; 4.55, 1H, d, *J* = 4.8 Hz, δ_C 67.9, d, CH-8). The magnitude of the ^{1}H-^{1}H COSY spectrum led to the observation of long-range correlations, including the assignments of vicinal coupling with H-5 and proton H-7 on the *cis*-substituted double bond, as well as homoallylic couplings with H-8 and CH$_3$-11. A comparison of the ^{1}H and ^{13}C NMR data of **1** with those of phaseolorin D (**2**) [52] revealed that both had the same chromone core, except for the presence of one trisubstituted double bond at C-6 (δ 140.5) and C-7 (δ 122.3) instead of sp^3 methine (C-6) and sp^3 methylene (C-7) in **2**. Confirming evidence was obtained from the ^{1}H-^{1}H COSY correlation from olefinic proton (δ_H 5.61, H-7) to the oxygenated methine (δ_H 4.69, H-8) and HMBC correlations from H$_3$-11 to C-5, C-6 and C-7 (Figure 5).
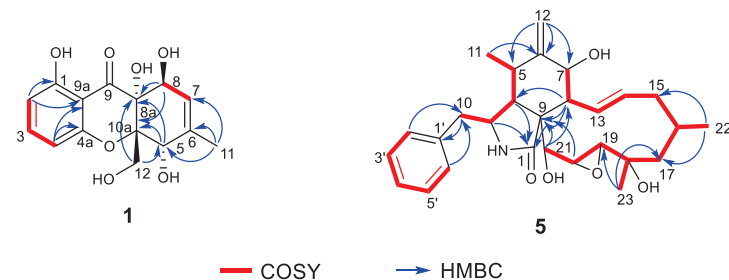

Figure 5. Key COSY and HMBC correlations of Compounds **1** and **5**.

Table 1. ^{1}H (400 MHz) and ^{13}C (100 MHz) NMR data of 1 and 2 in CD$_3$OD.

Position	1		2	
	δ_C Type	δ_H (*J* in Hz)	δ_C Type	δ_H (*J* in Hz)
1	163.2, C		163.4, C	
2	109.3, CH	6.43, d, 8.2	109.7, CH	6.44, d, 8.2
3	138.9, CH	7.38, t, 8.2	139.0, CH	7.39, t, 8.2
4	108.7, CH	6.52, d, 8.2	109.5, CH	6.55, d, 8.2
4a	160.8, C		160.3, C	
5	74.3, CH	4.69, brs	74.6, CH	4.29, m
6	140.5, C		29.2, CH	2.34, m
7	122.3, CH	5.61, dq, 4.8,1.7	32.0, CH$_2$	1.57, dt, 14.8, 2.8 2.43, m
8	67.9, CH	4.55, d, 4.8	68.6, CH	4.44, t, 3.6
8a	74.5, C		85.4, C	
9	197.2, C		196.2, C	
9a	108.4, C		108.6, C	
10a	86.5, C		76.4, C	
11	19.2, CH$_3$	1.86, d, 1.7	18.1, CH$_3$	1.32, d, 7.8
12	64.1, CH$_2$	H$_a$ 4.12, d, 13.2 H$_b$ 4.03, d, 13.2	60.5, CH$_2$	H$_a$ 3.83, d, 13.5 H$_b$ 4.28, m

In the NOESY experiment of **1** (Figure 6), the correlations of H$_2$-12/H-5 indicated the same spatial orientation. Biogenetically, the configuration of **1** was deduced to be the same as that of **2**, and the calculated ECD spectrum method can be used to predict the absolute configuration of C-8a and C-10a, respectively (Figure 7). Consequently, the absolute configuration of C-5 was assigned to be *S*. However, neither the lack of NOE between H-5/H-8 nor the adjacent coupling constant of *J*$_{7,8eq}$ = 4.8 Hz between H-7 and H-8 supported the relative configuration between H-5 and H-8. To solve this problem, the δ_C values of two plausible epimers, namely 5*S*,5a*S*,8*S*,8a*R*-**1** and 5*S*,5a*S*,8*R*,8a*R*-**1** (8-*epi*-**1**), were performed after the optimization of the selected conformers at the B3LYP/6-31G(d) level. The results showed that the calculated ^{13}C NMR spectrum of the truncated model 5*S*,5a*S*,8*S*,8a*R* -**1** perfectly matched with the experimental one (Figure 8). Therefore, the configuration of **1** was conclusively assigned and given the tentative name phaseolorin J.
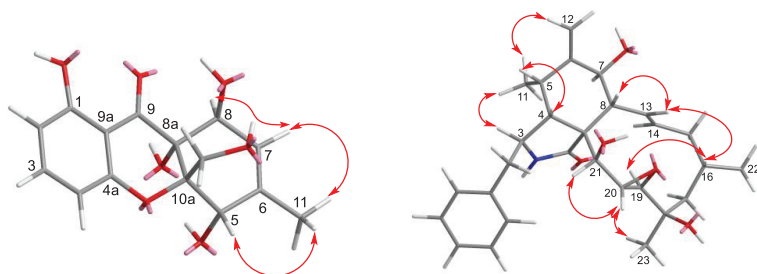
Figure 6. Key NOESY correlations of compounds **1** and **5**.
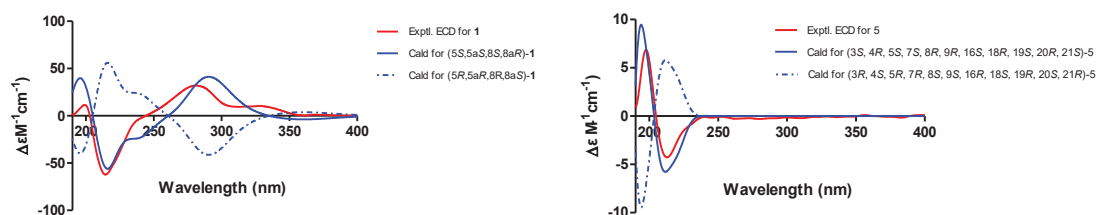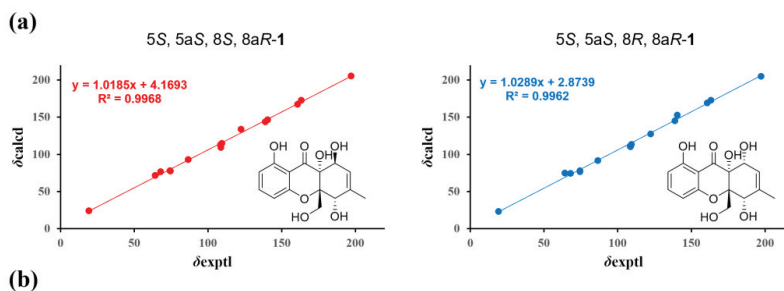
Figure 7. Experimental and calculated electronic circular dichroism (ECD) spectra of **1** and **5**.

(a)

(b)

DP4+ probability of ^{13}C NMR of **1**		
Plausible isomer	5*S*, 5a*S*, 8*S*, 8a*R*-**1**	5*S*, 5a*S*, 8*R*, 8a*R*-**1**
DP4+	99.23%	0.77%

Figure 8. ^{13}C NMR calculation results of two plausible epimers (**1** and 8-*epi*-**1**) at the B3LYP/6-31G(d) level: (**a**) linear correlation plots of calculated and experimental 13C values; (**b**) DP4+ probability of ^{13}C values of **1**.

Phomoparagin D (**5**) was obtained as a colorless amorphous powder. The molecular formula of **5** was established as $C_{28}H_{37}NO_5$ from its HRESIMS (*m/z* 506.2304 [M + K] $^+$, calcd for $C_{28}H_{37}NO_5K$ 506.2303. The ^{1}H NMR spectrum (Table 2) showed proton signals for a mono substituted phenyl at δ_H (7.22−7.31, 5H), a tertiary methyl at δ_H (0.92, 3H, s, H$_3$-23), two secondary methyl groups at δ_H (0.80, 3H, d, *J* = 6.7 Hz, H$_3$-11; 1.02, 3H, d, *J* = 6.8 Hz, H$_3$-22), an exocyclic methylene group at δ_H (5.22 and 5.01, 2H, both s, H$_2$-12), four oxygenated methine groups at δ_H (3.82, 1H, d, *J* = 10.8 Hz, H-7; 3.21, 1H, d, *J* = 2.4 Hz, H-19; 2.99, 1H, m, H-20; 3.43, 1H, s, H-21), and two olefinic methine groups at δ_H (5.72, 1H, d, *J* = 15.5 Hz, 9.5 Hz, H-13; 5.54, 1H, m, H-14). The ^{13}C NMR and DEPT spectra (Table 1) of compound **5** displayed 28 carbons, including 3 sp^3 methyls, 3 sp^3 methylenes, 9 sp^3 methines, 2 sp^3 quaternary carbons, 1 sp^2 exocyclic methylene, 7 sp^2 olefinic methines, and 3 sp^2 quaternary carbons (2 olefinic carbon and 1 amide carbonyl). The carbon profile and characteristic ^{1}H NMR signals, as well as the 2D NMR spectra of **5** revealed that it has a similar indole-based cytochalasin skeleton as that of cytochalasin J (**6**), which was first reported in 1981 as deacetylcytochalasin H from the same *Phomopsis* sp. [53]. The main difference between the two compounds is the lack of the typical C$_{19}$-C$_{20}$ double bond (δ_H 5.76, δ_C 129.3, d, CH-19; δ_H 5.85, δ_C 137.2, d, CH-20) in the macrocycle ring of the latter that was replaced by a 19, 20-epoxide ring (δ_H 3.21 (d, *J* =2.4 Hz), δ_C 63.1, CH-19; δ_H 2.99, m, δ_C 57.7, CH-20) in **5**. The existence of the epoxide ring was deduced by the analysis of its HRESIMS data, and the molecular weight of **5** was 16 mass units larger than that of **6**. This finding was supported by the ^{1}H-^{1}H COSY correlations of H-7/H-8/H-13/ H-14/ H-15/ H-16/ H-17/ H-18/ H-19/H-20/H-21, along with the HMBC correlations from H$_3$-23 (δ_H 0.92, 3H, s) to C-17, C-18 and C-19, and H-21 (δ_H 3.43, 1H, s) to C-8, C-9, C-19

and C-20 (Figure 5). The diagnostic ROESY correlations (Figure 6) positioned H-3, H$_3$-11, H-7, H$_3$-22, H$_3$-23, H-20, and H-21 on the α-face and H-4, H-5, H-8, H-14, H-16, and H-19 on the β-face of **5**, whereas the absolute configuration was assigned by a comparison of the experimental and simulated electronic circular dichroism (ECD) spectra generated by the time-dependent density functional theory (TDDFT) calculations at the B3LYP/6-31+G(d,p) level using the Gaussian 09 program. The experimental ECD spectrum (CH$_3$OH) for 3*S*, 4*R*, 5*S*, 7*S*, 8*R*, 9*R*, 16*R*, 16*R*, 19*R*, 20*S*, and 21*R* -**5** matched well with the calculated spectrum (Figure 7), which confirmed the unambiguous assignment of the absolute configuration of **5**, and the trivial name phomoparagin D was assigned. The possible biogenetic pathway of phomoparagin D (**5**) was postulated (Scheme 1), which might arise from cytochalasin J (**6**) by a different set of catalyzed reactions.

**Table 2.** ^{1}H (400 MHz) and ^{13}C (100 MHz) NMR data of **5** and **6** in CD$_3$OD.

Position	5		6	
	δ$_C$ Type	δ$_H$ (*J* in Hz)	δ$_C$ Type	δ$_H$ (*J* in Hz)
1	178.4, C		178.7, C	
3	55.3, CH	3.37, dd, 6.1, 3.5	55.1, CH	3.31, m
4	51.9, CH	2.46, dd, 5.1, 3.5	50.8, CH	2.61, m
5	33.8, CH	2.75, m	34.0, CH	2.92, m
6	151.7, C		151.9, C	
7	72.7, CH	3.82, d, 10.8	72.5, CH	3.83, d, 10.7
8	45.8, CH	2.89, d, 10.1	50.2, CH	2.88, m
9	56.1, C		54.9, C	
10	44.8, CH$_2$	H$_a$ 2.86, dd, 10.3, 6.2H$_b$ 2.77, m	46.6, CH$_2$	H$_a$ 2.92, mH$_b$ 2.59, dd, 13.6, 8.2
11	13.8, CH$_3$	0.80, d, 6.7	14, CH$_3$	1.11, d, 6.7
12	113.1, CH$_2$	H$_a$ 5.22, s H$_b$ 5.01, s	113.1, CH$_2$	H$_a$ 5.34, s H$_b$ 5.12, s
13	131.2, CH	5.72, dd, 15.5, 9.5	129.4, CH	5.73, dd, 15.5, 9.8
14	135.4, CH	5.54, m	138.7, CH	5.33, m
15	43.7, CH$_2$	H$_a$ 2.05, dd, 12.4, 5.6H$_b$ 1.65, d, 12.4	45, CH$_2$	H$_a$ 2.02, mH$_b$ 1.81, m
16	28.7, CH	1.87, m	29.4, CH	1.80, m
17	48.7, CH$_2$	H$_a$ 1.75, dd, 14.8, 3.2H$_b$ 1.45, dd, 14.8, 3.8	55, CH$_2$	H$_a$ 1.90, dd, 14.4, 3.4H$_b$ 1.57, dd, 14.4, 3.3
18	73.6, C		75.1, C	
19	63.1, CH	3.21, d, 2.4	137.5, CH	5.75, dd, 16.8, 2.2
20	57.7, CH	2.99, m	132.2, CH	6.03, dd, 16.8, 2.6
22	26.2, CH$_3$	1.02, d, 6.8	26.7, CH$_3$	1.04, d, 6.6
23	23.5, CH$_3$	0.92, s	31.8, CH$_3$	1.36, s
1′	138.5, C		137.5, C	
2′/6′	131.2, CH	7.22, d, 7.2	131.1, CH	7.15, dd, 8.0, 1.3
3′/5′	129.6, CH	7.31, t, 7.2	129.5, CH	7.32, dd, 8.0, 7.1
4′	128.0, CH	7.25, dt, 7.2, 3.6	127.8, CH	7.24, dd, 7.1, 1.3

A plausible biosynthesis of compounds **1**–**11** was proposed, as shown in Schemes 1 and 2. More than 4000 chromones have been isolated and structurally elucidated from natural origin until now, and they are biosynthesized by the type III polyketide synthases (PKSs) [54]. Compounds **1** and **2** isolated from *P. asparagi* DHS-48 are assumed to be derived from one acetyl-CoA starter and seven molecules of malonyl-CoA extender units to form an octaketide that undergoes Claisen condensation and cyclization to yield anthraquinone precursors such as emodin, even though it was not isolated in this study. Oxidative cleavage, cyclization via epoxidation, and nucleophilic attack by a hydroxyl group to give the ring-closed dihydroxanthone involved the epimerization of C-10a. The subsequent keto–enol equilibrium and redox would provide compounds **1** and **2**, referring to the reports made

by Rönsberg et al. [55]. Previous feeding experiments with sodium ^{13}C-labeled acetate by Lösgen et al. [56] in 2007 revealed that a heptaketide precursor is involved in the biosynthesis of **3** and **4**, which are analogues to phomochromenones D-G isolated in our previous study [46], implying some cryptic post-synthesis modification genes were stimulated by the currently adopted epigenetic manipulation for the production of those metabolites previously unobserved or merely increased sufficiently under epigenetic control to be detected. Cytochalasins **5–11** might rationally share a common biosynthetic precursor as we previously described via polyketide synthase (PKS)/nonribosomal peptide synthetase (NRPS) hybrid machinery [38]. The stimulated metabolite **5** was is likely to be also derived from **6** by epoxidation, meanwhile **9** feasibly converted through catalytic dehydration.
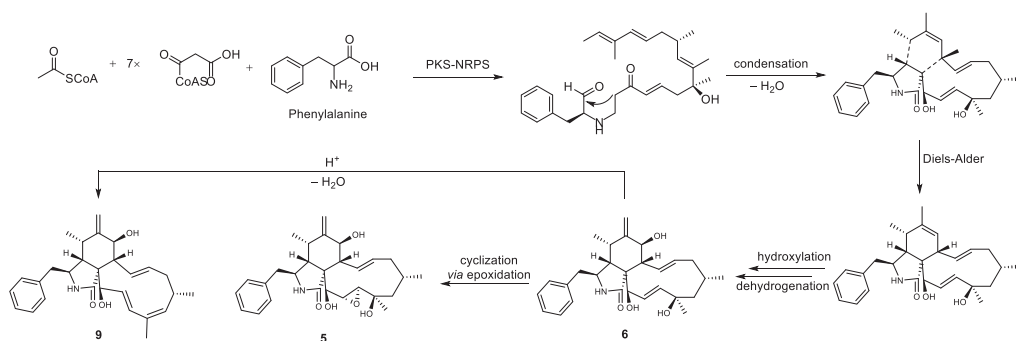
Scheme 1. Proposed biosynthetic pathway for compounds **5** and **9** from **6**.
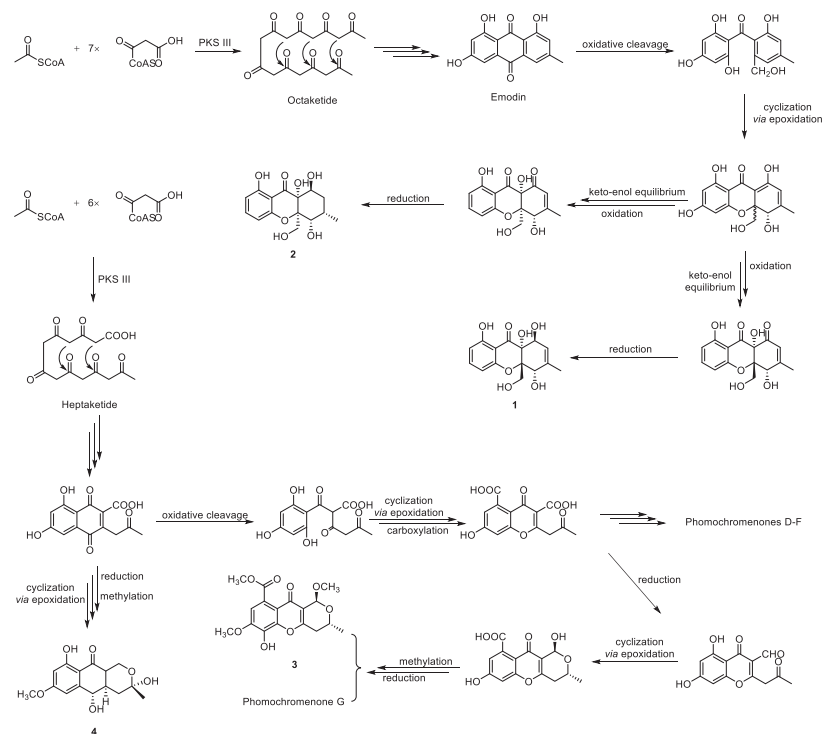
Scheme 2. Proposed biosynthetic pathway for compounds **1–4**.

2.3. Biological Activity of Compounds

The immunosuppressive assay showed that compounds **1** and **8** exhibited moderate-to-weak inhibitory activity against ConA-induced T and LPS-induced B murine splenic lymphocytes in vitro, with the IC_{50} values of 42 and 88 μM and 15 and 110 μM (Table 3), respectively, whereas the other investigated compounds showed no apparent inhibitory effect. Additionally, compound **5** showed significant in vitro cytotoxicity against human cancer cell lines Hela, with an IC_{50} value of 5.8 μM, and showed moderately significant in vitro cytotoxicity against human cancer cell lines HepG2, with an IC_{50} value of 59 μM (Table 4), respectively, which was comparable with the positive controls adriamycin and fluorouracil. These results suggested that the 19,20-epoxide ring in compound 5 is essential for its inhibition of tumor cell proliferation compared with compounds **6–11**.

Table 3. Immunosuppressive activities of tested compounds.

Compound	IC_{50} (μM) [a]	
	ConA-Induced T-Cell Proliferation	**LPS-Induced B-Cell Proliferation**
1	42.35 ± 2.49	88.19 ± 2.59
8	14.71 ± 0.47	109.95 ± 5.68
2–7, 9–11	-	-
cyclosporin A [b]	4.39 ± 0.02	25.11 ± 0.43

[a] Data are presented as mean ± SD from three separate experiments. [b] Positive control. '-' stands for no inhibitory effect at 200 μM.

Table 4. Antitumor activity test of tested compounds.

Compound	IC_{50} (μM) [a]	
	HepG2	**Hela**
5	59.14 ± 15.79	5.82 ± 0.82
1–4, 6–11	-	-
Adriamycin [b]	-	0.95 ± 0.61
Fluorouracil [c]	176 ± 28.8	-

[a] Data are presented as mean ± SD from three separate experiments. [b] Hela cell positive control. [c] Hepg2 cell positive control. '-' stands for no inhibitory effect at 200 μM.

3. Materials and Methods

3.1. General Procedures

The specific rotations were obtained on an ATR-W2 HHW5 digital Abbe refractometer (Shanghai Physico-optical Instrument Factory, Shanghai, China). The UV spectra were determined using a Shimadzu UV-2600 PC spectrophotometer (Shimadzu Corporation, Tokyo, Japan), while the ECD spectra were measured on a JASCO J-715 spectra polarimeter (Japan Spectroscopic, Tokyo, Japan). The 1H, 13C, and 2D NMR spectra were recorded on a Bruker AV 400 NMR spectrometer using TMS as an internal standard. High-resolution ESI-MS was performed on an LCMS-IT-TOF instrument (Shimadzu Corporation, Tokyo, Japan) using peak matching. TLC and column chromatography (CC) were carried out over silica gel (200–400 mesh, Qingdao Marine Chemical Inc., Qingdao, China) or Sephadex-LH-20 (18−110 μm, Merck, Darmstadt, Germany), respectively. HPLC analysis was measured on Wasters e2695 (Waters Corporation, Milford, MA, USA) using a C18 column (Waters, 5 μm, 10 × 150 mm). Semi-preparative HPLC was achieved on an Agilent Technologies 1200LC instrument with a C18 column (Agilent Technologies 10 mm × 250 mm). High-speed centrifugation was performed using a TGL-16B Anting centrifuge (Anting Scientific instrument Factory, Shanghai, China). The constant temperature water bath was in HH-2 thermostat water baths (Hervey Biotechnology Corporation, Jinan, China). Liquid fermentation was carried out in an ATL-03202 High-precision CNC shaking machine (Shanghai Kanxin Instrument and Equipment Corporation, Shanghai, China). The purity of the isolated

compounds was determined via high-performance liquid chromatography (HPLC), which was performed on an Agilent 1200 instrument and a reverse-phase column (4.6 × 150 mm, 5 μm). The UV wavelength for detection was 210 nm. All the crude extracts and compounds were eluted with a flow rate of 0.8 mL·min^{-1} over a 50 min gradient (solvents: A, H$_2$O; B, MeOH), as follows: 0–5min, 25% B; 5–15 min, 25–30% B; 15–30 min, 30–55% B; 30–40 min, 55–75% B; 40–50 min, 70–90% B (Figure S45).

3.2. Fungal Material

The endophytic fungi *Phomopsis asparagi* DHS-48 was isolated with a PDA medium from the fresh root of the mangrove plant Rhizophora mangle, collected in October 2015 in Dong Zhai Gang-Mangrove Garden on Hainan Island, China. The strain was isolated under sterile conditions from the inner tissue of the root, following an isolation protocol described previously [57], and the fungi (strain no.DHS-8) was identified using a molecular biological protocol via the DNA amplification and sequencing of the ITS region (GenBank Accession no.MT126606). A voucher strain was deposited at one of the authors' laboratories (J.X.).

3.3. Epigenetic Manipulation and Culture Condition

For the epigenetic manipulation experiments, fungal mycelia and spores were initially inoculated onto Petri dishes containing potato dextrose agar (PDA) at 28 °C for 5 days. Then, a single colony was inoculated into a 100 mL potato dextrose broth (PDB) (in 500 mL Erlenmeyer flasks with continuous shaking for ten days at 28 °C) and the PDA plates (15 mL agar media inverted incubated for five days at 28 °C) were treated with different concentrations (0, 10, 50, and 100 μM) of the DNMT inhibitor 5-aza and the HDAC inhibitor sodium butyrate, or a combination of the two, while the control cultures were treated with vehicle only (filter-sterilized H$_2$O). The quantity of biomass is an essential parameter in the determination of a suitable epigenetic modifier or its optimal addition. After filtering the PDB liquid medium, the mycelium precipitate was washed three times with distilled water and lyophilized to constant weight as dry biomass. For the fungi that grow on PDA, the direct measurement of fungal biomass is hampered because the fungi penetrate into and bind themselves tightly to the solid-substrate particles. The indirect method based on the nucleic acid contents was adopted according to Liu's method [58], with some modifications. The pure mycelium of 0.05, 0.1, 0.15, 0.2, 0.25, and 0.3 g was extracted by adding 25 mL of 5% trichloroacetic acid solution in a water bath at 80 °C for 25 min with constant stirring and then cooled in an ice bath at 8000 r/min, centrifuged at 4 °C for 15 min, and diluted 5 times. The OD value was measured at 260 nm with 1% trichloroacetic acid as the blank control. Finally, dry biomass was quantified based on a standard curve between the nucleic acid content and dry biomass ranging from 0.05 to 0.3 g with y = 4.3543x − 0.0158 (R^2 = 0.998). All the culture groups were prepared and measured in 3 replicates. The HPLC profiles of the EtOAc extracts of the fungi cultivated in the presence of different epigenetic agents were tested. The cultures were extracted three times with EtOAc (50 mL × 3 for each PDA plate, 250 mL × 3 for each PDB flask). The EtOAc-soluble materials were passed over organic membranes and then subjected to HPLC analysis under conditions mentioned in Section 3.1.

3.4. Extraction Isolation

The fungus was cultivated on PDA by adding 50 μM sodium butyrate at 28 °C for 7 days. Then, a single colony was inoculated in an autoclaved rice solid-substrate medium in Erlenmeyer flasks (130 × 1 L), each containing 100 g of rice, 100 mL of 0.3% of saline water, and 50 μM sodium butyrate and fermented at 28 °C for 28 days. Briefly, 130 flasks of cultures were extracted 3 times with 400 mL of EtOAc, and the filtrate was evaporated under reduced pressure to yield a crude extract of 20 g. The crude extracts were analyzed using HPLC and ^{1}H NMR. The EtOAc extracts were chromatographed on silica gel column chromatography (CC) using a step gradient elution process with CH$_2$Cl$_2$-MeOH (0–100%) to provide nine fractions (Fr. 1–Fr. 9). Fr. 3 was subjected to open silica gel CC using

gradient elution with CH_2Cl_2-EtOAc (6:1–1:2, v/v) to yield seven fractions. Fr. 3.1–Fr. 3.7. Fr. 3.4 were purified with semi-preparative reversed-phase HPLC using MeOH-H_2O (70:30, v/v) to afford compound **10** (6 mg) (Figures S38–S40) and compound **7** (6 mg) (Figures S29–S31). In addition, Fr. 3.5 was separated via silica gel CC using CH_2Cl_2-EtOAc (3:1, v/v) and purified via semi-preparative reversed-phase HPLC using MeOH-H_2O (70:30, v/v) to afford compound **11** (7 mg) (Figures S41–S43). Fr. 4 was separated via open silica gel CC using gradient elution with CH_2Cl_2-EtOAc (3:1–1:1, v/v) to obtain three fractions (Fr. 4.1–Fr. 4.3). Fr. 4.2 was chromatographed on a Sephadex LH-20 CC by eluting with MeOH to yield three fractions (Fr. 4.2.1–Fr. 4.2.3). Fr. 4.2.1 was purified using a silica gel flash column with CH_2Cl_2-EtOAc (2:1, v/v) as the eluent to obtain compound **8** (11.8 mg) (Figures S32–S34) and compound **9** (3 mg) (Figures S35–S37). Fr. 4.2.2 was subjected to Sephadex LH-20 CC using MeOH-CH_2Cl_2 (1:1, v/v) as an eluent to obtain compound **6** (5.9 mg) (Figures S26–S28). Fr. 5 was subjected to open silica gel CC using gradient elution with CH_2Cl_2-EtOAc (4:1–1:2, v/v) to yield five fractions Fr. 5.1–Fr. 5.5. Fr. 5.3 was subsequently subjected to Sephadex LH-20 CC using MeOH-CH_2Cl_2 (1:1, v/v) as an eluent to give six fractions Fr. 5.3.1–Fr. 5.3.6. Fr. 6 was separated through silica gel elution using CH_2Cl_2-EtOAc (2:1, v/v) to obtain six fractions (Fr. 6.1–Fr. 6.6). Fr. 6.3 was purified with Sephadex LH-20 CC using MeOH-CH_2Cl_2 (1:1, v/v) to yield compound **4** (12 mg) (Figures S23–S25). Fr. 6.4 was subjected to reversed-phase HPLC (MeOH-H_2O 70:30, v/v) to obtain compound **3** (5 mg) (Figures S20–S22). Fr. 6.5 was subjected to open silica gel CC using gradient elution with CH_2Cl_2-EtOAc (4:1–1:2, v/v) to give five fractions (Fr. 6.5.1–Fr. 6.5.5). Additionally, promising Fr. 6.5.4 was purified with reversed-phase HPLC (MeOH-H_2O, 70:30 to 100:0, v/v) to furnish compound **2** (7 mg) (Figures S17–S19) and compound **1** (6 mg) (Figures S1–S8). Fr.7 was subjected to open silica gel CC using gradient elution with CH_2Cl_2-EtOAc (1:1, v/v) to yield six fractions Fr. 7.1–Fr. 7.6. Fr. 7.3 was subjected to Sephadex LH-20 CC using MeOH-CH_2Cl_2 (1:1, v/v) as an eluent to obtain compound **5** (15 mg) (Figures S9–S16).

Phaseolorin J (**1**): light yellow amorphous powder (MeOH); $[\alpha]^{20}_D$ +160 (c 0.0001, MeOH); UV (MeOH) λ_{max} 214 nm (the absorptions due to aromatic rings); ^1H and ^{13}C NMR data, see Table 1; HRESIMS m/z 331.0781 [M + Na]$^+$ (calcd for $C_{15}H_{16}O_7Na$ 331.0788).

Phomoparagin D (**5**): colorless amorphous powder (MeOH); $[\alpha]^{20}_D$ +60 (c 0.0001, MeOH); UV (MeOH) λ_{max} 206 nm (the absorptions due to aromatic rings); ^1H and ^{13}C NMR data, see Table 1; HRESIMS m/z 506.2304 [M + K]$^+$ (calcd for $C_{28}H_{37}NO_5K$ 506.2303).

3.5. Theory and Calculation Details

Specific Monte Carlo conformational searches were run by employing Spartan's 14 software using the Merck molecular force field (MMFF). Conformers with a Boltzmann population of over 0.4% were chosen for ECD (Tables S1–S4) and ^{13}CNMR (Tables S5–S9) calculations. Then, the conformers were initially optimized at the B3LYP/6-31G(d) level in the gas phase using the PCM polarizable conductor calculation model. The stable conformations obtained at the B3LYP/6-31G(d) level were further used in magnetic shielding constants. The theoretical calculation of ECD was conducted in MeOH using the time-dependent density functional theory (TD-DFT) at the B3LYP/6-31+g (d, p) level for all the conformers of compounds **1** and **5**. The ECD spectra were generated using the program SpecDis 1.6 (University of Würzburg, Würzburg, Germany) and GraphPad Prism 5 (University of California, San Diego, USA) from dipole-length rotational strengths by applying Gaussian band shapes with sigma = 0.3 eV.

3.6. Cytotoxicity Assay

HepG2 (liver cancer cell line) and Hela (cervical cancer cell line) were purchased from the Type Culture Collection of the Chinese Academy of Sciences, Shanghai, China. The cells were grown in an RPMI-1640 culture medium. Cytotoxicity against HepG2 cells and HeLa cells was evaluated using the 3-(4,5-dimethylthiazol-2-yl)-2,5-diphenyltetrazolium bromide (MTT) (Sigma-Aldrich, Missouri, St. Louis, MO, USA) method, as described previously [45].

In addition, 5-fluorouracil (5-FU) (Beijing Solarbio Science and Technology Co., Ltd., 99.8%) (Beijing, China) and adriamycin (Shanghai Macklin Biochemical Co., Ltd, 99.8%) (Shanghai, China) were used as positive controls, respectively.

3.7. Isolation and Culture of Spleen Lymphocytes

The BALB/c female mice were sacrificed via cervical dislocation, and their spleens were removed aseptically. The splenocytes were washed using RPMI1640 supplemented with penicillin/streptomycin (100 U/mL and 100 μg/mL, respectively) and 10% heat-inactivated FBS, and collected in a centrifuge tube. The erythrocytes were removed for 3 min with an erythrocyte lysis buffer. The cells were plated at a density of 5×10^6 cells/mL or 1×10^7 cells/mL. Cell numbers were performed using a hemocytometer, and cell viability was determined using the trypan-blue dye exclusion technique; cell viability showed more than 95%. The culture media were kept in a humidified atmosphere of 5% CO_2 at 37 °C.

3.8. Cell Activity and Cell Proliferation

In each 96-well cell culture plate, 100 μL of lymphocyte suspension was inoculated with a concentration of $1*10^7$ cells/mL in each well, and the culture was left overnight in a 37 °C, 5% CO_2 incubator to stabilize the cells. Then, the compounds or positive control (CsA) diluted in a complete medium to different concentrations were added to each well, resulting in the final concentrations of 1, 5, 10, 15, 20, 30, and 40 μM, respectively. The final concentrations of the compounds in the anti-proliferation assay were 20 μM, 35 μM, 50 μM, 70 μM, and 100 μM. After 72 or 48 h incubation in the incubator, the effect of the compounds on the survival rate and anti-proliferation of splenocytes was analyzed using the CCK-8 method.

3.9. Statistical Analysis

All the cell data are presented as the mean standard deviation of the means (S.D.), and a one-way analysis of variance (ANOVA) test was used to evaluate the statistical significance of differences between the groups using GraphPad Prism.

4. Conclusions

Collectively, the mangrove endophytic fungus *Phomopsis asparagi* DHS-48 was effectively stimulated using an HDAC inhibitor (sodium butyrate) to produce two new compounds, named phaseolorin J (**1**) and phomoparagin D (**5**), along with nine known chromones (**2**–**4**) and cytochalasins (**6**–**11**). All the isolates were evaluated for their immuno-suppressive and cytotoxic activities. Among them, compounds **1** and **8** showed moderately inhibitory activity against the proliferation of ConA-induced T and LPS-induced B murine spleen lymphocytes, and compound **5** exerted comparative or better in vitro cytotoxicity against the tested human cancer cell lines than the positive control. Thus, this study demonstrates that epigenetic manipulation appears to have a large potential for enhancing the production and/or accumulation of new chemodiversity from mangrove endophytic fungi.

^{1}H-NMR of cytochalasin J (**6**). Figure S27: ^{13}C-NMR of cytochalasin J (**6**). Figure S28: HR-ESI-MS of cytochalasin J (**6**). Figure S29: ^{1}H-NMR of cytochalasin J$_1$ (**7**). Figure S30: ^{13}C-NMR of cytochalasin J$_1$ (**7**). Figure S31: HR-ESI-MS of cytochalasin J$_1$ (**7**). Figure S32: ^{1}H-NMR of cytochalasin H (**8**). Figure S33: ^{13}C-NMR of cytochalasin H (**8**). Figure S34: HR-ESI-MS of cytochalasin H (**8**). Figure S35: ^{1}H-NMR of cytochalasin J$_2$ (**9**). Figure S36: ^{13}C-NMR of cytochalasin J$_2$ (**9**). Figure S37: HR-ESI-MS of cytochalasin J$_2$ (**9**). Figure S38: ^{1}H-NMR of cytochalasin J$_3$ (**10**). Figure S39: ^{13}C-NMR of cytochalasin J$_3$ (**10**). Figure S40: HR-ESI-MS of cytochalasin J$_3$ (**10**). Figure S41: ^{1}H-NMR of phomopchalasin D (**11**). Figure S42: ^{13}C-NMR of phomopchalasin D (**11**). Figure S43: HR-ESI-MS of phomopchalasin D (**11**). Figure S44: Overlay of HPLC profiles of EtOAc extracts of *Phomopsis asparagi* DHS-48 cultivated in PDA treated with different epigenetic agents. Figure S45: HPLC spectrum for the purity of tested compounds. Table S1: Gibbs free energies[a] and equilibrium populations[b] of low-energy conformers of phaseolorin J (**1**). Table S2: Cartesian coordinates for the low-energy reoptimized MMFF conformers of phaseolorin J (**1**) at B3LYP/6-31G(d,p) level of theory in gas. Table S3: Gibbs free energies[a] and equilibrium populations[b] of low-energy conformers of phomoparagin D (**5**). Table S4: Cartesian coordinates for the low-energy reoptimized MMFF conformers of phomoparagin D (**5**) at B3LYP/6-31G(d,p) level of theory in gas. Table S5: The calculated ^{13}C NMR data for isomers of phaseolorin J (**1**). Table S6: DFT-optimized structures and thermodynamic parameters for low-energy conformers of **1**. Table S7: DFT-optimized structures and thermodynamic parameters for low-energy conformers of 8-*epi*-**1**. Table S8: Optimized Z-matrixes of **1** in the gas phase (Å) at B3LYP/6-31G(d) level. Table S9: Optimized Z-matrixes of 8-*epi*-**1** in the gas phase (Å) at B3LYP/6-31G(d) level.

References

1. Xu, J. Bioactive natural products derived from mangrove-associated microbes. *Rsc. Adv.* **2015**, *5*, 841–892. [CrossRef]
2. Xu, J. Biomolecules Produced by Mangrove-Associated Microbes. *Curr. Med. Chem.* **2011**, *18*, 5224–5266. [CrossRef] [PubMed]
3. Bugni, T.S.; Ireland, C.M. Marine-Derived Fungi: A Chemically and Biologically Diverse Group of Microorganisms. *Nat. Prod. Rep.* **2004**, *21*, 143–163. [CrossRef]
4. Xu, J.; Yi, M.; Ding, L.; He, S. A Review of Anti-Inflammatory Compounds from *Marine Fungi*, 2000–2018. *Mar. Drugs* **2019**, *17*, 636. [CrossRef] [PubMed]
5. Wu, M.J.; Xu, B.F.; Guo, Y.W. Unusual Secondary Metabolites from the Mangrove Ecosystems: Structures, Bioactivities, Chemical, and Bio-syntheses. *Mar. Drugs.* **2022**, *20*, 535. [CrossRef] [PubMed]
6. Choque, E.; Klopp, C.; Valiere, S.; Raynal, J.; Mathieu, F. Whole-Genome Sequencing of *Aspergillus tubingensis* G131 and Overview of Its Secondary Metabolism Potential. *BMC Genom.* **2018**, *19*, 200. [CrossRef]
7. Nützmann, H.W.; Reyes-Dominguez, Y.; Scherlach, K.; Schroeckh, V.; Horn, F.; Gacek, A.; Schümann, J.; Hertweck, C.; Strauss, J.; Brakhage, A.A. Bacteria-Induced Natural Product Formation in the Fungus *Aspergillus nidulans* Requires Saga/Ada-Mediated Histone Acetylation. *Proc. Natl. Acad. Sci. USA* **2011**, *108*, 14282–14287. [CrossRef]
8. Pfannenstiel, B.T.; Keller, N.P. On Top of Biosynthetic Gene Clusters: How Epigenetic Machinery Influences Secondary Metabolism in Fungi. *Biotechnol. Adv.* **2019**, *37*, 107345. [CrossRef]
9. Rutledge, P.J.; Challis, G.L. Discovery of Microbial Natural Products by Activation of Silent Biosynthetic Gene Clusters. *Nat. Rev. Microbiol.* **2015**, *13*, 509–523. [CrossRef]
10. Skellam, E. Strategies for Engineering Natural Product Biosynthesis in Fungi. *Trends Biotechnol.* **2019**, *37*, 916. [CrossRef]
11. Bode, H.B.; Bethe, B.; Höfs, R.; Zeeck, A. Big Effects from Small Changes: Possible Ways to Explore Nature's Chemical Diversity. *Chem. BioChem.* **2002**, *3*, 619–627. [CrossRef]
12. Liu, Y.Z.; Lu, C.H.; Shen, Y.M. Guanacastane-Type Diterpenoids from *Coprinus plicatilis*. *Phytochem. Lett.* **2014**, *7*, 161–164. [CrossRef]

13. Wang, W.J.; Li, D.Y.; Li, Y.C.; Hua, H.M.; Ma, E.L.; Li, Z.L. Caryophyllene Sesquiterpenes from the Marine-Derived Fungus *Ascotricha* sp. ZJ-M-5 by the One Strain–Many Compounds Strategy. *J. Nat. Prod.* **2014**, *77*, 1367–1371. [CrossRef]

14. Keller, N.P. Fungal Secondary Metabolism: Regulation, Function and Drug Discovery. *Nat. Rev. Microbiol.* **2019**, *17*, 167–180. [CrossRef] [PubMed]

15. Lyu, H.N.; Liu, H.W.; Keller, N.P.; Yin, W.B. Harnessing Diverse Transcriptional Regulators for Natural Product Discovery in Fungi. *Nat. Prod. Rep.* **2020**, *37*, 6–16. [CrossRef]

16. Reyes, F.; Bills, G.F.; Durán-Patrón, R. Strategies for the Discovery of Fungal Natural Products. *Front. Microbiol.* **2022**, *13*, 897756.

17. Berger, S.L.; Kouzarides, T.; Shiekhattar, R.; Shilatifard, A. An Operational Definition of Epigenetics. *Genes Dev.* **2009**, *23*, 781–783.

18. Wu, J.S.; Shi, X.H.; Zhang, Y.H.; Yu, J.Y.; Fu, X.M.; Li, X.; Chen, K.X.; Guo, Y.W.; Shao, C.L.; Wang, C.Y. Co-Cultivation With 5-Azacytidine Induced New Metabolites From the Zoanthid-Derived Fungus *Cochliobolus lunatus*. *Front. Chem.* **2019**, *7*, 763–770.

19. Mafezoli, J.; Xu, Y.M.; Hilário, F.; Freidhof, B.; Espinosa Artiles, P.; dos Santos, L.C.; de Oliveira, M.C.F.; Gunatilaka, A.A.L. Modulation of Polyketide Biosynthetic Pathway of the Endophytic Fungus, *Anteaglonium* sp. FL0768, by Copper (II) and Anacardic Acid. *Phytochem. Lett.* **2018**, *28*, 157–163.

20. Niu, S.W.; Liu, D.; Shao, Z.Z.; Proksch, P.; Lin, W.H. Eremophilane-Type Sesquiterpenoids in a Deep-Sea Fungus *Eutypella* sp. Activated by Chemical Epigenetic Manipulation. *Tetrahedron* **2018**, *74*, 7310–7325.

21. Sharma, V.; Singamaneni, V.; Sharma, N.; Kumar, A.; Arora, D.; Kushwaha, M.; Bhushan, S.; Jaglan, S.; Gupta, P. Valproic Acid Induces Three Novel Cytotoxic Secondary Metabolites in *Diaporthe* sp., an Endophytic Fungus from *Datura inoxia* Mill. *Bioorgan. Med. Chem. Lett.* **2018**, *28*, 2217–2221. [CrossRef] [PubMed]

22. Shi, T.; Shao, C.L.; Liu, Y.; Zhao, D.L.; Cao, F.; Fu, X.M.; Yu, J.Y.; Wu, J.S.; Zhang, Z.K.; Wang, C.Y. Terpenoids From the Coral-Derived Fungus *Trichoderma harzianum* (XS-20090075) Induced by Chemical Epigenetic Manipulation. *Front. Microbiol.* **2020**, *11*, 572–583. [CrossRef] [PubMed]

23. Zhang, S.X.; Fang, H.; Yin, C.P.; Wei, C.L.; Hu, J.W.; Zhang, Y.L. Antimicrobial Metabolites Produced by *Penicillium mallochii* CCH01 Isolated From the Gut of *Ectropis oblique*, Cultivated in the Presence of a Histone Deacetylase Inhibitor. *Front. Microbiol.* **2019**, *10*, 2186–2193. [CrossRef] [PubMed]

24. Asai, T.; Chung, Y.M.; Sakurai, H.; Ozeki, T.; Chang, F.R.; Wu, Y.C.; Yamashita, K.; Oshima, Y. Highly Oxidized Ergosterols and Isariotin Analogs from an Entomopathogenic Fungus, *Gibellula formosana*, Cultivated in the Presence of Epigenetic Modifying Agents. *Tetrahedron* **2012**, *68*, 5817–5823. [CrossRef]

25. Niu, S.W.; Liu, D.; Shao, Z.Z.; Liu, J.R.; Fan, A.L.; Lin, W.H. Chemical Epigenetic Manipulation Triggers the Production of Sesquiterpenes from the Deep-Sea Derived *Eutypella* Fungus. *Phytochemistry* **2021**, *192*, 112978. [CrossRef] [PubMed]

26. Wu, J.S.; Yao, G.S.; Shi, X.H.; Rehman, S.U.; Xu, Y.; Fu, X.M.; Zhang, X.L.; Liu, Y.; Wang, C.Y. Epigenetic Agents Trigger the Production of Bioactive Nucleoside Derivatives and Bisabolane Sesquiterpenes From the Marine-Derived Fungus *Aspergillus versicolor*. *Front. Microbiol.* **2020**, *11*, 85–93. [CrossRef] [PubMed]

27. Beau, J.; Mahid, N.; Burda, W.N.; Harrington, L.; Shaw, L.N.; Mutka, T.; Kyle, D.E.; Barisic, B.; Van Olphen, A.; Baker, B.J. Epigenetic tailoring for the production of anti-infective cytosporones from the marine fungus *Leucostoma persoonia*. *Mar. Drugs* **2012**, *10*, 762–774. [CrossRef]

28. Demers, D.H.; Knestrick, M.A.; Fleeman, R.; Tawfik, R.; Azhari, A.; Souza, A.; Baker, B.J. Exploitation of mangrove endophytic fungi for infectious disease drug discovery. *Mar. Drugs* **2018**, *16*, 376. [CrossRef]

29. Farr, D.F.; Castlebury, L.A.; Rossman, A.Y. Morphological and molecular characterization of *Phomopsis vaccinii* and additional isolates of *Phomopsis* from blueberry and cranberry in the eastern United States. *Mycologia* **2002**, *94*, 494–504. [CrossRef]

30. Yan, B.C.; Wang, W.G.; Hu, D.B.; Sun, X.; Kong, L.M.; Li, X.N.; Du, X.; Luo, S.H.; Liu, Y.; Li, Y.; et al. Phomopchalasins A and B, two cytochalasans with polycyclic-fused skeletons from the endophytic fungus *Phomopsis* sp. shj2. *Org. Lett.* **2016**, *18*, 1108–1111. [CrossRef]

31. Shang, Z.; Raju, R.; Salim, A.A.; Khalil, Z.G.; Capon, R.J. Cytochalasins from an australian marine sediment-derived *Phomopsis* sp. (cmb-m0042f): Acid-mediated intramolecular cycloadditions enhance chemical diversity. *J. Org. Chem.* **2017**, *82*, 9704–9709. [CrossRef] [PubMed]

32. Wagenaar, M.M.; Clardy, J. New Antibiotic and Cytotoxic Dimers Produced by the Fungus *Phomopsis longicolla* Isolated from an Endangered Mint. *J. Nat. Prod.* **2001**, *64*, 1006–1009. [CrossRef] [PubMed]

33. Li, Z.J.; Yang, H.Y.; Li, J.; Liu, X.; Ye, L.; Kong, W.S.; Tang, S.Y.; Du, G.; Liu, Z.H.; Zhou, M.; et al. Isopentylated diphenyl ether derivatives from the fermentation products of an endophytic fungus *Phomopsis fukushii*. *J. Antibiot.* **2018**, *71*, 359–362. [CrossRef] [PubMed]

34. Elsässer, B.; Krohn, K.; Flörke, U.; Root, N.; Aust, H.J.; Draeger, S.; Schulz, B.; Antus, S.; Kurtán, T. X-ray Structure Determination, Absolute Configuration and Biological Activity of Phomoxanthone A. *Eur. J. Org. Chem.* **2005**, *2005*, 4563–4570. [CrossRef]

35. Horn, W.S.; Simmonds, M.S.J.; Schwartz, R.E.; Blaney, W.M. Phomopsichalasin, a novel antimicrobial agent from an endophytic *Phomopsis* sp. *Tetrahedron* **1995**, *51*, 3969–3978. [CrossRef]

36. Xie, S.; Wu, Y.; Qiao, Y.; Guo, Y.; Wang, J.; Hu, Z.; Zhang, Q.; Li, X.; Huang, J.; Zhou, Q.; et al. Protoilludane, illudalane, and botryane sesquiterpenoids from the endophytic fungus *Phomopsis* sp. tj507a. *J. Nat. Prod.* **2018**, *81*, 1311–1320. [CrossRef]

37. Tan, Q.W.; Fang, P.H.; Ni, J.C.; Gao, F.; Chen, Q.J. Metabolites Produced by an Endophytic *Phomopsis* sp. and Their Anti-TMV Activity. *Molecules* **2017**, *22*, 2073. [CrossRef]

38. Feng, Z.; Zhang, X.X.; Wu, J.W.; Wei, C.W.; Feng, T.; Zhou, D.D.; Wen, Z.C.; Xu, J. Immunosuppressive Cytochalasins from the Mangrove Endophytic Fungus *Phomopsis asparagi* DHS-48. *Mar. Drugs* **2022**, *20*, 526. [CrossRef]

39. Xu, Z.Y.; Xiong, B.X.; Xu, J. Chemical investigation of secondary metabolites produced by mangrove endophytic fungus *Phyllosticta capitalensis*. *Nat. Prod. Res.* **2019**, *35*, 1561–1565. [CrossRef]

40. Hemberger, Y.; Xu, J.; Wray, V.; Proksch, P.; Wu, J.; Bringmann, G. Pestalotiopens A and B: Stereochemically challenging flflexible sesquiterpene-cyclopaldic acid Hybrids from *Pestalotiopsis* sp. *Chem. Eur. J.* **2013**, *19*, 15556–15564. [CrossRef]

41. Deng, Q.; Li, G.; Sun, M.Y.; Yang, X.; Xu, J. A new antimicrobial sesquiterpene isolated from endophytic fungus *Cytospora* sp. from the Chinese mangrove plant *Ceriops tagal*. *Nat. Prod. Res.* **2020**, *34*, 1404–1408. [CrossRef] [PubMed]

42. Sun, M.Y.; Zhou, D.D.; Wu, J.W.; Zhou, J.; Xu, J. Sdy-1 Executes Antitumor Activity in HepG2 and HeLa Cancer Cells by Inhibiting the Wnt/β-Catenin Signaling Pathway. *Mar. Drugs* **2022**, *20*, 125. [CrossRef] [PubMed]

43. Wei, C.W.; Deng, Q.; Sun, M.Y.; Xu, J. Cytospyrone and Cytospomarin: Two New Polyketides Isolated from Mangrove Endophytic Fungus, *Cytospora* sp. *Molecules* **2020**, *25*, 4224. [CrossRef] [PubMed]

44. Xu, J.; Kjer, J.; Sendker, J.; Wray, V.; Guan, H.; Edrada, R.; Lin, W.H.; Wu, J.; Proksch, P. Chromones from the Endophytic Fungus *Pestalotiopsis* sp. Isolated from the Chinese Mangrove Plant *Rhizophora Mucronata*. *J. Nat. Prod.* **2009**, *72*, 662–665. [CrossRef] [PubMed]

45. Zhou, J.; Li, G.; Deng, Q.; Zheng, D.Y.; Yang, X.B.; Xu, J. Cytotoxic Constituents from the Mangrove Endophytic *Pestalotiopsis* sp. Induce G (0)/G (1) Cell Cycle Arrest and Apoptosis in Human Cancer Cells. *Nat. Prod. Res.* **2018**, *32*, 2968–2972. [CrossRef]

46. Wei, C.W.; Sun, C.X.; Feng, Z.; Zhang, X.X.; Xu, J. Four New Chromones from the Endophytic Fungus *Phomopsis asparagi* DHS-48 Isolated from the Chinese Mangrove Plant *Rhizophora mangle*. *Mar. Drugs* **2021**, *19*, 348. [CrossRef]

47. Xu, Z.Y.; Wu, X.; Li, G.; Feng, Z.; Xu, J. Pestalotiopisorin B, a New Isocoumarin Derivative from the Mangrove Endophytic Fungus *Pestalotiopsis* sp. HHL101. *Nat. Prod. Res.* **2020**, *34*, 1002–1007. [CrossRef]

48. Zhang, X.X.; Li, G.; Deng, Q.; Xu, Z.Y.; Cen, J.R.; Xu, J. Vomifoliol Isolated from Mangrove Plant Ceriops Tagal Inhibits the NFAT Signaling Pathway with CN as the Target Enzyme in vitro. *Bioorgan. Med. Chem. Lett.* **2021**, *48*, 128235. [CrossRef]

49. Chen, S.H.; Guo, H.; Jiang, M.H.; Wu, Q.L.; Li, J.; Shen, H.J.; Liu, L. Mono- and Dimeric Xanthones with Anti-Glioma and Anti-Inflammatory Activities from the Ascidian-Derived Fungus *Diaporthe* sp. SYSU-MS4722. *Mar. Drugs* **2022**, *20*, 51. [CrossRef]

50. Huang, M.X.; Li, J.; Liu, L.; Yin, S.; Wang, J.; Lin, Y.C. Phomopsichin A-D; four new chromone derivatives from mangrove endophytic fungus *Phomopsis* sp. 33. *Mar. Drugs* **2016**, *14*, 215. [CrossRef]

51. Wijeratne, E.K.; Bashyal, B.P.; Gunatilaka, M.K.; Arnold, A.E.; Gunatilaka, A.L. Maximizing chemical diversity of fungal metabolites: Biogenetically related heptaketides of the endolichenic fungus *Corynespora* sp. *J. Nat. Prod.* **2010**, *73*, 1156–1159. [CrossRef] [PubMed]

52. Guo, H.; Liu, Z.M.; Chen, Y.C.; Tan, H.B.; Li, S.N.; Li, H.H. Chromone-derived polyketides from the deep-sea fungus *Diaporthe phaseolorum* fs431. *Mar. Drugs* **2019**, *17*, 182. [CrossRef] [PubMed]

53. Cole, R.J.; Wells, J.M.; Cox, R.H.; Cutler, H.G.J. Isolation and biological properties of deacetylcytochalasin H from *Phomopsis* sp. *Agric. Food Chem.* **1981**, *29*, 205–206. [CrossRef]

54. Bisht, R.; Bhattacharyya, A.; Shrivastava, A.; Saxena, P. An overview of the medicinally important plant type III PKS derived polyketides. *Front. Plant Sci.* **2021**, *12*, 746908. [CrossRef]

55. Rönsberg, D.; Debbab, A.; Mándi, A.; Vasylyeva, V.; Böhler, P.; Stork, B.; Proksch, P. Pro-apoptotic and immunostimulatory tetrahydroxanthone dimers from the endophytic fungus *Phomopsis longicolla*. *J. Org. Chem.* **2013**, *78*, 12409–12425. [CrossRef] [PubMed]

56. Lösgen, S.; Schlörke, O.; Meindl, K.; Herbst-Irmer, R.; Zeeck, A. Structure and biosynthesis of chaetocyclinones, new polyketides produced by an endosymbiotic fungus. *Eur. J. Org. Chem.* **2010**, *2007*, 2191–2196. [CrossRef]

57. Zhou, J.; Diao, X.; Wang, T.; Chen, G.; Lin, Q.; Yang, X.; Xu, J. Phylogenetic diversity and antioxidant activities of culturable fungal endophytes associated with the mangrove species *Rhizophora stylosa* and *R. mucronata* in the South China Sea. *PLoS ONE* **2018**, *13*, e0197359. [CrossRef]

58. Liu, G.; Xu, Z.N.; Cen, P.L. A Morphologically Structured Model for Mycelial Growth and Secondary Metabolite Formation. *Chin. J. Chem. Eng.* **2000**, *8*, 46–51.

Article

New Chlorinated Metabolites and Antiproliferative Polyketone from the Mangrove Sediments-Derived Fungus *Mollisia* sp. SCSIO41409

Jian Cai [1,2,†], Xueni Wang [1,3,†], Xia Gan [3,4], Qian Zhou [3], Xiaowei Luo [4], Bin Yang [1,2], Yonghong Liu [1,2], Disna Ratnasekera [5,*] and Xuefeng Zhou [1,2,*]

1   CAS Key Laboratory of Tropical Marine Bio-resources and Ecology, Guangdong Key Laboratory of Marine Materia Medica, South China Sea Institute of Oceanology, Chinese Academy of Sciences, Guangzhou 510301, China
2   University of Chinese Academy of Sciences, Beijing 100049, China
3   Guangxi Zhuang Yao Medicine Center of Engineering and Technology, Guangxi University of Chinese Medicine, Nanning 530200, China
4   Institute of Marine Drugs, Guangxi University of Chinese Medicine, Nanning 530200, China
5   Department of Agricultural Biology, Faculty of Agriculture, University of Ruhuna, Matara 81000, Sri Lanka
*   Correspondence: disnar@agbio.ruh.ac.lk (D.R.); xfzhou@scsio.ac.cn (X.Z.)
†   These authors contributed equally to this work.

Abstract: Two new chlorinated metabolites, 8-chlorine-5-hydroxy-2,3-dimethyl-7-methoxychromone (**1**) and 3,4-dichloro-1*H*-pyrrole-2,5-dione (**3**), and eight known compounds (**2** and **4**–**9**) were isolated from the mangrove sediments-derived fungus *Mollisia* sp. SCSIO41409. Their structures were elucidated by physicochemical properties and extensive spectroscopic analysis. The absolute configuration of stemphone C (**4**) was established for the first time by the X-ray crystallographic analysis. Compounds **3** and **4** showed different intensity of antimicrobial activities against several pathogenic fungi and bacteria, and antiproliferative activities against two human prostate cancer cell lines (IC_{50} values 2.77 to 9.60 μM). Further, stemphone C (**4**) showed a reducing PC-3 cell colony formation, inducing apoptosis and blocking the cell cycle at S-phase in a dose-dependent manner; thus, it could be considered as a potential antiproliferative agent and a promising anti-prostate cancer lead compound.

Keywords: mangrove sediments-fungus; *Mollisia* sp.; chlorinated metabolites; prostate cancer; antimicrobial

1. Introduction

Mangrove forests are a complex ecosystem, and the microbes in mangrove sediments play an important role in the biogeochemical cycles of mangrove ecosystems [1]. The high diversity of mangrove environments has contributed to high microbial diversity, which is an important source of bioactive natural products [2–4]. Research on secondary metabolites from mangrove sediments-derived microbes has yielded many natural products with novel structures and significant pharmacological activities [5–8]. In particular, halogenated compounds obtained from mangrove-derived microbes, especially chlorine-containing metabolites, have received a great deal of attention [9–11].

Mollisia is a taxonomically neglected discomycete genus (Helotiales, Leotiomycetes) in decaying plant tissues or root soil. The natural products from the genus *Mollisia* were not well explored and were limited to few publications. Mollisinols A and B, two new metabolites were isolated from the endophytic fungus *Mollisia* sp., derived from the root bark of *Ardisia cornudentata* Mez [3]. Ophiobolin C, isolated from *Mollisia* sp. (GB5328) from the dead bark of *Tsuga canadensis*, was an inhibitor of binding with human CCR5 receptor and exhibited an IC_{50} value of 40 μM [12]. KS-504 compounds, three novel inhibitors of Ca^{2+} and calmodulin-dependent cyclic nucleotide phosphodiesterase were

isolated from *Mollisia ventosa* KAC-1 148 [13]. Mollisianitrile, a new antibiotic was isolated from *Mollisa* sp. A59–96 [14]. Benesudon, isolated from *Mollisia bensuada*, possessed antimicrobial, cytotoxic, and phytotoxic activities [15]. Mollisin, a dichloronaphthoquinone derivative produced by the fungus *Mollisia caesia* [16]. In our study, we explored potential bioactive secondary metabolites from a mangrove sediment-derived fungal strain, *Mollisia* sp. SCSIO41409, isolated from a mangrove sediment sample in Hainan Island, China. During our search for potentially diverse and bioactive secondary metabolites from mangrove fungal sources [10,17–19], two new chlorinated metabolites (**1** and **3**), and seven known polyketides (**2** and **4–9**) (Figure 1) were isolated and identified from a mangrove sediment-derived fungus *Mollisia* sp. SCSIO41409. These compounds were examined for antimicrobial and antiproliferative activities. Herein, we report the details of the isolation, structural elucidation, and biological evaluation of all isolated compounds.
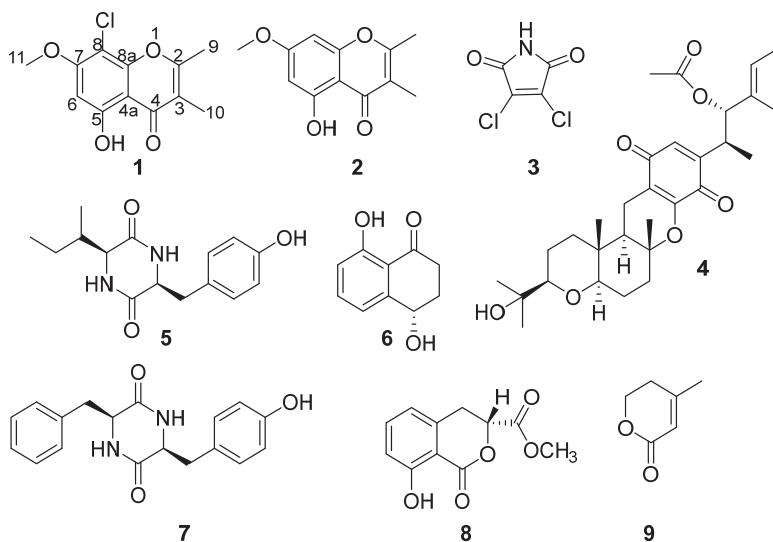

Figure 1. Structures of compounds **1–9**.

2. Results

2.1. Structural Determination

Compound **1** was isolated as a white needle crystal and had the molecular formula $C_{12}H_{11}ClO_4$ as determined by the HRESIMS spectrum, which showed a cluster of protonated ion peaks at *m/z* 255.0422/257.0394 [M + H]$^+$ with the ratio of 3:1, indicative of a monochlorinated compound. The 1D NMR (Table 1) and HSQC spectrum of **1** showed signals of a carbonyl carbon (δ_C 181.1), seven non-protonated *sp*^{2} carbons (δ_C 163.9, 160.0, 159.9, 151.6, 114.6, 103.7 and 97.4), one aromatic methine ($\delta_{H/C}$ 6.62/95.9), one oxygenated methyl ($\delta_{H/C}$ 3.94/57.0), and two methyls ($\delta_{H/C}$ 2.42/18.3 and 1.91/8.8). The above-mentioned data combined with seven degrees of unsaturation suggested that **1** presented a chromone skeleton. The above NMR characteristics showed great similarity to those of the co-isolated **2**, which was reported as a chromone compound. The main difference was the presence of the chlorine atom instead of a hydrogen atom at C-8 in **1** and this deduction was supported by the above 2D NMR data. The HMBC correlations (Figure 2) from H$_3$-9 to C-2 and C-3, from H$_3$-10 to C-2, C-3, and C-4, revealed that the methyl groups CH$_3$-9 and CH$_3$-10 were located at C-2 and C-3, respectively. The HMBC correlations from 5-OH to C-4a, C-5, and C-6 indicated the location of the phenolic hydroxyl group (C-5). The chemical shift of C-8 (δ_C 97.4) revealed the substitution of chlorine instead of the oxygenated methyl, which was attached at C-8. The methoxy group was deduced to link with C-7 by the HMBC signal of H$_3$-11/C-7 and the chemical shift of C-7 (δ_C 159.9). The X-ray crystal structure of

1 (CDCC 2221470), obtained by slow evaporation in CH$_3$OH, further confirmed the above elucidation of the planar structure. Compound **1** was unambiguously characterized as shown in Figure 1 and defined as 8-chlorine-5-hydroxy-2,3-dimethyl-7-methoxychromone.

Compound **3** was isolated as a red needle crystal, and its molecular formula of C$_4$HCl$_2$NO$_2$ was determined by HRESIMS data at *m/z* 163.9318 [M–H]$^-$ (calcd for C$_4$Cl$_2$NO$_2$, 163.9312). The analysis of its structure accurately from the NMR spectrum was difficult, because of its symmetrical structure and simplicity of carbons (δ_C 164.1, 132.8) and hydrogens (δ_H 11.71 (s, 1H)). However, we obtained X-ray crystal data (Cu Kα radiation) of **3**, and the structure was accurately determined as 3,4-dichloro-1*H*-pyrrole-2,5-dione (Figure 3). Compound **3** has been previously identified as a synthetic product, which was synthesized to illustrate the insecticidal structure-activity relationship of the *N*-amino-maleimide derivatives [20]. Here we are reporting the first time this compound explored from nature, as a new metabolite or new natural product.

Compound **4**, obtained as yellow needles, was found to have the molecular formula C$_{30}$H$_{42}$O$_7$ on the basis of HRESIMS data at *m/z* 515.3003 [M+H]$^+$ (calcd C$_{30}$H$_{43}$O$_7$, 515.3003). The ^{13}C NMR and DEPT data displayed 30 carbon signals including eight methyls, five methylenes, two *sp*^{3} methine, two *sp*^{2} methine, three oxygenated *sp*^{3}, one *sp*^{3} quaternary, two oxygenated *sp*^{3} quaternary, four *sp*^{2} quaternary and three carbonyls. Detailed comparison of the above NMR data with the literature [21], **4** was identified as stemphone C. However, the absolute configuration of **4** had not been reported. We determined the absolute configuration of **4** as 4*S*, 5*S*, 13*R*, 14*R*, 17*R*, 18*R*, 21*R* (Figure 3) by X-ray crystallographic analysis using Cu Kα radiation.

Meanwhile, the other seven known compounds were identified as 5-hydroxy-2,3-dimethyl-7-methoxychromone (**2**) [22], *cis*-cyclo (Tyr-Ile) (**5**) [23],4,8-dihydroxy-1-tetralone (**6**) [24], cyclo (Phe-Tyr) (**7**) [25], tenuissimasatin (**8**) [26], 4-methyl-5,6-dihydro-2H-pyran-2-one (**9**) [27], respectively, by comparison of their NMR data (supplementary information) with previous reports.
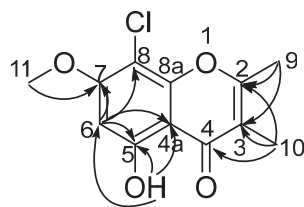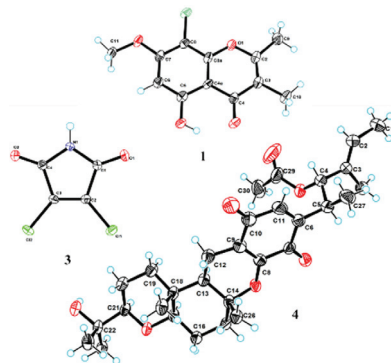

Figure 2. Key HMBC (arrows) correlations of **1**.

Figure 3. X-ray single-crystal structures of compounds **1**, **3**, and **4**.

Table 1. The NMR data of compound **1** (500 and 125 MHz, δ in ppm, DMSO-d_6).

Pos.	δ_C Type	δ_H (*J* in Hz)	HMBC
2	163.9, C		
3	114.6, C		
4	181.1, C		
4a	103.7, C		
5	160.0, C		
6	95.9, CH	6.62 (s)	4a, 5, 7, 8
7	159.9, C		
8	97.4, C		
8a	151.6, C		
9	18.3, CH3	2.42 (s)	2, 3
10	8.8, CH3	1.91 (s)	2, 3, 4
11	57.0, CH3	3.94 (s)	7
5-OH		13.09 (s)	4a, 5, 6

2.2. Antimicrobial and Antiproliferative Activities

All of the obtained compounds were evaluated for the activities of pathogenic fungi and bacteria commonly found in crop plants (Table 2). Compound **3** exhibited antifungal activities against *Botrytis cinerea*, *Verticillium dahlia* kieb., *Fusarium graminearum* schw., *Fusarium oxysporum* f.sp. niveum, *Rhizoctonia solani,* and *Septoria nodorum* Berk., with the MIC values of 25–50 µg/mL. Compound **4** exhibited antibiotic activity against bacteria *Erysipelothrix rhusiopathiae* WH13013 and *Streptococcus suis* SC19, with the MIC values of 1.56 and 6.25 µg/mL. In particular, the strength of **4** against *E. rhusiopathiae* was stronger than that of penicillin with the MIC value of 6.25 µg/mL.

Table 2. Antifungal, antibacterial, and cytotoxic activities of **3** and **4**.

Activities	Strains or Cells	3	4	Positive
Antifungal (MIC, µg/mL)	*B. cinerea*	25	>100	12.50 [a]
	V. dahlia	25	>100	12.50 [a]
	F. graminearum	50	>100	12.50 [a]
	F. oxysporum	50	>100	>100 [a]
	R. solani	50	>100	100 [a]
	S. nodorum	25	50	12.50 [a]
Antibacterial (MIC, µg/mL)	*E. rhusiopathiae*	>100	1.56	6.25 [b]
	S. aureus	100	>100	6.25 [b]
	S. suis	100	6.25	1.56 [b]
	E. coli	>100	>100	50.00 [c]
Cytotoxic (IC$_{50}$, µM)	22Rv1	8.35	5.81	0.03 [d]
	PC-3	9.60	2.77	0.12 [d]
	HepG2	/	7.11	178.60 [d]
	A549	/	11.68	29.95 [d]
	Hela	/	11.47	/
	WPMY-1	/	5.53	0.51 [d]
	MC3T3-E1	/	3.63	/

[a] Cycloheximide; [b] Penicillin; [c] Streptomycin; [d] Docetaxel

Two human prostate cancer cell lines, PC-3 (androgen receptor negative) and 22Rv1 (androgen receptor positive), were used in the antiproliferative assay for all the obtained compounds. Compound **3** exhibited antiproliferative activity against 22Rv1 and PC-3 cells with IC$_{50}$ values of 8.35 and 9.60 µM, respectively, while **4** showed activities against 22Rv1 and PC-3 cells with IC$_{50}$ values of 5.81 and 2.77 µM, respectively. In order to evaluate whether **4** selectively inhibits prostate cancer cells, we screened other cancer cells for antiproliferative activity. The result showed that **4** was also active against other cells (HepG2, A549, Hela, WPMY-1, MC3T3-E1) with IC$_{50}$ values of 3.63–11.68 µM. Thus, **4**

had the most significant effect on PC-3 cells compared to other compounds with broader inhibitory activity.

To further evaluate the inhibitory effect of **4** on PC-3 cells, we performed a plate clone formation assay. The results showed that **4** significantly inhibited the formation of clonal colonies of PC-3 cells and its inhibitory effect was positively correlated with the dose (Figure 4). In addition, we examined the effect of **4** on PC-3 cell apoptosis by flow cytometry. It was revealed that **4** could significantly induce apoptosis in PC-3 cells. As shown in Figure 5, when PC-3 cells were treated with 10 μM of **4** for 48 h, 14.64% of the cells were induced to early apoptosis and 36.84% of the cells were induced to late apoptosis. This finding suggests that the induction of apoptosis in PC-3 cells is a mode of action for the production of antiproliferative activity by **4**.
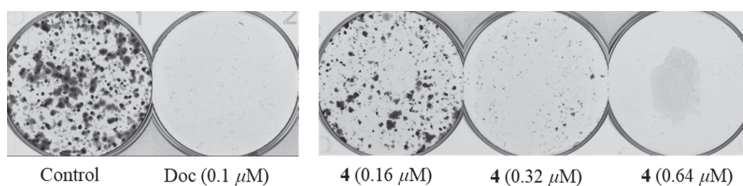

Figure 4. Compound **4** reduced PC-3 cells colony formation in a dose-dependent manner.
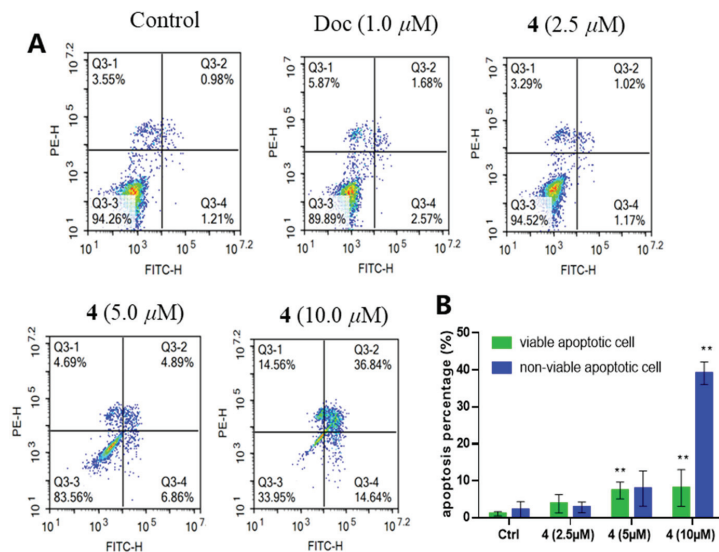

Figure 5. Compound **4** triggered PC-3 cells apoptosis in a dose-dependent manner (**A**,**B**). All results were presented as mean ± standard deviation (SD). Statistical significance was determined with One-Way ANOVA. ** $p < 0.01$ was considered statistically significant.

To identify the inhibitory process of the proliferation of prostate cancer cells, we detected the cell cycle distribution of PC-3 cells. As shown in Figure 6, when treated with the M-phase blocker docetaxel, a large number of PC-3 cells were blocked in M-phase, with a dramatic increase in the ratio of G2/M, up to 71.23 percent. However, unlike in the case of docetaxel, the percentage of S-phase was significantly increased in cells treated with **4**. When the concentration of **4** reached 10 μM, the percentage of cells in the S-phase was as high as 59.14 percent. These results suggested that **4** blocked the cell cycle at S-phase, impairing cell proliferation. Consequently, it is revealed that **4** is a promising lead compound for pharmacotherapy of prostate cancer.
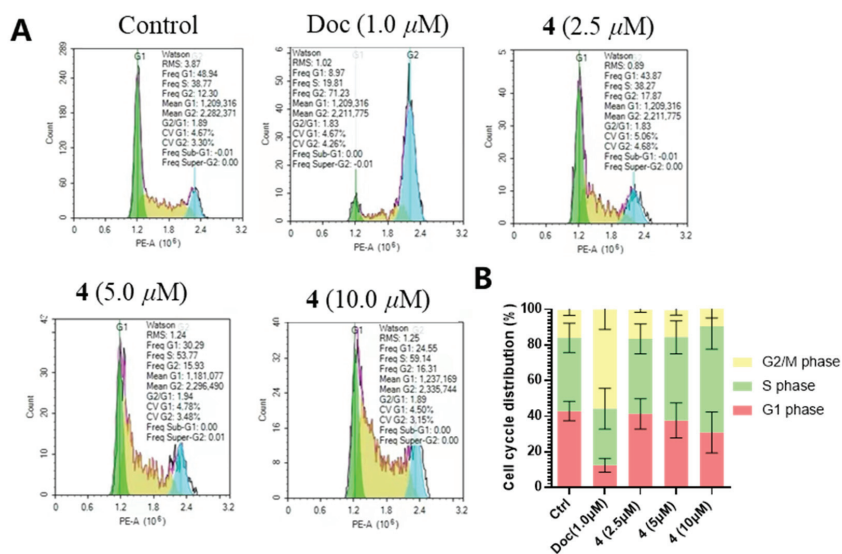
Figure 6. Compound **4** induced PC-3 cell cycle arresting at S phase (**A**,**B**). All results were presented as mean $\pm$ standard deviation (SD).

3. Discussion

Marine organisms and microorganisms living in extreme marine environments were considered to be important sources of halogenated compounds [28]. Chlorinated metabolites, as a key part of the halogenated compounds, have demonstrated a wide range of significant activities. Due to the high concentration of chloride ions in mangrove ecosystem, many chlorinated compounds have been excavated from mangrove-derived microorganisms [9–11]. In this study, two new chlorinated metabolites, **1** and **3**, were isolated from mangrove sediments-derived fungus. Although 3,4-dichloro-1*H*-pyrrole-2,5-dione (**3**) has been previously reported as a synthetic product, it was discovered as a new metabolite of natural origin in our study. So, mangrove sediments-derived microbes have proved to be a promising source of novel and unique chlorine-containing bioactive secondary metabolites.

An important result of this study is the discovery of stemphone C (**4**) with significant anti-prostate cancer activity in vitro. Stemphone C (**4**) had been reported from an *Aspergillus* strain as a potentiator of imipenem activity against methicillin-resistant *Staphylococcus aureus*, with other stemphone derivatives [21,29]. Stemphone was found to inhibit over contraction of portal vein, induced by high glucose levels [30], and its derivatives were also revealed to inhibit lipid droplet accumulation in macrophages [31]. In our study, stemphone C (**4**) exhibited obvious antimicrobial activity against the bacteria *Erysipelothrix rhusiopathiae* WH13013, with the MIC value of 1.56 μg/mL. In addition, obvious antiproliferative activities of stemphone C (**4**) were also revealed against two prostate cancer cell lines (PC-3 and 22Rv1) and three other cancer cell lines (HepG2, WPMY-1, and MC3T3-E1), with IC_{50} values less than 10 μM. Furthermore, it showed reducing PC-3 cells colony formation, inducing apoptosis, and blocking the cell cycle at S-phase in a dose-dependent manner. Our study showed that stemphone C (**4**) could be considered as a potential antiproliferative agent, especially as a promising anti-prostate cancer lead compound. Importantly, we could able to determine the absolute configuration of **4**, the first time in this study, which is necessary for further development of this active compound.

4. Materials and Methods

4.1. General Experimental Procedures

The UV and IR spectra were recorded on a Shimadzu UV-2600 PC spectrometer (Shimadzu, Beijing, China) and an IR Affinity-1 spectrometer (Shimadzu), respectively. Optical rotations were determined with an Anton Paar MPC 500 (Anton, Graz, Austria) polarimeter. High resolution electrospray ionization mass spectroscopy (HRESIMS) spectra were acquired on a Bruker maXis Q-TOF mass spectrometer (Bruker BioSpin International AG, Fällanden, Swizerland). The NMR spectra were recorded on a Bruker Avance spectrometer (Bruker) operating at 500 and 700 MHz for ^{1}H NMR and 125 and 175 MHz for ^{13}C NMR that used tetramethylsilane as an internal standard. Semipreparative high-performance liquid chromatography (HPLC) was performed on the Hitachi Primaide with a DAD detector, using an ODS column (YMC-pack ODS-A, 10 × 250 mm, 5 μm). Column chromatography was performed over silica gel (200–300 mesh) (Qingdao Marine Chemical Factory, Qingdao, China). Spots were detected on TLC (Qingdao Marine Chemical Factory) under 254 nm UV light. All solvents employed were of analytical grade (Tianjin Fuyu Chemical and Industry Factory, Tianjin, China).

4.2. Fungal Material

The fungal strain *Mollisia* sp. SCSIO41409 was isolated from a mangrove sediment sample, collected from the Hongsha River estuary near South China Sea, in Sanya city, Hainan Island. The fungus was identified according to the internally transcribed spacer (ITS) region sequence data of the rDNA (supplementary information), and the sequence was deposited in GenBank with the accession number OP872608. A voucher specimen was deposited in the CAS Key Laboratory of Tropical Marine Bioresources and Ecology, South China Sea Institute of Oceanology, Chinese Academy of Sciences, Guangzhou, China.

4.3. Fermentation and Extraction

The fungal strain was cultured in 200 mL seed medium (1.5% malt extract, 1.5% sea salt) in 500 mL Erlenmeyer flasks at 28 °C for 3 days on a rotary shaker (180 rpm). A large-scale fermentation was incubated statically at 26 °C for 60 days using a rice medium (150 g rice, 1.5% sea salt, 150 mL H_2O) in the 1 L flask (×53). The whole fermented culture was extracted with EtOAc three times to afford a brown extract (197.2 g).

4.4. Isolation and Purification

The crude extract was chromatographed over a silica gel column eluted with petroleum ether /CH_2Cl_2 (0–100%, *v/v*) and CH_2Cl_2/CH_3OH (0–100%, *v/v*) to obtain eleven fractions (Frs. 1–11) based on TLC properties. Fr. 2 was subjected to semipreparative HPLC (63%CH_3CN/H_2O, 2.5 mL/min) to afford **2** (3.7 mg, t_R = 18.6 min) and **1** (9.1 mg, t_R = 27.0 min). Fr. 4 was separated by semipreparative HPLC (40% MeCN/H_2O, 2.5 mL/min) to afford **9** (7.1 mg, t_R = 6.5 min), **8** (4.1 mg, t_R = 8.1 min), **3** (27.8 mg, t_R = 11.1 min). Fr. 5 was separated by semipreparative HPLC (37% MeCN/H_2O, 2.5 mL/min) to afford **6** (8.6 mg, t_R = 9.8 min). **4** (8.0 mg, t_R = 24.0 min) was obtained from Fr. 6 by semipreparative HPLC eluting with 76% CH_3CN/H_2O (2.5 mL/min). Fr. 10 was separated by semipreparative HPLC (23% MeCN/H_2O, 2.5 mL/min) to afford **7** (22.0 mg, t_R = 19.0 min) and **5** (9.0 mg, t_R = 12.0 min).

4.5. Spectroscopic Data of Compounds

8-chlorine-5-hydroxy-2,3-dimethyl-7-methoxychromone (**1**): white needles, m.p. 196–198 °C; UV (CH_3OH) λ_{max} (log ε) 327 (3.54), 282 (3.49), 259 (4.10), 244 (4.15), 204 (4.11) nm; IR (film) ν_{max} 3734, 2926, 2855, 1717, 1653, 1558, 1437, 1207, 1182, 1103, 820 cm^{-1}; ^{1}H and ^{13}C NMR data as shown in Table 1; HRESIMS *m/z* 255.0422 [M + H]$^+$ (calcd for $C_{12}H_{12}ClO_4^+$, 255.0419).

3,4-dichloro-1*H*-pyrrole-2,5-dione (**3**): red needles, m.p. 173–175 °C; UV (CH_3OH) λ_{max} (log ε) 235.60 (0.80), 229.20 (0.79) nm; IR (film) ν_{max} 3204, 1732, 1609, 1331, 1047,

1026, 851, 735, 673, 550 cm^{-1}; ^{1}H NMR (700 MHz, DMSO-d_6) δ 11.71 (s, 1H); ^{13}C NMR (175 MHz, DMSO) δ 164.06, 132.82. HRESIMS data at m/z 163.9318 [M–H]$^{-}$ (calcd for C$_4$Cl$_2$NO$_2$, 163.9312).

4.6. X-ray Crystallographic Analysis

The clear light colorless crystal of **1** was obtained in MeOH by slow evaporation. Crystallographic data for the structure has been deposited in the Cambridge Crystallographic Data Centre. Copies of the data can be obtained, free of charge, on application to CCDC, 12 Union Road, Cambridge CB21EZ, UK [fax: +44(0)-1223-336033 or e-mail: deposit@ccdc.cam.ac.uk].

Crystal data for **1**: 2C$_{12}$H$_{11}$ClO$_4$, Mr = 509.31, crystal size 0.3 × 0.03 × 0.02 mm^3, triclinic, a = 10.3781 (6) Å, b = 10.7434 (9) Å, c = 11.7251 (8) Å, α = 94.077(6)°, β = 101.693 (5)°, γ = 118.572 (7)°, V = 1102.59 (14) Å^3, Z = 4, T = 100.00 (10) K, space group P-1, μ(Cu Kα) = 3.099 mm^{-1}, D_{calc} = 1.534 g/cm^3, 3879 reflections measured (7.852° $\leq$ 2Θ $\leq$ 133.17°), 3879 unique (R_{sigma} = 0.0731). The final R_1 values were 0.0733 (I > 2σ(I)). The final wR(F^2) values were 0.2186 (I > 2σ(I)). The final R_1 values were 0.1004 (all data). The final wR(F^2) values were 0.2360 (all data). The goodness of fit on F^2 was 1.059 (CCDC 2221470).

Crystal data for **3**: 2C$_4$HCl$_2$NO$_2$, Mr = 165.96, crystal size 0.09 × 0.06 × 0.06 mm^3, monoclinic, a = 7.11690 (10) Å, b = 8.03280 (10) Å, c = 10.2446 (2) Å, α = 90°, β = 99.9790(10)°, γ = 90°, V = 576.809 (16) Å^3, Z = 4, T = 100.00 (10) K, space group $P2_1/c$, μ(Cu Kα) = 9.446 mm^{-1}, D_{calc} = 1.911 g/cm^3, 2500 reflections measured (12.63° $\leq$ 2Θ $\leq$ 148.6°), 1126 unique (R_{sigma} = 0.0272). The final R_1 values were 0.0239 (I > 2σ(I)). The final wR(F^2) values were 0.0666 (I > 2σ(I)). The final R_1 values were 0.0246 (all data). The final wR(F^2) values were 0.0671 (all data). The goodness of fit on F^2 was 1.092 (CCDC 2221370).

Crystal data for **4**: 2C$_{30}$H$_{42}$O$_7$·CH$_3$OH, Mr = 1061.31, crystal size 0.06 × 0.06 × 0.05 mm^3, orthorhombic, a = 6.37690 (10) Å, b = 19.5291 (3) Å, c = 49.6907 (8) Å, α = 94.077(6)°, β = 101.693(5)°, γ = 118.572(7)°, V = 1102.59 (14) Å^3, Z = 4, T = 100.01 (10) K, space group P-1, μ(Cu Kα) = 3.099 mm^{-1}, D_{calc} = 1.534 g/cm^3, 3879 reflections measured (7.852° $\leq$ 2Θ $\leq$ 133.17°), 3879 unique (R_{sigma} = 0.0731). The final R_1 values were 0.0733 (I > 2σ(I)). The final wR(F^2) values were 0.2186 (I > 2σ(I)). The final R_1 values were 0.1004 (all data). The final wR(F^2) values were 0.2360 (all data). The goodness of fit on F^2 was 1.020. The flack parameter was 0.18 (9) (CCDC 2221376).

4.7. Antibacterial Activity Assay

The antimicrobial activities against six fungi (Botrytis cinerea, Verticillium dahlia kieb., Fusarium graminearum schw., Fusarium oxysporum f.sp. niveum, Rhizoctonia solani, and Septoria nodorum Berk.) and four bacteria (Escherichia coli ATCC 25922, Staphylococcus aureus ATCC 25923, Streptococcus suis SC19, Erysipelothrix rhusiopathiae WH13013) were evaluated in 96-well plates with a twofold serial dilution method described previously [32]. Cycloheximide and penicillin were used as positive controls against fungi and bacteria, respectively.

4.8. Cytotoxicity Bioassay

Cell viability was analyzed by 3-(4,5)-dimethylthiahiazo (-z-y1)-3,5-di-phenytetrazoliu mromide (MTT) assay as previously described [33]. In brief, cells were seeded in a 96-well plate at a density of 5 × 10^3 per well overnight and treated with compounds for demand time. OD$_{570}$ values were detected using a Hybrid Multi-Mode Reader (Synergy H1, BioTek, Santa Clara, CA, USA). The experiment was independently repeated three times.

4.9. Plate Clone Formation Assay

PC-3 cells were seeded in the six-well plate at a density of 1000 cells per well overnight, then cells were treated with DMSO (0.1 %, *v/v*), docetaxel (0.1 μM), compound **4** (0.16 μM, 0.32 μM, and 0.64 μM), respectively, for demand time. The cell clone colony formation was observed after two weeks of treatment. Cells were fixed with 4% formaldehyde for 30 min

and washed with PBS buffer, then stained with crystal violet stain solution for 30 min. The dye solution was removed and washed the cells with PBS buffer again. Cell colonies were recorded and analyzed by the colony count analysis system (GelCount, Oxford Optronix, Oxford, UK). The experiment was repeated three times independently.

4.10. Apoptosis and Cell Cycle Assay

PC-3 cells were seeded in the six-well plate at a density of 2.0×10^5 cells/well and incubated overnight and treated with DMSO (0.1 %, v/v), docetaxel (1.0 μM), compound **4** (2.5 μM, 5.0 μM, 10 μM), respectively, for 48 h. Then, cells were collected and stained with annexin V-FITC and PI solution, following the manufacturer's manual (BMS500FI-300, Thermo Fisher Scientific, Waltham, MA, USA). Apoptotic rates and cell cycle distribution of PC-3 cells were examined and analyzed by flow cytometer (NovoCyte, Agilent, Santa Clara, CA, USA). Each experiment was repeated three times independently.

5. Conclusions

In conclusion, nine polyketides, including two new chlorinated metabolites 8-chlorine-5-hydroxy-2,3-dimethyl-7-methoxychromone (**1**) and 3,4-dichloro-1*H*-pyrrole-2,5-dione (**3**), were isolated from the mangrove-sediment-derived fungus *Mollisia* sp. SCSIO41409. The X-ray single-crystal diffraction analysis and absolute configuration of (4*S*, 5*S*, 13*R*, 14*R*, 17*R*, 18*R*, 21*R*)-stemphone C (**4**) were described for the first time. Compounds **3** and **4** showed different intensities of antimicrobial activities and antiproliferative activities. Further experiments revealed that **4** could significantly reduce PC-3 cells colony formation, induce apoptosis, and block the cell cycle at the S phase in a dose-dependent manner. Stemphone C (**4**) could be considered as a potential antiproliferative agent and a promising anti-prostate cancer lead compound.

References

1. Li, K.; Chen, S.; Pang, X.; Cai, J.; Zhang, X.; Liu, Y.; Zhu, Y.; Zhou, X. Natural products from mangrove sediments-derived microbes: Structural diversity, bioactivities, biosynthesis, and total synthesis. *Eur. J. Med. Chem.* **2022**, *230*, 114117. [CrossRef] [PubMed]
2. Zhou, H.; Zhu, T.; Cai, S.; Gu, Q.; Li, D. Drimane Sesquiterpenoids from the Mangrove-Derived Fungus Aspergillus ustus. *Chem. Pharm. Bull.* **2011**, *59*, 762–766. [CrossRef] [PubMed]
3. Fan, N.W.; Chang, H.S.; Cheng, M.J.; Chan, H.Y.; Hsieh, S.Y.; Liu, T.W.; Chen, S.W.; Yuan, G.F.; Chen, I.S. New Metabolites from the Endophytic Fungus *Mollisia* sp. *Chem. Nat. Compd.* **2016**, *52*, 585–590. [CrossRef]
4. Li, K.; Su, Z.; Gao, Y.; Lin, X.; Pang, X.; Yang, B.; Tao, H.; Luo, X.; Liu, Y.; Zhou, X. Cytotoxic Minor Piericidin Derivatives from the Actinomycete Strain Streptomyces psammoticus SCSIO NS126. *Mar. Drugs* **2021**, *19*, 428. [CrossRef]
5. Zhang, Y.-M.; Li, H.-Y.; Hu, C.; Sheng, H.-F.; Zhang, Y.; Lin, B.-R.; Zhou, G.-X. Ergosterols from the Culture Broth of Marine Streptomyces anandii H41-59. *Mar. Drugs* **2016**, *14*, 84. [CrossRef]

6.   Liu, Y.; Li, X.-M.; Meng, L.-H.; Jiang, W.-L.; Xu, G.-M.; Huang, C.-G.; Wang, B.-G. Bisthiodiketopiperazines and Acorane Sesquiterpenes Produced by the Marine-Derived Fungus Penicillium adametzioides AS-53 on Different Culture Media. *J. Nat. Prod.* **2015**, *78*, 1294–1299. [CrossRef] [PubMed]

7.   Yurchenko, A.N.; Smetanina, O.F.; Ivanets, E.V.; Kalinovsky, A.I.; Dyshlovoy, S.A. Pretrichodermamides D–F from a marine algicolous fungus Penicillium sp. KMM 4672. *Mar. Drugs* **2016**, *14*, 122. [CrossRef] [PubMed]

8.   Dai, J.; Chen, A.; Zhu, M.; Qi, X.; Tang, W.; Liu, M.; Li, D.; Gu, Q.; Li, J. Penicisulfuranol A, a novel C-terminal inhibitor disrupting molecular chaperone function of Hsp90 independent of ATP binding domain. *Biochem. Pharmacol.* **2019**, *163*, 404–415. [CrossRef]

9.   Chen, S.; Cai, R.; Liu, Z.; Cui, H.; She, Z. Secondary metabolites from mangrove-associated fungi: Source, chemistry and bioactivities. *Nat. Prod. Rep.* **2021**, *39*, 560–595. [CrossRef]

10.   Luo, X.; Lin, X.; Tao, H.; Wang, J.; Li, J.; Yang, B.; Zhou, X.; Liu, Y. Isochromophilones A–F, cytotoxic chloroazaphilones from the marine mangrove endophytic fungus Diaporthe sp. SCSIO 41011. *J. Nat. Prod.* **2018**, *81*, 934–941. [CrossRef]

11.   Ren, X.; Chen, C.; Ye, Y.; Xu, Z.; Zhao, Q.; Luo, X.; Liu, Y.; Guo, P. Anti-inflammatory compounds from the mangrove endophytic fungus Amorosia sp. SCSIO 41026. *Front. Microbiol.* **2022**, *13*, 976399. [CrossRef] [PubMed]

12.   Jayasuriya, H.; Herath, K.B.; Ondeyka, J.G.; Polishook, J.D.; Bills, G.F.; Dombrowski, A.W.; Springer, M.S.; Siciliano, S.; Malkowitz, L.; Sanchez, M.; et al. Isolation and Structure of Antagonists of Chemokine Receptor (CCR5). *J. Nat. Prod.* **2004**, *67*, 1036–1038. [CrossRef]

13.   Nakanishi, S.; Ando, K.; Kawamoto, I.; Yasuzawa, T.; Sano, H.; Kase, H. KS-504 compounds, novel inhibitors of Ca^{2+} and calmodulin-dependent cyclic nucleotide phosphodiesterase from mollisia ventosa. *J. Antibiot.* **1989**, *42*, 1775–1783. [CrossRef] [PubMed]

14.   Weber, D.; Sterner, O.; Anke, T. Mollisianitrile, a New Antibiotic from Mollisia sp. A59-96. *Z. Für Nat. C* **2007**, *62*, 567–570. [CrossRef] [PubMed]

15.   Thines, E.; Arendholz, W.-R.; Anke, H.; Sterner, O. Benesudon, a New Antibiotic Fungal Metabolite from Cultures of Mollisia benesuada (Tul.) Phill. *J. Antibiot.* **1997**, *50*, 13–17. [CrossRef] [PubMed]

16.   Van Der Kerk, G.J.M.; Overeem, J.C. Mollisin, a dichloronaphthoquinone derivative produced by the fungus: Mollisia caesia. *Recl. Trav. Chim. Pays-Bas.* **1957**, *76*, 425–436. [CrossRef]

17.   Cai, J.; Chen, C.; Tan, Y.; Chen, W.; Luo, X.; Luo, L.; Yang, B.; Liu, Y.; Zhou, X. Bioactive Polyketide and Diketopiperazine Derivatives from the Mangrove-Sediment-Derived Fungus Aspergillus sp. SCSIO41407. *Molecules* **2021**, *26*, 4851. [CrossRef] [PubMed]

18.   Cai, J.; Wang, X.; Yang, Z.; Tan, Y.; Peng, B.; Liu, Y.; Zhou, X. Thiodiketopiperazines and Alkane Derivatives Produced by the Mangrove Sediment–Derived Fungus Penicillium ludwigii SCSIO 41408. *Front. Microbiol.* **2022**, *13*, 857041. [CrossRef]

19.   Chen, C.; Chen, W.; Tao, H.; Yang, B.; Zhou, X.; Luo, X.; Liu, Y. Diversified Polyketides and Nitrogenous Compounds from the Mangrove Endophytic Fungus Penicillium steckii SCSIO 41025. *Chin. J. Chem.* **2021**, *39*, 2132–2140. [CrossRef]

20.   Song, X.; Liu, C.; Chen, P.; Zhang, H.; Sun, R. Natural Product-Based Pesticide Discovery: Design, Synthesis and Bioactivity Studies of N-Amino-Maleimide Derivatives. *Molecules.* **2018**, *23*, 1521. [CrossRef]

21.   Koyama, N.; Nagahiro, T.; Yamaguchi, Y.; Masuma, R.; Tomoda, H.; Omura, S. Stemphones, Novel Potentiators of Imipenem Activity against Methicillin-resistant Staphylococcus aureus, Produced by Aspergillus sp. FKI-2136. *J. Antibiot.* **2005**, *58*, 695–703. [CrossRef] [PubMed]

22.   Tanahashi, T.; Takenaka, Y.; Nagakura, N.; Hamada, N. 2,3-Dialkylchromones from Mycobiont Cultures of the Lichen Graphis scripta. *Heterocycles* **2000**, *53*, 1589. [CrossRef]

23.   Harizani, M.; Katsini, E.; Georgantea, P.; Roussis, V.; Ioannou, E. New Chlorinated 2,5-Diketopiperazines from Marine-Derived Bacteria Isolated from Sediments of the Eastern Mediterranean Sea. *Molecules* **2020**, *25*, 1509. [CrossRef]

24.   Kokubun, T.; Veitch, N.C.; Bridge, P.D.; Simmonds, M.S. Dihydroisocoumarins and a tetralone from Cytospora eucalypticola. *Phytochemistry* **2003**, *62*, 779–782. [CrossRef] [PubMed]

25.   Lu, X.; Shen, Y.; Zhu, Y.; Xu, Q.; Liu, X.; Ni, K.; Cao, X.; Zhang, W.; Jiao, B. Diketopiperazine constituents of marine Bacillus subtilis. *Chem. Nat. Compd.* **2009**, *45*, 290–292. [CrossRef]

26.   Fang, Z.F.; Yu, S.S.; Zhou, W.Q.; Chen, X.G.; Ma, S.G.; Li, Y.; Qu, J. A new isocoumarin from metabolites of the endophytic fungus Alternaria tenuissima (Nees & T. Nees: Fr.) Wiltshire. *Chin. Chem. Lett.* **2012**, *23*, 317–320. [CrossRef]

27.   Mao, Z.; Zhang, W.; Wu, C.; Feng, H.; Peng, Y.; Shahid, H.; Cui, Z.; Ding, P.; Shan, T. Diversity and antibacterial activity of fungal endophytes from Eucalyptus exserta. *BMC Microbiol.* **2021**, *21*, 155. [CrossRef] [PubMed]

28.   Niu, S.; Liu, D.; Shao, Z.; Huang, J.; Fan, A.; Lin, W. Chlorinated metabolites with antibacterial activities from a deep-sea-derived *Spiromastix* fungus. *RSC Adv.* **2021**, *11*, 29661–29667. [CrossRef]

29.   Yamazaki, H.; Koyama, N.; Omura, S.; Tomoda, H. Structure-activity Relationships of Stemphones, Potentiators of Imipenem Activity against Methicillin-resistant Staphylococcus aureus. *J. Antibiot.* **2008**, *61*, 426–441. [CrossRef]

30.   Nobe, K.; Miyatake, M.; Nobe, H.; Sakai, Y.; Takashima, J.; Momose, K. Novel diacylglycerol kinase inhibitor selectively suppressed an U46619-induced enhancement of mouse portal vein contraction under high glucose conditions. *J. Cereb. Blood Flow Metab.* **2004**, *143*, 166–178. [CrossRef]

31.   Koyama, N.; Kobayashi, K.; Yamazaki, H.; Hiroshi, T. Inhibition of Lipid Droplet Accumulation in Mouse Macrophages by Stemphone Derivatives. *J. Antibiot.* **2008**, *61*, 509–514. [CrossRef] [PubMed]

32.   Wan, Z.; Fang, W.; Shi, L.; Wang, K.; Zhang, Y.; Zhang, Z.; Wu, Z.; Yang, Z.; Gu, Y. Novonestmycins A and B, two new 32-membered bioactive macrolides from Streptomyces phytohabitans HBERC-20821. *J. Antibiot.* **2014**, *68*, 185–190. [CrossRef] [PubMed]
33.   Wang, X.; Zhu, J.; Yan, H.; Shi, M.; Zheng, Q.; Wang, Y.; Zhu, Y.; Miao, L.; Gao, X. Kaempferol inhibits benign prostatic hyperplasia by resisting the action of androgen. *Eur. J. Pharmacol.* **2021**, *907*, 174251. [CrossRef] [PubMed]

Article

Secondary Metabolites with Antifungal Activities from Mangrove Derived Fungus *Monascus purpureus* WMD2424

Ming-Der Wu [1,†], **Jih-Jung Chen** [2,3,†] and **Ming-Jen Cheng** [4,*]

1. Bioresource Collection and Research Center (BCRC), Food Industry Research and Development Institute (FIRDI), Hsinchu 300, Taiwan
2. Department of Pharmacy, School of Pharmaceutical Sciences, National Yang Ming Chiao Tung University (NYCU), Taipei 112, Taiwan
3. Department of Medical Research, China Medical University Hospital, China Medical University, Taichung 404, Taiwan
4. Department of Life Science, Fu Jen Catholic University, New Taipei City 242, Taiwan
* Correspondence: chengfirdi@gmail.com
† These authors contributed equally to this work.

Abstract: The mold *Monascus*, also called red yeast rice, anka, or koji, has been used as the natural food coloring agent and food additives for more than 1000 years in Asian countries. It has also been used in Chinese herbology and traditional Chinese medicine due to its easing digestion and antiseptic effects. However, under different culture conditions, the ingredients in *Monascus*-fermented products may be changed. Therefore, an in-depth understanding of the ingredients, as well as the bioactivities of *Monascus*-derived natural products, is important. Here, through the thorough investigation into the chemical constituents of *M. purpureus* wmd2424, five previously undescribed compounds, monascuspurins A–E (**1–5**), were isolated from the EtOAc extract of mangrove-derived fungus *Monascus purpureus* wmd2424 cultured in RGY medium. All the constituents were confirmed via HRESIMS and 1D- and 2D-NMR spectroscopy. Their antifungal activity was also evaluated. Our results showed that four constituents (compounds **3–5**) possessed mild antifungal activity against *Aspergillus niger*, *Penicillium italicum*, *Candida albicans*, and *Saccharomyces cerevisiae*. It is worth mentioning that the chemical composition of the type strain *Monascus purpureus* wmd2424 has never been studied.

Keywords: *Monascus purpureus* wmd2424; Monascaceae; isoquinoline; antifungal activities

1. Introduction

Throughout human history, food has been used to satisfy hunger and provide nutrition. Nowadays, food can be widely used not only to eliminate diseases, but also to improve the quality of life. Finding beneficial food resources from the wisdom of your ancestors is a fairly effective strategy.

Despite plants, fungi (e.g., *Actinomucor* spp., *Amylomyces* spp., *Rhizopus* spp., *Monascus* spp., *Neurospora* spp., *Aspergillus* spp., *Penicillium* spp., *Torulopsis* spp., *Trichosporon* spp., and *Zygosaccharomyces* spp.) also take an important place in producing various food products in fermented forms [1]. Fungi of the genus *Monascus* (Monascaceae) have been used to ferment rice in Asia for centuries. It has been widely utilized as food additives, natural food coloring agent, food antiseptic, and healthy food for nearly two thousand years [2,3]. The production of red yeast rice was used as a Chinese folk medicine, recorded in old Chinese literature as a means of easing digestion and soothing pain. *Monascus* first became known in the West back in 1884, when van Tieghem introduced the usage of red powder (*Monascus ruber*) in Java local populations. Until 1979, Endo et al. isolated monacolin K analogues from *M. ruber* and opened up the investigation of ingredients and bioactivities from *Monascus* [4]. Monacolin K is the same compound as cholesterol-lowering medicine

lovastatin, which has been approved by the FDA to become the first commercial statin in 1987 [5].

Monascus-fermented rice, also called anka, koji, or red yeast rice, is obtained via the fermentation of rice with fungi of the genus *Monascus*, mainly *M. purpureus, M. pilosus, M. ruber, M. kaoliang,* and *M. anka* [3]. Recently, *Monascus*-fermented rice has been reported for various biological functions. For example, they are helpful for metabolism-related disease with cholesterol-lowering effects [6], cardiovascular diseases [6], and diabetes [7,8]. Also, much evidence has also depicted their anti-inflammation activity [9–11], which is also highly associated with cardiovascular disease [12], cancer [13–17], diabetes [18,19], and Alzheimer's disease [20,21]. Some investigations reveal the anti-microorganism activity of red yeast rice such as anti-bacteria [22–29] and anti-HCV [30]. In recent years, the phytochemical investigation of *Monascus* species have has resulted in the isolation and identification of azaphilones (yellow, orange, and red pigments), monacolins, flavonoids, fatty acids, organic acids, dimerumic acid, and γ-aminobutyric acid, etc. [9,14,27,31–34]. However, studies on the secondary metabolites of *Monascus* grown in fermentation conditions other than red yeast rice are limited. We recently isolated an unpublished novel strain, named WMD2424, from the mangrove wetland in Chiayi County, which had a unique morphology and possessed antimicrobial activities as determined by our preliminary screening. This strain was determined to be *Monascus purpureus* based on its phenotypic and genotypic data (Figure 1).
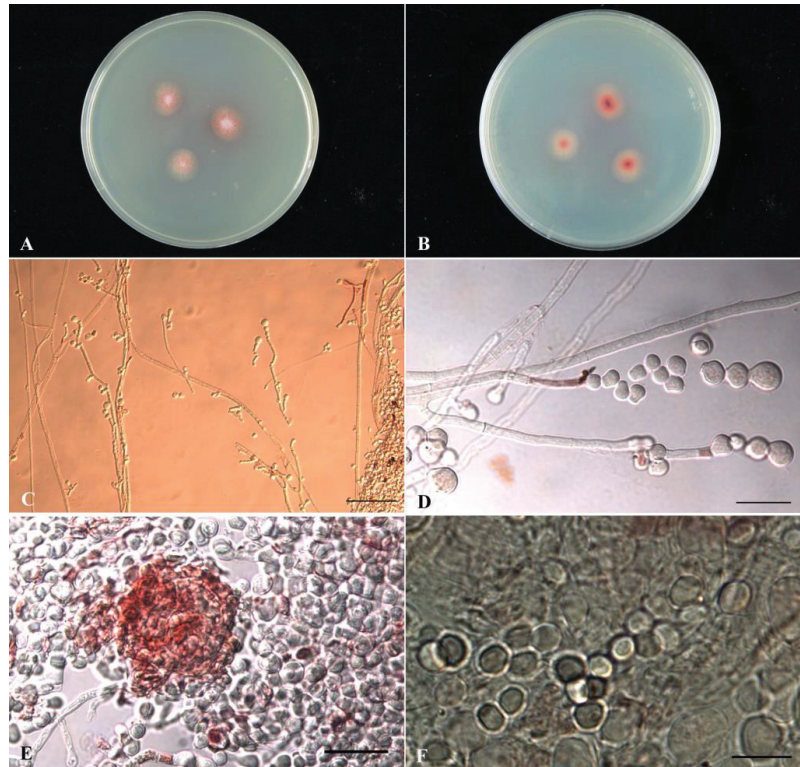

Figure 1. (**A**,**B**) Colony morphology, CYA, 25 °C, cultured for 7 days, (**A**) the front of the colony; (**B**) the back of the colony. (**C**–**F**) Microstructure: (**C**) hyphae and branches (bar = 100 μm); (**D**) conidiophores and conidia (bar = 25 μm); (**E**) ascocarp (bar = 25 μm); (**F**) ascospores (bar = 10 μm).

As part of our continuing efforts to explore the chemical diversity of marine fungal metabolites, *Monascus purpureus* WMD2424, fermented using RGY medium (3% rice starch, 7% glycerol, 1.5% polypeptone, 3% soybean powder, 0.2% MgSO$_4$, and 0.2% NaNO$_3$), was investigated. The scaled-up fermentation and extensive chromatographic separation of the EtOAc extract resulted in the isolation of 5 new metabolites, monascuspurins A–E (**1**–**5**), and their antifungal activity was also evaluated. Herein, we report the structural determination of the new compounds (Figure 2) and the bioactivities of these compounds.
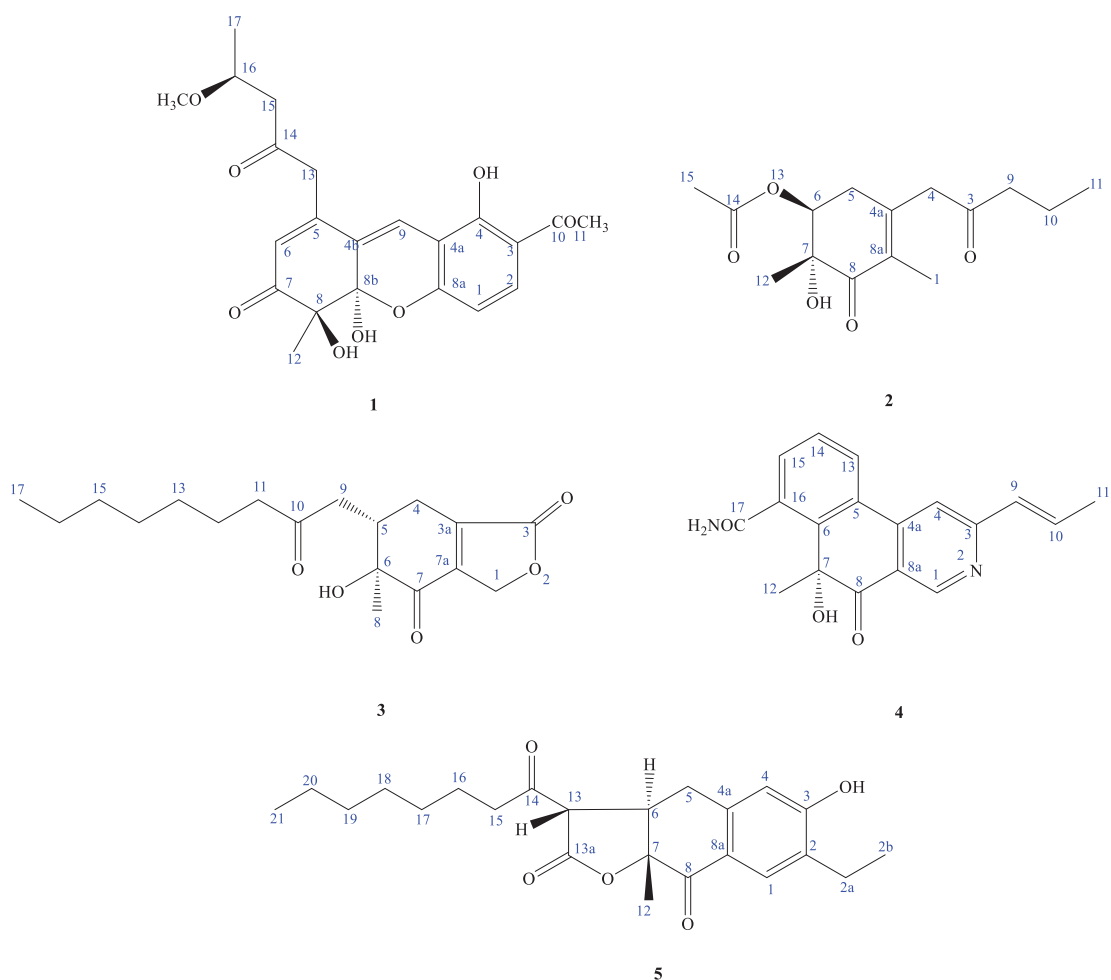
Figure 2. Compounds **1**–**5**, isolated from *Monascus purpureus* wmd2424.

2. Results

2.1. Taxonomic Identification (Phenotypic and Genotypic Data) of Monascus purpureus wmd2424

The sample WMD2424 is a filamentous fungal strain collected from the Chiayi mangrove wetland, inoculated in CYA medium, and cultured at 25 °C for 7 days. The diameter of the colony on the CYA plate is 15 mm, and the front color of the colony is reddish orange; the colony is velutinous, without radial grooves (sulcate), exudate (exudate), and soluble pigment (soluble pigment); the back of the colony is reddish orange. Observed under an optical microscope, the mycelium has a septate, and the thin wall is colorless; the conidia

are colorless, and the wall is smooth; conidia (conidia) grow on the top or lateral hyphae, with several clusters, pear-shaped, and a truncated bottom, 8.1–16.7 × 6.3–15.5 μm in size, with smooth walls that are colorless; the outer walls of the ascomata are light red but all immature; the same condition was found after 14 days of culture, and only one ascoma was found. The fruit contains ascospores, and the ascospores have a smooth, colorless outer wall and a broad oval shape, with a size of 4.3–5.6 × 3.8–4.8 μm. Partial sequence analysis of the β-tubulin gene fragment was carried out. The total length of the sequence was 1019 bp, compared with the GenBank database, and analyzed and judged with reference to the taxonomic literature. The results showed that the sequence similarity with Monascus purpureus wmd2424 was 99.88% (838/839). The strain was identified as Monascus purpureus according to the colony culture morphology, microstructural characteristics and partial sequence analysis of β-tubulin gene fragment.

2.2. Structure Elucidation of Compounds

Compound **1** was obtained as oil with an $[\alpha]^{26}_D$: +34.2 (*c* 0.01, CHCl$_3$). The molecular formula was established as C$_{22}$H$_{24}$O$_8$ via HRESIMS, indicating 11 degrees of unsaturation. The UV spectrum showed maximum absorption at 268 and 360 nm. The IR spectrum showed absorptions at 3406, 1710, and 1680 cm^{-1}, corresponding to the hydroxyl group and carbonyl groups. The ^{1}H NMR spectroscopic data (Table 1) of **1** show three methyl groups, including one singlet at δ_H 1.48 (3H, s, H-12), one triplet at δ_H 1.28 (3H, t, *J* = 6.4 Hz, H-17), and one acetyl at δ_H 2.60 (3H, s, H-11). It also showed two methylene groups [δ_H 2.72 (1H, d, *J* = 16.2 Hz, H-15), 2.75 (1H, d, *J* = 16.2 Hz, H-15), 3.72 (1H, d-like, *J* = 17.0 Hz, CH$_2$-13), 3.77 (1H, d-like, *J* = 17.0 Hz, CH$_2$-13)], one oxymethine [δ_H 4.25 (1H, m, H-16)], one *meta*-coupling aromatic ring at δ_H 6.68 (1H, dd, *J* = 8.8 Hz, H-1) and 7.71 (1H, d, *J* = 8.8 Hz, H-2), two olefinic protons at δ_H 5.94 (1H, s, H-6) and 7.53 (1H, s, H-9), one intramolecular hydrogen bond at δ_H 13.4 (1H, s, OH-4), and two hydroxyl groups at δ_H 3.50 (1H, s, OH-8 or OH-8b) and 4.15 (1H, s, OH-8b or OH-8). The ^{1}H (Table 1), 2D-NMR (Figures 3 and 4), IR, and UV spectra showed that compound **1** was a xanthene derivative similar to xanthonoides as monasxanthone A [35]. The molecular weight of **1** is 30 units more than **1** and showed another proton peak at δ_H 4.25 (1H, m, H-16) and 3.21 (3H, s, OCH$_3$-16), suggesting the existence of a methoxy group in **1**. The NMR spectra of **1** represent a 4-methoxy-2-oxopentyl moiety at C-5 position in **1** instead of a pentan-2-one in monasxanthone A. Thus, the structure of **1** was elucidated as 7-acetyl-4,8-dihydroxy-1-(4-methoxy-2-oxopentyl)-4-methyl-4,4a-dihydro-3*H*-xanthen-3-one and named monascuspurin A. The relative configuration of **1** was deduced from the NOESY spectrum (Figure 4). The absolute configuration of **1** was further established as (8*S*,8b*R*,16*S*), for the experimental electronic circular dichroism (ECD) curve was in line with its theoretical curve, which was calculated by using the time-dependent density functional theory (TD-DFT) approach [36] (Figure 5).

Table 1. ^{1}H-NMR data for Compounds **1–5** in CDCl$_3$ (δ in ppm, *J* in Hz, and 600 MHz in CDCl$_3$).

No.	1	2	3	4	5
1	6.68 (1H, dd, *J* = 8.8)	1.76 (3H, q, *J* = 1.2)	4.89 (1H, dd, *J* = 18.0, 4.5) 5.05 (1H, dd, *J* =18.0, 3.3)	9.05 (1H, s)	7.91 (1H, s)
2	7.71 (1H, d, *J* = 8.8)				
2a					2.64 (3H, q, *J* = 7.2)
2b					1.26 (3H, *J* = 7.2)
4		3.33 (1H, d, *J* = 16.8) 3.48 (1H, d, *J* = 16.8)	2.10–2.12 (1H, m) 2.95, d (1H, dd, *J* = 19.0, 4.5, 3.3)	7.59 (1H, s)	6.63 (1H, s)
5		2.49 (1H, ddd, *J* = 18.0, 10.7, 1.2 Hz, H$_{ax}$-5) 2.53 (1H, ddd, *J* = 18.0, 6.2, 1.2 Hz, H$_{eq}$-5)	2.80–2.82 (1H, m)		3.15 (1H, dd, *J* =16.0, 4.2, H-eq) 2.92 (1H, dt, *J* = 16.0, 12.3, H-ax)
6	5.94 (1H, s)	4.83 (1H, dd, *J* = 10.7, 6.2)			3.34 (1H, td, *J* = 12.6, 4.2)
8			1.24 (3H, s)		
9	7.53 (1H, d, *J* = 8.8)	2.45 (2H, t, *J* = 7.8)	2.49–2.52 (1H, m) 3.03 (1H, dd, *J* = 18.0, 3.2)	6.65 (1H dq, *J* = 15.6, 1.8)	
10		1.61 (2H, sextet, *J* = 7.8)		7.13 (1H, dd, *J* = 15.6, 6.8)	
11		0.92 (3H, t, *J* = 7.8)	2.44–2.47 (2H, m)	2.05 (3H, dd, *J* = 6.8, 1.8)	
12		1.38 (3H, s)	1.55–1.60 (2H, m)	1.85 (3H, s)	1.47 (3H, s)
13	3.72 (1H, d-like, *J* = 17.0), 3.77 (1H, d-like, *J* = 17.0)		1.20–1.35 (2H, m)	8.04 (1H, dd, *J* = 7.8)	3.72 (3H, d, *J* = 12.6)
14			1.20–1.35 (2H, m)	7.70 (1H, t, *J* = 7.8)	
15	2.72 (1H, d, *J* = 16.2), 2.75 (1H, d, *J* = 16.2)	2.09 (3H, s)	1.20–1.35 (2H, m)	7.90 (1H, dd, *J* = 7.8, 0.6)	2.65/3.03 (each 1H, dt, *J* = 18.0, 7.2)
16	4.25 (1H, m)		1.20–1.35 (2H, m)		1.64 (2H, pentet, *J* = 7.2)
17	1.28 (3H, t, *J* = 6.4)		0.90 (3H, t, *J* = 7.2)		1.30–1.33 (2H, m)
18					1.30–1.33 (2H, m)

Table 1. *Cont.*

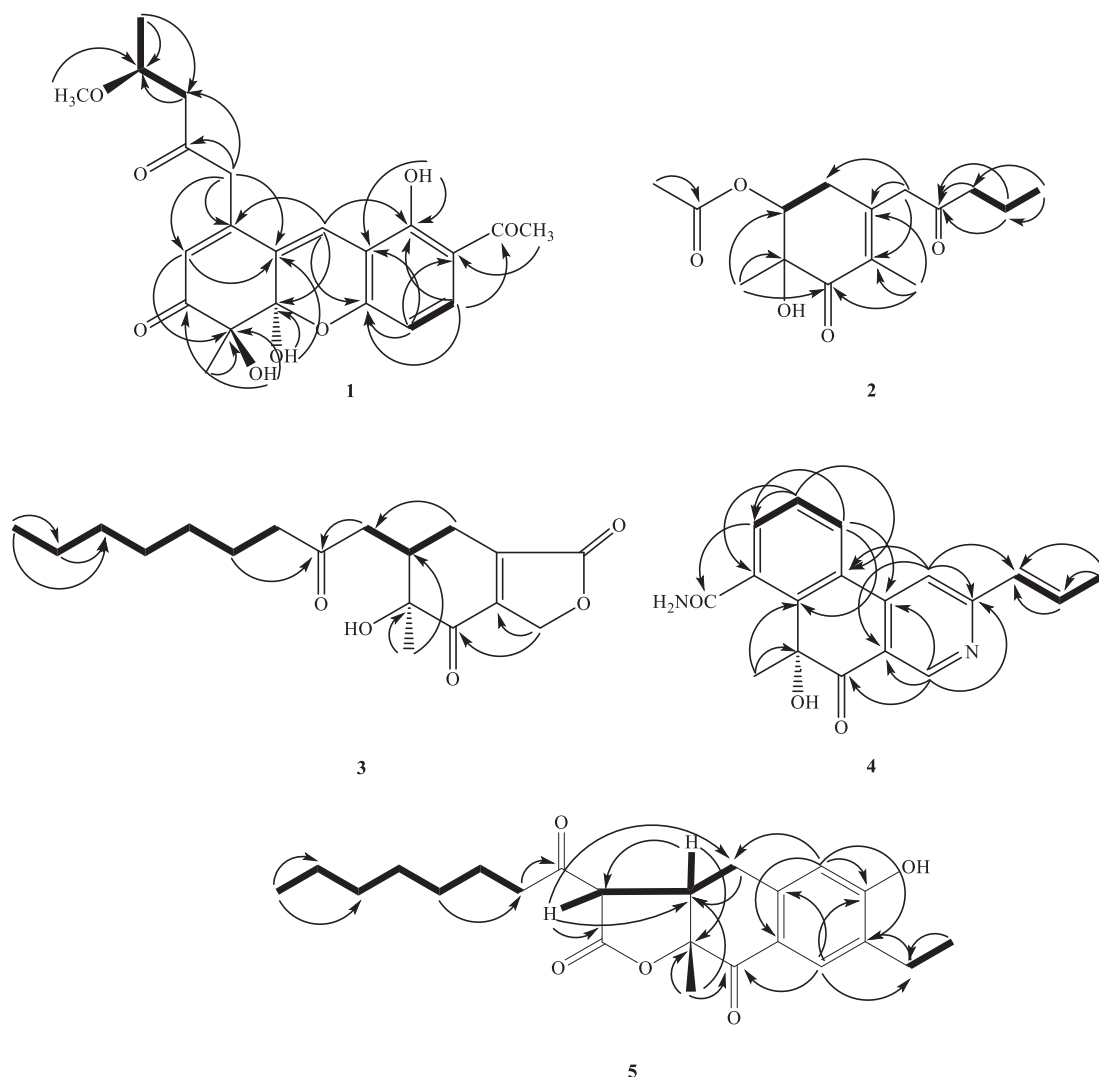| No.	1	2	3	4	5
19					1.30–1.33 (2H, m)
20					1.30–1.33 (2H, m)
21					0.91 (3H, t, J =7.2)
OH-3					5.42 (1H, br s)
OCH$_3$	16.21 (3H, s)				
OH-4	13.4 (1H, s)				
OH-8	3.50 (1H, br s)/4.15 (1H, br s)				
OH-8b	4.15 (1H, br s)/3.50 (1H, br s)				

Figure 3. Key COSY (^{1}H–^{1}H) and HMBC (^{1}H→^{13}C) correlations of compounds **1–5**.

Compound **2** was obtained as an optically active colorless oil. [α]^{26}$_D$: +54.2 (*c* 0.01, CHCl$_3$). The molecular formula was determined as C$_{15}$H$_{22}$O$_5$ (five degrees of unsaturation) via HR-ESI-MS (*m/z* 305.13598, ([M+Na]$^+$, C$_{21}$H$_{30}$NaO$_5^+$; calcd. 305.13592)), which was in agreement with the ^{1}H- and ^{13}C-NMR data (Table 1). The UV spectrum absorption λ$_{max}$ (MeOH) at 242 nm, and a strong IR absorption at 1675 cm^{-1}, as well as the observation of the featuring carbon resonances [δ$_C$ 132.1 (C-8a), 146.2 (C-4a), and 195.1 (C-8)] in the ^{13}C-NMR spectrum (Table 1), revealed the presence of an α,β-unsaturated carbonyl functionality in **1**. The remaining IR spectrum revealed the presence of the OH group (3410 cm^{-1}), and ester (1715 cm^{-1}), respectively. The ^{1}H-NMR spectrum of **2** exhibited signals attributed to one allylic Me (δ$_H$ 1.76 (3H, q, *J* = 1.2 Hz, Me-1), signals of α-methylene protons of one ketone [δ$_H$ 3.33/3.48 (each 1H, d, *J* = 16.8 Hz, CH$_2$-4), 2.45 (2H, t, *J* = 7.8 Hz, CH$_2$-9)], one β-methylene signals of ketone (δ$_H$ 1.61 (2H, sextet, *J* = 7.8 Hz, CH$_2$-10)), one aliphatic CH$_2$

proton (δ_H 2.49 (1H, ddd, J = 18.0, 10.7, 1.2 Hz, Hax-5) and 2.53 (1H, ddd, J = 18.0, 6.2, 1.2 Hz, Heq-5)]), one oxymethine [δ_H 4.83 (1H, dd, *J* = 10.7, 6.2 Hz, H-6)], one acetoxy group [δ_H 2.09 (3H, s, H-15)], and one terminal Me moiety (δ_H 0.92 (3H, t, *J* = 7.8 Hz, H-11)). Fifteen C-atom signals (Table 2) corresponding to six quaternary C-atoms (including three carbonyl groups, one oxygenated quaternary carbon), one OCH, two olefinic carbons, four CH_2, and four CH_3 groups were observed in the ^{13}C-NMR and DEPT spectra.
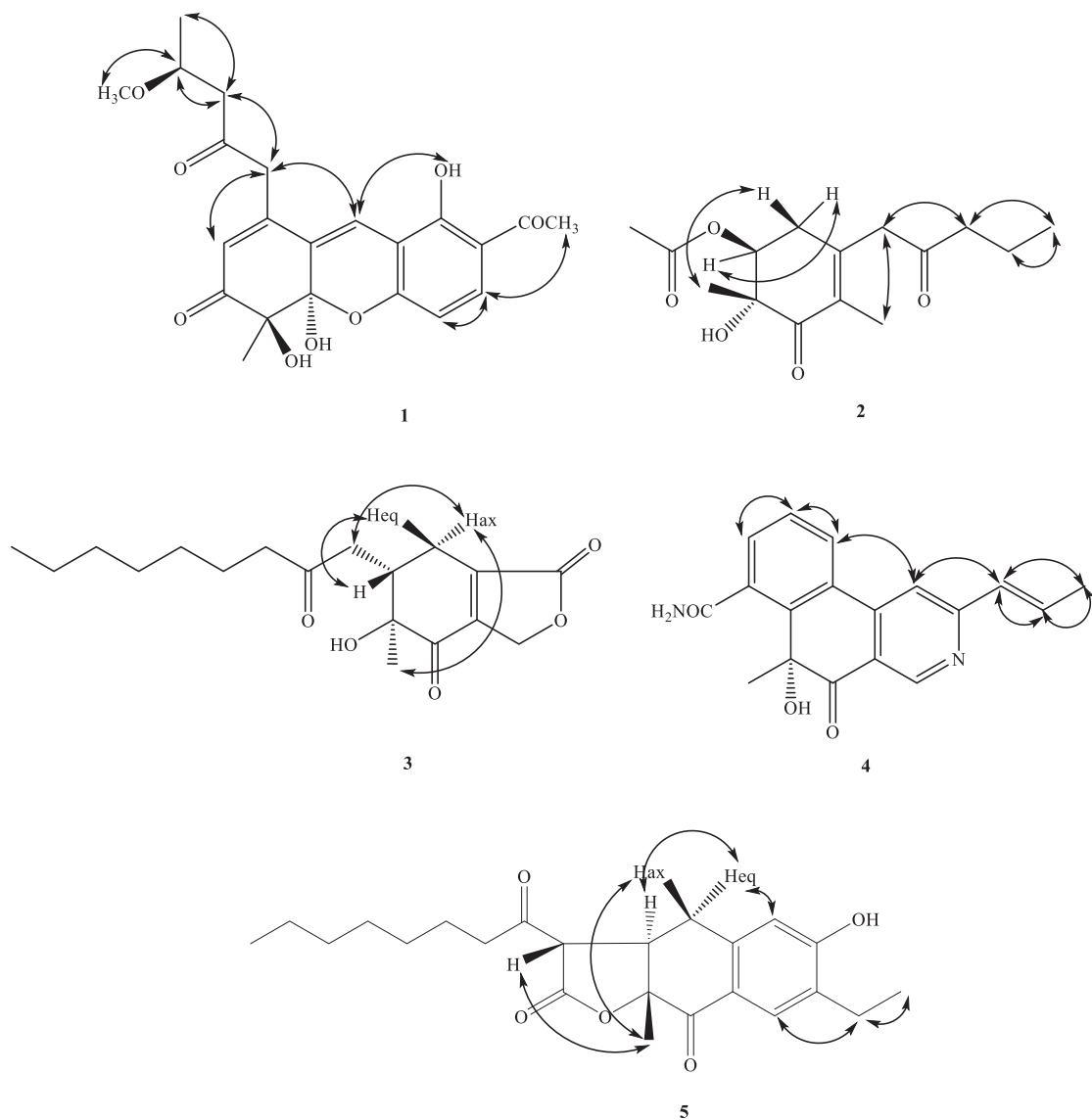

Figure 4. Key NOESY correlations (↔) of compounds **1**–**5**.
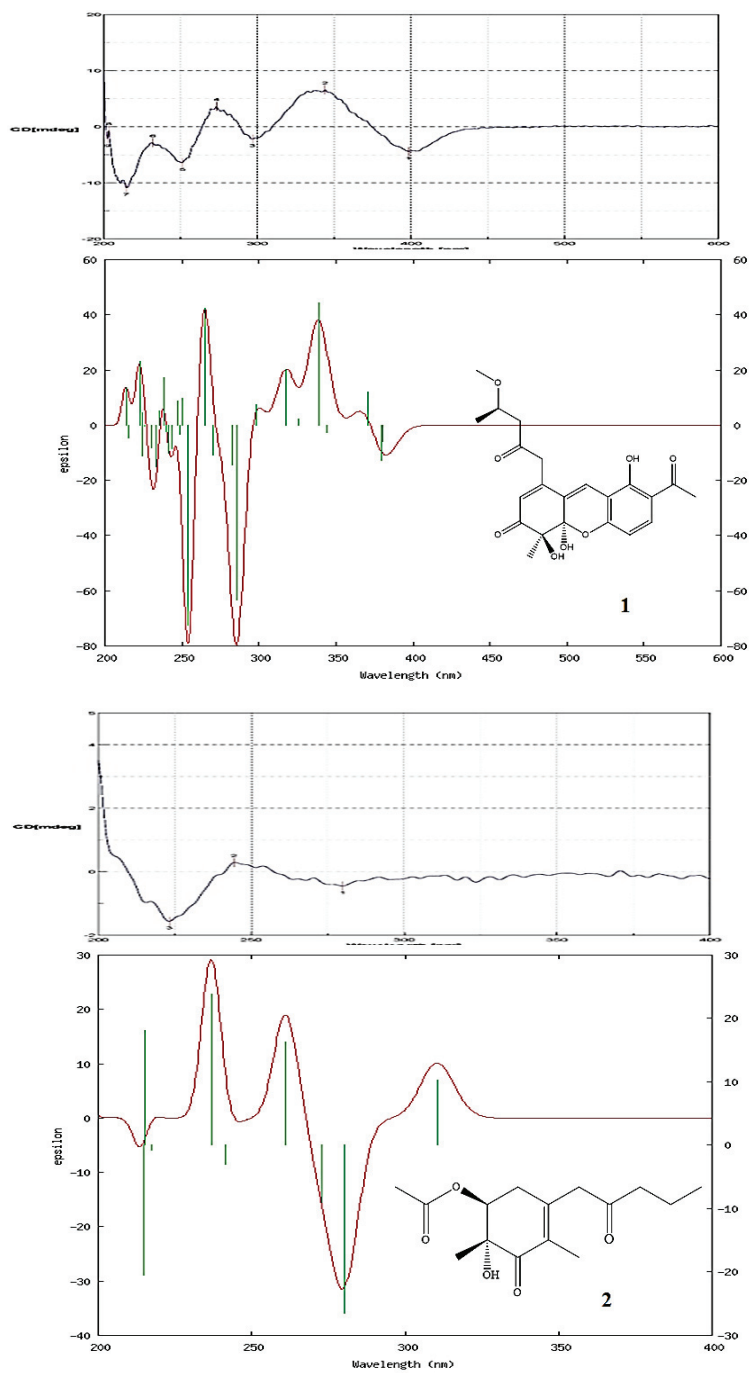
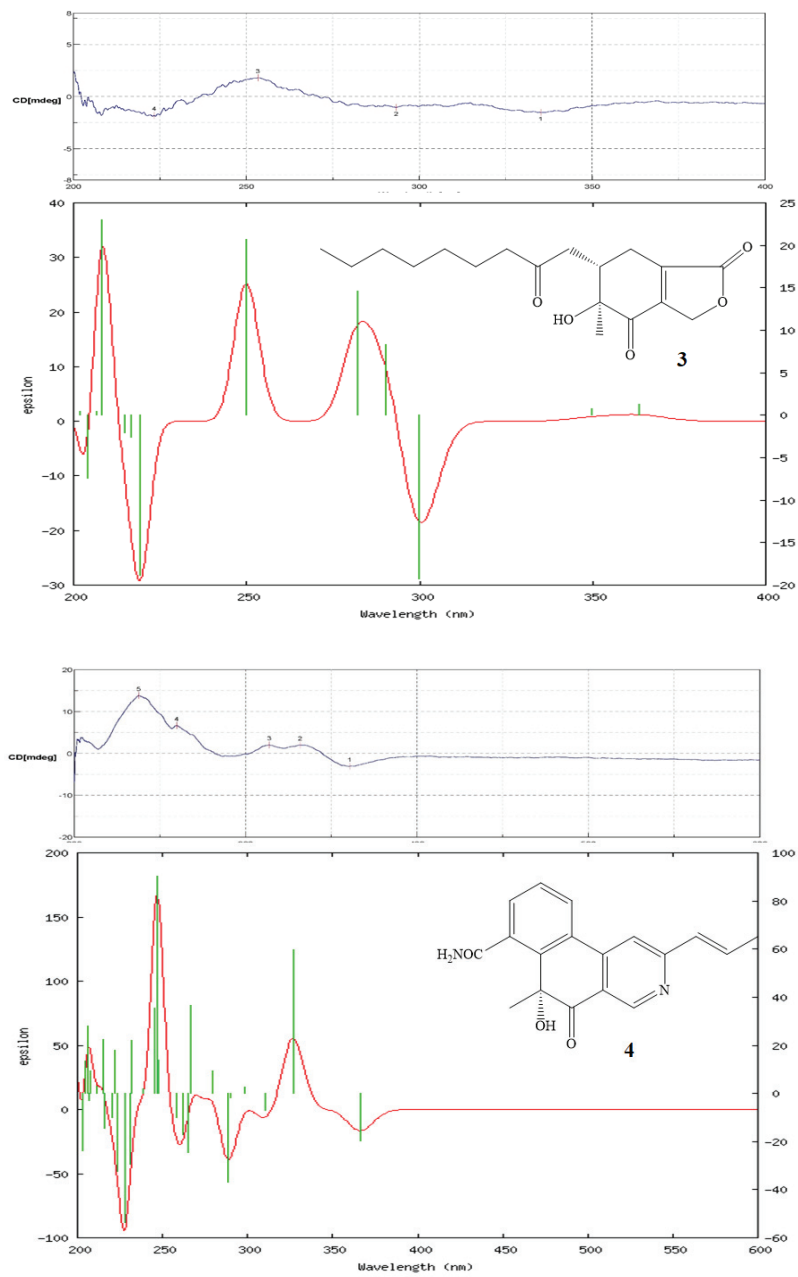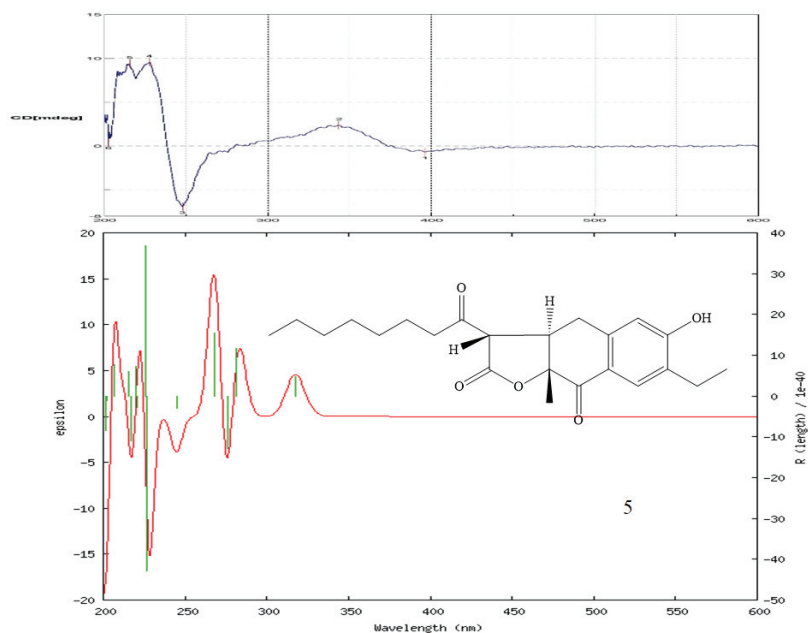**Figure 5.** *Cont.*

Figure 5. *Cont.*

Figure 5. Experimental CD spectra (upper) and the calculated ECD (lower) spectra of compounds **1–5**.

The ^{1}H- and ^{13}C-NMR spectra of **2** (Tables 1 and 2) were similar to those of monaphilone C [31], except that an acetoxy moiety at C-6 of **2** replaced a 2-oxoheptyl moiety at C-6 of monaphilone C. The planner structure of **2** was confirmed using the COSY and HMBC experiments (Figure 3). The stereochemistry of **2** was proposed on the basis of the NOESY experiments (Figure 4). The H-6/CH$_3$-12 has no correlation in the NOESY spectrum (Figure 4) represented acetoxy group and CH$_3$-12 are *syn*-form. The physicochemical data and NMR spectra of compound **2** and the known compound monapurpureusone [31] are similar; the only difference is that the specific rotation of monapurpureusone is negative, while the specific rotation of **2** is positive, and it can be inferred that the two are stereoisomers. On comparing the reference to the (6*S*,7*R*)-configuration of FK17-P2b ($[\alpha]^{26}_D$: + 26.0 (c 0.1, MOH)) [37], the relative configuration of **2** can be assigned as *rel*-(6*S*,7*R*)-configuration, and named monascuspurin B. The absolute configuration of **2** was defined via a comparison of the experimental and calculated ECD data (Figure 5). Therefore, the absolute configuration of **2** was undoubtedly determined as (6*S*,7*R*).

Compound **3** was isolated as oil with $[\alpha]^{26}_D$: +74.2 (c 0.01, CHCl$_3$). Its molecular formula was determined to be C$_{18}$H$_{26}$O$_5$ based on the HRESIMS [M+Na]$^+$ peak at 345.16780 (Calcd.: C$_{18}$H$_{26}$O$_5$, 345.16779), referring six degrees of unsaturation. The maximum absorption of an IR spectrum showed the presence of the hydroxyl group (3410 cm^{-1}), γ-lactone (1770 cm^{-1}), and α,β-unsaturated C=O (1715 cm^{-1}). The UV spectrum exhibited the absorption band at 285 nm. The CD spectrum showed a positive Cotten effect at 250 nm and depict the negative Cotten effect at 225, 290, and 335 nm.

Table 2. ^{13}C-NMR data for compounds **2–5** (δ in ppm, 150 MHz for ^{13}C NMR in CDCl$_3$).

No.	1	2	3	4	5
1	108.8	12.3	67.2	149.8	130.4
2	134.0				130.0
2a					22.0
2b					14.2
3	114.8	205.4	170.9	161.8	159.0
3a			144.5		
4	161.2	48.8	25.9	114.0	115.8
4a	110.2	146.8		143.5	140.9
4b	125.3				
5	149.2	37.9	40.7	126.7	30.2
6	123.5	67.9	63.2	151.0	43.1
7	198.4	85.1	198.5	84.9	84.2
7a			148.9		
8	79.8	195.6	19.2	192.8	192.1
8a	157.3	132.0		122.7	124.7
8b	97.2				
9	122.7	45.0	41.8	131.8	
10	203.1	17.2	209.1	137.2	
11	26.6	13.6	43.4	18.8	
12	23.0	16.2	23.5	27.3	17.4
13	48.9		29.0	129.1	54.9
13a			29.0		170.9
14	206.1	170.2	29.0	132.3	203.9
15	50.3	21.3	31.4	127.8	42.8
16	73.4		22.4	125.8	23.5
17	23.0		13.9	168.5	29.1
18					29.1
19					31.7
20					22.8
21					13.9

The ^{1}H-NMR spectrum (Table 1) displayed an oxononyl group at [δ_H 0.90 (3H, t, J = 7.2 Hz, H-17), 1.20–1.35 (8H, m, H-13~H-16), 1.55–1.60 (2H, m, H-12), 2.44–2.46 (2H, m, H-11)], one methyl group [δ_H 1.24 (3H, s, H-8)], signals of the α-methylene protons of one ketone [δ_H 2.49–2.52 (1H, m, 1H of CH$_2$-9), 3.03 (1H, dd, J = 18.0, 3.2 Hz, 1H of CH$_2$-9), and 2.44–2.47 (2H, m, CH$_2$-11)], one oxymethylene [δ_H 4.89 (1H, dd, J = 18.0, 4.5 Hz, 1H of CH$_2$-1), 5.05 (1H, dd, J = 18.0, 3.3 Hz, 1H of CH$_2$-1)], one non-equivalent methylene proton at [δ_H 2.10–2.12 (1H, m, 1 H of CH$_2$-4), 2.95 (1H, ddd, J = 19.0, 4.5, 3.3 Hz, 1 H of CH$_2$-4)], and one methine [δ_H 2.80–2.82 (1H, m, H-5)]. Eighteen C-atom signals (Table 2) corresponding to six quaternary C-atoms, one CH, nine CH$_2$, and two CH$_3$ groups, were observed in the ^{13}C-NMR and DEPT spectra. Since four out of six unsaturation equivalents were accounted for via the above-mentioned ^{13}C-NMR data, **1** was inferred to have two rings (one as a six-membered and another as a five-membered ring). In addition, two rings

were further determined as a cyclohex-2-enone skeleton combined with one γ-lactone ring via the detail HMBC and COSY analyses.

The ^{1}H- and ^{13}C-NMR spectra of **3** (Table 1) were similar to those of monaphilone A [31]; the major difference was the presence of signals for an γ-lactone attached to C-3a and 7a in **3**, instead of signals for a 4*H*-pyran group in monaphilone A [31]. HMBC correlations between the H-atom signals at δ_H 4.89/5.05 (CH$_2$(1)) and the C-atom signals at δ_C 198.3 (C-7) once indicated that the γ-lactone was located at C-3a and 7a of the cyclohex-2-enone ring. The relative configuration of **3** was derived using a NOESY spectrum (Figure 4) and a comparison with similar compounds [31], the relative configuration of which was based on a NOESY analyses. No NOEs for H-5/Me$_{ax}$-8 and H$_{ax}$-4 indicated that Me-8 and H$_{ax}$-4 were on the same side of the molecular plane, tentatively assumed as α-orientation.

The H-5 was occupied at axial β-oriented, which was further confirmed by the NOE H-5/H$_{eq}$-4. The relative configuration at C-5 and 6 were determined to be (5*S**,6*S**) based on the correlation between the [α]$_D$ value and the known configuration at C-5/C-6 for monaphilone A type derivatives [31]. In order to determine the absolute configuration of **3**, the theoretical electronic circular dichroism (ECD) spectra of 4 possible stereoisomers were calculated using a time-dependent density-functional theory (TDDFT) calculation, and the calculated ECD curve of (5*S*,6*S*) revealed good agreement with the experimental spectrum of **2** (Figure 5). Therefore, the absolute configuration of **3** was assigned as (5*S*,6*S*) and named as monascuspurin C.

Compound **4** was obtained as colorless oil. The molecular formula was determined as C$_{18}$H$_{16}$N$_2$O$_3$ on the basis of the [M+Na]$^+$ peak at *m/z* 331.10588 (calcd. 331.10586 for C$_{18}$H$_{16}$NaN$_2$O$_3$) in its HR-ESI-MS. The UV absorptions (λ$_{max}$ 220, 252, and 312 nm) confirmed the presence of a pyridine moiety [38]. IR absorption bands were assigned to amide (3400 cm^{-1}), multiple carbonyls C=O (1712 and 1656 cm^{-1}), and the pyridine ring (1589, 1535, and 1458 cm^{-1}) functional groups. Twelve indices of hydrogen deficiency (IHD) were determined from the molecular formula, ^{13}C-NMR (Table 2), and DEPT spectra. The CD spectrum showed positive Cotten effect at 240, 262, 319, and 333 nm, and negative Cotten effect at 365 nm.

Interpretation of the ^{1}H-NMR spectrum of **4** (Table 1) exhibited the signals of one 2,4,5-trisubstituted pyridine ring [δ_H 9.03 (1H, *s*, H-1), 7.59 (*s*, H-4)], one trans-propenyl unit [δ_H 2.05 (3H, dd, *J* = 6.8, 1.8 Hz, H-11), 6.65 (1H dq, *J* = 15.6, 1.8 Hz, H-9), 7.13 (1H, dq, *J* = 15.6, 6.8 Hz, H-10)], one Me group [δ_H 1.85 (3H *s*, Me-12)], as well as one ABC system aromatic ring [δ_H 7.70 (1H, t, *J* = 8.0 Hz, H-14), 7.90 (1H, dd, *J* = 8.0, 0.8 Hz, H-15), and 8.04 (1H, dd, *J* = 8.0, 0.8 Hz, H-13)]. The ^{13}C and DEPT NMR spectra indicated (Table 2) that compound **4** is a pyridine derivative with signals for 18 C-atoms, which were classified as nine quaternary C-atoms comprising six olefinic C-atoms, one amide C-atom (δ_C 168.5 (C-17), one ketone groups (δ_C 192.8 (C-8)), one oxygenated quaternary carbon [δ_C 84.9 (C-7)], one Me group (δ_C 27.3 (C-12), and one trans-propenyl unit [δ_C 131.8 (C-9), 137.2 (C-10), 18.8 (C-11)].

The ^{1}H- and ^{13}C-NMR spectra of **4** (Table 1) were similar to those of monascopyridine C and D [38]; the major difference was the presence of signals for ABC system aromatic ring attached between C-5 and C-6 in **4**, instead of signals for an alkyl groups in monascopyridine C and D. HMBC correlations between the H-atom signals at δ_H 8.04 (H-13) and the C-atom signals at δ_C 151.0 (C-6), and 143.5 (C-4a) and δ_H 7.70 (H-14) and the C-atom signals at δ_C 126.7 (C-5), indicated that the ABC system aromatic ring was bounded at C-5 and 6. The other key correlations of HMBC were illustrated in Figure 3.

Furthermore, the attachment of the amide to C-17, the methyl group to C-7, and the trans-propenyl group located at C-3, were disclosed according to the HMBC cross-peaks of δ_H 7.90 (H-15)/δ_C 168.5 (C-17), δ_H 1.85 (H-12) to C-6/C-7/C-8, and δ_H 7.59 (H-4) to C-9.

On the basis of the evidence, the entire structure of **4** was confirmed and named monascuspurin D. The relative configuration at C-7 was determined to be 7*R* based on the correlation between the [α]$^{26}_D$:+ 15.9 (*c* 0.01, CHCl$_3$) and the known configuration at C-7 for (*R*)-2-hydroxy-2-methylcyclohexanone derivatives [39]. The absolute configuration of

4 was defined via a comparison of the experimental and calculated ECD data (Figure 5). Therefore, the absolute configuration of **4** was determined as 7*R*.

Compound **5** was obtained as an optically active oil. $[\alpha]^{26}_D$: +56.7 (*c* 0.01, CHCl$_3$). The molecular formula was determined as C$_{23}$H$_{30}$O$_5$ on the basis of the [*M*+H]$^+$ peak at *m*/*z* 409.19912 (calcd. 409.19909 for C$_{23}$H$_{30}$NaO$_5$) in its HR-ESI-MS. The UV absorptions (λ_{max} 235 and 285 nm) confirmed the presence of a benzenoid nucleus. The bands at 3400, 1780, 1695, and 1615/1577 cm^{-1} in the IR spectrum revealed the presence of a hydroxyl group, γ-lactone, and aromatic ring, respectively. Nine indices of hydrogen deficiency (IHD) were determined from the molecular formula, ^{13}C-NMR (Table 1), and DEPT spectra. The ^{1}H-NMR and ^{13}C-NMR spectra (Table 2) of **5** were similar to those of ankaflavin [9], except that a 2-ethylphenol group of **5** replaced a (*E*)-6-(prop-1-en-1-yl)-2*H*-pyran group at C-4a–C-8a of ankaflavin. Further confirmation using the HMBC correlations (Figure 3) of H-1/C-3, 4a, 2a, H-4/C-2, 3, 5, 8a, and H-2b/C-2, 2a, verified the junction of the 2-ethylphenol unit at C-4a and C-8a. The correlations of H-1/H-2a and H-4/CH$_2$-5 were also observed in the NOESY experiment (Figure. 4) and further supported the position of each aromatic substitution. The ^{1}H- and ^{13}C-NMR, COSY (Figure 3), NOESY (Figure 4), HSQC, and HMBC (Figure 3) experiments confirmed the structure as 7-ethyl-3-hexanoyl-6-hydroxy-9a-methyl-3a,9adihydronaphtho[2,3-*b*]furan-2,9(3*H*,4*H*)-dione, and designated monascuspurin E.

The dextrorotatory optical activity of **5**, gathered from the NOESY spectrum (Figure 4), indicates that Hax-5 is correlated to H-12 and H-13, and H-6 has no NOE contacts with Hax-5, H-12, and H-13. It can be concluded that Hax-5, H-12, and H-13 are on the same side, and H-6, H-12, and H-13 are on the opposite side, and once again it indicated that the relative configuration of **5** is (6*R*,7*R*,13*S*), as in the case of ankaflavin [9]. In order to determine the absolute configuration of **5**, the theoretical ECD spectra of all possible stereoisomers were calculated using the TDDFT calculation, and the calculated ECD curve of the isomer (6*R*,7*R*,13*S*) revealed a good agreement with the experimental one (Figure 5). Therefore, the absolute configuration of **5** was assigned as (6*R*,7*R*,13*S*)-form and named as monascuspurin E.

3. Discussion

Red yeast rice has been used in food and traditional Chinese medicine since ancient times. In recent years, research has also found that red yeast rice bacteria can produce many active secondary metabolites. In order to further explore the efficacy of different strains of red yeast rice and expand the application range of red yeast rice, in this study, a strain wmd2424 was isolated from the mangrove forest in Chiayi Wetland, and the strain was identified as *Monascus purpureus* via the results of colony culture morphology, microstructural characteristics, and partial sequence analysis of the β-tubulin gene fragment. After liquid fermentation using RGY medium, extraction with ethyl acetate, and analysis of its metabolites, a total of six new compounds were obtained.

To the best of our knowledge, this is the first report of isoquinoline-type metabolites from the edible fungi genus *Monascus*. These results demonstrate that *Monascus* produces unique and diverse metabolites in different fermentation conditions and soil-derived collections. Therefore, in a special ecological environment, more natural products with biological activity may be found by searching for *Monascus* species.

Biological Studies

Culture broth from *M. purpureus* wmd2424 was tested for antifungal activity against the following fungi: *Aspergillus niger* (BCRC-31512), *Penicillium italicum* (BCRC-30567), *Candida albicans* (BCRC-21538), and *Saccharomyces cerevisiae* (BCRC-20822). The antifungal data are shown in Table 3 and the clinically used antifungal drug ketoconazole was employed as a positive control.

Table 3. Antifungal activity of five sufficient compounds isolated from the culture broth of *A. punica* 04107M (diameter of the zone of growth-inhibitory fungicidal zone is given in mm, including the diameter of the disk, which is 8 mm).

Test Microorganism	Isolated Compounds					
	1	**2**	**3**	**4**	**5**	**Ketoconazole**
A. niger	15.4 ± 0.7	29.1 ± 3.5	29.3 ± 1.9	32.0 ± 1.8	27.5 ± 2.8	34.2 ± 1.8
P. italicum	17.8 ± 1.2	28.5 ± 2.1	29.4 ± 1.4	28.3 ± 3.1	17.5 ± 2.2	35.9 ± 2.3
C. albicans	16.2 ± 5.4	27.6 ± 3.9	36.2 ± 3.6	31.2 ± 3.5	28.0 ± 3.1	39.3 ± 3.1
S. cerevisiae	12.9 ± 1.1	30.1 ± 4.0	21.9 ± 2.5	28.2 ± 2.8	27.3 ± 1.4	34.2 ± 1.1

Inhibitory zone diameter (mm); ± inhibitory zone; positive control (STD): ketoconazole. Each value represents the mean ± SD.

Our results indicate that compounds **3–5** have moderate antifungal activity compared to ketoconazole, with **1** being weaker. From the results of the antifungal tests, the following conclusions can be drawn about these isolates: (a) within the novel strain, the 2,3-dimethylcyclohex-2-en-1-one (compound **2**) and γ-lactone (compound **3**) showed antifungal activities with inhibition zones of 29, 28, 27, and 30 mm, and 29, 29, 36, and 21 mm against *Aspergillus niger* (BCRC-31512), *Penicillium italicum* (BCRC-30567), *Candida albicans* (BCRC-21538), and *Saccharomyces cerevisiae* (BCRC-20822), respectively. (b) The xanthonoids (compound **1**) exhibited weak antifungal activities against the *Aspergillus niger* (BCRC-31512), *Penicillium italicum* (BCRC-30567), *Candida albicans* (BCRC-21538), and *Saccharomyces cerevisiae* (BCRC-20822) strains. (c) The other type of isoquinoline, Monascuspurin D (compound **4**), indicated effective inhibition zones of 32, 28, 31, and 28 mm against *Aspergillus niger* (BCRC-31512), *Penicillium italicum* (BCRC-30567), *Candida albicans* (BCRC-21538), and *Saccharomyces cerevisiae* (BCRC-20822), respectively. (d) The azaphilone compound **5** exhibited moderate antifungal activities against the *Aspergillus niger* (BCRC-31512) and *Candida albicans* (BCRC-21538) strains (Table 3).

The inhibitory activity of compounds **3–5** against *A. niger*, *P. italicum*, *C. albicans*, and *S. cerevisiae* was further tested using the method described in the experimental section (Table 4). Compound **2** has inhibitory activity against *S. cerevisiae*, with MIC values of 43.45 μg/mL. Compound **3** has inhibitory activity against *C. albicans*, with an MIC value of 32.87 μg/mL. Compound **4** was found to have moderate inhibitory activity against the *A. niger*, and *C. albican* strains with MIC values ranging from 29.65 and to 58.43 μg/mL. They were less biologically active than the reference compound, ketoconazole, which had MIC values of 4.10, 5.34, 10.88, and 3.57 μg/mL against *A. niger*, *P. italia*, *C. albicans*, and *S. cerevisiae*, respectively. In this bioassay, no antifungal activity (MIC > 100) was observed for compound **5** at concentrations below 100 μg/mL.

Table 4. MIC values of compounds **2–5** in μg/mL against four fungi strains.

Compounds	*A. niger*	*P. italicum*	*C. albicans*	*S. cerevisiae*
2	>100	>100	>100	43.45 ± 2.33 [a]
3	>100	>100	32.87 ± 2.19 [a]	>100
4	29.65 ± 3.54 [a]	>100	58.43 ± 1.51 [a]	>100
5	>100	>100	>100	>100
Ketoconazole	4.10 ± 0.84 [a]	5.34 ± 2.56 [a]	10.88 ± 5.67 [a]	3.57 ± 0.98 [a]

[a] Each value represents the mean ± SD.

4. Materials and Methods

4.1. General Experimental Procedures

For the TLC, we used silica gel 60 F254-precoated plates (Merck); for column chromatography (CC), we used silica gel 60 (70–230 or 230–400 mesh, Merck) and Spherical C18 100A Reversed Phase Silica Gel (RP-18) (particle size: 20–40 μm) (Silicycle). For the HPLC analysis, we used a spherical C18 column (250 mm × 10 mm, 5 μm) (Waters) and LDC-Analytical-III apparatus. For the UV spectra, we used a Jasco UV-240 spectrophotometer, with λmax (log ε) in nm. For optical rotation, we used a Jasco DIP-370 polarimeter, in CHCl3. For the IR spectra, we used a Perkin-Elmer-2000 FT-IR spectrophotometer, with ν in cm^{-1}. For the 1H-, 13C-, and 2D-NMR spectra, we used Varian-VNMRS-600 and Varian-Unity-Plus-400 spectrometers; δ in ppm relative to Me4Si, J in Hz. For the ESI and HRESIMS, we used a Bruker APEX-II mass spectrometer, in *m/z*.

4.2. Microorganism, Cultivation, and Preparation of the Strain

This WMD2424 strain was isolated from the mangrove wetland collected in Chiayi County, Taiwan, using HV agar and cultured at 28 °C for 3 weeks. A voucher specimen was immersed in 15% glycerol–water solution at −80 °C and deposited at the Bioresource Collection and Research Center (BCRC) of the Food Industry Research and Development Institute (FIRDI). Analysis of the ITS rDNA using the BLAST database screening provided a 99.9% match with *Monascus purpureus*, whose sequence has been submitted to GenBank.

To each 500-mL flask containing 150 mL of liquid RGY medium (3% rice starch, 7% glycerol, 1.5% polypeptone, 3% soybean powder, 0.2% MgSO4, and 0.2% NaNO3) were added 10 mL of fungal inocula and incubated at 25° for 2 weeks on a rotary shaker at the speed of 100 circles/min without illumination. A total of 14.0 L of fungal fermented broth was harvested and then filtered to remove fungal mycelium.

4.3. Isolation and Characterization of Secondary Metabolites

Liquid fermentate of M. purpureus (14.0 L) was extracted with BuOH to yield a BuOH extract (16.9 g), which was partitioned in EtOAc–H2O (1:1; 2 L × 3) to produce an EtOAc-soluble fraction (8.9 g) and an H2O-soluble fraction. The active EtOAc-soluble fraction (8.9 g) was subjected to silica gel column chromatography (CC) using CH2Cl2–MeOH (100:1) as the primary eluent, gradually increasing the eluent polarity with MeOH to produce 10 fractions (Frs. 1–Frs. 10). Fr. 2 was subjected to RP-18 silica gel CC using H2O–acetone (2:1) as the eluent to produce 5 fractions (Frs. 2-1–2-5), Fr. 2-5 (432 mg) was subjected to silica gel CC using CH2Cl2–EtOAc (3:1) as the eluent to produce 4 fractions (Frs. 2-5-1–Frs. 2-5-4), Fr. 2-5-3 was further subjected to silica gel CC using CH2Cl2–EtOAc (2:1) as the eluent to give **1** (1.2 mg) and **2** (3.0 mg). Fr. 3 was subjected to RP-18 silica gel CC using H2O–acetone (1:1) as the eluent to obtain 8 fractions (Frs. 3-1–3-8), Fr.3-8 was further subjected to silica gel CC using CH2Cl2–acetone (1:1) as the eluent to give 11 fractions (Frs. 3-8-1–Frs. 3-8-11), Fr. 3-8-10 was purified with prep. TLC (CH2Cl2/EtOAc 6:1) to obtain **4** (1.8 mg). Fr. 5 (1132 mg) was subjected to RP-18 silica gel CC using H2O–acetone (1:1) as the eluent to give **3** (1.2 mg) and **5** (3.3 mg).

Monascuspurin A (compound **1**): Oil. $[\alpha]^{26}$D: +34.2 (*c* 0.01, CHCl3). UV (MeOH) λmax (log ε) 268 (4.11), 360 (3.89) nm. IR νmax (neat) 3406 (OH), 1710, 1680 (C=O), 1615, 1450, 1406 (aromatic ring) cm^{-1}. CD (MeOH) λext 215 (Δε −10.9), 232 (Δε −4.2), 251 (Δε −7.9), 273 (Δε +5.2), 296 (Δε −2.3), 342 (Δε +7.3), 400 (Δε −6.7) nm. ESI-MS *m/z* 439 [M+Na]$^+$. 1H NMR (600 MHz, CDCl3): see Table 1. HRESI-MS *m/z*: 439.13640 [M+Na]$^+$ (calculated for C22H24O8Na, 439.13636).

Monascuspurin B (compound **2**): Oil. $[\alpha]^{26}$D: + 54.2 (*c* 0.01, CHCl3). UV (MeOH): 242 (3.98) nm. IR (neat): 3410 (OH), 1715 (C=O), 1675 (C=O) cm^{-1}. CD (MeOH) λext 225 (Δε −1.9), 241 (Δε +0.9), 282 (Δε −0.3) nm. 1H NMR (600 MHz, CDCl3): see Table 1; 13C NMR (150 MHz, CDCl3): see Table 2. ESI-MS *m/z* 305 [M+Na]$^+$. HRESI-MS *m/z*: 305.13598 [M+Na]$^+$, (calculated for C15H22O5Na, 305.13592).

Monascuspurin C (compound **3**): Oil. $[\alpha]^{26}_{D}$: +74.2 (*c* 0.01, CHCl$_3$). UV (MeOH): 285 (3.26) nm. IR (Neat): 3410 (OH), 1770, 1715 (C=O) cm^{-1}. CD (MeOH) λ_{ext} ($\Delta\varepsilon$): 225 ($\Delta\varepsilon$ −1.89), 250 ($\Delta\varepsilon$ +1.79), 290 ($\Delta\varepsilon$ −1.08), 335 ($\Delta\varepsilon$ −1.69) nm. ^{1}H-NMR (600 MHz, CDCl3): see Table 1; ^{13}C-NMR (150 MHz, CDCl$_3$): see Table 2. ESI-MS *m/z* 345 [M+Na]$^+$. HRESI-MS *m/z*: 345.16780 [M+Na]$^+$, C$_{18}$H$_{26}$O$_5$ (calculated for C$_{15}$H$_{13}$O, 345.16779).

Monascuspurin D (compound **4**): oil; $[\alpha]^{26}_{D}$: + 15.9 (*c* 0.01, CHCl$_3$); UV (MeOH): 220 (4.01), 252 (4.22), 312 (3.89) nm; IR (neat): 3400 (OH), 1712, 1656 (C=O), 1589, 1535, 1458 (pyridine) cm^{-1}; CD (MeOH) λ_{ext} ($\Delta\varepsilon$) 240 ($\Delta\varepsilon$ +13.19), 262 ($\Delta\varepsilon$ +5.13), 319 ($\Delta\varepsilon$ +1.98), 333 ($\Delta\varepsilon$ +2.01), 365 ($\Delta\varepsilon$ −2.81) nm. ^{1}H-NMR (600 MHz, CDCl$_3$): see Table 1; ^{13}CNMR (150 MHz, CDCl$_3$): see Table 2; ESI-MS *m/z* 331 [M+Na]$^+$; HRESIMS *m/z* 331.10588 [M+Na]$^+$ (calculated for C$_{18}$H$_{16}$NO$_4$, 331.10586).

Monascuspurin E (compound **5**): oil; $[\alpha]^{26}_{D}$: +56.7 (*c* 0.01, CHCl$_3$); UV (MeOH): 235 (4.22), 285 (3.89) nm; IR (neat): 3400 (OH), 1780, 1695 (C=O), 1615, 1577 (aromatic ring) cm^{-1}; ^{1}H-NMR (600 MHz, CDCl$_3$): see Table 1; ^{13}C-NMR (150 MHz, CDCl$_3$): see Table 2; ESI-MS *m/z* 409 [M+Na]$^+$; HRESIMS *m/z* 409.19912 [M+Na]$^+$ (calculated for C$_{23}$H$_{30}$O$_5$Na, 409.19909).

Computational Methods

The theoretical ECD curves of compounds **1**–**5** were calculated by using Gaussian 09, Revsion E.01. software. Conformational searches were performed using Spartan'14 software with the Molecular Merck force field (MMFF). ECD spectra of conformers with a Boltzmann distribution over 2% were calculated via the TD-DFT method at the B3LYP/6.311+G (d,p) level in MeOH. According to a Gaussian band shape with a 0.2 eV exponential half-width from the dipole-length dipolar and rotational strengths, the theoretical ECD spectra were generated using the SpecDis 3.0.

4.4. Antifungal Activity Assays

The assays tested for the presence of microorganisms. The in vitro antifungal activity of compounds **1**–**5** was tested against a panel of laboratory control strains belonging to the Bioresource Collection and Research Center (BCRC) in Hsinchu, Taiwan, namely, the fungal organisms *Aspergillus niger* (BCRC-31512), *Penicillium italicum* (BCRC-30567), *Candida albicans* (BCRC-21538), and *Saccharomyces cerevisiae* (BCRC-20822).

4.4.1. Via Disk Diffusion Assay

Antifungal susceptibility testing of the isolated compounds was performed with the following strains: *Aspergillus niger*, *Penicillium italicum*, *Candida albicans*, and *Saccharomyces cerevisiae* using the disk diffusion method and the following CLSI guidelines were applied: M44-A and M44-S2 for yeasts [40,41] and M-51P for filamentous fungi. A standard disk of ketoconazole was used as a positive control, while a disk imbued with 50 µL of pure DMSO was used as a negative control. The diameters of the inhibition zones were measured in millimeters by means of a slide caliper. Each test was performed in triplicate, and the results were analyzed for statistical significance [40–42].

4.4.2. Via Broth Dilution Assay

The MIC determination for the antifungal assay was performed according to the Clinical and Laboratory Standard Institute (CLSI) using the broth dilution assay method [43–45]. Extract stock solutions and partitions were prepared in 5% DMSO, and twofold serial dilutions were prepared in RPMI in 96-well microtiter plates (Corning Incorporated, Corning, NY, USA). The final concentrations ranged from 0.98 to 2.000 g mL^{-1}. Test organisms (100 µL) were added to each well in microtiter plates. The growth control contained medium and inoculum. Blank controls contained medium only. The microtiter plates were then incubated at 35 °C and the endpoints were read after 48 h. The lowest concentration for each test compound at which color change occurred was recorded as its primary MIC value. The average of primary values from three individual tests were calculated, and the average was taken as the final MIC value for each of the test compounds.

5. Conclusions

Red yeast rice is a well-known material which has been widely used for decades, but the chemistry and bioactivity of the constituents are still not so clear. Previous investigation of *Monascus* species had isolated different skeleton constituents, mainly azaphilones and monacolin analogs. However, some minor compounds such as benzenoid derivatives or other types of compounds from *Monascus* species have received less attention. Accordingly, it is still worth investigating the ingredients and bioactivity of red yeast rice.

In this report, we committed to explore unusual skeleton compounds in *M. purpureus* wmd2424, and successfully found new xanthonoid, cyclohexenone, γ-lactone, isoquinoline, and azaphilone skeleton compounds. Xanthonoids are yellow pigments in a C_6-C_1-C_6 system and restricted in a few families of higher plants, some fungi and lichens, and has seldom been found in *Monascus* spp. [46] This is the second report of isolating xanthonoids from *Monascus spp*, which represent different yellow azaphilone pigments (monascin, ankaflavin) from this genus. The structures of these isolates were determined using spectroscopic experiments. The BuOH soluble fraction from the *M. purpureus* wmd2424 fermentation broth was tested for antifungal activities. Our results indicated that compounds **3–5** displayed moderate antifungal activities against *Aspergillus niger*, *Penicillium italicum*, *Candida albicans*, and *Saccharomyces cerevisiae*. It is worth mentioning that the chemical composition of *M. purpureus* wmd2424 has never been studied. The result indicated *M. purpureus* wmd2424 could produce more metabolites with extensive antifungal activity, and that its metabolites in other mediums were worth being studied further.

Author Contributions: M.-J.C. designed the research and performed the research; M.-D.W. conducted the biological assays; M.-J.C. and J.-J.C. performed the isolation and structure elucidation of the constituents; and M.-J.C. organized the data and wrote the paper. All authors have read and agreed to the published version of the manuscript.

Conflicts of Interest: The authors declare no conflict of interest.

References

1. Nout, M.J.R.; Aidoo, K.E. Asian fungal fermented food. In *Industrial Applications*; Hofrichter, M., Ed.; Springer: Berlin/Heidelberg, Germany, 2011; pp. 29–58.
2. Liu, B.H.; Wu, T.S.; Su, M.C.; Chung, C.P.; Yu, F.Y. Evaluation of citrinin occurrence and cytotoxicity in *Monascus* fermentation products. *J. Agric. Food Chem.* **2005**, *53*, 170–175. [CrossRef] [PubMed]
3. Ma, J.; Li, Y.; Ye, Q.; Li, J.; Hua, Y.; Ju, D.; Zhang, D.; Cooper, R.; Chang, M. Constituents of red yeast rice, a traditional Chinese food and medicine. *J. Agric. Food Chem.* **2000**, *48*, 5220–5225. [CrossRef] [PubMed]
4. Endo, A. Monacolin K, a new hypocholesterolemic agent produced by a *Monascus* species. *J. Antibiot.* **1979**, *32*, 852–854. [CrossRef] [PubMed]
5. Endo, A. A historical perspective on the discovery of statins. *P. Jpn. Acad. B-PHYS.* **2010**, *86*, 484–493. [CrossRef] [PubMed]
6. Lee, C.L.; Tsai, T.Y.; Wang, J.J.; Pan, T.M. In vivo hypolipidemic effects and safety of low dosage Monascus powder in a hamster model of hyperlipidemia. *Appl. Microbiol. Biotechnol.* **2006**, *70*, 533–540. [CrossRef]
7. Li, X.; Liu, C.; Duan, Z.; Guo, S. HMG-CoA reductase inhibitors from *Monascus*-fermented rice. *J. Chem.* **2013**, *2013*, 6. [CrossRef]
8. Shi, Y.C.; Pan, T.M. Anti-diabetic effects of *Monascus purpureus* NTU 568 fermented products on streptozotocin-induced diabetic rats. *J. Agric. Food Chem.* **2010**, *58*, 7634–7640. [CrossRef]
9. Akihisa, T.; Tokuda, H.; Yasukawa, K.; Ukiya, M.; Kiyota, A.; Sakamoto, N.; Suzuki, T.; Tanabe, N.; Nishino, H. Azaphilones, furanoisophthalides, and amino acids from the extracts of *Monascus pilosus*-fermented rice (red-mold rice) and their chemopreventive effects. *J. Agric. Food Chem.* **2005**, *53*, 562–565. [CrossRef]
10. Hsu, L.C.; Liang, Y.H.; Hsu, Y.W.; Kuo, Y.H.; Pan, T.M. Anti-inflammatory properties of yellow and orange pigments from *Monascus purpureus* NTU 568. *J. Agric. Food Chem.* **2013**, *61*, 2796–2802. [CrossRef]

11. Yasukawa, K.; Takahashi, M.; Natori, S.; Kawai, K.I.; Yamazaki, M.; Takeuchi, M.; Takido, M. Azaphilones inhibit tumor promotion by 12-*O*-tetradecanoylphorbol-13-acetate in two-stage carcinogenesis in mice. *Oncology* **1994**, *51*, 108–112. [CrossRef]
12. Cottone, S.; Lorito, M.; Riccobene, R.; Nardi, E.; Mulè, G.; Buscemi, S.; Geraci, C.; Guarneri, M.; Arsena, R.; Cerasola, G. Oxidative stress, inflammation and cardiovascular disease in chronic renal failure. *J. Nephrol.* **2008**, *21*, 175–179.
13. Hong, M.Y.; Seeram, N.P.; Zhang, Y.; Heber, D. Anticancer effects of Chinese red yeast rice versus monacolin K alone on colon cancer cells. *J. Nutr. Biochem.* **2008**, *19*, 448–458. [CrossRef] [PubMed]
14. Zhu, L.; Yau, L.F.; Lu, J.G.; Zhu, G.Y.; Wang, J.R.; Han, Q.B.; Hsiao, W.L.; Jiang, Z.H. Cytotoxic dehydromonacolins from red yeast rice. *J. Agric. Food Chem.* **2012**, *60*, 934–939. [CrossRef]
15. Chang, W.T.; Chuang, C.H.; Lee, W.J.; Huang, C.S. Extract of *Monascus purpureus* CWT715 fermented from sorghum liquor biowaste inhibits migration and invasion of SK-Hep-1 human hepatocarcinoma cells. *Molecules* **2016**, *21*, 1691. [CrossRef] [PubMed]
16. Chiu, H.W.; Chen, M.H.; Fang, W.H.; Hung, C.M.; Chen, Y.L.; Wu, M.D.; Yuan, G.F.; Wu, M.J.; Wang, Y.J. Preventive effects of *Monascus* on androgen-related diseases: Androgenetic alopecia, benign prostatic hyperplasia, and prostate cancer. *J. Agric. Food Chem.* **2013**, *61*, 4379–4386. [CrossRef] [PubMed]
17. Lee, J.S.; Kim, H.C.; Park, S.W.; So, H.S.; Woo, C.Y.; Choi, J.H.; Kim, S.H.; Kim, S.J.; Oh, Y.M. A case of isolated pulmonary mucormycosis in an immunocompetent host. *Tuberc. Respir. Dis.* **2013**, *74*, 269–273. [CrossRef] [PubMed]
18. Wellen, K.E.; Hotamisligil, G.S. Inflammation, stress, and diabetes. *J. Clin. Invest.* **2005**, *115*, 1111–1119. [CrossRef] [PubMed]
19. Leonie, K.H.; Lesley, V.C. Adipose tissue macrophages, low grade inflammation and insulin resistance in human obesity. *Curr. Pharm. Des.* **2008**, *14*, 1225–1230.
20. Kamer, A.R.; Craig, R.G.; Dasanayake, A.P.; Brys, M.; Glodzik-Sobanska, L.; de Leon, M.J. Inflammation and Alzheimer's disease: Possible role of periodontal diseases. *Alzheimers Dement.* **2008**, *4*, 242–250. [CrossRef]
21. Vasto, S.; Candore, G.; Listì, F.; Balistreri, C.R.; Colonna-Romano, G.; Malavolta, M.; Lio, D.; Nuzzo, D.; Mocchegiani, E.; Di Bona, D.; et al. Inflammation, genes and zinc in Alzheimer's disease. *Brain Res. Rev.* **2008**, *58*, 96–105. [CrossRef]
22. Martínková, L.; J°zlová, P.; Veselý, D. Biological activity of polyketide pigments produced by the fungus *Monascus*. *J. Appl. Microbiol.* **1995**, *79*, 609–616.
23. Martínková, L.; Patáková-Jůzlová, P.; Krent, V.; Kucerová, Z.; Havlícek, V.; Olsovský, P.; Hovorka, O.; Ríhová, B.; Veselý, D.; Veselá, D.; et al. Biological activities of oligoketide pigments of *Monascus purpureus*. *Food Addit. Contam.* **2001**, *16*, 15–24. [CrossRef] [PubMed]
24. Kim, C.; Jung, H.; Kim, J.H.; Shin, C.S. Effect of *monascus* pigment derivatives on the electrophoretic mobility of bacteria, and the cell adsorption and antibacterial activities of pigments. *Colloids Surf. B* **2006**, *47*, 153–159. [CrossRef] [PubMed]
25. Zhao, G.P.; Li, Y.Q.; Yang, J.; Cui, K.Y. Antibacterial characteristics of orange pigment extracted from *Monascus* pigments against *Escherichia coli*. *Czech J. Food Sci.* **2016**, *34*, 197–203. [CrossRef]
26. Kim, C.; Jung, H.; Kim, Y.O.; Shin, C.S. Antimicrobial activities of amino acid derivatives of *monascus* pigments. *FEMS Microbiol. Lett.* **2006**, *264*, 117–124. [CrossRef] [PubMed]
27. Jůzlová, P.; Martínková, L.; Křen, V. Secondary metabolites of the fungus *Monascus*: A review. *J. Ind. Microbiol.* **1996**, *16*, 163–170. [CrossRef]
28. Wong, H.C.; Koehler, P.E. Production and isolation of an antibiotic from *Monascus purpureus* and its relationship to pigment production. *J. Food Sci.* **1981**, *46*, 589–592. [CrossRef]
29. Fabric, C.E.; Santerre, A.L.; Loret, M.O.; Baberian, R.; Pareilleux, A.; Goma, G.; Blanc, P.J. Production and food applications of the red pigments of *Monascus ruber*. *J. Food Sci.* **1993**, *58*, 1099–1102.
30. Sun, J.M.; Kim, S.J.; Kim, G.W.; Rhee, J.K.; Kim, N.D.; Jung, H.; Jeun, J.; Lee, S.H.; Han, S.H.; Shin, C.S.; et al. Inhibition of hepatitis C virus replication by Monascus pigment derivatives that interfere with viral RNA polymerase activity and the mevalonate biosynthesis pathway. *J. Antimicrob. Chemother.* **2011**, *67*, 49–58. [CrossRef]
31. Hsu, Y.W.; Hsu, L.C.; Liang, Y.H.; Kuo, Y.H.; Pan, T.M. Monaphilones A−C, three new antiproliferative azaphilone derivatives from *Monascus purpureus* NTU 568. *J. Agric. Food Chem.* **2010**, *58*, 8211–8216. [CrossRef]
32. Jongrungruangchok, S.; Kittakoop, P.; Yongsmith, B.; Bavovada, R.; Tanasupawat, S.; Lartpornmatulee, N.; Thebtaranonth, Y. Azaphilone pigments from a yellow mutant of the fungus *Monascus kaoliang*. *Phytochemistry* **2004**, *65*, 2569–2575. [CrossRef] [PubMed]
33. Loret, M.-O.; Morel, S. Isolation and structural characterization of two new metabolites from *Monascus*. *J. Agric. Food Chem.* **2010**, *58*, 1800–1803. [CrossRef] [PubMed]
34. Kim, D.; Ku, S. Beneficial effects of *Monascus* sp. KCCM 10093 pigments and derivatives: A mini review. *Molecules* **2018**, *23*, 98. [CrossRef] [PubMed]
35. Wu, H.C.; Chen, Y.F.; Cheng, M.J.; Wu, M.D.; Chen, Y.L.; Chang, H.S. Investigations into Chemical Components from *Monascus purpureus* with Photoprotective and Anti-Melanogenic Activities. *J. Fungi* **2021**, *7*, 619. [CrossRef]
36. Diedrich, C.; Grimme, S. Systematic investigation of modern quantum chemical methods to predict electronic circular dichroism spectra. *J. Phys. Chem. A* **2003**, *107*, 2524–2539. [CrossRef]
37. Ma, M.Z.; Ge, H.J.; Yi, W.W.; Wu, B.; Zhang, Z.Z. Bioactive drimane sesquiterpenoids and isocoumarins from the marine-derived fungus *Penicillium minioluteum* ZZ1657. *Tetrahedron Lett.* **2020**, *61*, 151504. [CrossRef]

38. Knecht, A.; Cramer, B.; Humpf, H.-U. New *Monascus* metabolites: Structure elucidation and toxicological properties studied with immortalized human kidney epithelial cells. *Mol. Nutr. Food. Res.* **2006**, *50*, 314–321. [CrossRef]
39. Takikawa, H.; Hachisu, Y.; Bode, J.W.; Suzuki, K. Catalytic enantioselective crossed aldehyde-ketone benzoin cyclization. *Angew. Chem. Int. Ed. Engl.* **2006**, *45*, 3492–3494. [CrossRef]
40. Clinical and Laboratory Standards Institute. *Method for Antifungal Disk Diffusion Susceptibility Testing of Yeasts, Approved Guideline, CLSI Document M44-A*; Clinical and Laboratory Standards Institute: Wayne, PA, USA, 2004.
41. Clinical and Laboratory Standards Institute. *Zone Diameter Interpretive Standards, Corresponding Minimal Inhibitory Concentration (MIC) Interpretive Breakpoints, and Quality Control Limits for Antifungal Disk Diffusion Susceptibility Testing of Yeasts, Informational Supplement, CLSI Document M44-S2*, 2nd ed.; Clinical and Laboratory Standards Institute: Wayne, PA, USA, 2008.
42. Clinical and Laboratory Standards Institute. *Method for Antifungal Disk Diffusion Susceptibility Testing of Filamentous Fungi, Proposed Guideline, CLSI Document M51-P*; Clinical and Laboratory Standards Institute: Wayne, PA, USA, 2008.
43. Clinical and Laboratory Standards Institute. *Reference Method for Broth Dilution Antifungal Susceptibility Testing of Yeasts, Approved Standard, CLSI Document M27-A3*, 3rd ed.; Clinical and Laboratory Standards Institute: Wayne, PA, USA, 2008.
44. Clinical and Laboratory Standards Institute. *Reference Method for Broth Dilution Antifungal Susceptibility Testing of Yeasts, Informational Supplement, CLSI Document M27-S3*, 3rd ed.; Clinical and Laboratory Standards Institute: Wayne, PA, USA, 2008.
45. Clinical and Laboratory Standards Institute. *Reference Method for Broth Dilution Antifungal Susceptibility Testing of Filamentous Fungi, Approved Standard, CLSI Document M38-A2*, 2nd ed.; Clinical and Laboratory Standards Institute: Wayne, PA, USA, 2008.
46. Velíšek, J.; Davídek, J.; Cejpek, K. Biosynthesis of food constituents: Natural pigments. Part 2—A review. *Czech J. Food Sci.* **2008**, *26*, 73–98. [CrossRef]

MDPI